TIROS IV
RADIATION DATA CATALOG
AND
USERS' MANUAL

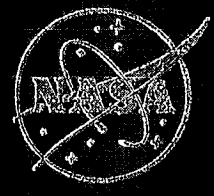

GODDARD SPACE FLIGHT CENTER
GREENBELT, MARYLAND

TIROS IV
RADIATION DATA CATALOG
AND
USERS' MANUAL

By
Staff Members
of the
Aeronomy and Meteorology Division
Goddard Space Flight Center
National Aeronautics and Space Administration

December 15, 1963

FOREWORD

This combination Catalog and Users' Manual represents a new documentation format for the TIROS IV five-channel medium resolution scanning radiometer experiment. It replaces the two separate companion volumes which were published previously for TIROS II and TIROS III.

Many members of the staff of the Aeronomy and Meteorology Division contributed to the success of the TIROS IV medium resolution radiometer experiment. Valuable contributions in the areas of laboratory measurements of materials and computer programming for data processing came from the National Weather Satellite Center, U. S. Weather Bureau, whose efforts are gratefully acknowledged.

The task of assembling the information contained in this manual into written form suitable for publication was largely accomplished by the following members of the Aeronomy and Meteorology Division:

Mr. Virgil G. Kunde, Editor	Mr. George Nicholas
Mr. W. R. Bandeen	Mr. R. E. Samuelson
Miss Musa Halev	Mrs. I. Persano Strange
Mr. Robert Hite	Mr. Harold P. Thompson

The efforts of the above individuals are hereby acknowledged.

The preparation of the material presented in Appendix A and Appendix B was accomplished mainly through the efforts of Mr. Saul Adelman and Mr. Fred Siskind.

ABSTRACT

The TIROS IV Meteorological Satellite contains a medium resolution scanning radiometer. Two of the channels of this instrument are sensitive to reflected solar radiation and the remaining two respond to emitted thermal radiation from the earth and its atmosphere. The two thermal channels are calibrated in terms of equivalent blackbody temperatures, and the reflected solar radiation channels in terms of effective radiant emittances. The calibration data, along with orbital and attitude data and the radiation data from the satellite, were incorporated in a computer program for an IBM 7090 which was used to produce, in binary form, the "Final Meteorological Radiation Tape" which is the basic repository of all radiation data.

After launch, the radiometer displayed the same degradation of response characteristics as did its predecessors in TIROS II and TIROS III. The onset of degradation results in a departure of the data from the prelaunch laboratory calibration. The cause of degradation has not been determined, and the matter is still being studied at the Goddard Space Flight Center.

Before work with the TIROS IV radiation data is attempted, an understanding of the radiometer, its calibration, and the problems encountered in the experiment, especially from response degradation, is essential. The instrumentation design, development work, and the calibrations herein described were performed by the Goddard Space Flight Center staff, whereas the computer and programming efforts were carried out jointly by the staffs of the National Weather Satellite Center, U. S. Weather Bureau, and the Goddard Space Flight Center.

In this Catalog-Manual, the radiometer and its calibration, data processing, the "Final Meteorological Radiation Tape", the observed degradation patterns, and possible corrections for degradation are discussed. The Catalog-Manual also includes, in two forms, documentation of each orbit of successfully reduced radiation data acquired by TIROS IV. One method of presentation is the Index of Final Meteorological Radiation Tapes and the other is a Subpoint Track Summary of Available Radiation Data in diagrammatic form.

TABLE OF CONTENTS

LIST OF FIGURES

LIST OF TABLES

LIST OF COMMON SYMBOLS

A^c Cumulative quasi-global albedo

A^i Quasi-global albedo

A_λ Spectral Absorptivity of the thermistor detector

D Digital Number: scale 0 to 127

F Number of cycles-per-second above the base frequency of a given 50 cps subcarrier band

ΔF The flight measured space-level (both directions viewing outer space) minus the ground-calibrated "space-level" (both directions viewing blackbodies of liquid nitrogen temperatures (—196°C) in terms of cycles-per-second of a given 50 cps subcarrier band

F_{SC} Output frequency of the voltage controlled oscillator

J_λ Spectral radiant intensity of visible light source, i.e., a standard tungsten lamp or the sun (watts/steradian/micron)

P^c Cumulative quasi-global emitted radiant power

$\overline{P}^c$ Cumulative quasi-global effective emitted radiant power

P^i Quasi-global emitted radiant power

$\overline{P}^i$ Quasi-global effective emitted radiant power

R_λ^B Spectral reflectivity of the black half of the chopper disk

R_λ^M Spectral reflectivity of the aluminized half of the chopper disk

R_λ^P Spectral reflectivity of the radiometer prism

R_λ The ratio $\dfrac{R_\lambda^B}{R_\lambda^M}$

R Distance from the visible light source to the center of the diffuse reflector

T_{BB} Equivalent blackbody temperature (degrees Kelvin)

T_C Radiometer housing temperature

T_E Satellite electronics temperature

W Total outgoing longwave flux

$W_\lambda(T)$ Spectral radiant emittance (the Planck function) for a blackbody of temperature T (watts/meter^2/micron)

$\overline{W}$ Effective radiant emittance (watts/meter^2)—defined by equation (2) for channels 1 and 2, and defined by equation (6) for channels 3 and 5

$\overline{W}^*$ Defined by equation (7)

V_{RAD} Output voltage of the the radiometer

f_λ Spectral transmission of the filter-lens combinations in the radiometer

r Constant in equation (8)

r_λ Spectral reflectivity of the diffuse reflector employed in the calibration of the visible channels

s Constant in equation (8)
Ω Solid angle of the sun as viewed from the earth
γ Incidence angle of radiation from visible light source impinging upon diffuse reflector employed in the calibration of the visible channels
λ Wavelength in microns
ϕ_λ Effective spectral response of the radiometer defined by equation (1)
$\Delta\phi$ Right ascension of the sun minus the right ascension of the orbital ascending node
δT_{BB} Channel 2 additive temperature corrections for floor and wall side

I. INTRODUCTION

The TIROS IV Meteorological Satellite was injected into orbit on February 8, 1962. Its mean orbital characteristics are listed in Table I.

TABLE I

Perigee Altitude	710 km
Apogee Altitude	845 km
Anomalistic Period	100.40 min.
Inclination	48.30°

The experiments flown in the satellite include two television cameras and three radiometers. The radiometers measure emitted thermal and reflected solar radiation from the earth and its atmosphere. One is a low resolution non-scanning instrument having two detectors, one white and the other black. A second radiometer is the University of Wisconsin's heat balance experiment.

This manual is concerned only with the third radiation measuring device, a five-channel medium resolution scanning radiometer, which responds to radiation in four different spectral regions. Two of these channels respond to emitted thermal radiation from the earth and its atmosphere and the other two channels respond to reflected solar radiation. The remaining channel, on TIROS IV only, was used to transmit a redundant time reference signal, thereby eliminating the broad band thermal radiation data which were transmitted via this channel in TIROS II and TIROS III. The two thermal radiation channels are calibrated in terms of equivalent blackbody temperatures and the reflected solar radiation channels in terms of effective radiant emittances.

The radiation data from the medium resolution radiometer experiment are processed together with orbital position and attitude information and calibration data on an IBM 7090 computer to produce a binary "Final Meteorological Radiation (FMR) Tape" which is the basic repository of the radiation data in terms of equivalent blackbody temperature or effective radiant emittance. An Index of all FMR tapes and a diagrammatic Subpoint Track Summary of the available radiation data for each orbit are included at the end of this Catalog-Manual.

Before attempting to interpret the radiation data from TIROS IV which are contained on the FMR tape, careful consideration should be given to all points discussed in this manual. An understanding of the significance of the equivalent blackbody temperatures or effective radiant emittance values and a familiarity with the principle of the radiometer, its peculiarities, and the method of calibration are essential. Before attempting to utilize the radiation data the effects of instrumental response degradation on the data must also be considered.

This combination Catalog and Users' Manual represents a new documentation format, replacing the two separate volumes which were published for the TIROS II and TIROS III five-channel radiometer experiments.[1,2,3,4] The previous separate catalogs described and illustrated in detail the several basic mapping programs which are available upon request for the further machine processing which is required of the FMR Tapes before the data can be subjected to manual analysis and interpretation. In view of the foregoing and because a catalog of the TIROS II and TIROS III type can contain at best only a small fraction of the available data before the size of the volume becomes prohibitively large, it was decided not to publish mapped samples of data from TIROS IV, which would be similar to samples already published from previous satellites.

Instead, persons wishing to utilize radiation data in any of the standard mapping formats illustrated in the TIROS II and TIROS III Catalogs may request single copies in limited quantities by writing to:

TIROS Radiation Data, Code 651
Aeronomy and Meteorology Division
NASA Goddard Space Flight Center
Greenbelt, Maryland, 20771

When requesting such data the following information should be given *(See Frame top of page 2)*. All terms are discussed fully in subsequent parts of this manual.

Routinely, a data population map, indicating the number of individual measurements contained in each grid point average, will accompany each data coverage grid print map as well as a sample latitude-longitude overlay for geographically locating the data. Persons having additional questions concerning the data or the data reduction system, may obtain further information by writing to the above address.

For persons having access to computer facilities, copies of the FMR Tapes, containing the originally reduced data in their entirety, may be obtained at cost by writing to:

National Weather Records Center
Asheville, North Carolina

Television pictures taken concurrently with the radiation data may also be obtained from the National Weather Records Center.

1. Satellite: (e.g., TIROS II, III, or IV)
2. Read-Out Orbit No.:—(cf. Index of FMR Tapes)
3. Channel No.: (e.g., Channel 2, 8.0-12.0 microns; Channel 3, 0.2-6.0 microns; etc.)
4. Calendar Date (of Equator Crossing): (cf. Index of FMR Tapes)
5. Time Interval (Beginning and Ending) of Data Requested, in GMT: (cf. Index of FMR Tapes, Subpoint Track Summaries, and/or Orbital Overlays)
6. Format: Listings (Program MS 500) or Grid Print Maps. When requesting grid print maps list also:

   a. Map Base and Approximate Scale
      (1) Polar Stereographic, Low Resolution (AW 950)
      (2) Polar Stereographic, High Resolution (MS 501)
      (3) Multi-Resolution Mercator (MSC 2)
          5.0 degrees per mesh interval—1/40 million (approx.)
          2.5 degrees per mesh interval—1/20 million (approx.)
          1.25 degrees per mesh interval—1/10 million (approx.)

   b. Maximum sensor nadir angle: (unless otherwise specified, 58° will be used)

   c. Field Values and Contouring: (unless otherwise specified, all maps will include field values and contouring except Mercator Maps of scales larger than 1/20 million which will contain no field values or controuring; reference Section IV of TIROS III Catalog)

The availability of such pictures is documented in the Key to Meteorological Records Documentation No. 5.34, "Catalogue to Meteorological Satellite Data—TIROS IV Television Cloud Photography", copies of which may be obtained from the Superintendent of Documents, U. S. Government Printing Office, Washington 25, D. C.

II. DESCRIPTION OF THE MEDIUM RESOLUTION RADIOMETER EXPERIMENT

2.1 *Principle of the Radiometer*[5,6]

The principle of the radiometer is illustrated in Figure 1 where the components of a single channel are pictured. The fields of view of the channels are approximately coincident, each being about five degrees wide at the half-power point of the response. The optical axis of each channel is bi-directional 180° apart. As the half-aluminized, half-black chopper disk rotates, radiation from first one direction and then the other reaches the thermistor bolometer detector. This results in a chopped output which is amplified and rectified, giving a DC signal which (neglecting electronic noise and possible optical imbalance) is theoretically proportional to the difference in energy flux viewed in the two directions. Variations in the amplitude of the radiometer signal are converted into subcarrier frequency deviations and stored by means of a miniature magnetic tape recorder. When the satellite is interrogated, while within range of a Command and Data Acquisition Station, the information is telemetered back to earth where it is recorded on magnetic tape. The further processing of these magnetic tapes is discussed in Section IV of this manual.

The radiometer is mounted in the satellite such that the optical axes are inclined 45° to the satellite spin axis. (The viewing directions are designated "wall" and "floor" according to their orientation in the satellite.) When one optic views the earth, the other views outer space. Thus, the outer space radiation level (assumed to be zero) can be used as a reference. When both optics are viewing outer space, the resultant signal is designated as the "space-viewed level." Theoretically, this signal should be zero, but in reality is not, due to electronic noise and any initial optical imbalance, plus subsequent changes in balance caused by the degradation of certain channels after the laboratory calibration.

As the satellite rotates on its axis, the radiometer scan pattern on the surface of the earth is defined by the intersection of a 45° half-angle cone and a sphere. This pattern ranges from a circle when the spin vector is parallel to the orbital radius vector, to two hyperbola-like branches when the spin vector is perpendicular to the radius vector. The orbital motion of the satellite provides the scan advance. When viewing vertically downward from a height of about 780 km, the spatial resolution of the radiometer is about 68 km, i.e., the "spot" on earth viewed

by the radiometer has a diameter of about 68 km.

2.2 *Description of the Sensors*

The nominal channel bandwidths for the TIROS IV medium resolution radiometer are given in Table II.

TABLE II

Channel	Nominal Bandwidth (microns)	Nature of Band
1	6.0 - 6.5	Water vapor absorption
2	8.0 -12.0	Atmospheric window
3	0.2 - 6.0	Reflected solar radiation
4		Time reference channel for TIROS IV
5	0.55-0.75	Response of the TV system

In the 6.0 to 6.5 micron channel a maximum of absorption due to water vapor is encountered. Energy in this channel is therefore received mainly from the highest altitudes where water vapor may be found in the atmosphere. In contrast, the energy received in the 8.0 to 12.0 micron channel is received mainly from either the earth's surface and/or clouds since absorption due to any of the atmospheric constituents—except ozone which covers only a minor portion of this channel—is very small. The total solar energy reflected from the earth is contained in the 0.2 to 6.0 micron channel. The 0.55 to 0.75 micron channel is of interest because it covers only a narrow spectral region very near the maximum of the solar energy distribution, and it is similar in its spectral response to the TV cameras carried on the satellite.

The interpretation of the radiation data in terms of physically significant quantities has been presented in the literature.[7-24]

2.3 *Geographic Limitations of Data Utilization*

Care should be exercised in the use of the correlation of the radiation data with geographic location, such as attempted comparisons with synoptic situations. Uncertainties in attitude lead to an estimated maximum error of 1° to 2° in great circle arc. At a nadir angle of 0°, a 2° error would result in a position error on the surface of the earth of less than 20 miles. At a nadir angle of 60°, a 2° error corresponds to an error of more than 200 miles. It should be emphasized that such errors result in distortion as well as translation, and a simple linear shift of the data is in general not sufficient for correction. [25-30]

In addition to attitude errors, time errors also contribute to difficulties in geographic correlation. The principal sources of time errors are: mistakes at the ground station in transmission of the end-of-tape pulse, erroneous sensing by the analog-to-digital converter of the end-of-tape pulse, and the necessity of counting through noise on the relative satellite clock frequency. These errors are generally estimated to be less than ten seconds in TIROS IV. However, users are cautioned to be watchful for those rare cases where there still might be larger errors of the order of one minute or more. Time errors also result in distortion as well as translation.

III. CALIBRATION

Before considering the calibration flow sequence, it is necessary to discuss two quantities which are fundamental to the calibration. These are the effective spectral response and the effective radiant emittance.

3.1 *Effective Spectral Response*

The radiation received by the radiometer is modified by the various elements in the optical train before being absorbed by the bolometer detector. These include the reflecting properties of the prism and chopper, the transmission characteristics of filters and lenses, and the absorption properties of the detector. By assuming equal optical properties and temperature for both sides of the prism, an effective spectral response, ϕ_λ, can be defined as

$$\phi_\lambda = R_\lambda^P \ (R_\lambda^M - R_\lambda) \ f_\lambda A_\lambda \qquad (1)$$

In the actual computation of ϕ_λ, either the above expression or the expression

$$\phi_\lambda = R_\lambda^P (1 - R_\lambda) \ f_\lambda A_\lambda \qquad (2)$$

was used. The use of equation (2) assumes the reflectivity of the aluminized half of the chopper disk is independent of wavelength

The materials used in the lens and filter of each channel are given in Table III.

The spectral absorptivity of the thermistor detectors was determined by measurements made on sample Barnes Engineering Company bolometers of the same type as used in the radiometer. For all channels, the quantity A_λ was taken as the average of measurements made by the Barnes Engineering Company

on 10 bolometers in the spectral region, 0.3 to 16 microns, and by the Naval Ordnance Laboratory, Corona, California, on 9 bolometers in the region 0.5 to 30 microns. The two sets of measurements were normalized at 13 microns.

A discussion of the final values of ϕ_λ derived for each channel follows:

CHANNEL 1

The function f_λ was taken from Barnes Engineering Company measurements made on the channel 1 filter of the TIROS IV radiometer in combination with plane samples of the germanium lens elements. The Barnes measurement for the transmission of the germanium immersion lens used in this channel is also incorporated in the f_λ function. The function R_λ^P was taken from a Barnes measurement on a good $\lambda/4$ front-surfaced aluminum mirror. The value $(R_\lambda^M - R_\lambda)$ was a Barnes measurement made on the channel 1 chopper disk of the TIROS IV radiometer. The effective spectral response for channel 1 is given in Figure 2 and Table IV.

CHANNEL 2

The filter transmission was taken from measurements made on a similar filter by the Meteorological Satellite Laboratory of the U.S. Weather Bureau. The transmission of the germanium doublet lens was obtained by squaring a measurement made by Barnes on a plane sample of lens material having a thickness equivalent to the mean thickness of one of the lens elements. The product of filter-lens combination was used as the function f_λ. The quantity R_λ was taken from measurements performed at the Meteorological Satellite Laboratory of the U.S. Weather Bureau. The measurement of R_λ was made on a sample similar to the chopper disk of the radiometer. The function R_λ^P was taken from a Barnes measurements on a good $\lambda/4$ front-surfaced aluminum mirror. Beyond 16 microns, due to lack of measurements, the reflectivity was assumed to be constant at the 16 micron value. The effective spectral response for channel 2 is given in Figure 3 and Table V.

CHANNEL 3

The function f_λ was obtained from transmission measurements made by Barnes on the sapphire (Al_2O_3) and barium fluoride (BaF_2) lens. The value $(R_\lambda^M - R_\lambda^B)$ was measured by Barnes on the channel 3 chopper disk of the TIROS IV radiometer. The function R_λ^P was taken from an average of measurements taken by Barnes on the two reflecting surfaces of the prisms from radiometers 102A and 103A and from a Barnes measurements on a good $\lambda/4$ front-surfaced aluminum mirror. The effective spectral response is given in Figure 4 and Table VI.

CHANNEL 4

For reasons discussed in an earlier section, channel 4 was used for other purposes on TIROS IV thereby eliminating the infrared data for this channel.

CHANNEL 5

The transmission of the sapphire (Al_2O_3) and silicon dioxide (SiO_2) lens and interference filters were taken from Barnes measurements. The product of the above transmissivities is the function f_λ. The value $(R_\lambda^M - R_\lambda^B)$ was taken from the Barnes measurement on the channel 3, TIROS IV, radiometer. The function R_λ^P was taken from an average of measurements taken byBarnes on the two reflecting surfaces of the prisms from radiometers 102A and 103A and from a Barnes measurement on a good $\lambda/4$ front-surfaced aluminum mirror. The effective spectral response is given in Figure 5 and Table VII.

3.2 *Effective Radiant Emittance*

The pre-flight calibration of the two emitted thermal radiation channels (channels 1 and 2) was carried out by simulating the space-referenced earth signal in the laboratory. The radiometer's field of view is filled in one direction by a blackbody target at liquid nitrogen temperature (80°K) — which is essentially equivalent to the space reference—while the field of view in the other direction is filled with a blackbody target whose temperature is varied over the range expected when viewing the earth and its atmosphere. Thus, the infrared measurements are in terms of an "equivalent temperature, T_{BB}" of a blackbody filling the field of view which would cause the same response from the radiometer. Since the spectral response of the radiometer is assumed to be known from the spectral characteristics of the individual reflecting, refracting, and transmitting components of the optic, that portion of the radiant emittance of the

source which falls within the spectral response curve of the instrument can be calculated. This quantity is defined as the effective radiant emittance, $\overline{W}$ ($\frac{watts}{m^2}$), and can be written as

$$\overline{W} = \int_o^{\infty} \cdot W_\lambda (T_{BB})\, \phi_\lambda \, d\lambda \qquad (3)$$

The data from the two emitted thermal radiation channels can therefore be expressed either as T_{BB} in degrees Kelvin or as $\overline{W}$ in watts per square meter of radiant emittance within the spectral response curve of the channel. The $\overline{W}$ vs. T_{BB} functions for channels1 and 2 are given in Tables VIII and IX and in Figures 6 and 7.

In calibrating the reflected solar radiation channels (channels 3 and 5) one direction of the channels is merely masked with black tape to simulate space. To simulate reflected solar radiation from the earth and its atmosphere, a white diffuse reflector of known spectral reflectivity is illuminated at normal incidence from a standard lamp of known spectral intensity at a measured distance away, thus determining the spectral radiant emittance from the reflector. With the illuminated reflector filling the field of view, the output signal from each channel is measured. The spectral radiant emittance from the reflector is integrated over the spectral response curves of the solar channels to yield that portion of the radiation viewed to which each channel responds. The result of such integration is the "effective radiant emittance, $\overline{W}$." Thus, the reflected solar radiation measurements are in terms of that portion of diffuse radiation from a target filling the field of view to which each channel responds, $\overline{W}$. In order to interpret these measurements in terms of reflectance (loosely, "albedo"), we must know the effective radiant emittance, $\overline{W}^*$, which would be measured by each channel if the field of view were filled by a perfectly diffuse surface of unit reflectivity when illuminated by one solar constant at normal incidence. The expressions for $\overline{W}$ and $\overline{W}^*$ for channels 3 and 5 are defined in Section 3.6.2.

3.3 *Radiation Data Flow Sequence*

The radiation data flow sequence is shown in Figure 8. The sequence from satellite through ground station is illustrated in Figure 8(a). When an effective radiant emittance $\overline{W}$ is viewed by one side of the radiometer while the other side views outer space, and with a radiometer housing temperature, T_C, a radiometer output voltage V_{RAD} is obtained. This relationship, $V_{RAD} = f(\overline{W}, SIDE, T_C)$, is shown schematically in Figure 8b. This signal, V_{RAD}, is fed into a voltage controlled oscillator which produces an output frequency F_{sc} when the oscillator electronics temperature is T_E. This relationship, $F_{sc} = f(V_{RAD}, T_E)$, is shown schematically in Figure 8c, and is shown in Figures 9–12 for channels 1, 2, 3, and 5.

At the ground station the frequency F_{sc}, now increased by a factor of 30, is fed into a demodulator, the output of which enters an analog-to-digital converter which converts F_{sc} to a digital number, D. The conversion formula is

$$D = \frac{127}{50} F \qquad (4)$$

and is shown schematically in Figure 8d. The resulting digital number D and the temperature's T_E and T_C, which are also telemetered from the satellite, are used to obtain the value $\overline{W}$ (or T_{BB}) for channels 1 and 2 and the value $\overline{W}$ for channels 3 and 5 from the calibration data as indicated below.

In practice, for the purpose of simplifying the data reduction, each channel is calibrated for different values of T_C while maintaining a fixed relationship between T_E and T_C rather than calibrating the radiometer and each oscillator as separate units to obtain the transfer functions shown in Figures 8b and 8c. In addition, each oscillator is calibrated as a function of T_E to obtain the transfer function as shown in Figure 8c.

3.4 *Relation Between Electronics and Radiometer Housing Temperatures*

In effect, the calibration of the TIROS IV radiometer-oscillator system was made with the relationship between T_E and T_C being maintained as

$$T_E = T_C + 5°C \qquad (5)$$

The TIROS IV calibration curves which are presented in the manual are therefore valid when T_E and T_C satisfy equation (5).

The validity of the TIROS IV calibration with regard to equation (5) was checked using the flight data for T_E and T_C. The temperature comparison of T_E and T_C for TIROS IV is shown in Figure 13. It can be seen from Figure 13 that there is some variation of T_E and T_C from equation (5) and the maximum variation is about 5°C. The effects of this variation on the radiation data are

estimated as follows. The effect on $\overline{W}$ and T_{BB} of a 5° temperature variation from the calibrated T_C and T_E relation was computed previously for the TIROS III radiometer oscillators. The relative change in $\overline{W}$ and T_{BB} for the above 5° variation is approximately the same for TIROS III and TIROS IV. Therefore, the computations (Table X) made for TIROS III may be used to a good approximation for TIROS IV. From Table X, the maximum average temperature difference in channels 1 and 2 is 0.8°K, while the maximum average difference in effective radiant emittances for channels 3 and 5, in percentage of one solar constant radiated from a diffuse source, is 0.2%.

3.5 *Space-Viewed Level*

Although there is no specified on-board calibration mechanism on the TIROS IV radiometer, the "space-viewed level" can be considered to be a single-point check-of-calibration while in orbit. Any observed shift in the space viewed level after the original calibration is sufficient but not necessary to indicate a change in the calibration of the instrument (i.e., knowledge of the shift of a given point on a curve is sufficient to indicate a change in position of the curve whereas knowledge of the lack of a shift of the point is not sufficient to preclude a rotation of the curve about the point). It is important, therefore, to include a measurement of space viewed levels in the calibration of the instrument. Within the spectral regions of sensitivity of the emitted thermal radiation channels, radiation from a blackbody target at liquid nitrogen temperatures is practically the equivalent of the radiation levels of outer space. To simulate space radiation for the two reflected solar radiation channels, one need only turn off the lights in the laboratory. In the calibration procedure, which is described below, the space-viewed level is calibrated as a function of radiometer housing temperature.

3.6. *Target Blackbody Temperature, T_{BB}, and Target Effective Radiant Emittance, $\overline{W}$, vs. Digital Number, D.*

The TIROS IV radiometer and its associated electronics package were calibrated as a system. In the original calibration, the radiometer was placed in a high vacuum chamber while the electronics canister was placed in a thermally-controlled environmental chamber. Between the original calibration carried out at the Goddard Space Flight Center during the period 19-22 December 1961 and the launch of the satellite on 8 February 1962 several check-of-calibration measurements of all channels were made under varying conditions of pressure (ambient as well as high vacuum) and of housing and infrared target temperatures. These measurements indicated that, whereas the original calibration of channels 1 and 2 remained essentially unchanged, channels 3 and 5 suffered a consistent and progressive decrease in response. The resultant calibration curves shown in this manual represent the status of the calibration as of 25 January 1962, the date when the final check-of-calibration measurements were made before launch.

The following discussion concerns the techniques employed in the original calibration carried out at the Goddard Space Flight Center.

3.6.1 *Emitted Thermal Radiation Channels 1 and 2.* Two laboratory blackbody targets, placed in a container so that liquid or gaseous nitrogen could flow around them, were used in the calibration procedure.

At a certain radiometer housing temperature, T_C, regulated by the temperature of alcohol flowing through tubes in thermal contact with the radiometer housing in the vacuum chamber, liquid nitrogen at —196°C was pumped through the tubes in one target while the temperature of the nitrogen flowing through tubes in the other target was varied from —196°C to about +40°C.

This procedure was carried out at four different radiometer housing temperatures (0°, 16°, 24°, and 35°C) while viewing the warm target respectively through the wall and floor sides of the radiometer. The calibration curves for T_C = 7°C were interpolated from the calibration curves for T_C = 0°C and 16°C. The temperatures of each target were recorded by means of thermocouples. Using the frequency to digital number conversion shown schematically in Figure 8d, a curve of T_{BB} vs. D was constructed for each channel on both wall and floor sides, at varying values of T_C (Figures 14–23). If the quantity $\overline{W}$ is desired, it may be determined from the $\overline{W}$ vs. T_{BB} graphs for each channel (Figures 6 and 7). The complete calibration procedure is shown schematically in Figure 34a.

3.6.2 *Reflected Solar Radiation Channels 3 and 5.* A tungsten filament lamp calibrated by the Bureau of Standards was used in the calibration procedure as a standard source. Radiation from the lamp was diffusely reflected from a sheet of white Kodak paper of known spectral reflectivity. The output signal of each channel was read with the illuminated paper normal to rays from the

lamp and completely filling one field of view of the radiometer. The other field of view was covered with black tape. In order to obtain more than one point per calibration, the white paper was placed at different distances from the tungsten filament source lamp. The effective radiant emittance was computed using

$$\overline{W} = \frac{\cos \gamma}{R^2} \int_0^{\infty} J_\lambda \, r_\lambda \, \phi_\lambda \, d\lambda \qquad (6)$$

A curve of $\overline{W}$ vs. V_{RAD} was then constructed, with T_C being the ambient temperature of the room in which the calibration was made. In order to construct $\overline{W}$ vs. F_{sc} curves at various values of T_C, it was necessary to make additional measurements in vacuum where T_C could be controlled. Two targets consisting of diffusers illuminated by light bulbs, one target for each of the wall and floor sides, were used for both channels in this calibration. The voltages could be regulated. A certain range of voltages were selected and measurements at the various values of T_C were made of each voltage, recording corresponding radiometer voltage and output frequency at each level. Measurements were made by illuminating alternately both wall and floor sides, keeping the lights off on the side that was to simulate space viewing. In order to correlate the vacuum measurements with the tungsten-filament lamp source measurements, it was necessary to make one set of vacuum measurements at the same T_C that existed for the air measurements. By relating bulb voltage levels to $\overline{W}$ at the air measurements, $\overline{W}$ vs. F_{sc} curves were constructed for $T_C = 0°$, 7°, 16°, 24° and 35°C. A comparison calibration was made using rays from the mid-day sun as the visible light source, and the results agreed within 5% of the tungsten lamp calibration. As indicated above, check-of-calibration measurements subsequent to the original calibration indicated a consistent and progressive decrease in the response of channels 3 and 5. The resulant calibration curves for these channels (Figures 24–33) represent their calibration as of 25 January 1962 the date the final check-of-calibration measurements were made.

In order to calculate the reflectance (loosely, "albedo") from the incident solar radiation of a spot on earth viewed by the radiometer, one must know $\overline{W}^*$, the particular value of $\overline{W}$ which would be measured if the spot viewed were a perfectly diffuse reflector, having unit reflectivity, and illuminated by solar radiation at normal incidence. Using Equation (6) for this calculation, and setting $\gamma = 0°$, $R = 1$ astronomical unit, $r_\lambda = 1$, and $J_\lambda = W_\lambda(T) \times$ (cross-sectional area of sun)$/\pi$, we have

$$\overline{W}^* = \frac{\Omega}{\pi} \int_0^{\infty} W_\lambda \, (T) \, \phi_\lambda \, d\lambda \qquad (7)$$

Calculations of $\overline{W}^*$ were made taking the sun as a 5800°K blackbody for Channel 3 and a 6000°K blackbody for Channel 5. The complete calibration procedure is shown schematically in Figure 34(b).

Recent tests on the anisotropy of the white Kodak paper indicate that it may not be a good diffuse source due to the inclusion of a specular reflectance component in the total reflectance. The magnitude of the anisotropic properties of the Kodak paper and the ensuing effects on the calibration of channels 3 and 5 are under study.

3.7 *Field of View Measurements*

The Barnes Engineering Company made field of view measurements of the various channels of the TIROS IV radiometer. A line source consisting of a filament wire, 0.040 inches in diameter, was used. The line source remained in a plane perpendicular to the geometric axes, about 57.3 inches from the thermistor bolometers in the wall direction (where 1 inch normal diplacement ~1°). The line source was moved from right to left looking out from the radiometer in the wall direction (horizontal field of view measurements) and from top (up) to bottom (down) in the wall direction (vertical field of view measurements). The line source was kept normal to its direction of motion across the field of view during both horizontal and vertical measurements. These measurements are shown in Figures 35 and 36. Laboratory measurements for the floor side are not available.

3.8 *Summary of the Calibration*

When a certain value of effective radiant emmitance $\overline{W}$ or equivalent blackbody temperature T_{BB} is viewed by the radiometer housing temperature an output signal F_{sc} results. If T_E and T_C are within ± 5°C of the relationship

$$T_E = T_C + 5°C$$

only a negligible error in T_{BB} or $\overline{W}$ is introduced. From F_{sc} and T_C, which is measured independently, the measured value of effective radiant emittance ($\overline{W}$) or equivalent

blackbody temperature (T_{BB}) can be determined from the calibration curves.

The calibration for each side of each channel is carried out for five parametric values of T_c; hence, it is necessary to interpolate between the two transfer functions bracketing an actual value of T_c to arrive at the calibration for a given orbital period.

IV. RADIATION DATA PROCESSING

4.1 *Information Flow in the Satellite* [5, 31]

The radiation experiment instrumentation is independent of the television camera system except for power, command, certain timing signals and antennas (Figure 37). The output of the five medium resolution radiometer channels is fed into five subcarrier oscillators. These voltage controlled oscillators are of the phase shift type with symmetric amplifiers in the feedback loops, the gains of which are controlled by the balanced input signal. A sixth channel is provided for telemetry of the wide angle low resolution sensor data, the University of Wisconsin's heat balance data, environmental temperatures, instrumentation canister pressure, and calibration. In channel 6, a mechanical commutator switches resistive sensors in one branch of a phase shift oscillator. The seventh channel, a tuning fork oscillator, serves as a reference frequency and timing signal. As discussed previously, the signal of channel 7 is also repeated on channel 4. During the remainder of this Catalog-Manual any discussion concerning channel 7 will mention only channel 7 explicitly, although it is true that channel 4 could also be used for the same purpose. The outputs from these seven different channels are summed and the resultant composite signal equalized in a record amplifier which drives the head of a miniature tape recorder. An oscillator provides an alternating current bias to the record head and the signal required for the erase head. For convenience, erase of the magnetic tape occurs immediately before recording. The record spectrum extends from 100 cps to 550 cps. The tape recorder is an endless loop, two-speed design running at 0.4 ips record and 12 ips playback speed. The endless loop records continuously, day and night, except during a playback sequence. A hysteresis synchronous motor generates torque in the record mode through a mylar belt speed reduction. The fourth subharmonic of the tuning fork oscillator, generated by flip flops, drives a cam shaft which activates a bank of micro switches connected to the five commutated subchannels of the time-sharing sixth channel. Each is sampled for six seconds and the fifth includes a group of seven to be subcommutated.

Playback is initiated upon command by applying power to a direct current motor. A magnetized flywheel generates a frequency proportional to the motor speed. A frequency discriminator feeds the error signal to the stabilized power supply of the motor and closes the servo loop. Playback speed is essentially constant from 0° to 50°C. A low flutter and wow of 2.5% peak-to-peak, measured without frequency limitations, is achieved by using precision bearings and ground-in-place shafts having tolerances of better than 50 parts per million. A command pulse activates the playback motor, the playback amplifier, and the 238 Mc FM telemetry transmitter feeding the duplexer and antenna.

In order to permit comparison of the low resolution measurements with TV pictures, each TV shutter action generates a 1.5 second pulse which is recorded as an amplitude modulation of the channel 7 timing signal.

There are nine solar cells mounted behind narrow slits for north-angle determination. These slits have an opening angle of close to 180° in planes through the spin axis. The sun illumination generates pulses as long as illumination parallel to the spin axis is avoided. One of these sensors generates a 0.5 second pulse in addition to the north indicator code so that spin rate information and a measure of relative sun position is available. Again, this pulse is recorded as an amplitude modulation of channel 7.

Reconstruction of the radiation information vitally depends on its correlation with absolute time. An accurate, but relative, timing signal is provided by the tuning fork oscillator and a crude one by the sun pulses except when the satellite is in the earth's umbra. Absolute time is transmitted to the satellite and recorded on the tape as a one second dropout of channel 7. This pulse is designated as the End-of-Tape (E.O.T.) and its occurrence is known within milliseconds of absolute time.

4.2 *Information Flow at the Command and Data Acquisition* [5,31] *Station*

Upon interrogation, the 238 Mc carrier is received by an antenna, and the composite signal is recorded on magnetic tape and, simultaneously, fed to a "Quick Look" demodu-

lator (Figure 38a). At the same time, the envelope of channel 7 and the clipped signal of channel 2 are graphically recorded. The 8.0–12.0 micron "events" on the graphic record show alternately the earth and sky scan intervals as the satellite spins and progresses along the orbit, and the channel 7 envelope shows the three distinctive types of AM pulses impressed on the clock frequency during the record; namely, the sun sensor pulses, the TV camera pulses, and the "end-of-tape" pulse. Auxiliary uses of the radiation data include determination of the spin axis attitude in space and the times when television pictures were taken and recorded in the satellite, to be read out later over a ground station (Figures 38b and 38c).

The magnetic tapes are routinely mailed every day to the Aeronomy and Meteorology Division, GSFC, in Greenbelt, Maryland.

4.3 *Information Flow at the Data Processing Center* [5,31]

At the Data Processing Center of the Aeronomy and Meteorology Division, the master tape containing the composite radiation signal is demultiplexed, demodulated, and fed into an analog-to-digital converter (Figure 39). Canister pressure is read separately. The analog-to-digital converter produces a magnetic "Radiation Data Tape" made up of 36 bit words suitable for an IBM 7090 computer. The magnetic "Radiation Data Tapes" are then sent to the Data Reduction Center of the Aeronomy and Meteorology Division.

4.4 *Information Flow at the Data Reduction Center* [5]

The IBM 7090 computer program requires inputs from three sources to produce, in binary form, the "Final Meteorological Radiation (FMR) Tapes". One source is the "Radiation Data Tape" containing radiation data and satellite environmental parameters in digital form. Another source is the calibration data for converting digital information to meaningful physical units. The third source is the "Orbital Tape" from the NASA Space Computing Center containing satellite position and attitude data. The FMR tape then is the basic repository of data from the medium resolution scanning radiometer. In order to study and utilize the scanning radiometer data, appropriate computer programs must be written to "talk" to the FMR tape and provide for printing out data, punching cards, or producing maps. The format of the FMR tape and the make-up of the IBM 7090 computer program which produces it are discussed in detail in sections 4.5 and 4.6.

4.5 *Format of the "Final Meterological Radiation Tape"*

TIROS IV radiation data are available on low density, binary tapes prepared on an IBM 7090 computer. The FMR tape is the product of a computer program whose input is the orbital data, digitized radiation data, and TIROS IV radiometer calibration data. The make-up of this program is discussed in section 4.6. The FMR tape contains calibrated radiation measurements, geographical locations associated with the radiation measurements, orbital data, solar emphemeris, and satellite temperatures. The exact format of these data is described below. The purpose of this section is to emphasize certain features that will aid programmers in utilizing these data.

Each orbit of radiation data is treated as a file which contains a documentation record plus data records that represent approximately one minute intervals of time. The documentation record is the first record of each file and contains 14 data words whose format is described below. Dref is defined as the number of days between zero hour of September 1, 1957, and zero hour of launch date. TIROS IV time counts zero time as zero hour at Greenwich on the day of launch, thus launch time is given in GMT and launch day is zero day, with succeeding days numbered sequentially. However, if the satellite life extends beyond about 100 days, the value of dref is redefined by adding approximately 100, while the TIROS IV day is decreased by the same amount.

Each record of data covers approximately one minute of time, and the data are found in the decrement (D) and address (A) of each data word. The record terminates with the end of swath in progress at 60.0 seconds past the minute specified in words 1D, 1A, and 2D. In the case of satellite-earth orientation such that the radiometer continuously scans the earth for more than one rotation of the satellite, the record will terminate with the end of the revolution in progress at 60.0 seconds past the minute specified in words 1D, 1A and 2D. The End of File gap will be duplicated at the end of the last file on each FMR tape.

For each earth viewing swath, the radiation measured from channel 1 (6.0–6.5μ) and channel 2 (8.0–12.0μ) is reported as equivalent blackbody temperature in °K, while the radiation measured from channel 3 (0.2–

729-166 O - 64 - 2

6.0μ) and channel 5 (0.55–0.75μ) is reported as effective radiant emittance in watts/meter^2. Channel 4 has been retained in the FMR tape format with its input set to zero. For each fifth measurement in a swath, the point on earth being "viewed" by the radiometer is defined in terms of latitude and longitude. These computations are based on the best available estimate of satellite attitude.

In order that the user may distinguish between data from the wall and floor sides of the satellite, the data words containing the measured energy are labeled with a 1 in position 19 when the wall side of the satellite is viewing the earth. The user should realize that if the signal from the satellite becomes noisy, swath sizes, as interpreted by the computer, may become abnormal and the data can be labeled and located incorrectly. In order to flag abnormal data, minus signs are inserted for the following three reasons:

1. A measurement within a swath whose digital response falls below the arbitrarily defined threshold between earth and space. (The end of a swath is arbitrarily defined by three consecutive measurements falling below the threshold.)

2. An entire swath is labeled with minus signs when the observed swath size falls outside of the theoretical swath size $\pm 25\%$. The theoretically computed swath size is based on the best available estimate of satellite attitude, height, and spin rate.

3. The entire swath is labeled with minus signs when it is either the first or last swath in the close mode. (In the closed scanning mode the radiometer continuously scans over the earth for more than one spin rotation without viewing the horizon or space.)

FORMAT OF FINAL METEOROLOGICAL RADIATION TAPE

Documentation Record

Word No.	Quantity	Units	Scaling	Remarks
1	Dref		$B = 35$	Number of days between zero hour of Sept. 1, 1957, and zero hour of launch day.
2	Date			Date of Interrogation expressed as a packed word, i.e., February 8, 1962 would be $(020862)_{10}$ or $(021076)_8$. These numbers are shifted to extreme right side of the data word.
3	Day	TIROS IV Day	$B = 35$	Start time of this file of radiation data.
4	Hour	Z Hour	$B = 35$	
5	Minute	Z Minute	$B = 35$	
6	Seconds	Z Seconds	$B = 26$	
7	Day	TIROS IV Day	$B = 35$	Time of Interrogation, i.e., end time of this file of radiation data.
8	Hour	Z Hour	$B = 35$	
9	Minute	Z Minute	$B = 35$	
10	Seconds	Z Seconds	$B = 26$	
11	Satellite Spin Rate	Deg/Sec	$B = 26$	Satellite spin rate.
12	Frequency	35,72,144	$B = 35$	Data sampling frequency (cycles of a 550 cps tuning fork)
13	Orbit No.		$B = 35$	Orbit No. at time of Interrogation
14	Station Code		$B = 35$	Code defining ground station ("1" for Wallops Island, Va., "2" San Nicholas Island, Calif.)

1D	Day		$B = 17$	TIROS IV Day
1A	Hour		$B = 35$	Z time in day specified in word ID
2D	Minute		$B = 17$	
2A	GHA	Degrees	$B = 29$	Greenwich hour angle and declination of sun at time specified in words 1D, 1A, and 2D. 90° are added to declination to yield positive numbers.
3D	Decl.	Degrees	$B = 11$	
3A	T_C	Degrees K	$B = 35$	Reference temperature of the medium resolution radiometer.
4D	T_K	Degrees K	$B = 17$	Reference temperature of maindeck electronics.
4A	Height	Kilometers	$B = 35$	Height of satellite at time specified in words 1D, 1A, and 2D.
5D	Latitude	Degrees	$B = 11$	Latitude of subsatellite point at time specified in words 1D, 1A, 2D. 90° are added to all latitudes to yield positive numbers.
5A	Longitude	Degrees	$B = 29$	Longitude of subsatellite point at time specified in words 1D, 1A, 2D. Longitudes are reported as 0 to 360°, with west being positive.
6D	Seconds		$B = 8$	Seconds past time specified in words 1D, 1A, 2D when first earth viewing response is detected, and every fifth response thereafter.
6A	Latitude	Degrees	$B = 29$	Latitude of subsatellite point at time specified in words 1D, 1A, 2D, 6D. 90° are added to all latitudes to yield positive numbers.
7D	Longitude	Degrees	$B = 11$	Longitude of subsatellite point at time specified in words 1D, 1A, 2D, 6D. Longitudes are reported as 0 to 360°, with west being positive.
7A	Latitude	Degrees	$B = 29$	Latitude of point on earth being "viewed" by radiometer at time specified in words 1D, 1A, 2D, 6D. 90° are added to all latitudes to yield positive numbers.
8D	Longitude	Degrees	$B = 11$	Longitude of point on earth being "viewed" by radiometer at time specified in words 1D, 1A, 2D, 6D. Longitudes are reported as 0 to 360°, with west being positive.
8A	Nadir Angle	Degrees	$B = 29$	Nadir angle of optic axis from radiometer to point specified in words 7A, 8D.
9D	Azimuth Angle	Degrees	$B = 11$	Azimuth angle of optic axis from radiometer to point specified in word 7A, 8D. This angle is measured clockwise and expressed as a positive number.

9A	Zero			
10D	T_{BB} (ch. 1)	Degrees K	$B = 14$	Measurement by each of the five medium resolution channels at time specified in 1D, 1A, 2D, 6D when radiometer is "viewing" point on earth specified in words 7A, 8D.
10A	T_{BB} (ch. 2)	Degrees K	$B = 32$	
11D	$\overline{W}$ (ch. 3)	Watts/m^2	$B = 14$	
11A	Zero		$B = 32$	
12D	$\overline{W}$ (ch. 5)	Watts/m^2	$B = 14$	
12A	Zero			
13D	T_{BB} (ch. 1)	Degrees K	$B = 14$	The data sample immediately following the measurement recorded in words 10D-12A.
13A	T_{BB} (ch. 2)	Degrees K	$B = 32$	
14D	$\overline{W}$ (ch. 3)	Watts/m^2	$B = 14$	
14A	Zero		$B = 32$	
15D	$\overline{W}$ (ch. 5)	Watts/m^2	$B = 14$	
15A	Zero			
16D	T_{BB} (ch. 1)	Degrees K	$B = 14$	The data sample immediately following the measurement recorded in words 13D-15A.
16A	T_{BB} (ch. 2)	Degrees K	$B = 32$	
17D	$\overline{W}$ (ch. 3)	Watts/m^2	$B = 14$	
17A	Zero		$B = 32$	
18D	$\overline{W}$ (ch. 5)	Watts/m^2	$B = 14$	
18A	Zero			
19D	T_{BB} (ch. 1)	Degrees K	$B = 14$	The data sample immediately following the measurement recorded in words 16D-18A.
19A	T_{BB} (ch. 2)	Degrees K	$B = 32$	
20D	$\overline{W}$ (ch. 3)	Watts/m^2	$B = 14$	
20A	Zero		$B = 32$	
21D	$\overline{W}$ (ch. 5)	Watts/m^2	$B = 14$	
21A	Zero			
22D	T_{BB} (ch. 1)	Degrees K	$B = 14$	The data sample immediately following the measurement recorded in words 19D-21A.
22A	T_{BB} (ch. 2)	Degrees K	$B = 32$	
23D	$\overline{W}$ (ch. 3)	Watts/m^2	$B = 14$	
23A	Zero		$B = 32$	
24D	$\overline{W}$ (ch. 5)	Watts/m^2	$B = 14$	
24A	Zero			

The block of data from words 6D to 24A will be repeated, thus defining every fifth measurement in a swath. The address of the third word in the last response of a swath will contain 010101010101010 to signal end of record. A "look ahead" feature was incorporated into TIROS IV data reduction, and if the End of Tape signal occurs within an earth-viewing swath, that entire swath is discarded. Each time the swath terminates, two words (N and $N+1$) will follow the last "earth viewing" response with the following format:

Word No.	Quantity	Units	Scaling	Remarks
ND	Code	111111111111111		Code indicating end of swath
NA	Nadir Angle	Degrees	$B = 29$	The minimum nadir angle that occurred in the previously defined swath
(N+1)D	Latitude	Degrees	$B = 11$	Latitude of point on earth being "viewed" by radiometer when the minimum nadir angle occurred. 90° are added to all latitudes to yield positive numbers
(N+1)A	Longitude	Degrees	$B = 29$	Longitude of point on earth being "viewed" by radiometer when minimum nadir angle occurred. Longitudes are reported as 0 to 360°, with west being positive.

Occasionally dropouts are encountered and the corresponding data records contain no radiation data. This event is relatively rare in TIROS IV data, but in such cases the radiation data record contains only five words (1D to 5A) which document the record with respect to time. In such records, the datum in the address of the third word (T_C) is destroyed by the End of Record code.

A flow diagram to aid in interpreting this format is shown in Figure 40. It is seen that the format is analogous to four "nested loops" (in programming language), i.e., groups of five responses, entire swaths, one-minute records, and files. It is pointed out that a particular swath (and, hence, a particular record and a particular file) can end either on the "anchor data response" or on any of the four following non-geographically located data responses and that Figure 40 merely illustrates one possible combination of ending responses.

4.6 *IBM 7090 Computer Flow Diagram*

The FMR tape as described in the previous section is prepared with an IBM 7090 computer program whose input consists of orbital data, digital radiation data, and TIROS IV radiometer calibration data. The flow charts shown in Figure 41 outline the logical steps in this program and thus gives some insight into the mechanics of preparing these tapes. The flow chart has been greatly condensed since it is impossible to present a detailed flow chart within the space limitations of this publication.

The first phase of this program sets up the documentation data and then reads the entire file of radiation data to compute the start time from the end-of-tape time and the data sampling frequency. Given the starting and ending times, the program then searches the orbital tape to find orbital data (subsatellite point, height, nadir angle, right ascension, and declination) covering the same time interval. These data are then arranged in tables as a function of time so that interpolation subroutines can be used in the second phase to obtain values of the orbital characteristics for any specified time.

At this point, an optional feature allows the program to accept the attitude data from the orbital tape, or an alternate estimate of the attitude from a second documentation card. If the alternate attitude is accepted, the nadir angles are recomputed.

The second phase of the program reduces the digitized radiation data into useful meteorological data. This begins with a detailed examination of the radiation data to distinguish between earth and space viewed data. This distinction is based on an arbitrarily defined threshold value applied to channel 2. Both sensors are assumed to be viewing space when the measured radiation falls below the threshold value, and one sensor is viewing the earth when the measured radiation exceeds the threshold value. The end of swath is arbitrarily defined as three consecutive space-viewed measurements.

For each earth-viewing swath, the program proceeds to determine which sensor is viewing the earth, computes the latitude and longitude of the point on earth being "viewed" by the radiometer for each fifth measurement in the swath; and converts the digitized data into radiation units for each measurement in the swath. The data words containing radiation measurements contain a "1" in position 19 when the wall sensor is viewing the earth.

Each record on the FMR tape covers approximately one minute of time and terminates with the end of swath in progress at 60.0 seconds past the minute. When the end of tape is encountered, the program writes the last data record and reinitializes in preparation for the next orbit of radiation data.

V. RADIATION DATA COVERAGE AND DOCUMENTATION

5.1 *Radiation Data Coverage*

The discussion in this section concerning the radiation data coverage parallels the discussion given by Wood and Widger[32] on the photographic coverage by the TIROS satellite.

The geographical area from which significant meteorological radiation data are obtained by TIROS IV is limited in latitudinal extent mainly to the area between about 48°N and 48°S latitude. The latitude limitation is due to the 48° inclination of the orbit of the satellite to the equatorial plane.

A longitudinal limitation is imposed on obtaining radiation data due to the location of the data acquisition stations. This is because the range at which each station can contact the satellite and acquire data is limited to line of sight from the ground to satellite. To obtain as noise-free data as possible the antenna elevation angles are generally limited to 10° above the horizon. In Figure 42 the data acquisition circles for a 10° antenna elevation angle at Wallops

Island and San Nicolas Island acquisition stations are shown plotted on a Mercator Projection World Map.

Figure 42 also shows the trace of the subpoint tracks for 8 successive orbits. This series of subpoint tracks shows that the maximum number of successive orbits that may be interrogated by the acquisition stations is 8. If orbit (N) can just be acquired by the Wallops Island station, then orbit (N+8) is the first orbit which cannot be acquired by the San Nicolas Island station. The dashed line in Figure 42 shows the last orbit which may be acquired by San Nicholas Island. Therefore, only a maximum of 8 successive orbits (N through N+7) may be interrogated in any interrogation day and orbits with ascending nodes between longitudes 75°E and 85°W cannot be acquired by either station. The interrogation day includes all orbits interrogated in the series of 8 consecutive orbits which come within range of the Command and Data Acquisition stations during each 24-hour period, as shown in Figure 42. The interrogation day can and often does occur on two separate calendar days. The shaded area of Figure 42 shows the geographical areas where nearly all radiation data are acquired. The unshaded regions between 48°N and 48°S latitude show the longitude limitations on the acquisition of data due to the location of the acquisition stations. Because of the inclination of the sensors to the spin vector and/or the precession of the spin vector some data are acquired in the unshaded regions to about 63°N or 63°S latitude. However, the number of data samples acquired in this area is small compared to the number acquired in the shaded area.

Further latitude limitations are imposed on obtaining reflected solar radiation measurements because of the need for solar illumination. Because of the slight bulge of the earth at the equator, the satellite orbital plane precesses in right ascension at the rate of —4.43 deg/day. This is illustrated in Figure 43, where the spin vector and orbital plane orientation for selected orbits of TIROS IV, as viewed from the sun, are shown. The quantity $\Delta\phi$ is defined as the right ascension of the sun minus the right ascension of the orbital ascending node. Due to the precession of the orbital plane and the movement of the earth in its orbit, a complete cycle of the precession of the plane of the satellite's orbit relative to the sun (synodic period) is completed in about 66.5 days.

For any single day the plane of the satellite orbit remains nearly fixed in absolute space while the earth rotates within the orbit. Thus, at a given latitude and considering only solar illumination, reflected solar radiation could be obtained for all longitudes during any single day. The precession of the orbital plane causes the illuminated latitudes, as seen by the satellite, to change during one synodic period as described below. In the following discussion the solar illuminated area, where radiation data are available, is defined by requiring the solar zenith angle to be less than 70° and the radiometer optical nadir angle to be less than 58°. The following discussion is concerned only with the availability of reflected solar radiation measurements.

The time of the TIROS IV launch has been chosen so that the northern part of the orbit is on the side of the earth nearest the sun (Figure 43a) and reflected solar radiation data can be obtained from about 20°S latitude to 55°N latitude. After about 15 days, the orbital plane has precessed to a $\Delta\phi$ of 180° (Figure 43b) which means that the descending node occurs on the meridian of the subsolar point. At this time, reflected solar radiation data can be obtained from about 61°S to 51°N latitude.

By TIROS IV Day 31, or 31 sequential days following launch day, the orbital plane has precessed to a $\Delta\phi$ of 270° (Figure 43c) and the southern part of the orbit is over the sunlit side of the earth. At this time reflected solar radiation data can be obtained only in the Southern Hemisphere from about 63°S to 0° latitude and the satellite is over the Northern Hemisphere only at night. On TIROS IV Day 48, $\Delta\phi$ is equal to 0° (Figure 43d) and the ascending node of the orbit is on the sunlit side of the earth. At this time, reflected solar radiation data are available from about 56.5°S to 60°N latitude. Continued precession until TIROS IV Day 65 moves the orbit to a $\Delta\phi$ of 90° (Figure 43e) where the reflected solar radiation data coverage is from about 0°N to 63°N latitude. At this time, the satellite is in the Southern Hemisphere only at night. On about TIROS IV Day 66.5, the orbital plane has the same orientation as at launch. The whole precession cycle then repeats with the synodic period of about 66.5 days throughout the satellite lifetime. The northern and southern latitude limits of reflected solar radiation coverage can vary from one synodic period to the next due to the changing subsolar point.

The reflected solar radiation coverage for TIROS IV is summarized in Figure 44 where

the shaded area indicates the illuminated latitudes for each TIROS IV Day. Disregarding the solar illumination requirement, the medium resolution radiometer latitude coverage as shown in Figure 44 would be from about 63°S to 63°N latitude. Knowing this, we can see in Figure 44 that during two time intervals of TIROS IV reflected solar radiation data could not be acquired due to inadequate solar illumination. During the first time interval, centered on TIROS IV Day 5, the subsolar point was in the Southern Hemisphere at a declination of about —14°, thus reducing the coverage in the Northern Hemisphere from 63°N latitude to about 56°N latitude. During the second time interval, centered on TIROS IV Day 105, the subsolar point was in the Northern Hemisphere at about +20° declination thus reducing the coverage in the Southern Hemisphere from about 63°S latitude to about 50°S latitude.

5.2 *Documentation of Radiation Data*

The radiation data available on the FMR tapes have been documented in an Index of Final Meteorological Radiation Tapes. This Index, which is found in Appendix A, lists information for the orbital ascending node, the spin vector attitude, and the spin rate for every TIROS IV orbit for which radiation data are available. The time interval for which radiation data are available in each processed orbit is also listed in Appendix A.

For each interrogation day, the time interval for the radiation data on the FMR tape is summarized diagrammatically on the subpoint tracks for that day. Information concerning the minimum nadir angle is also included. The presentations are located in Appendix B. and identified by calendar date. With the data in this form, the user can quickly find the applicable orbits and approximate the geographical area of radiation data coverage.

VI. PRE-LAUNCH AND POST-LAUNCH OBSERVATIONS AND DEVELOPMENTS

6.1 *Pre-Launch Degradation of Channels 3 and 5*

As indicated in Section 3.6, the response of channels 3 and 5 apparently degraded before launch, based upon check-of-calibration measurements made between 22 December 1961 and 25 January 1962, whereas the original calibration of channels 1 and 2 remained essentially unchanged.

6.2 *Post-Launch Degradation of Channels 1, 2, 3, and 5*

There is strong evidence that all channels of the medium resolution radiometers flown on TIROS II and TIROS III, as well as on TIROS IV, degraded in response in some way after going into orbit. The post-launch degradation has been observed in two ways. First, as pointed out in Section 3.5, the space-viewed level can be considered to be a single-point check of calibration, and any shift observed in this level after the original calibration indicates that a change has occurred in the system. A shift could be caused by an imbalance which develops between the floor and wall optical paths in one of the emitted thermal radiation channels, or by a drift of the transfer functions of the satellite-borne electronics associated with either the reflected solar or emitted thermal radiation channels. Because the ground demodulation equipment is readily accessible and constantly checked and aligned, the possibility of its contributing to a persistent shift in the space-viewed level can be discounted.

The weight of evidence to date indicates that the primary cause of shifts of the space-viewed levels of the thermal radiation channels has been an imbalance which developed between the floor and wall paths of the optics. We shall define this type of degradation as "asymmetrical optical degradation." Because the shift in the space-viewed level due to asymmetrical optical degradation results from chopped thermal radiation emitted from components of the radiometer within the passband of the filter, it follows that this type of degradation cannot be a cause of a shift in the space-viewed levels of the reflected solar radiation channels which are not sensitive in the infrared. A drift in the satellite-borne radiometer preamplifier or associated oscillator could of course cause a shift in the space-viewed levels of the reflected solar radiation channels, but to date there have been no appreciable shifts in these channels, inferring that the electronics are relatively stable. The shifts of the space-viewed levels, ΔF, of the thermal radiation channels of TIROS IV are shown in Figure 45. The very small level of indicated asymmetrical optical degradation for these channels compared to their counterparts in TIROS III is seen by comparison with pages 68 and 69 of the TIROS III Radiation Data Users' Manual[4] (e.g., at orbit 1000 the ΔF

of $\sim$ 1 c.p.s. for channel 1, TIROS IV, compares with a ΔF of $\sim$ 30 c.p.s. for channel 1, TIROS III; and the ΔF of $\sim$ 0.5 c.p.s. for channel 2, TIROS IV, compares with a ΔF of $\sim$ 2.5 c.p.s. for channel 2, TIROS III).

Another type of degradation may exist for all channels without any shift occurring in the space-viewed level. In the absence of an on-board calibration, this type of degradation has been indicated by the behavior of large quantities of data analyzed statistically by a computer program originally designed to study the "quasi-global" heat balance. Throughout this document the term "quasi-globe" shall refer to that portion of the world observed by the radiometer under the constraints of the TIROS orbit i.e., the broad zone between 55°N latitude and 55°S latitude, with the exception of those areas which can not be acquired due to the locations of the Command and Data Acquisition stations. The heat balance program was designed to convert individual measurements from channels 2 and 4 to total outgoing long-wave flux, W, by the methods given by Wark, Yamamoto, and Leinesch[20] and to average the calculations accumulated throughout a sustained period (e.g. a month) over time and area to yield the "cumulative quasi-global emitted radiant power, p^c," (in units of 10^{14} watts). The program was also designed to calculate reflectances from individual measurements from channels 3 and 5 according to the Lambert cosine law and to average the calculations accumulated throughout a sustained period over time and area to yield the "cumulative quasi-global albedo, A^c." The primary purpose of the heat balance program thus has not been fulfilled due to the evidence of degradation which it revealed. We shall define this type of degradation as "symmetrical optical degradation."

Two specific characteristics of the heat balance program should be pointed out:

1 The accumulation of measurements over a sustained period masks the true magnitude of the day by day changes in the instrument, and

2 The conversion of channel 2 and 4 measurements to total outgoing long-wave flux masks the true magnitude of the instrumental degradation.

Concerning the second characteristic, the Wark, Yamamoto, Leinesch[20] conversion from a channel 2 or 4 measurement to total outgoing long-wave flux, W, can be approximated by the linear expression (incorporating a mean value for the limb darkening effect)

$$W = r + s\,\overline{W} \qquad (8)$$

where r and s are constants of positive sign. To utilize the results from the heat balance program in investigating instrumental degradation the two characteristics above must be eliminated by further manual manipulation of the computer output. A full discussion of the heat balance program, of the methods of analysis of its output for investigating instrumental degradation, and of the models which attempt to correct the degraded measurements is found in the "TIROS III Radiation Data Users' Manual Supplement[33]" and will not be repeated here.

Results from channels 2 (8-12μ) and the channels 4 (8-30μ) of TIROS II and III and from channel 2 (8-12μ) of TIROS IV are shown in Figure 46. Intermediate cumulative averages (e.g. days 0-3, days 0-6, days 0-9, etc.) were printed out approximately every 3 days by the computer as it developed each cumulative average over about a 30 day period. The intermediate values are the interconnected circled dots, and a 30 day cumulative average is the final circled dot in each string of points. The initiation of a new cumulative average is indicated by a break in the interconnecting lines. Thus five separate sequences of cumulative averages for channel 2 of TIROS IV, each extending over a period of about 30 days, are shown in Figure 46. It is seen that there is an apparent decrease with time of the cumulative quasi-global emitted radiant power to about day 42 (22 March 1962; orbit 600) after which the power stabilizes and remains sensibly constant at a value of about 963 x 10^{14} watts. Values of the cumulative quasi-global emitted radiant power for the thermal radiation channels of TIROS II and III show decreases over the first 600 orbits also, but at even greater rates. For comparison, quasi-global emitted radiant power values were calculated from London[34] and are shown by arrows near the lower left-hand corner of Figure 46. Because London investigated only the Northern Hemisphere, opposite seasons from 0° to 55°N were combined as an approximation to represent the quasi-globe from 55°S to 55°N.

In treating data from the reflected solar radiation channels the program calculated cumulative averages of quasi-global albedo, A^c, over successive periods of only 9 days with intermediate cumulative averages printed out approximately every 3 days. In

Figure 46 fifteen separate sequences of A^c for the reflected solar radiation channels of TIROS IV are shown. The values of albedo along the ordinate on the right are positioned such that the resulting absorbed solar radiation [Insolation over the quasi-globe x (1-albedo)] coincides with the ordinate on the left. Again it is seen that there is an apparent decrease with time of albedo after which the 0.2–6.0μ channel of TIROS IV seems to stabilize while albedo values from the 0.55-0.75μ channel values continue to decrease. It is difficult to interpret the reflected solar radiation results in light of the progressive decrease of response of both channels which occurred before launch (up to 25 January 1962). There may well have been continued decreases during the two weeks that elapsed between the last check of calibration and launch. On the other hand perhaps factors present during launch or during the first few days (or even hours) of exposure to the space environment contribute to the apparently low initial values of A^c in Figure 46.

Because of the angular motion of the spin vector of TIROS over the celestial sphere,[30] occasionally the 45° half-angle conical figure, generated by the radiometer axis in the wall direction as the satellite spins, intersects the direct rays of the sun. Under these conditions, direct solar rays impinge upon the sensors from the wall direction momentarily once during each satellite rotation. Such an unfavorable satellite-sun geometry may exist for one or two days until it is eliminated by a change in the attitude of the spacecraft. There were four periods in the history of TIROS IV when such an unfavorable geometry occurred, viz., the periods including the orbits numbered 300-328 (TIROS IV days 21-23), 1005-1039 (days 70-72), 1335-1360 (days 93-95) and 1555-1590 (days 108-111). When solar interference was severe, the data were not reduced. However, in several orbits where there was no interference with the long-wave channels and only marginal interference with the short-wave channels the data were reduced. In Figure 46 the sharp gradients and divergencies in the data from the two short-wave channels near days 21, 72, and 110 apparently are the results of marginal contamination from the direct rays of the sun.

In interpreting Figure 46 it must be emphasized that radiative equilibrium can not be assumed for the quasi-globe, that is, one can not equate absorbed solar radiation with emitted terrestrial radiation to yield the quasi-global heat balance. Heat is lost from the quasi-globe by other means than radiation, primarily through meridional wind and ocean current components crossing the 55°N and 55°S boundaries. Calculations from London's data indicate that the annual quasi-global excess of absorbed solar radiation over emitted terrestrial radiation is 70×10^{14} watts. It is tempting to try to infer the quasi-global albedo by extrapolating the TIROS IV 8.0–12.0μ curve back to the ordinate, keeping in mind the following two assumptions: (1) that the intercept value of total flux was correctly derived from satellite measurements, which at the time of launch were undegraded and represented accurately a quasi-global mean value, and (2) that this value of emitted terrestrial radiation plus 70×14^{14} watts represents the net quasi-global heat loss. The TIROS IV curve extrapolated backward in time intersects the ordinate at 1025×10^{14} watts. The net quasi-global loss then becomes $(1025 + 70) \times 10^{14} = 1095 \times 10^{14}$ watts, and the albedo required to replenish 1095×10^{14} watts with absorbed solar radiation is 30.7%. (This value is 2.8% lower than the quasi-global annual albedo of 33.5% calculated from London's data.)

6.2.1 *Channel 1* The history of the frequency differences, ΔF, between the in-flight and calibrated space-viewed levels as a function of orbit number is shown in the upper half of Figure 45. Due to the way in which the plotted points were acquired, ΔF is about 1 c.p.s. higher in the figure than it actually was. Therefore, the in-flight and calibrated space-viewed levels are approximately the same to about orbit 900, after which the in-flight space-viewed level increases slightly, resulting in a ΔF of about 1.5 c.p.s. at orbit 2039.

The cumulative quasi-global effective emitted radiant power $\overline{P}^c$ for channel 1 was obtained using the computer program described in Section 6.2. It was possible to specify the constants $r = o, s = 1$ in equation (8) thus averaging values of $\overline{W}$ directly in the program. However, it was still necessary to eliminate the cumulative characteristic of the program output to yield the quasi-global effective emitted radiant power, $\overline{P}^i$. (The quasi-global effective emitted radiant power, $\overline{P}^i$, is equal to the mean quasi-global effective radiant emittance, $\overline{W}_{ave}$, multiplied by 4.1785×10^{14} meters^2, the area between 55°N and 55°S.) Values of $\overline{P}^i$ for approximately every 20 orbits are plotted in Figure 47. Although there is wide scatter among the individual points, there is an apparent decrease of about 18% in the values of $\overline{P}^i$ throughout the life-

time of the satellite. Since channel 1 responds to emission from water vapor, a correct interpretation of Figure 47 demands a knowledge of the time and space variations in the global distribution of water vapor to separate possible meteorological factors from instrumental degradation. Because of our lack of knowledge of the behavior of water vapor on a global scale and because of the large scatter of the individual points, we have not attempted to construct a correction nomogram for channel 1 measurements. However, one may infer from Figure 47 that some instrumental degradation is taking plaec.

6.2.2 *Channel 2* The history of ΔF is shown in the lower half of Figure 45. Here the plotted points reflect the true value of ΔF, never deviating more than 1 c.p.s. from zero.

Individual values of the quasi-global emitted radiant power, P^i, for approximately every 20 orbits were derived from the cumulative averages of Figure 46 by the method described in the TIROS III Supplement[33] and a smooth curve was drawn through them in Figure 48. By its very nature, P^i is expected to remain fairly constant with time and not be strongly affected by meteorological changes.

As can be seen from Figure 48, P^i decreases by about 6% during the first six weeks after launch and then remains fairly constant during the remainder of the experiment's lifetime. The 6% decrease in P^i could possibly be explained by changing meteorological conditions, such as increasing cloud cover, for the six week period rather than by degradation effects in channel 2. However, it is felt that the percentage increase in the quasi-global albedo necessary to decrease P^i by 6% is not very likely to occur. Furthermore, the curves for P^i for channels 2 of TIROS II and TIROS III shown in Figure 46 exhibit a decrease which is similar timewise but of larger magnitude —a decrease which cannot be caused by meteorological conditions alone and must be due to degradation. Also, the shape of the curve of Figure 48 in the region of decreasing P^i suggests rather strongly a degradation pattern. Therefore, the decline of P^i is attributed to symmetrical optical degradation of the response of channel 2.

From the degradation curve of P^i, and assuming that the space-level remained at its calibrated value (which is essentially true as seen in Figure 45) a symmetrical optical degradation model has been developed and applied to channel 2. From this model the corrections, δT_{BB}, have been derived. These corrections, shown in Figure 49, are to be added to the wall and floor T_{BB} measurements contained on the FMR tape. For example, from Figure 49, it is seen that an equivalent blackbody temperature of 280°K measured by channel 2 during orbit 300 should be increased by 4°K, yielding a corrected measurement of 284°K. The correction nomogram in Figure 49 was tested and essentially confirmed in a comparision of satellite measurements with measurements from a balloonborne experiment flown by the University of Michigan on 2 June 1962 (see Section 6.2.3 below).

It is to be emphasized that the above corrections are only simplified attempts at correcting for several complicated degradation mechanisms which are not yet fully understood. However, the corrections offered in Figure 49 represent a realistic approach in correcting for degradation.

6.2.3 *Channel 3 and Channel 5* Values of quasi-global albedo A^i for channels 3 and 5 were derived from the cumulative quasi-global albedos A^c of Figure 46 by the method described in the TIROS III Supplement[33] and smooth curves were drawn through them in Figures 50 and 51. In Figure 50, A^i for channel 3 as a function of orbit number is indicated by the solid line. Error bars indicate approximately one standard deviation. It is difficult to obtain a representative value for A^i during the first few days after launch because only a small amount of data over a limited geographical area can be obtained and therefore the initial portion of the curve cannot be determined very accurately. Figure 50 indicates that A^i for channel 3 decreased strongly during the first week after launch. This decrease is attributed to degradation of the channel 3 response. After about orbit 600 the curve levels off indicating that the instrumental response has stabilized and does not degrade further. There is additional evidence which indicates that the decrease in A^i is due to degradation. First, A^i for channel 3 of TIROS III showed a decrease in time similar to that of Figure 50. Second, and more conclusive, is the observed degradation in the response of channel 3 before launch.

The plot of A^i vs. orbit number for channel 5 is shown in Figure 51. By the same arguments used for channel 3, it is concluded that the response of channel 5 shows degradation. However, in contrast to channel 3, values of A^i from channel 5 continue to decrease to the end of the experiment.

The degradation of the response of channels 3 and 5 indicated above was substantiated by a separate experiment. A five channel radiometer, similar to the one carried on TIROS IV, was flown on a balloon by the University of Michigan (under contract to NASA) over South Dakota on 2 June 1962. The duration of the flight was from sunrise to sunset. Radiation data from the same area were obtained by the TIROS IV five channel radiometer on orbit 1642 at $21^h\ 43^m$ *GMT* of the same day. By comparing the measurements obtained from a given area by both radiometers, some indication as to degradation in the satellite radiometer can be determined. Complications in the comparison of the measurements occur due to the time variation between the measurements, different viewing angles, and the different altitudes of the two radiometers.

The comparison indicates that the balloon measurements of channel 3 and channel 5 are higher than the satellite measurements taken over the same areas by factors of about 1.84 ± 0.14 and 2.15 ± 0.15 respectively. Comparative channel 5 data from the two radiometers are shown in Figure 52. Since the balloon-borne radiometer was carefully calibrated, both before and after the flight with no evidence of change, the factors cited above can be interpreted as absolute correction factors. Thus from Figure 50 the corrected channel 3 value of A_i at orbit 1642 becomes

$$A^i = 1.84 \times 16.5 = 30.4\%$$

and from Figure 51 the corrected channel 5 value of A^i at orbit 1642 becomes

$$A^i = 2.15 \times 13 = 28.0\%$$

The channel 3 value of A^i compares favorably with the 30.7% albedo inferred from extrapolated channel 2 data in Section 6.2 above, whereas the channel 5 value of A^i is somewhat lower. As a first approximation, one can assume a value of $A^i = 29 \pm 4\%$ and calculate degradation correction factors as a function of time from Figures 50 and 51 for channels 3 and 5 respectively. It can be seen that the channel 3 correction factor would remain constant after orbit 600 whereas the channel 5 correction factor would increase constantly with time.

The correction factors discussed above were derived on the assumption that the degradation involves only a wavelength-independent decrease in the instrumental response, symmetrical with respect to floor and wall sides, and linearly proportional to effective radiation intensity, with no drift in the satellite-borne electronics. Caution must be exercised in applying factors, based upon broad averages, to individual measurements extending over the entire instrumental dynamic range from the lowest to the highest intensities. Any departure of the system from the assumption of linear proportionality to the effective radiation intensity could introduce appreciable errors in individual measurements which are higher or lower than the mean. Plans to use computer techniques to investigate the behavior of the intensity distribution of the measurements with time, looking for non-linearities in the instrumental degradation are now going forward. However, it was decided to publish the work to date now, rather than hold publication of the Catalog-Manual until further results are obtained. Therefore, the correction factors suggested above are perforce incomplete and must be applied with caution. However, they should be of use as a guide in interpreting data from the reflected solar radiation channels. In the last analysis, any efforts of the type described above are poor substitutes for an active and adequate means of checking the calibration of the orbiting instrument. Such an on-board calibration device is now being designed, and it is planned to include it in the next TIROS medium resolution experiment, scheduled to be launched in 1964.

6.3 *Estimate of the Accuracy of the Data*

Inaccuracies in the data are caused not only by the degradation of the various channels after the original calibration, but also by such effects as wow and flutter in the magnetic tape, noise, drift of T_E and T_C from their assumed relationship, and uncertainties in the original calibration.

The estimates of accuracy given below apply to the mid-range of target intensities. As can be seen from the figures of F_{sc} vs. T_{BB}, the accuracy of the thermal channels suffers at very low target temperatures.

6.3.1 *Channel 1* The estimated relative accuracy of T_{BB} measurements is $\pm$ 2°K, and the estimated absolute accuracy is $\pm$ 5°K immediately after launch, after which some degradation in instrumental response apparently occurs.

6.3.2 *Channel 2* The estimated relative accuracy of T_{BB} measurements is $\pm$ 2°K, and the estimated absolute accuracy is $\pm$4°K after launch, increasing to an estimated $\pm$6°K in later orbits after applying corrections from Figure 49.

6.3.3 *Channel 3 and Channel 5* The estimated relative accuracy of $\overline{W}$ measurements is $\pm$ 20 w/m^2 and $\pm$ 3 w/m^2 respectively. Because of the history of pre-launch as well as post-launch degradation, no estimates of absolute accuracy are given.

6.4 *Infrared Radiation Experiment Lifetime*

After orbit 1728, the satellite record mechanism began to fail and many of the later orbits had no end-of-tape pulse. As a result, only 41 orbits were digitized after orbit 1728. At orbit 2039 the record system completely failed and this was the last orbit of radiation data digitized for TIROS IV.

VII. CONCLUSIONS

The major limitation of the TIROS IV medium resolution radiometer experiment is the uncertainty in the absolute values of the measurements, resulting from the post-launch degradation of the instrumental response. The degradation corrections given in Section VI can serve as a guide for interpreting the data in terms of absolute values. However, because they were derived from large-scale averages, caution should be exercised in applying them to individual measurements, especially those near the high or low extremes of the instrumental dynamic range.

In studies involving comparative measurements over many days, the data from channel 2 (8-12μ) and channel 3 (0.2-6μ) after orbit 600 should be used wherever possible because the degradation in the response of these two channels appears to stabilize and remain constant after that time.

The data from all channels are of value throughout the history of the radiometer experiment for studies involving relative measurements over a short period of time, for example the contrast mapping of cloud systems.

TABLE III.—*Filter and Lens Materials*

	Channel 1	Channel 2	Channel 3	Channel 5
Lens 1	Germanium immersion lens detector, first surface coated with pure ZnS of λ/4 optical thickness at 6.3μ.	Germanium with both surfaces coated with pure ZnS of λ/4 optical thickness at 10μ.	Synthetic Barium Fluoride (BaF_2) with no coatings.	Pure Quartz (SiO_2) with no coatings.
Lens 2	Germanium with both surfaces coated with pure ZnS of λ/4 optical thickness at 6.3μ.	Germanium with both surfaces coated with pure ZnS of λ/4 optical thickness at 10μ.	Synthetic Sapphire (Al_2O_3) with no coatings.	Synthetic Sapphire (Al_2O_3) with no coatings.
Lens 3	Germanium with both surfaces cotaed with pure ZnS of λ/4 optical thickness at 6.3μ.	None	None	None
Filter 1	Narrow band, OCLI, interference type centered at 6.3μ, outer filter surfaces of Al_2O_3 substrate, inner filter has 14 alternate multilayers of Ge and SiO.	Indium Antimonide (InSb), both surfaces coated with pure ZnS of λ/4 optical thickness at 10μ.	None	Narrow band Infrared industries Type 259,-011,513
Filter 2	None	Arsenic Trisulfide (As_2S_3) glass, uncoated 0.5mm plane piece.	None	Narrow band Infrared Industries Type 259,-011,608
Filter 3	None	None	None	Infrared Industries chance glass ON-20 1/8 inch thick.

TABLE IV.—*Effective Spectral Response, Channel 1*

λ (Microns)	$\phi\lambda$
5.6	0
5.7	.002
5.8	.009
5.9	.037
6.0	.110
6.1	.162
6.2	.194
6.3	.207
6.4	.211
6.5	.169
6.6	.081
6.7	.027
6.8	.010
6.9	.004
7.0	0

TABLE V.—*Effective Spectral Response, Channel 2*

λ (Microns)	$\phi\lambda$	λ (Microns)	$\phi\lambda$
7.1	0	15.0	.007
7.5	.081	15.5	.022
8.0	.210	16.0	.064
8.5	.303	16.5	.072
9.0	.384	17.0	.068
9.5	.398	17.5	.058
10.0	.358	18.0	.048
10.5	.332	18.5	.037
11.0	.312	19.0	.029
11.5	.308	19.5	.024
12.0	.261	20.0	.018
12.5	.193	20.5	.013
13.0	.131	21.0	.008
13.5	.055	21.5	.005
14.0	.012	22.0	.001
14.5	.001	22.5	0

TABLE VI.—*Effective Spectral Response, Channel 3*

λ (Microns)	$\phi\lambda$	λ (Microns)	$\phi\lambda$
.25	.122	3.50	.714
.30	.353	4.00	.614
.40	.520	4.10	.580
.50	.588	4.20	.561
.80	.403	4.30	.547
.90	.421	4.50	.532
1.00	.478	5.00	.410
1.40	.572	5.50	.250
1.60	.605	6.00	.116
2.00	.650	6.20	.053
2.60	.642	6.50	.022
2.80	.646	6.90	0
3.00	.638		

TABLE VII.—*Effective Spectral Response, Channel 5*

λ (Microns)	$\phi\lambda$	λ (Microns)	$\phi\lambda$
.350	.001	.775	.008
.475	.003	.800	.001
.500	.021	.825	.000
.525	.104	1.100	.002
.550	.276	1.130	.011
.563	.290	1.200	.006
.575	.275	1.600	.010
.600	.200	1.800	.029
.607	.195	2.000	.050
6.25	.225	2.120	.050
.650	.262	2.210	.044
.660	.267	2.300	.047
.675	.256	2.400	.054
.700	.176	2.500	.058
.710	.159	2.600	.056
.730	.187	2.700	.014
.750	.091	2.750	.002
.765	.022	2.800	.000

TABLE VIII.—T_{BB} *vs.* $\overline{W}$, *Channel 1*

T_{BB} (°K)	W (watts/m²)
170	.0069
190	.0280
210	.0876
230	.2247
250	.4962
270	.9748
290	1.7460
310	2.9010
330	4.5350
350	6.7380
370	9.5960

TABLE IX.—T_{BB} *vs.* $\overline{W}$, *Channel 2*

T_{BB} (°K)	W (watts/m²)
170	1.87
190	4.05
210	7.71
230	13.32
250	21.30
270	31.98
290	45.64
310	62.46
330	82.57
350	106.00

TABLE X.—*Changes in Blackbody Temperature and Effective Radiant Emittance Due to Differences of* T_C *From* T_E. *Calculations Made for TIROS III Radiometer*

Channel	T_E (°C)	T_C (°C)	Side	F (cps)	T_{BB} (°K)	ΔT_{BB}	$\overline{W}$ (w/m²)	$\overline{W}/\overline{W}^*$	$\Delta(\overline{W}/\overline{W}^*)$
1	0	0	Floor	130	247.5	0			
	5	0		130.2	248.0	0.5			
	5	5		130.2	245.5	0			
	0	5		130	245.0	0.5			
	0	0	Wall	130	254.3	0			
	5	0		130.2	254.8	0.5			
	5	5		130.2	246.1	0			
	0	5		130	245.5	0.6			
Av.						0.52			
2	0	0	Floor	185	235.5	0			
	5	0		185.3	236.3	0.8			
	5	5		185.3	233.1	0			
	0	5		185	232.4	0.7			
	0	0	Wall	185	239.2	0			
	5	0		185.3	240.0	0.8			
	5	5		185.3	234.8	0			
	0	5		185	233.9	0.9			
Av.						0.8			
3	0	0	Floor	248			232.5	.304	0
	5	0		248.1			233.5	.306	.002
	5	5		248.1			207	.271	0
	0	5		248			206	.270	.001
	0	0	Wall	248			283	.371	0
	5	0		248.1			284.5	.372	.001
	5	5		248.1			230	.301	0
	0	5		248			228	.298	.003
Av.									.002
5	0	0	Floor	386			71.4	.657	0
	5	0		385.9			71.2	.656	.001
	5	5		385.9			63.2	.582	0
	0	5		386			63.4	.584	.002
	0	0	Wall	386			75.6	.696	0
	5	0		385.9			75.3	.693	.003
	5	5		385.9			65.8	.606	0
	0	5		386			66.0	.608	.002
Av.									.002

VIII. REFERENCES

1. "TIROS II Radiation Data Catalog." Goddard Space Flight Center, Greenbelt, Md., 15 August 1961, 356 pp.
2. "TIROS II Radiation Data Users' Manual." Goddard Space Flight Center, Greenbelt, Md., 15 August 1961, 57 pp.
3. "TIROS III Radiation Data Catalog." Goddard Space Flight Center, Greenbelt, Md., 15 December 1962, 388 pp.
4. "TIROS III Radiation Data Users' Manual." Goddard Space Flight Center, Greenbelt, Md., August 1962, 71 pp.
5. Bandeen, W. R., R. A. Hanel, John Licht, R. A. Stampfl, and W. G. Stroud. "Infrared and Reflected Solar Radiation Measurements from the TIROS II Meteorological Satellite." *J. of Geophys. Res., 66,* 3169-3185, October 1961.
6. Hanel, R. A., and W. G. Stroud. "Infrared Imaging from Satellites." *J. of the SMPTE, 69,* 25-26, January 1960.
7. Bandeen, W. R., B. J. Conrath, W. Nordberg, and H. P. Thompson. "A Radiation View of Hurricane Anna from the TIROS Meteorological Satellite." pp 224-233 in *Proceedings of the First International Symposium on Rocket and Satellite Meteorology, Washington, April, 1962,* edited by H. Wexler and J. E. Caskey, Jr., North-Holland Publishing Co., Amsterdam, 1963. (Also, NASA TN D-1713, Goddard Space Flight Center, Greenbelt, Maryland, April 1963.)
8. Bandeen, W. R., V. Kunde, W. Nordberg and H. P. Thompson. "TIROS III Meteorological Satellite Radiation Observations of a Tropical Hurricane." (To be published in Tellus.)
9. Fritz, Sigmund, and Jay S. Winston. "Synoptic Use of Radiation Measurements from Satellite TIROS II." *Monthly Weather Review, 90,* 1-9, January 1962.
10. Furukawa, P. M., P. A. Davis, and W. Viezee. "An Examination of some TIROS II Radiation Data and Related Studies." Final Report, Contract No. AF 19(628)-322, Stanford Research Institute, Menlo Park, California, July 1962.
11. Greenfield, S. M. and W. W. Kellogg. "Calculations of Atmospheric Infrared Radiation as seen from a Meteorological Satellite." *J. of Meteor., 17,* 283-289, June 1960.
12. Hanel, R. A. and D. Q. Wark. "TIROS II Radiation Experiment and Its Physical Significance." *J. Opt. Soc. Am.,* 51, 1394-1399, December 1961.
13. London, Julius. "Satellite Observations of Infrared Radiation." Scientific Report No. 1, Contract No. AF 19(604)-5955, College of Engineering, New York University, New York 53, N. Y., December 1959.
14. London, Julius, Katsuyuki Ooyama, and Herbert Viebrock. "Satellite Observations of Infrared Radiation." Scientific Report No. 2, Contract No. AF 19(604)-5955, College of Engineering, New York University, New York 53, N. Y., July 1960.
15. London, Julius, Katsuyuki Ooyama, and Herbert Viebrock. "Satellite Observations of Infrared Radiation." Final Report, Contract No. AF(604)-5955, College of Engineering, New York University, New York 53, N. Y., October 1961.
16. Möller, Fritz. "Einige vorläufige Auswertungen der Strahlungsmessungen von TIROS II." *Arch. f. Met., Geophys. u. Biokl., 12,* Ser. B. 78-94, July 1962. (Also "Some Preliminary Evaluations of TIROS II Radiation Measurements." Univ. München, Meteorologisches Inst., München 13, Amalienstr. 52/III, Germany, January 1962.)
17. Nordberg, W., W. R. Bandeen, B. J. Conrath, V. Kunde and I. Persano, "Preliminary Results of Radiation Measurements from the TIROS III Meteorological Satellite." *J. of the Atmos. Sciences, 19,* 20-30, January 1962.
18. Prabhakara, C. and S. I. Rasool. "Evaluation of TIROS Infrared Data." pp 234-246 in *Proceedings of the First International Symposium on Rocket and Satellite Meteorology, Washington, April 1962,* edited by H. Wexler and J. E. Caskey, Jr., North-Holland Publishing Co., Amsterdam, 1963.
19. Wark, D. Q. "On Indirect Temperature Soundsings of the Stratosphere from Satellites." *J. of Geophys., Research, 66,* 77-82, January 1961.
20. Wark, D. Q., G. Yamamoto and J. H. Lienesch. "Methods of Estimating Infrared Flux and Surface Temperature from Meteorological Satellites." *J. of the Atmos. Sciences, 19,* 369-384, September 1962. (Also "Infrared Flux and Surface Temperature Determinations from TIROS Radiometer Measurements." Meteorological Satellite Laboratory Report No. 10, U. S. Weather Bureau, Washington, D. C., August 1962.)
21. Wexler, R. "Satellite Observations of Infrared Radiation." First Semi-Annual Technical Summary Report, Contract No. AF 19(604)-5968, Allied Research Assoc., Inc., Boston, Mass., December 24, 1959.
22. Wexler, R. "Satellite Observations of Infrared Radiation." Second Semi-Annual Technical Summary Report, Contract No. AF 19(604)-5968, Allied Research Assoc., Inc., Boston, Mass., June 30, 1960.
23. Wexler, R. "Interpretation of Satellite Observations of Infrared Radiation." Scientific Report No. 1, Contract No. AF 19(604)-5968, Allied Research Assoc., Inc., Boston, Mass., April 20, 1961.
24. Wexler, R. "Interpretation of TIROS II Radiation Measurements." Final Report, Contract No. AF 19(604)-5968, Allied Research Assoc., Inc., Boston, Mass., May 31, 1962.
25. "TIROS II Radiation Data Users' Manual Supplement." Goddard Space Flight Center, Greenbelt, Md., 15 May 1962, 13 pp.
26. Doolittle, R. C., L. Miller and I. Ruff. "Geographic Locations of Cloud Features." Appendix A of "Final Report on the TIROS I Meteorological Satellite System," Part II by Staff, Meteorological Satellite Laboratory, U.S. Weather Bureau, in *NASA Technical Report R-131, 1962.*
27. Bristor, C. L., E. G. Albert and J. B. Jones. "Problems in Mapping Data from Meteorological Satellites." *Space Research II, Proceedings of*

the Second International Space Science Symposium, Florence, Italy, April 10-14, 1961, North-Holland Publishing Company, Holland.
28. Hubert, L. F. "TIROS I: Camera Attitude Data, Analysis of Location Errors, and Deviation of Correction for Calibration." *Meteorological Satellite Laboratory Report No. 14,* U. S. Weather Bureau.
29. Dean C. "Attitude Determination from Picture Data." "TIROS I: An Operational Evaluation of a New Meteorological Tool." Second Semi-Annual Technical Summary Report, Contract AF 19(604)-5581, Allied Research Associates, Inc., June 30, 1960.
30. Bandeen, William R. and Warren P. Manger. "Angular Motion of the TIROS I Meteorological Satellite due to Magnetic and Gravitational Torques." *J. of Geophys. Res., 65,* 2992-2995, September 1960.
31. Davis, J., R. Hanel, R. Stampfl, M. Strange, and M. Townsend. "Telemetering IR Data from the TIROS II Meteorological Satellite." NASA TN D-1293, Goddard Space Flight Center, Greenbelt, Maryland.
32. Widger, Jr., W. K. and C. P. Wood. "An Explanation of the Limitations to the Coverage Provided by TIROS." *Weatherwise, 14,* No. 6, December 1961.
33. *TIROS III Radiation Data Users' Manual Supplement—Correction Models for Instrumental Response Degradation*" Goddard Space Flight Center, Greenbelt, Md., 1 December 1963.
34. London, Julius. "A Study of the Atmospheric Heat Balance." Final Report, Contract No. AF 19(122)-165, College of Engineering, New York University, New York 53, N. Y. July 1957.

729-166 O - 64 - 3

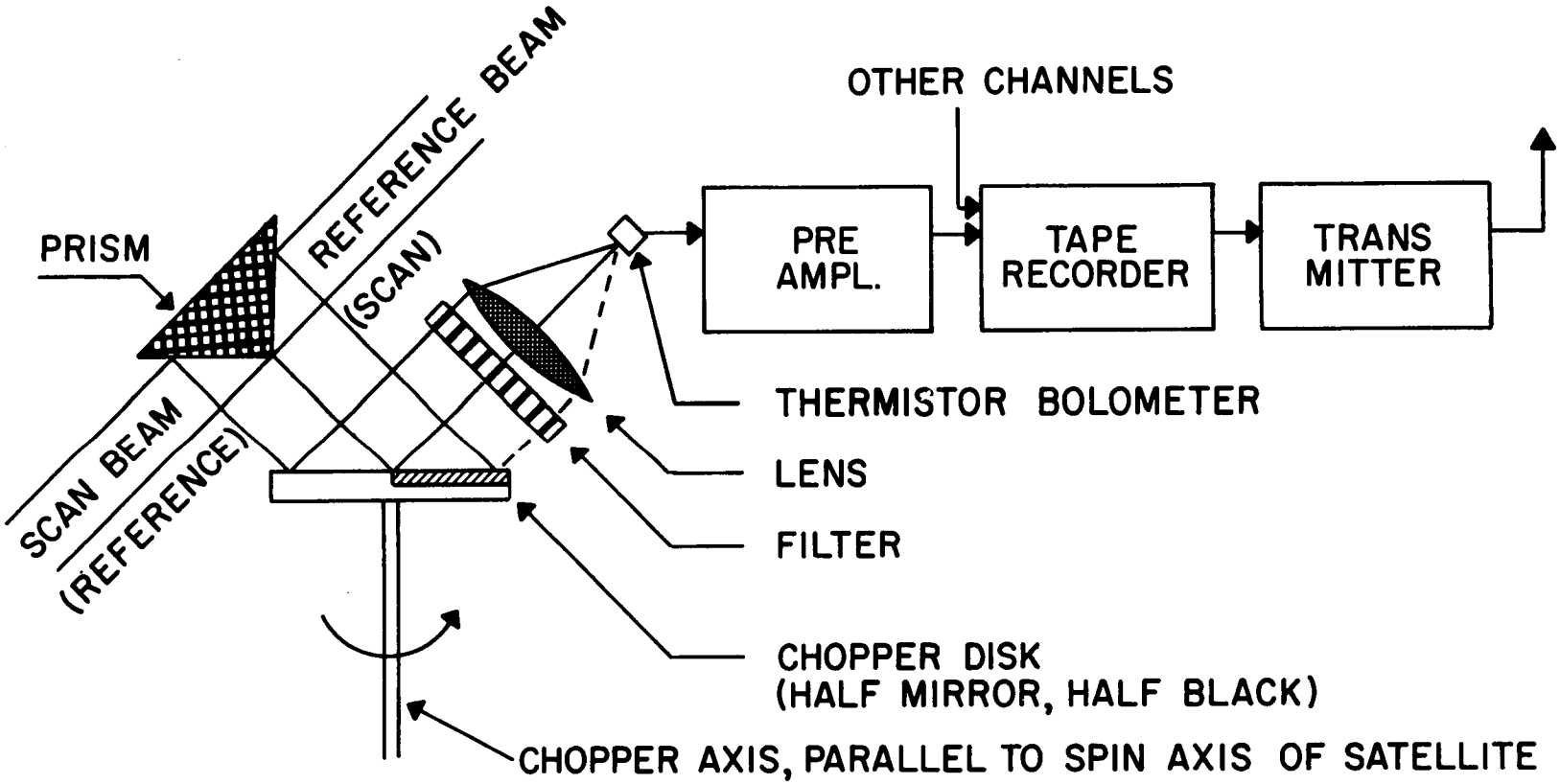

Figure 1—Block diagram of one channel of the medium resolution scanning radiometer.

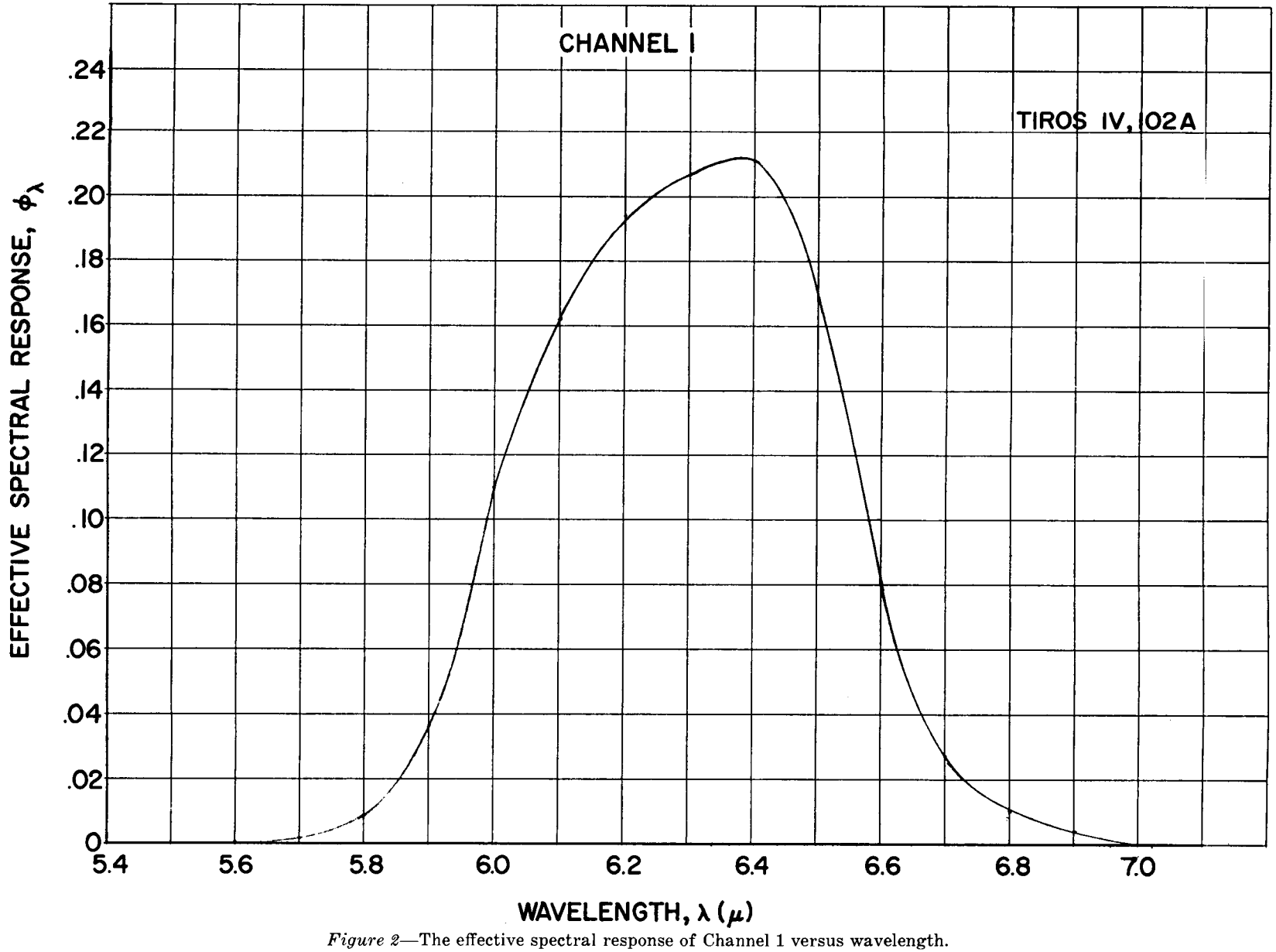

Figure 2—The effective spectral response of Channel 1 versus wavelength.

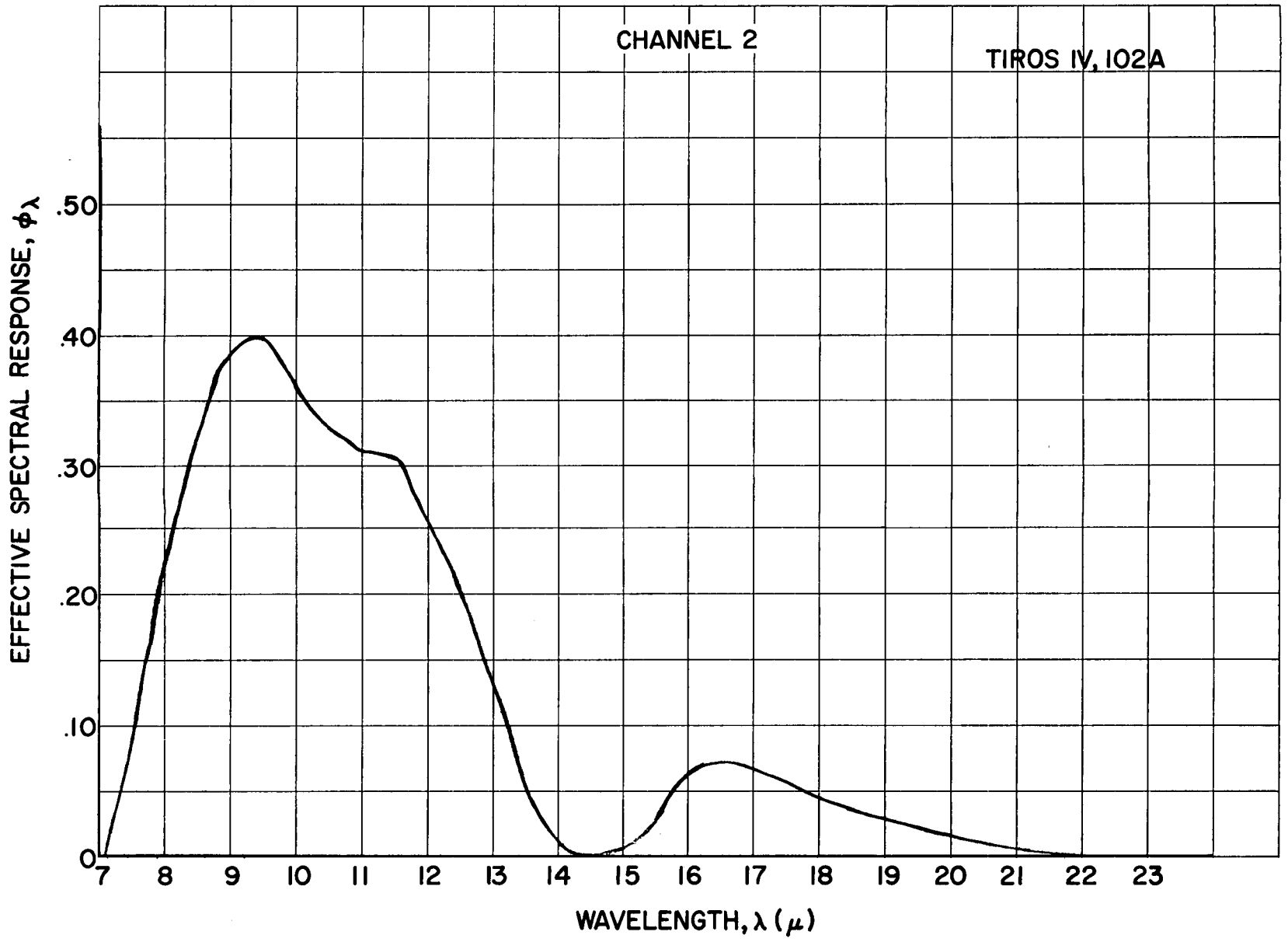

Figure 3—The effective spectral response of Channel 2 versus wavelength.

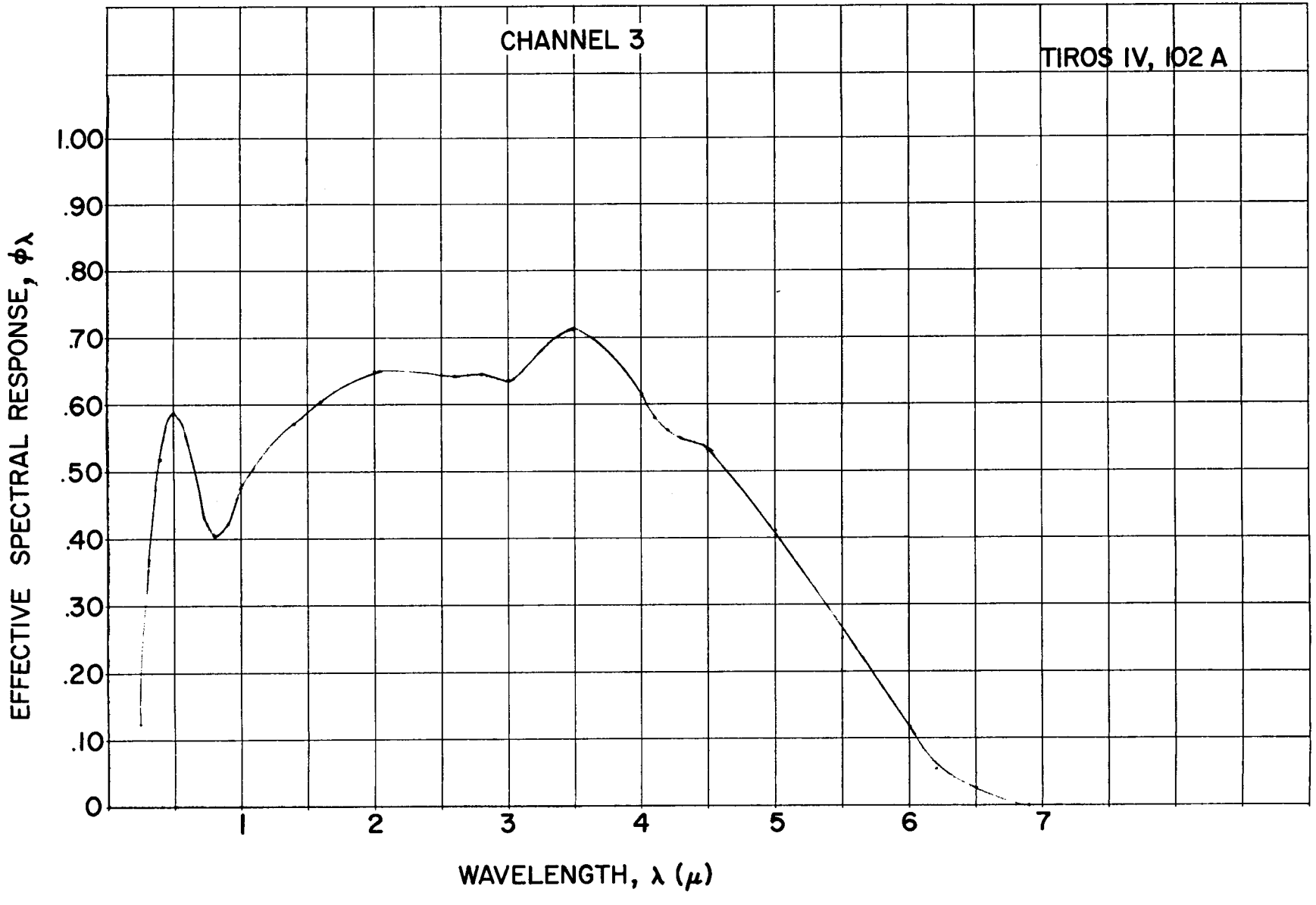

Figure 4—The effective spectral response of Channel 3 versus wavelength.

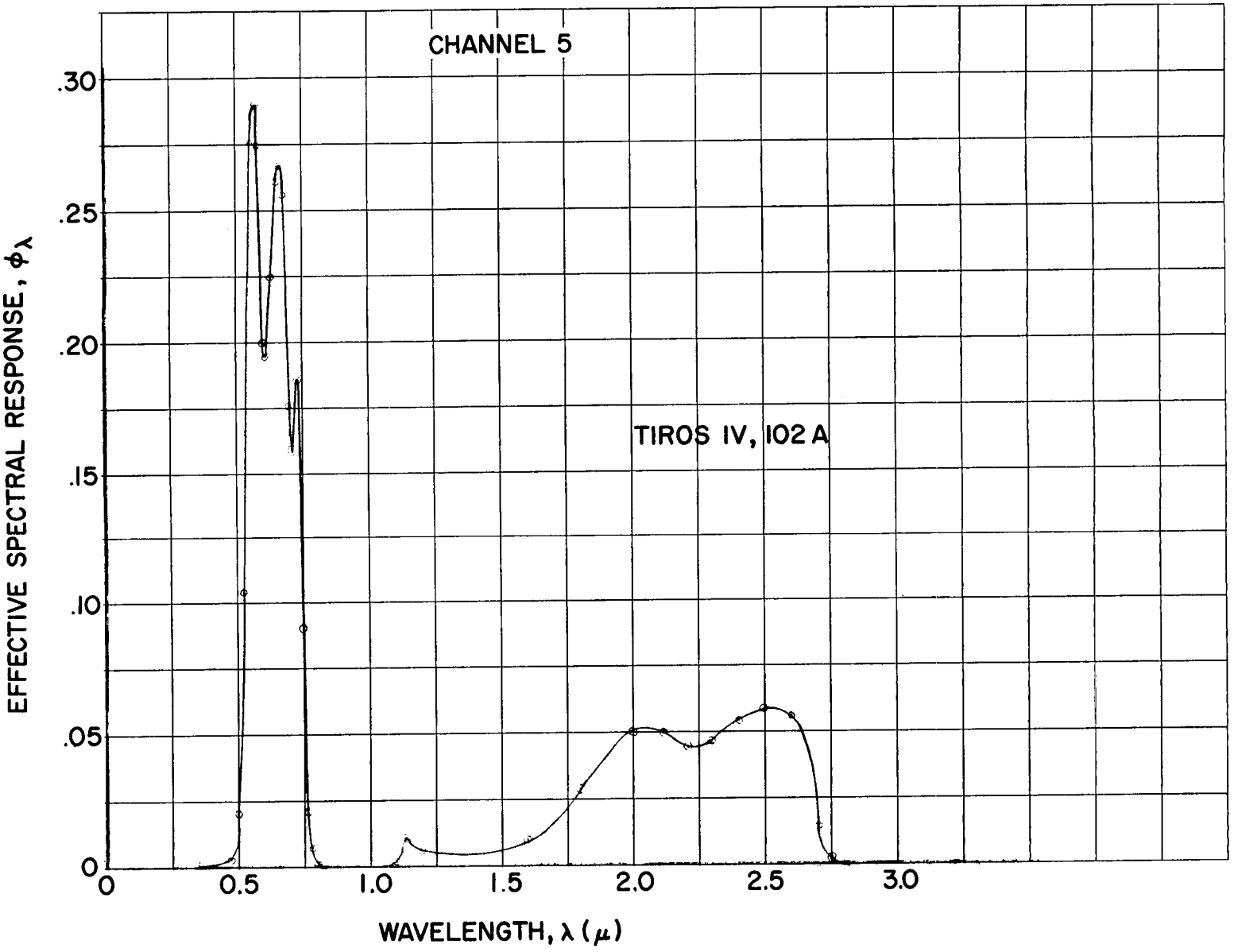

Figure 5—The effective special response of Channel 5 versus wavelength.

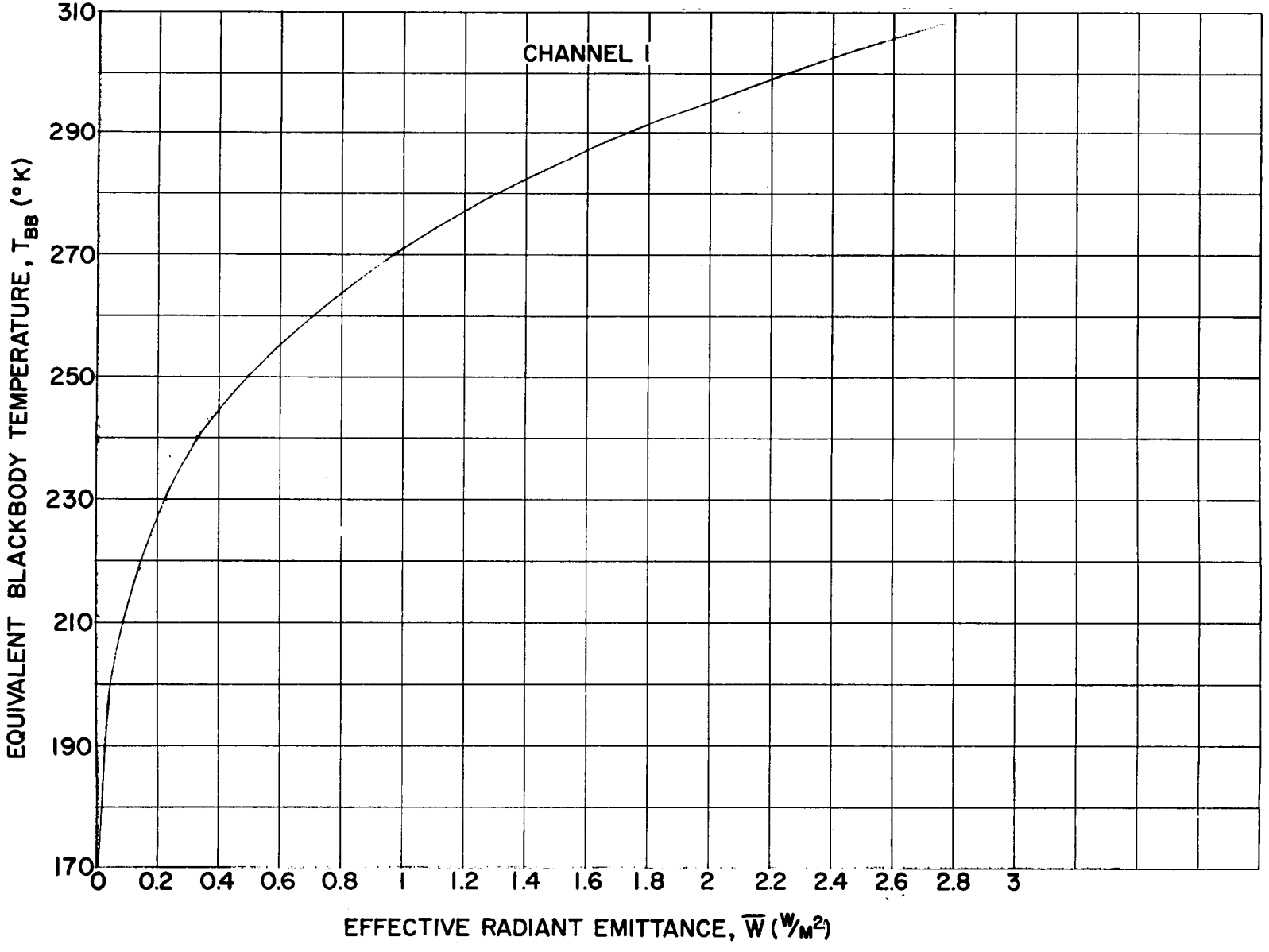

Figure 6—The effective radiant emittance of Channel 1 versus equivalent blackbody temperature.

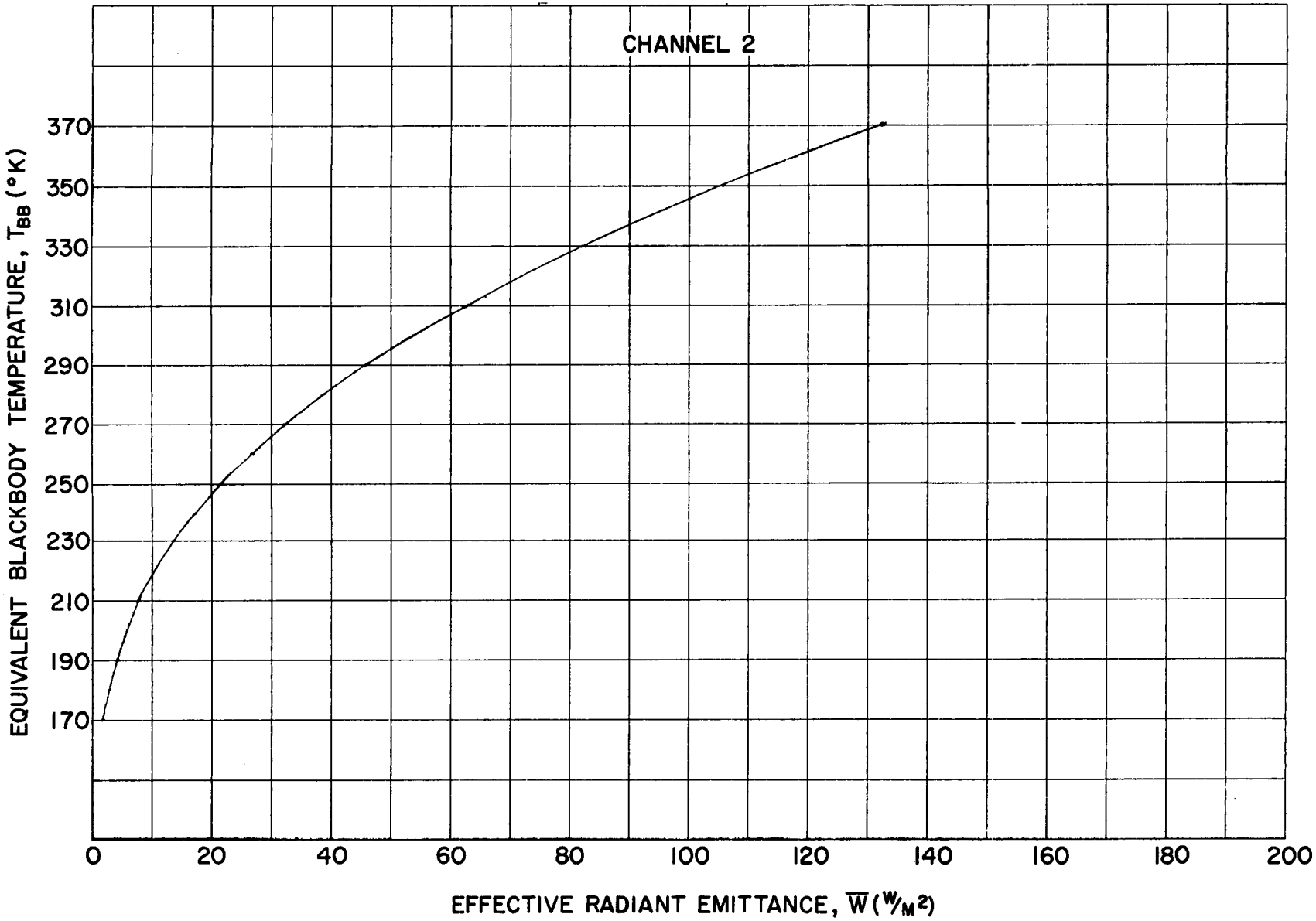

Figure 7—The effective radiant emittance of Channel 2 versus equivalent blackbody temperature.

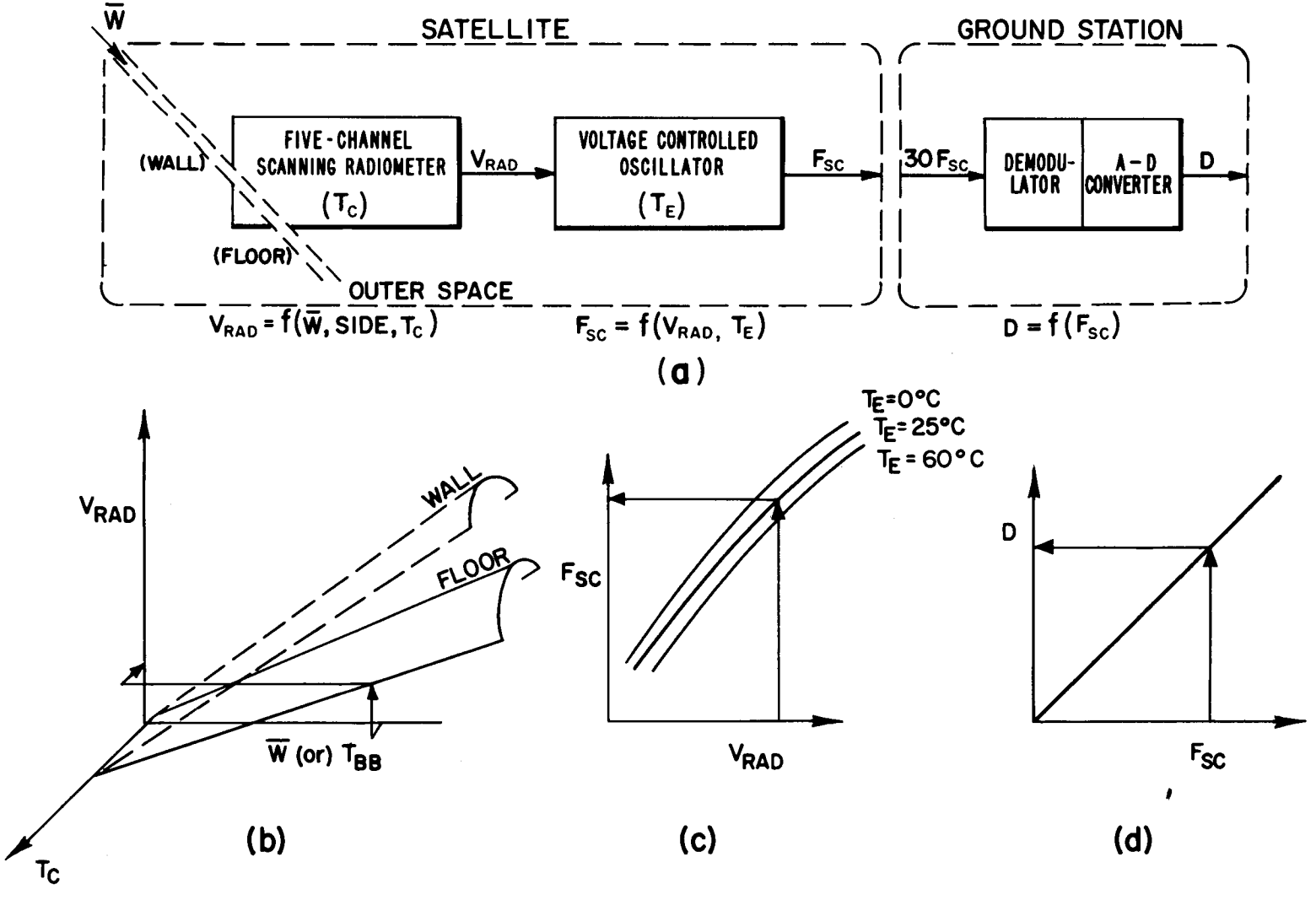

Figure 8—(*a*) Schematic representation of transfer functions associated with instrumentation in the satellite and at the ground station.
(*b*) Three-dimensional representation of the response of the five-channel scanning radiometer.
(*c*) The response of the voltage controlled oscillator shown as a parametric function of the electronics temperature T_E.
(*d*) Conversion from subcarrier frequency to digital number.

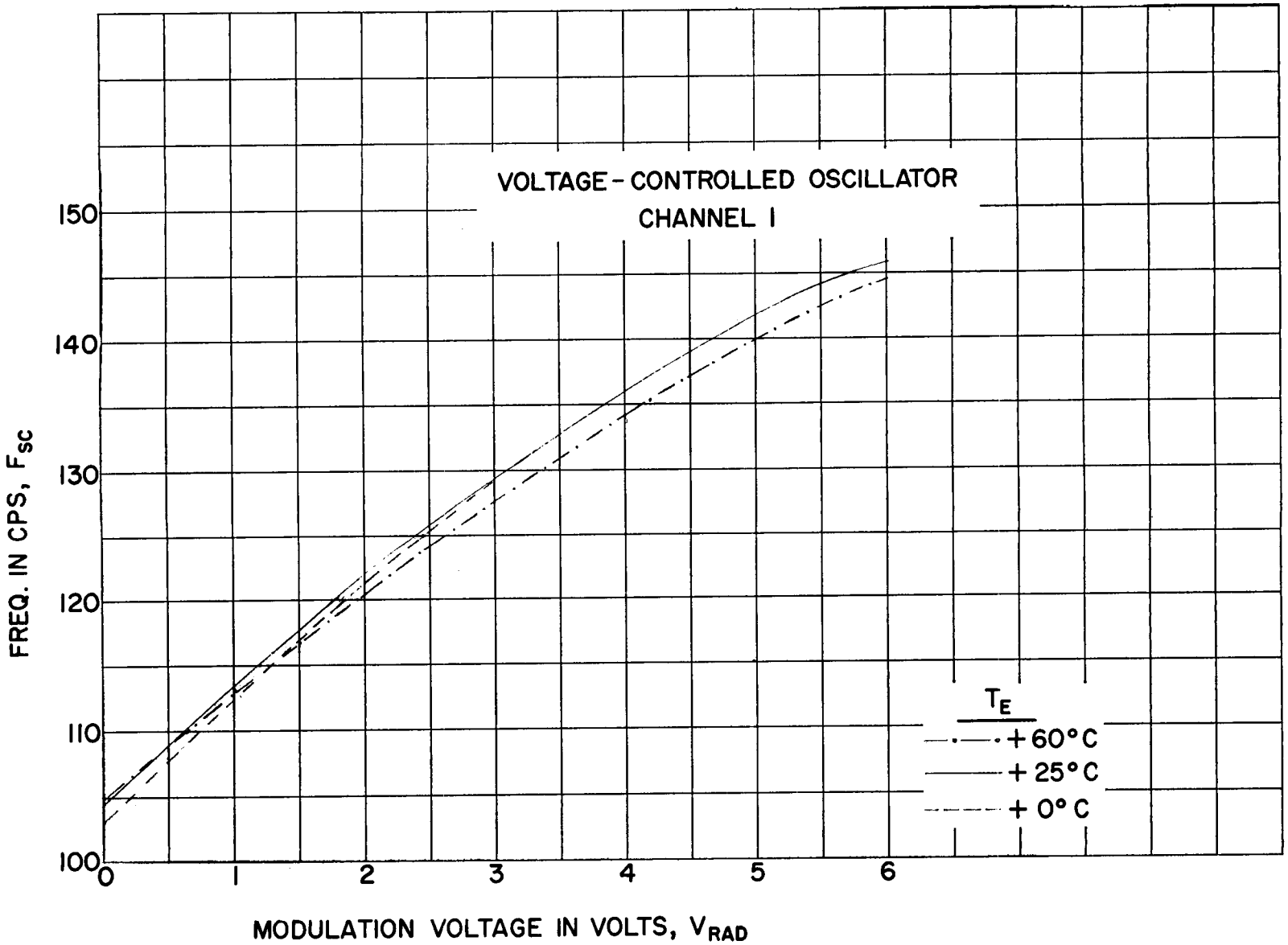

Figure 9—The response of the voltage controlled oscillator for Channel 1 shown as a parametric function of the electronics temperature, T_E.

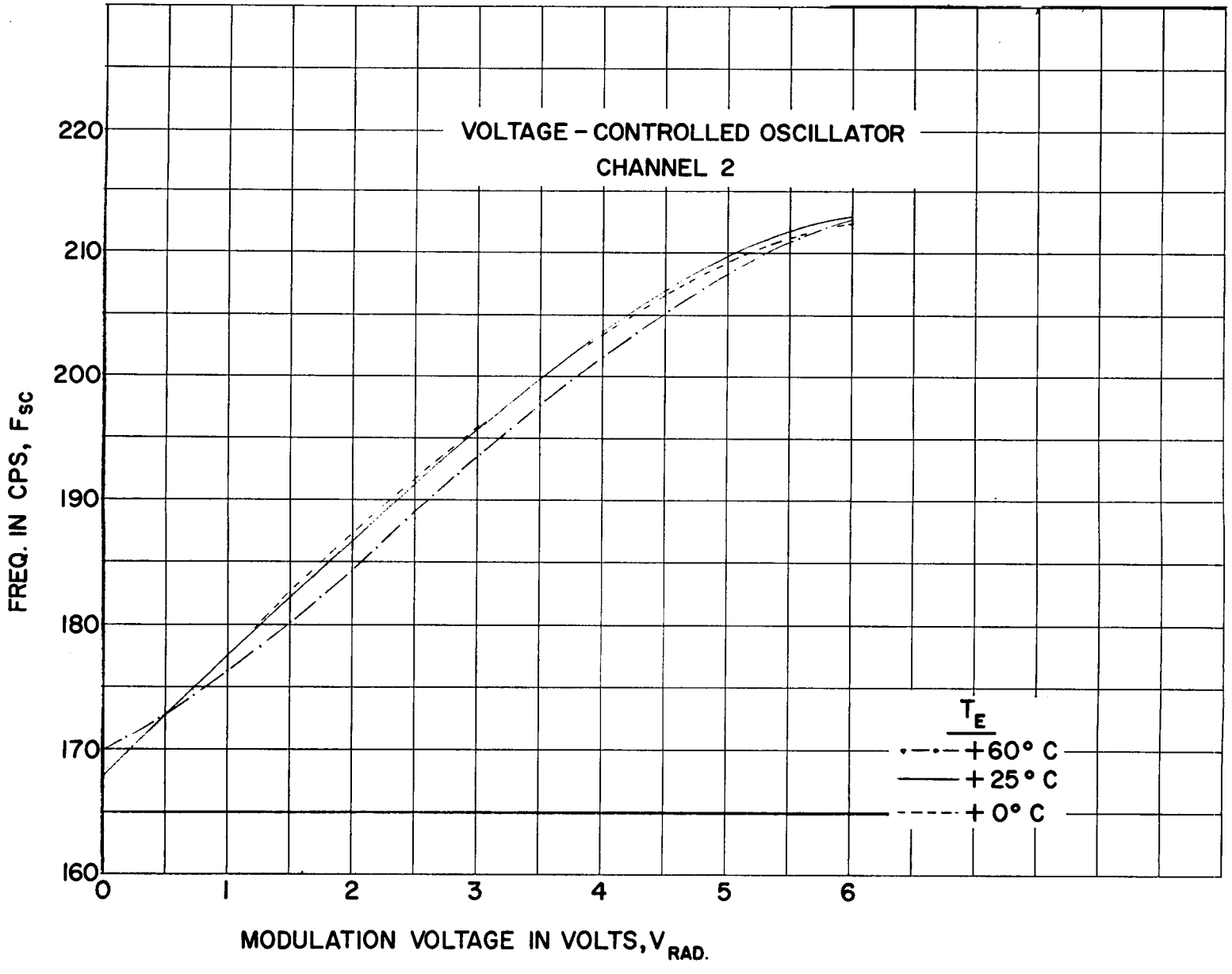

Figure 10—The response of the voltage controlled oscillator for Channel 2 shown as a parametric function of the electronics temperature, T_E.

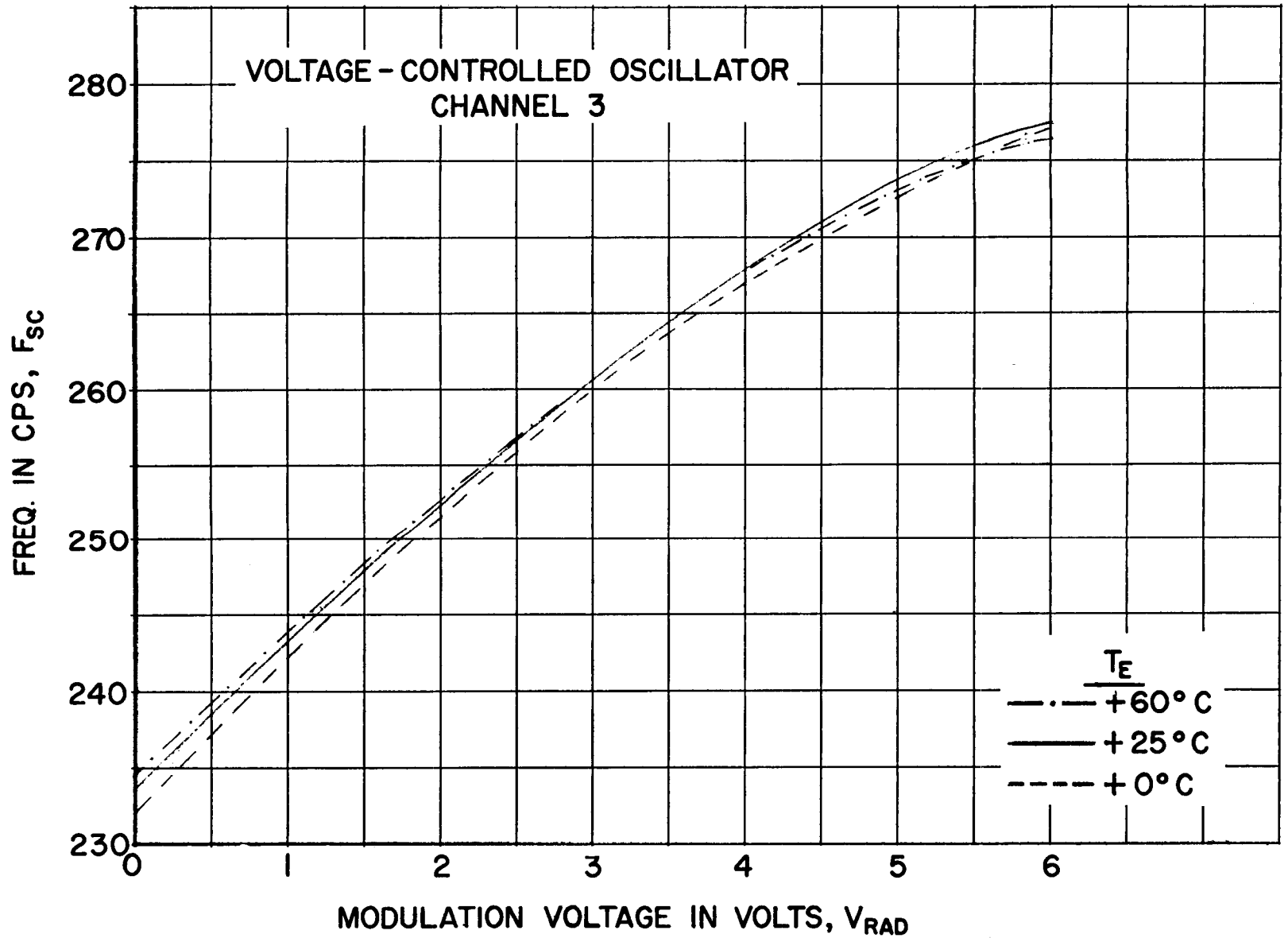

Figure 11—The response of the voltage controlled oscillator for Channel 3 shown as a parametric function of the electronics temperature, T_E.

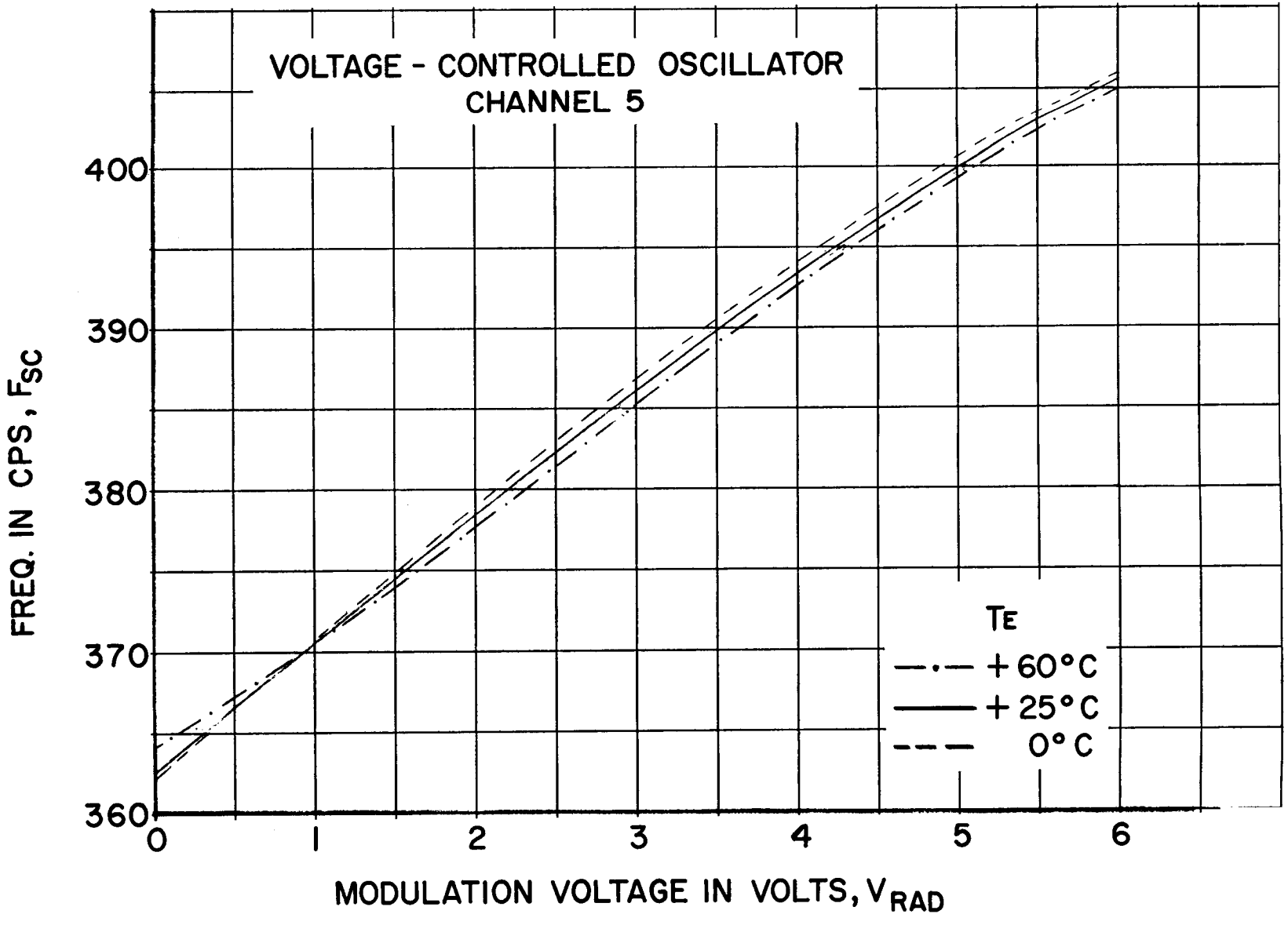

Figure 12—The response of the voltage controlled oscillator for Channel 5 shown as a parametric function of the electronics temperature, T_E.

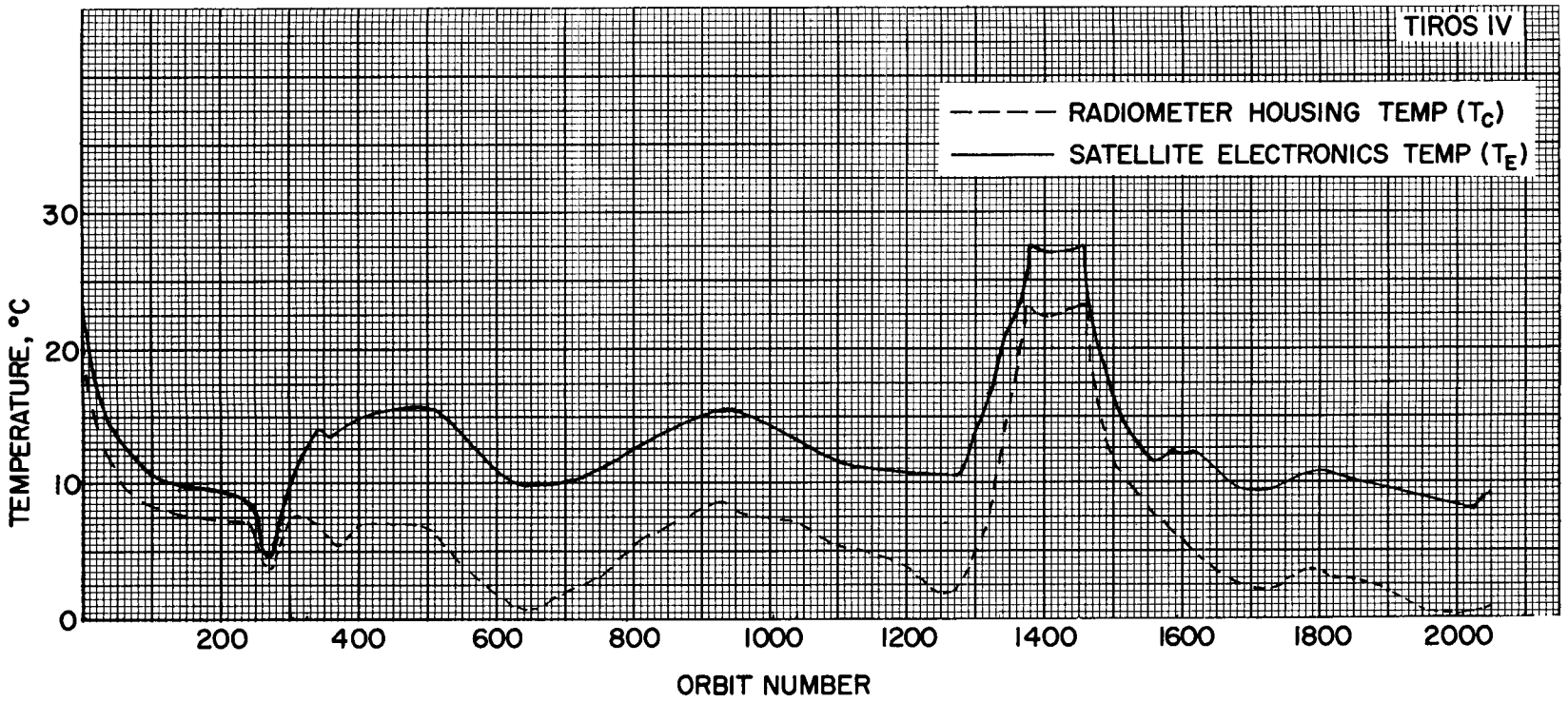

Figure 13—A temperature comparison of T_C and T_E for TIROS IV.

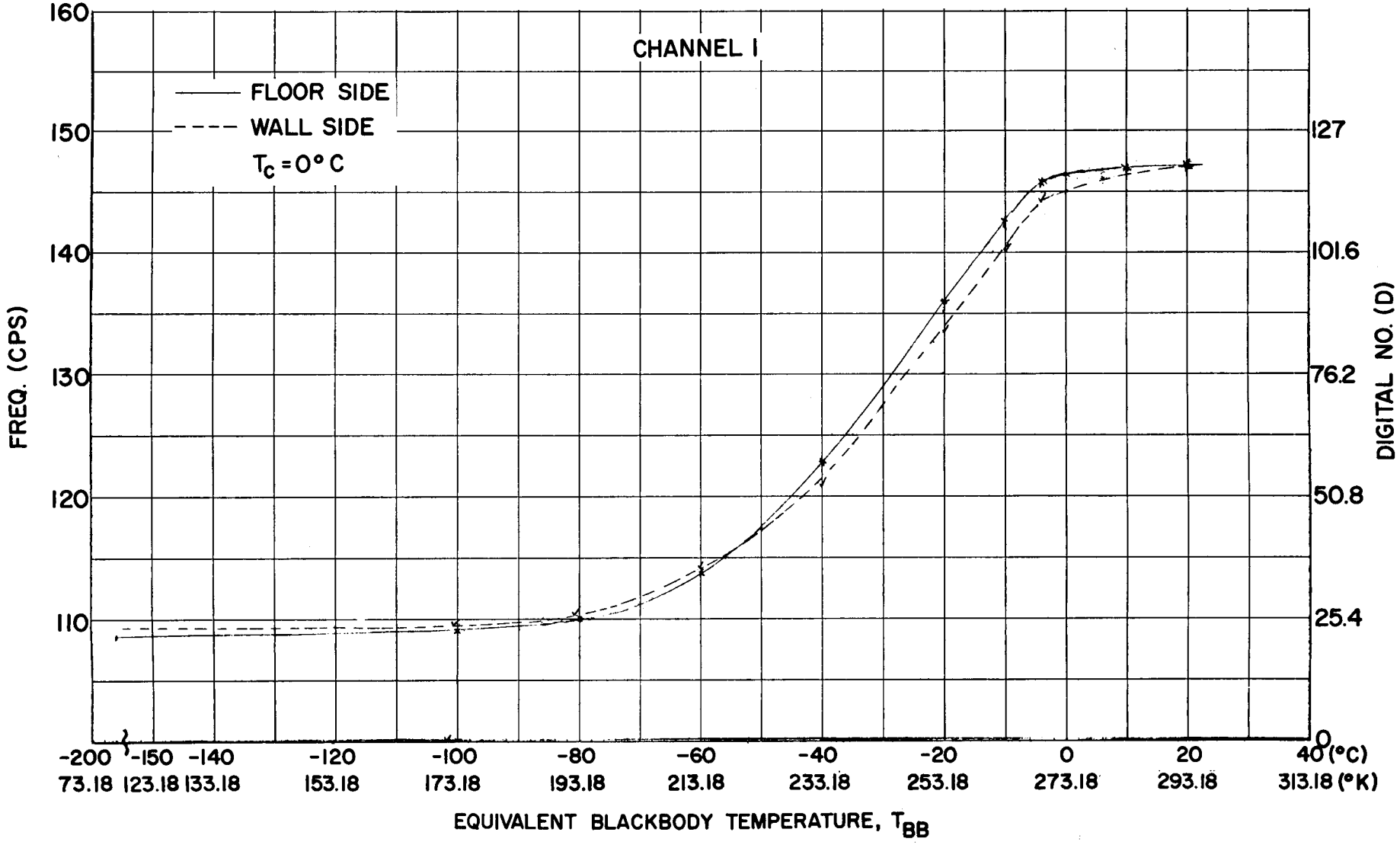

Figure 14—Subcarrier frequency and digital number versus blackbody temperature for wall and floor sides, Channel 1. (T_c = 0°C)

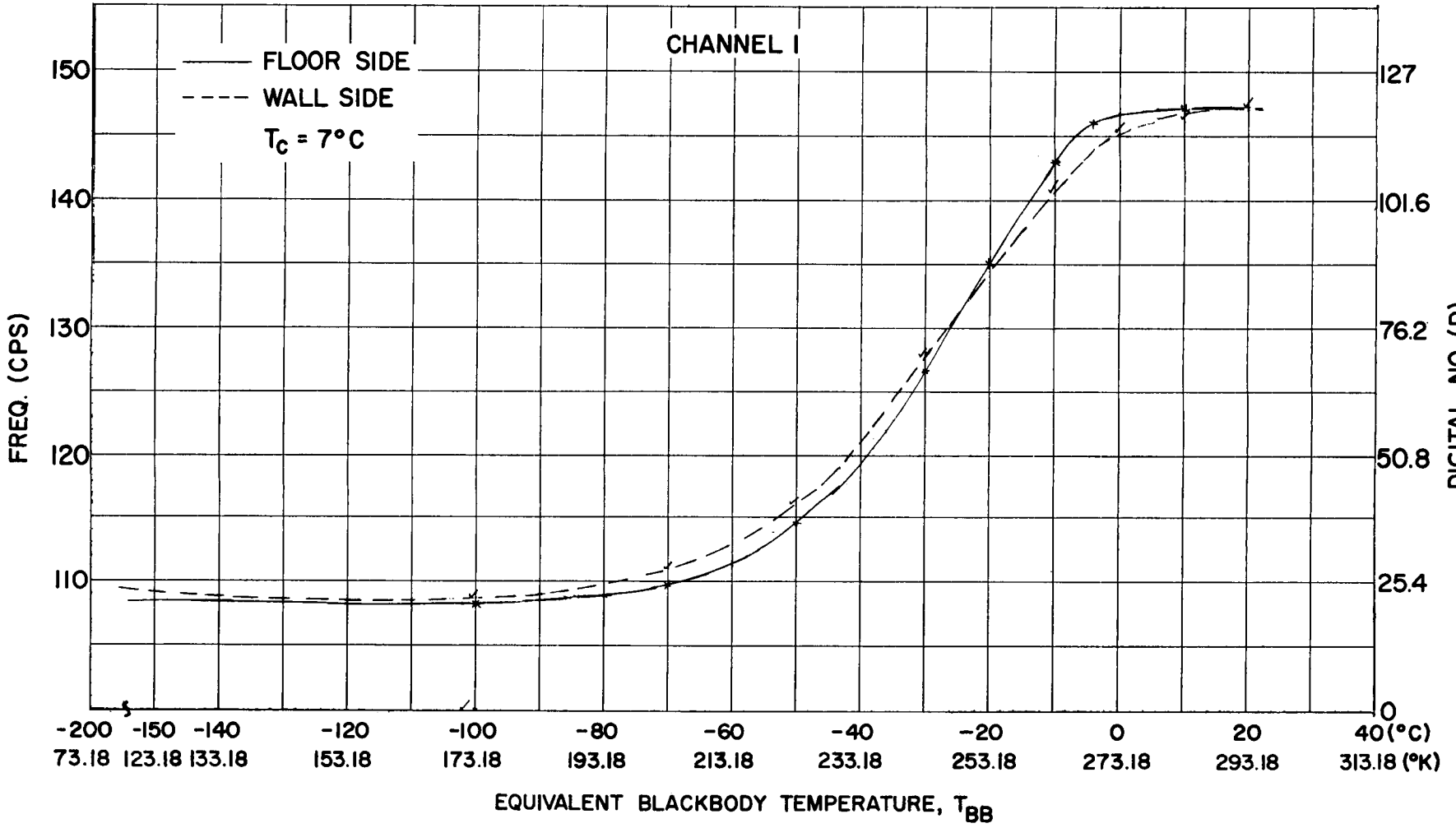

Figure 15—Subcarrier frequency and digital number versus blackbody temperature for wall and floor sides, Channel 1. (T_c = 7°C)

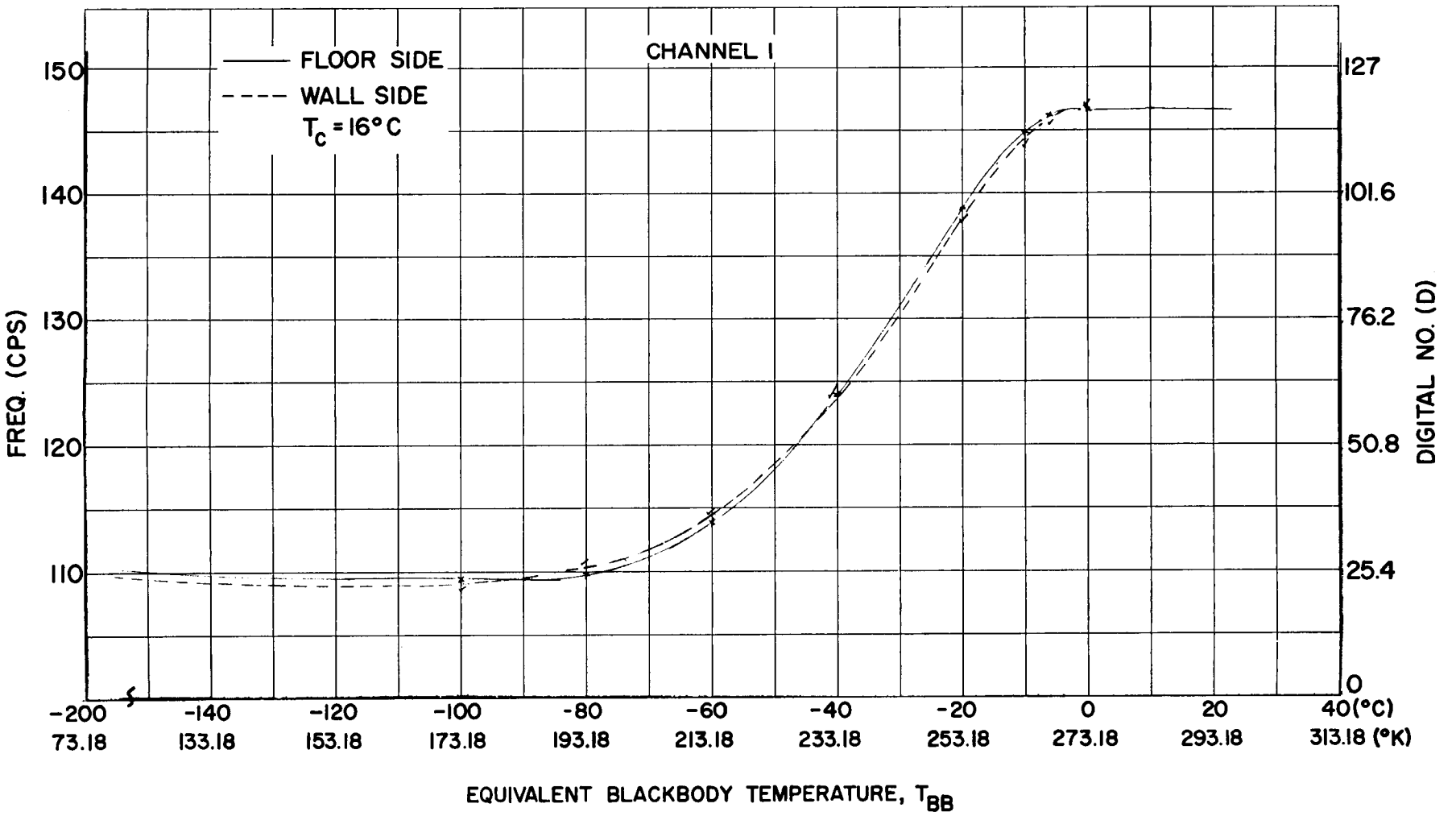

Figure 16—Subcarrier frequency and digital number versus blackbody temperature for wall and floor sides, Channel 1. ($T_c = 16°C$)

729-166 O - 64 - 4

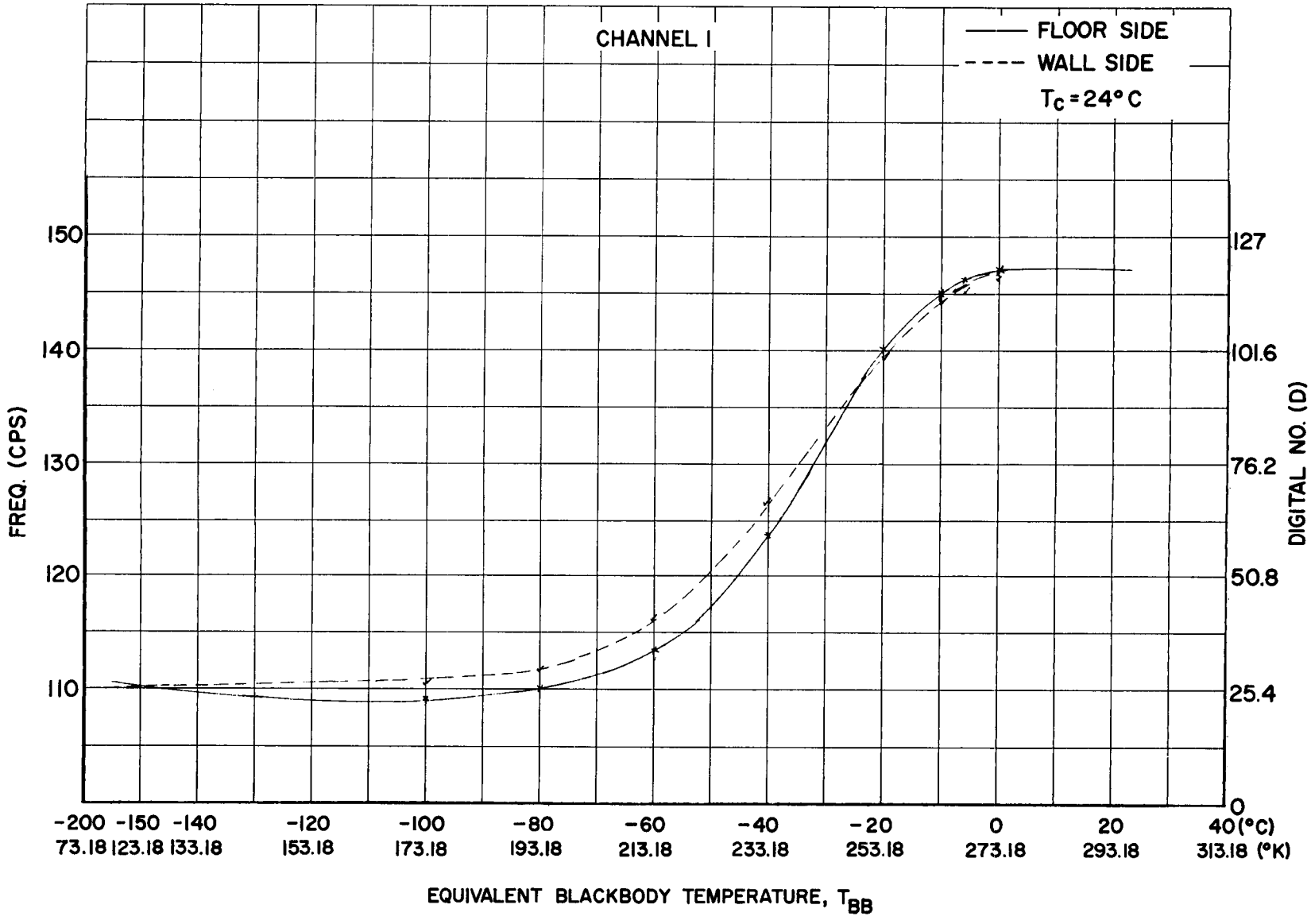

Figure 17—Subcarrier frequency and digital number versus blackbody temperature for wall and floor sides, Channel 1. (T_c = 24°C)

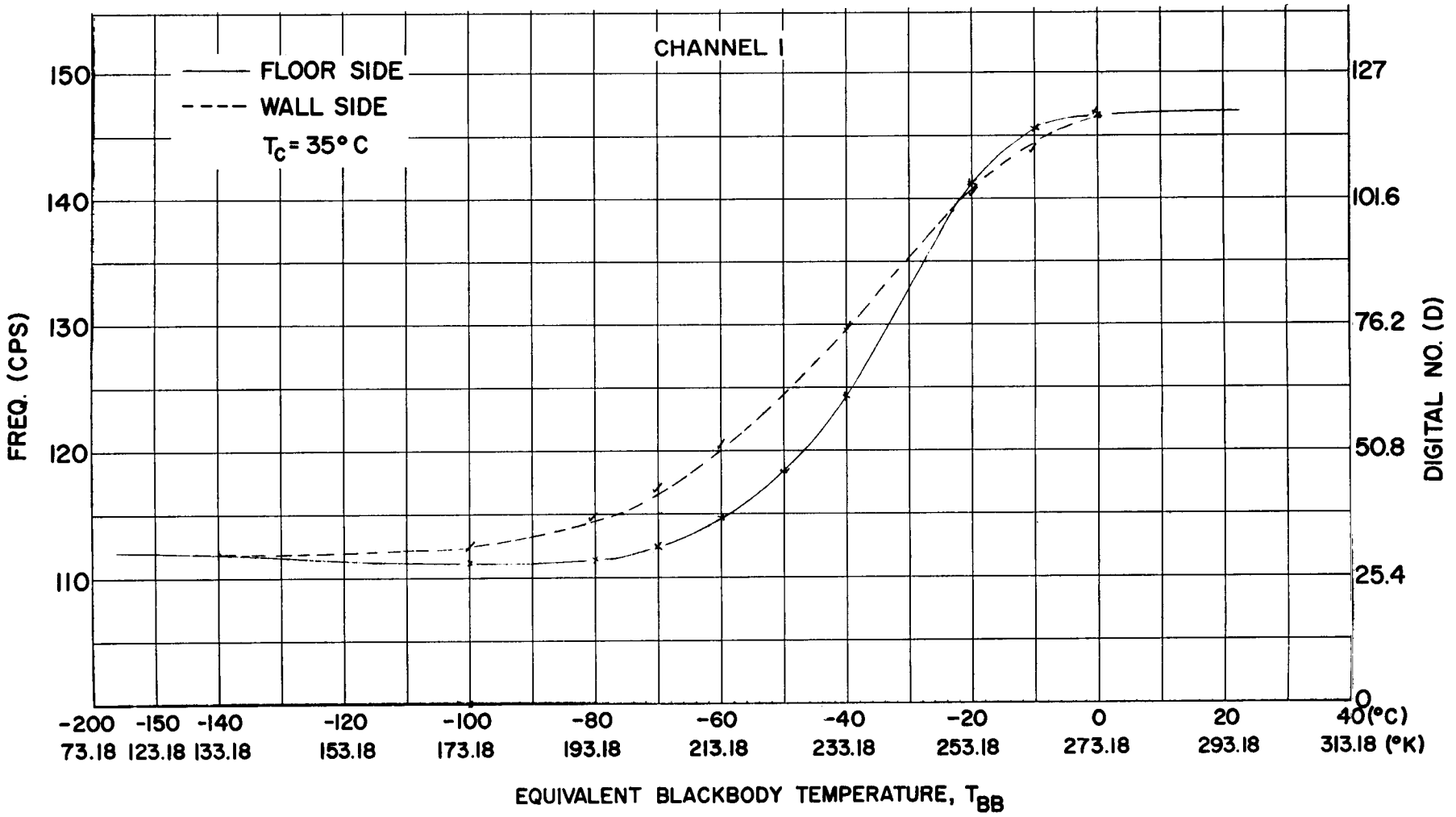

Figure 18—Subcarrier frequency and digital number versus blackbody temperature for wall and floor sides, Channel 1. (T_c = 35°C)

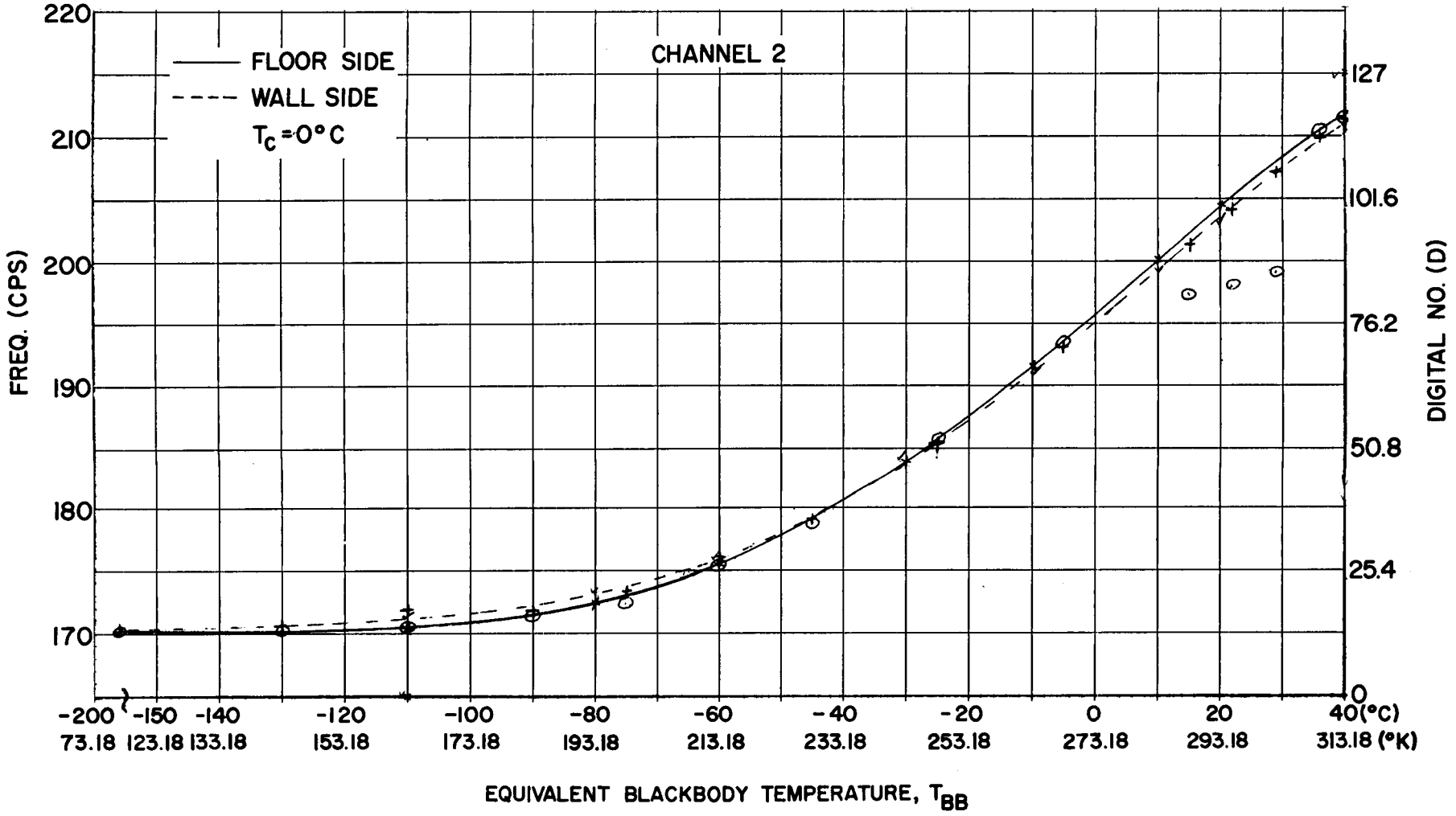

Figure 19—Subcarrier frequency and digital number versus blackbody temperature for wall and floor sides, Channel 2. (T_c = 0°C)

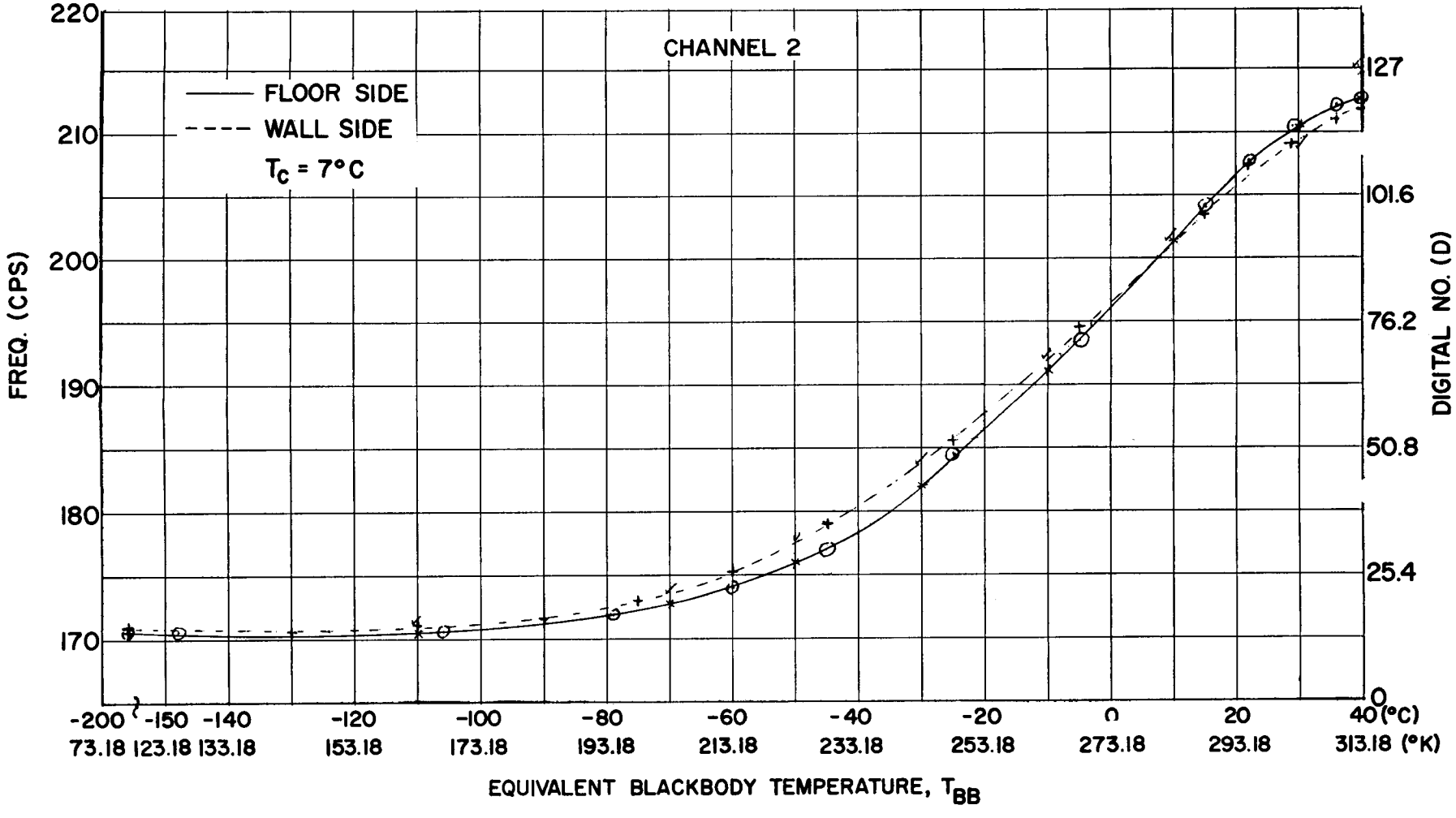

Figure 20—Subcarrier frequency and digital number versus blackbody temperature for wall and floor sides, Channel 2. (T_C = 7°C)

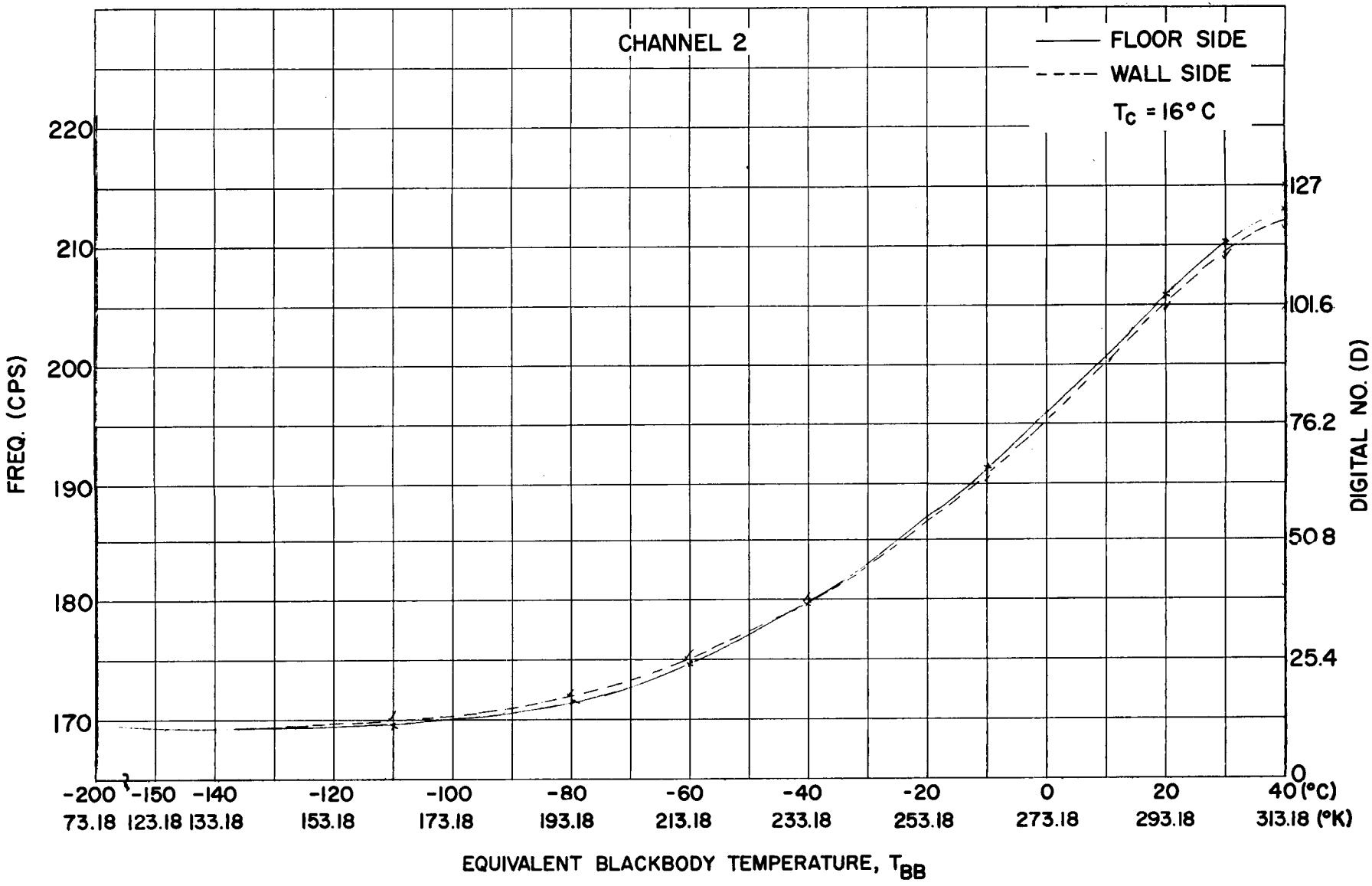

Figure 21—Subcarrier frequency and digital number versus blackbody temperature for wall and floor sides, Channel 2. (T_c = 16°C)

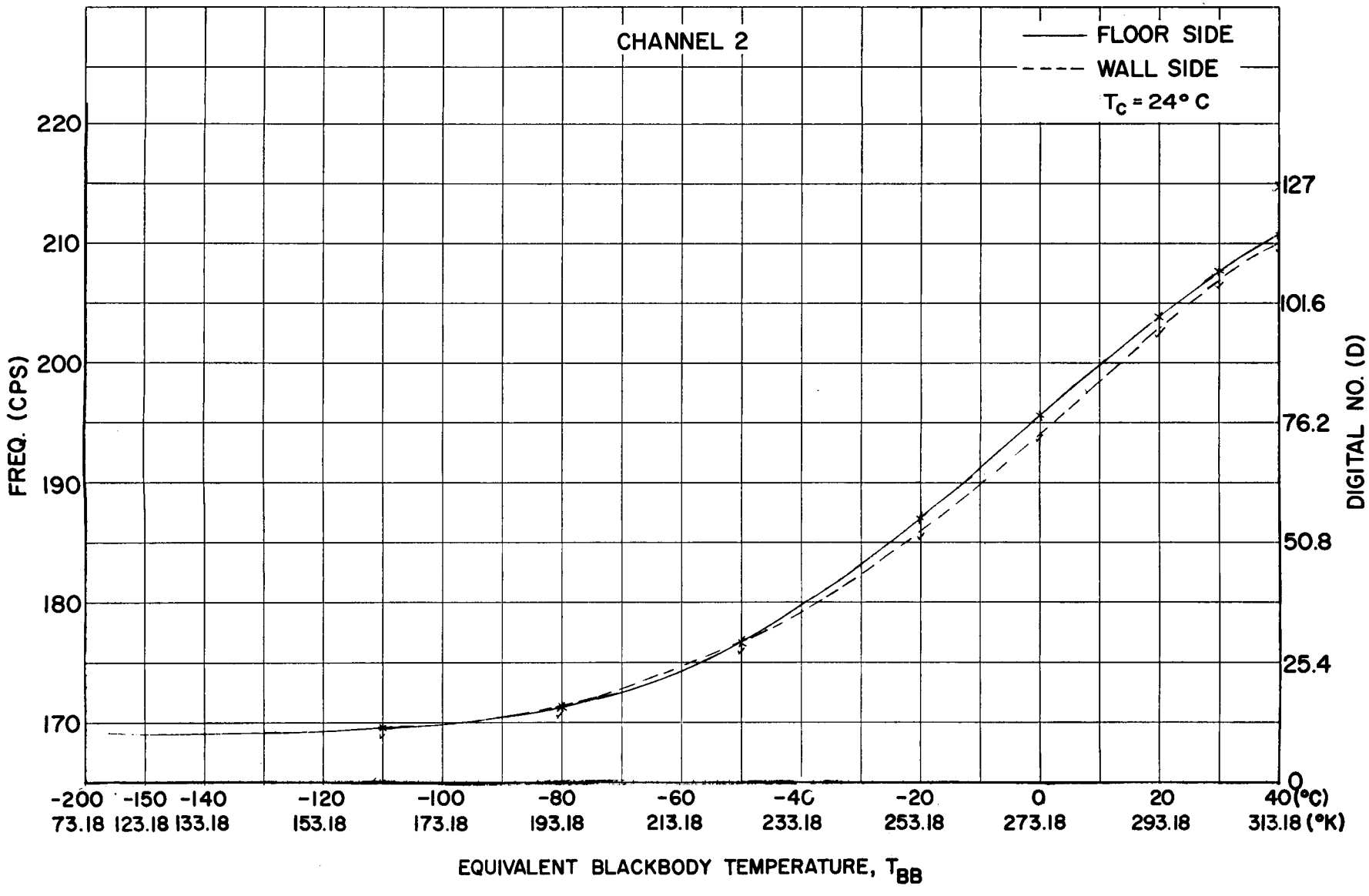

Figure 22—Subcarrier frequency and digital number versus blackbody temperature for wall and floor sides, Channel 2. (T_c = 24°C)

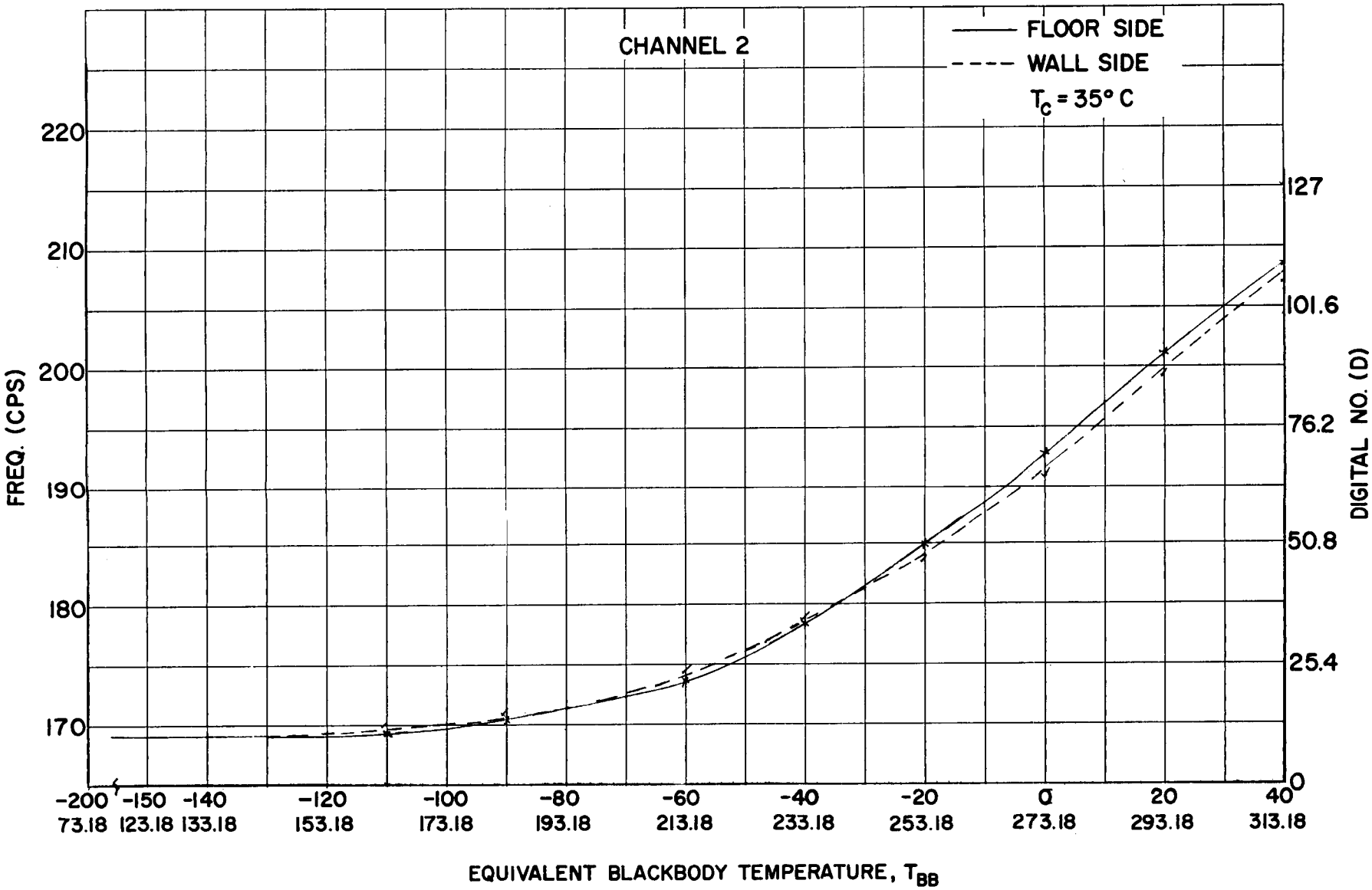

Figure 23—Subcarrier frequency and digital number versus blackbody temperature for wall and floor sides, Channel 2. (T_C = 35°C)

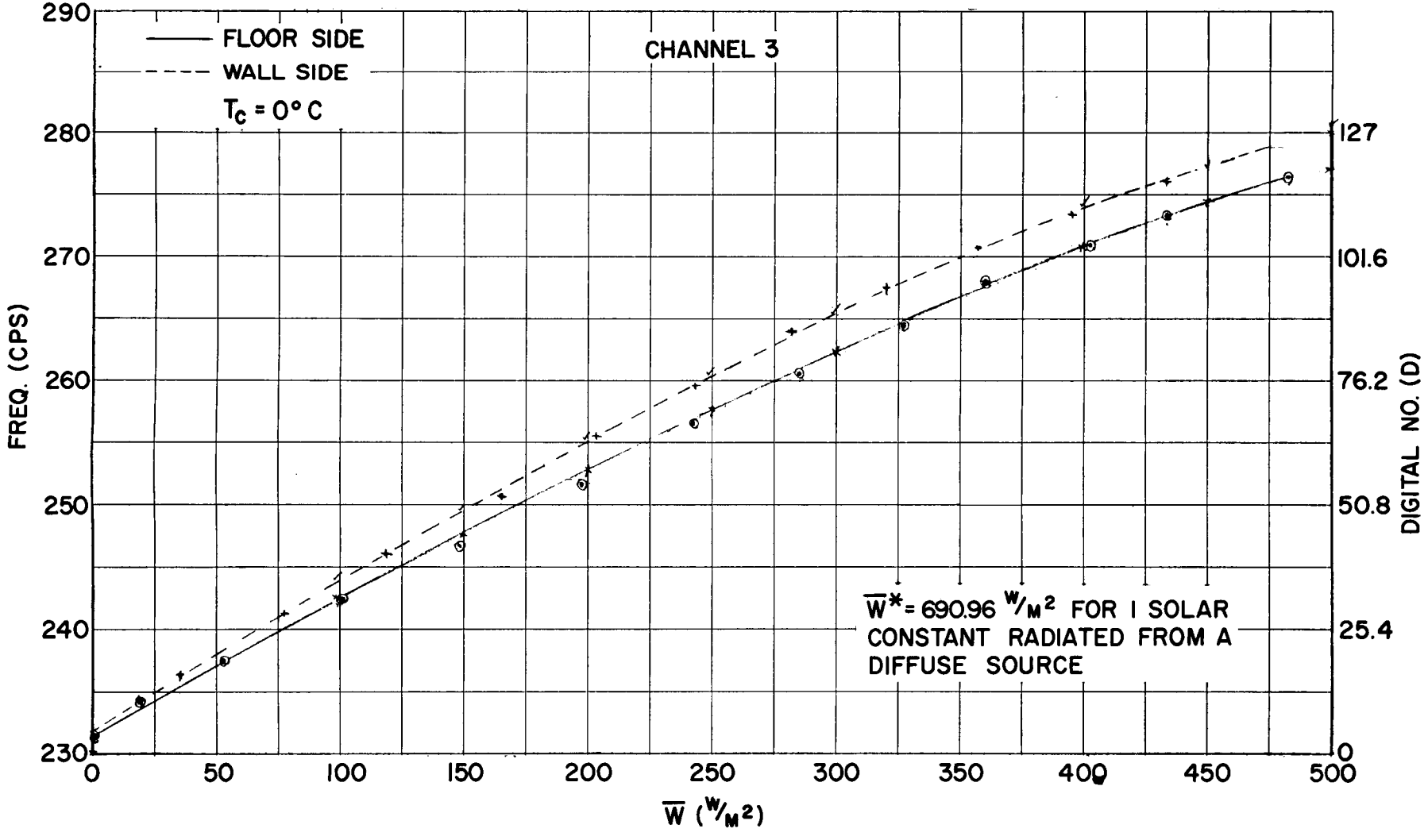

Figure 24—Subcarrier frequency and digital number versus effective radiant emittance for wall and floor sides, Channel 3. (T_c = 0°C)

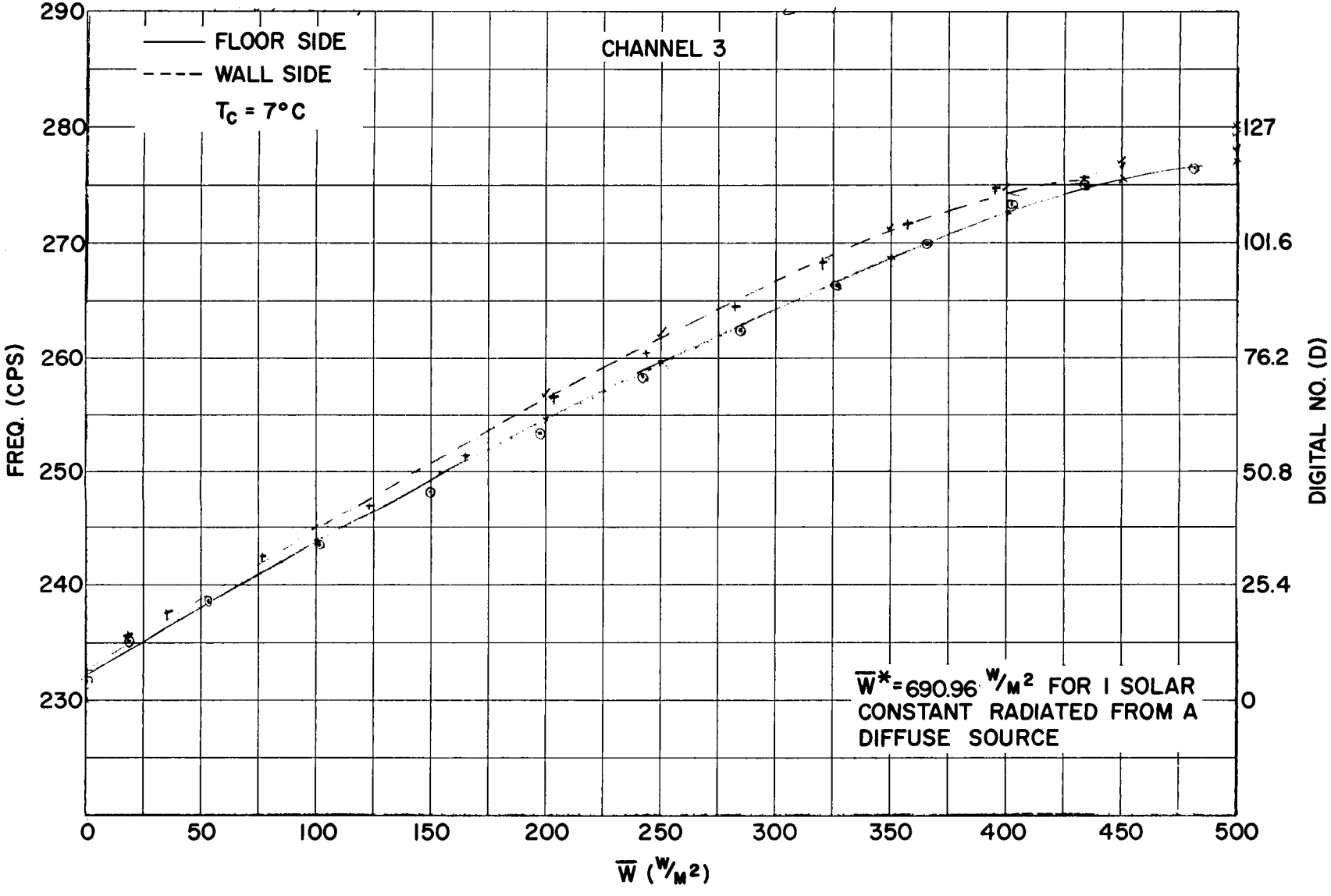

Figure 25—Subcarrier frequency and digital number versus effective radiant emittance for wall and floor sides, Channel 3. (T_C = 7°C)

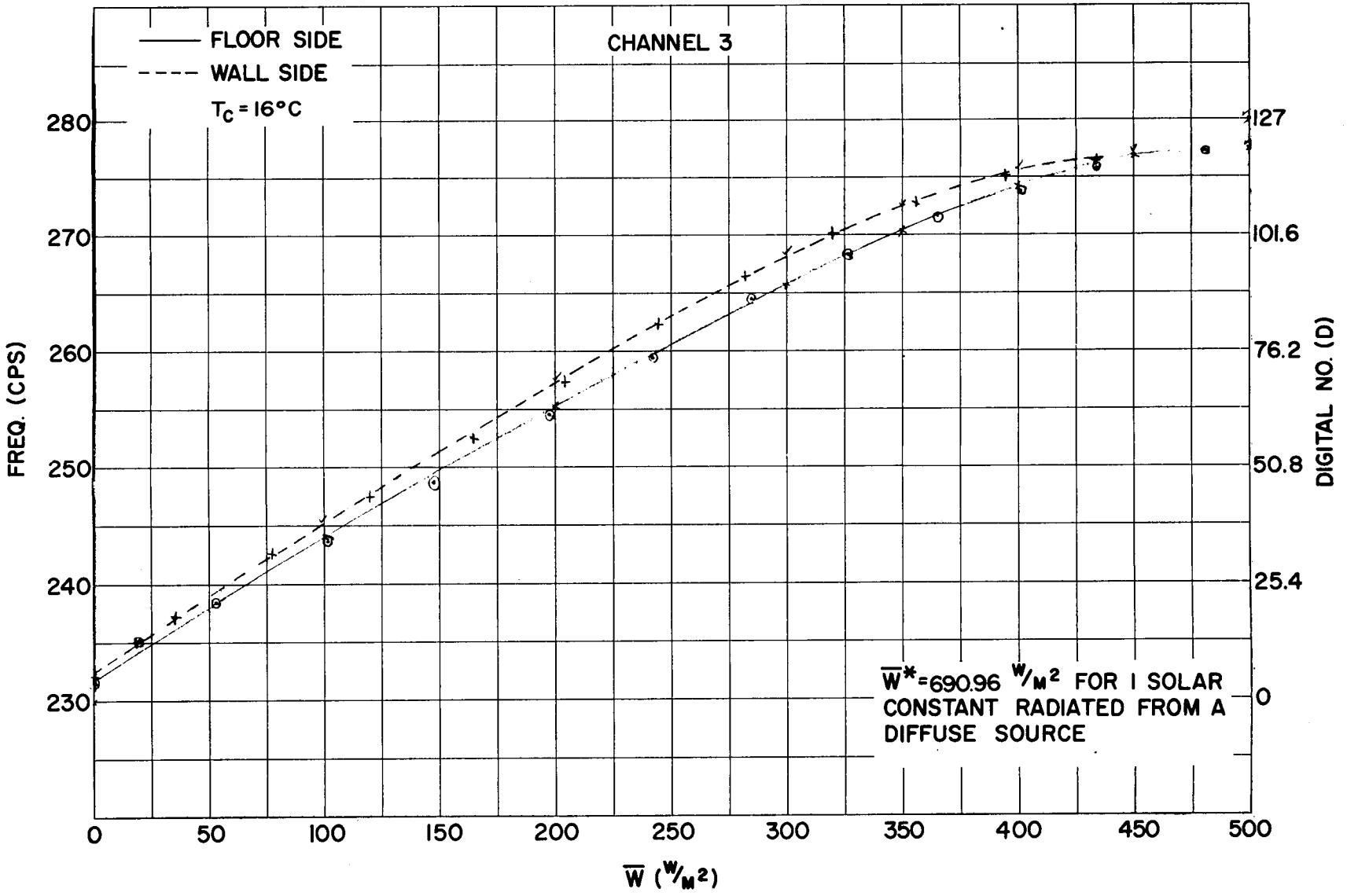

Figure 26—Subcarrier frequency and digital number versus effective radiant emittance for wall and floor sides, Channel 3. (T_C = 16°C)

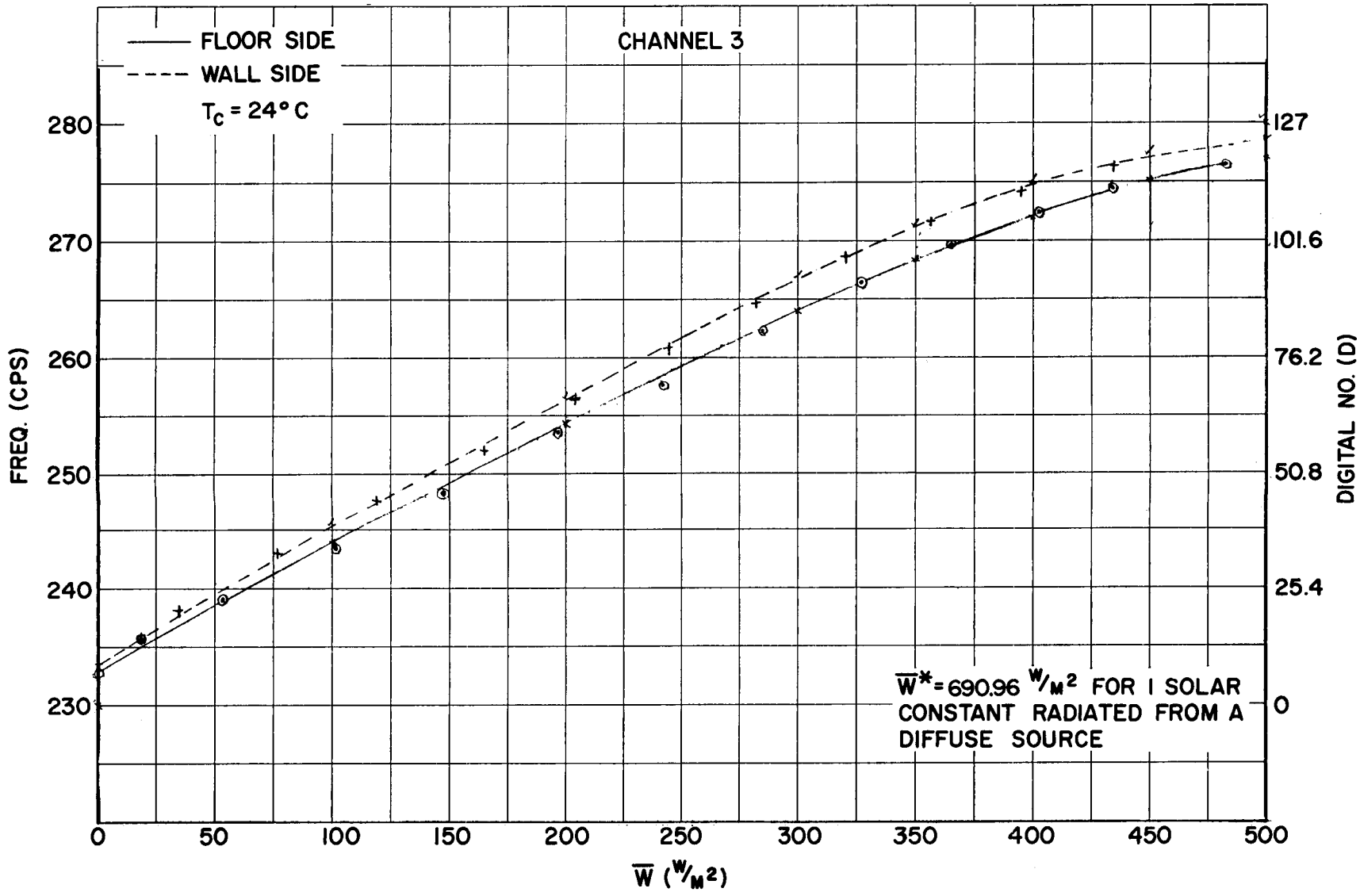

Figure 27—Subcarrier frequency and digital number versus effective radiant emittance for wall and floor sides, Channel 3. (T_C = 24°C)

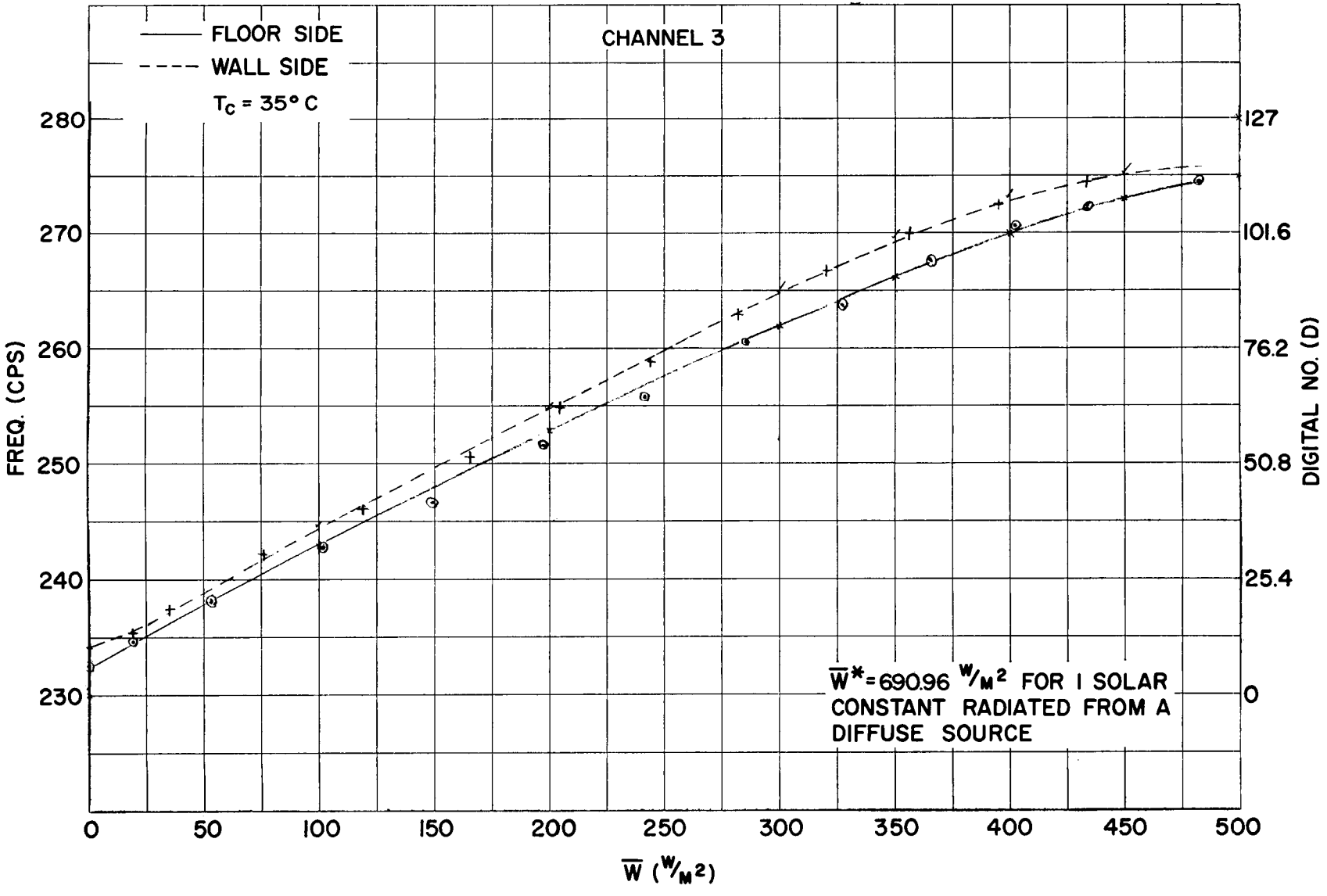

Figure 28—Subcarrier frequency and digital number versus effective radiant emittance for wall and floor sides, Channel 3. (T_c = 35°C)

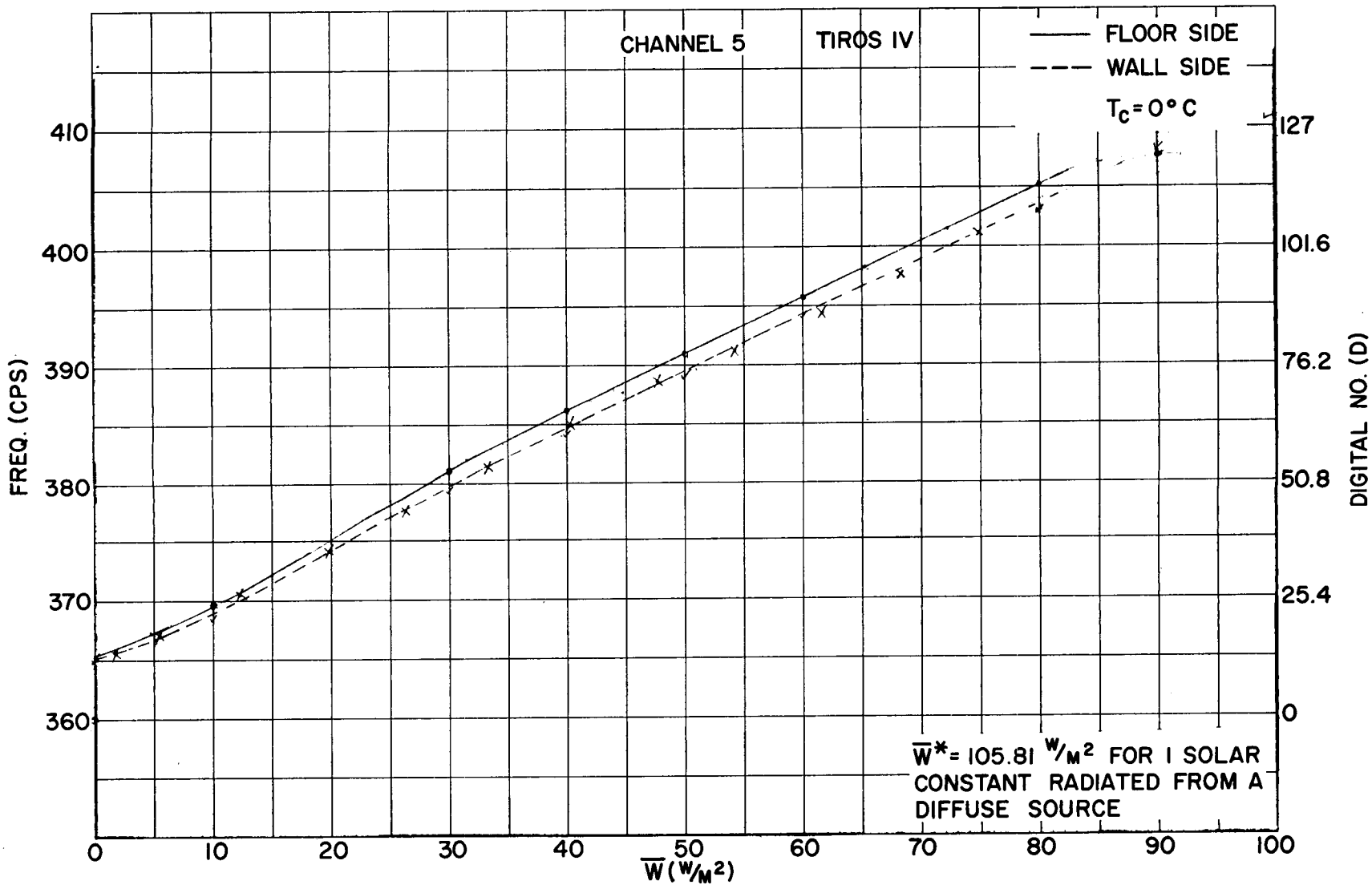

Figure 29—Subcarrier frequency and digital number versus effective radiant emittance for wall and floor sides, Channel 5. ($T_c = 0°C$)

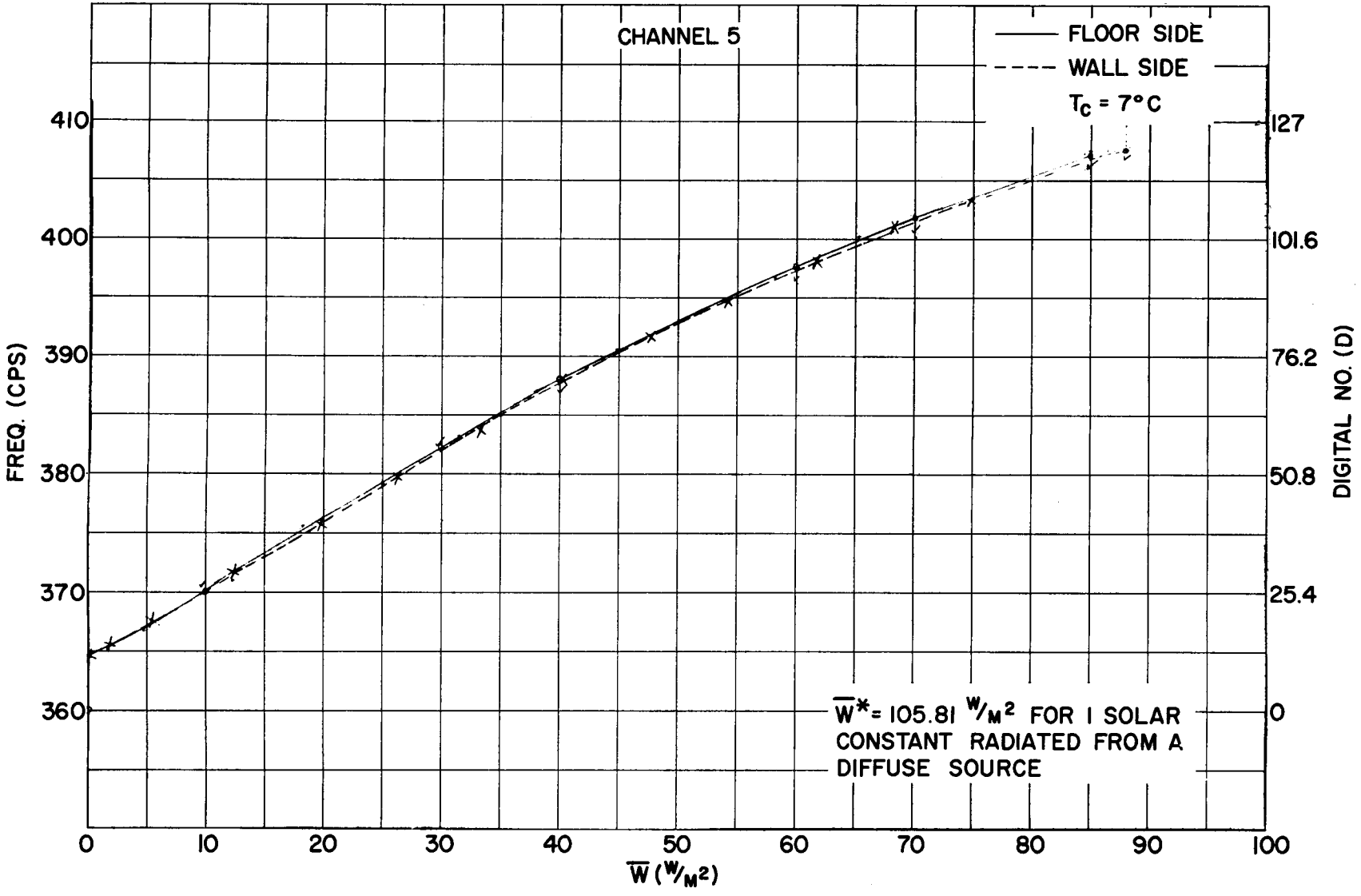

Figure 30—Subcarrier frequency and digital number versus effective radiant emittance for wall and floor sides, Channel 5. (T_c = 7°C)

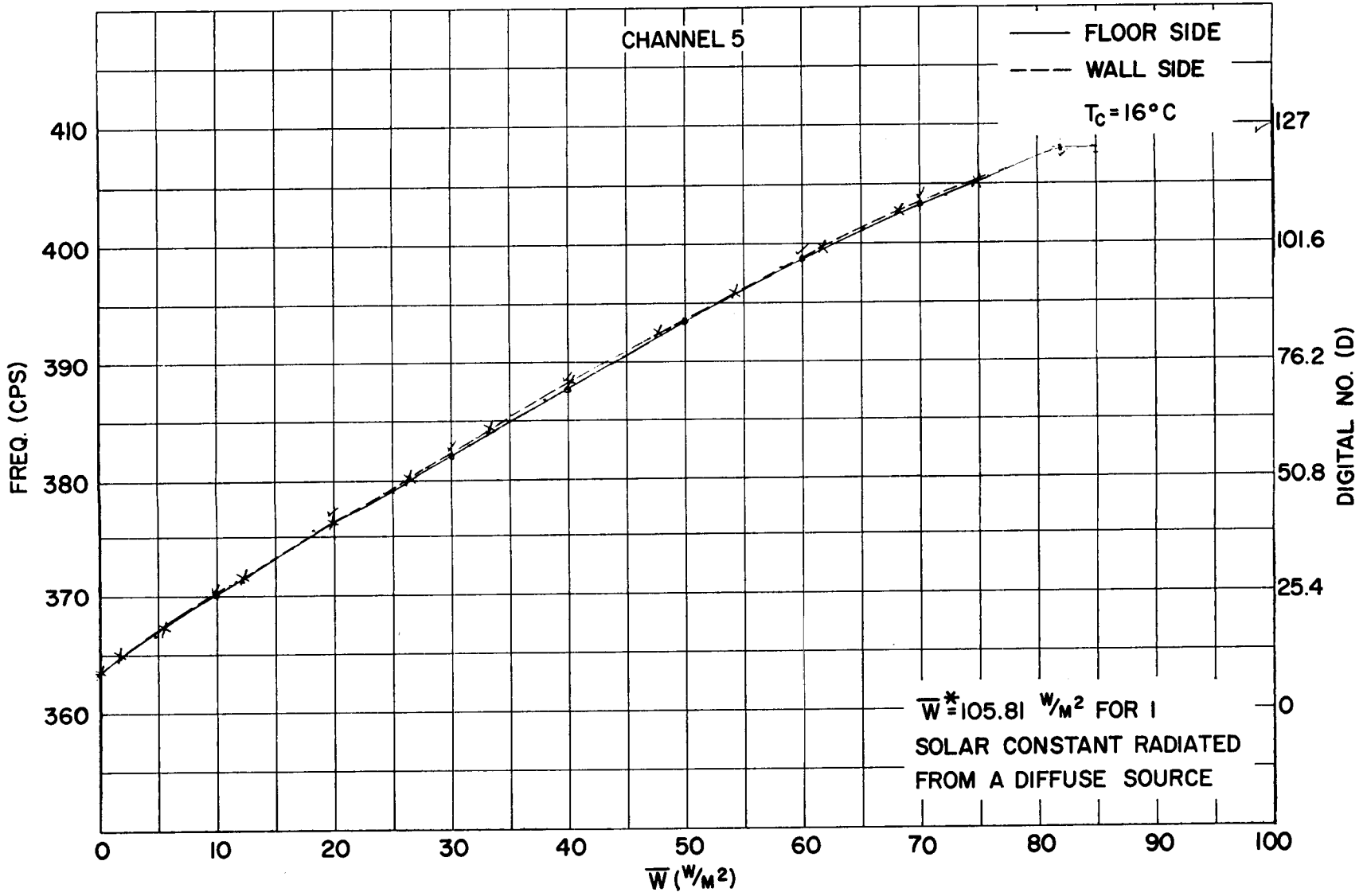

Figure 31—Subcarrier frequency and digital number versus effective radiant emittance for wall and floor sides, Channel 5. (T_c = 16°C)

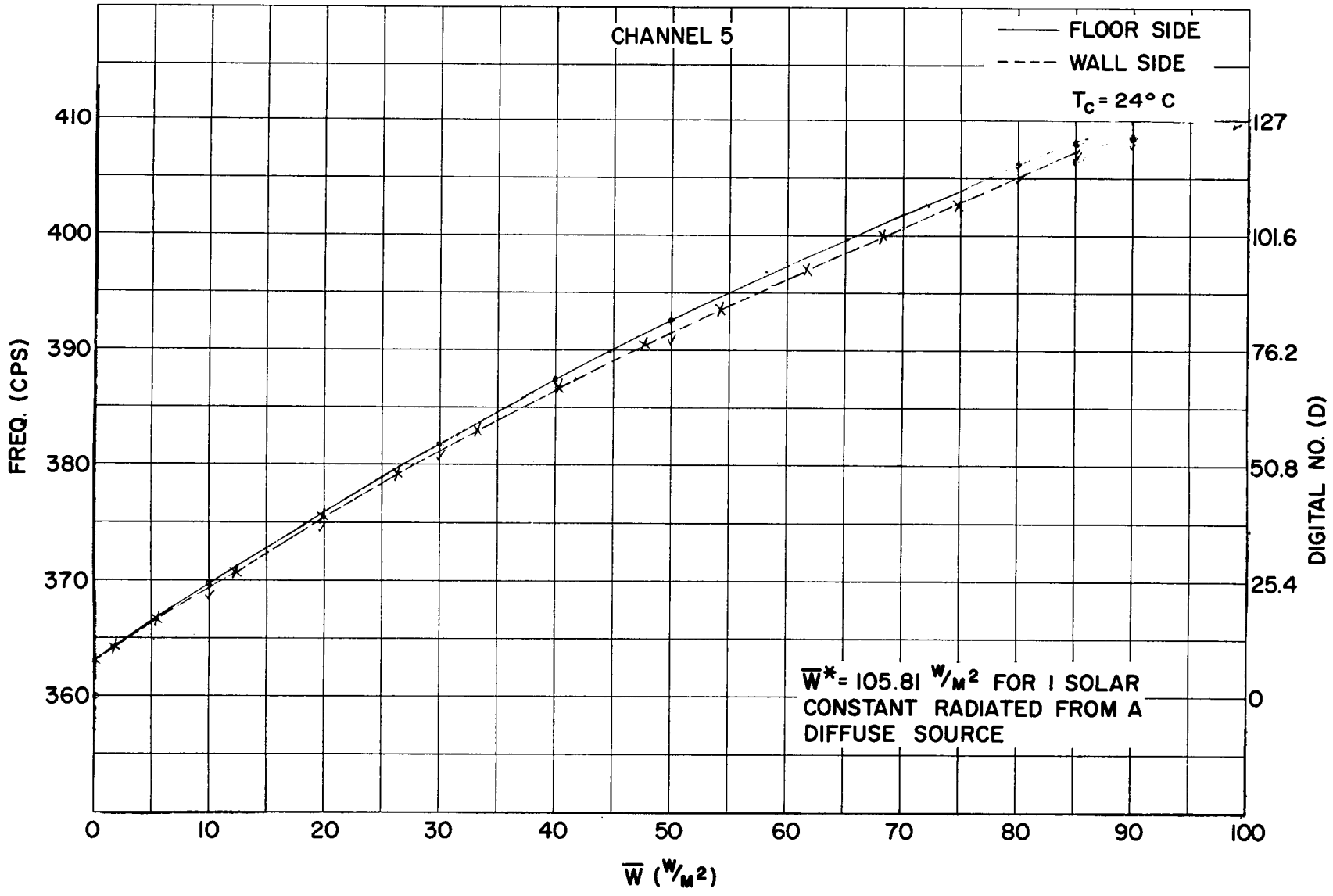

Figure 32—Subcarrier frequency and digital number versus effective radiant emittance for wall and floor sides, Channel 5. (T_c = 24°C)

729-166 O - 64 - 5

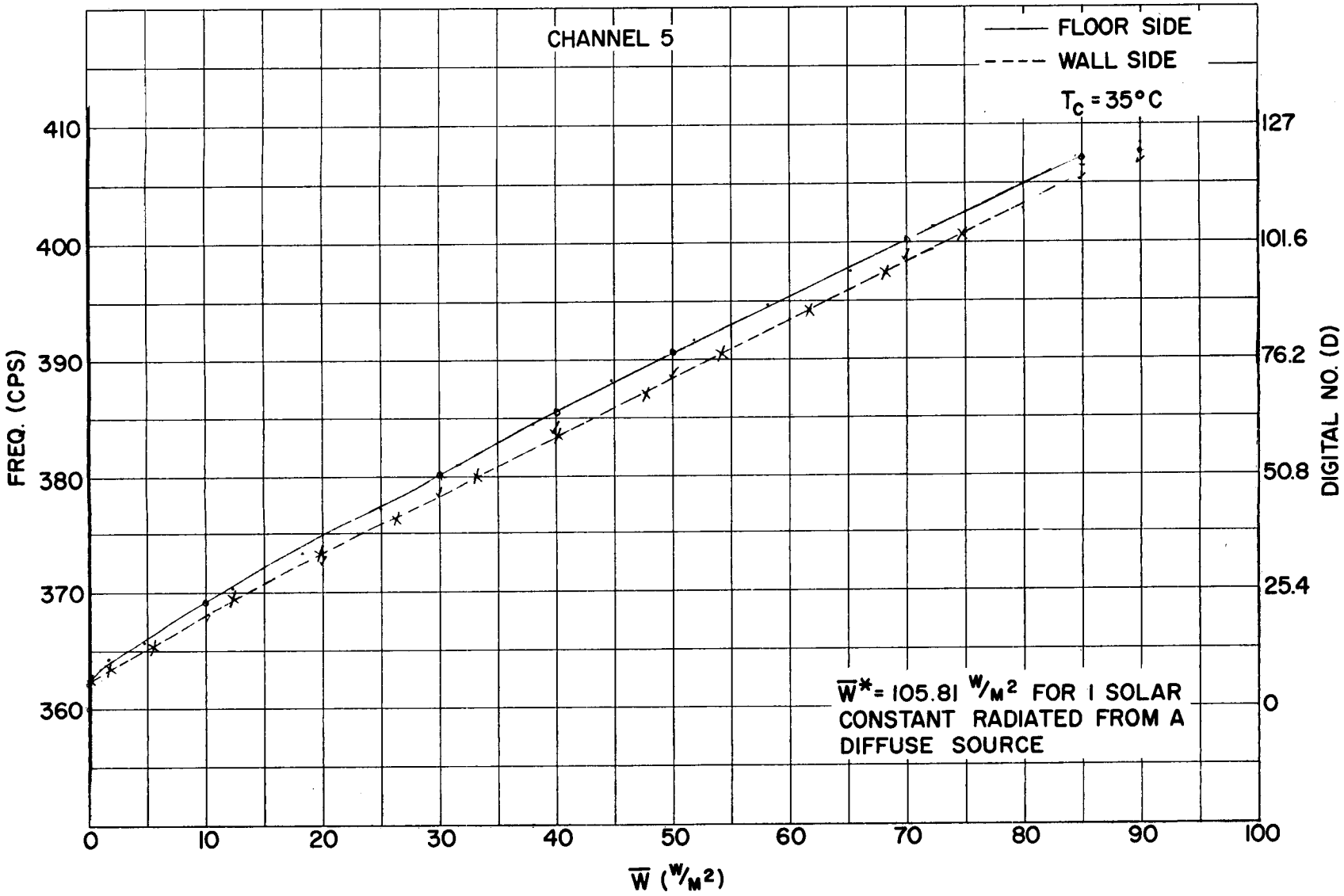

Figure 33—Subcarrier frequency and digital number versus effective radiant emittance for wall and floor sides, Channel 5. (T_c = 35°C)

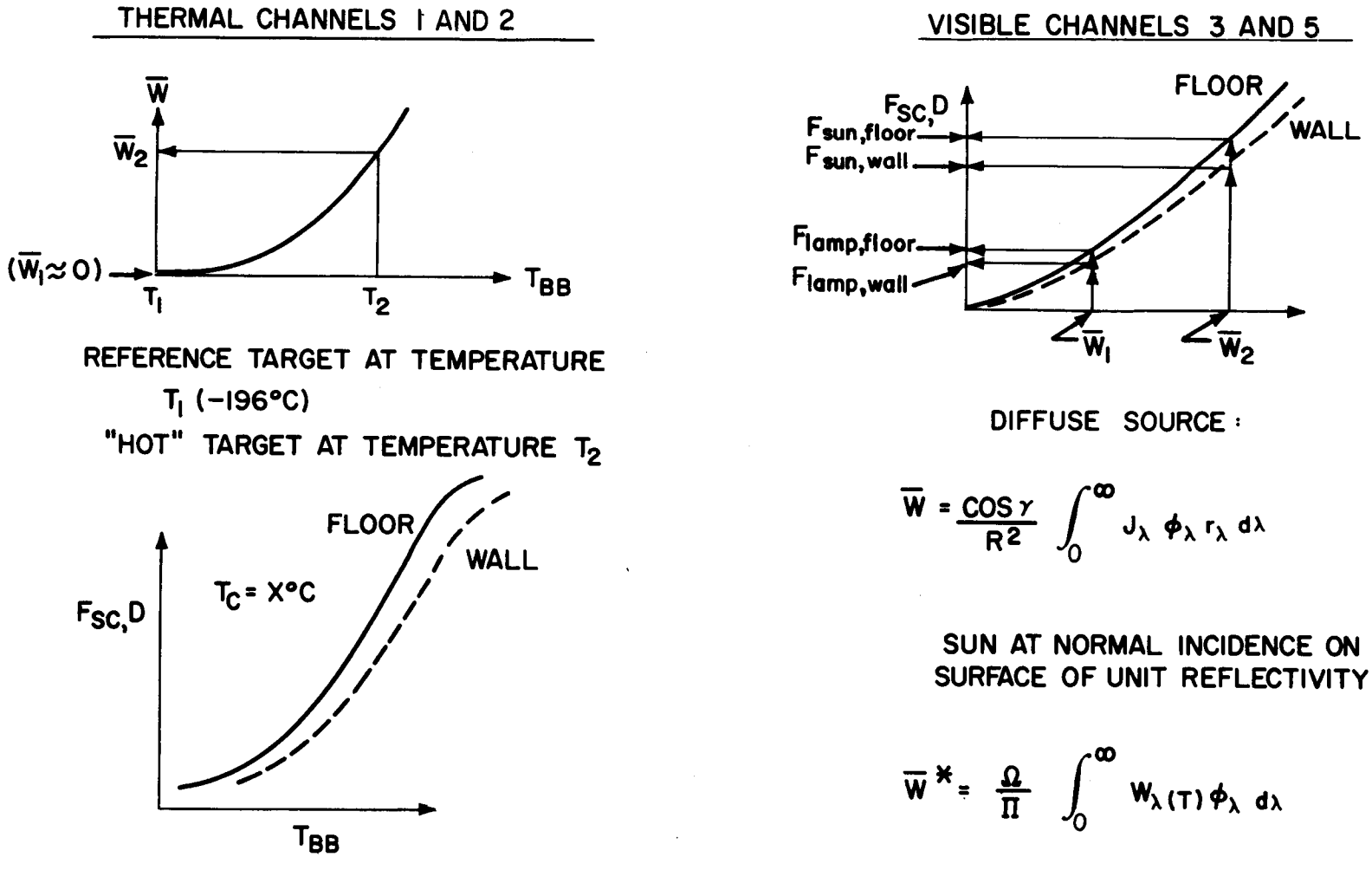

Figure 34—(*a*) Calibration of the emitted thermal radiation Channels 1 and 2.
(*b*) Calibration of the reflected solar radiation Channels 3 and 5.

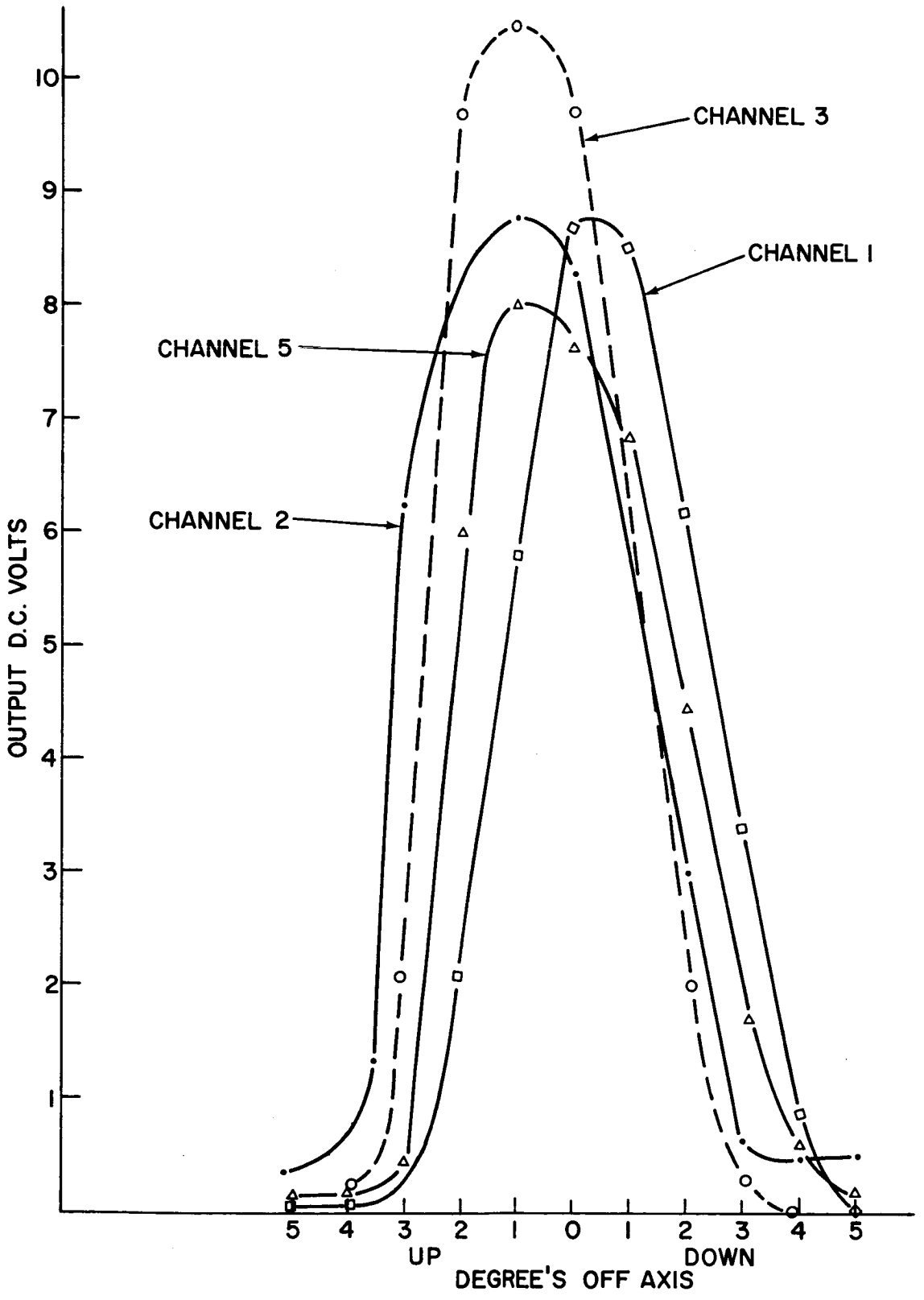

Figure 35—Vertical field of view measurements.

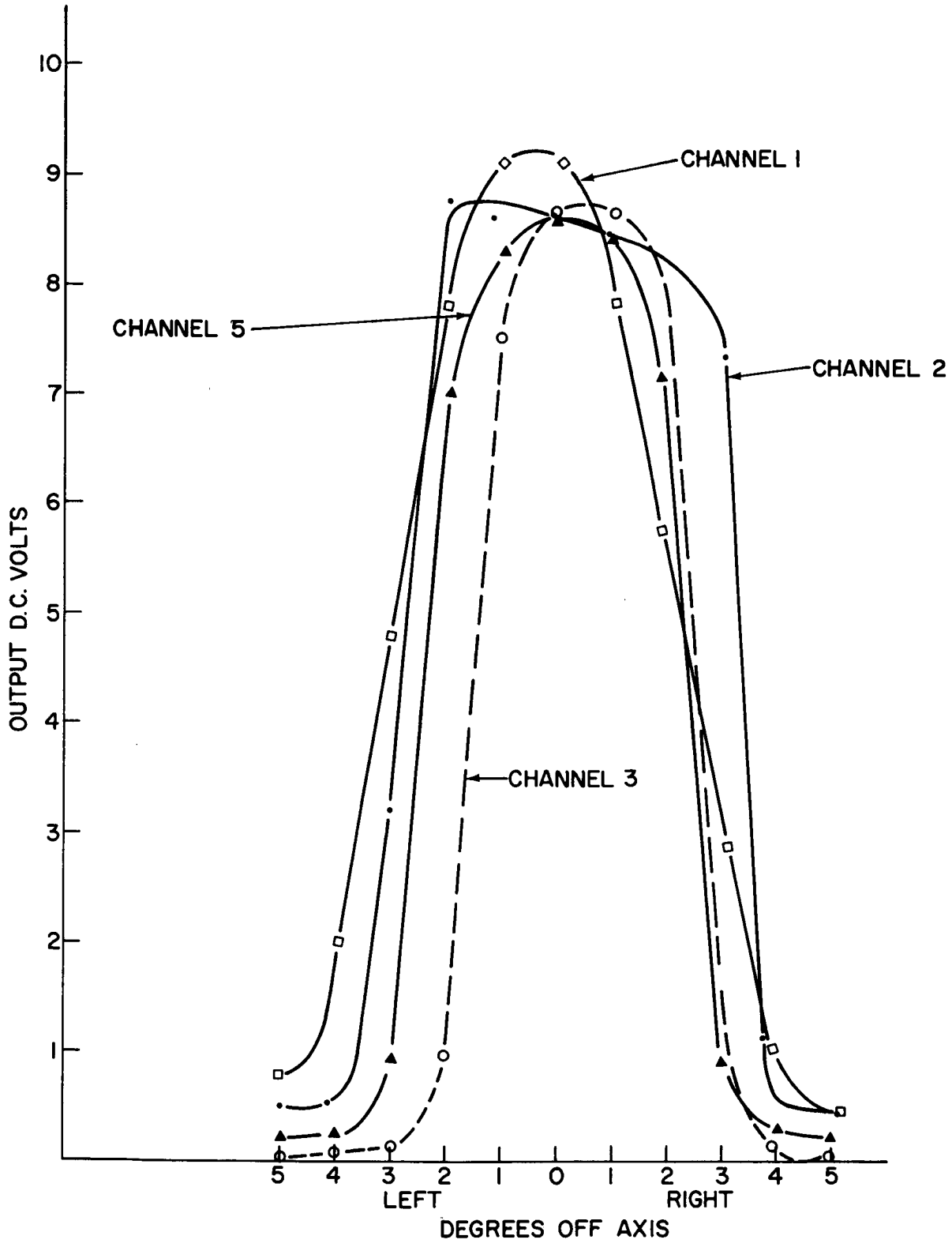

Figure 36—Horizontal field of view measurements.

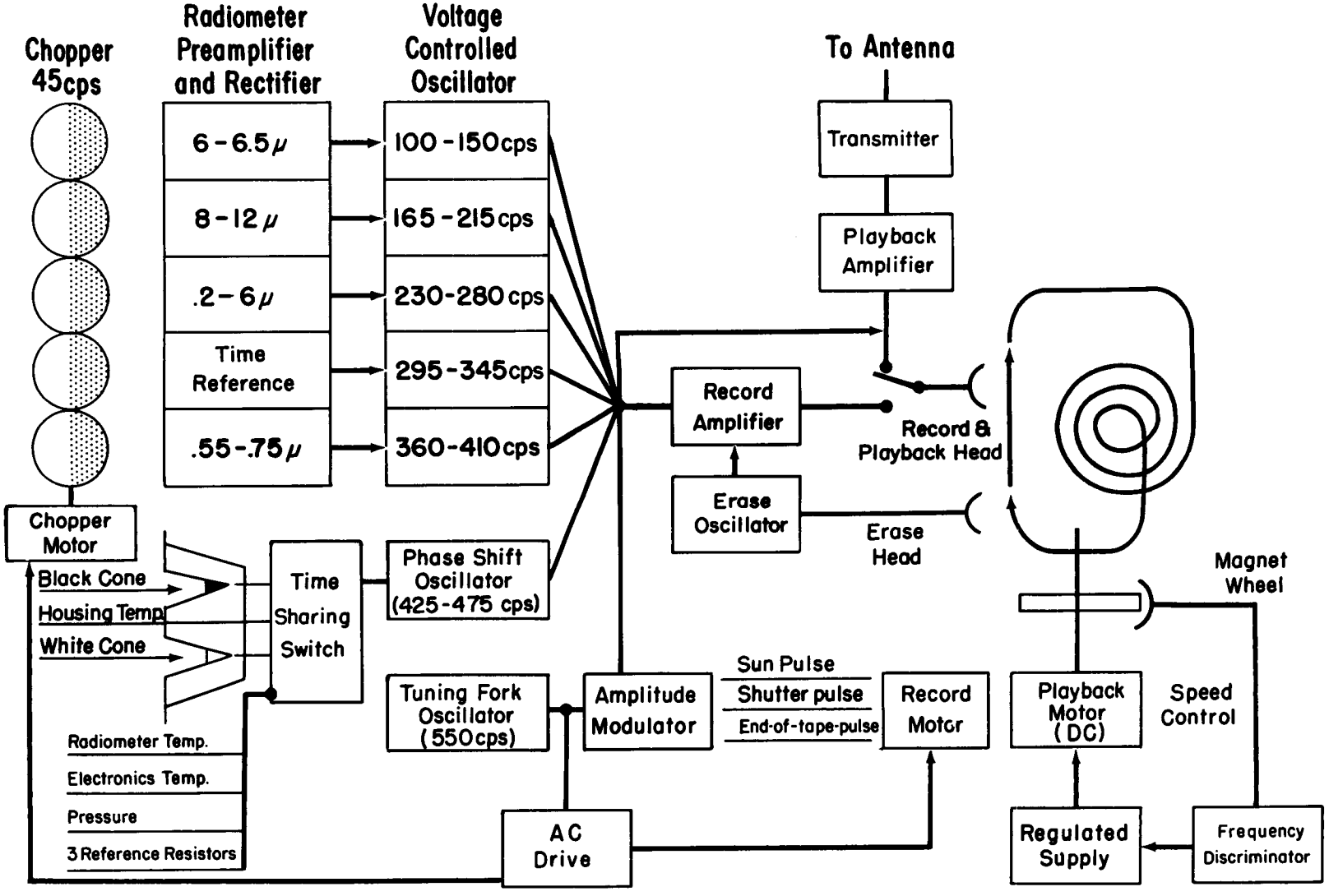

Figure 37—Block diagram of the radiation experiment in the satellite.

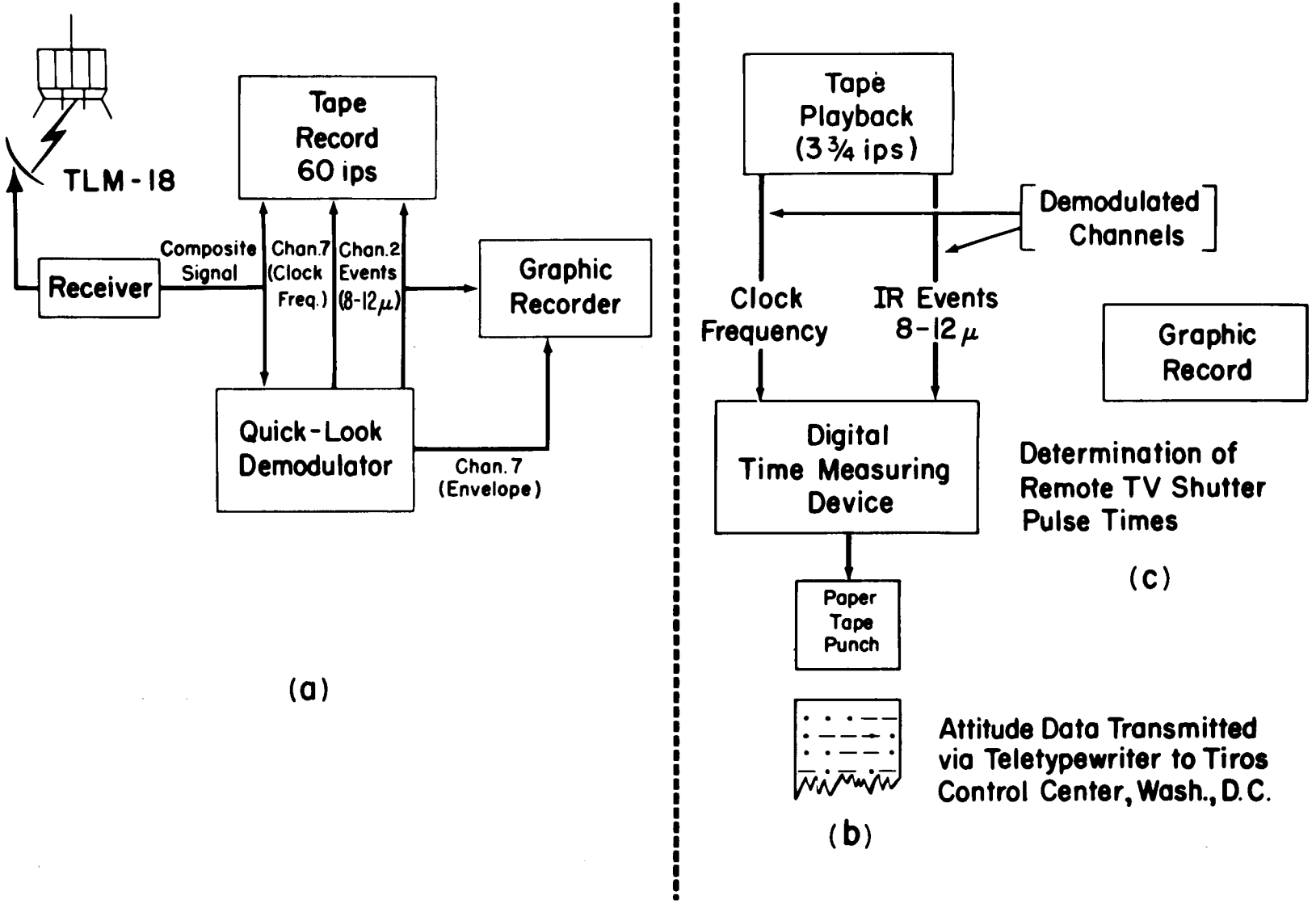

Figure 38—Block diagram of information flow at a Command and Data Acquisition station including auxiliary uses of the radiation data.

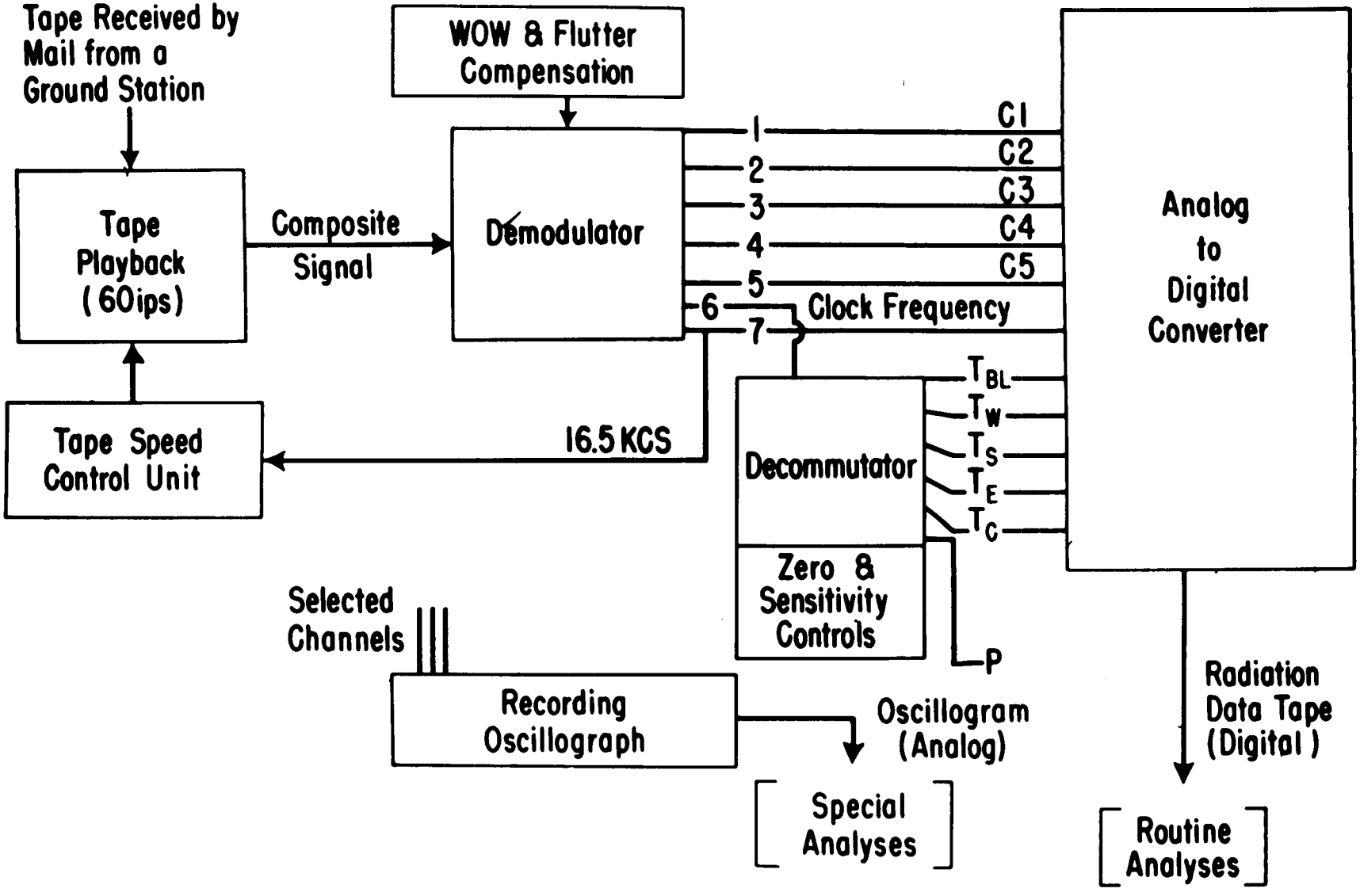

Figure 39—Block diagram of information flow at the Data Processing Center in producing a digital magnetic tape for computer input.

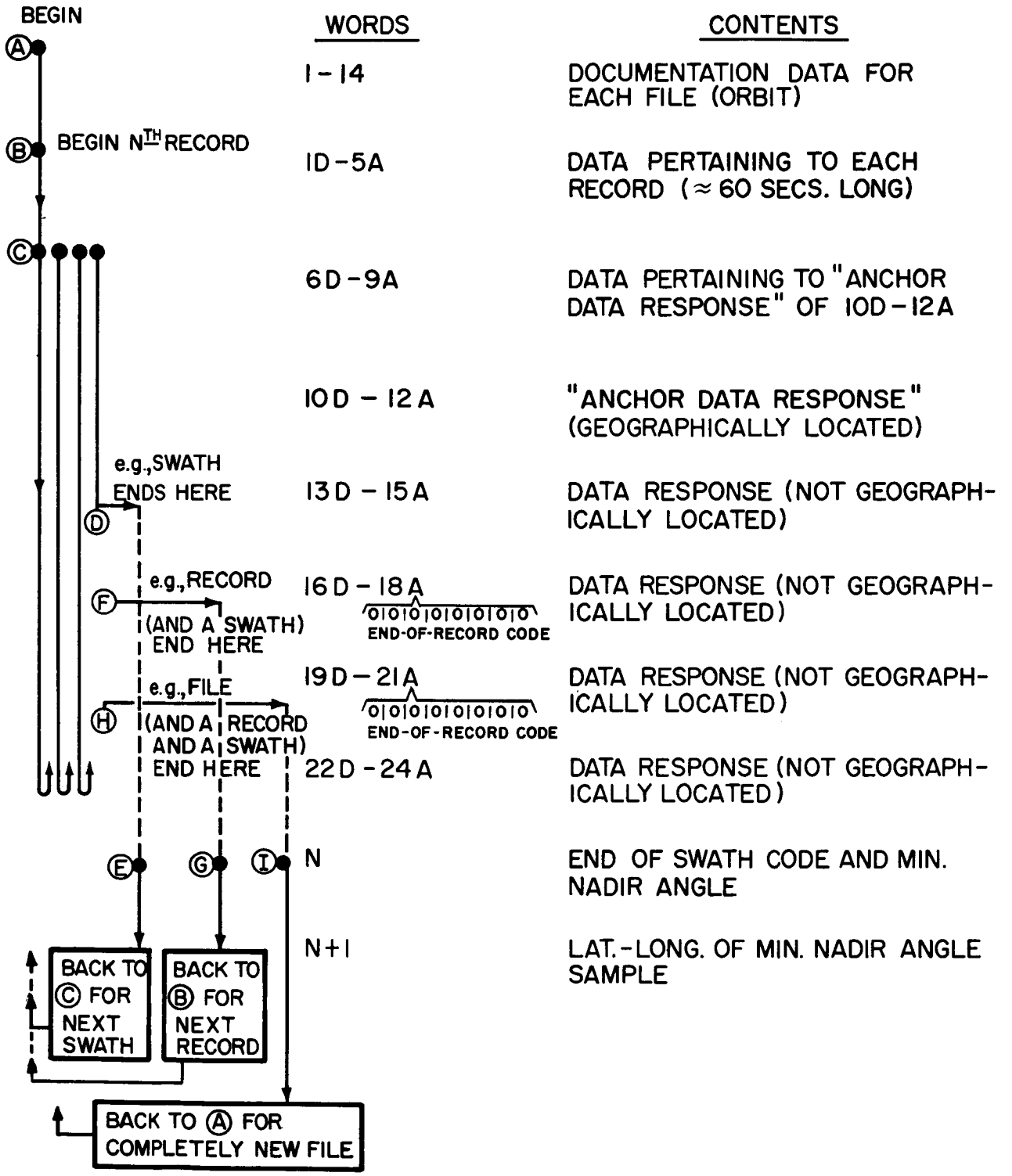

Figure 40—Diagram for interpretation of FMT Tape format.

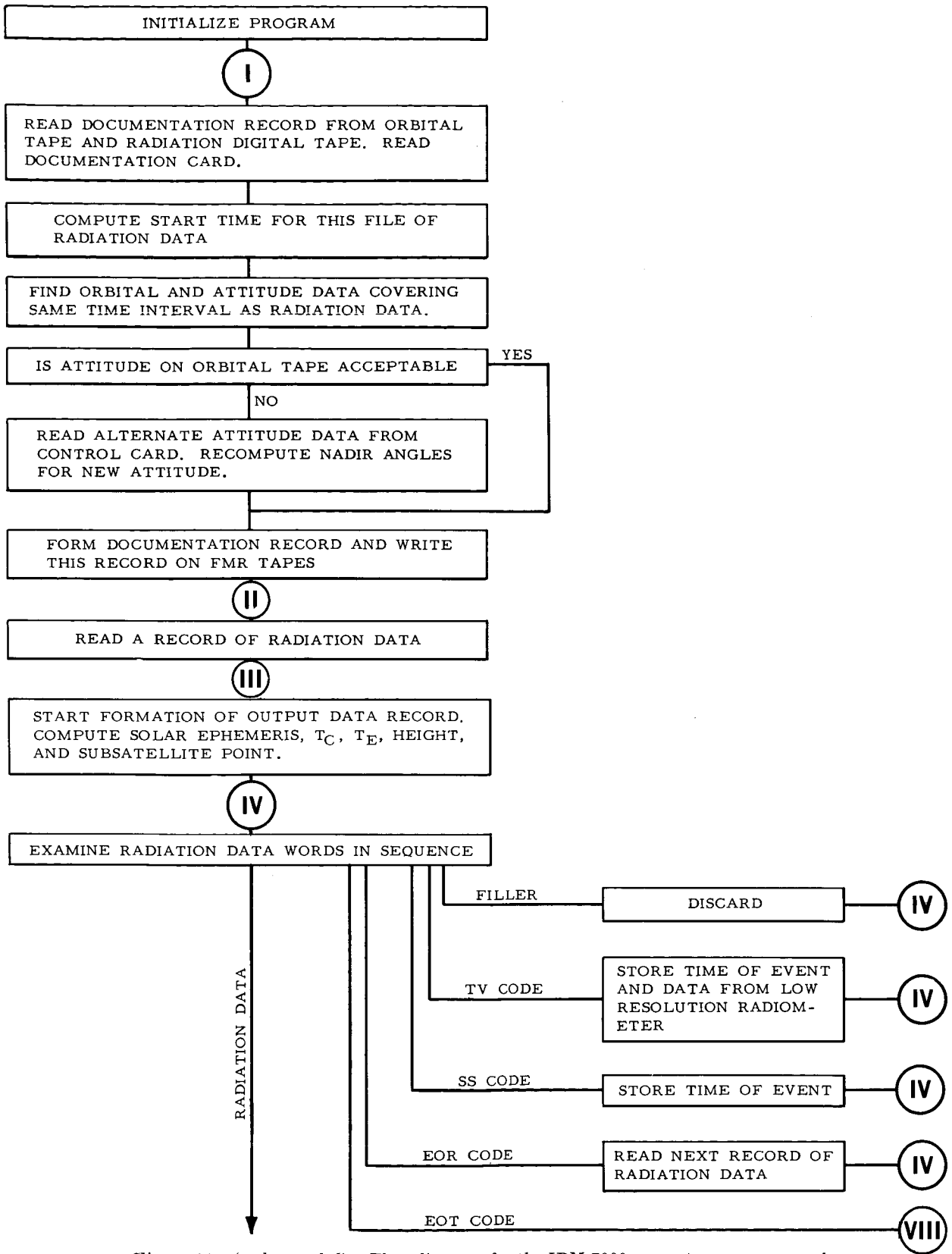

Figure 41—(*a*, *b*, *c* and *d*)—Flow diagram for the IBM 7090 computer program used in reducing the radiation data.

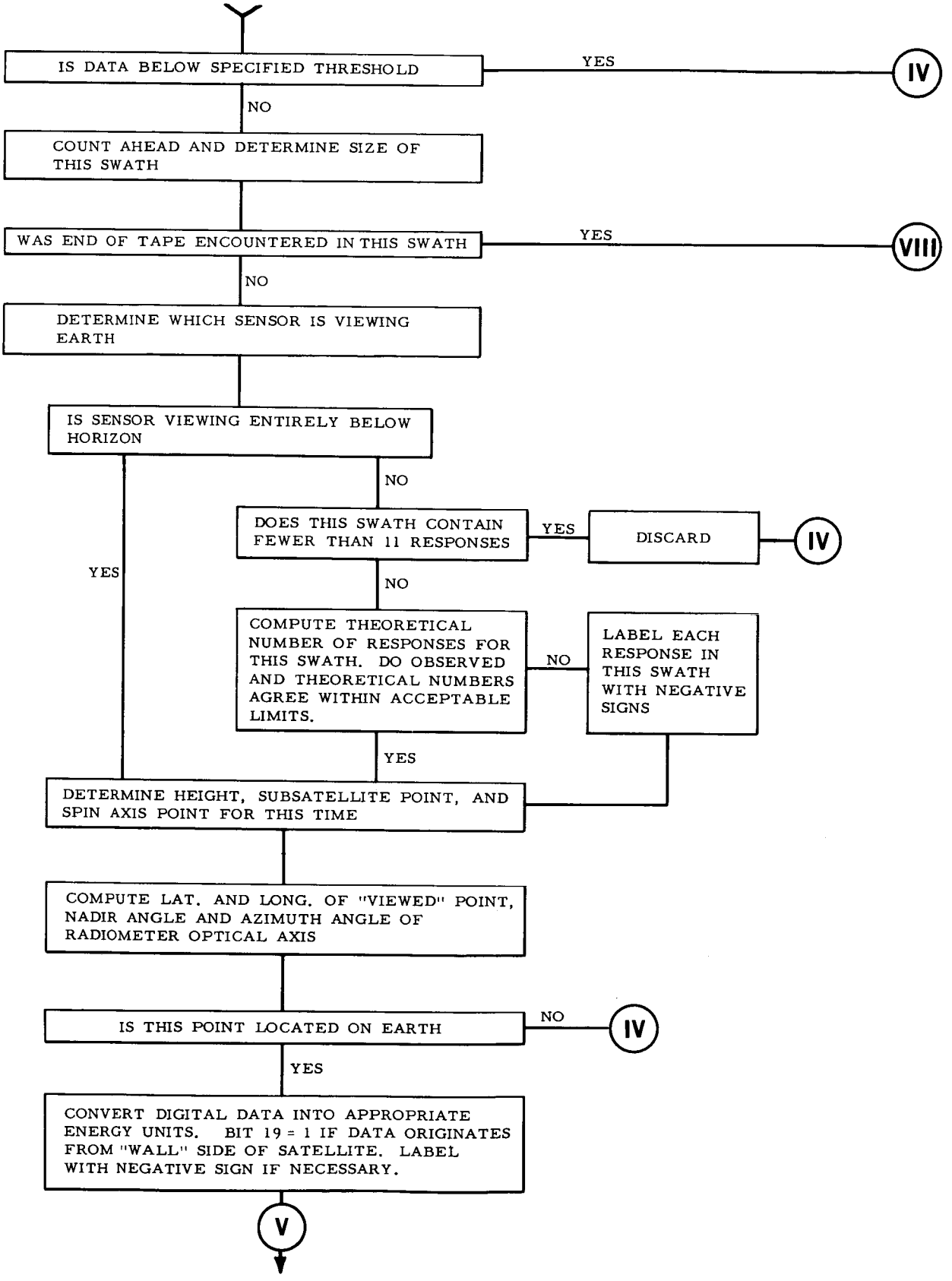
IS DATA BELOW SPECIFIED THRESHOLD
YES
IV
NO
COUNT AHEAD AND DETERMINE SIZE OF THIS SWATH
WAS END OF TAPE ENCOUNTERED IN THIS SWATH
YES
VIII
NO
DETERMINE WHICH SENSOR IS VIEWING EARTH
IS SENSOR VIEWING ENTIRELY BELOW HORIZON
YES
NO
DOES THIS SWATH CONTAIN FEWER THAN 11 RESPONSES
YES
DISCARD
IV
NO
COMPUTE THEORETICAL NUMBER OF RESPONSES FOR THIS SWATH. DO OBSERVED AND THEORETICAL NUMBERS AGREE WITHIN ACCEPTABLE LIMITS.
NO
LABEL EACH RESPONSE IN THIS SWATH WITH NEGATIVE SIGNS
YES
DETERMINE HEIGHT, SUBSATELLITE POINT, AND SPIN AXIS POINT FOR THIS TIME
COMPUTE LAT. AND LONG. OF "VIEWED" POINT, NADIR ANGLE AND AZIMUTH ANGLE OF RADIOMETER OPTICAL AXIS
IS THIS POINT LOCATED ON EARTH
NO
IV
YES
CONVERT DIGITAL DATA INTO APPROPRIATE ENERGY UNITS. BIT 19 = 1 IF DATA ORIGINATES FROM "WALL" SIDE OF SATELLITE. LABEL WITH NEGATIVE SIGN IF NECESSARY.
V

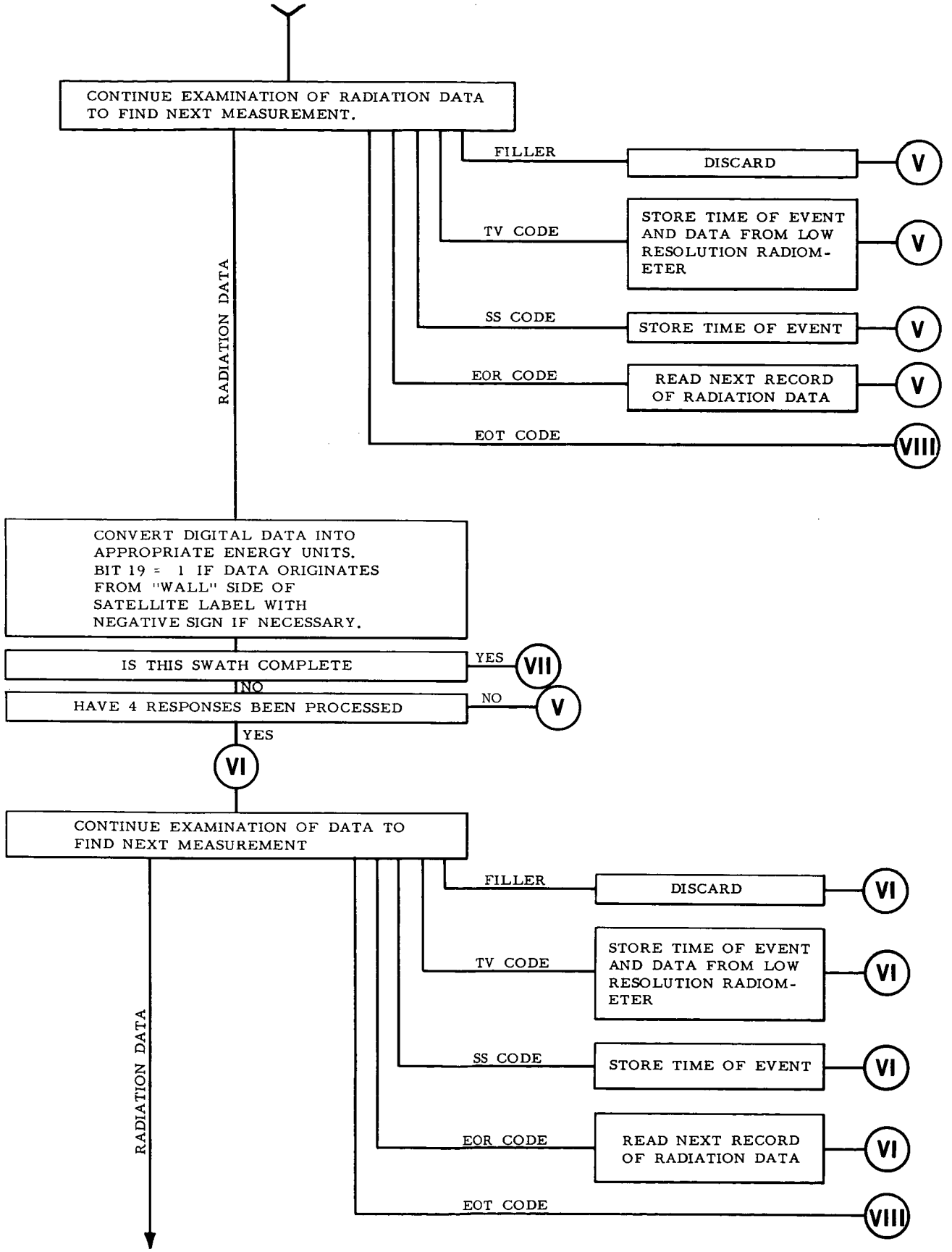
CONTINUE EXAMINATION OF RADIATION DATA TO FIND NEXT MEASUREMENT.
FILLER
DISCARD
V
TV CODE
STORE TIME OF EVENT AND DATA FROM LOW RESOLUTION RADIOM-ETER
V
SS CODE
STORE TIME OF EVENT
V
EOR CODE
READ NEXT RECORD OF RADIATION DATA
V
EOT CODE
VIII
RADIATION DATA
CONVERT DIGITAL DATA INTO APPROPRIATE ENERGY UNITS. BIT 19 = 1 IF DATA ORIGINATES FROM "WALL" SIDE OF SATELLITE LABEL WITH NEGATIVE SIGN IF NECESSARY.
IS THIS SWATH COMPLETE
YES
VII
NO
HAVE 4 RESPONSES BEEN PROCESSED
NO
V
YES
VI
CONTINUE EXAMINATION OF DATA TO FIND NEXT MEASUREMENT
FILLER
DISCARD
VI
TV CODE
STORE TIME OF EVENT AND DATA FROM LOW RESOLUTION RADIOM-ETER
VI
SS CODE
STORE TIME OF EVENT
VI
EOR CODE
READ NEXT RECORD OF RADIATION DATA
VI
EOT CODE
VIII
RADIATION DATA

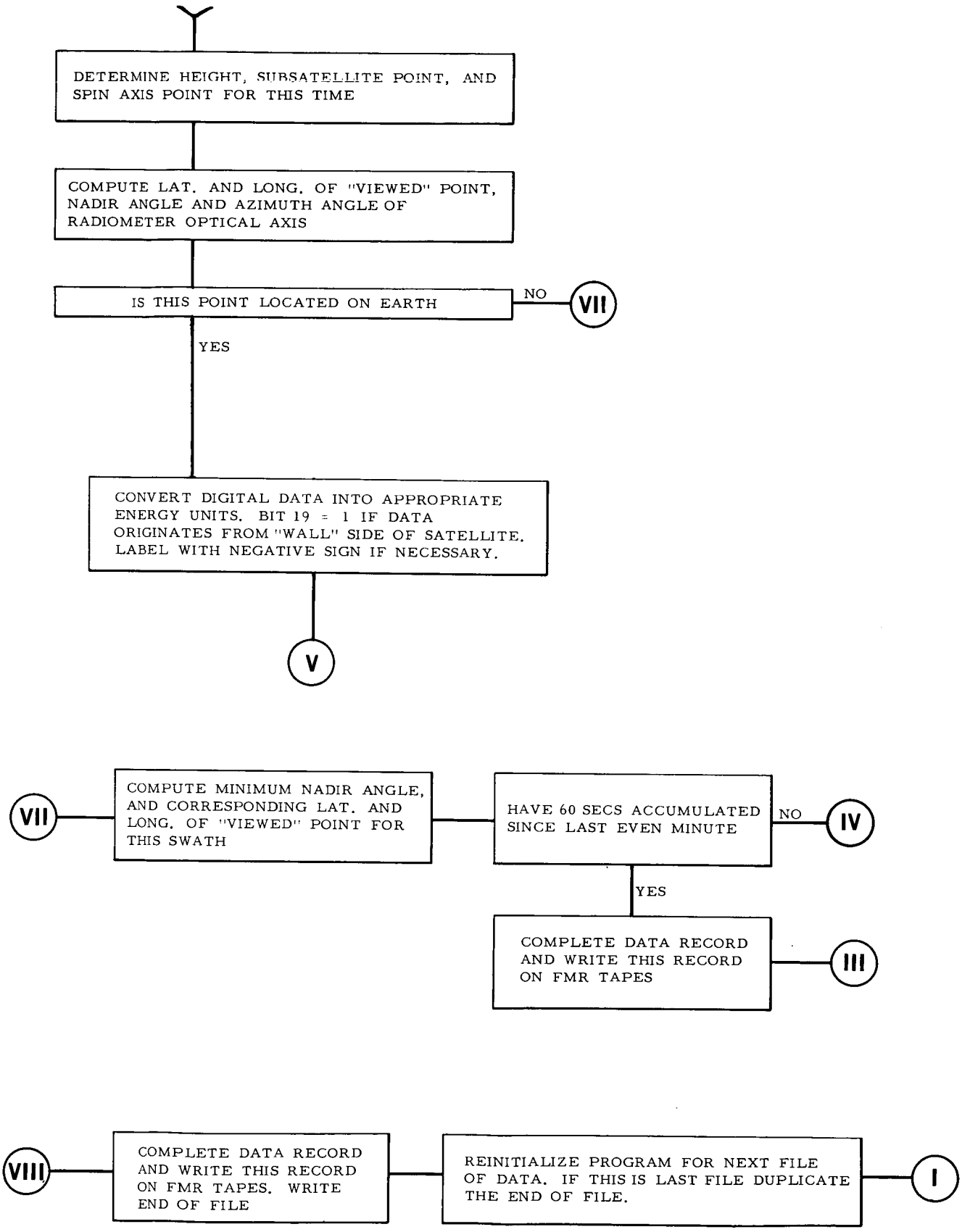
DETERMINE HEIGHT, SUBSATELLITE POINT, AND SPIN AXIS POINT FOR THIS TIME
COMPUTE LAT. AND LONG. OF "VIEWED" POINT, NADIR ANGLE AND AZIMUTH ANGLE OF RADIOMETER OPTICAL AXIS
IS THIS POINT LOCATED ON EARTH
NO
VII
YES
CONVERT DIGITAL DATA INTO APPROPRIATE ENERGY UNITS. BIT 19 = 1 IF DATA ORIGINATES FROM "WALL" SIDE OF SATELLITE. LABEL WITH NEGATIVE SIGN IF NECESSARY.
V
VII
COMPUTE MINIMUM NADIR ANGLE, AND CORRESPONDING LAT. AND LONG. OF "VIEWED" POINT FOR THIS SWATH
HAVE 60 SECS ACCUMULATED SINCE LAST EVEN MINUTE
NO
IV
YES
COMPLETE DATA RECORD AND WRITE THIS RECORD ON FMR TAPES
III
VIII
COMPLETE DATA RECORD AND WRITE THIS RECORD ON FMR TAPES. WRITE END OF FILE
REINITIALIZE PROGRAM FOR NEXT FILE OF DATA. IF THIS IS LAST FILE DUPLICATE THE END OF FILE.
I

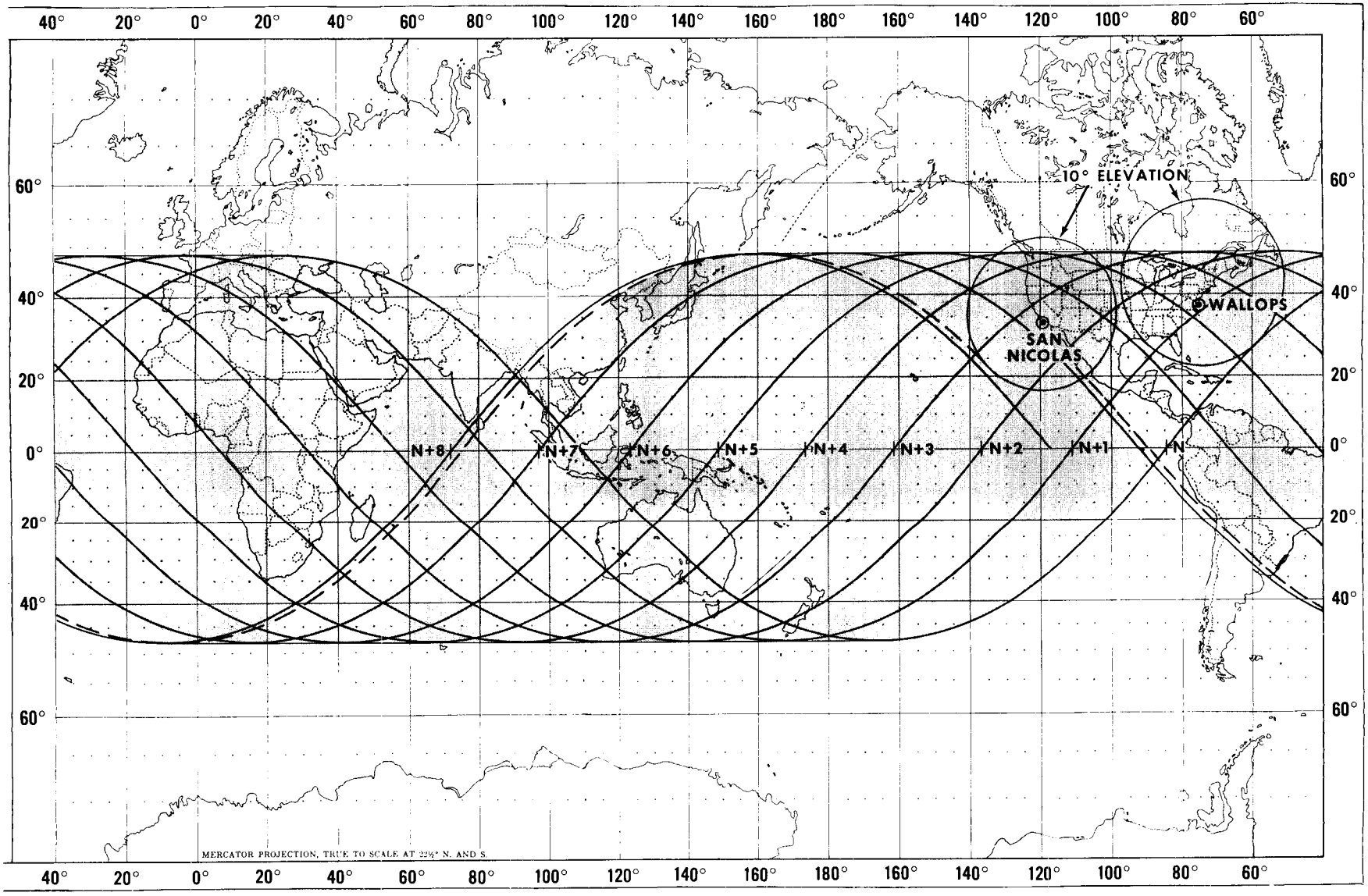

Figure 42—Nominal world-wide radiation data coverage. The shaded area shows the geographical areas from which nearly all radiation data are acquired. The data acquisition circles for a 10° antenna elevation angle at the CDA stations are also shown.

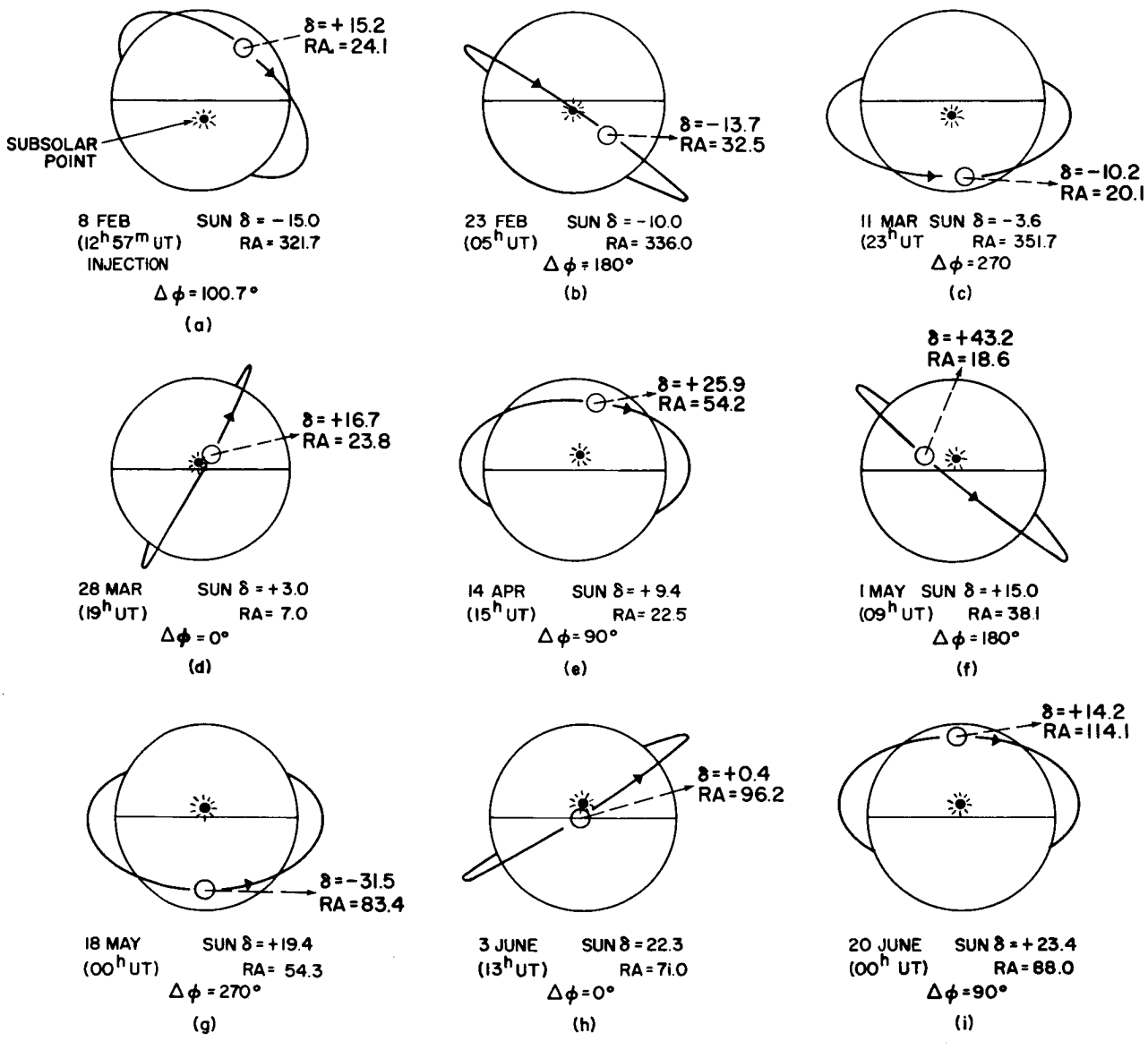

Figure 43—(*a*, *b*, *c*, *d*, *e*, *f*, *g*, *h* and *i*)—Cosmic view of the earth and the precessing TIROS IV orbital plane. The celestial coordinates of the sun and the satellite spin vector are shown for each selected day. The time is given to the nearest hour GMT and corresponds to the given value of $\Delta\phi$.

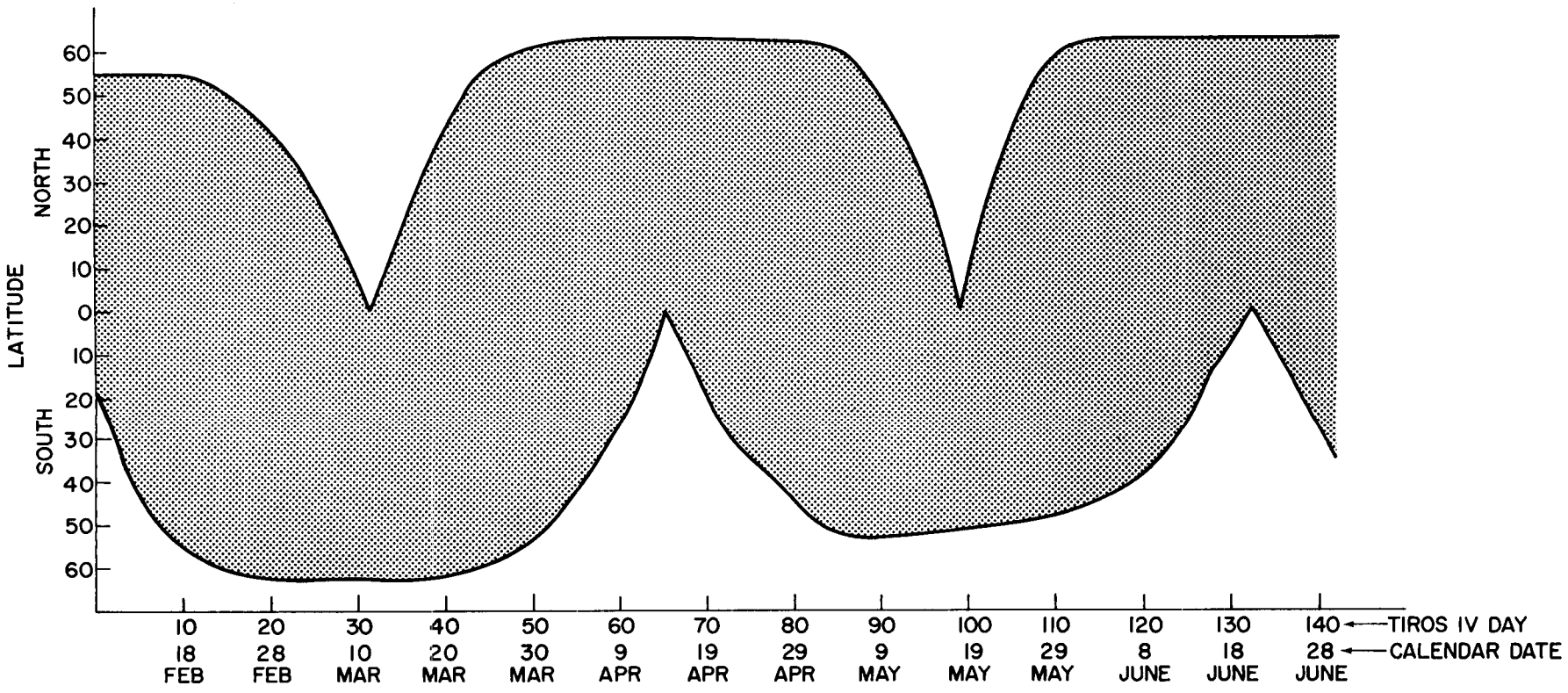

Figure 44—Solar illuminated latitudes for TIROS IV.

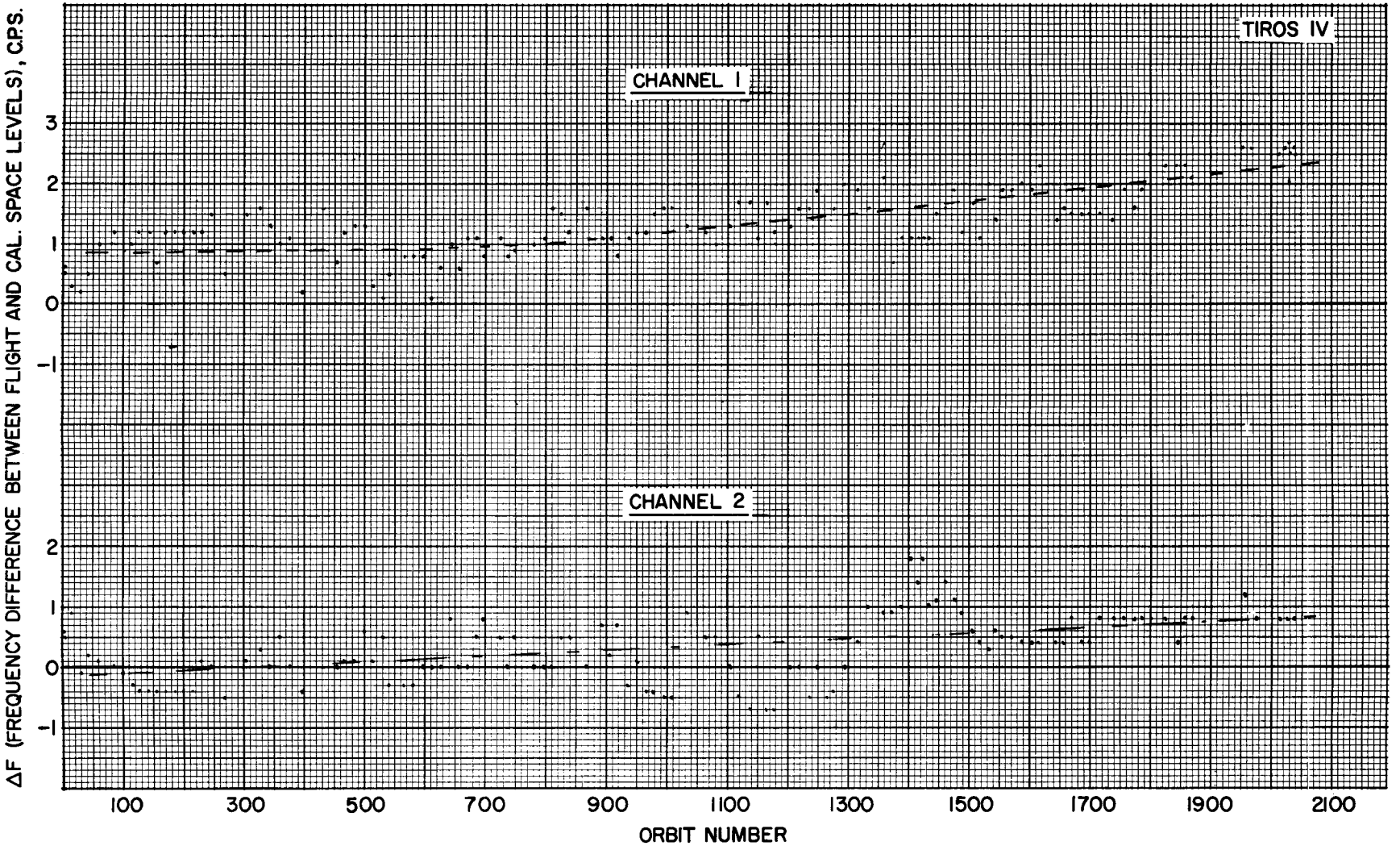

Figure 45—Frequency difference between flight and calibrated space level vs. orbit number for Channel 1 and Channel 2.

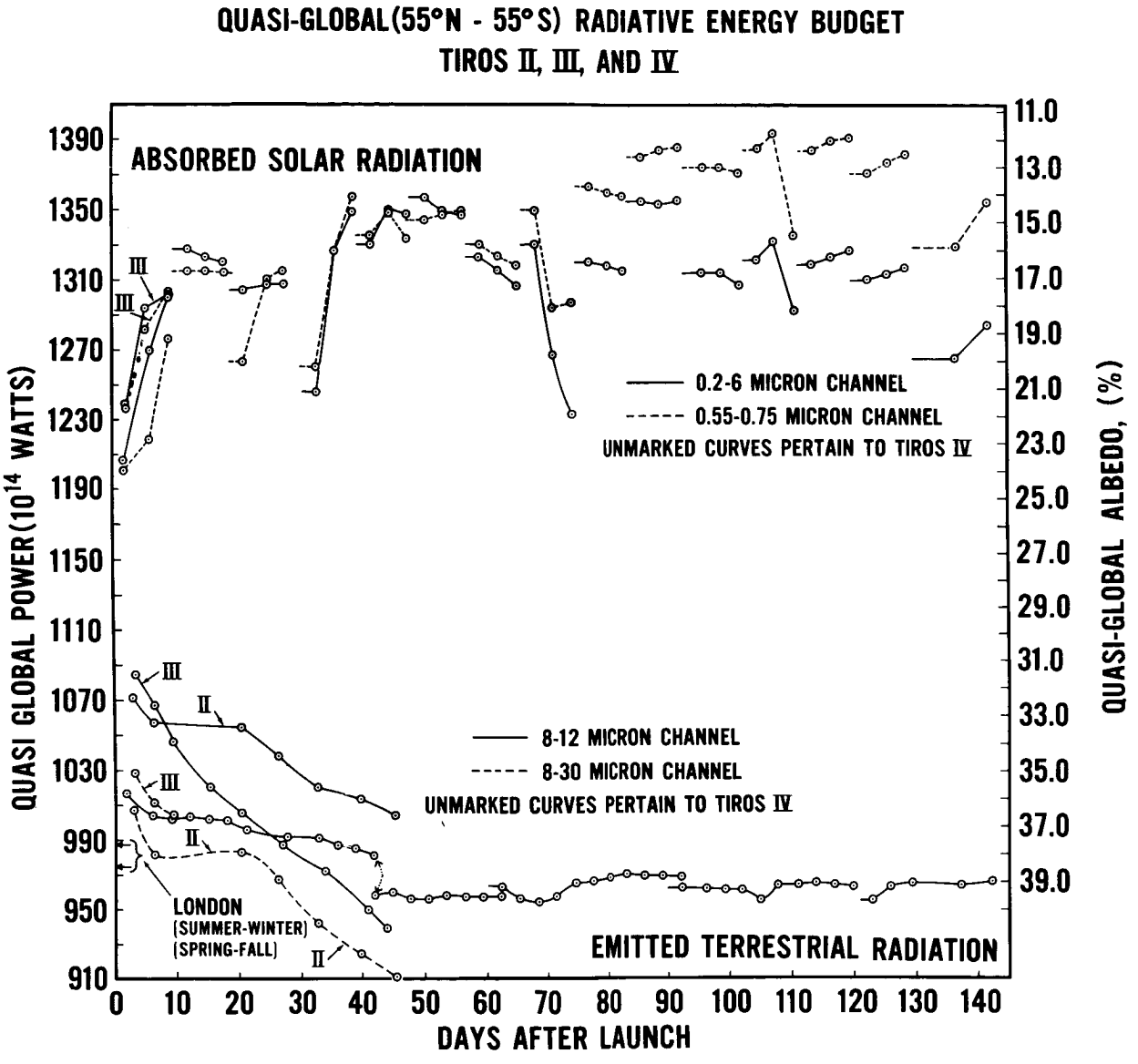

Figure 46—Quasi-global (55°N-55°S) radiative energy budget, TIROS II, III and IV. Quasi-global emitted radiant power along the left ordinate and quasi-global albedo along the right ordinate are plotted as a function of days after launch. Absorbed solar energy [Insolation over the quasi-globe x (1-albedo)] coincides with the left ordinate. The large difference between absorbed solar radiation and emitted terrestrial radiation indicates a degradation of the instrumental calibration.

729-166 O - 64 - 6

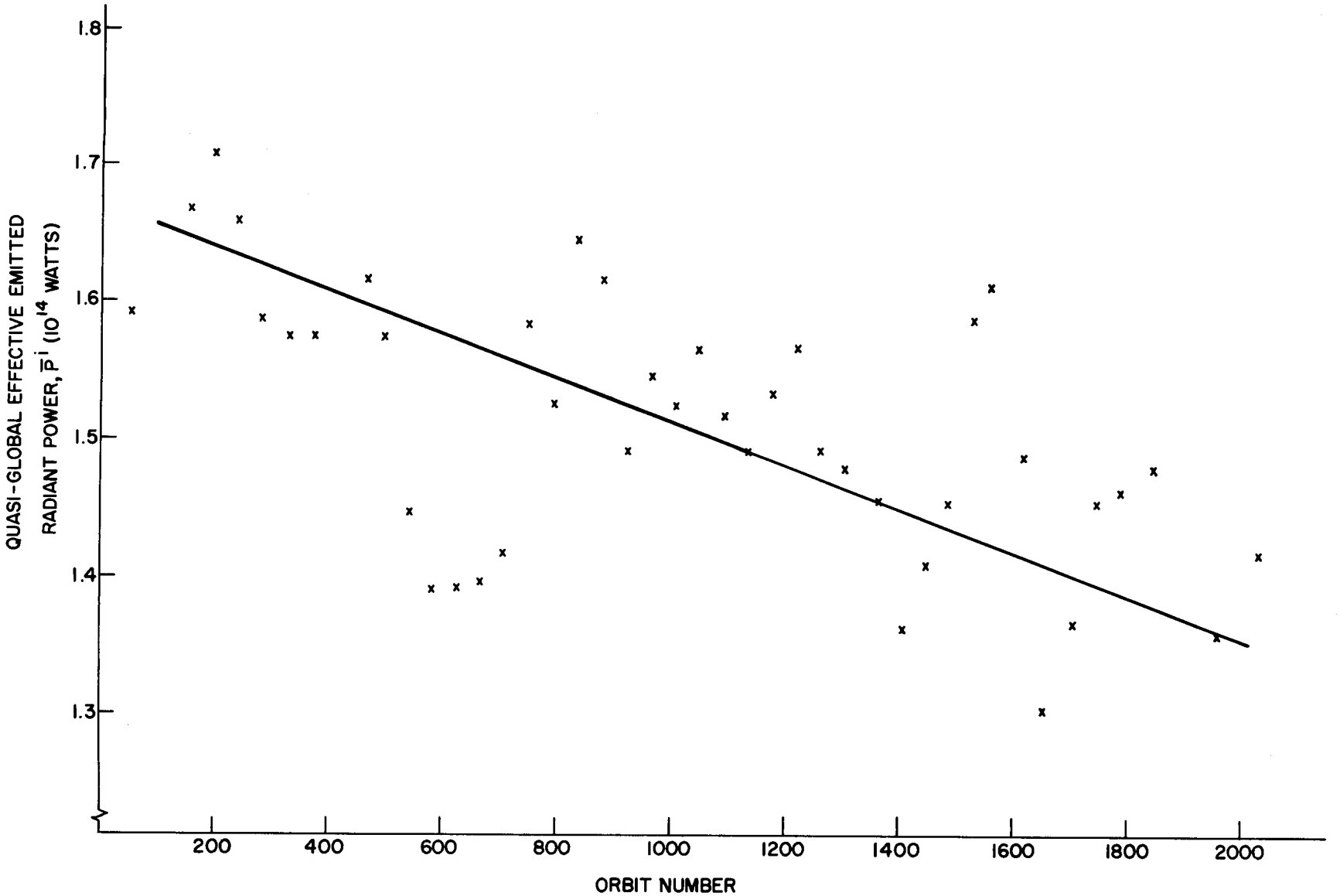

Figure 47—The quasi-global effective emitted radiant power determined from Channel 1 is shown as a function of orbit number.

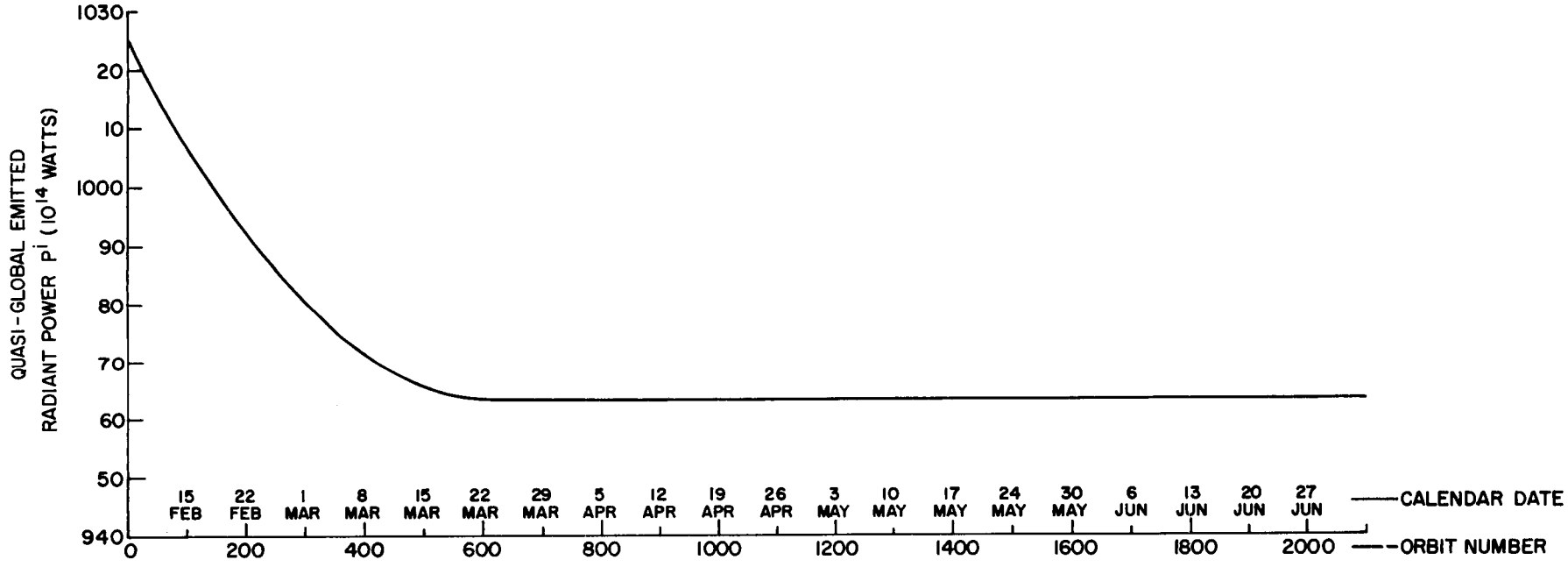

Figure 48—The quasi-global emitted radiant power determined from Channel 2 as a function of orbit number.

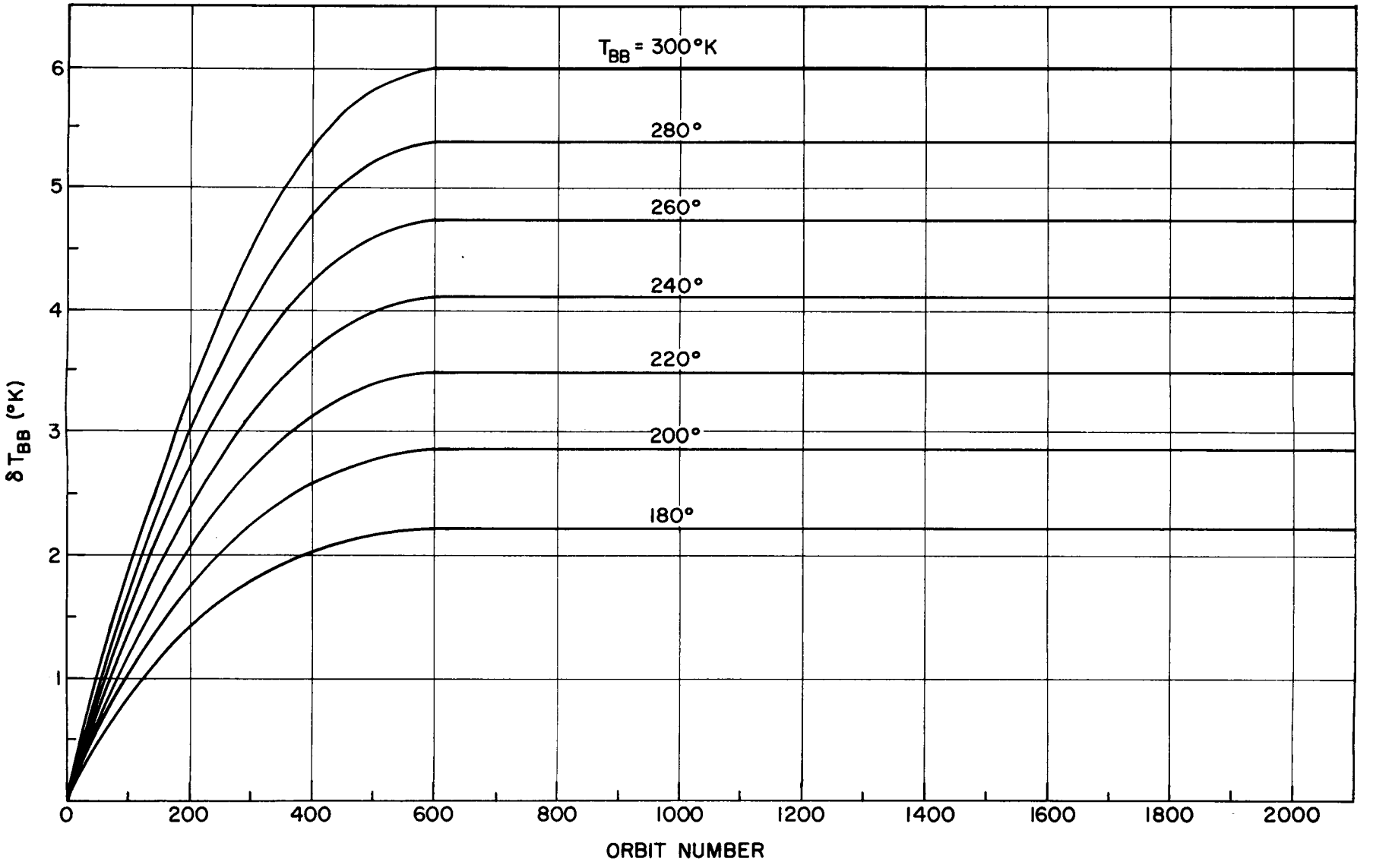

Figure 49—Corrections (δT_{BB}) to be added to Channel 2 wall or floor measurements of T_{BB} as a function of orbit number.

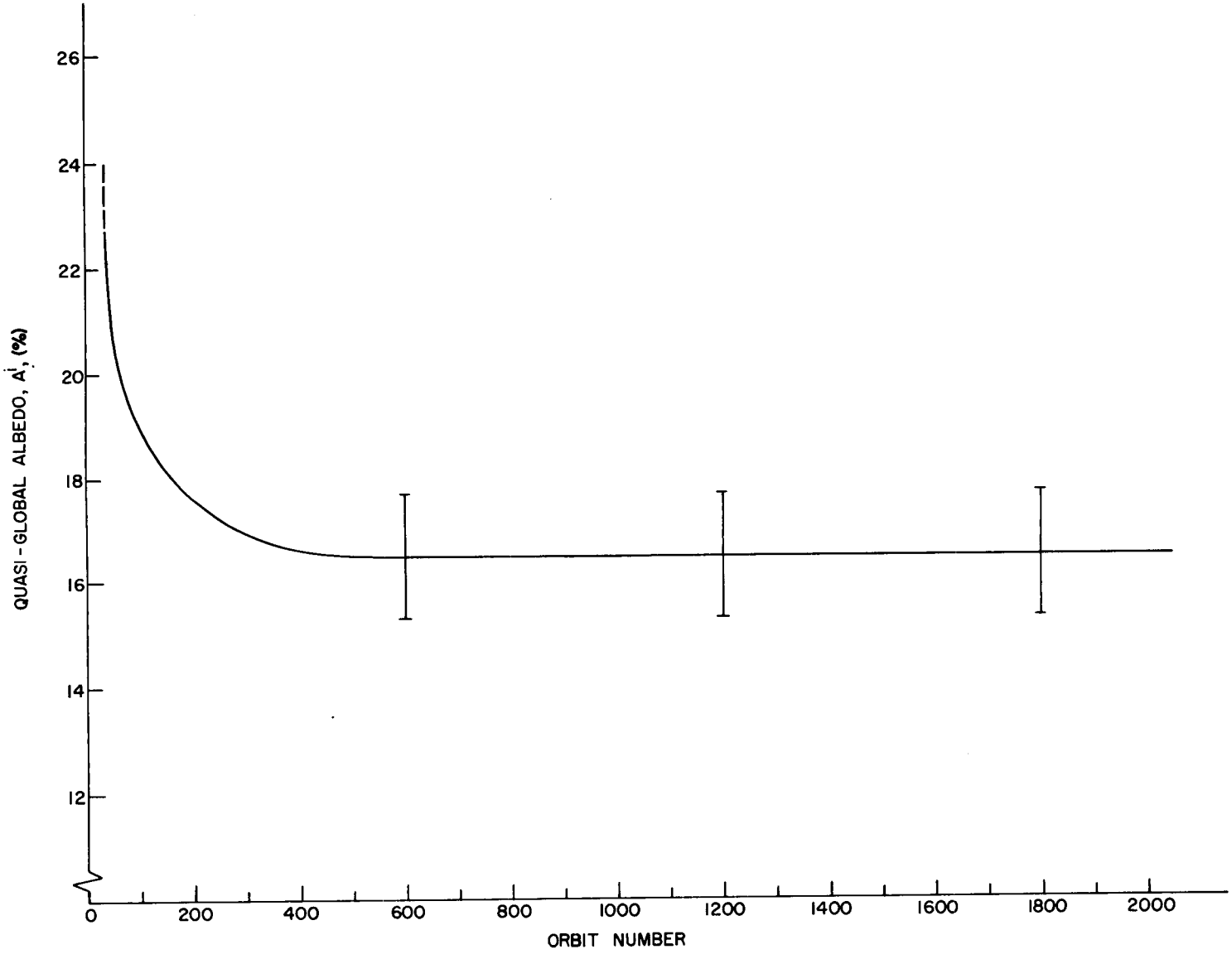

Figure 50—The quasi-global albedo of Channel 3, as a function of orbit number. Error bars indicate approximately one standard deviation.

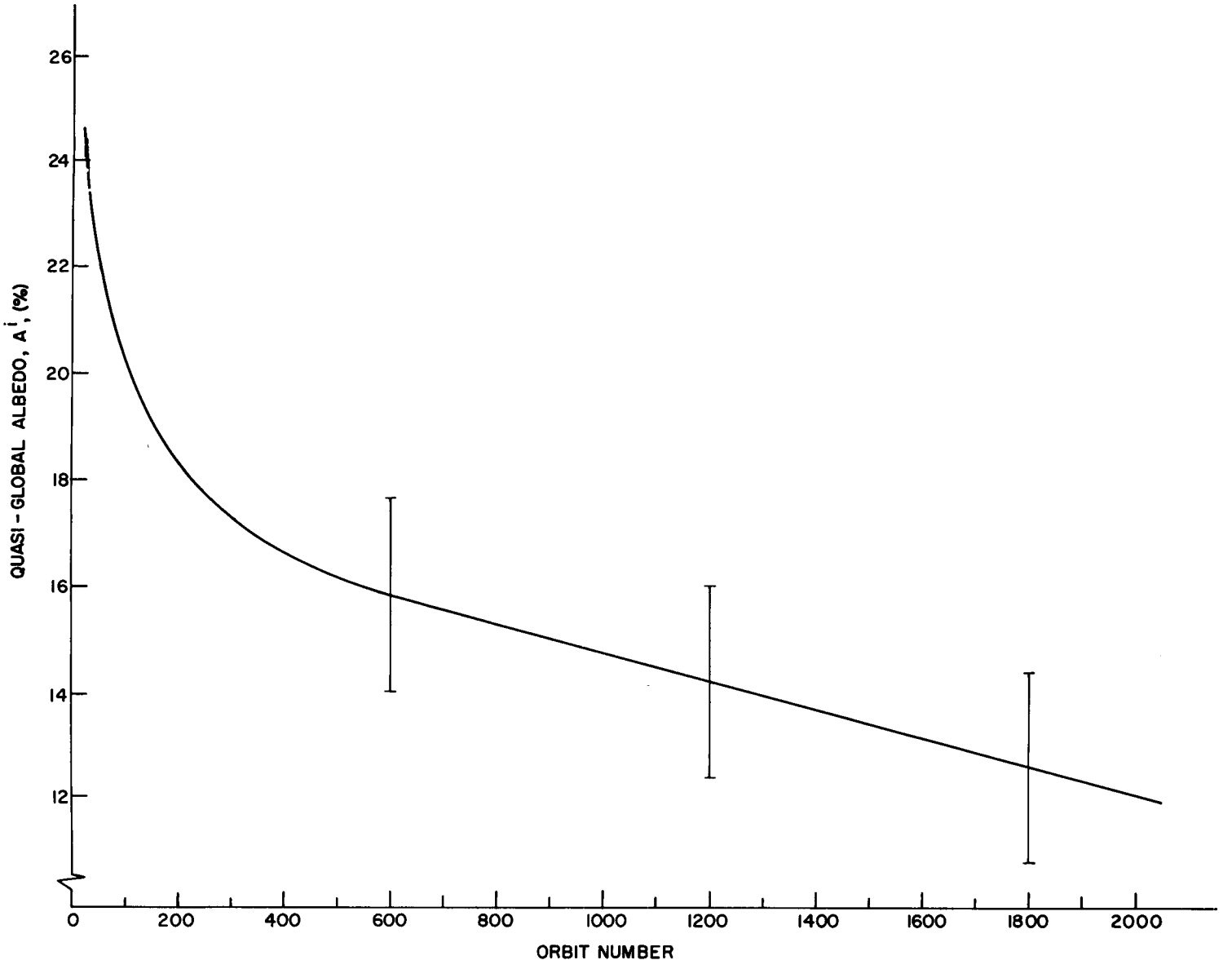

Figure 51—The quasi-global albedo of Channel 5, as a function of orbit number. Error bars indicate approximately one standard deviation.

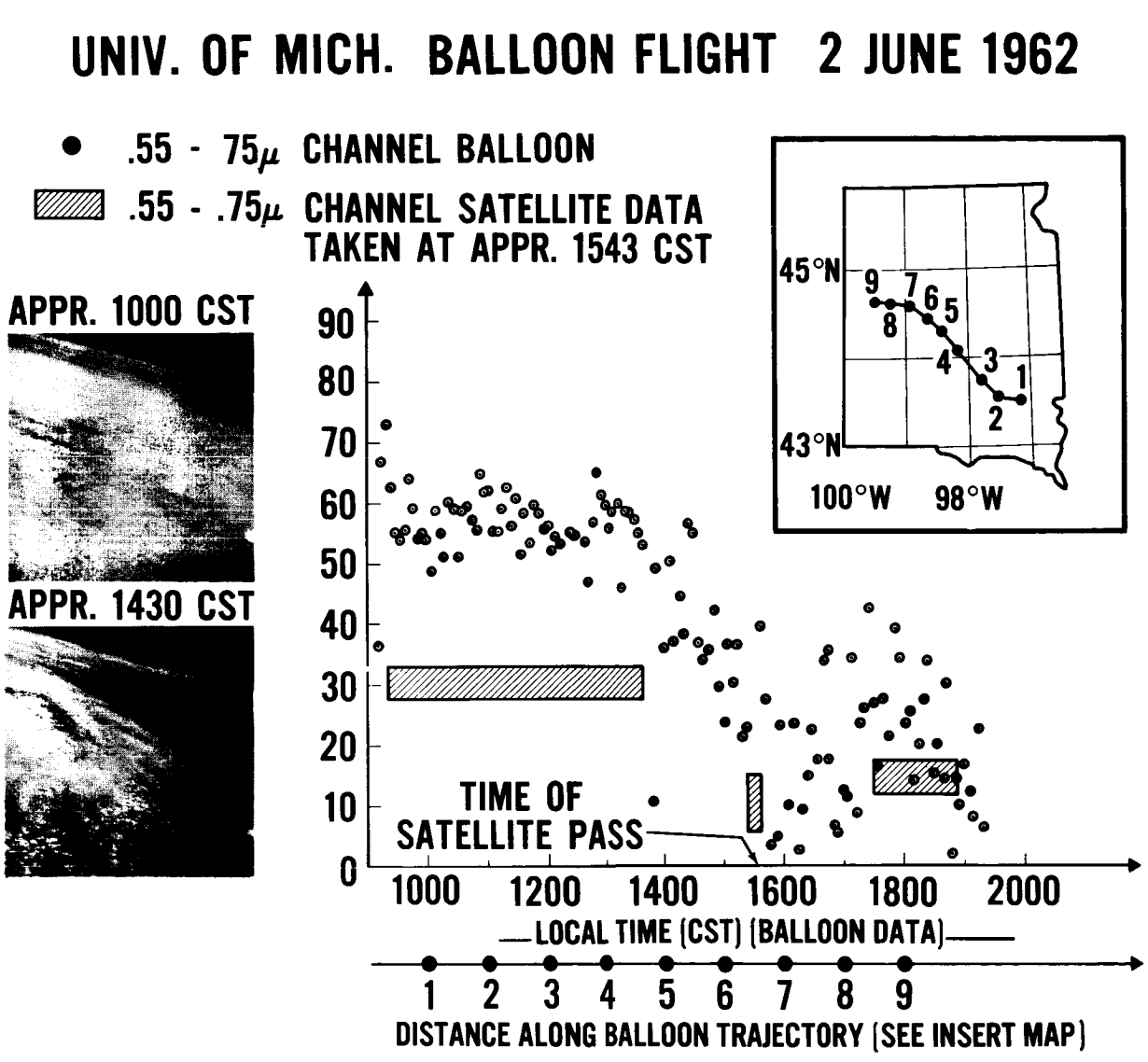

Figure 52—Comparison of results from Channel 5 of the TIROS IV radiometer with those from Channel 5 of a similar balloon-borne instrument indicating degradation of the response of the TIROS sensor by a factor of about 2.15. Percent reflectance along the ordinate is plotted as a function of local time for the balloon data. The sub-balloon points over South Dakota as a function of time are shown by the second abscissa in conjunction with the insert map. The upper photographic insert taken by a camera on the balloon shows an overcast stratus deck with some overlying cirrus prevailing at the beginning of the flight. The lower insert shows broken cells of stratocumulus with thin cirrus later in the flight. The marked decrease in measured reflectances at this time is indicated on the graph.

APPENDIX A

INDEX OF FINAL METEOROLOGICAL RADIATION TAPES

All of the 132 FMR tapes, containing data from 732 individual orbits of TIROS IV, are tabulated on the following pages. The FMR tapes for TIROS IV are numbered from 201 through 332. TIROS II and TIROS III radiation data are contained on the first 200 numbered tapes.

The Index is designed to be used in conjunction with the Mercator Projection World Maps in Appendix B and the master subpoint track overlay in the pocket at the rear of the volume. The subpoint track is subdivided into one minute time intervals referred to ascending node time, with the "minus" and "plus" indicators corresponding to "before" and "after" ascending node time respectively.

The Index is divided into two basic sections. One section contains information concerning the attitude of the satellite and the location of the subpoint track as a function of time for each orbit listed on the FMR tape. The second section of the Index contains information which gives the time for which radiation data are available on the FMR tape for each orbit listed. The nomenclature used in the Index is defined below.

INDEX NOMENCLATURE

Heading	Explanation
Orbit No.	The orbit number from launch to the first ascending node is designated zero, thereafter the number increases by one at each ascending node.
CDA Sta.	Control and Data Acquisition Station. "W" is the Wallops Island, Virginia station and "N" is the San Nicholas Island, California station.
Satellite Equator Crossing at Orbital Ascending Node (ANO)	
Earth longitude	The longitude on earth at which the satellite crossed the equatorial plane going from south to north, measured in degrees from 0° to 180° west and 0° to 180° east.
Hours; minutes; seconds; (GMT)	Greenwich Mean Time of the occurrence of ANO in hours, minutes and seconds.
Calendar date	Date on which the ascending node of a given orbit occurred.
TIROS IV Day	The TIROS IV Day advances 1 for each succeeding calendar day after February 8, 1962, the day of launch, which is designated "TIROS IV Day 0."
Spin Vector Attitude	
Decl.	Celestial co-ordinates of declination and right ascension of the satellite spin vector. The tabulated value for each orbit are for the time of ascending node. As these values change only slightly throughout one orbit, the value at the time of ANO is adequate, for most purposes, throughout the entire orbit.
R. A.	
η_o	Satellite attitude in a system which has the orbital co-ordinates chosen as a reference system. η_o is the minimum satellite nadir angle during an orbital period and t_o is the time of occurrence of η_o. Positive or negative values of η_o indicate that the camera axis is pointed north or south of the subpoint track, respectively, while t_o is given in minutes after ANO.
t_o	

Heading	Explanation
Spin rate	Rate of rotation of satellite about its spin axis.
Time Interval of File on FMR Tape	
Begin	The beginning time of the radiation data available on an FMR tape in minutes with respect to the time of the occurrence of the ANO. Negative values indicate that the data were acquired before the ANO was reached.
End	The end time of the radiation data available on the FMR tape. This value is given in absolute time (GMT) and in minutes with respect to the ANO. Positive values indicate that the data were acquired after the ANO.
Drop-Outs	The time of the dropout (where no radiation data are available due to system noise, etc.) is listed in minutes with respect to the ANO, either minus or plus.
FMR Tape Reel No.	Number of the magnetic tape reel on which an orbit is located.

To illustrate the use of the tabulated material, the entry in the row for orbit No. 286 indicates that when TIROS IV passed within range of the Wallops Island, Virginia, Command and Data Acquisition Station (abbreviated W) radiation data were telemetered from the satellite. The ascending node (ANO) of orbit 286 was earth longitude 174.4°E when TIROS IV crossed the equatorial plane going from south to north at 10:42:28 GMT on February 28, 1962 which, being the twentieth day after launch, is "TIROS IV Day 20." The declination and right ascension of the spin vector were, respectively, 23.0 degrees south of the celestrial equator and 39.3 degrees east of the Vernal Equinox. The minimum satellite nadir angle of the orbit was 25.1 degrees and occurred 74.2 minutes after the ANO (or 11:56:40 GMT). The negative value of η_0 indicates that the intersection of the spin (camera) axis with the earth (the terrestrial principal point) lay south of the subpoint track. The spin rate of the satellite was 70.117 degrees per second. The Index also shows that the FMR tape data began 62.7 minutes before the ascending node (09:39:46) and ended 30.6 minutes after the ascending node, or 11:13:03 GMT. Further it is seen that a dropout occurs on the tape between —7.5 and —6.5 minutes with respect to the orbital ascending node (i.e., 10:34:58 GMT to 10:35:58 GMT). Finally, it is seen that these data are recorded on FMR Tape Reel No. 220.

The spin vector celestial coordinates and the satellite spin rate are also presented in graphical form in Figures A1 and A2. Both figures are based on the data presented in the Index.

READOUT ORBIT											TIME INTERVAL OF FILE ON FMR TAPE					
Orbit No.	CDA Sta.	Satellite Equator Crossing at Orbital Ascending Node (ANO)				Spin Vector Attitude				Spin Rate (deg./sec.)	Begin	End		Dropouts, Minutes w/r/t ANO		FMR Tape Reel No.
		Earth Longitude (degrees)	Hours; Minutes; Seconds (GMT)	Calendar Date	Julian Date	Decl. (deg.)	R.A. (deg.)	η_o (deg.)	t_o (min. after ANO)		Minutes w/r/t ANO	Hours; Minutes; Seconds (GMT)	Minutes w/r/t ANO	From –	To –	
0001	N	132.0 W	14:18:03	2-8-62	0	15.1	24.2	1.8	43.4	50.784	–64.4	14:25:03	7.0			201
0001	W	132.0 W	14:18:03	2-8-62	0	15.1	24.2	1.8	43.4	50.784	–64.4	14:25:03	7.0			201
0002	W	157.4 W	15:58:20	2-8-62	0	15.0	24.2	1.7	43.5	50.779	–69.6	16:21:03	22.7			201
0003	W	177.1 E	17:38:38	2-8-62	0	14.8	24.2	1.6	43.6	50.769	–62.8	18:07:03	28.4			201
0004	W	151.7 E	19:18:56	2-8-62	0	14.7	24.2	1.4	43.8	50.759	–24.3	19:52:03	33.1			201
0006	N	100.8 E	22:39:31	2-8-62	0	14.5	24.2	1.2	44.0	50.749	–54.8	23:15:03	35.5			201
0014	W	102.8 W	12:01:53	2-9-62	1	13.3	24.6	0.4	44.6	50.689	–80.8	12:14:57	13.1			202
0015	W	128.3 W	13:42:10	2-9-62	1	13.1	24.6	–0.2	44.8	50.679	–77.7	13:58:03	15.9			202
0016	W	153.7 W	15:22:28	2-9-62	1	13.0	24.6	–0.5	44.9	50.674	–27.6	15:44:03	21.6			202
0017	W	179.2 W	17:02:46	2-9-62	1	12.9	24.6	–0.6	45.0	50.664	–66.5	17:29:03	26.3			202
0021	N	79.0 E	23:43:57	2-9-62	1	12.3	24.7	–1.0	45.3	50.634	–52.0	00:24:03	40.1			202
0028	W	99.1 W	11:26:03	2-10-62	2	11.2	25.0	–2.1	45.9	50.579	–78.9	11:40:27	14.4			203
0029	W	124.6 W	13:06:21	2-10-62	2	11.1	25.0	–2.2	46.1	50.574	–50.6	13:20:56	14.6			203
0030	W	150.0 W	14:46:39	2-10-62	2	10.9	25.0	–2.4	46.1	50.569	–73.3	15:06:03	19.4			203
0031	N	175.5 W	16:26:57	2-10-62	2	10.8	25.0	–2.5	46.3	50.559	–35.2	16:42:03	15.1			203
0035	N	82.7 E	23:08:08	2-10-62	2	10.2	25.1	–3.1	46.6	50.529	–53.5	23:47:03	38.9			203
0042	W	95.4 W	10:50:12	2-11-62	3	9.2	25.4	–4.2	47.3	50.474	–59.5	10:59:03	8.9			204
0043	W	120.9 W	12:30:30	2-11-62	3	9.1	25.4	–4.4	47.5	50.469	–79.5	12:44:27	14.0			204
0045	W	171.8 W	15:51:06	2-11-62	3	8.8	25.4	–4.6	47.6	50.449	–68.5	16:16:27	25.4			204
0046	N	162.8 E	17:31:23	2-11-62	3	8.6	25.4	–4.8	47.6	50.444	–69.4	17:54:27	23.1			204
0049	N	86.4 E	22:32:17	2-11-62	3	8.2	25.5	–5.2	48.0	50.424	–55.3	23:10:03	37.8			204

0056	W	91.8 W	10:14:21	2-12-62	4	7.2	25.9	- 6.4	48.6	50.374	-83.2	10:24:33	10.2			205
0058	W	142.7 W	13:34:57	2-12-62	4	6.9	25.9	- 6.7	48.8	50.359	-75.4	13:53:03	18.1			205
0059	N	168.1 W	15:15:15	2-12-62	4	6.8	25.9	- 6.8	49.0	50.354	- 3.4	15:28:03	12.8			205
0060	N	166.4 E	16:55:32	2-12-62	4	6.6	25.9	- 7.0	49.1	50.344	-72.9	17:16:03	20.5			205
0061	W	141.0 E	18:35:50	2-12-62	4	6.5	25.9	- 7.1	49.1	50.339	-41.8	19:14:03	38.2			205
0062	N	115.5 E	20:16:08	2-12-62	4	6.3	25.9	- 7.3	49.2	50.329	-56.4	20:48:33	32.4			205
0063	N	90.1 E	21:56:26	2-12-62	4	6.2	26.0	- 7.5	49.3	50.324	-55.9	22:33:03	36.6			205
0085	W	109.9 W	10:42:57	2-14-62	6	3.1	26.8	-11.1	51.3	50.174	-72.0	10:56:33	13.6			206
0086	W	135.3 W	12:23:15	2-14-62	6	3.0	26.8	-11.2	51.4	50.169	-73.3	12:42:03	18.8			206
0087	W	160.8 W	14:03:32	2-14-62	6	2.8	26.8	-11.4	51.5	50.159	-70.6	14:27:03	23.5			206
0088	N	173.8 E	15:43:50	2-14-62	6	2.7	26.8	-11.5	51.6	50.154	-70.6	16:02:03	18.2			206
0099	W	106.2 W	10:07:06	2-15-62	7	1.2	27.2	-13.3	52.6	50.079	-79.7	10:20:33	13.5			207
0100	W	131.6 W	11:47:23	2-15-62	7	1.1	27.2	-13.5	52.8	50.069	-75.1	12:05:03	17.7			207
0101	W	157.1 W	13:27:41	2-15-62	7	1.0	27.2	-13.6	52.9	50.064	-69.1	13:52:03	24.4			207
0102	N	177.5 E	15:07:59	2-15-62	7	0.9	27.2	-13.7	53.0	50.059	-70.4	15:25:03	17.1			207
0103	N	152.0 E	16:48:17	2-15-62	7	0.7	27.2	-13.9	53.1	50.054	-66.4	17:14:33	26.3			207
0103	W	152.0 E	16:48:17	2-15-62	7	0.7	27.2	-13.9	53.1	50.054	-66.4	17:14:33	26.3			207
0104	N	126.6 E	18:28:34	2-15-62	7	0.6	27.2	-14.0	53.2	50.044	-59.9	18:59:33	31.0			207
0113	W	102.5 W	09:31:16	2-16-62	8	-0.6	27.6	-15.5	54.0	49.984	-78.4	09:44:33	13.3			208
0114	W	128.0 W	11:11:34	2-16-62	8	-0.7	27.6	-15.7	54.1	49.979	-76.5	11:28:03	16.5			208
0115	W	153.4 W	12:51:51	2-16-62	8	-0.8	27.6	-15.8	54.2	49.969	-70.0	13:15:03	23.2			208
0116	W	178.9 W	14:32:09	2-16-62	8	-1.0	27.6	-15.9	54.3	49.964	-65.1	15:00:03	28.9			208
0117	N	155.7 E	16:12:27	2-16-62	8	-1.1	27.6	-16.1	54.4	49.959	-66.5	16:37:03	25.6			208
0118	N	130.2 E	17:52:45	2-16-62	8	-1.2	27.6	-16.2	54.5	49.949	-62.3	18:22:33	29.8			208
0127	W	98.8 W	08:55:25	2-17-62	9	-2.3	28.0	-17.6	55.3	49.894	-82.1	09:06:57	11.5			209
0128	W	124.3 W	10:35:42	2-17-62	9	-2.4	28.0	-17.8	55.4	49.889	-39.0	10:49:03	13.4			209
0129	W	149.7 W	12:16:00	2-17-62	9	-2.6	28.0	-17.9	55.5	49.879	-73.0	12:36:03	20.1			209

READOUT ORBIT											TIME INTERVAL OF FILE ON FMR TAPE					FMR Tape Reel No.
Orbit No.	CDA Sta.	Satellite Equator Crossing at Orbital Ascending Node (ANO)				Spin Vector Attitude				Spin Rate (deg./sec.)	Begin	End		Dropouts, Minutes w/r/t ANO		
		Earth Longitude (degrees)	Hours; Minutes; Seconds (GMT)	Calendar Date	Julian Date	Decl. (deg.)	R.A. (deg.)	η_o (deg.)	t_o (min. after ANO)		Minutes w/r/t ANO	Hours; Minutes; Seconds (GMT)	Minutes w/r/t ANO	From –	To –	
0130	W	175.2 W	13:56:18	2-17-62	9	–2.7	28.0	–18.1	55.7	49.874	–67.1	14:22:03	25.8			209
0132	W	133.9 E	17:16:54	2-17-62	9	–2.9	28.0	–18.3	55.9	49.869	–57.2	17:53:03	36.2			209
0141	W	95.2 W	08:19:34	2-18-62	10	–4.0	28.3	–19.7	56.6	49.804	–52.6	08:30:33	11.0			210
0142	W	120.6 W	09:59:51	2-18-62	10	–4.1	28.3	–19.8	56.7	49.799	–41.9	10:14:03	14.2			210
0143	W	146.1 W	11:40:09	2-18-62	10	–4.2	28.3	–20.0	56.8	49.794	–72.3	12:01:03	21.9			210
0144	W	171.5 W	13:20:27	2-18-62	10	–4.3	28.3	–20.1	57.0	49.789	–67.2	13:46:03	25.6			210
0145	W	163.0 E	15:00:45	2-18-62	10	–4.4	28.3	–20.2	57.1	49.784	–61.5	15:32:33	31.8			210
0146	W	137.6 E	16:41:02	2-18-62	10	–4.5	28.3	–20.4	57.2	49.774	–56.3	17:17:03	36.0			210
0155	W	91.5 W	07:43:42	2-19-62	11	–5.4	28.7	–21.7	58.0	49.719	–39.6	07:52:33	8.9			211
0156	W	116.9 W	09:24:00	2-19-62	11	–5.5	28.7	–21.9	58.1	49.714	–67.3	09:39:03	15.1			211
0157	W	142.4 W	11:04:18	2-19-62	11	–5.6	28.7	–22.0	58.2	49.709	–72.7	11:24:03	19.8			211
0158	W	167.8 W	12:44:36	2-19-62	11	–5.7	28.7	–22.2	58.3	49.704	–66.9	13:10:03	25.5			211
0159	W	166.7 E	14:24:53	2-19-62	11	–5.7	28.7	–22.3	58.4	49.699	–61.0	14:56:03	31.2			211
0160	W	141.3 E	16:05:11	2-19-62	11	–5.8	28.7	–22.4	58.6	49.689	–57.0	16:41:03	35.9			211
0170	W	113.3 W	08:48:09	2-20-62	12	–6.7	29.0	–23.9	59.4	49.629	–23.1	09:01:33	13.4			212
0171	W	138.7 W	10:28:27	2-20-62	12	–6.8	29.0	–24.1	59.5	49.619	–74.4	10:47:03	18.6			212
0172	W	164.2 W	12:08:45	2-20-62	12	–6.8	29.0	–24.2	59.6	49.614	–69.2	12:33:03	24.3			212
0173	W	170.4 E	13:49:02	2-20-62	12	–6.9	29.0	–24.3	59.7	49.609	–63.6	14:19:03	30.0			212
0174	W	144.9 E	15:29:20	2-20-62	12	–7.0	29.0	–24.4	59.8	49.604	–57.7	16:05:03	35.7			212
0184	W	109.6 W	08:12:18	2-21-62	13	–7.8	29.4	–25.8	60.7	49.549	–80.7	08:24:33	12.3			213
0185	W	135.0 W	09:52:36	2-21-62	13	–7.9	29.4	–26.0	60.8	49.544	–86.2	10:10:03	17.5			213

0186	W	160.5 W	11:32:53	2-21-62	13	– 7.9	29.4	–26.1	60.9	49.539	–69.5	11:57:03	24.2			213
0187	W	174.1 E	13:13:11	2-21-62	13	– 8.0	29.4	–26.2	61.1	49.529	–64.0	13:42:33	29.4			213
0188	W	148.6 E	14:53:29	2-21-62	13	– 8.2	29.4	–26.2	61.2	49.524	–58.8	15:28:03	34.6			213
0189	N	123.2 E	16:33:47	2-21-62	13	– 8.5	29.4	–26.2	61.3	49.519	–60.6	17:05:03	31.3			213
0190	N	97.7 E	18:14:04	2-21-62	13	– 8.8	29.6	–26.2	61.4	49.514	–43.9	18:50:03	36.0			213
0198	W	105.9 W	07:36:27	2-22-62	14	–10.7	30.8	–26.3	62.8	49.474	–81.3	07:48:33	12.1			214
0199	W	131.4 W	09:16:44	2-22-62	14	–10.9	30.9	–26.4	63.0	49.469	–25.5	09:34:03	17.3			214
0200	N	156.8 W	10:57:02	2-22-62	14	–11.1	30.9	–26.5	63.1	49.464	–30.6	11:09:33	12.5			214
0201	W	177.7 E	12:37:20	2-22-62	14	–11.3	30.9	–26.6	63.2	49.459	–64.8	13:06:03	28.7			214
0202	W	152.3 E	14:17:38	2-22-62	14	–11.5	30.9	–26.7	63.4	49.454	–56.6	14:54:33	36.9			214
0212	W	102.2 W	07:00:35	2-23-62	15	–13.8	32.6	–26.8	64.9	49.404	–35.5	07:12:03	11.5			215
0213	W	127.7 W	08:40:53	2-23-62	15	–13.9	32.7	–26.8	65.0	49.399	–76.7	08:57:03	16.2			215
0214	N	153.1 W	10:21:11	2-23-62	15	–14.1	32.7	–26.8	65.1	49.394	–77.9	10:31:03	9.9			215
0215	W	178.6 W	12:01:29	2-23-62	15	–14.2	32.8	–26.8	65.3	49.389	–65.5	12:29:03	27.6			215
0217	N	130.5 E	15:22:04	2-23-62	15	–14.7	32.9	–26.8	65.4	49.379	–62.6	15:52:33	30.5			215
0226	W	98.6 W	06:24:44	2-24-62	16	–16.3	34.7	–27.1	67.0	49.329	–57.2	06:35:33	10.8			216
0228	N	149.5 W	09:45:20	2-24-62	16	–16.5	34.8	–27.1	67.2	49.319	–83.3	09:55:03	9.7			216
0229	W	174.9 W	11:25:37	2-24-62	16	–16.6	34.9	–27.1	67.3	49.314	–21.3	11:53:03	27.4			216
0230	W	159.6 E	13:05:55	2-24-62	16	–16.8	34.9	–27.1	67.4	49.309	–12.4	13:37:03	31.1			216
0231	N	134.2 E	14:46:13	2-24-62	16	–16.9	35.0	–27.1	67.5	58.787	–62.7	15:16:33	30.3			216
0232	N	108.7 E	16:26:31	2-24-62	16	–17.1	35.1	–27.1	67.6	58.782	–58.5	17:01:03	34.5			216
0240	W	94.9 W	05:48:53	2-25-62	17	–17.4	36.7	–25.8	68.0	58.762	–32.7	05:59:33	10.7			217
0241	W	120.3 W	07:29:11	2-25-62	17	–17.5	36.8	–25.8	68.1	58.762	– 3.4	07:43:03	13.9			217
0243	W	171.2 W	10:49:46	2-25-62	17	–18.0	36.9	–25.4	68.2	58.757	–66.2	11:16:03	26.3			217
0244	W	163.3 E	12:30:01	2-25-62	17	–18.2	37.2	–25.2	68.4	58.752	–61.7	13:01:47	31.8			217
0245	W	137.9 E	14:10:22	2-25-62	17	–18.4	37.4	–25.0	68.6	70.357	–42.6	14:47:03	36.7			217
0254	W	91.2 W	05:13:02	2-26-62	18	–19.9	38.2	–24.5	71.0	70.307	–67.9	05:24:03	11.0			218

READOUT ORBIT											TIME INTERVAL OF FILE ON FMR TAPE					FMR Tape Reel No.
Orbit No.	CDA Sta.	Satellite Equator Crossing at Orbital Ascending Node (ANO)				Spin Vector Attitude				Spin Rate (deg./sec.)	Begin	End		Dropouts, Minutes w/r/t ANO		
		Earth Longitude (degrees)	Hours; Minutes; Seconds (GMT)	Calendar Date	Julian Date	Decl. (deg.)	R.A. (deg.)	η_o (deg.)	t_o (min. after ANO)		Minutes w/r/t ANO	Hours; Minutes; Seconds (GMT)	Minutes w/r/t ANO	From –	To –	
0255	W	116.6 W	06:53:19	2-26-62	18	−20.1	38.6	−24.5	71.2	70.302	−78.9	07:07:03	13.7			218
0258	W	167.0 E	11:54:13	2-26-62	18	−20.6	39.5	−24.4	71.8	70.282	−62.3	12:25:03	30.8			218
0259	W	141.5 E	13:34:31	2-26-62	18	−20.8	39.8	−24.3	72.0	70.277	−45.0	14:10:27	35.9			218
0269	W	113.0 W	06:17:26	2-27-62	19	−24.0	46.1	−24.1	74.5	70.217	−80.1	06:30:33	13.1			219
0270	W	138.4 W	07:57:44	2-27-62	19	−23.8	45.9	−24.5	74.5	70.212	−74.7	08:16:03	18.3			219
0271	W	163.9 W	09:38:02	2-27-62	19	−23.8	45.6	−24.5	74.7	70.207	−67.9	10:03:03	25.0			219
0272	W	170.7 E	11:18:20	2-27-62	19	−23.7	45.4	−24.5	74.6	70.202	−62.1	11:49:03	30.7			219
0273	W	145.2 E	12:58:37	2-27-62	19	−23.7	45.1	−24.6	74.6	70.197	−55.3	13:36:33	37.9			219
0275	N	94.3 E	16:19:13	2-27-62	19	−23.4	44.2	−24.9	74.5	70.187	+28.2	16:58:33	39.3			219
0283	W	109.3 W	05:41:35	2-28-62	20	−23.2	40.1	−25.1	74.3	70.137	−80.0	05:55:03	13.5			220
0284	W	134.7 W	07:21:53	2-28-62	20	−23.1	39.8	−25.1	74.3	70.132	−73.2	07:41:03	19.2			220
0286	W	174.4 E	10:42:28	2-28-62	20	−23.0	39.3	−25.1	74.2	70.117	−62.7	11:13:03	30.6	− 7.5	− 6.5	220
0287	W	148.9 E	12:22:46	2-28-62	20	−22.9	39.0	−25.2	74.2	70.112	−56.8	12:59:23	36.6			220
0288	N	123.5 E	14:03:04	2-28-62	20	−22.8	38.7	−25.4	74.1	70.107	−58.3	14:36:03	33.0			220
0289	N	98.0 E	15:43:21	2-28-62	20	−22.7	38.3	−25.5	74.1	70.102	−37.2	16:22:03	38.7			220
0298	W	131.1 W	06:46:01	3- 1-62	21	−22.2	34.0	−25.9	73.8	70.047	−74.7	07:04:33	18.5	−47.0	−46.0	221
0299	N	156.5 W	08:26:19	3- 1-62	21	−22.1	33.5	−26.0	73.8	70.042	−69.3	08:50:03	23.7			221
0300	W	178.0 E	10:06:37	3- 1-62	21	−22.1	33.3	−26.1	73.7	70.037	−63.8	10:36:03	29.4			221
0301	W	152.6 E	11:46:55	3- 1-62	21	−22.0	33.0	−26.2	73.7	70.027	−59.0	12:21:03	34.1			221
0302	W	127.1 E	13:27:12	3- 1-62	21	−21.8	32.7	−26.3	73.6	70.022	−30.7	14:05:33	38.4			221
0303	N	101.7 E	15:07:30	3- 1-62	21	−21.6	32.3	−26.5	73.6	70.017	−55.4	15:45:03	37.6			221

0325	W	98.3 W	03:54:01	3- 3-62	23	−19.5	22.6	−28.3	72.9	69.892	−82.7	04:04:33	10.5			222
0327	W	149.2 W	07:14:36	3- 3-62	23	−19.4	22.1	−28.4	72.8	69.882	−71.1	07:37:03	22.5			222
0328	W	174.6 W	08:54:54	3- 3-62	23	−19.3	21.8	−28.5	72.7	69.877	−64.1	09:23:33	28.7			222
0329	W	159.9 E	10:35:12	3- 3-62	23	−19.2	21.6	−28.7	72.9	69.872	−61.8	11:07:03	31.9			222
0330	W	134.5 E	12:15:29	3- 3-62	23	−19.0	21.4	−28.9	72.9	69.867	−54.1	12:54:03	38.6			222
0339	W	94.6 W	03:18:09	3- 4-62	24	−17.8	17.5	−29.9	72.5	69.817	−71.5	03:29:33	11.4			223
0340	W	120.0 W	04:58:27	3- 4-62	24	−17.8	16.9	−30.0	72.4	69.812	−77.4	05:14:33	16.1			223
0341	W	145.5 W	06:38:45	3- 4-62	24	−17.7	16.7	−30.0	72.4	69.807	−72.1	07:00:03	21.3			223
0342	W	170.9 W	08:19:03	3- 4-62	24	−17.6	16.4	−30.1	72.6	69.797	+11.4	08:46:33	27.5			223
0343	W	163.6 E	09:59:20	3- 4-62	24	−17.5	16.3	−30.2	72.5	69.792	−59.9	10:33:03	33.7			223
0344	W	138.2 E	11:39:38	3- 4-62	24	−17.5	16.2	−30.2	72.5	69.787	−55.0	12:17:33	37.9			223
0345	N	112.7 E	13:19:56	3- 4-62	24	−17.5	16.2	−30.4	72.7	69.782	−54.9	13:55:57	36.0			223
0346	N	87.3 E	15:00:14	3- 4-62	24	−17.5	16.3	−30.5	72.8	69.772	−52.5	15:40:33	40.6			223
0353	W	90.9 W	02:42:18	3- 5-62	25	−17.4	16.5	−30.6	73.5	69.732	−74.0	02:53:33	11.3			224
0354	W	116.4 W	04:22:36	3- 5-62	25	−17.4	16.5	−30.7	73.6	69.727	−77.8	04:38:03	15.5			224
0355	W	141.8 W	06:02:54	3- 5-62	25	−17.4	16.5	−30.7	73.7	69.722	−72.3	06:24:03	21.2			224
0356	W	167.3 W	07:43:11	3- 5-62	25	−17.4	16.5	−30.8	73.9	69.717	+ 9.7	08:11:03	27.9			224
0357	W	167.3 E	09:23:29	3- 5-62	25	−17.4	16.5	−30.8	73.9	69.712	−59.6	09:57:03	33.6			224
0358	W	141.8 E	11:03:47	3- 5-62	25	−17.4	16.5	−30.8	74.0	69.707	−54.7	11:42:03	38.3	+ 0.2	+ 3.2	224
0359	N	116.4 E	12:44:05	3- 5-62	25	−17.4	16.5	−30.9	74.1	69.702	−58.3	13:19:03	35.0			224
0360	N	90.9 E	14:24:22	3- 5-62	25	−17.3	16.5	−30.9	74.2	69.697	−52.6	15:04:03	39.7			224
0368	W	112.7 W	03:46:45	3- 6-62	26	−17.1	16.7	−31.2	75.0	69.647	−77.9	04:01:33	14.8			225
0369	W	138.1 W	05:27:03	3- 6-62	26	−17.1	16.7	−31.2	75.1	69.642	−73.0	05:47:33	20.5			225
0372	N	145.5 E	10:27:56	3- 6-62	26	−17.0	16.7	−31.3	75.4	69.622	− 6.0	10:56:03	28.1			225
0373	N	120.1 E	12:08:14	3- 6-62	26	−17.0	16.7	−31.3	75.6	69.617	−58.5	12:42:33	34.3			225
0374	N	94.6 E	13:48:32	3- 6-62	26	−17.0	16.7	−31.3	75.6	69.612	−53.2	14:28:33	40.0			225
0383	N	134.4 W	04:51:12	3- 7-62	27	−16.7	16.8	−31.5	76.6	69.562	−20.5	05:01:03	9.9			226

READOUT ORBIT											TIME INTERVAL OF FILE ON FMR TAPE					FMR Tape Reel No.
Orbit No.	CDA Sta.	Satellite Equator Crossing at Orbital Ascending Node (ANO)				Spin Vector Attitude				Spin Rate (deg./sec.)	Begin	End		Dropouts, Minutes w/r/t ANO		
		Earth Longitude (degrees)	Hours; Minutes; Seconds (GMT)	Calendar Date	Julian Date	Decl. (deg.)	R.A. (deg.)	η_o (deg.)	t_o (min. after ANO)		Minutes w/r/t ANO	Hours; Minutes; Seconds (GMT)	Minutes w/r/t ANO	From –	To –	
0384	N	159.9 W	06:31:29	3- 7-62	27	–16.6	16.8	–31.5	76.6	69.557	–77.1	06:46:03	14.6			226
0385	N	174.7 E	08:11:47	3- 7-62	27	–16.6	16.8	–31.5	76.7	69.552	–71.8	08:33:03	21.3			226
0386	N	149.2 E	09:52:05	3- 7-62	27	–16.6	16.8	–31.4	76.8	69.542	– 3.1	10:20:03	28.0			226
0387	N	123.7 E	11:32:23	3- 7-62	27	–16.6	16.8	–31.4	76.9	69.537	+ 1.6	12:05:33	33.2			226
0388	N	98.3 E	13:12:40	3- 7-62	27	–16.6	16.8	–31.4	76.9	69.532	+ 9.5	13:51:03	38.4			226
0397	N	130.8 W	04:15:20	3- 8-62	28	–16.2	16.8	–31.2	78.0	69.482	–18.8	04:25:03	9.7			227
0398	N	156.2 W	05:55:38	3- 8-62	28	–16.2	16.8	–31.2	77.9	69.477	–79.6	06:09:03	13.4			227
0438	W	94.3 W	00:47:29	3-11-62	31	–14.5	16.6	–30.6	81.8	69.181	–82.3	00:58:33	11.1			228
0452	W	90.6 W	00:11:38	3-12-62	32	– 9.9	20.4	–31.8	84.8	69.081	–82.5	00:22:33	10.9			229
0466	W	87.0 W	23:36:05	3-12-62	32	– 3.3	23.2	–34.2	87.9	68.976	–79.4	23:48:03	12.0			230
0467	W	112.5 W	01:16:23	3-13-62	33	– 2.7	23.3	–34.4	88.1	68.971	–79.1	01:29:03	12.7			230
0469	N	163.4 W	04:36:59	3-13-62	33	– 2.5	23.2	–34.5	88.3	68.956	–11.1	04:52:33	15.6			230
0473	N	94.8 E	11:18:11	3-13-62	33	– 2.5	23.0	–33.7	88.6	68.926	–16.1	11:57:33	39.4			230
0480	W	83.3 W	23:00:16	3-13-62	33	– 2.5	22.6	–32.6	89.2	68.876	–22.2	23:10:33	10.3			231
0481	W	108.8 W	00:40:34	3-14-62	34	– 2.6	22.6	–32.6	89.2	68.866	–79.4	00:54:03	13.5			231
0482	W	134.2 W	02:20:52	3-14-62	34	– 2.6	22.5	–32.4	89.2	68.861	–74.9	02:39:33	18.7			231
0483	W	159.7 W	04:01:10	3-14-62	34	– 2.6	22.4	–32.3	89.3	68.856	–67.1	04:26:33	25.4			231
0484	W	174.9 E	05:41:27	3-14-62	34	– 2.6	22.4	–32.2	89.4	68.846	–61.0	06:12:33	31.1			231
0485	W	149.4 E	07:21:45	3-14-62	34	– 2.6	22.3	–32.0	89.5	68.836	–57.6	07:57:33	35.8			231
0495	W	105.1 W	00:04:44	3-15-62	35	– 2.6	21.6	–30.7	90.0	68.766	–80.1	00:17:33	12.8	–71.7	–69.7	232
0497	W	156.0 W	03:25:20	3-15-62	35	– 2.6	21.5	–30.4	90.2	68.751	–68.9	03:49:33	24.2			232

0498	W	178.5 E	05:05:38	3-15-62	35	– 2.6	21.4	–30.2	90.3	68.741	–63.5	05:35:33	29.9			232
0499	W	153.1 E	06:45:56	3-15-62	35	– 2.6	21.4	–30.0	90.4	68.736	– 1.9	07:21:33	35.6			232
0500	W	127.6 E	08:26:14	3-15-62	35	– 2.6	21.3	–29.9	90.5	68.726	–54.2	09:05:33	39.3			232
0509	W	101.5 W	23:28:55	3-15-62	35	– 2.6	21.0	–28.3	91.1	68.666	–80.2	23:41:33	12.6	–71.9	–67.9	233
0510	W	126.9 W	01:09:13	3-16-61	36	– 2.6	21.0	–28.1	91.1	68.656	–76.7	01:26:33	17.3			233
0511	W	152.4 W	02:49:31	3-16-62	36	– 2.6	20.9	–28.0	91.2	68.651	–70.1	03:12:33	23.0			233
0512	W	177.8 W	04:29:48	3-16-62	36	– 2.5	20.9	–27.9	91.3	68.646	–63.2	04:59:33	29.8	–51.8	–50.8	233
0513	W	156.7 E	06:10:06	3-16-62	36	– 2.5	20.8	–27.8	91.4	68.636	–62.2	06:41:13	31.1			233
0514	W	131.3 E	07:50:24	3-16-62	36	– 2.4	20.8	–27.6	91.4	68.631	–53.1	08:29:33	39.2			233
0515	N	105.8 E	09:30:42	3-16-62	36	– 2.4	20.7	–27.5	91.6	68.626	+13.3	10:07:33	36.9			233
0516	N	80.4 E	11:11:00	3-16-62	36	– 2.3	20.7	–27.3	91.5	68.616	–34.8	11:53:33	42.6			233
0524	W	123.2 W	00:33:23	3-17-62	37	– 1.7	20.7	–26.2	92.3	68.561	–77.3	00:49:33	16.2			234
0525	W	148.7 W	02:13:41	3-17-62	37	– 1.6	20.7	–26.1	92.4	68.556	–68.5	02:36:33	23.9			234
0526	W	174.1 W	03:53:59	3-17-62	37	– 1.6	20.7	–26.0	92.5	68.546	–67.0	04:20:33	26.6			234
0527	W	160.4 E	05:34:17	3-17-62	37	– 1.5	20.6	–25.8	92.5	68.541	– 2.9	06:08:33	34.3			234
0528	W	135.0 E	07:14:35	3-17-62	37	– 1.5	20.6	–25.7	92.6	68.536	+ 4.1	07:53:33	40.0			234
0529	N	109.5 E	08:54:53	3-17-62	37	– 1.4	20.6	–25.5	92.7	68.526	–56.2	09:29:33	34.7			234
0530	N	84.1 E	10:35:11	3-17-62	37	– 1.4	20.6	–25.4	92.8	68.521	–53.9	11:15:33	40.3			234
0537	W	94.1 W	22:17:16	3-17-62	37	– 0.8	20.6	–24.3	93.3	68.471	–82.0	22:27:33	10.3			235
0538	W	119.6 W	23:57:34	3-17-62	37	– 0.7	20.6	–24.2	93.4	68.461	–78.7	00:12:03	14.5			235
0539	W	145.0 W	01:37:52	3-18-62	38	– 0.6	20.6	–24.0	93.5	68.456	–73.6	01:58:03	20.2			235
0540	W	170.5 W	03:18:10	3-18-62	38	– 0.6	20.6	–23.9	93.6	68.451	–67.5	03:44:03	25.9			235
0541	W	164.1 E	04:58:28	3-18-62	38	– 0.5	20.5	–23.8	93.6	68.448	–61.4	05:30:33	32.1			235
0542	W	138.6 E	06:38:46	3-18-62	38	– 0.4	20.5	–23.6	93.8	68.436	+13.7	07:17:09	38.4			235
0553	W	141.3 W	01:02:03	3-19-62	39	0.5	20.5	–21.9	94.7	68.361	–73.2	01:22:33	20.5			236
0555	W	167.7 E	04:22:39	3-19-62	39	0.6	20.5	–21.6	94.9	68.346	–62.2	04:54:03	31.4			236
0558	N	91.4 E	09:23:32	3-19-62	39	0.8	20.4	–21.1	95.0	68.326	–52.8	10:03:33	40.0			236

729-166 O - 64 - 7

READOUT ORBIT											TIME INTERVAL OF FILE ON FMR TAPE					FMR Tape Reel No.
Orbit No.	CDA Sta.	Satellite Equator Crossing at Orbital Ascending Node (ANO)				Spin Vector Attitude				Spin Rate (deg./sec.)	Begin	End		Dropouts, Minutes w/r/t ANO		
		Earth Longitude (degrees)	Hours; Minutes; Seconds (GMT)	Calendar Date	Julian Date	Decl. (deg.)	R.A. (deg.)	η_o (deg.)	t_o (min. after ANO)		Minutes w/r/t ANO	Hours; Minutes; Seconds (GMT)	Minutes w/r/t ANO	From –	To –	
0565	W	86.8 W	21:05:38	3-19-62	39	1.6	20.5	−20.2	95.7	68.276	−84.6	21:14:33	8.9			237
0566	W	112.2 W	22:45:53	3-19-62	39	1.7	20.5	−20.1	95.8	68.271	−45.8	22:59:03	13.2			237
0567	W	137.7 W	00:26:10	3-20-62	40	1.7	20.5	−19.9	95.8	68.266	−61.1	00:43:03	16.9			237
0568	W	163.1 W	02:06:28	3-20-62	40	1.8	20.5	−19.8	95.8	68.256	−70.8	02:29:03	22.6			237
0569	W	171.4 E	03:46:46	3-20-62	40	1.9	20.4	−19.7	96.1	68.251	−63.2	04:17:03	30.3			237
0571	N	120.5 E	07:07:22	3-20-62	40	2.0	20.4	−19.3	96.1	68.236	−58.7	07:41:33	34.2			237
0572	N	95.1 E	08:47:40	3-20-62	40	2.1	20.4	−19.2	96.1	68.231	−54.6	09:26:33	38.9			237
0580	W	108.5 W	22:10:03	3-20-62	40	3.0	20.6	−17.9	96.8	68.176	−80.1	22:23:33	13.5			238
0581	W	134.0 W	23:50:21	3-20-62	40	3.1	20.5	−17.7	97.1	68.166	−74.4	00:09:33	19.2			238
0582	W	159.4 W	01:30:39	3-21-62	41	3.2	20.5	−17.6	97.1	68.156	−68.4	01:55:33	24.9			238
0583	W	175.1 E	03:10:57	3-21-62	41	3.3	20.5	−17.4	97.1	68.151	−62.7	03:41:33	30.6			238
0584	W	149.6 E	04:51:15	3-21-62	41	3.4	20.5	−17.3	97.3	68.146	−40.9	05:27:33	36.3			238
0585	N	124.2 E	06:31:33	3-21-62	41	3.4	20.5	−17.1	97.3	68.136	−57.1	07:04:33	33.0			238
0586	N	98.7 E	08:11:51	3-21-62	41	3.5	20.5	−16.9	97.3	68.131	−54.2	08:50:33	38.7			238
0595	W	130.3 W	23:14:32	3-21-62	41	4.5	20.7	−15.4	98.1	68.071	−77.0	23:31:03	16.5			239
0596	W	155.8 W	00:54:50	3-22-62	42	4.6	20.7	−15.2	98.3	68.061	−70.7	01:17:33	22.7			239
0597	W	178.8 E	02:35:08	3-22-62	42	4.7	20.7	−15.1	98.3	68.056	−64.9	03:03:33	28.4			239
0598	W	153.3 E	04:15:26	3-22-62	42	4.8	20.6	−14.9	98.3	68.051	−37.1	04:50:33	35.1			239
0600	N	102.4 E	07:36:01	3-22-62	42	5.0	20.6	−14.6	98.6	68.036	−55.9	08:13:33	37.5			239
0608	W	101.2 W	20:58:25	3-22-62	42	5.9	20.9	−13.2	99.3	67.981	−81.4	21:10:33	12.1	−69.4	−68.4	240
0609	W	126.7 W	22:38:43	3-22-62	42	6.0	20.9	−13.0	99.4	67.971	−66.7	22:54:33	15.8			240

0610	W	152.1 W	00:19:01	3-23-62	43	6.1	20.9	−12.9	99.5	67.966	−69.8	00:42:33	23.5			240
0611	W	177.6 W	01:59:19	3-23-62	43	6.2	20.9	−12.7	99.5	67.956	−66.9	02:27:03	27.7			240
0612	W	157.0 E	03:39:37	3-23-62	43	6.3	20.9	−12.6	99.7	67.951	−62.0	04:10:03	30.4			240
0622	W	97.5 W	20:22:36	3-23-62	43	7.6	21.1	−10.8	0.1	67.876	−80.0	20:36:03	13.5			241
0623	W	123.0 W	22:02:54	3-23-62	43	7.7	21.1	−10.7	0.3	67.871	−76.9	22:19:33	16.7			241
0624	W	148.4 W	23:43:12	3-23-62	43	7.8	21.1	−10.5	0.3	67.866	−71.3	00:05:33	22.4			241
0625	W	173.9 W	01:23:30	3-24-62	44	7.9	21.1	−10.4	0.4	67.856	− 8.2	01:50:03	26.5			241
0626	W	160.7 E	03:03:47	3-24-62	44	8.0	21.1	−10.2	0.5	67.851	−33.2	03:37:33	33.8			241
0628	N	109.7 E	06:24:23	3-24-62	44	8.2	21.1	− 9.9	0.6	67.836	−17.1	07:01:33	37.2			241
0636	W	93.9 W	19:46:47	3-24-62	44	9.3	21.5	− 8.5	1.4	67.776	−33.6	19:58:33	11.8			242
0637	W	119.3 W	21:27:05	3-24-62	44	9.4	21.5	− 8.3	1.4	67.771	−75.7	21:45:03	18.0			242
0638	W	144.8 W	23:07:23	3-24-62	44	9.5	21.5	− 8.2	1.6	67.766	−72.1	23:29:27	22.1			242
0639	W	170.2 W	00:47:40	3-25-62	45	9.6	21.5	− 8.0	1.6	67.756	− 1.7	01:15:33	27.9			242
0640	W	164.3 E	02:27:58	3-25-62	45	9.7	21.5	− 7.9	1.7	67.751	+ 1.4	03:00:33	32.6			242
0642	N	113.4 E	05:48:34	3-25-62	45	9.9	21.5	− 7.5	1.8	67.736	−56.9	06:23:03	34.5			242
0643	N	88.0 E	07:28:52	3-25-62	45	10.0	21.5	− 7.4	1.9	67.726	−53.6	08:08:03	39.2			242
0650	W	90.2 W	19:10:58	3-25-62	45	11.0	21.9	− 6.1	2.5	67.676	−82.1	19:21:33	10.6			243
0651	W	115.7 W	20:51:16	3-25-62	45	11.1	21.9	− 6.0	2.6	67.671	−77.4	21:07:33	16.3	−67.3	−66.3	243
0652	W	141.1 W	22:31:34	3-25-62	45	11.3	21.9	− 5.8	2.7	67.666	−73.1	22:51:33	20.0			243
0653	W	166.6 W	00:11:51	3-26-62	46	11.4	21.9	− 5.7	2.8	67.656	−67.1	00:38:33	27.7			243
0654	W	168.0 E	01:52:09	3-26-62	46	11.5	21.9	− 5.5	2.9	67.651	−62.8	02:23:03	30.9			243
0655	W	142.5 E	03:32:27	3-26-62	46	11.6	21.9	− 5.3	3.0	67.641	−57.1	04:09:03	36.6			243
0657	N	91.6 E	06:53:03	3-26-62	46	11.8	22.0	− 5.0	3.2	67.631	−54.2	07:32:33	39.5			243
0665	W	112.0 W	20:15:27	3-26-62	46	13.0	22.4	− 3.7	4.0	67.571	−57.3	20:30:33	15.1			244
0666	W	137.4 W	21:55:45	3-26-62	46	13.1	22.5	− 3.5	4.0	67.566	−19.1	22:15:03	19.3			244
0667	W	162.9 W	23:36:04	3-26-62	46	13.2	22.5	− 3.4	4.1	67.556	−68.3	00:01:33	25.5			244
0668	W	171.7 E	01:16:22	3-27-62	47	13.4	22.5	− 3.2	4.2	67.551	+ 3.8	01:49:03	32.7			244

READOUT ORBIT											TIME INTERVAL OF FILE ON FMR TAPE					FMR Tape Reel No.
Orbit No.	CDA Sta.	Satellite Equator Crossing at Orbital Ascending Node (ANO)				Spin Vector Attitude				Spin Rate (deg./sec.)	Begin	End		Dropouts, Minutes w/r/t ANO		
		Earth Longitude (degrees)	Hours; Minutes; Seconds (GMT)	Calendar Date	Julian Date	Decl. (deg.)	R.A. (deg.)	η_o (deg.)	t_o (min. after ANO)		Minutes w/r/t ANO	Hours; Minutes; Seconds (GMT)	Minutes w/r/t ANO	From –	To –	
0669	W	146.2 E	02:56:40	3-27-62	47	13.5	22.5	– 3.1	4.3	67.546	–56.8	03:33:33	36.9			244
0670	N	120.7 E	04:36:58	3-27-62	47	13.6	22.5	– 2.9	4.4	67.536	–58.3	05:10:33	33.6			244
0671	N	95.3 E	06:17:16	3-27-62	47	13.7	22.5	– 2.8	4.5	67.531	–52.7	06:57:33	40.3	+20.7	+21.7	244
0679	W	108.3 W	19:39:39	3-27-62	47	14.9	23.0	– 1.5	5.1	67.471	–77.7	19:54:03	14.4			245
0680	W	133.8 W	21:19:57	3-27-62	47	15.1	23.1	– 1.3	5.3	67.466	–72.5	21:40:03	20.1			245
0683	W	149.9 E	02:20:51	3-28-62	48	15.4	23.1	– 0.9	5.6	67.441	+17.7	02:56:33	35.7			245
0684	N	124.4 E	04:01:09	3-28-62	48	15.5	23.1	– 0.7	5.6	67.436	–58.7	04:33:03	31.9			245
0685	N	99.0 E	05:41:27	3-28-62	48	15.7	23.2	– 0.6	5.8	67.431	–55.0	06:19:03	37.6			245
0696	W	179.0 E	00:04:44	3-29-62	49	17.2	23.9	1.2	6.8	67.351	–63.4	00:34:33	29.8			246
0697	W	153.5 E	01:45:02	3-29-62	49	17.3	23.9	1.4	7.0	67.341	–59.2	02:19:03	34.0			246
0698	N	128.1 E	03:25:20	3-29-62	49	17.4	23.9	1.5	6.9	67.336	–60.7	03:57:33	32.2			246
0699	N	102.6 E	05:05:38	3-29-62	49	17.6	24.0	1.7	7.1	67.331	+ 4.2	05:42:33	36.9			246
0707	W	101.0 W	18:28:02	3-29-62	49	18.7	24.6	3.0	7.7	67.276	–72.5	18:39:33	11.5			247
0708	W	126.4 W	20:08:20	3-29-62	49	18.8	24.7	3.1	7.9	67.271	–74.1	20:26:03	17.7			247
0709	W	151.9 W	21:48:38	3-29-62	49	18.9	24.7	3.2	8.1	67.266	–68.3	22:12:33	23.9			247
0710	W	177.3 W	23:28:56	3-29-62	49	19.1	24.8	3.4	8.1	67.261	–64.9	23:57:33	28.6			247
0711	W	157.2 E	01:09:14	3-30-62	50	19.2	24.8	3.5	8.3	67.256	–42.1	01:46:03	36.8			247
0722	W	122.8 W	19:32:31	3-30-62	50	20.6	25.7	5.2	9.2	67.181	–63.1	19:46:03	13.5			248
0723	W	148.2 W	21:12:49	3-30-62	50	20.8	25.8	5.3	9.4	67.176	–68.5	21:37:03	24.2			248
0724	W	173.7 W	22:53:07	3-30-62	50	20.9	25.8	5.5	9.4	67.171	–65.3	23:21:03	27.9			248
0725	W	160.9 E	00:33:25	3-31-62	51	21.0	25.8	5.6	9.5	67.166	–60.7	01:06:33	33.1			248

0726	W	135.4 E	02:13:43	3-31-62	51	21.1	25.9	5.7	9.6	67.161	−55.1	02:51:33	37.8			248
0735	W	93.7 W	17:16:25	3-31-62	51	22.3	26.9	7.0	10.6	67.101	−82.8	17:27:33	11.1			249
0736	W	119.1 W	18:56:43	3-31-62	51	22.4	26.9	7.2	10.7	67.096	−72.5	19:16:03	19.3			249
0737	W	144.6 W	20:37:00	3-31-62	51	22.5	27.0	7.3	10.8	67.091	−69.3	21:00:33	23.6			249
0738	W	170.0 W	22:17:18	3-31-62	51	22.6	27.1	7.4	10.9	67.081	−65.2	22:45:03	27.8			249
0739	W	164.5 E	23:57:36	3-31-62	51	22.7	27.1	7.6	10.9	67.076	−60.4	00:30:33	33.0			249
0740	W	139.1 E	01:37:54	4- 1-62	52	22.8	27.2	7.7	11.0	67.071	−55.4	02:15:33	37.7			249
0741	N	113.6 E	03:18:12	4- 1-62	52	23.0	27.2	7.8	11.1	67.066	−56.2	03:53:33	35.4			249
0742	N	88.2 E	04:58:30	4- 1-62	52	23.1	27.3	7.9	11.2	67.061	−52.2	05:38:33	40.1			249
0749	W	90.0 W	16:40:36	4- 1-62	52	24.0	28.2	8.9	12.1	67.011	−82.9	16:50:33	10.0			250
0750	W	115.4 W	18:20:54	4- 1-62	52	24.1	28.3	9.0	12.1	67.006	−74.7	18:38:03	17.2			250
0751	W	140.9 W	20:01:12	4- 1-62	52	24.2	28.4	9.1	12.2	67.001	−70.1	20:23:03	21.9			250
0752	W	166.3 W	21:41:30	4- 1-62	52	24.3	28.5	9.3	12.3	66.996	−67.4	22:07:33	26.1			250
0753	W	168.2 E	23:21:48	4- 1-62	52	24.4	28.5	9.4	12.4	66.986	−60.7	23:53:33	31.8			250
0754	W	142.7 E	01:02:06	4- 2-62	53	24.5	28.6	9.5	12.4	66.981	−56.1	01:38:33	36.5			250
0755	N	117.3 E	02:42:24	4- 2-62	53	24.6	28.7	9.6	12.6	66.976	−58.3	03:16:33	34.2			250
0764	W	111.8 W	17:45:05	4- 2-62	53	25.6	29.8	10.7	13.6	66.916	−80.1	17:58:33	13.5			251
0765	W	137.2 W	19:25:23	4- 2-62	53	25.7	29.9	10.9	13.6	66.911	−74.5	19:44:33	19.2			251
0766	W	162.7 W	21:05:41	4- 2-62	53	25.8	30.0	11.0	13.8	66.906	−67.6	21:30:33	24.9			251
0767	W	171.9 E	22:45:58	4- 2-62	53	25.9	30.1	11.1	13.8	66.896	−61.7	23:17:33	31.6			251
0768	W	146.4 E	00:26:16	4- 3-62	54	26.0	30.2	11.2	14.0	66.891	−56.9	01:02:33	36.3	−57.3	−56.3	251
0778	W	108.1 W	17:09:16	4- 3-62	54	27.1	31.6	12.3	15.2	66.831	+ 9.5	17:25:03	15.8			252
0779	W	133.6 W	18:49:34	4- 3-62	54	27.1	31.7	12.4	15.2	66.821	−20.3	19:07:03	17.5			252
0780	W	159.0 W	20:29:52	4- 3-62	54	27.2	31.8	12.5	15.3	66.816	−67.1	20:55:03	25.2			252
0781	W	175.5 E	22:10:10	4- 3-62	54	27.3	31.9	12.6	15.4	66.811	−64.2	22:39:03	28.9			252
0782	W	150.1 E	23:50:28	4- 3-62	54	27.4	31.9	12.7	15.5	66.806	−58.0	00:26:03	35.6			252
0783	N	124.6 E	01:30:46	4- 4-62	55	27.5	32.0	12.8	15.7	66.796	−58.9	02:02:33	31.8			252

READOUT ORBIT											TIME INTERVAL OF FILE ON FMR TAPE					FMR Tape Reel No.
Orbit No.	CDA Sta.	Satellite Equator Crossing at Orbital Ascending Node (ANO)				Spin Vector Attitude				Spin Rate (deg./sec.)	Begin	End		Dropouts, Minutes w/r/t ANO		
		Earth Longitude (degrees)	Hours; Minutes; Seconds (GMT)	Calendar Date	Julian Date	Decl. (deg.)	R.A. (deg.)	η_o (deg.)	t_o (min. after ANO)		Minutes w/r/t ANO	Hours; Minutes; Seconds (GMT)	Minutes w/r/t ANO	From –	To –	
0784	N	99.2 E	03:11:04	4- 4-62	55	27.6	32.2	12.8	15.7	66.791	–56.0	03:48:33	37.5			252
0792	W	104.4 W	16:33:27	4- 4-62	55	28.3	33.4	13.7	16.5	66.741	–68.3	16:48:03	14.6			253
0793	W	129.9 W	18:13:45	4- 4-62	55	28.3	33.6	13.8	16.7	66.736	–77.1	18:30:03	16.3			253
0794	W	155.3 W	19:54:03	4- 4-62	55	28.4	33.7	13.9	16.9	66.731	–69.6	20:18:03	24.0			253
0795	W	179.2 E	21:34:21	4- 4-62	55	28.4	33.8	14.0	16.9	66.721	–64.1	22:03:33	29.2			253
0796	W	153.8 E	23:14:39	4- 4-62	55	28.5	33.9	14.1	17.1	66.716	–55.5	23:52:03	37.4			253
0798	N	102.8 E	02:35:15	4- 5-62	56	28.7	34.1	14.2	17.2	66.706	–54.5	03:14:03	38.8			253
0806	W	100.8 W	15:57:39	4- 5-62	56	29.2	35.4	14.9	18.1	66.661	– 7.8	16:10:03	12.4			254
0807	W	126.2 W	17:37:57	4- 5-62	56	29.3	35.6	15.0	18.3	66.656	–73.8	17:57:03	19.1			254
0808	W	151.7 W	19:18:15	4- 5-62	56	29.3	35.7	15.1	18.4	66.651	–71.5	19:40:03	21.8			254
0809	W	177.1 W	20:58:32	4- 5-62	56	29.3	35.8	15.2	18.5	66.640	–65.4	21:26:03	27.5			254
0810	W	157.4 E	22:38:50	4- 5-62	56	29.4	35.9	15.3	18.6	66.635	–57.2	23:15:03	36.2			254
0811	W	132.0 E	00:19:08	4- 6-62	57	29.4	36.0	15.3	18.6	66.630	–55.7	00:56:03	36.9			254
0812	N	106.5 E	01:59:26	4- 6-62	57	29.5	36.2	15.4	18.8	66.625	–54.2	02:38:33	39.1			254
0813	N	81.1 E	03:39:44	4- 6-62	57	29.6	36.3	15.4	19.0	66.620	–50.3	04:21:27	41.7	– 9.7	– 8.7	254
0821	W	122.6 W	17:02:08	4- 6-62	57	30.0	37.7	16.1	19.8	66.575	–78.0	17:17:33	15.4			255
0822	W	148.0 W	18:42:26	4- 6-62	57	30.0	37.8	16.1	20.0	66.570	–72.9	19:03:03	20.6	–41.4	–40.4	255
0823	W	173.5 W	20:22:44	4- 6-62	57	30.0	38.0	16.2	20.0	66.560	–64.3	20:52:03	29.3			255
0824	W	161.1 E	22:03:02	4- 6-62	57	30.0	38.1	16.3	20.2	66.555	+ 7.3	22:35:03	32.0			255
0825	W	135.6 E	23:43:20	4- 6-62	57	30.1	38.2	16.3	20.4	66.550	–55.2	00:21:33	38.2			255
0837	W	169.8 W	19:46:55	4- 7-62	58	30.4	40.2	17.0	21.8	66.480	–64.9	20:15:33	28.6			256

0838	W	164.8 E	21:27:13	4- 7-62	58	30.4	40.3	17.1	21.8	66.475	−63.2	21:58:03	30.3			256
0839	W	139.3 E	23:07:31	4- 7-62	58	30.4	40.4	17.1	22.0	66.470	−43.2	23:43:03	35.5			256
0849	W	115.2 W	15:50:31	4- 8-62	59	30.5	42.2	17.5	23.2	66.415	−81.5	16:02:03	11.5			257
0850	W	140.7 W	17:30:49	4- 8-62	59	30.5	42.3	17.6	23.2	66.410	−74.0	17:50:33	19.7			257
0852	W	168.4 E	20:51:24	4- 8-62	59	30.5	42.6	17.6	23.5	66.395	−58.8	21:26:03	34.7			257
0853	W	143.0 E	22:31:42	4- 8-62	59	30.5	42.7	17.7	23.6	66.390	−57.5	23:07:03	35.4			257
0863	W	111.6 W	15:14:42	4- 9-62	60	30.4	44.4	17.9	24.8	66.330	−79.3	15:29:03	14.4			258
0864	W	137.0 W	16:55:00	4- 9-62	60	30.4	44.6	17.9	25.0	66.325	−76.4	17:12:30	17.5			258
0866	W	172.1 E	20:15:36	4- 9-62	60	30.3	44.8	18.0	25.1	66.315	+ 3.5	20:49:03	33.5			258
0867	W	146.6 E	21:55:54	4- 9-62	60	30.3	44.9	18.0	25.1	66.310	−59.3	22:30:03	34.2	+ 2.1	+ 3.1	258
0877	W	107.9 W	14:38:54	4-10-62	61	30.0	46.6	18.0	26.3	66.255	−79.9	14:51:33	12.7			259
0878	W	133.3 W	16:19:12	4-10-62	61	30.0	46.8	18.0	26.5	66.250	−30.0	16:35:03	15.9			259
0879	W	158.8 W	17:59:30	4-10-62	61	29.9	46.9	18.1	26.5	66.240	−68.8	18:22:03	22.5			259
0880	W	175.7 E	19:39:48	4-10-62	61	29.9	47.0	18.1	26.7	66.235	−46.7	20:12:57	33.2			259
0881	W	150.3 E	21:20:26	4-10-62	61	29.8	47.1	18.0	26.8	66.230	−59.2	21:54:03	34.0			259
0882	N	124.8 E	23:00:24	4-10-62	61	29.8	47.2	18.0	26.9	66.225	−60.4	23:32:33	32.2	− 0.4	+ 0.6	259
0891	W	104.2 W	14:03:06	4-11-62	62	29.4	48.7	17.9	27.9	66.175	−83.1	14:13:03	10.0			260
0892	W	129.7 W	15:43:24	4-11-62	62	29.3	48.8	17.9	28.1	66.170	−77.4	15:58:33	15.2			260
0893	W	155.1 W	17:23:42	4-11-62	62	29.2	49.0	17.9	28.2	66.160	−72.0	17:45:03	21.4			260
0894	W	179.4 E	19:04:00	4-11-62	62	29.2	49.0	17.9	28.3	66.155	−61.9	19:35:33	31.6			260
0895	W	154.0 E	20:44:18	4-11-62	62	29.1	49.2	17.9	28.4	66.150	−58.8	21:19:03	34.8			260
0896	N	128.5 E	22:24:36	4-11-62	62	29.0	49.3	17.9	28.6	66.145	−59.8	22:58:03	33.5			260
0897	N	103.1 E	00:04:54	4-12-62	63	29.0	49.4	17.8	28.6	66.140	−57.6	00:40:03	35.2			260
0905	W	100.6 W	13:27:17	4-12-62	63	28.4	50.7	17.6	29.6	66.100	− 4.7	13:38:03	10.8			261
0906	W	126.0 W	15:07:35	4-12-62	63	28.4	50.8	17.6	29.7	66.090	−79.2	15:21:33	14.0			261
0907	W	151.5 W	16:47:53	4-12-62	63	28.3	50.9	17.6	29.8	66.085	−71.8	17:09:33	21.7			261
0908	W	176.9 W	18:28:11	4-12-62	63	28.2	51.0	17.6	30.0	66.080	−66.5	18:54:33	26.3			261

READOUT ORBIT											TIME INTERVAL OF FILE ON FMR TAPE					FMR Tape Reel No.
Orbit No.	CDA Sta.	Satellite Equator Crossing at Orbital Ascending Node (ANO)				Spin Vector Attitude				Spin Rate (deg./sec.)	Begin	End		Dropouts, Minutes w/r/t ANO		
		Earth Longitude (degrees)	Hours; Minutes; Seconds (GMT)	Calendar Date	Julian Date	Decl. (deg.)	R.A. (deg.)	η_o (deg.)	t_o (min. after ANO)		Minutes w/r/t ANO	Hours; Minutes; Seconds (GMT)	Minutes w/r/t ANO	From –	To –	
0909	W	157.6 E	20:08:29	4-12-62	63	28.1	51.1	17.5	30.0	66.075	–56.7	20:45:03	36.6			261
0910	W	132.2 E	21:48:47	4-12-62	63	28.1	51.2	17.5	30.1	66.070	–56.0	22:26:33	37.4			261
0911	N	106.7 E	23:29:05	4-12-62	63	28.0	51.4	17.4	30.2	66.065	–55.2	00:07:03	38.0			261
0912	N	81.3 E	01:09:23	4-13-62	64	27.9	51.5	17.4	30.4	66.060	–54.5	01:48:03	38.7			261
0919	W	96.9 W	12:51:28	4-13-62	64	27.3	52.6	17.1	31.2	66.020	–82.4	13:02:33	11.1			262
0920	W	122.3 W	14:31:46	4-13-62	64	27.2	52.7	17.0	31.4	66.015	–74.8	14:47:33	15.8			262
0921	N	147.8 W	16:12:04	4-13-62	64	27.1	52.8	17.0	31.4	66.010	–79.1	16:23:33	11.5			262
0922	N	173.3 W	17:52:22	4-13-62	64	27.0	52.8	17.0	31.6	66.005	–74.8	18:09:33	17.2			262
0923	N	161.3 E	19:32:40	4-13-62	64	26.9	52.9	16.9	31.6	66.000	–70.1	19:55:33	22.9	+11.3	+12.3	262
0924	W	135.8 E	21:12:58	4-13-62	64	26.9	53.0	16.9	31.8	65.995	–56.4	21:49:03	36.1	+ 0.0	+ 2.0	262
0926	N	84.9 E	00:33:34	4-14-62	65	26.7	53.3	16.7	31.9	65.985	–54.4	01:12:03	38.5			262
0933	W	93.2 W	12:15:40	4-14-62	65	26.0	54.3	16.3	32.8	65.945	–81.5	12:26:57	11.5			263
0934	W	118.7 W	13:55:57	4-14-62	65	25.9	54.3	16.2	33.0	65.940	–77.5	14:11:33	15.6			263
0935	W	144.1 W	15:36:15	4-14-62	65	26.0	54.2	16.1	33.0	65.935	–70.8	15:59:03	22.8			263
0936	W	169.6 W	17:16:33	4-14-62	65	26.3	54.0	15.8	32.9	65.930	–67.7	17:42:33	26.0	–52.6	–51.6	263
0937	W	165.0 E	18:56:51	4-14-62	65	26.6	53.7	15.4	32.9	65.925	–62.5	19:27:33	30.7			263
0938	W	139.5 E	20:37:09	4-14-62	65	26.9	53.5	15.2	32.8	65.915	–56.3	21:11:03	33.9			263
0939	N	114.1 E	22:17:27	4-14-62	65	27.1	53.1	15.0	32.8	65.910	–58.8	22:51:33	34.1			263
0940	N	88.6 E	23:57:45	4-14-62	65	27.3	52.6	14.9	32.7	65.905	–52.8	00:38:27	40.7			263
0947	W	89.6 W	11:39:51	4-15-62	66	29.8	49.0	13.1	32.1	65.870	–83.2	11:50:03	10.2			264
0948	W	115.0 W	13:20:09	4-15-62	66	30.2	48.6	12.8	32.1	65.865	– 8.4	13:32:03	11.9			264

0949	W	140.5 W	15:00:27	4-15-62	66	30.6	48.4	12.4	32.0	65.855	−76.1	15:19:03	18.6			264
0950	W	165.9 W	16:40:45	4-15-62	66	30.9	48.1	12.1	32.0	65.850	−68.3	17:05:33	24.8	−51.8	−50.8	264
0951	W	168.6 E	18:21:02	4-15-62	66	31.2	47.8	11.8	31.9	65.845	−64.1	18:50:33	29.5			264
0952	W	143.2 E	20:01:20	4-15-62	66	31.5	47.5	11.6	31.9	65.840	−60.2	20:35:03	33.7			264
0953	N	117.7 E	21:41:38	4-15-62	66	31.7	47.1	11.4	31.8	65.835	−59.7	22:15:33	33.9			264
0962	W	111.3 W	12:44:20	4-16-62	67	34.8	41.8	9.3	31.1	65.785	−62.6	13:00:03	15.7			265
0963	W	136.8 W	14:24:38	4-16-62	67	35.2	41.4	9.0	31.1	65.780	−75.3	14:42:03	17.4			265
0964	W	162.3 W	16:04:56	4-16-62	67	35.5	41.1	8.7	31.0	65.775	−67.8	16:28:33	23.6			265
0965	W	172.3 E	17:45:14	4-16-62	67	35.8	40.8	8.4	31.0	65.770	−65.5	18:12:33	27.3			265
0966	W	146.9 E	19:25:31	4-16-62	67	36.0	40.4	8.2	30.9	65.765	−60.3	19:58:03	32.5			265
0967	N	121.4 E	21:05:49	4-16-62	67	36.2	39.9	8.1	30.9	65.755	−60.0	21:38:33	32.7			265
0968	N	95.9 E	22:46:09	4-16-62	67	36.4	39.3	8.0	30.6	65.750	−57.2	23:22:33	36.4			265
0976	W	107.7 W	12:08:33	4-17-62	68	39.0	33.8	6.3	30.0	65.710	−83.2	12:19:33	11.0			266
0977	W	133.1 W	13:48:51	4-17-62	68	39.4	33.3	6.0	29.6	65.705	−77.8	14:04:33	15.7	+ 1.2	+ 2.2	266
0978	W	158.6 W	15:29:09	4-17-62	68	39.7	32.9	5.8	29.6	65.695	−71.4	15:51:33	22.4			266
0979	W	176.0 E	17:09:27	4-17-62	68	39.9	32.5	5.6	29.6	65.690	−66.8	17:36:03	26.6			266
0980	W	150.5 E	18:49:45	4-17-62	68	40.1	32.0	5.4	29.5	65.685	−60.0	19:22:33	32.8	− 1.8	− 0.8	266
0981	N	125.1 E	20:30:02	4-17-62	68	40.3	31.5	5.3	29.5	65.680	−62.3	21:01:32	31.5			266
0982	N	99.6 E	22:10:20	4-17-62	68	40.4	30.8	5.2	29.4	65.675	−56.7	22:47:03	36.7			266
0991	W	129.5 W	13:13:02	4-18-62	69	43.0	23.9	3.6	28.5	65.625	−64.8	13:31:03	18.0			267
0993	W	179.6 E	16:33:38	4-18-62	69	43.5	22.9	3.2	28.4	65.615	−53.9	17:03:33	29.5			267
0994	W	154.2 E	18:13:56	4-18-62	69	43.7	22.4	3.0	28.3	65.610	−62.6	18:45:03	31.1	− 3.9	− 2.9	267
0995	N	128.7 E	19:54:14	4-18-62	69	43.8	21.8	3.0	28.3	65.605	−58.6	20:26:03	31.8			267
0996	N	103.3 E	21:34:32	4-18-62	69	43.9	21.0	3.0	28.2	65.600	−26.8	22:10:33	36.0			267
1004	W	100.3 W	10:56:55	4-19-62	70	45.6	13.9	1.9	27.1	65.550	−73.8	11:07:33	10.6			268
1005	W	125.8 W	12:37:13	4-19-62	70	45.8	13.2	1.7	27.0	65.540	−78.3	12:51:03	13.8			268
1006	W	151.3 W	14:17:31	4-19-62	70	46.0	12.6	1.6	27.0	65.530	−12.8	14:42:03	24.5			268

READOUT ORBIT											TIME INTERVAL OF FILE ON FMR TAPE					FMR Tape Reel No.
Orbit No.	CDA Sta.	Satellite Equator Crossing at Orbital Ascending Node (ANO)				Spin Vector Attitude				Spin Rate (deg./sec.)	Begin	End		Dropouts, Minutes w/r/t ANO		
		Earth Longitude (degrees)	Hours; Minutes; Seconds (GMT)	Calendar Date	Julian Date	Decl. (deg.)	R.A. (deg.)	η_o (deg.)	t_o (min. after ANO)		Minutes w/r/t ANO	Hours; Minutes; Seconds (GMT)	Minutes w/r/t ANO	From –	To –	
1007	W	176.7 W	15:57:49	4-19-62	70	46.2	12.0	1.4	26.9	65.525	–43.7	16:26:03	28.2			268
1009	W	132.4 E	19:18:25	4-19-62	70	46.4	10.7	1.3	26.8	65.515	–11.3	19:54:33	36.1			268
1018	W	96.7 W	10:21:06	4-20-62	71	46.4	10.6	1.1	27.4	65.455	–82.6	10:32:03	11.0			269
1019	W	122.1 W	12:01:24	4-20-62	71	46.4	10.6	1.0	27.4	65.445	–80.7	12:14:03	12.7			269
1020	W	147.6 W	13:41:42	4-20-62	71	46.4	10.7	1.0	27.5	65.440	–68.6	14:06:03	24.3			269
1021	W	173.0 W	15:22:00	4-20-62	71	46.4	10.8	0.9	27.5	65.430	–28.2	15:49:33	27.6			269
1023	W	136.1 E	18:42:36	4-20-62	71	46.4	10.9	0.8	27.6	65.420	–58.4	19:17:33	35.0	– 1.6	– 0.6	269
1032	W	93.0 W	09:45:17	4-21-62	72	46.3	11.7	0.4	28.2	65.355	–84.2	09:54:57	9.7			270
1033	W	118.5 W	11:25:35	4-21-62	72	46.3	11.8	0.3	28.4	65.350	–79.3	11:38:33	13.0			270
1034	W	143.9 W	13:05:53	4-21-62	72	46.3	11.8	0.3	28.4	65.345	–54.3	13:27:03	21.2			270
1035	W	169.4 W	14:46:11	4-21-62	72	46.3	11.9	0.2	28.5	65.335	–54.9	15:13:03	26.9			270
1036	W	165.2 E	16:26:29	4-21-62	72	46.3	12.0	0.2	28.6	65.330	–32.3	16:58:33	32.1			270
1037	W	139.7 E	18:06:47	4-21-62	72	46.3	12.0	0.3	28.7	65.325	–59.2	18:41:03	34.3			270
1039	N	88.8 E	21:27:23	4-21-62	72	46.3	12.2	– 0.4	28.9	65.310	–55.3	22:06:03	38.7			270
1046	W	89.3 W	09:09:28	4-22-62	73	46.2	12.8	– 0.7	29.3	65.265	–81.8	09:21:03	11.6			271
1048	W	140.2 W	12:30:04	4-22-62	73	46.2	12.9	– 0.8	29.4	65.250	–26.9	12:50:03	20.0			271
1049	W	165.7 W	14:10:22	4-22-62	73	46.2	13.0	– 1.0	29.4	65.245	–66.9	14:36:33	26.2			271
1051	W	143.4 E	17:30:58	4-22-62	73	46.2	13.1	– 1.1	29.5	65.230	–60.2	18:04:03	33.1			271
1053	N	92.5 E	20:51:33	4-22-62	73	46.2	13.2	– 1.2	29.7	65.215	–54.1	21:31:03	39.5			271
1061	W	111.1 W	10:13:57	4-23-62	74	46.0	13.8	– 1.9	30.3	65.165	–77.9	10:29:03	15.1			272
1062	W	136.6 W	11:54:15	4-23-62	74	46.0	13.9	– 2.0	30.4	65.155	–22.6	12:12:03	17.8			272

1063	W	162.0 W	13:34:33	4-23-62	74	46.0	14.0	− 2.0	30.5	65.150	−66.7	14:01:03	26.5			272
1064	W	172.5 E	15:14:50	4-23-62	74	46.0	14.0	− 2.2	30.6	65.145	−64.1	15:44:03	29.2			272
1067	N	96.2 E	20:15:44	4-23-62	74	46.0	14.2	− 2.4	30.8	65.125	−56.5	20:52:03	36.3			272
1075	W	107.5 W	09:38:07	4-24-62	75	45.7	14.8	− 3.2	31.4	65.075	−57.8	09:48:33	10.4			273
1077	W	158.4 W	12:58:43	4-24-62	75	45.7	14.9	− 3.3	31.4	65.060	− 3.3	13:24:33	25.8			273
1079	W	150.7 E	16:19:19	4-24-62	75	45.7	15.0	− 3.5	31.5	65.045	−11.7	16:51:33	32.2			273
1080	N	125.3 E	17:59:37	4-24-62	75	45.7	15.1	− 3.6	31.6	65.040	−61.6	18:31:03	31.4			273
1081	N	99.8 E	19:39:54	4-24-62	75	45.7	15.1	− 3.8	31.6	65.030	−59.1	20:14:03	34.2			273
1089	W	103.8 W	09:02:18	4-25-62	76	45.5	15.6	− 4.6	32.2	64.980	−82.8	09:12:33	10.3			274
1090	W	129.2 W	10:42:36	4-25-62	76	45.4	15.7	− 4.7	32.3	64.970	−75.4	11:00:33	18.0			274
1091	W	154.7 W	12:22:54	4-25-62	76	45.4	15.8	− 4.8	32.4	64.965	−73.7	12:42:27	19.6			274
1092	W	179.9 E	14:03:11	4-25-62	76	45.4	15.8	− 4.9	32.4	64.960	−66.0	14:29:03	25.9			274
1093	W	154.4 E	15:43:29	4-25-62	76	45.4	15.9	− 5.0	32.5	64.950	+10.2	16:15:03	31.6			274
1103	W	100.1 W	08:26:28	4-26-62	77	45.2	16.4	− 6.2	33.0	64.885	−82.8	08:36:03	9.6			275
1104	W	125.6 W	10:06:46	4-26-62	77	45.1	16.4	− 6.3	33.2	64.875	−80.2	10:20:03	13.3			275
1105	W	151.0 W	11:47:04	4-26-62	77	45.1	16.5	− 6.4	33.2	64.870	−67.5	12:07:03	20.0			275
1106	W	176.5 W	13:27:22	4-26-62	77	45.1	16.5	− 6.5	33.3	64.860	−11.1	13:59:33	32.2			275
1107	W	158.1 E	15:07:40	4-26-62	77	45.1	16.6	− 6.6	33.3	64.855	−37.7	15:41:33	33.9			275
1108	W	132.6 E	16:47:58	4-26-62	77	45.1	16.6	− 6.8	33.4	64.845	−44.9	17:24:03	36.1			275
1117	W	96.5 W	07:50:39	4-27-62	78	44.8	17.1	− 7.8	34.1	64.785	−83.0	08:00:33	9.9			276
1118	W	121.9 W	09:30:57	4-27-62	78	44.8	17.1	− 8.0	34.0	64.775	−78.4	09:44:03	13.1			276
1119	W	147.4 W	11:11:15	4-27-62	78	44.7	17.1	− 8.1	34.0	64.770	−75.1	11:30:03	18.8			276
1120	W	172.8 W	12:51:32	4-27-62	78	44.7	17.1	− 8.2	34.2	64.760	−65.2	13:20:03	28.5			276
1121	W	161.7 E	14:31:50	4-27-62	78	44.7	17.2	− 8.3	34.2	64.755	−58.1	15:06:03	34.2			276
1122	W	136.3 E	16:12:08	4-27-62	78	44.7	17.2	− 8.5	34.3	64.745	−56.5	16:49:03	36.9			276
1123	N	110.8 E	17:52:26	4-27-62	78	44.6	17.3	− 8.6	34.4	64.740	−57.9	18:28:03	35.6			276
1124	N	85.4 E	19:32:44	4-27-62	78	44.6	17.3	− 8.7	34.5	64.735	−53.4	20:13:03	40.3			276

READOUT ORBIT											TIME INTERVAL OF FILE ON FMR TAPE					FMR Tape Reel No.
Orbit No.	CDA Sta.	Satellite Equator Crossing at Orbital Ascending Node (ANO)				Spin Vector Attitude				Spin Rate (deg./sec.)	Begin	End		Dropouts, Minutes w/r/t ANO		
		Earth Longitude (degrees)	Hours; Minutes; Seconds (GMT)	Calendar Date	Julian Date	Decl. (deg.)	R.A. (deg.)	η_o (deg.)	t_o (min. after ANO)		Minutes w/r/t ANO	Hours; Minutes; Seconds (GMT)	Minutes w/r/t ANO	From –	To –	
1131	W	92.8 W	07:14:49	4-28-62	79	44.4	17.6	- 9.6	34.8	64.685	-84.1	07:24:33	9.7			277
1132	W	118.2 W	08:55:07	4-28-62	79	44.4	17.6	- 9.8	34.9	64.675	-79.9	09:09:03	13.9			277
1133	W	143.7 W	10:35:25	4-28-62	79	44.3	17.6	- 9.9	34.9	64.670	-73.8	10:55:03	19.6			277
1134	W	169.1 W	12:15:43	4-28-62	79	44.3	17.7	-10.0	35.0	64.665	-66.5	12:43:03	27.3			277
1135	W	165.4 E	13:56:01	4-28-62	79	44.3	17.7	-10.2	35.0	64.655	-42.9	14:28:33	32.5			277
1136	W	140.0 E	15:36:19	4-28-62	79	44.3	17.7	-10.3	35.2	64.650	-56.3	16:12:03	35.7			277
1145	W	89.1 W	06:38:59	4-29-62	80	44.0	18.0	-11.6	35.5	64.585	-84.5	06:48:33	9.6			278
1146	W	114.6 W	08:19:17	4-29-62	80	43.9	18.0	-11.7	35.7	64.580	- 6.4	08:31:03	11.8			278
1147	W	140.0 W	09:59:35	4-29-62	80	43.9	18.1	-11.8	35.7	64.575	-75.3	10:17:03	17.5			278
1148	W	165.5 W	11:39:53	4-29-62	80	43.9	18.1	-12.0	35.8	64.565	-67.4	12:06:03	26.2			278
1149	W	169.1 E	13:20:11	4-29-62	80	43.9	18.1	-12.1	35.9	64.555	-65.3	13:48:33	28.4			278
1150	W	143.6 E	15:00:29	4-29-62	80	43.9	18.1	-12.2	36.0	64.550	-57.7	15:35:33	35.1			278
1151	N	118.2 E	16:40:47	4-29-62	80	43.9	18.2	-12.4	36.0	64.545	-57.2	17:16:03	35.2			278
1152	N	92.7 E	18:21:04	4-29-62	80	43.8	18.2	-12.6	36.0	64.535	-54.7	19:00:03	39.0			278
1160	W	110.9 W	07:43:27	4-30-62	81	43.6	18.4	-13.7	36.4	64.480	-74.8	07:54:33	11.1			279
1161	W	136.3 W	09:23:45	4-30-62	81	43.6	18.4	-13.9	36.4	64.475	-76.7	09:40:03	16.3			279
1162	W	161.8 W	11:04:03	4-30-62	81	43.6	18.4	-14.0	36.5	64.465	-70.1	11:27:03	23.0			279
1163	W	172.8 E	12:44:21	4-30-62	81	43.5	18.4	-14.2	36.6	64.455	-59.8	13:17:33	33.2	-51.4	-50.4	279
1164	W	147.3 E	14:24:39	4-30-62	81	43.5	18.4	-14.3	36.6	64.450	-58.5	14:59:03	34.4			279
1165	N	121.8 E	16:04:57	4-30-62	81	43.5	18.4	-14.5	36.8	64.445	-59.4	16:39:03	34.1	-35.0	-34.0	279
1166	N	96.4 E	17:45:15	4-30-62	81	43.5	18.5	-14.6	36.8	64.435	-57.3	18:21:03	35.8			279

1174	W	107.2 W	07:07:38	5- 1-62	82	43.3	18.6	−15.8	37.1	64.380	−58.4	07:19:03	11.4			280
1175	W	132.7 W	08:47:55	5- 1-62	82	43.2	18.6	−16.0	37.2	64.375	−74.5	09:05:33	17.6	+15.1	+16.1	280
1176	W	158.1 W	10:28:13	5- 1-62	82	43.2	18.6	−16.1	37.3	64.370	−62.7	10:50:33	22.3			280
1177	W	176.4 E	12:08:31	5- 1-62	82	43.2	18.6	−16.3	37.3	64.360	−66.6	12:35:33	27.0			280
1178	W	151.0 E	13:48:49	5- 1-62	82	43.1	18.6	−16.4	37.4	64.355	−57.4	14:24:23	35.6			280
1188	W	103.5 W	06:31:47	5- 2-62	83	42.9	18.7	−18.0	37.9	64.285	−81.0	06:42:33	10.8			281
1189	W	129.0 W	08:12:05	5- 2-62	83	42.9	18.7	−18.2	38.0	64.280	−75.4	08:29:33	17.5			281
1190	W	154.5 W	09:52:23	5- 2-62	83	42.9	18.7	−18.3	38.0	64.270	−69.9	10:15:33	23.2			281
1191	W	179.9 W	11:32:41	5- 2-62	83	42.9	18.7	−18.5	38.1	64.265	−67.2	11:59:03	26.4			281
1192	W	154.6 E	13:12:59	5- 2-62	83	42.8	18.7	−18.6	38.1	64.260	−62.3	13:44:33	31.4			281
1202	W	99.9 W	05:55:57	5- 3-62	84	42.6	18.7	−20.3	38.5	64.185	−82.4	06:05:03	9.1			282
1203	W	125.3 W	07:36:15	5- 3-62	84	42.3	18.8	−20.3	38.7	64.180	−76.6	07:52:03	15.8			282
1204	W	150.8 W	09:16:33	5- 3-62	84	42.0	18.8	−20.3	38.7	64.170	−72.2	09:37:33	21.0			282
1205	W	176.2 W	10:56:51	5- 3-62	84	41.7	18.8	−20.3	38.9	64.165	−67.7	11:22:03	25.2			282
1206	W	158.3 E	12:37:09	5- 3-62	84	41.5	18.8	−20.3	39.1	64.155	−60.1	13:10:03	32.9			282
1207	N	132.9 E	14:17:27	5- 3-62	84	41.2	18.9	−20.4	39.1	64.150	−61.4	14:47:27	30.0			282
1208	N	107.4 E	15:57:45	5- 3-62	84	40.9	19.1	−20.5	39.2	64.140	−37.2	16:32:33	34.8			282
1217	W	121.7 W	07:00:25	5- 4-62	85	37.8	20.0	−20.9	40.5	64.070	− 1.2	07:14:33	14.1			283
1218	W	147.1 W	08:40:43	5- 4-62	85	37.5	20.0	−20.9	40.6	64.065	−69.8	09:00:33	19.8			283
1219	W	172.6 W	10:21:01	5- 4-62	85	37.2	20.1	−20.9	40.7	64.055	−69.0	10:45:03	24.0			283
1220	W	162.0 E	12:01:19	5- 4-62	85	36.9	20.1	−21.0	40.9	64.050	−63.3	12:31:07	29.8			283
1221	N	136.5 E	13:41:36	5- 4-62	85	36.7	20.1	−21.0	40.9	64.040	−65.3	14:09:33	28.0			283
1222	N	111.1 E	15:21:54	5- 4-62	85	36.4	20.2	−21.1	41.1	64.035	−57.1	15:56:03	34.2	−38.9	−37.9	283
1230	W	92.5 W	04:44:17	5- 5-62	86	33.6	20.9	−21.6	42.2	63.974	−14.4	04:54:33	10.3			284
1231	W	118.0 W	06:24:35	5- 5-62	86	33.3	20.9	−21.6	42.4	63.964	−81.4	06:37:03	12.5			284
1233	W	168.9 W	09:45:10	5- 5-62	86	32.7	20.9	−21.6	42.6	63.954	−70.7	10:10:33	25.4			284
1234	W	165.7 E	11:25:28	5- 5-62	86	32.4	20.9	−21.6	42.7	63.944	−63.5	11:55:33	30.1			284

READOUT ORBIT											TIME INTERVAL OF FILE ON FMR TAPE					FMR Tape Reel No.
Orbit No.	CDA Sta.	Satellite Equator Crossing at Orbital Ascending Node (ANO)				Spin Vector Attitude				Spin Rate (deg./sec.)	Begin	End		Dropouts, Minutes w/r/t ANO		
		Earth Longitude (degrees)	Hours; Minutes; Seconds (GMT)	Calendar Date	Julian Date	Decl. (deg.)	R.A. (deg.)	η_o (deg.)	t_o (min. after ANO)		Minutes w/r/t ANO	Hours; Minutes; Seconds (GMT)	Minutes w/r/t ANO	From –	To –	
1235	W	140.2 E	13:05:46	5- 5-62	86	32.1	20.9	-21.7	42.8	63.934	-59.7	13:40:22	34.6			284
1236	N	114.8 E	14:46:04	5- 5-62	86	31.8	20.9	-21.7	42.9	63.929	-60.3	15:19:03	33.0			284
1237	N	89.3 E	16:26:22	5- 5-62	86	31.5	21.0	-21.8	43.1	63.924	+ 2.4	17:05:33	39.2			284
1244	W	88.9 W	04:08:27	5- 6-62	87	29.0	21.4	-22.2	44.0	63.869	-84.6	04:17:33	11.1			285
1245	W	114.3 W	05:48:44	5- 6-62	87	28.7	21.4	-22.2	44.2	63.864	-82.0	06:00:43	12.0			285
1246	W	139.8 W	07:29:02	5- 6-62	87	28.4	21.4	-22.2	44.4	63.854	-36.3	07:46:13	17.2	+16.0	+17.0	285
1247	W	165.2 W	09:09:20	5- 6-62	87	28.1	21.5	-22.2	44.4	63.849	- 7.9	09:32:43	23.4			285
1248	W	169.3 E	10:49:38	5- 6-62	87	27.8	21.5	-22.2	44.6	63.839	-65.0	11:18:13	28.6			285
1249	W	143.9 E	12:29:56	5- 6-62	87	27.5	21.5	-22.3	44.6	63.834	-59.6	13:03:43	33.8			285
1250	N	118.4 E	14:10:14	5- 6-62	87	27.2	21.5	-22.4	44.8	63.824	-57.8	14:44:33	34.3			285
1259	W	110.6 W	05:12:54	5- 7-62	88	24.1	21.8	-22.9	46.1	63.759	-79.5	05:26:33	13.7			286
1260	W	136.1 W	06:53:12	5- 7-62	88	23.8	21.8	-22.9	46.2	63.749	-75.5	07:11:13	18.0			286
1261	W	161.5 W	08:33:30	5- 7-62	88	23.5	21.8	-22.9	46.3	63.744	-69.2	08:56:43	23.2			286
1262	W	173.0 E	10:13:47	5- 7-62	88	23.2	21.8	-22.9	46.4	63.734	-42.9	10:45:43	31.9			286
1263	W	147.6 E	11:54:05	5- 7-62	88	23.0	21.9	-22.9	46.4	63.729	-59.8	12:28:05	34.0			286
1273	W	107.0 W	04:37:02	5- 8-62	89	19.3	22.2	-23.5	48.1	63.654	-81.8	04:49:03	12.0			287
1274	W	132.4 W	06:17:20	5- 8-62	89	19.0	22.2	-23.5	48.2	63.649	-76.3	06:34:33	17.2	+15.7	+16.7	287
1275	W	157.9 W	07:57:38	5- 8-62	89	18.7	22.3	-23.5	48.3	63.639	- 3.2	08:21:25	23.8			287
1276	W	176.7 E	09:37:56	5- 8-62	89	18.4	22.3	-23.5	48.5	63.634	-63.8	10:07:03	29.1	-63.9	-62.9	287
1277	W	151.2 E	11:18:14	5- 8-62	89	18.7	22.3	-23.5	48.5	63.624	-61.4	11:50:03	31.8			287
1287	W	103.3 W	04:01:12	5- 9-62	90	14.8	22.5	-24.1	50.0	63.549	-81.7	04:13:03	11.9			288

1288	W	128.7 W	05:41:30	5- 9-62	90	14.5	22.5	-24.2	50.2	63.544	-77.1	05:58:03	16.6			288
1289	W	154.2 W	07:21:47	5- 9-62	90	14.2	22.6	-24.2	50.2	63.534	-70.8	07:44:33	22.8			288
1290	W	179.6 W	09:02:05	5- 9-62	90	13.9	22.6	-24.2	50.3	63.529	-64.9	09:30:33	28.5			288
1291	W	154.9 E	10:42:23	5- 9-62	90	13.7	22.7	-24.2	50.4	63.519	-60.2	11:15:03	32.7			288
1292	W	129.5 E	12:22:41	5- 9-62	90	13.4	22.7	-24.2	50.5	63.514	-55.8	13:00:03	37.4			288
1301	W	99.6 W	03:25:21	5-10-62	91	10.5	23.0	-24.9	51.9	63.444	-82.5	03:36:33	11.2			289
1302	W	125.1 W	05:05:39	5-10-62	91	10.2	23.0	-24.9	52.1	63.439	-77.7	05:21:03	15.4			289
1303	N	150.5 W	06:45:56	5-10-62	91	9.4	23.0	-24.5	52.3	63.429	-10.5	06:57:03	11.1			289
1304	W	176.0 W	08:26:14	5-10-62	91	8.6	23.0	-24.1	52.5	63.424	-65.1	08:54:33	28.3			289
1305	N	158.6 E	10:06:32	5-10-62	91	7.8	23.0	-23.8	52.7	63.419	-64.8	10:30:03	23.5			289
1316	W	121.4 W	04:29:48	5-11-62	92	- 2.0	25.2	-21.0	56.2	63.349	-77.6	04:45:33	15.8			290
1317	W	146.8 W	06:10:05	5-11-62	92	- 2.8	25.2	-20.7	56.4	63.339	-71.4	06:31:33	21.5			290
1318	W	172.3 W	07:50:23	5-11-62	92	- 3.5	25.2	-20.4	56.6	63.334	-66.0	08:17:33	27.2			290
1319	W	162.3 E	09:30:41	5-11-62	92	- 4.3	25.2	-20.0	56.8	63.329	-60.1	10:03:33	32.9			290
1320	N	136.8 E	11:10:59	5-11-62	92	- 5.6	25.3	-19.7	57.0	63.319	-55.7	11:48:33	37.6			290
1329	W	92.3 W	02:13:39	5-12-62	93	-12.7	28.8	-17.9	59.8	63.264	-22.7	02:24:03	10.4			291
1330	W	117.7 W	03:53:57	5-12-62	93	-13.4	29.1	-17.6	60.0	63.254	-70.5	04:08:03	14.1			291
1331	W	143.2 W	05:34:14	5-12-62	93	-14.1	29.2	-17.4	60.2	63.249	-71.3	05:55:33	21.3			291
1332	N	168.6 W	07:14:32	5-12-62	93	-14.7	29.3	-17.1	60.4	63.244	-70.5	07:29:33	15.0			291
1333	N	165.9 E	08:54:50	5-12-62	93	-15.4	29.4	-16.8	60.6	63.234	-72.2	09:16:33	21.7			291
1334	N	140.5 E	10:35:08	5-12-62	93	-16.1	29.6	-16.5	60.8	63.229	-64.6	11:03:03	27.9			291
1335	N	115.0 E	12:15:25	5-12-62	93	-16.9	29.9	-16.2	61.3	63.214	-62.1	12:47:03	31.6			291
1336	N	89.6 E	13:55:43	5-12-62	93	-17.7	30.3	-16.0	61.5	63.214	-53.7	14:34:03	38.3			291
1358	W	110.3 W	02:42:14	5-14-62	95	-31.1	43.4	-12.9	68.0	63.074	-79.4	02:56:33	14.3	-52.2	-51.2	292
1359	W	135.8 W	04:22:32	5-14-62	95	-31.4	44.4	-12.8	68.2	63.069	-74.9	04:41:33	19.0			292
1360	W	161.3 W	06:02:50	5-14-62	95	-31.8	45.0	-12.8	68.6	63.064	-69.3	06:27:33	24.7			292
1361	N	173.3 E	07:43:08	5-14-62	95	-32.2	45.4	-12.6	68.8	63.059	-71.2	08:03:33	20.4			292

READOUT ORBIT											TIME INTERVAL OF FILE ON FMR TAPE					FMR Tape Reel No.
Orbit No.	CDA Sta.	Satellite Equator Crossing at Orbital Ascending Node (ANO)				Spin Vector Attitude				Spin Rate (deg./sec.)	Begin	End		Dropouts, Minutes w/r/t ANO		
		Earth Longitude (degrees)	Hours; Minutes; Seconds (GMT)	Calendar Date	Julian Date	Decl. (deg.)	R.A. (deg.)	η_o (deg.)	t_o (min. after ANO)		Minutes w/r/t ANO	Hours; Minutes; Seconds (GMT)	Minutes w/r/t ANO	From –	To –	
1362	N	147.8 E	09:23:25	5-14-62	95	-32.6	45.9	-12.4	69.0	63.054	-67.7	09:50:03	26.6			292
1363	N	122.4 E	11:03:43	5-14-62	95	-33.0	46.4	-12.2	69.2	63.044	-60.8	11:36:33	32.8			292
1364	N	96.9 E	12:44:01	5-14-62	95	-33.5	47.2	-12.0	69.4	63.039	-55.9	13:21:33	37.5	- 3.0	- 1.0	292
1372	W	106.7 W	02:06:26	5-15-62	96	-35.8	55.3	-11.8	72.1	62.989	-80.2	02:19:33	13.1	-50.4	-49.4	293
1373	W	132.1 W	03:46:44	5-15-62	96	-35.9	56.1	-11.8	72.3	62.979	-66.3	04:05:33	18.8	+ 4.3	+ 5.3	293
1374	W	157.6 W	05:27:02	5-15-62	96	-36.0	56.7	-11.8	72.5	62.974	-68.7	05:51:33	24.5			293
1375	N	177.0 E	07:07:19	5-15-62	96	-36.1	57.3	-11.8	72.7	62.969	-70.0	07:26:33	19.2			293
1376	N	151.5 E	08:47:37	5-15-62	96	-36.3	57.8	-11.6	72.9	62.959	-67.1	09:13:33	25.9			293
1377	N	126.1 E	10:27:55	5-15-62	96	-36.6	58.5	-11.5	73.1	62.954	-61.1	11:00:33	32.6			293
1378	N	100.6 E	12:08:13	5-15-62	96	-36.8	59.4	-11.3	73.5	62.949	-55.7	12:45:33	37.3			293
1388	W	153.9 W	04:51:11	5-16-62	97	-36.3	69.6	-11.6	76.6	62.884	-41.8	05:12:33	21.4			294
1389	N	179.4 W	06:31:28	5-16-62	97	-36.2	70.2	-11.6	76.8	62.874	-59.5	06:50:33	19.1			294
1390	W	155.2 E	08:11:46	5-16-62	97	-36.1	70.8	-11.7	77.0	62.869	-57.0	08:48:03	36.3			294
1391	W	129.7 E	09:52:04	5-16-62	97	-36.1	71.4	-11.7	77.2	62.864	-55.1	10:30:03	38.0			294
1400	W	99.3 W	00:54:44	5-17-62	98	-33.6	80.4	-12.0	80.0	62.809	-83.4	01:05:03	10.3			295
1401	W	124.8 W	02:35:02	5-17-62	98	-33.1	81.0	-12.3	80.2	62.804	-77.1	02:51:26	16.4			295
1402	W	150.2 W	04:15:19	5-17-62	98	-32.6	81.5	-12.5	80.4	62.799	-70.8	04:37:33	22.2			295
1403	W	175.7 W	05:55:37	5-17-62	98	-32.2	82.0	-12.7	80.9	62.794	-64.3	06:24:33	28.9			295
1404	W	158.9 E	07:35:55	5-17-62	98	-31.9	82.4	-12.8	81.1	62.784	-63.3	08:06:03	30.1			295
1405	W	133.4 E	09:16:13	5-17-62	98	-31.7	83.0	-12.8	81.3	62.779	-54.7	09:54:33	38.3			295
1406	N	108.0 E	10:56:31	5-17-62	98	-31.5	83.4	-12.7	81.4	62.774	-55.9	11:29:03	32.5			295

1407	N	82.5 E	12:36:48	5-17-62	98	−31.5	83.4	−12.6	81.5	62.769	−53.0	13:17:03	40.3			295
1414	W	95.7 W	00:18:53	5-18-62	99	−31.5	83.4	−12.0	81.9	62.724	−81.2	00:30:33	11.7			296
1415	W	121.1 W	01:59:11	5-18-62	99	−31.5	83.4	−11.9	82.0	62.719	−77.3	02:15:33	16.4			296
1416	W	146.6 W	03:39:28	5-18-62	99	−31.4	83.4	−11.8	82.1	62.714	−70.8	04:01:33	22.1			296
1417	W	172.0 W	05:19:46	5-18-62	99	−31.4	83.3	−11.7	82.2	62.709	−65.2	05:47:33	27.8			296
1418	N	162.5 E	07:00:04	5-18-62	99	−31.4	83.3	−11.6	82.2	62.704	−67.6	07:23:33	23.5			296
1419	N	137.1 E	08:40:22	5-18-62	99	−31.4	83.3	−11.6	82.3	62.694	−62.0	09:10:33	30.2			296
1420	N	111.6 E	10:20:39	5-18-62	99	−31.4	83.3	−11.4	82.4	62.689	−58.3	10:55:03	34.4	+16.4	+17.4	296
1421	N	86.2 E	12:00:57	5-18-62	99	−31.4	83.3	−11.4	82.6	62.684	−53.1	12:40:33	39.6			296
1428	W	92.0 W	23:43:02	5-18-62	99	−31.3	83.3	−10.7	83.0	62.639	−81.5	23:54:03	11.0			297
1429	W	117.4 W	01:23:19	5-19-62	100	−31.3	83.3	−10.6	83.0	62.634	−81.0	01:35:03	11.7			297
1430	W	142.9 W	03:03:37	5-19-62	100	−31.3	83.3	−10.5	83.1	62.629	−72.5	03:24:33	20.9			297
1431	W	168.3 W	04:43:55	5-19-62	100	−31.3	83.3	−10.4	83.1	62.624	−66.1	05:10:33	26.6			297
1432	W	166.2 E	06:24:13	5-19-62	100	−31.3	83.3	−10.3	83.2	62.619	−60.7	06:56:33	32.3			297
1433	W	140.8 E	08:04:30	5-19-62	100	−31.3	83.3	−10.2	83.3	62.614	−56.2	08:41:33	37.1			297
1443	W	113.8 W	00:47:28	5-20-62	101	−30.9	83.3	− 9.2	84.0	62.549	−82.7	00:58:33	11.1			298
1444	W	139.2 W	02:27:46	5-20-62	101	−30.9	83.4	− 9.2	84.0	62.544	−74.5	02:46:33	18.8			298
1445	W	164.7 W	04:08:04	5-20-62	101	−30.8	83.4	− 9.0	84.1	62.539	−66.8	04:34:33	26.5			298
1446	W	169.9 E	05:48:22	5-20-62	101	−30.8	83.4	− 9.0	84.2	62.534	−61.2	06:20:33	32.2			298
1447	W	144.4 E	07:28:39	5-20-62	101	−30.8	83.4	− 8.8	84.4	62.524	−56.7	08:05:33	36.9			298
1457	W	110.1 W	00:11:37	5-21-62	102	−30.3	83.8	− 7.7	85.1	62.469	−79.1	00:25:33	13.9			299
1458	W	135.5 W	01:51:55	5-21-62	102	−30.3	83.8	− 7.5	85.2	62.464	−73.4	02:11:33	19.6			299
1459	W	161.0 W	03:32:13	5-21-62	102	−30.3	83.8	− 7.4	85.3	62.459	−67.8	03:57:33	25.3			299
1460	W	173.6 E	05:12:30	5-21-62	102	−30.2	83.8	− 7.3	85.4	62.454	−61.9	05:43:33	31.1			299
1461	W	148.1 E	06:52:48	5-21-62	102	−30.2	83.8	− 7.2	85.4	62.444	−57.5	07:28:33	35.8			299
1471	W	106.4 W	23:35:46	5-21-62	102	−29.7	84.2	− 6.1	86.2	62.384	−78.9	23:49:33	13.8			300
1472	W	131.8 W	01:16:03	5-22-62	103	−29.7	84.2	− 6.0	86.2	62.379	−73.9	01:34:33	18.5			300

729-166 O - 64 - 8

READOUT ORBIT											TIME INTERVAL OF FILE ON FMR TAPE					
Orbit No.	CDA Sta.	Satellite Equator Crossing at Orbital Ascending Node (ANO)				Spin Vector Attitude				Spin Rate (deg./sec.)	Begin	End		Dropouts, Minutes w/r/t ANO		FMR Tape Reel No.
		Earth Longitude (degrees)	Hours; Minutes; Seconds (GMT)	Calendar Date	Julian Date	Decl. (deg.)	R.A. (deg.)	η_o (deg.)	t_o (min. after ANO)		Minutes w/r/t ANO	Hours; Minutes; Seconds (GMT)	Minutes w/r/t ANO	From –	To –	
1473	W	157.3 W	02:56:21	5-22-62	103	-29.6	84.2	- 5.9	86.4	62.374	-68.7	03:20:33	24.2			300
1474	W	177.2 E	04:36:39	5-22-62	103	-29.6	84.2	- 5.8	86.4	62.369	-62.5	05:06:33	29.9			300
1475	N	151.8 E	06:16:57	5-22-62	103	-29.5	84.3	- 5.6	86.5	62.364	-61.4	06:43:33	26.6			300
1476	N	126.3 E	07:57:15	5-22-62	103	-29.5	84.3	- 5.5	86.6	62.354	-60.6	08:29:33	32.3			300
1477	N	100.9 E	09:37:32	5-22-62	103	-29.5	84.3	- 5.3	86.7	62.349	-51.6	10:15:33	38.0			300
1485	W	102.7 W	22:59:54	5-22-62	103	-29.0	84.7	- 4.3	87.3	62.304	-63.8	23:12:33	12.7			301
1486	W	128.2 W	00:40:12	5-23-62	104	-28.9	84.7	- 4.2	87.4	62.294	-75.7	00:57:33	17.4			301
1487	W	153.6 W	02:20:30	5-23-62	104	-28.9	84.7	- 4.0	87.5	62.289	-70.7	02:43:03	22.6			301
1488	W	179.1 W	04:00:48	5-23-62	104	-28.8	84.7	- 3.9	87.5	62.284	-63.1	04:30:33	29.8			301
1489	W	155.5 E	05:41:06	5-23-62	104	-28.8	84.7	- 3.8	87.6	62.279	-61.3	06:12:33	31.5			301
1490	W	130.0 E	07:21:23	5-23-62	104	-28.7	84.7	- 3.6	87.7	62.274	-55.0	07:59:33	38.2			301
1499	W	99.0 W	22:24:03	5-23-62	104	-28.1	85.1	- 2.3	88.4	62.219	-80.3	22:36:33	12.5			302
1500	W	124.5 W	00:04:21	5-24-62	105	-28.1	85.2	- 2.2	88.4	62.214	-75.4	00:21:33	17.2			302
1501	W	149.9 W	01:44:39	5-24-62	105	-28.0	85.2	- 2.1	88.5	62.209	-70.2	02:07:33	22.9			302
1503	W	159.1 E	05:05:15	5-24-62	105	-27.9	85.3	- 1.8	88.7	62.194	-58.9	05:39:56	34.7			302
1504	W	133.7 E	06:45:32	5-24-62	105	-27.8	85.3	- 1.7	88.8	62.189	-54.6	07:24:03	38.5			302
1513	W	95.4 W	21:48:12	5-24-62	105	-27.2	85.7	- 0.3	89.5	62.134	-81.4	22:00:03	11.9			303
1514	W	120.8 W	23:28:30	5-24-62	105	-27.2	85.7	- 0.3	89.6	62.129	-76.8	23:44:33	16.1			303
1515	W	146.3 W	01:08:48	5-25-62	106	-27.0	85.7	- 0.2	89.7	62.124	-72.2	01:30:33	21.8			303
1516	W	171.7 W	02:49:05	5-25-62	106	-27.0	85.8	0.3	89.7	62.119	-65.1	03:17:03	28.0			303
1517	W	162.8 E	04:29:23	5-25-62	106	-26.9	85.8	0.4	89.8	62.114	-59.8	05:02:33	33.2			303

1518	W	137.4 E	06:09:41	5-25-62	106	−26.8	85.8	0.5	89.9	62.104	−54.1	06:47:33	37.9			303
1519	N	111.9 E	07:49:59	5-25-62	106	−26.8	85.8	0.6	90.0	62.099	−54.0	08:25:33	35.6			303
1520	N	86.5 E	09:30:17	5-25-62	106	−26.7	85.9	0.8	90.0	62.094	−52.7	10:10:33	40.3			303
1527	W	91.7 W	21:12:21	5-25-62	106	−26.1	86.2	1.9	90.6	62.054	−82.2	21:23:33	11.2			304
1528	W	117.1 W	22:52:39	5-25-62	106	−26.0	86.2	2.0	90.7	62.044	−81.2	23:04:03	11.4			304
1529	W	142.6 W	00:32:57	5-26-62	107	−26.0	86.3	2.2	90.8	62.039	−75.2	00:50:33	17.6			304
1530	W	168.0 W	02:13:14	5-26-62	107	−25.9	86.3	2.3	90.8	62.034	−65.5	02:40:33	27.3			304
1531	W	166.5 E	03:53:32	5-26-62	107	−25.8	86.3	2.5	90.9	62.029	−59.0	04:26:33	33.0			304
1532	W	141.0 E	05:33:50	5-26-62	107	−25.8	86.3	2.6	91.0	62.024	+ 7.4	06:10:33	36.7			304
1533	N	115.6 E	07:14:08	5-26-62	107	−25.7	86.4	2.8	91.1	62.014	−37.2	07:48:33	34.4			304
1534	N	90.1 E	08:54:25	5-26-62	107	−25.6	86.4	3.0	91.1	62.009	−54.2	09:33:33	39.1			304
1541	W	88.0 W	20:36:30	5-26-62	107	−25.0	86.7	4.1	91.7	61.969	−30.9	20:47:33	11.1			305
1542	W	113.5 W	22:16:48	5-26-62	107	−24.9	86.7	4.3	91.8	61.964	−80.5	22:29:03	12.3			305
1543	N	138.9 W	23:57:05	5-26-62	107	−24.8	86.8	4.4	91.9	61.959	−67.1	00:07:33	10.5			305
1544	N	164.4 W	01:37:23	5-27-62	108	−24.8	86.8	4.6	91.9	61.954	−78.1	01:52:33	15.2			305
1545	N	170.2 E	03:17:41	5-27-62	108	−24.7	86.8	4.8	92.0	61.949	−71.0	03:39:33	21.9			305
1546	N	144.7 E	04:57:59	5-27-62	108	−24.6	86.8	4.9	92.1	61.939	−64.5	05:26:33	28.6			305
1547	N	119.3 E	06:38:17	5-27-62	108	−24.5	86.9	5.1	92.2	81.141	+ 3.1	07:12:33	34.3	+16.7	+18.7	305
1548	N	93.8 E	08:18:34	5-27-62	108	−24.5	86.9	5.3	92.2	81.134	−54.0	08:57:33	39.0	−34.6	−33.6	305
														+17.4	+19.4	
														+37.4	+38.4	
1555	W	84.3 W	20:00:39	5-27-62	108	−23.9	87.2	6.5	92.8	81.079	−80.4	20:12:33	11.9			306
1556	W	109.8 W	21:40:57	5-27-62	108	−23.8	87.2	6.7	92.9	81.071	−78.9	21:55:03	14.1			306
1557	W	135.2 W	23:21:14	5-27-62	108	−23.8	87.2	6.8	93.0	81.061	−74.3	23:40:03	18.8	−33.2	−32.2	306
														+17.8	+19.8	
1558	W	160.7 W	01:01:32	5-28-62	109	−23.7	87.3	7.0	93.0	81.056	−69.2	01:26:33	25.0	+17.5	+18.5	306
1559	N	173.9 E	02:41:50	5-28-62	109	−23.6	87.3	7.2	93.1	81.046	−59.8	03:02:33	20.7	+18.2	+19.2	306

READOUT ORBIT											TIME INTERVAL OF FILE ON FMR TAPE					FMR Tape Reel No.
Orbit No.	CDA Sta.	Satellite Equator Crossing at Orbital Ascending Node (ANO)				Spin Vector Attitude				Spin Rate (deg./sec.)	Begin	End		Dropouts, Minutes w/r/t ANO		
		Earth Longitude (degrees)	Hours; Minutes; Seconds (GMT)	Calendar Date	Julian Date	Decl. (deg.)	R.A. (deg.)	η_o (deg.)	t_o (min. after ANO)		Minutes w/r/t ANO	Hours; Minutes; Seconds (GMT)	Minutes w/r/t ANO	From –	To –	
1560	N	148.4 E	04:22:08	5-28-62	109	–23.5	87.3	7.4	93.2	81.041	–65.7	04:49:23	27.4	+17.9	+18.9	306
														–33.7	–32.7	
1562	N	97.5 E	07:42:43	5-28-62	109	–23.4	87.4	7.7	93.3	81.021	–49.0	08:23:46	41.1	+17.3	+21.3	306
1570	W	106.1 W	21:05:05	5-28-62	109	–22.7	87.7	9.2	93.9	80.961	–79.4	21:19:03	14.0	–33.1	–31.1	307
1588	N	155.8 E	03:10:23	5-30-62	111	– 9.4	91.0	6.6	98.3	80.821	–65.5	03:34:33	24.2	–32.4	–31.4	308
														–27.4	–26.4	
														+23.6	+24.6	
1590	N	104.9 E	06:30:59	5-30-62	111	– 9.0	91.1	6.8	98.6	80.801	–55.9	07:08:33	37.6	+23.0	+26.0	308
1591	N	79.4 E	08:11:16	5-30-62	111	– 8.8	91.2	7.0	98.8	80.796	–51.4	08:52:03	40.8	–27.3	–24.3	308
														+23.7	+24.7	
1598	W	98.8 W	19:53:21	5-30-62	111	– 7.6	91.9	8.4	99.4	80.741	–81.4	20:05:33	12.2	–76.4	–75.4	309
														–29.4	–28.4	
1599	W	124.2 W	21:33:39	5-30-62	111	– 7.5	91.9	8.5	99.6	80.731	–76.9	21:50:33	16.9	–75.6	–74.6	309
														–26.6	–25.6	
1600	W	149.7 W	23:13:56	5-30-62	111	– 7.3	92.0	8.7	99.6	80.726	–70.3	23:36:33	22.6			309
1601	W	175.1 W	00:54:14	5-31-62	112	– 7.2	92.0	8.9	99.8	80.721	–61.9	01:25:03	30.8	–25.2	–23.2	309
														+26.8	+27.8	
1602	N	159.4 E	02:34:32	5-31-62	112	– 7.1	92.0	9.1	100.0	80.711	–64.6	02:58:33	24.0	–26.5	–24.5	309
1603	N	134.0 E	04:14:50	5-31-62	112	– 7.0	92.1	9.2	100.0	80.701	–54.6	04:53:33	38.7	–25.8	–24.8	309
														+25.2	+26.2	

1604	N	108.5 E	05:55:07	5-31-62	112	– 6.8	92.2	9.4	100.1	80.696	–46.1	06:31:33	36.4	–30.1	–29.1	309
														–26.1	–25.1	
														+23.9	+25.9	
1605	N	83.1 E	07:35:25	5-31-62	112	– 6.7	92.2	9.7	100.1	80.686	–46.3	08:16:33	41.1	–26.4	–25.4	309
														–24.4	–23.4	
														+24.6	+26.6	
1612	W	95.1 W	19:17:30	5-31-62	112	– 5.5	92.9	11.0	0.7	80.631	–82.4	19:28:33	11.1	–74.5	–73.5	310
														–26.5	–24.5	
1613	W	120.5 W	20:57:47	5-31-62	112	– 5.3	93.0	11.2	0.7	80.626	–77.5	21:13:33	15.8			310
1614	W	146.0 W	22:38:05	5-31-62	112	– 5.2	93.0	11.3	0.9	80.621	–71.7	22:59:33	21.5			310
1615	W	171.4 W	00:18:23	6- 1-62	113	– 5.1	93.0	11.5	1.1	80.611	–65.1	00:46:33	28.2	–24.4	–23.4	310
1616	N	163.1 E	01:58:41	6- 1-62	113	– 5.0	93.1	11.7	1.0	80.601	–66.3	02:21:33	22.9	–24.7	–23.7	310
1617	N	137.7 E	03:38:58	6- 1-62	113	– 4.8	93.1	11.9	1.2	80.596	–63.6	04:08:33	29.6	–25.0	–24.0	310
														+26.0	+27.0	
1618	N	112.2 E	05:19:16	6- 1-62	113	– 4.7	93.2	12.0	1.3	80.586	–58.0	05:54:33	35.3	+26.7	+27.7	310
1619	N	86.8 E	06:59:34	6- 1-62	113	– 4.5	93.3	12.2	1.4	80.581	–37.9	07:39:33	40.0	–24.6	–23.6	310
														+26.4	+27.4	
1627	W	116.8 W	20:21:56	6- 1-62	113	– 3.3	94.0	13.7	2.3	80.516	–77.9	20:37:03	15.1	–23.9	–22.9	311
1628	W	142.3 W	22:02:14	6- 1-62	113	– 3.0	94.1	13.8	2.4	80.511	–71.8	22:23:33	21.3			311
1629	W	167.8 W	23:42:32	6- 1-62	113	– 2.9	94.1	14.0	2.5	80.501	–65.8	00:09:33	27.0	–23.5	–22.5	311
1630	W	166.8 E	01:22:50	6- 2-62	114	– 2.7	94.2	14.2	2.6	80.491	–60.6	01:55:33	32.7			311
1631	W	141.3 E	03:03:07	6- 2-62	114	– 2.6	94.2	14.4	2.6	80.486	–55.8	03:40:33	37.4	–23.1	–22.1	311
1632	N	115.9 E	04:43:25	6- 2-62	114	– 2.5	94.3	14.6	2.7	80.476	– 8.2	05:18:33	35.1	+27.6	+28.6	311
1640	W	87.7 W	18:05:47	6- 2-62	114	– 1.1	95.1	16.0	3.8	80.416	–82.6	18:16:33	10.8			312
1641	W	113.2 W	19:46:05	6- 2-62	114	– 1.0	95.2	16.2	3.8	80.406	–78.9	20:00:33	14.4			312
1642	W	138.6 W	21:26:23	6- 2-62	114	– 0.8	95.2	16.4	3.9	80.401	–72.5	21:47:03	20.7			312
1643	N	164.1 W	23:06:41	6- 2-62	114	– 0.7	95.3	16.5	4.1	80.391	–74.4	23:22:03	15.4	–71.7	–70.7	312

READOUT ORBIT											TIME INTERVAL OF FILE ON FMR TAPE					FMR Tape Reel No.
Orbit No.	CDA Sta.	Satellite Equator Crossing at Orbital Ascending Node (ANO)				Spin Vector Attitude				Spin Rate (deg./sec.)	Begin	End		Dropouts, Minutes w/r/t ANO		
		Earth Longitude (degrees)	Hours; Minutes; Seconds (GMT)	Calendar Date	Julian Date	Decl. (deg.)	R.A. (deg.)	η_o (deg.)	t_o (min. after ANO)		Minutes w/r/t ANO	Hours; Minutes; Seconds (GMT)	Minutes w/r/t ANO	From –	To –	
1644	N	170.5 E	00:46:58	6- 3-62	115	– 0.6	95.3	16.7	4.2	80.386	–72.3	01:08:03	21.1	–71.0	–70.0	312
														–22.0	–21.0	
1645	N	145.0 E	02:27:16	6- 3-62	115	– 0.5	95.4	16.9	4.2	80.376	+ 3.4	02:55:33	28.3			312
1646	N	119.6 E	04:07:34	6- 3-62	115	– 0.3	95.4	17.1	4.4	80.366	–58.6	04:42:03	34.5	+29.4	+30.4	312
1647	N	94.2 E	05:47:52	6- 3-62	115	– 0.2	95.5	17.3	4.4	80.356	–53.8	06:26:33	38.7			312
1654	W	84.0 W	17:29:56	6- 3-62	115	0.9	96.3	18.6	5.3	80.306	–83.9	17:39:33	9.6	–20.9	–18.9	313
1655	W	109.5 W	19:10:14	6- 3-62	115	1.1	96.4	18.7	5.4	80.301	–76.4	19:27:03	16.8	–21.2	–20.2	313
1656	W	134.9 W	20:50:32	6- 3-62	115	1.2	96.4	18.9	5.5	80.291	–74.4	21:09:33	19.0	–69.5	–68.5	313
														–20.5	–19.5	
1657	W	160.4 W	22:30:50	6- 3-62	115	1.3	96.5	19.1	5.6	80.281	–67.2	22:56:33	25.7			313
1658	W	174.1 E	00:11:07	6- 4-62	116	1.4	96.5	19.3	5.8	80.276	–61.0	00:42:33	31.4	–20.1	–19.1	313
1659	W	148.7 E	01:51:25	6- 4-62	116	1.5	96.6	19.4	5.8	80.266	–59.2	02:24:33	33.1	–20.4	–19.4	313
														+30.6	+31.6	
1669	W	105.8 W	18:34:23	6- 4-62	116	3.1	97.6	21.2	7.0	80.191	–80.7	18:47:03	12.7	–68.4	–67.4	314
1670	W	131.3 W	20:14:41	6- 4-62	116	3.2	97.7	21.3	7.1	80.181	–76.3	20:32:03	17.4	–18.7	–17.7	314
1672	N	177.8 E	23:35:17	6- 4-62	116	3.4	97.8	21.6	7.4	80.166	–73.8	23:54:33	19.3			314
1675	N	101.5 E	04:36:10	6- 5-62	117	3.8	98.0	22.1	7.8	80.141	–45.3	05:13:33	37.4	+32.8	+33.8	314
1683	W	102.1 W	17:58:32	6- 5-62	117	5.1	98.9	23.3	8.7	80.081	–82.0	18:10:03	11.5	–17.5	–16.5	315
1684	W	127.6 W	19:38:50	6- 5-62	117	5.2	99.0	23.5	8.8	80.071	–75.3	19:56:33	17.7			315
1685	W	153.1 W	21:19:08	6- 5-62	117	5.3	99.0	23.6	8.9	80.061	–71.5	21:41:03	21.9			315
1686	N	178.5 W	22:59:26	6- 5-62	117	5.4	99.1	23.8	9.0	80.056	–71.4	23:18:33	19.1	–66.4	–65.4	315

1687	N	156.1 E	00:39:43	6- 6-62	118	5.5	99.1	23.9	9.2	80.046	−68.3	01:04:33	24.8			315
1688	N	130.6 E	02:20:01	6- 6-62	118	5.6	99.2	24.1	9.2	80.041	−61.6	02:51:33	31.5			315
1690	N	79.7 E	05:40:37	6- 6-62	118	5.9	99.4	24.4	9.6	80.021	−52.5	06:21:33	40.9			315
1697	W	98.5 W	17:22:41	6- 6-62	118	6.9	100.3	25.4	10.5	79.966	−79.9	17:34:33	11.9	−15.7	−14.7	316
1698	W	123.9 W	19:02:59	6- 6-62	118	7.0	100.4	25.6	10.5	79.961	−77.0	19:19:33	16.6			316
1699	W	149.4 W	20:43:17	6- 6-62	118	7.1	100.4	25.7	10.7	79.951	−70.3	21:06:33	23.3			316
1700	W	174.8 W	22:23:35	6- 6-62	118	7.2	100.5	25.9	10.8	79.946	−64.5	22:52:33	29.0			316
1701	N	159.7 E	00:03:53	6- 7-62	119	7.3	100.6	26.0	10.9	79.941	−64.7	00:28:33	24.7	−64.9	−63.9	316
1702	N	134.3 E	01:44:10	6- 7-62	119	7.4	100.6	26.2	11.1	79.931	−61.2	02:14:33	30.4			316
1703	N	108.8 E	03:24:28	6- 7-62	119	7.5	100.7	26.3	11.2	79.921	−17.6	04:00:33	36.1			316
1704	N	83.4 E	05:04:46	6- 7-62	119	7.7	100.9	26.4	11.2	79.916	−52.4	05:45:33	40.8			316
1711	W	94.8 W	16:46:51	6- 7-62	119	8.5	101.8	27.5	12.1	79.866	−15.9	16:59:33	12.7			317
1712	W	120.3 W	18:27:08	6- 7-62	119	8.5	101.8	27.6	12.3	79.861	−77.3	18:43:33	16.4	−14.1	−13.1	317
1713	N	145.7 W	20:07:26	6- 7-62	119	8.6	101.9	27.8	12.5	79.856	−78.4	20:19:56	12.5			317
1714	N	171.2 W	21:47:44	6- 7-62	119	8.7	102.0	27.9	12.5	79.846	−75.4	22:04:33	16.8			317
1715	N	163.4 E	23:28:02	6- 7-62	119	8.7	102.0	28.1	12.7	79.841	−69.5	23:51:33	23.5			317
1716	N	137.9 E	01:08:20	6- 8-62	120	8.8	102.1	28.2	12.8	79.836	−18.3	01:38:33	30.2			317
1717	N	112.5 E	02:48:37	6- 8-62	120	8.9	102.2	28.3	12.9	79.826	−57.6	03:24:33	35.9			317
1718	N	87.0 E	04:28:55	6- 8-62	120	9.0	102.3	28.5	13.1	79.821	−51.2	05:09:33	40.6			317
1725	W	91.1 W	16:11:00	6- 8-62	120	9.9	103.2	29.2	14.0	79.771	−79.5	16:21:33	10.6	−62.0	−61.0	318
														−12.0	−11.0	
1726	W	116.6 W	17:51:18	6- 8-62	120	10.0	103.2	29.3	14.2	79.766	−77.5	18:06:33	15.3			318
1727	W	142.0 W	19:31:36	6- 8-62	120	10.1	103.3	29.4	14.4	79.761	−72.3	19:52:33	21.0	−61.6	−60.6	318
1739	W	87.5 W	15:35:09	6- 9-62	121	11.3	104.6	30.6	15.8	79.675	−64.5	15:43:03	7.9	−61.2	−59.2	319
														−10.2	- 9.2	
1741	W	138.4 W	18:55:45	6- 9-62	121	11.5	104.8	30.8	16.2	79.660	−73.7	19:15:33	19.8			319

READOUT ORBIT											TIME INTERVAL OF FILE ON FMR TAPE					FMR Tape Reel No.
Orbit No.	CDA Sta.	Satellite Equator Crossing at Orbital Ascending Node (ANO)				Spin Vector Attitude				Spin Rate (deg./sec.)	Begin	End		Dropouts, Minutes w/r/t ANO		
		Earth Longitude (degrees)	Hours; Minutes; Seconds (GMT)	Calendar Date	Julian Date	Decl. (deg.)	R.A. (deg.)	η_o (deg.)	t_o (min. after ANO)		Minutes w/r/t ANO	Hours; Minutes; Seconds (GMT)	Minutes w/r/t ANO	From –	To –	
1753	W	83.8 W	14:59:19	6-10-62	122	12.5	106.2	31.7	17.7	79.580	–64.6	15:08:33	9.2	–59.3	–57.3	320
														–54.3	–53.3	
1754	W	109.2 W	16:39:36	6-10-62	122	12.5	106.3	31.8	17.9	79.575	–78.5	16:50:03	10.5			320
1756	W	160.1 W	20:00:12	6-10-62	122	12.6	106.5	32.0	18.3	79.560	–71.0	20:22:03	21.9	–58.2	–56.2	320
1758	N	149.0 E	23:20:48	6-10-62	122	12.7	106.6	32.1	18.4	79.545	–67.6	23:46:03	25.3			320
1760	N	98.1 E	02:41:23	6-11-62	123	12.9	106.9	32.2	18.6	79.535	–56.8	03:16:03	34.7	–57.4	–56.4	320
1768	W	105.6 W	16:03:46	6-11-62	123	13.3	108.0	32.8	20.0	79.480	–70.1	16:13:33	9.8			321
1772	W	152.6 E	22:44:59	6-11-62	123	13.5	108.3	33.0	20.3	79.450	–60.8	23:17:27	32.5	–61.0	–60.0	321
1773	W	127.2 E	00:25:17	6-12-62	124	13.5	108.4	33.1	20.5	79.445	–53.2	01:04:03	38.8			321
1782	W	101.9 W	15:27:58	6-12-62	124	13.9	109.7	33.5	21.8	79.385	–64.1	15:39:03	11.1	–55.0	–54.0	322
1784	W	152.8 W	18:48:33	6-12-62	124	13.9	109.9	33.6	22.2	79.370	–68.1	19:09:03	20.5			322
1797	W	123.6 W	16:32:25	6-13-62	125	14.2	111.6	34.0	23.8	79.280	–81.3	16:45:03	12.6			323
1799	W	174.6 W	19:53:01	6-13-62	125	14.2	111.7	34.1	24.2	79.270	–68.4	20:18:03	25.0	–52.0	–51.0	323
1800	N	160.0 E	21:33:19	6-13-62	125	14.2	111.8	34.1	24.4	79.260	–64.4	21:55:03	21.7			323
1801	N	134.5 E	23:13:37	6-13-62	125	14.2	111.9	34.1	24.4	79.255	–65.6	23:41:03	29.4			323
1803	N	83.6 E	02:34:13	6-14-62	126	14.2	112.2	34.1	24.8	79.245	– 3.7	03:13:03	38.8			323
1824	W	90.9 W	13:40:28	6-15-62	127	13.9	113.6	34.2	27.3	79.120	–64.4	13:49:03	8.6	–48.5	–47.5	324
														–15.5	–14.5	
1825	W	116.3 W	15:20:45	6-15-62	127	13.9	113.6	34.1	27.5	79.115	–78.7	15:33:33	12.8			324
1827	N	167.2 W	18:41:21	6-15-62	127	13.9	113.6	34.1	27.7	79.105	–75.3	18:53:33	12.2			324
1841	N	163.6 W	18:05:31	6-16-62	128	13.8	113.8	33.5	29.0	79.020	–81.9	18:17:33	12.0	–46.5	–45.5	325

1854	W	134.4 W	15:49:24	6-17-62	129	13.8	113.9	32.7	30.4	78.945	−73.6	16:05:03	15.6	−45.4	−44.4	326
														−26.4	−25.4	
1855	N	159.9 W	17:29:42	6-17-62	129	13.8	113.9	32.6	30.6	78.940	−73.5	17:40:03	10.4	−45.7	−44.7	326
1868	W	130.8 W	15:13:34	6-18-62	130	13.8	114.0	31.5	31.7	78.860	−74.4	15:28:03	14.5			327
1869	N	156.2 W	16:53:52	6-18-62	130	13.8	114.0	31.4	31.9	78.855	−63.4	17:04:03	10.2			327
1953	N	134.2 W	13:18:52	6-24-62	136	15.7	114.1	18.4	38.4	78.310	−73.0	13:25:43	6.8	−37.9	−36.9	328
1957	N	124.0 E	20:00:04	6-24-62	136	15.8	114.1	17.6	38.7	78.280	−60.4	20:30:03	30.0	+11.9	+12.9	328
1967	W	130.5 W	12:43:03	6-25-62	137	16.3	114.0	15.5	39.5	78.220	−56.7	12:57:43	14.7			329
2011	N	170.4 W	14:16:10	6-28-62	140	15.4	115.1	7.2	42.5	77.915	−77.7	14:32:03	15.9			330
2012	W	164.1 E	15:56:28	6-28-62	140	15.1	115.1	7.1	42.6	77.905	−60.6	16:29:03	32.6	−33.5	−32.5	330
2013	W	138.7 E	17:36:46	6-28-62	140	15.0	115.2	7.0	42.7	77.900	−56.6	18:14:03	37.3	−33.8	−32.8	330
2014	N	113.2 E	19:17:04	6-28-62	140	14.7	115.2	6.9	42.9	77.890	−55.5	19:53:33	36.5			330
2015	N	87.8 E	20:57:22	6-28-62	140	14.5	115.4	6.7	42.9	77.885	−40.7	21:39:19	42.0			330
2022	W	90.4 W	08:39:28	6-29-62	141	12.7	116.2	6.1	44.0	77.835	−79.9	08:51:33	12.1			331
2023	W	115.8 W	10:19:45	6-29-62	141	12.5	116.3	6.0	44.0	77.825	−20.9	10:36:43	17.0	+16.2	+17.2	331
2024	W	141.3 W	12:00:03	6-29-62	141	12.2	116.3	5.9	44.2	77.820	−15.3	12:21:03	21.0			331
2025	W	166.7 W	13:40:21	6-29-62	141	12.0	116.3	5.9	44.4	77.815	−65.8	14:08:03	27.7			331
2028	N	116.9 E	18:41:15	6-29-62	141	11.3	116.4	5.5	44.5	77.790	−56.6	19:17:33	36.3			331
2029	N	91.5 E	20:21:33	6-29-62	141	11.1	116.5	5.4	44.7	77.780	−52.8	21:02:03	40.5			331
2037	W	112.2 W	09:43:56	6-30-62	142	9.0	117.3	4.7	45.8	77.725	−79.5	09:58:03	14.1	−30.9	−29.9	332
2039	W	163.1 W	13:04:32	6-30-62	142	8.5	117.3	4.5	46.0	77.710	−68.2	13:30:03	25.5			332

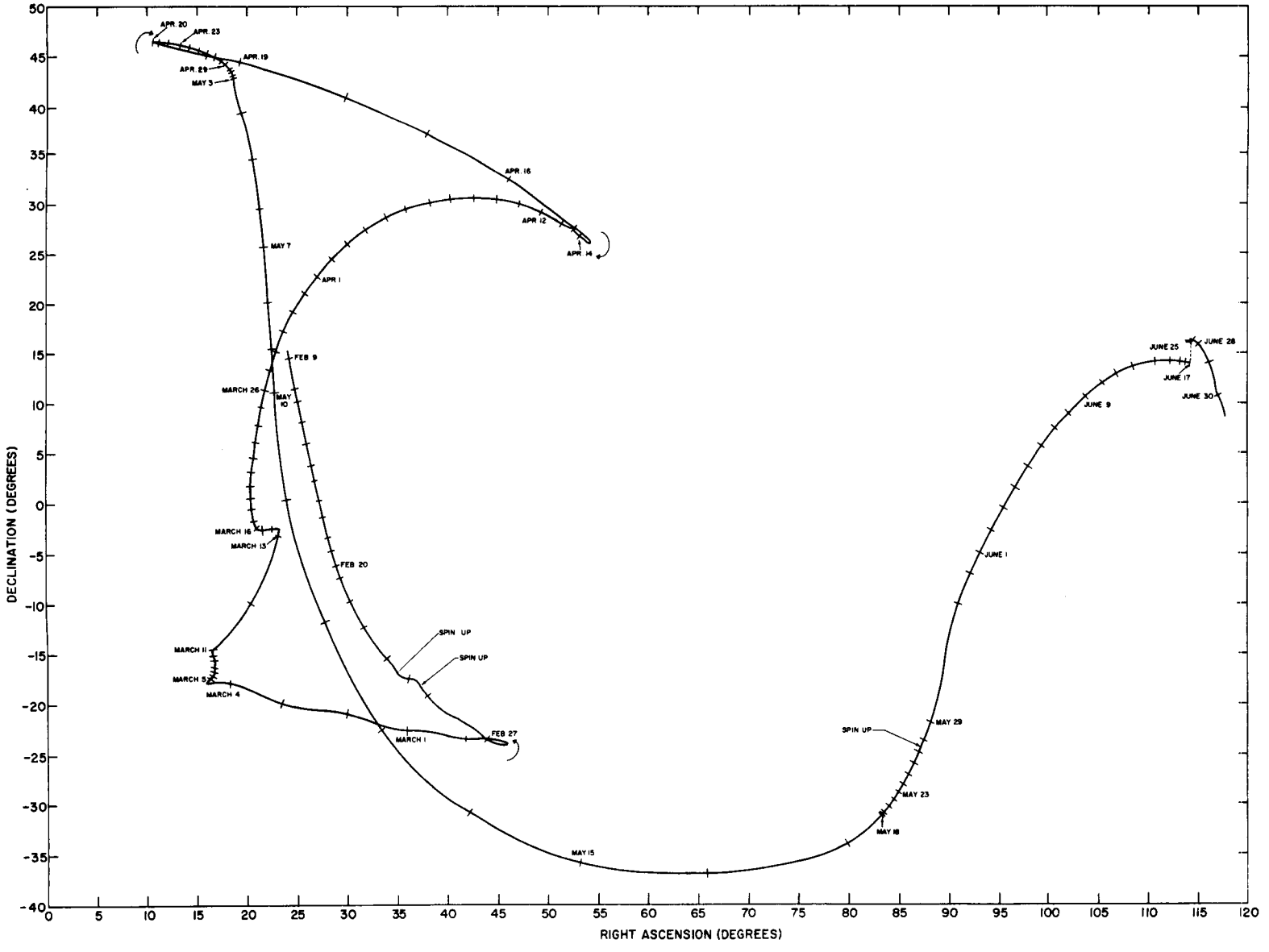

Figure A1—Observed motion of the TIROS IV spin vector on the celestial sphere. Each subdivision represents one day. Positions at 00 GMT each day are indicated.

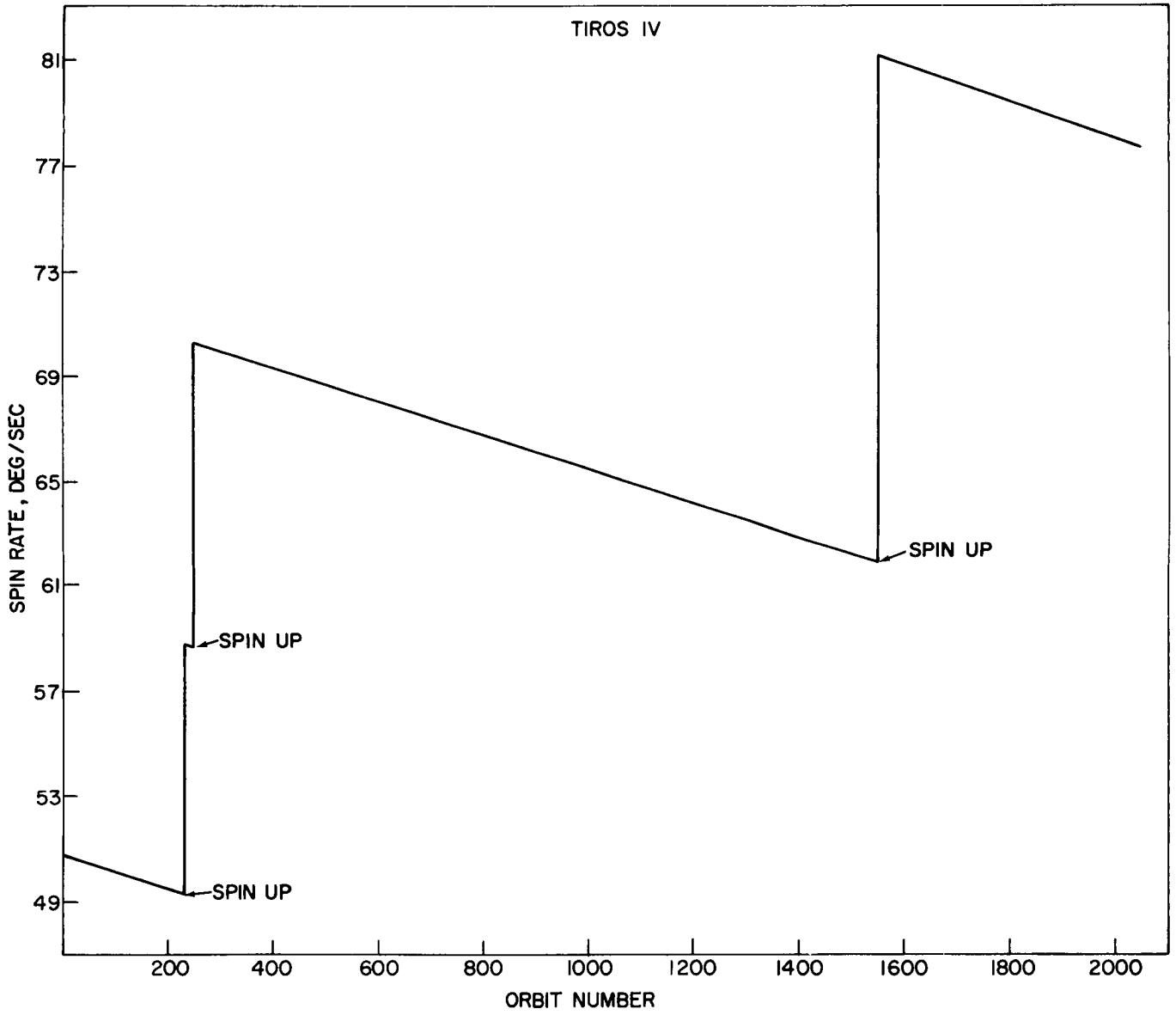

Figure A2—Time history of the TIROS IV spin rate.

APPENDIX B

SUBPOINT TRACK SUMMARY OF AVAILABLE RADIATION DATA

In this section, the time interval for which radiation data are available on the FMR tapes is summarized diagrammatically by means of subpoint tracks for each interrogation day. As discussed previously, an interrogation day may be contained within the calendar day or it may consist of parts of two calendar days. This method of presentation enables the data user to quickly apprise himself of the orbits containing data in an area of interest.

Before discussing the subpoint track summaries however, the various scanning modes of the TIROS radiometer and the relationship between the satellite nadir angle (the angle between the local vertical and satellite spin axis in the direction of the television cameras) and the optical axis of the medium resolution radiometer will be illustrated.

The three possible earth scanning patterns or modes of the TIROS radiometer may be characterized as follows (Figure B1):

(a) Closed Mode—All scan spots throughout a number of spin cycles of the satellite are earth viewed, either through the wall sensor or the floor sensor.

(b) Single Open Mode—Some scan spots of a spin cycle are space viewed and the remainder are earth viewed through the wall sensor only or through the floor sensor only.

(c) Alternating Open Mode—The scan spots of a spin cycle are a combination of space and earth viewed, alternately through the wall sensor and the floor sensor.

In Figure B2, on an earth cross-section, are shown nominal satellite nadir angle values bounding the various radiometer scanning modes. These values are for a height above the earth of about 717 km. It has been assumed that the spin vector coordinates remain constant throughout one orbit and that the minimum nadir angle is zero. Generally, the minimum nadir angle encountered throughout an orbit is not zero, thus diminishing the time period in the closed mode. In a number of orbits, the minimum nadir angle is greater than 19°, and hence there is no closed mode.

On the subpoint track summaries, each interrogation day is denoted by its calendar date or dates as the case may be. Dropouts are indicated by a symbol |--| where each dash represents one minute for which data are not available. Dropouts which occur at the beginning of tape have been left off the subpoint summaries. Each orbit is identified by orbit number and the time of occurrence of the ANO, to the hour and nearest minute in GMT. The symbol ⊙ indicates the point with respect to the orbital subpoint track where the minimum satellite nadir (η_0) angle for the interrogation day occurs. The orbit to which η_0 applies is indicated by a straight line drawn normal to that orbit and the value of η_0 to the nearest degree is also indicated. In cases where some ambiguity might arise as to the orbit to which η_0 applies, an arrow parallel to the applicable subpoint track is used (e.g. on page 138).

η_0 = —28° applies to Read-out orbit 0329). The spin-vector changes only slightly in declination and right ascension during one interrogation day and thus the minimum nadir angle is essentially constant and remains at approximately the same relative position to each orbit during one interrogation day.

To illustrate the use of the subpoint summaries, we use the same example as in Appendix A. If the master subpoint track overlay from the back of the Catalog-Manual is placed over the subpoint track for orbit 286 (page 136) with the ascending node at longitude 174.4°E, then the subpoint track shown is applicable to the data acquired during this interrogation. For a radiometer sensor nadir angle of 58°, the radiometer can acquire data from an area which is within 15° of great circle arc of the subpoint track. It can be seen that the data began 62.7 minutes before and ended 30.6 minutes after the ascending node time which was approximately 11:13 GMT. Also, a one minute dropout occurs between —6.5 and —7.5 minutes with respect to the ascending node time. The minimum nadir angle, to the nearest whole degree, and sufficiently accurate to apply to the entire day, was —25° on orbit 288. The intersection of the spin (camera) axis with the earth ⊙ lay south of the subpoint track as indicated by the negative value of η_0.

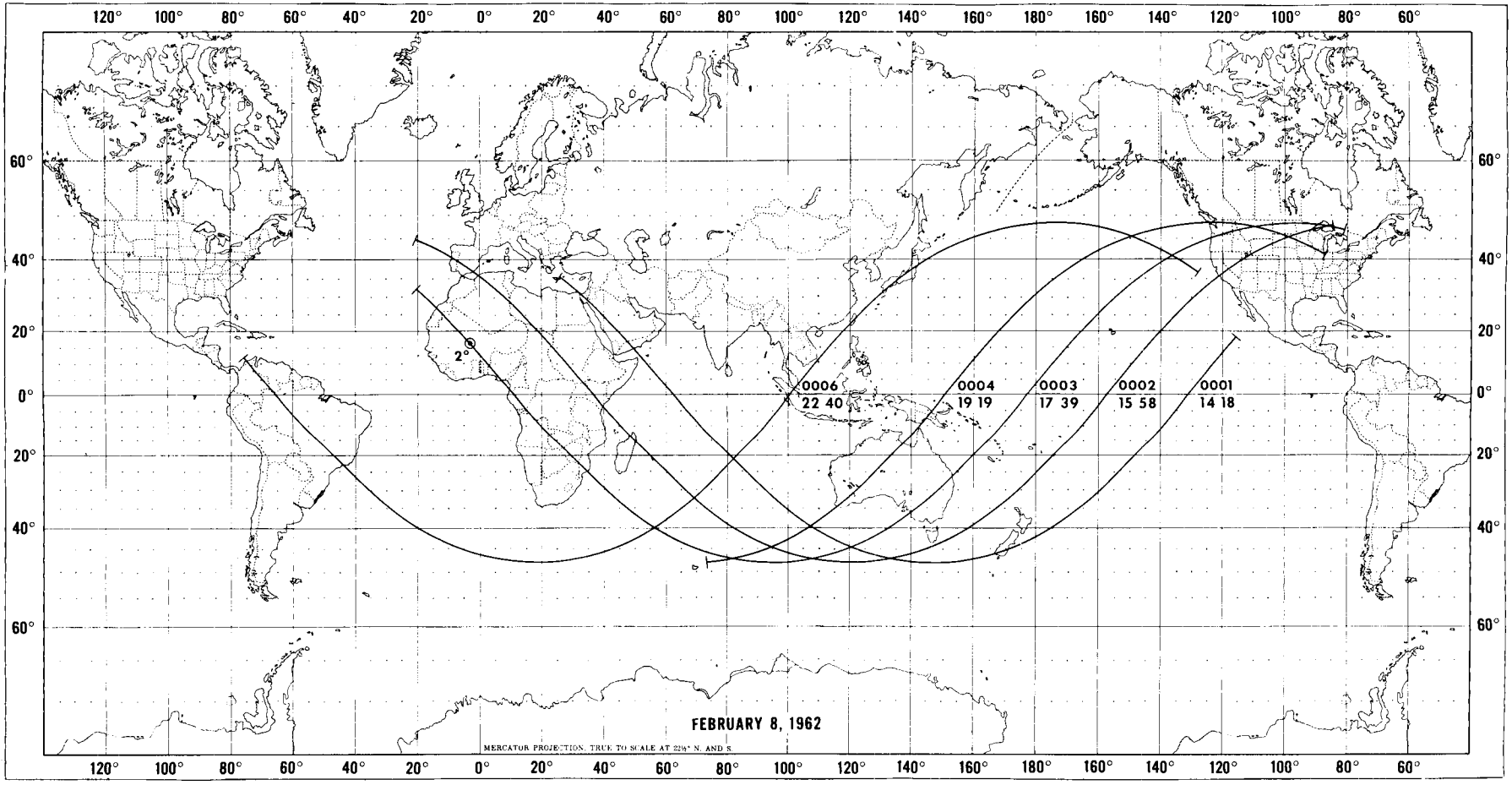
120° 100° 80° 60° 40° 20° 0° 20° 40° 60° 80° 100° 120° 140° 160° 180° 160° 140° 120° 100° 80° 60°
60°
40°
20°
0°
20°
40°
60°
2°
0006
22 40
0004
19 19
0003
17 39
0002
15 58
0001
14 18
FEBRUARY 8, 1962
MERCATOR PROJECTION. TRUE TO SCALE AT 22½° N. AND S.

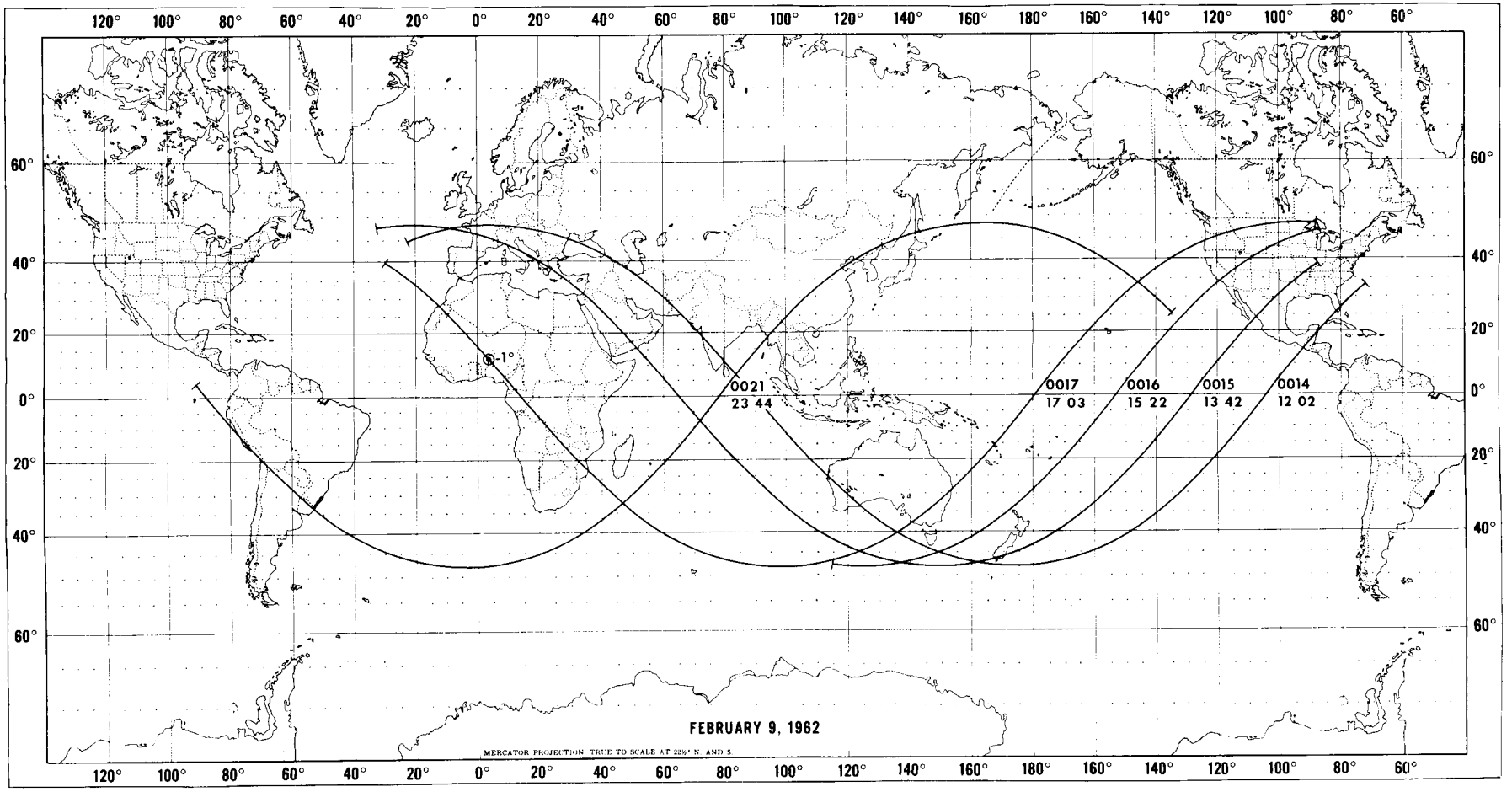
120° 100° 80° 60° 40° 20° 0° 20° 40° 60° 80° 100° 120° 140° 160° 180° 160° 140° 120° 100° 80° 60°
60°
40°
20°
0°
20°
40°
60°
1°
0021
23 44
0017
17 03
0016
15 22
0015
13 42
0014
12 02
FEBRUARY 9, 1962
MERCATOR PROJECTION, TRUE TO SCALE AT 22½° N. AND S.

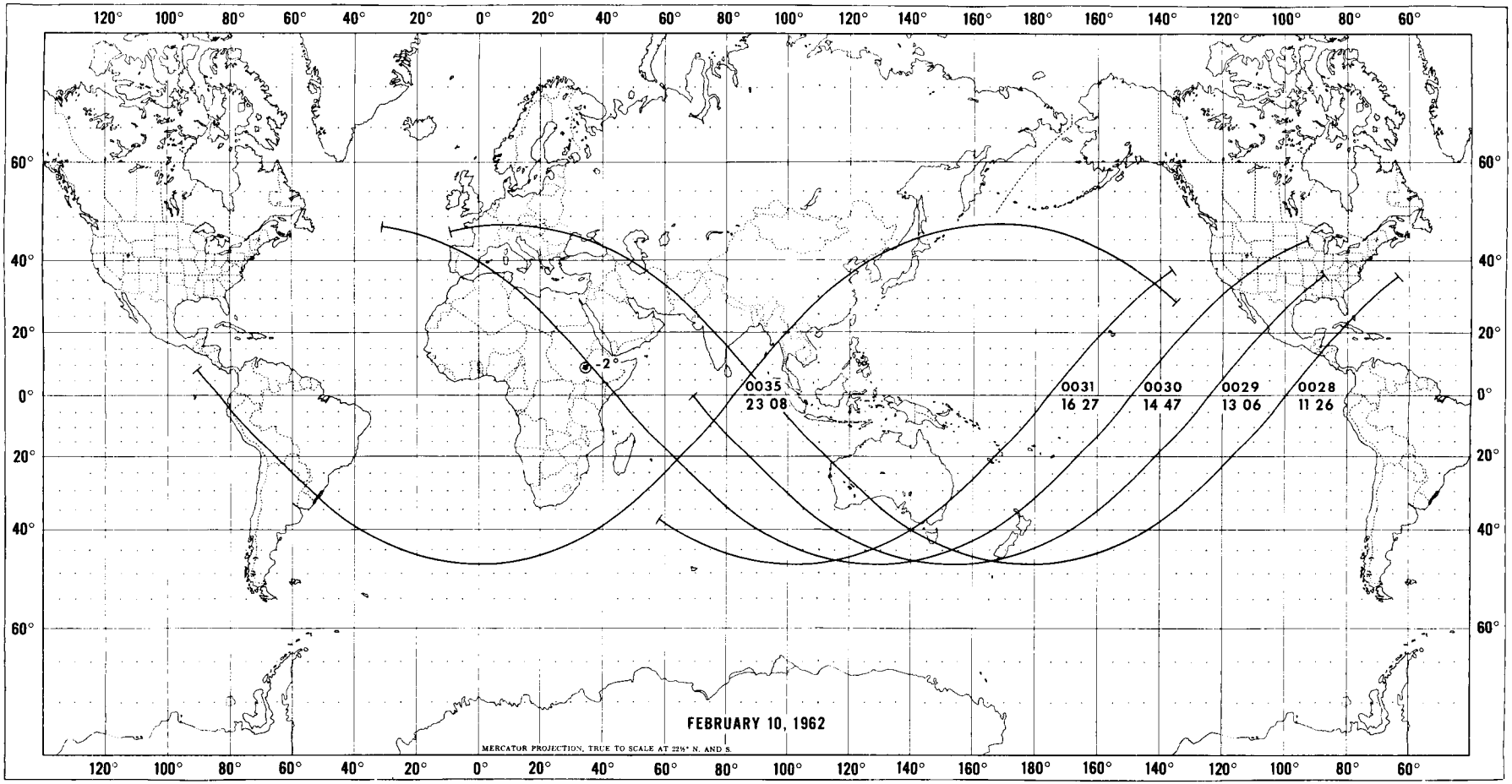
120° 100° 80° 60° 40° 20° 0° 20° 40° 60° 80° 100° 120° 140° 160° 180° 160° 140° 120° 100° 80° 60°
60°
40°
20°
0°
20°
40°
60°
-2°
0035
23 08
0031
16 27
0030
14 47
0029
13 06
0028
11 26
FEBRUARY 10, 1962
MERCATOR PROJECTION, TRUE TO SCALE AT 22½° N. AND S.

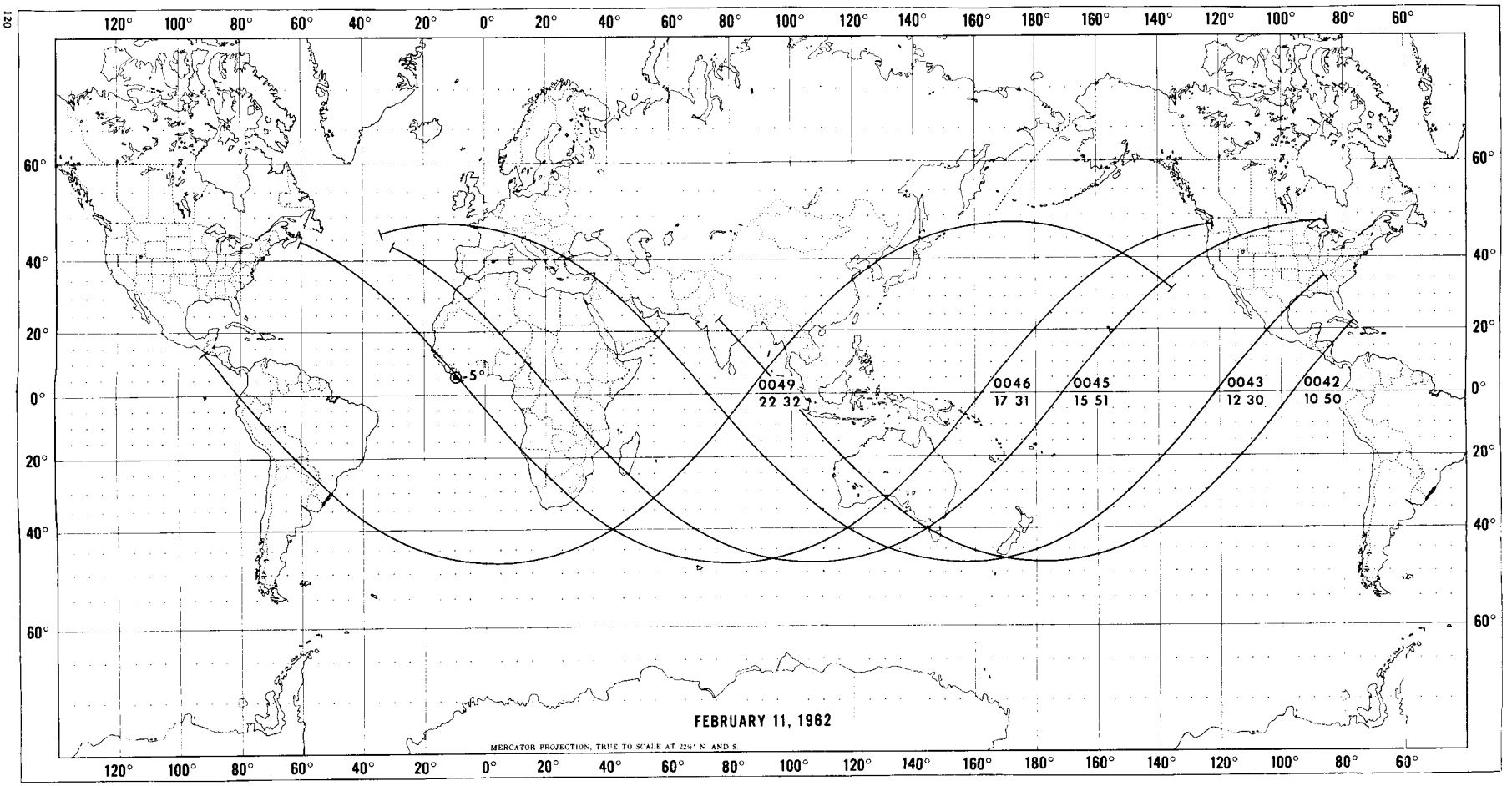
120° 100° 80° 60° 40° 20° 0° 20° 40° 60° 80° 100° 120° 140° 160° 180° 160° 140° 120° 100° 80° 60°
60°
40°
20°
0°
20°
40°
60°
-5°
0049
22 32
0046
17 31
0045
15 51
0043
12 30
0042
10 50
FEBRUARY 11, 1962
MERCATOR PROJECTION, TRUE TO SCALE AT 22½° N. AND S.

729-166 O - 64 - 9

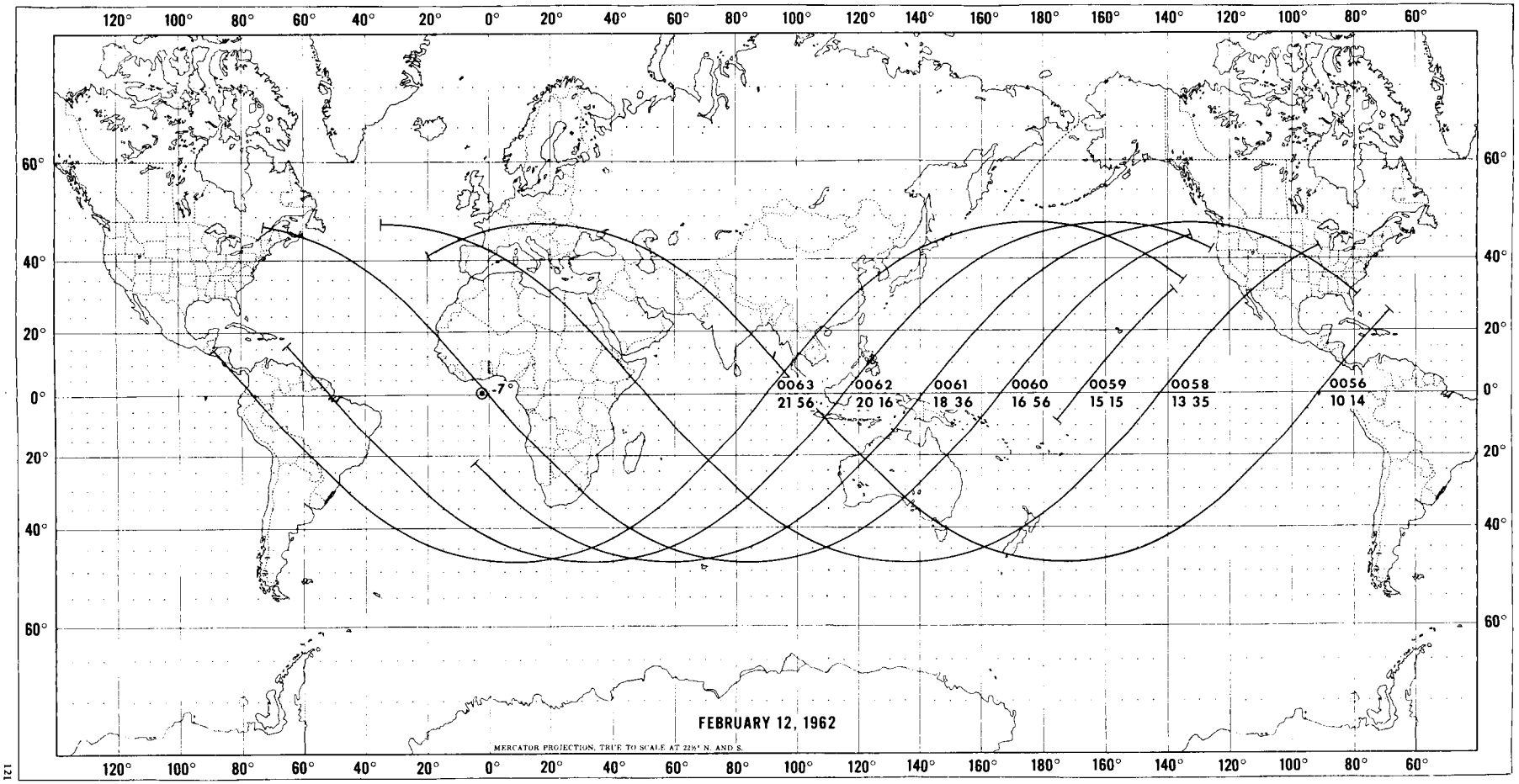
120° 100° 80° 60° 40° 20° 0° 20° 40° 60° 80° 100° 120° 140° 160° 180° 160° 140° 120° 100° 80° 60°
60°
40°
20°
0°
20°
40°
60°
-7°
0063
21 56
0062
20 16
0061
18 36
0060
16 56
0059
15 15
0058
13 35
0056
10 14
FEBRUARY 12, 1962
MERCATOR PROJECTION, TRUE TO SCALE AT 22½° N. AND S.

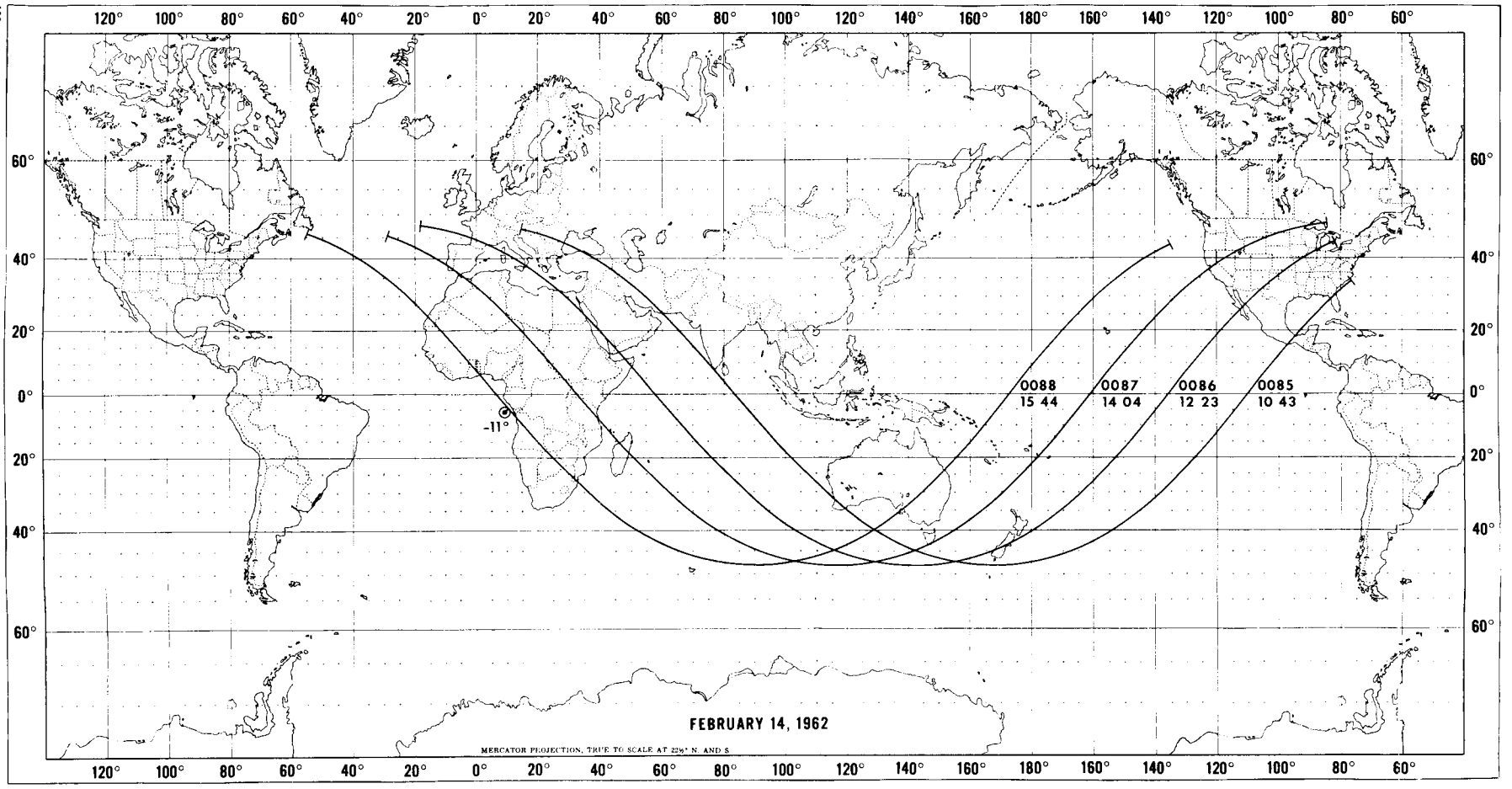
120° 100° 80° 60° 40° 20° 0° 20° 40° 60° 80° 100° 120° 140° 160° 180° 160° 140° 120° 100° 80° 60°
60°
40°
20°
0°
20°
40°
60°
-11°
0088
15 44
0087
14 04
0086
12 23
0085
10 43
FEBRUARY 14, 1962
MERCATOR PROJECTION, TRUE TO SCALE AT 22½° N. AND S.

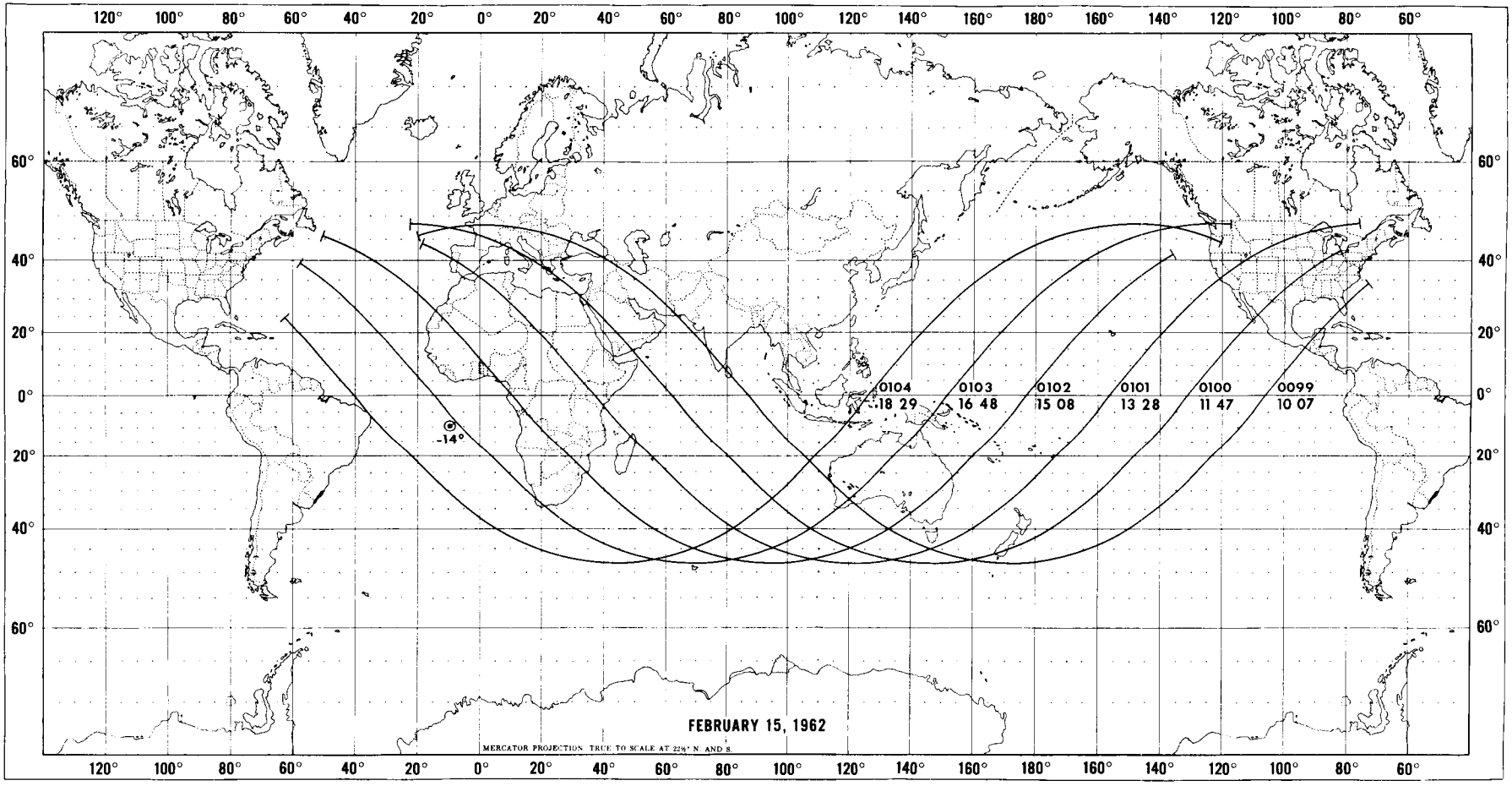
120° 100° 80° 60° 40° 20° 0° 20° 40° 60° 80° 100° 120° 140° 160° 180° 160° 140° 120° 100° 80° 60°
60°
40°
20°
0°
20°
40°
60°
0104
18 29
0103
16 48
0102
15 08
0101
13 28
0100
11 47
0099
10 07
-14°
FEBRUARY 15, 1962
MERCATOR PROJECTION TRUE TO SCALE AT 22½° N. AND S.

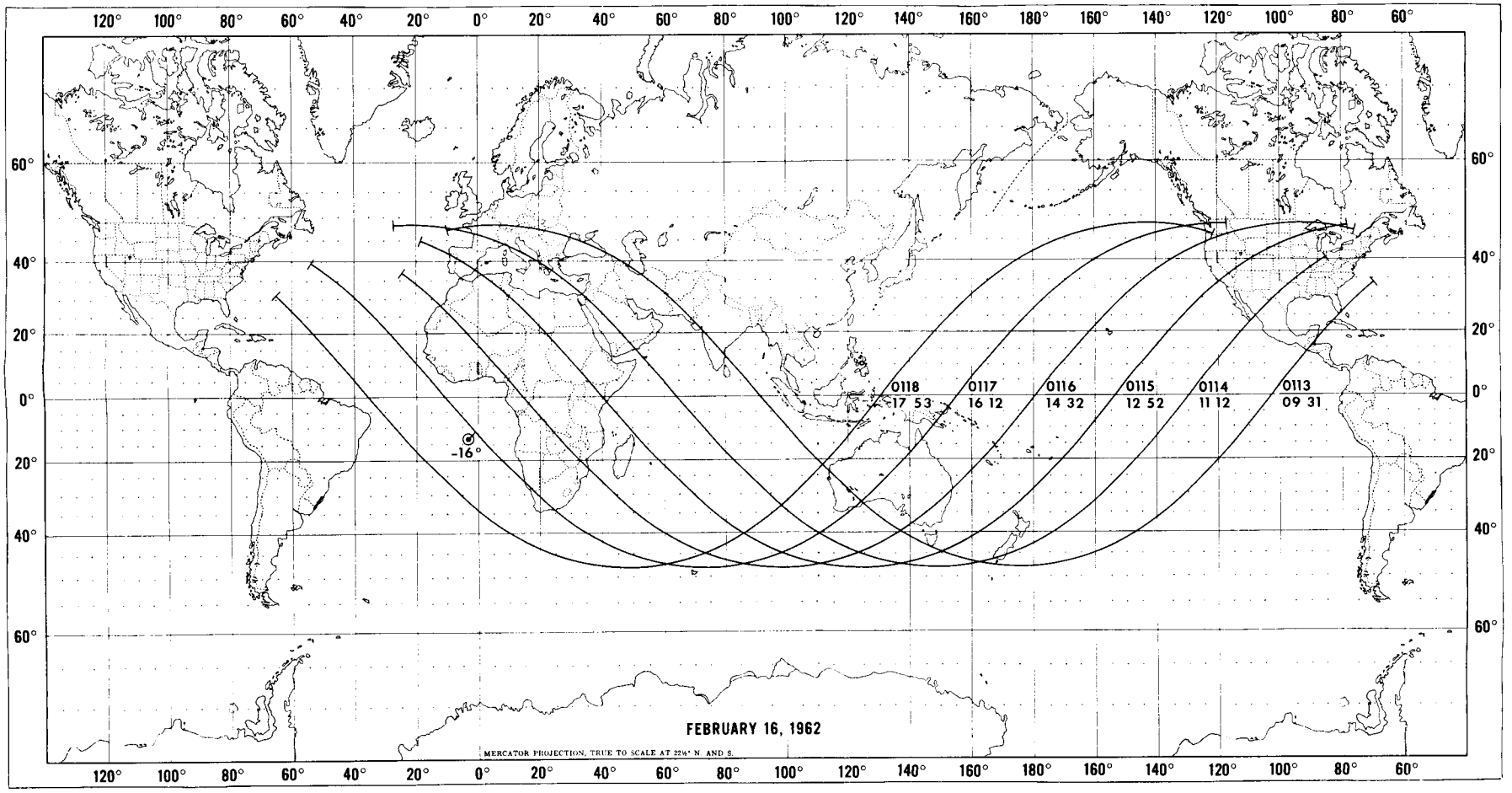
120° 100° 80° 60° 40° 20° 0° 20° 40° 60° 80° 100° 120° 140° 160° 180° 160° 140° 120° 100° 80° 60°
60°
40°
20°
0°
20°
40°
60°
0118
17 53
0117
16 12
0116
14 32
0115
12 52
0114
11 12
0113
09 31
-16°
FEBRUARY 16, 1962
MERCATOR PROJECTION, TRUE TO SCALE AT 22½° N. AND S.

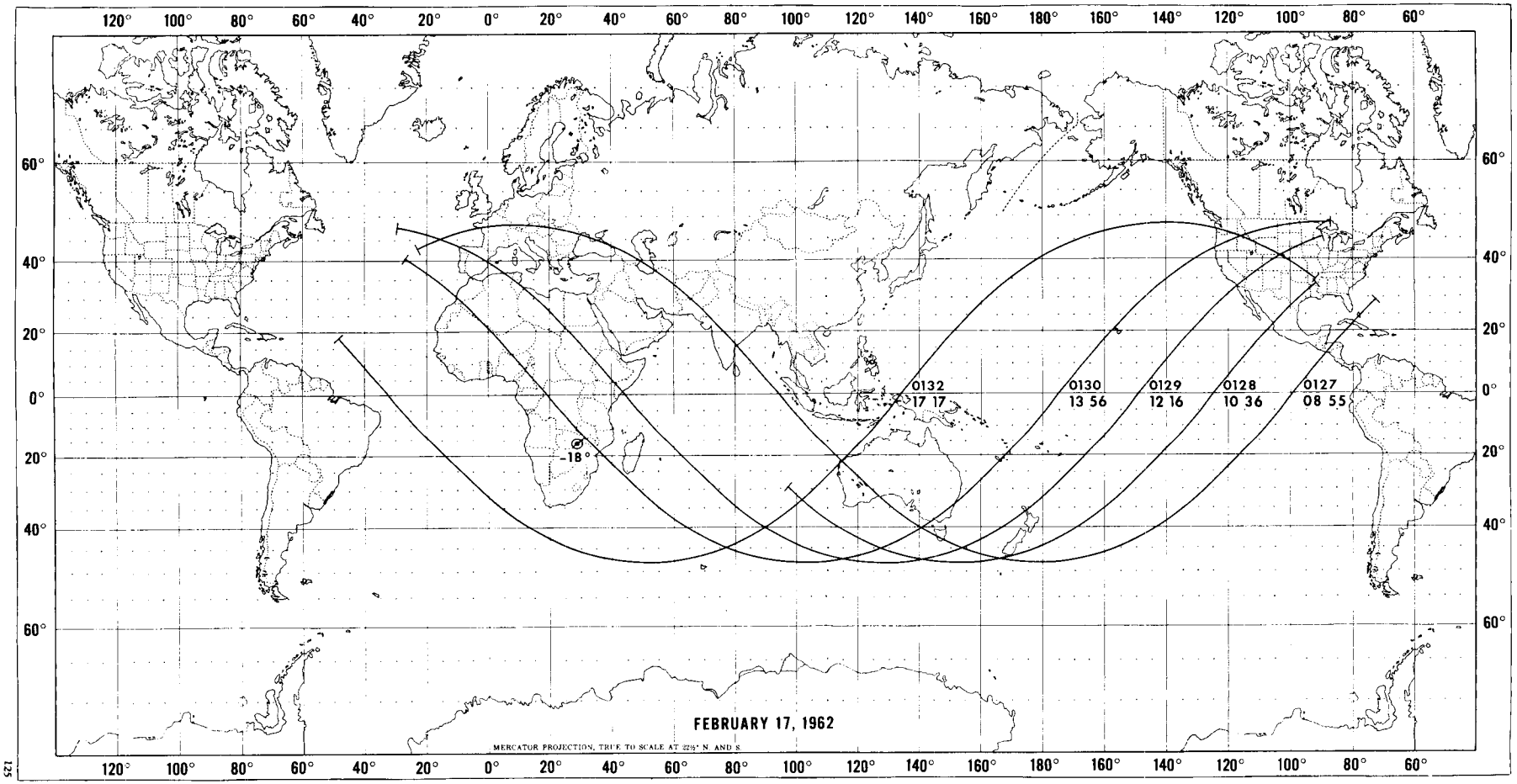
120° 100° 80° 60° 40° 20° 0° 20° 40° 60° 80° 100° 120° 140° 160° 180° 160° 140° 120° 100° 80° 60°
60°
40°
20°
0°
20°
40°
60°
0132
17 17
0130
13 56
0129
12 16
0128
10 36
0127
08 55
-18°
FEBRUARY 17, 1962
MERCATOR PROJECTION, TRUE TO SCALE AT 22½° N. AND S.

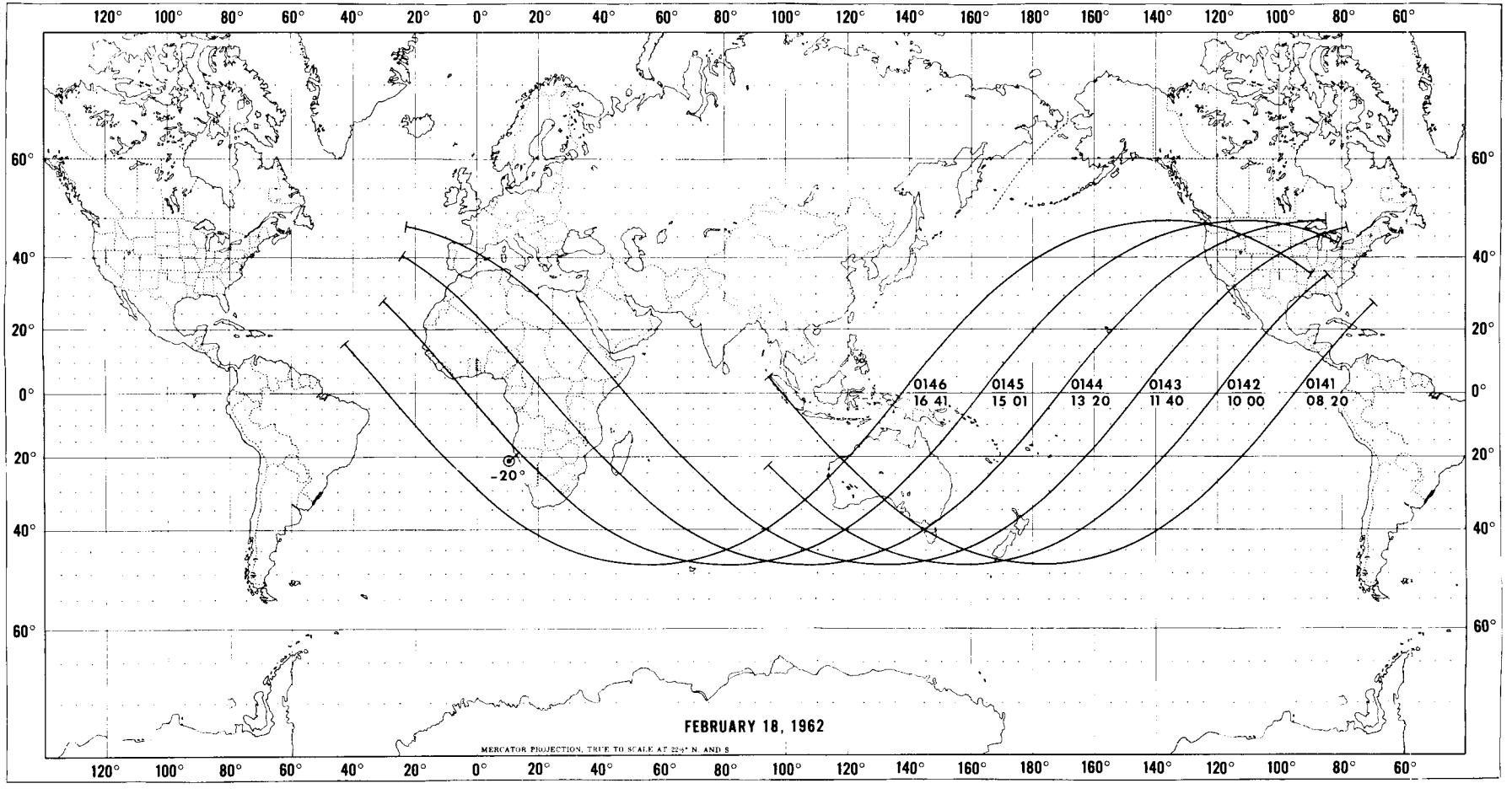
120° 100° 80° 60° 40° 20° 0° 20° 40° 60° 80° 100° 120° 140° 160° 180° 160° 140° 120° 100° 80° 60°
60°
40°
20°
0°
20°
40°
60°
0146
16 41
0145
15 01
0144
13 20
0143
11 40
0142
10 00
0141
08 20
-20°
FEBRUARY 18, 1962
MERCATOR PROJECTION, TRUE TO SCALE AT 22½° N. AND S.

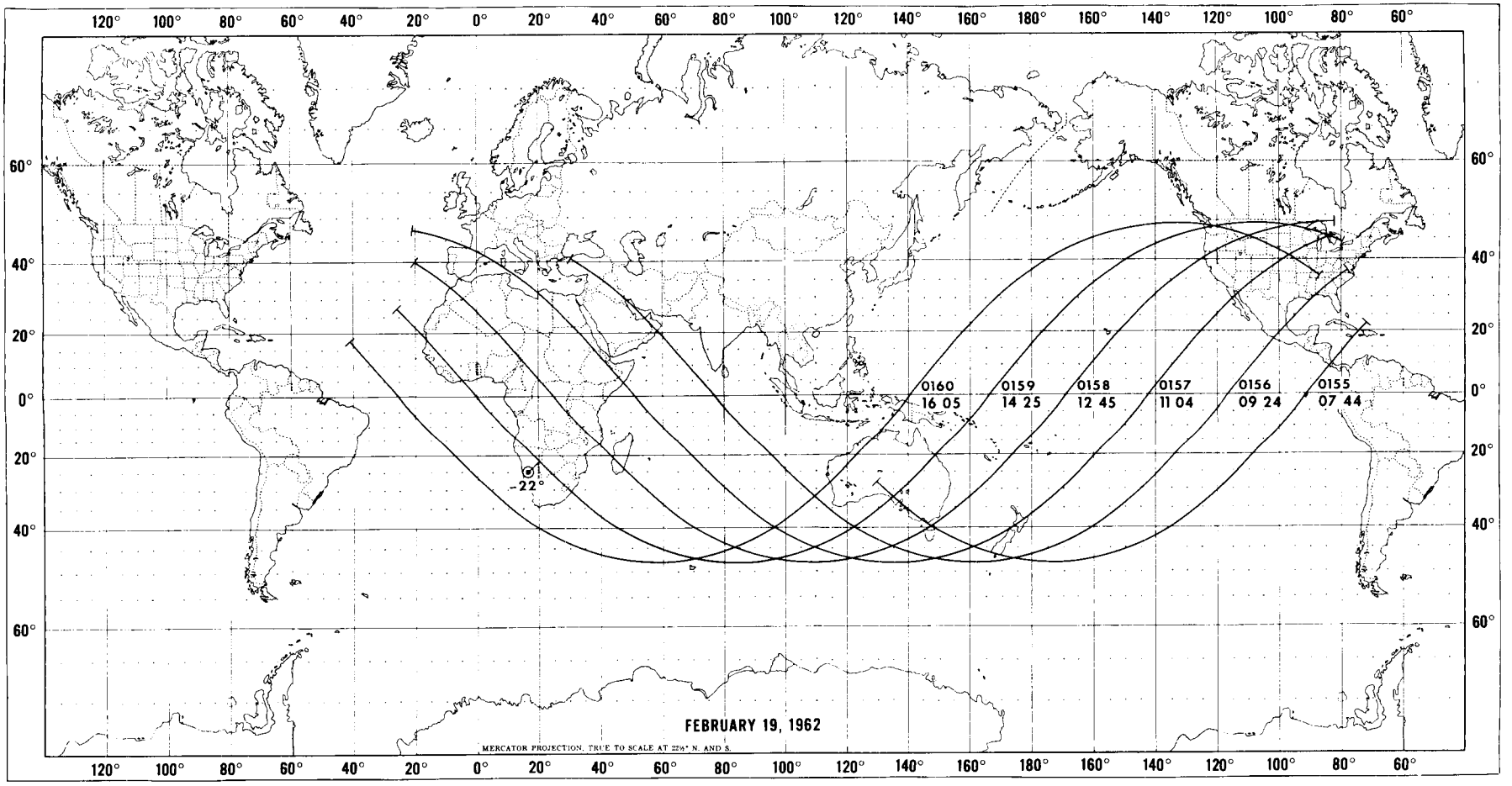
120° 100° 80° 60° 40° 20° 0° 20° 40° 60° 80° 100° 120° 140° 160° 180° 160° 140° 120° 100° 80° 60°
60°
40°
20°
0°
20°
40°
60°
0160
16 05
0159
14 25
0158
12 45
0157
11 04
0156
09 24
0155
07 44
-22°
FEBRUARY 19, 1962
MERCATOR PROJECTION, TRUE TO SCALE AT 22½° N. AND S.

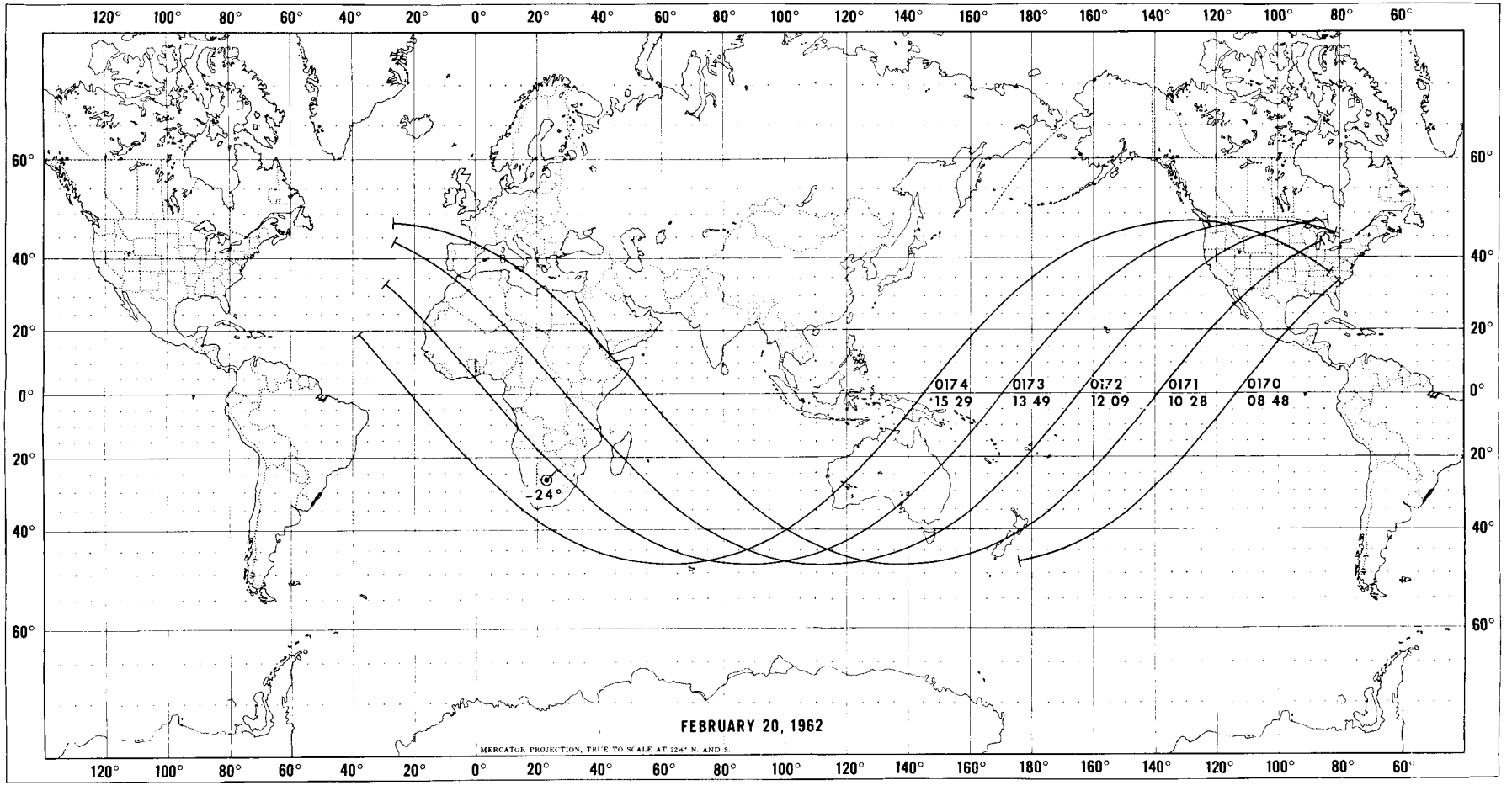
120° 100° 80° 60° 40° 20° 0° 20° 40° 60° 80° 100° 120° 140° 160° 180° 160° 140° 120° 100° 80° 60°
60°
40°
20°
0°
20°
40°
60°
0174
15 29
0173
13 49
0172
12 09
0171
10 28
0170
08 48
-24°
FEBRUARY 20, 1962
MERCATOR PROJECTION, TRUE TO SCALE AT 22½° N. AND S.

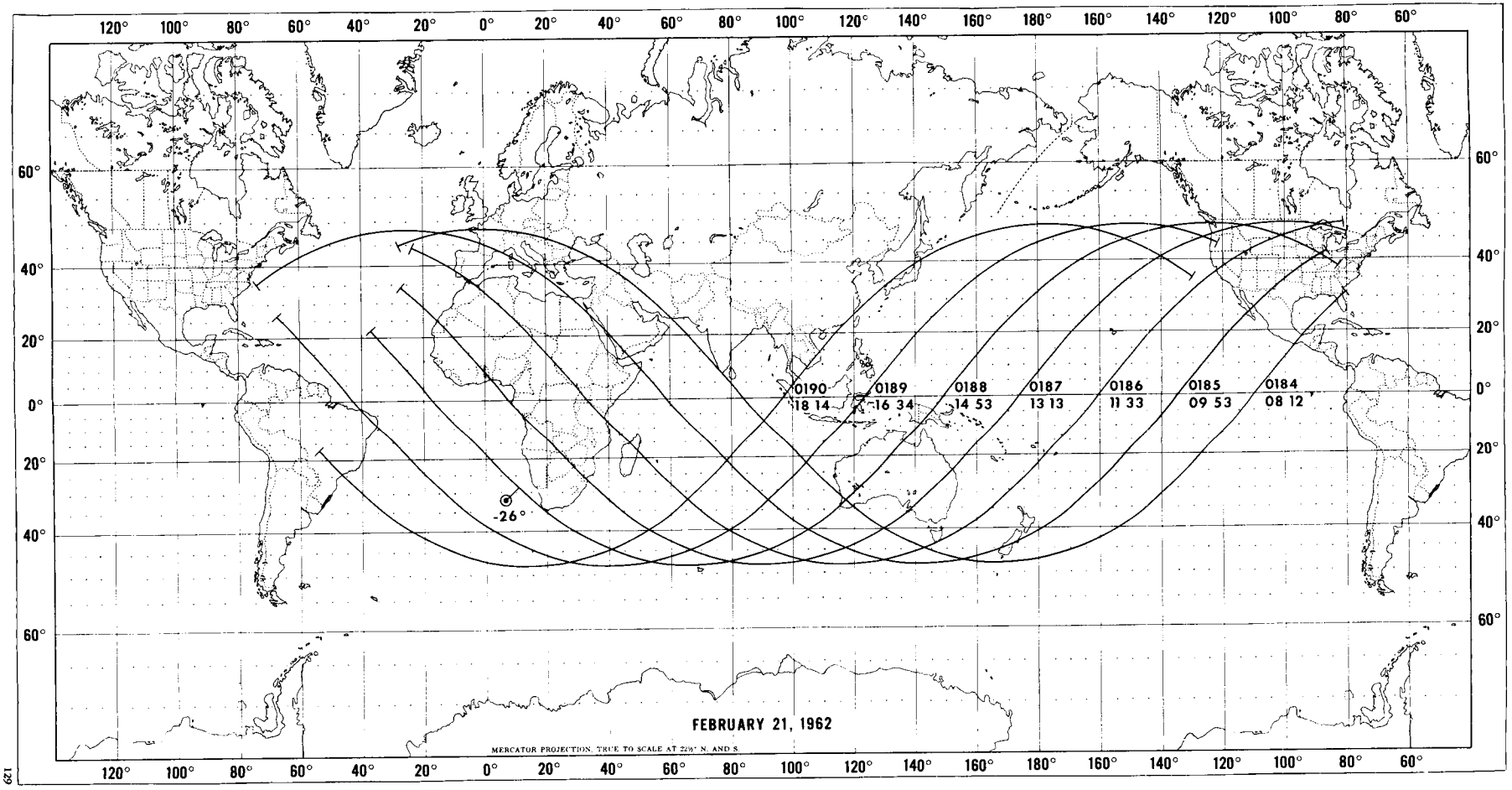
120° 100° 80° 60° 40° 20° 0° 20° 40° 60° 80° 100° 120° 140° 160° 180° 160° 140° 120° 100° 80° 60°
60°
40°
20°
0°
20°
40°
60°
0190 18 14
0189 16 34
0188 14 53
0187 13 13
0186 11 33
0185 09 53
0184 08 12
-26°
FEBRUARY 21, 1962
MERCATOR PROJECTION. TRUE TO SCALE AT 22½° N. AND S.

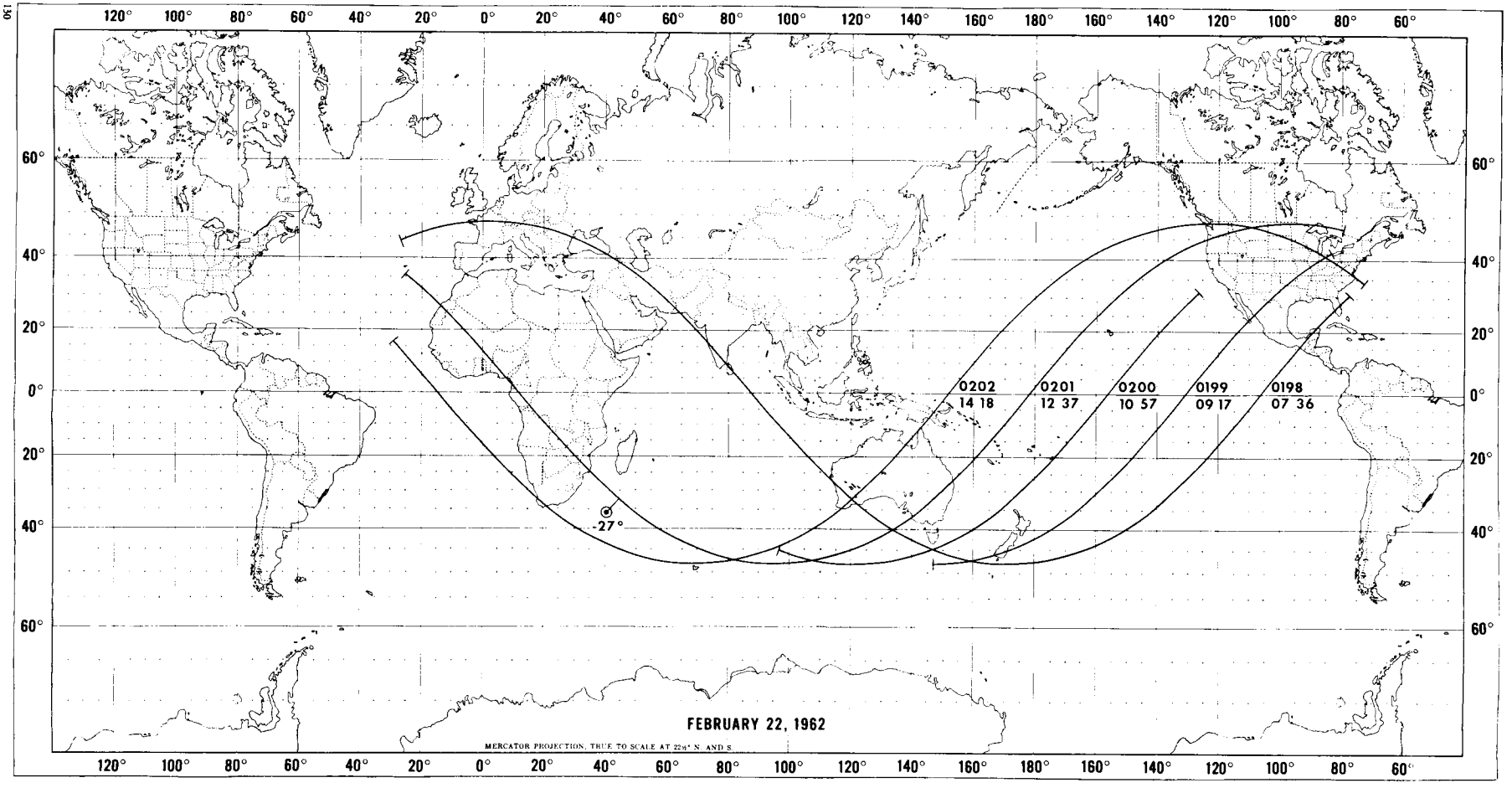
120° 100° 80° 60° 40° 20° 0° 20° 40° 60° 80° 100° 120° 140° 160° 180° 160° 140° 120° 100° 80° 60°
60°
40°
20°
0°
20°
40°
60°
0202
14 18
0201
12 37
0200
10 57
0199
09 17
0198
07 36
-27°
FEBRUARY 22, 1962
MERCATOR PROJECTION, TRUE TO SCALE AT 22½° N. AND S.

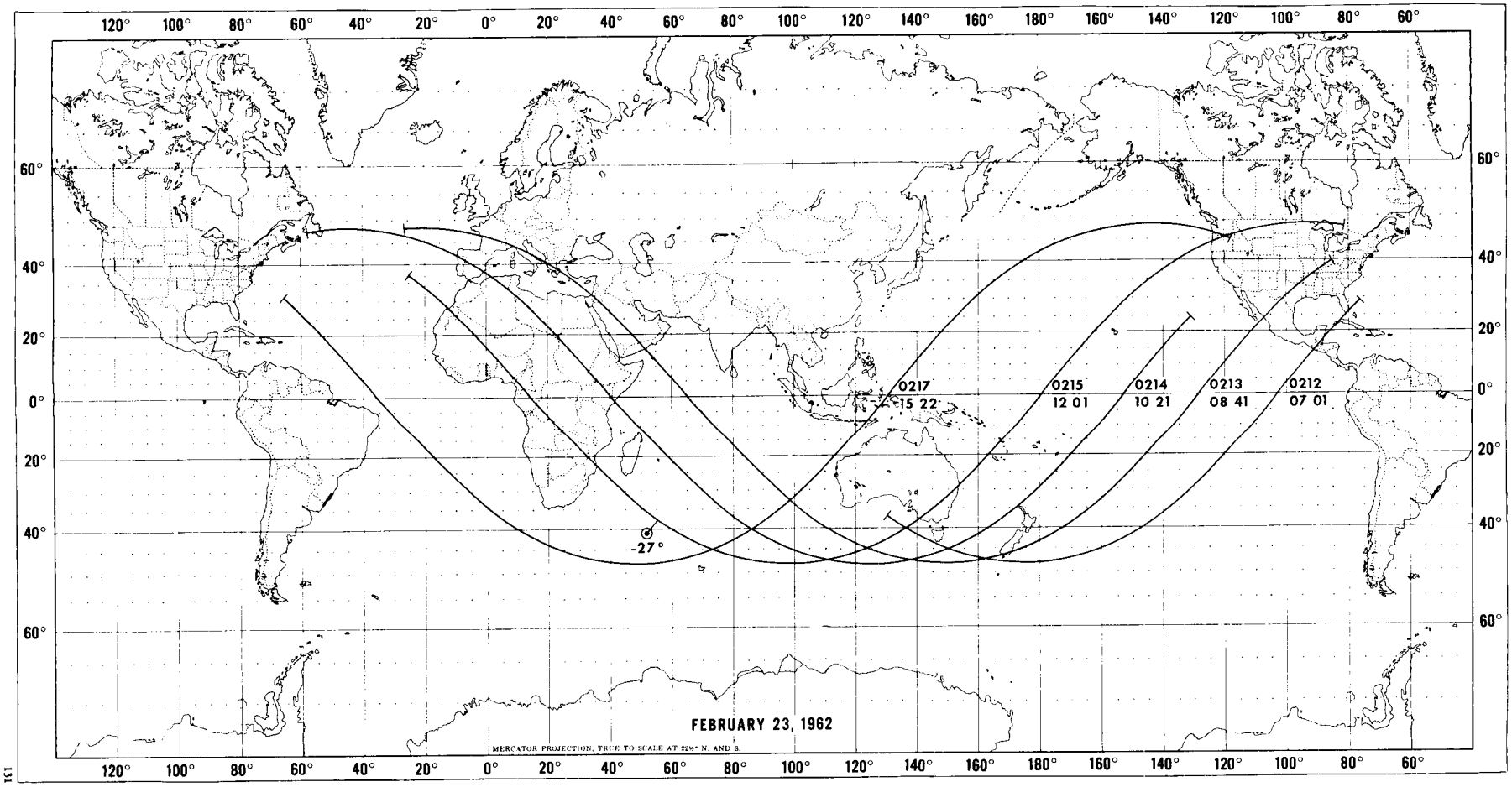
120° 100° 80° 60° 40° 20° 0° 20° 40° 60° 80° 100° 120° 140° 160° 180° 160° 140° 120° 100° 80° 60°
60°
40°
20°
0°
20°
40°
60°
0217
15 22
0215
12 01
0214
10 21
0213
08 41
0212
07 01
-27°
FEBRUARY 23, 1962
MERCATOR PROJECTION, TRUE TO SCALE AT 22½° N. AND S.

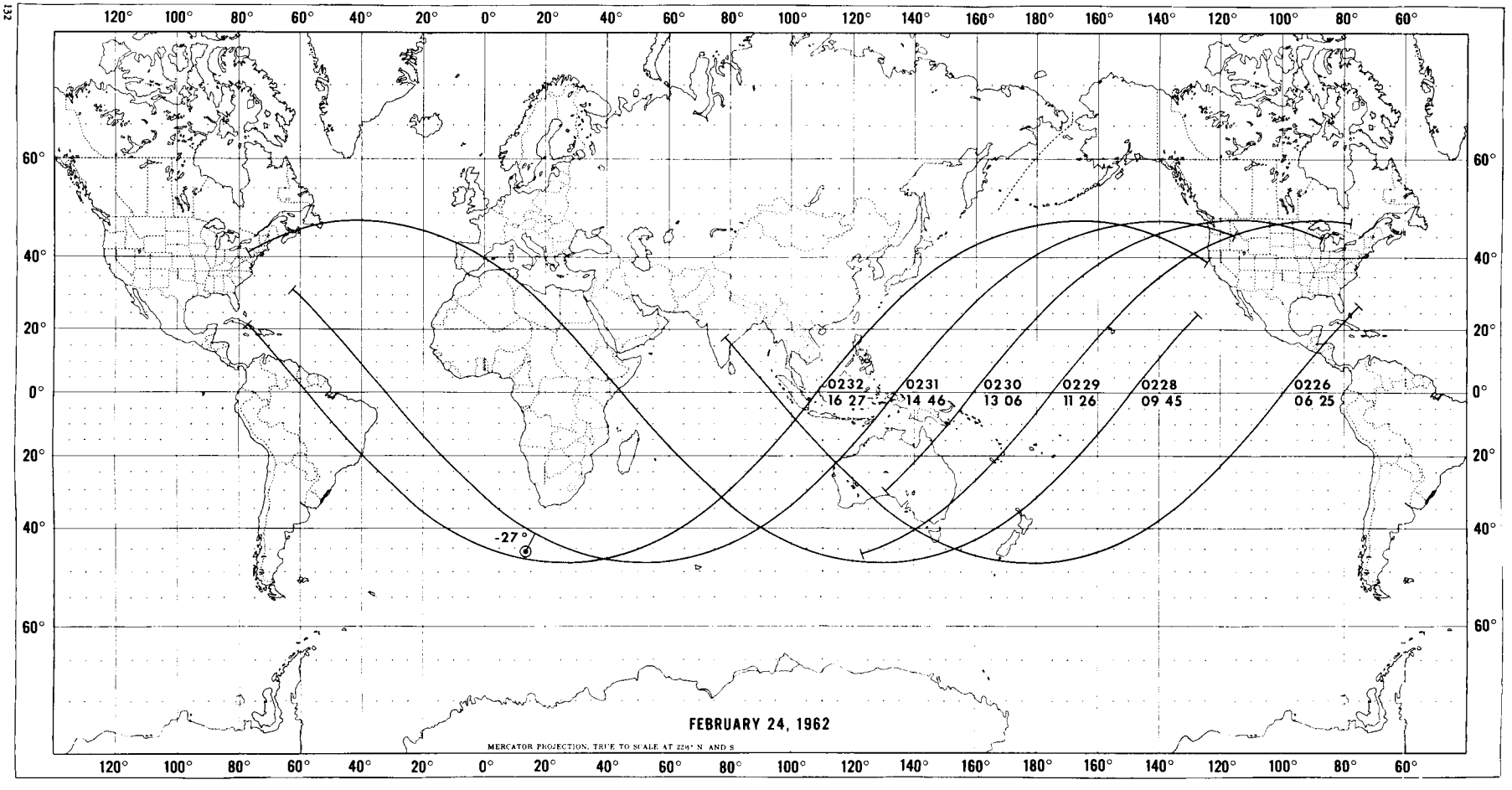
120° 100° 80° 60° 40° 20° 0° 20° 40° 60° 80° 100° 120° 140° 160° 180° 160° 140° 120° 100° 80° 60°
60°
40°
20°
0°
20°
40°
60°
0232
16 27
0231
14 46
0230
13 06
0229
11 26
0228
09 45
0226
06 25
-27°
FEBRUARY 24, 1962
MERCATOR PROJECTION, TRUE TO SCALE AT 22½° N AND S

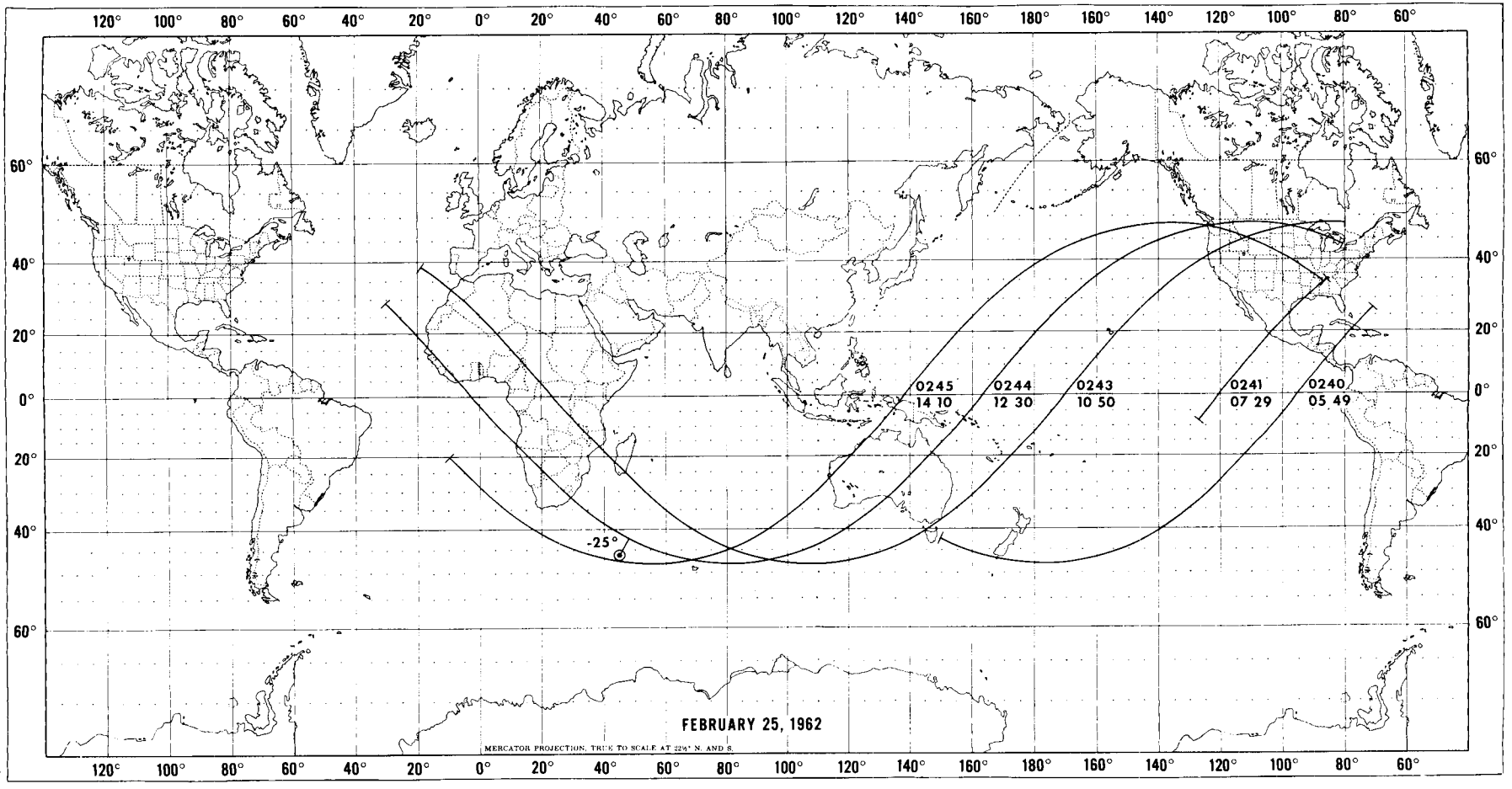
120° 100° 80° 60° 40° 20° 0° 20° 40° 60° 80° 100° 120° 140° 160° 180° 160° 140° 120° 100° 80° 60°
60°
40°
20°
0°
20°
40°
60°
0245
14 10
0244
12 30
0243
10 50
0241
07 29
0240
05 49
-25°
FEBRUARY 25, 1962
MERCATOR PROJECTION, TRUE TO SCALE AT 22½° N. AND S.

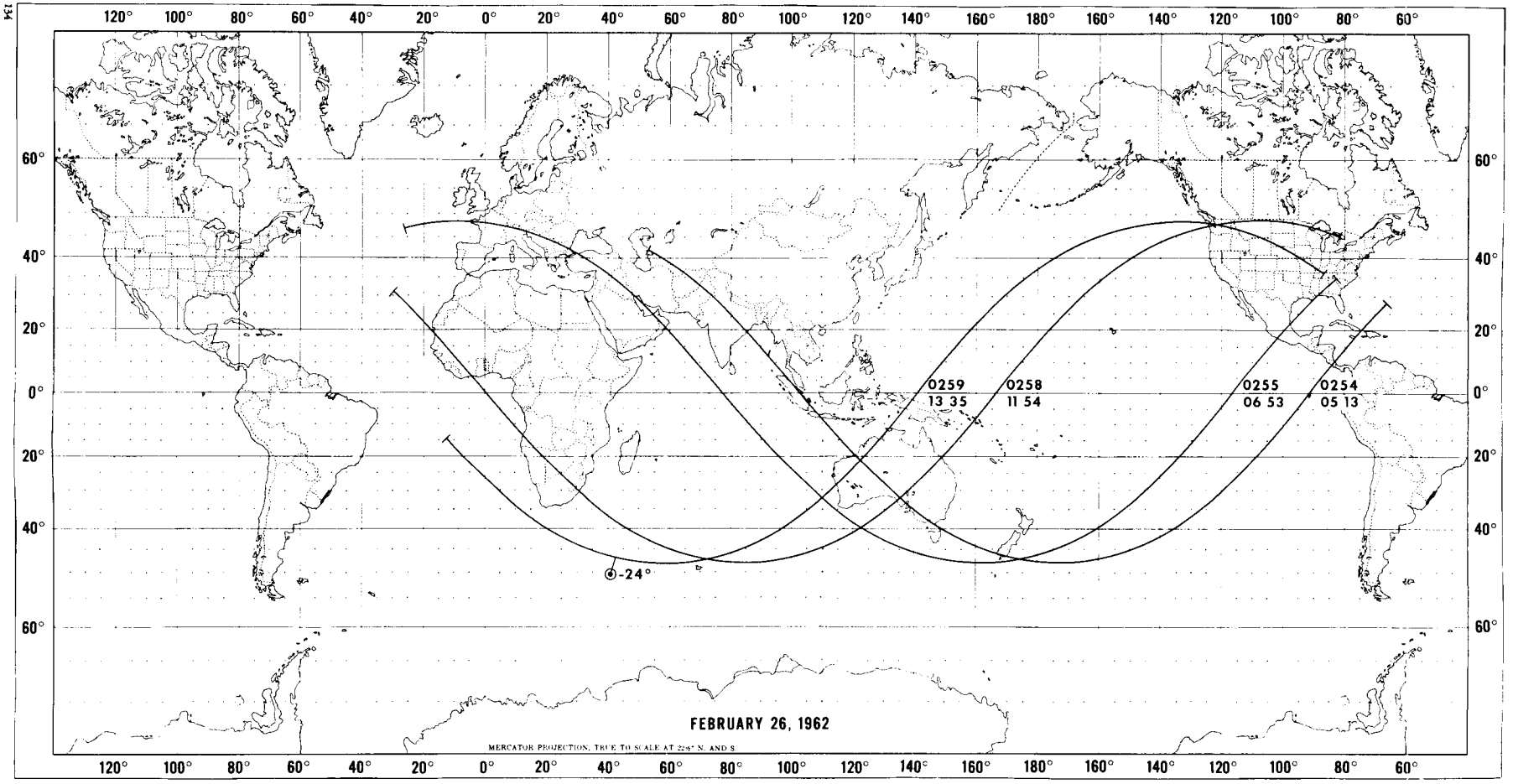
120° 100° 80° 60° 40° 20° 0° 20° 40° 60° 80° 100° 120° 140° 160° 180° 160° 140° 120° 100° 80° 60°
60°
40°
20°
0°
20°
40°
60°
0259
13 35
0258
11 54
0255
06 53
0254
05 13
-24°
FEBRUARY 26, 1962
MERCATOR PROJECTION, TRUE TO SCALE AT 22½° N. AND S.

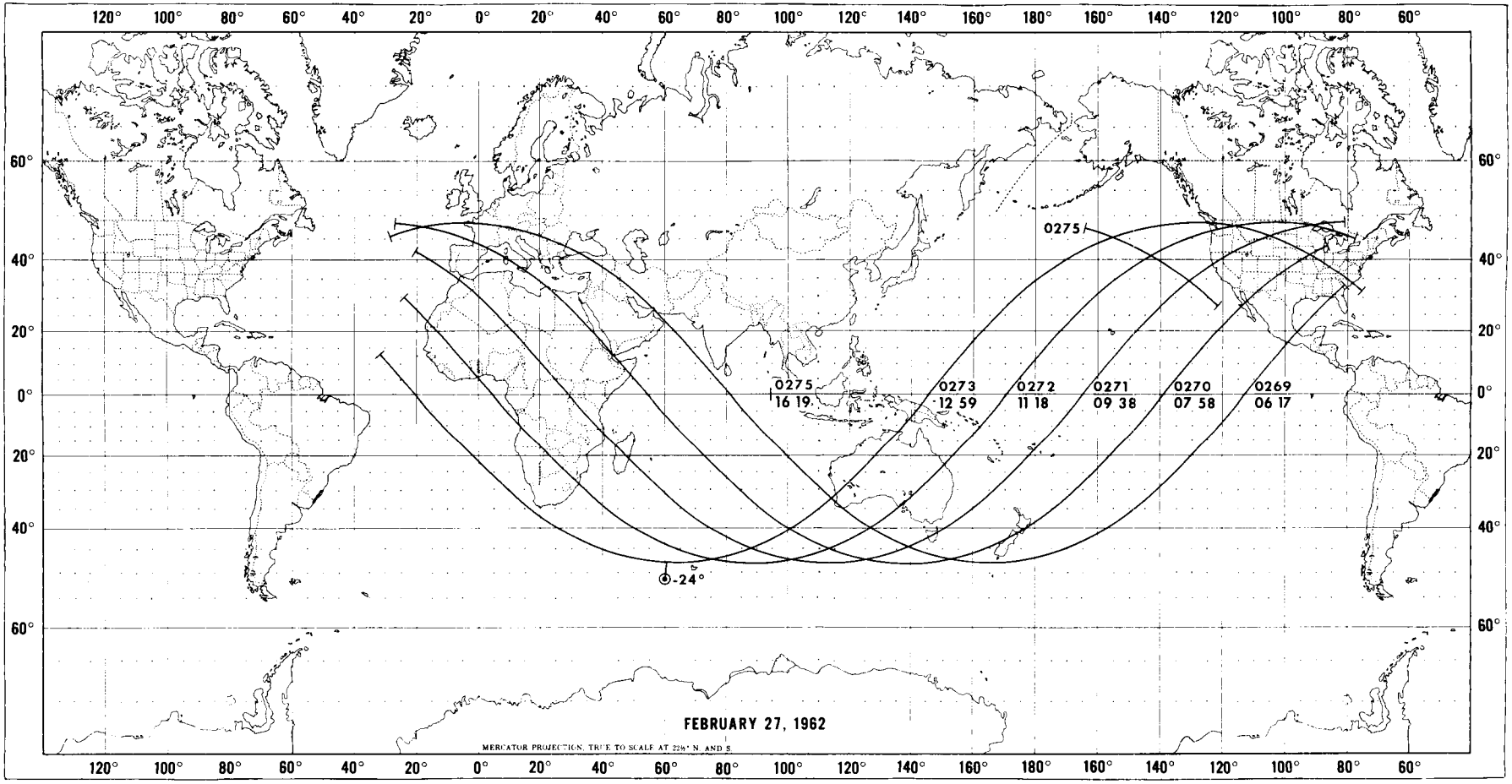
120° 100° 80° 60° 40° 20° 0° 20° 40° 60° 80° 100° 120° 140° 160° 180° 160° 140° 120° 100° 80° 60°
60°
40°
20°
0°
20°
40°
60°
0275
0275
16 19
0273
12 59
0272
11 18
0271
09 38
0270
07 58
0269
06 17
-24°
FEBRUARY 27, 1962
MERCATOR PROJECTION, TRUE TO SCALE AT 22½° N AND S

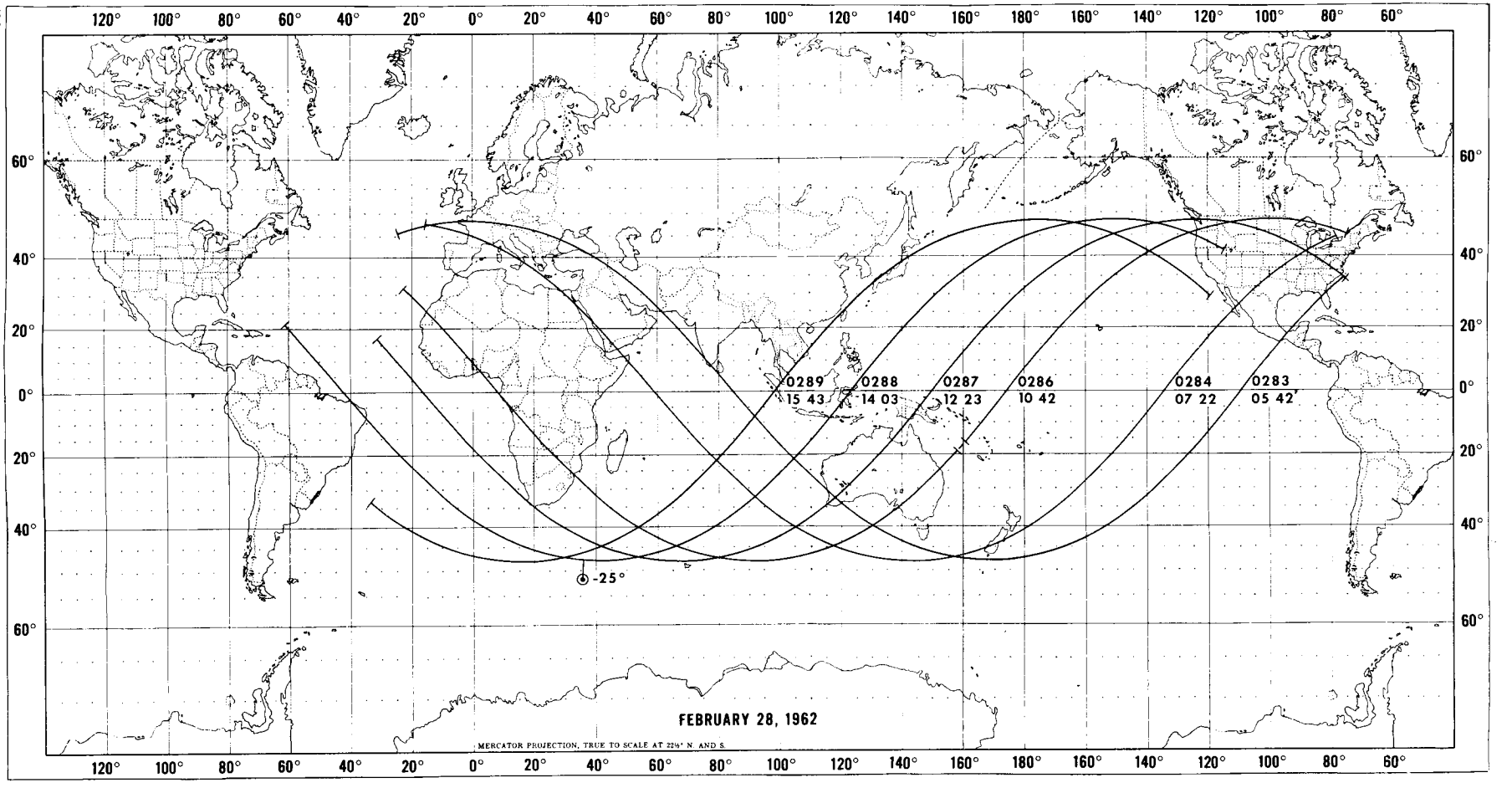
120° 100° 80° 60° 40° 20° 0° 20° 40° 60° 80° 100° 120° 140° 160° 180° 160° 140° 120° 100° 80° 60°
60°
40°
20°
0°
20°
40°
60°
0289
15 43
0288
14 03
0287
12 23
0286
10 42
0284
07 22
0283
05 42
-25°
FEBRUARY 28, 1962
MERCATOR PROJECTION, TRUE TO SCALE AT 22½° N. AND S.

729-166 O - 64 - 10

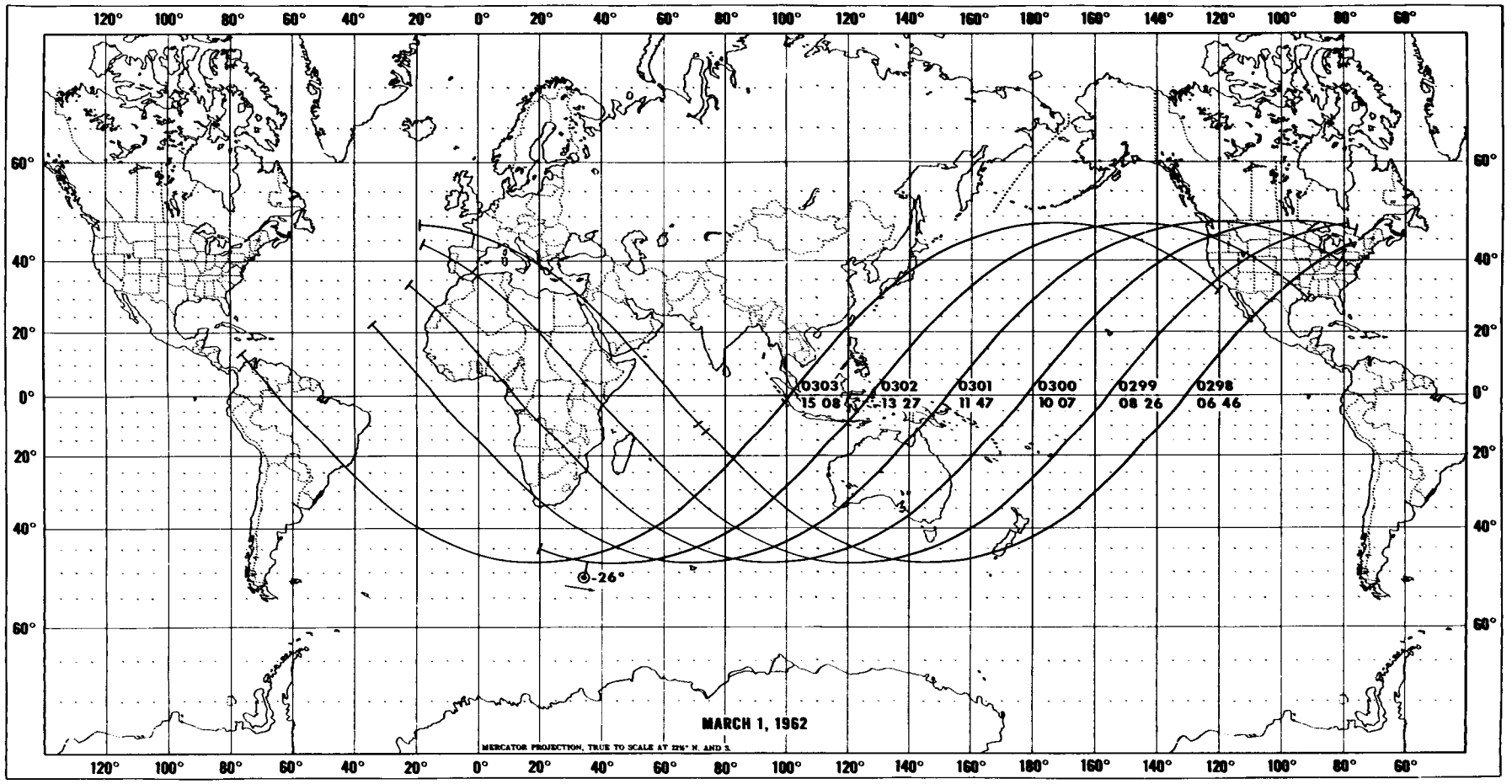

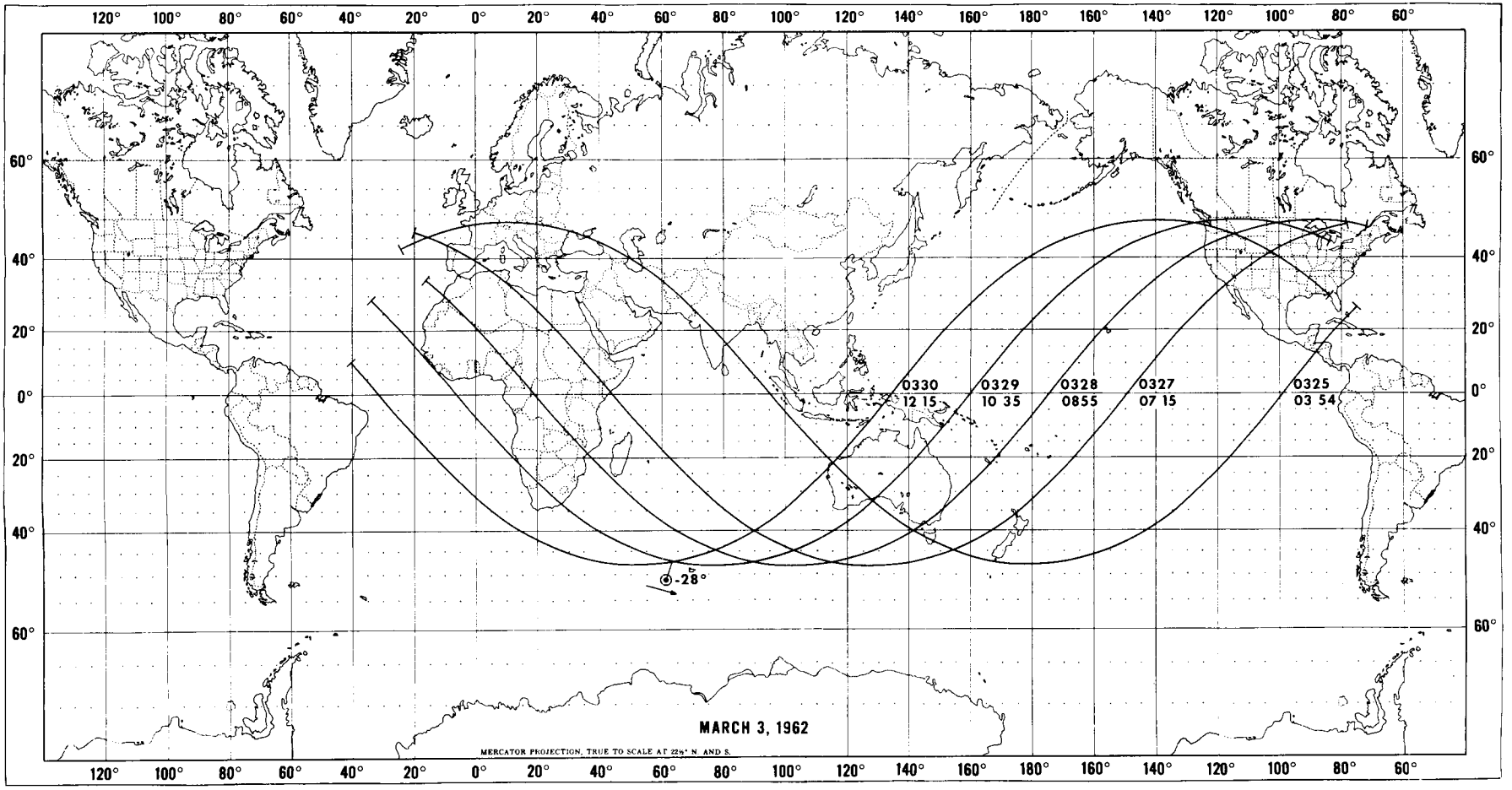
120° 100° 80° 60° 40° 20° 0° 20° 40° 60° 80° 100° 120° 140° 160° 180° 160° 140° 120° 100° 80° 60°
60°
40°
20°
0°
20°
40°
60°
0330
12 15
0329
10 35
0328
0855
0327
07 15
0325
03 54
-28°
MARCH 3, 1962
MERCATOR PROJECTION, TRUE TO SCALE AT 22½° N. AND S.

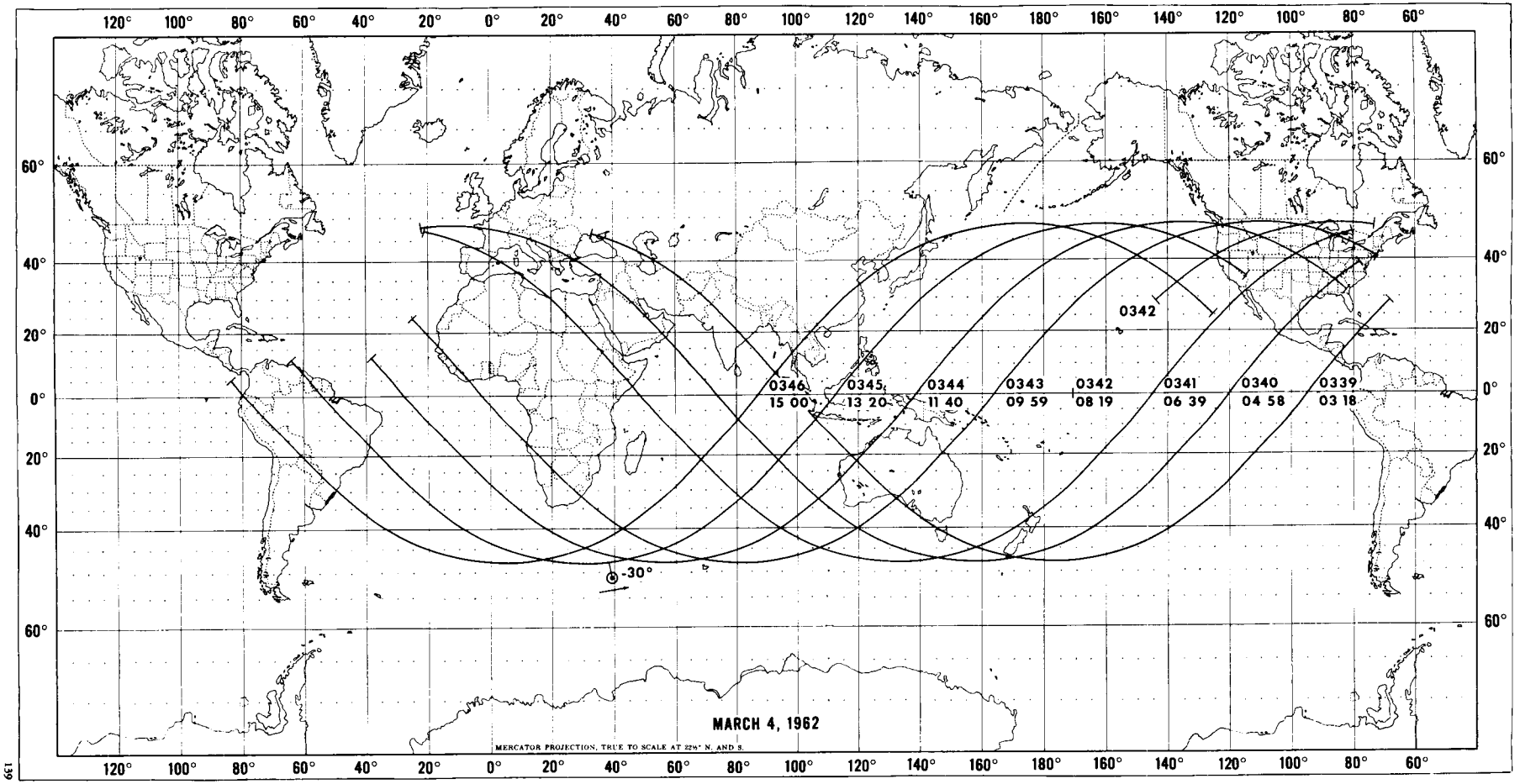
120° 100° 80° 60° 40° 20° 0° 20° 40° 60° 80° 100° 120° 140° 160° 180° 160° 140° 120° 100° 80° 60°
60°
40°
20°
0°
20°
40°
60°
0342
0346
15 00
0345
13 20
0344
11 40
0343
09 59
0342
08 19
0341
06 39
0340
04 58
0339
03 18
-30°
MARCH 4, 1962
MERCATOR PROJECTION, TRUE TO SCALE AT 22½° N. AND S.

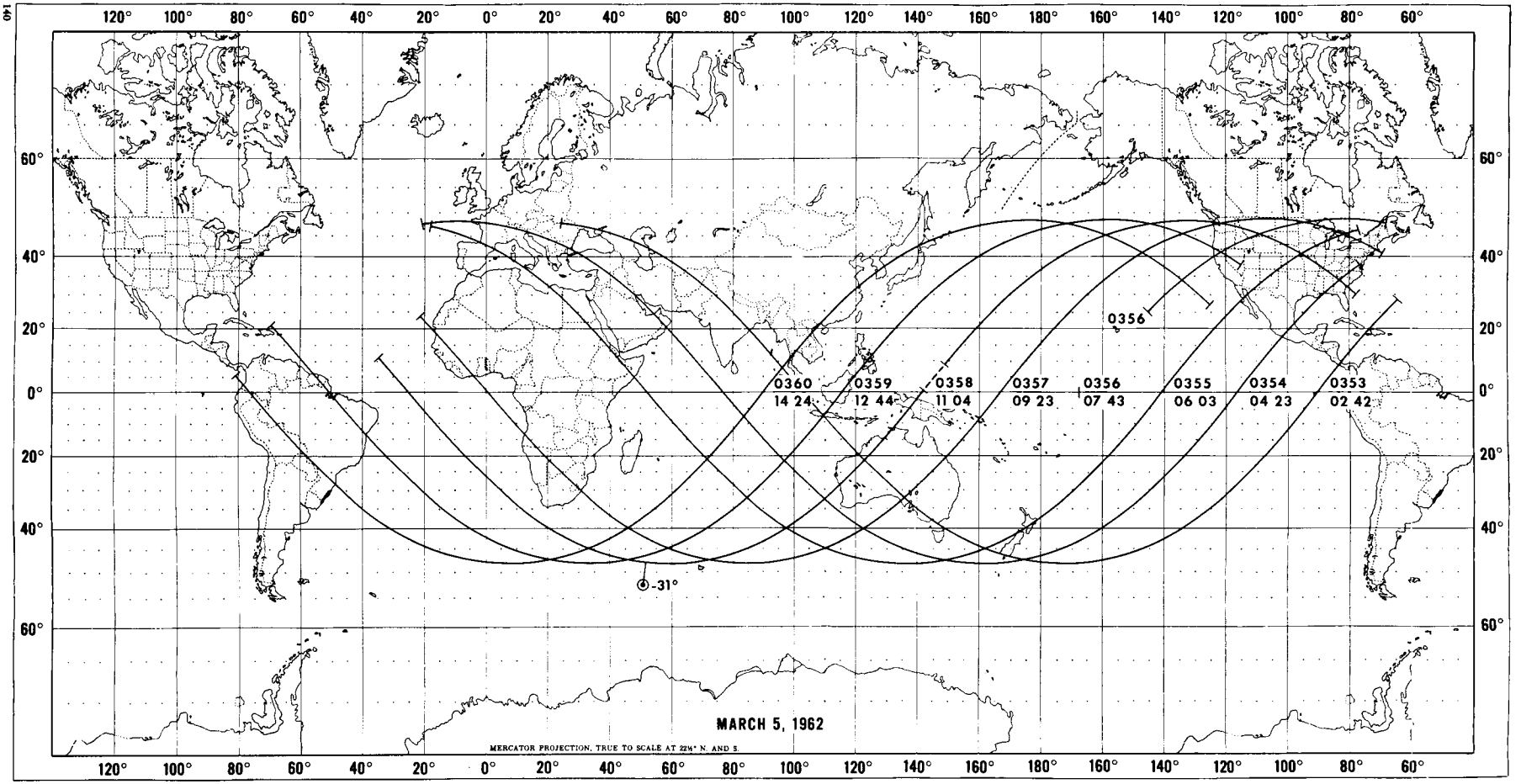
120° 100° 80° 60° 40° 20° 0° 20° 40° 60° 80° 100° 120° 140° 160° 180° 160° 140° 120° 100° 80° 60°
60°
40°
20°
0°
20°
40°
60°
0360
14 24
0359
12 44
0358
11 04
0357
09 23
0356
07 43
0355
06 03
0354
04 23
0353
02 42
0356
-31°
MARCH 5, 1962
MERCATOR PROJECTION, TRUE TO SCALE AT 22½° N. AND S.

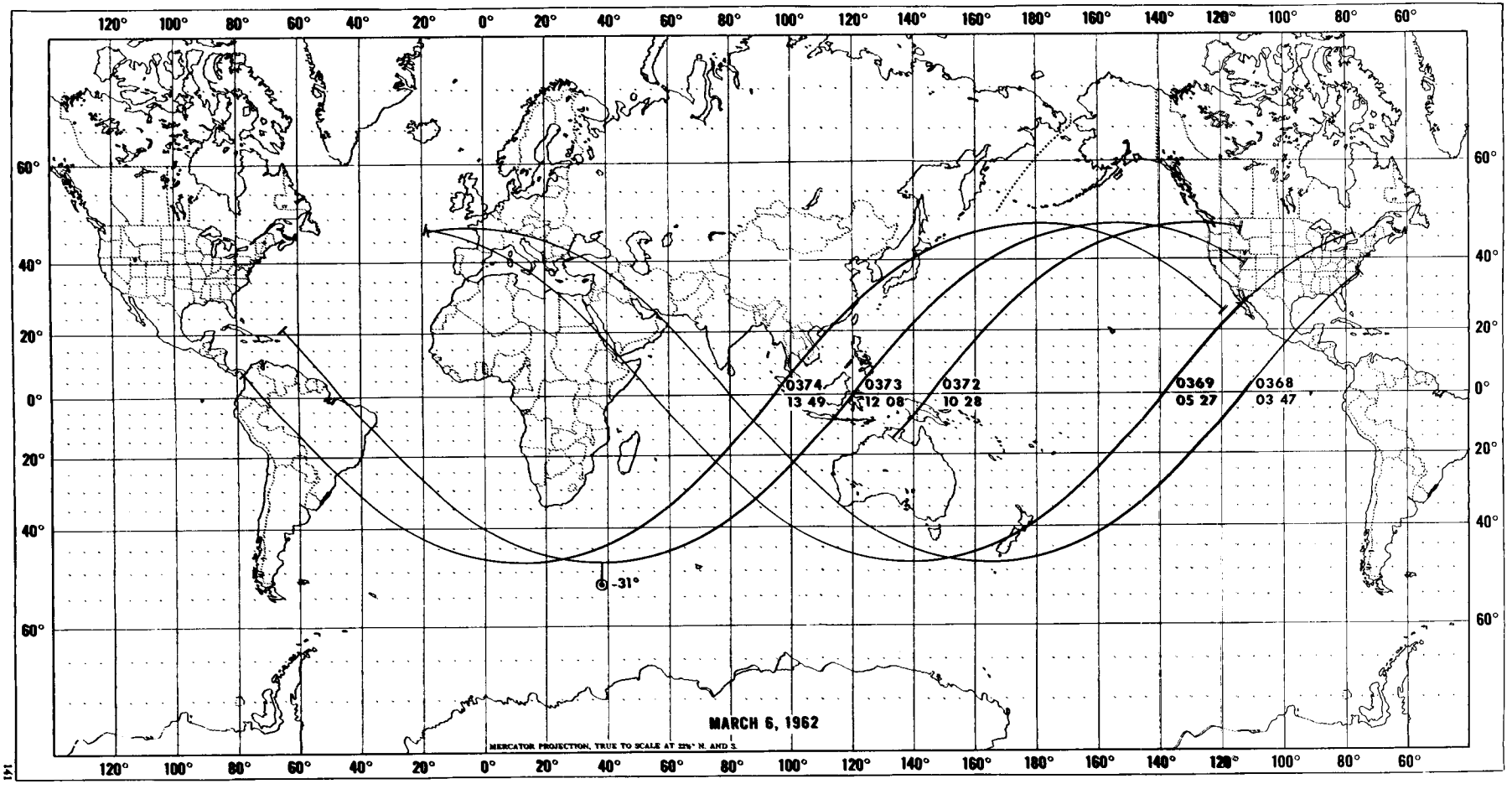
120° 100° 80° 60° 40° 20° 0° 20° 40° 60° 80° 100° 120° 140° 160° 180° 160° 140° 120° 100° 80° 60°
60°
40°
20°
0°
20°
40°
60°
0374
13 49
0373
12 08
0372
10 28
0369
05 27
0368
03 47
-31°
MARCH 6, 1962
MERCATOR PROJECTION, TRUE TO SCALE AT 22½° N. AND S.

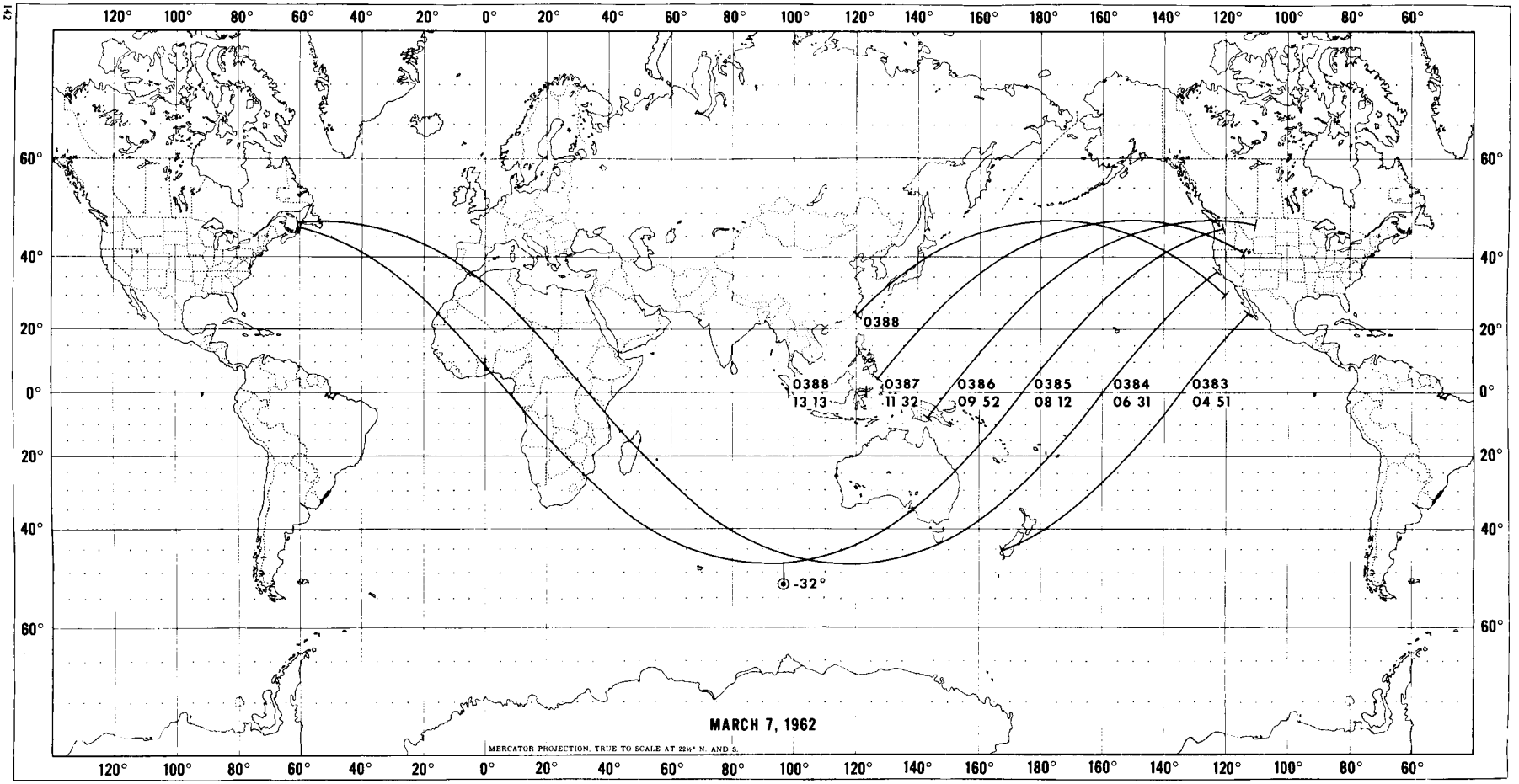
120° 100° 80° 60° 40° 20° 0° 20° 40° 60° 80° 100° 120° 140° 160° 180° 160° 140° 120° 100° 80° 60°
60°
40°
20°
0°
20°
40°
60°
0388
0388
13 13
0387
11 32
0386
09 52
0385
08 12
0384
06 31
0383
04 51
-32°
MARCH 7, 1962
MERCATOR PROJECTION, TRUE TO SCALE AT 22½° N. AND S.

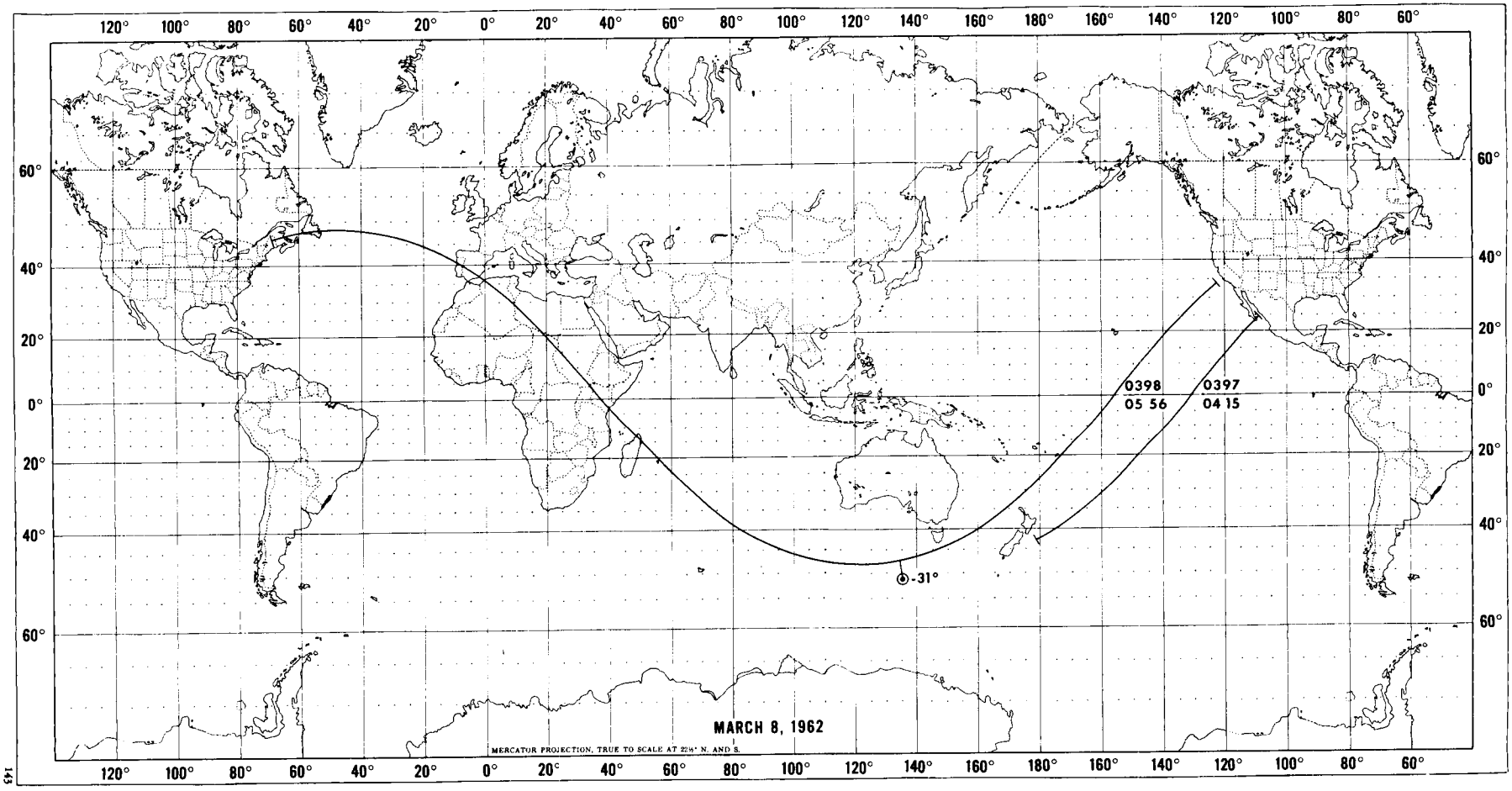
120° 100° 80° 60° 40° 20° 0° 20° 40° 60° 80° 100° 120° 140° 160° 180° 160° 140° 120° 100° 80° 60°
60°
40°
20°
0°
20°
40°
60°
0398
05 56
0397
04 15
-31°
MARCH 8, 1962
MERCATOR PROJECTION, TRUE TO SCALE AT 22½° N. AND S.

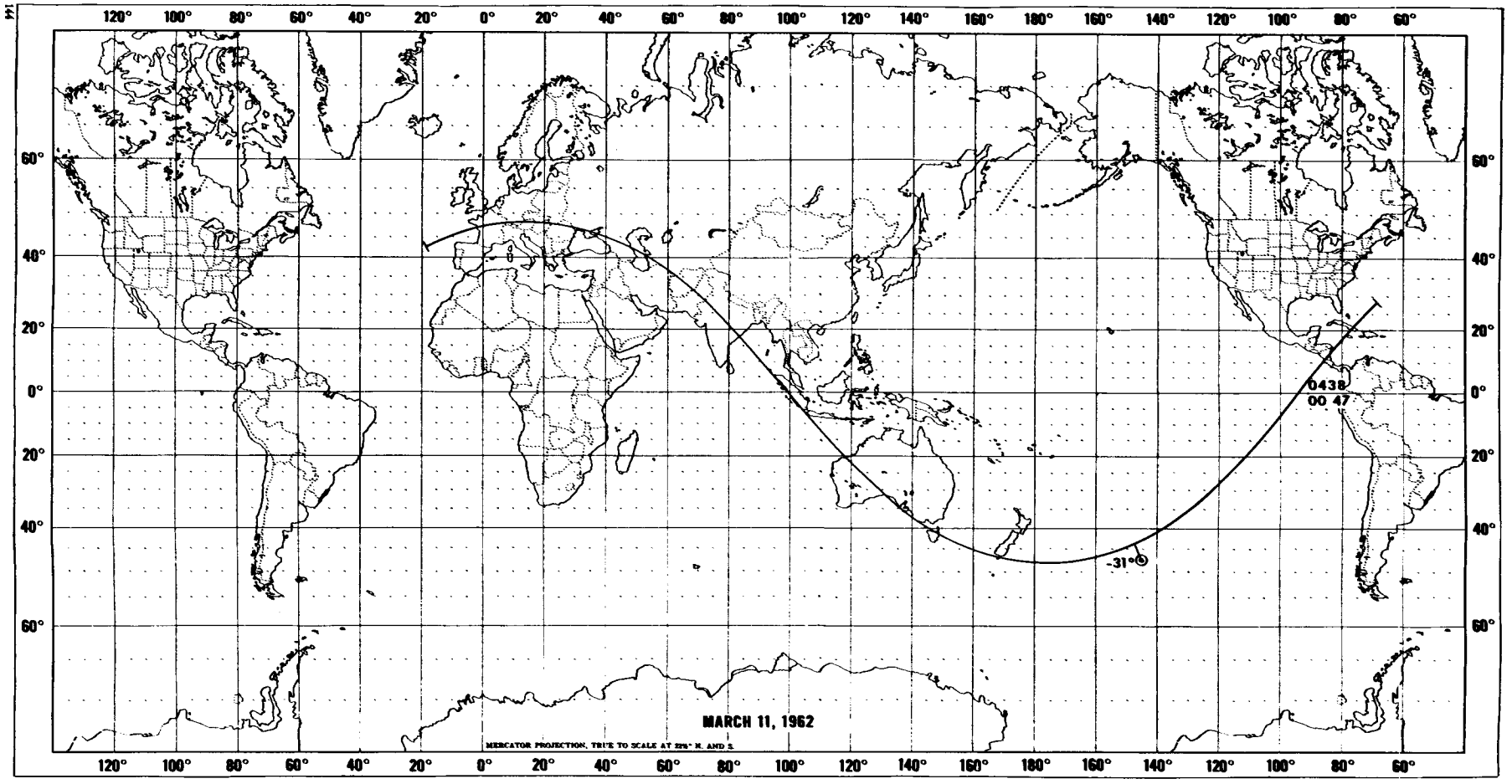
120° 100° 80° 60° 40° 20° 0° 20° 40° 60° 80° 100° 120° 140° 160° 180° 160° 140° 120° 100° 80° 60°
60°
40°
20°
0°
20°
40°
60°
0438
00 47
-31°
MARCH 11, 1962
MERCATOR PROJECTION, TRUE TO SCALE AT 32½° N. AND S.

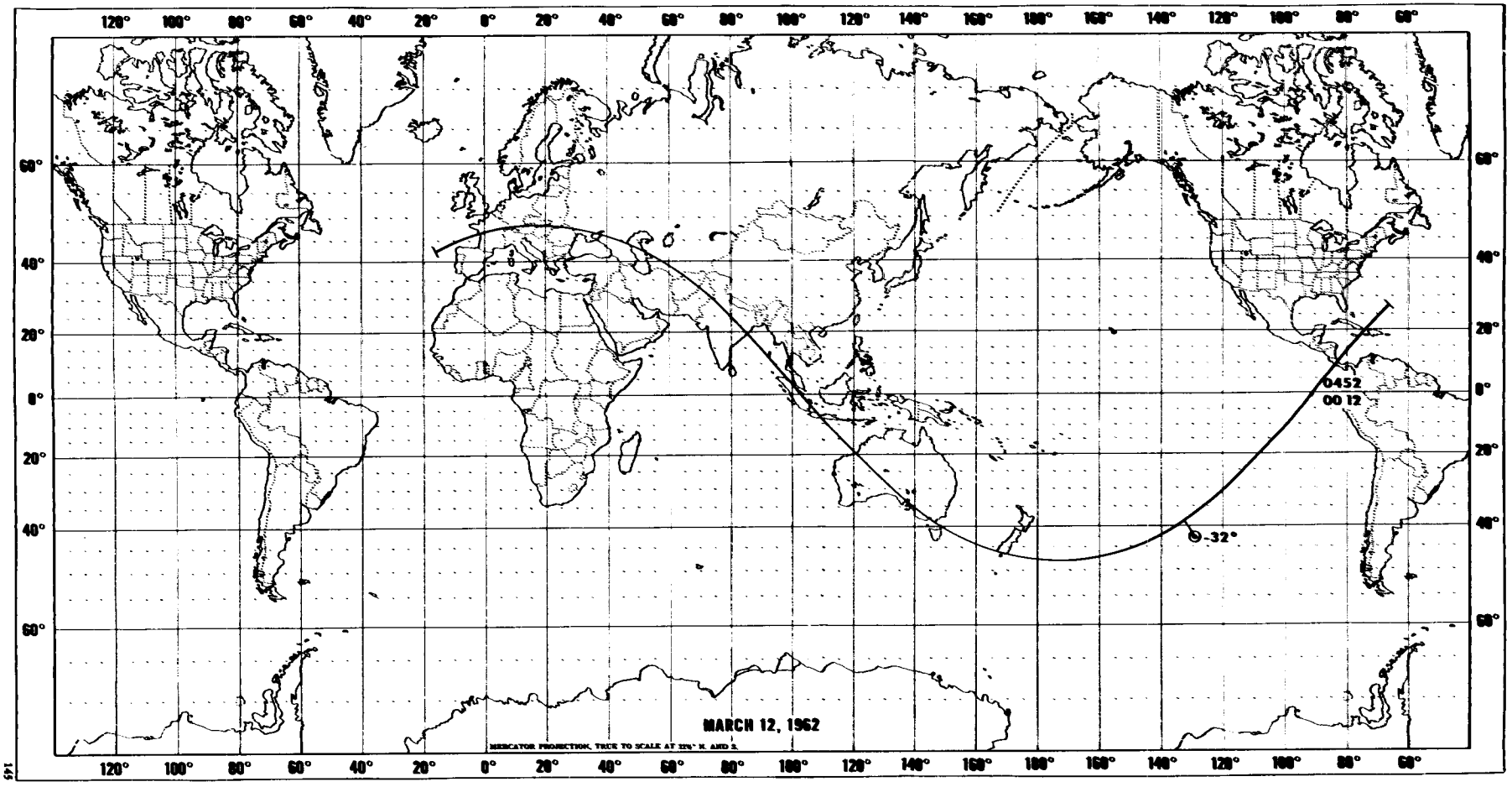
120° 100° 80° 60° 40° 20° 0° 20° 40° 60° 80° 100° 120° 140° 160° 180° 160° 140° 120° 100° 80° 60°
60°
40°
20°
0°
20°
40°
60°
0452
00 12
-32°
MARCH 12, 1962
MERCATOR PROJECTION, TRUE TO SCALE AT 32½° N. AND S.

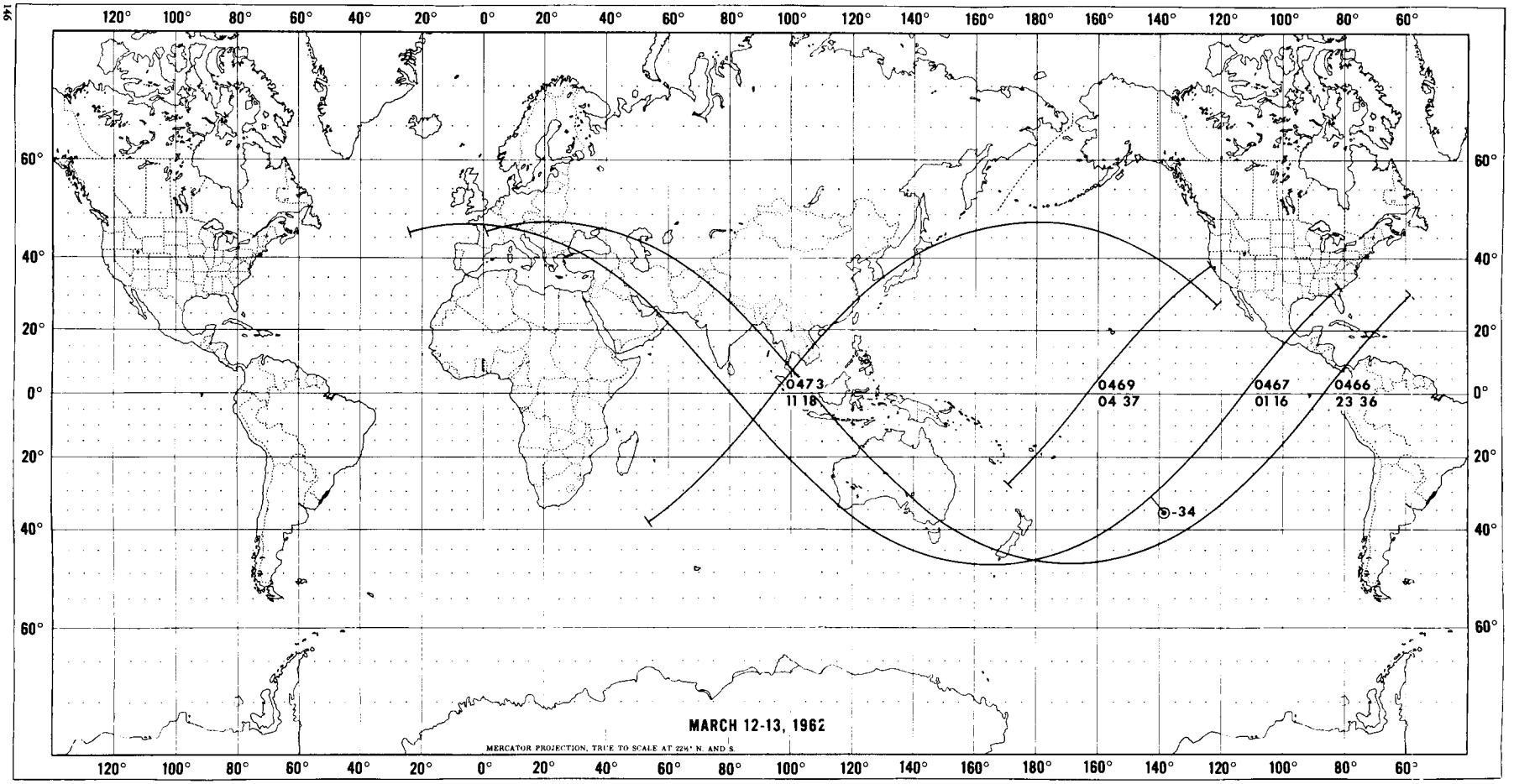
120° 100° 80° 60° 40° 20° 0° 20° 40° 60° 80° 100° 120° 140° 160° 180° 160° 140° 120° 100° 80° 60°
60°
40°
20°
0°
20°
40°
60°
0473
11 18
0469
04 37
0467
01 16
0466
23 36
-34
MARCH 12-13, 1962
MERCATOR PROJECTION, TRUE TO SCALE AT 22½° N. AND S.

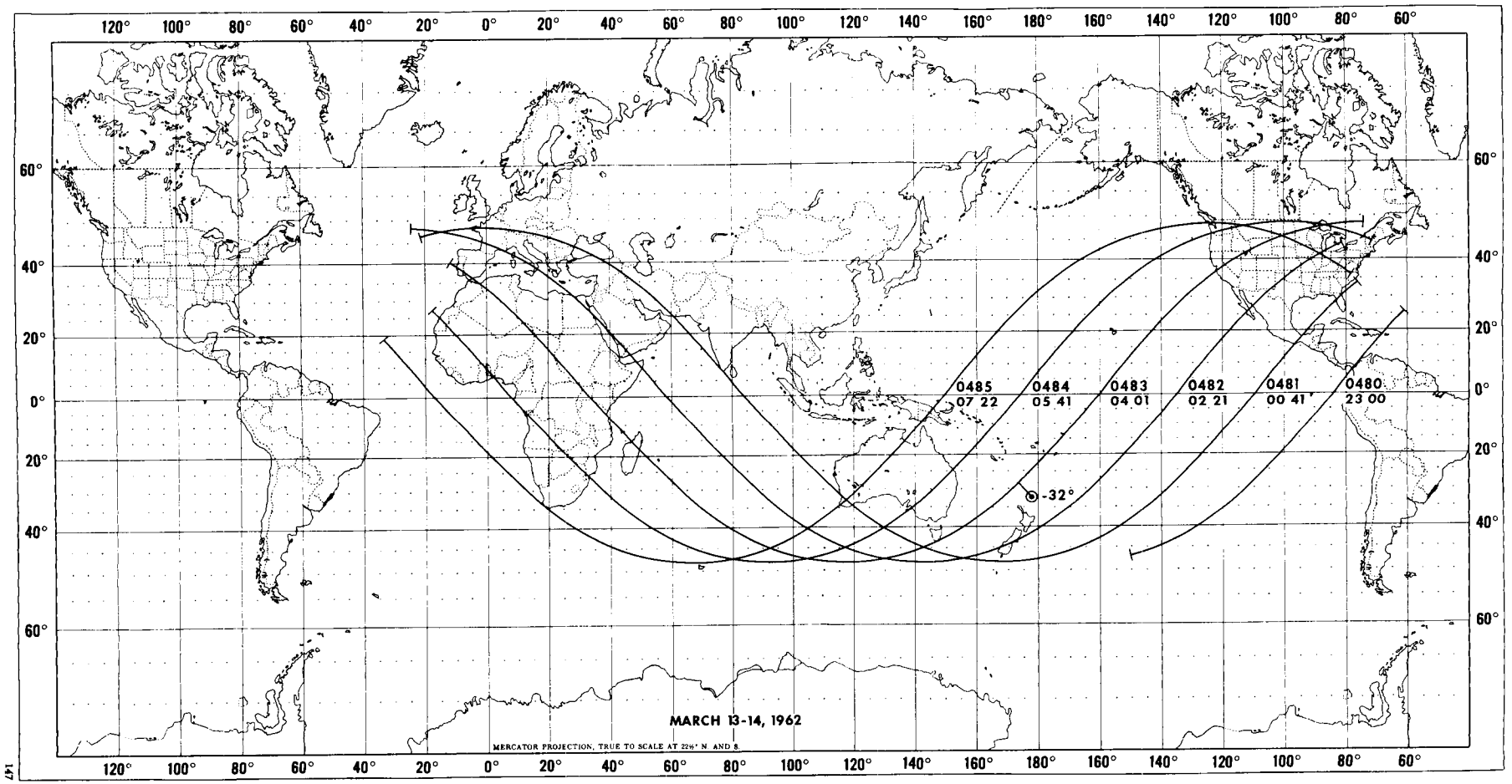
120° 100° 80° 60° 40° 20° 0° 20° 40° 60° 80° 100° 120° 140° 160° 180° 160° 140° 120° 100° 80° 60°
60°
40°
20°
0°
20°
40°
60°
0485
07 22
0484
05 41
0483
04 01
0482
02 21
0481
00 41
0480
23 00
-32°
MARCH 13-14, 1962
MERCATOR PROJECTION, TRUE TO SCALE AT 22½° N. AND S.

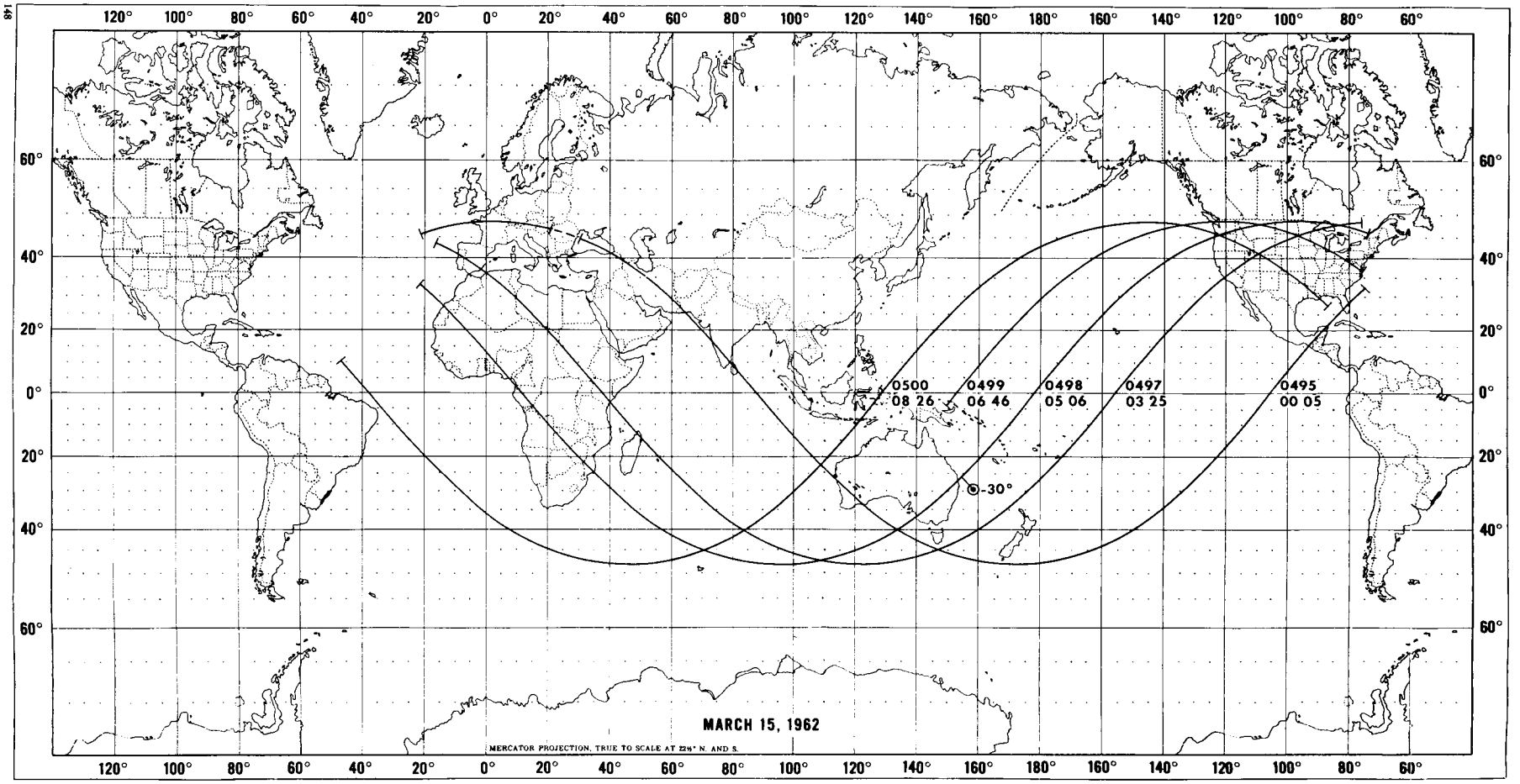
120° 100° 80° 60° 40° 20° 0° 20° 40° 60° 80° 100° 120° 140° 160° 180° 160° 140° 120° 100° 80° 60°
60°
40°
20°
0°
20°
40°
60°
0500
08 26
0499
06 46
0498
05 06
0497
03 25
0495
00 05
-30°
MARCH 15, 1962
MERCATOR PROJECTION, TRUE TO SCALE AT 22½° N. AND S.

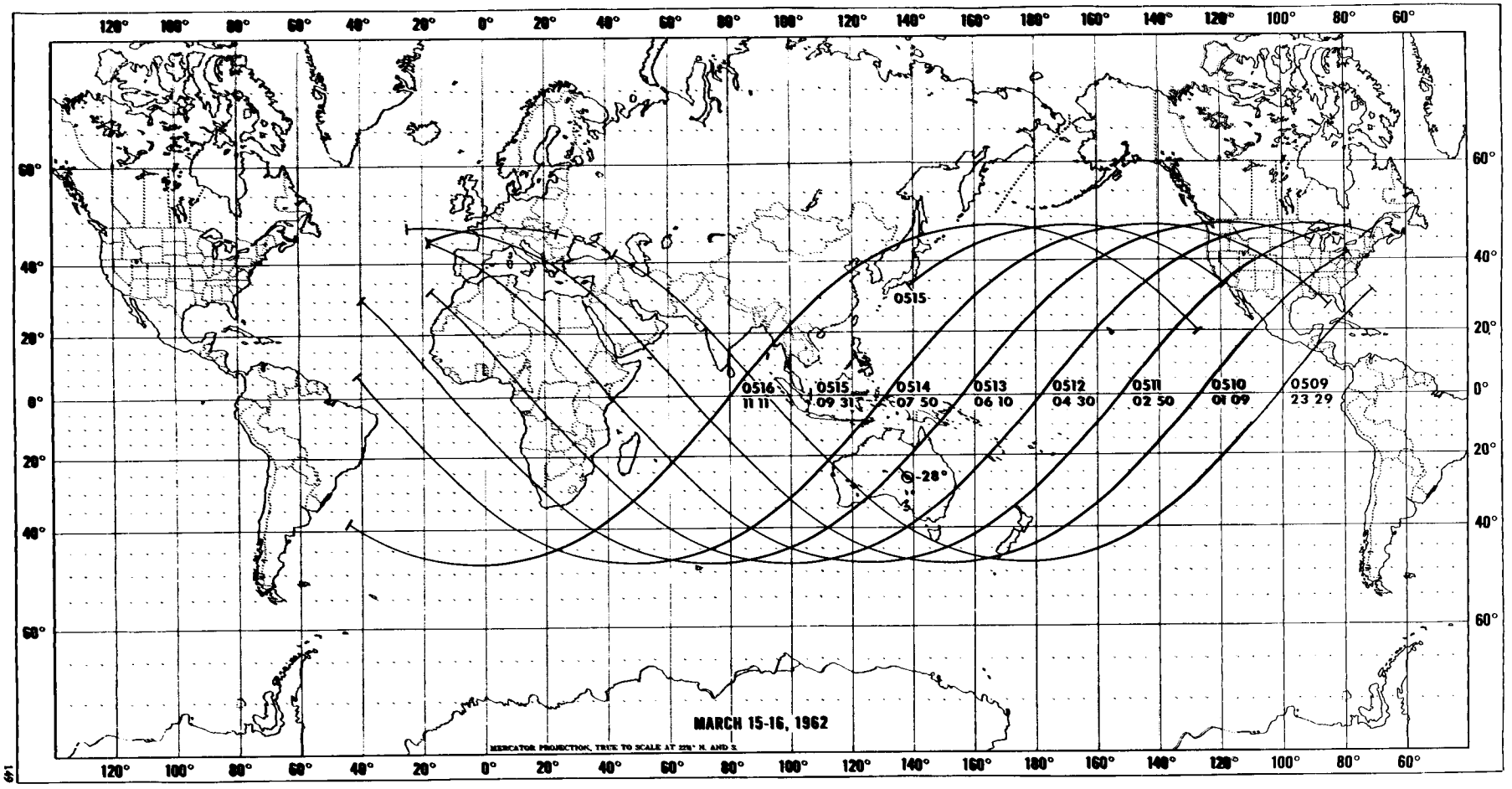
0516
11 11
0515
09 31
0514
07 50
0513
06 10
0512
04 30
0511
02 50
0510
01 09
0509
23 29
0515
-28°
MARCH 15-16, 1962
MERCATOR PROJECTION, TRUE TO SCALE AT 25½° N. AND S.

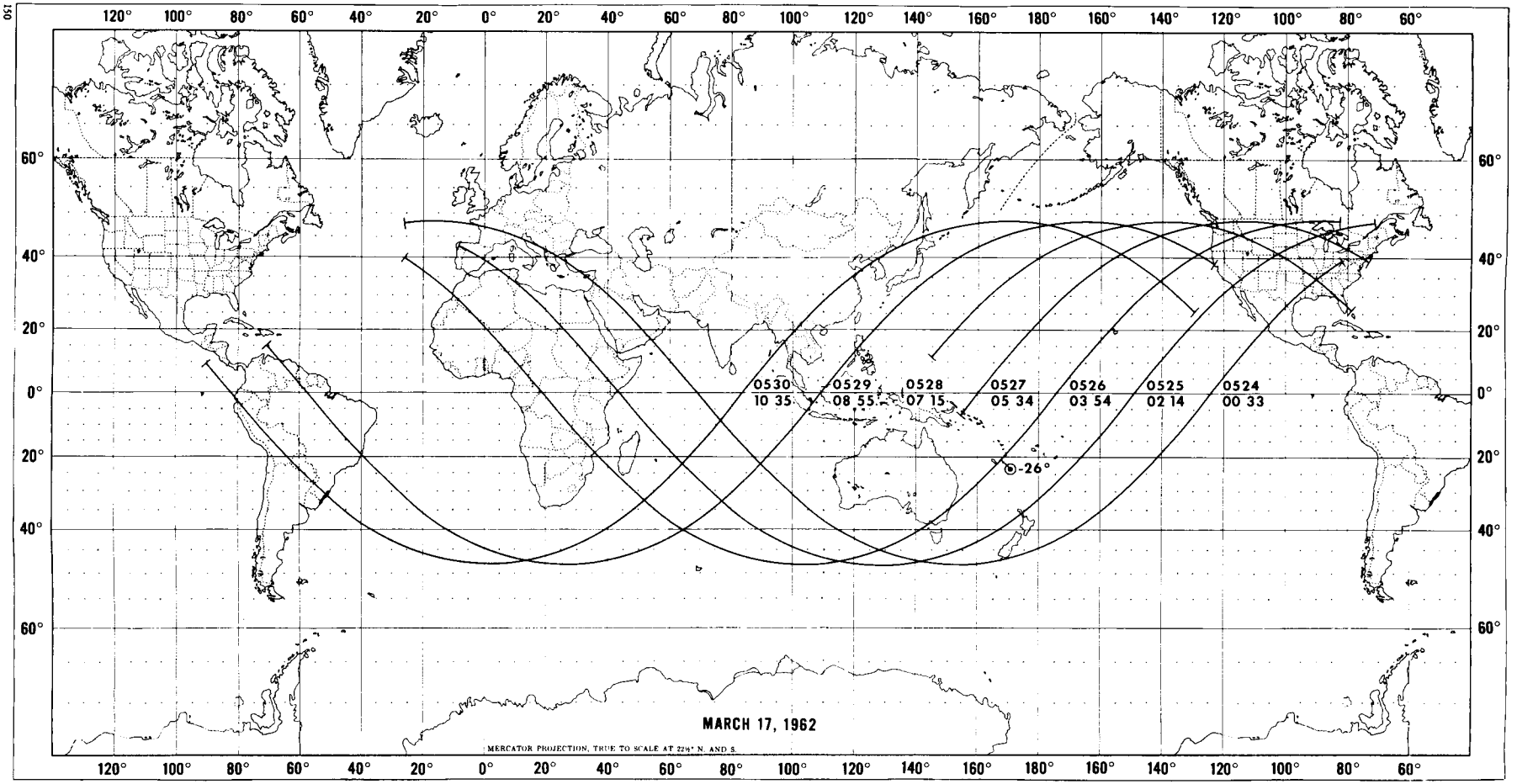
120° 100° 80° 60° 40° 20° 0° 20° 40° 60° 80° 100° 120° 140° 160° 180° 160° 140° 120° 100° 80° 60°
60°
40°
20°
0°
20°
40°
60°
0530
10 35
0529
08 55
0528
07 15
0527
05 34
0526
03 54
0525
02 14
0524
00 33
-26°
MARCH 17, 1962
MERCATOR PROJECTION, TRUE TO SCALE AT 22½° N. AND S.

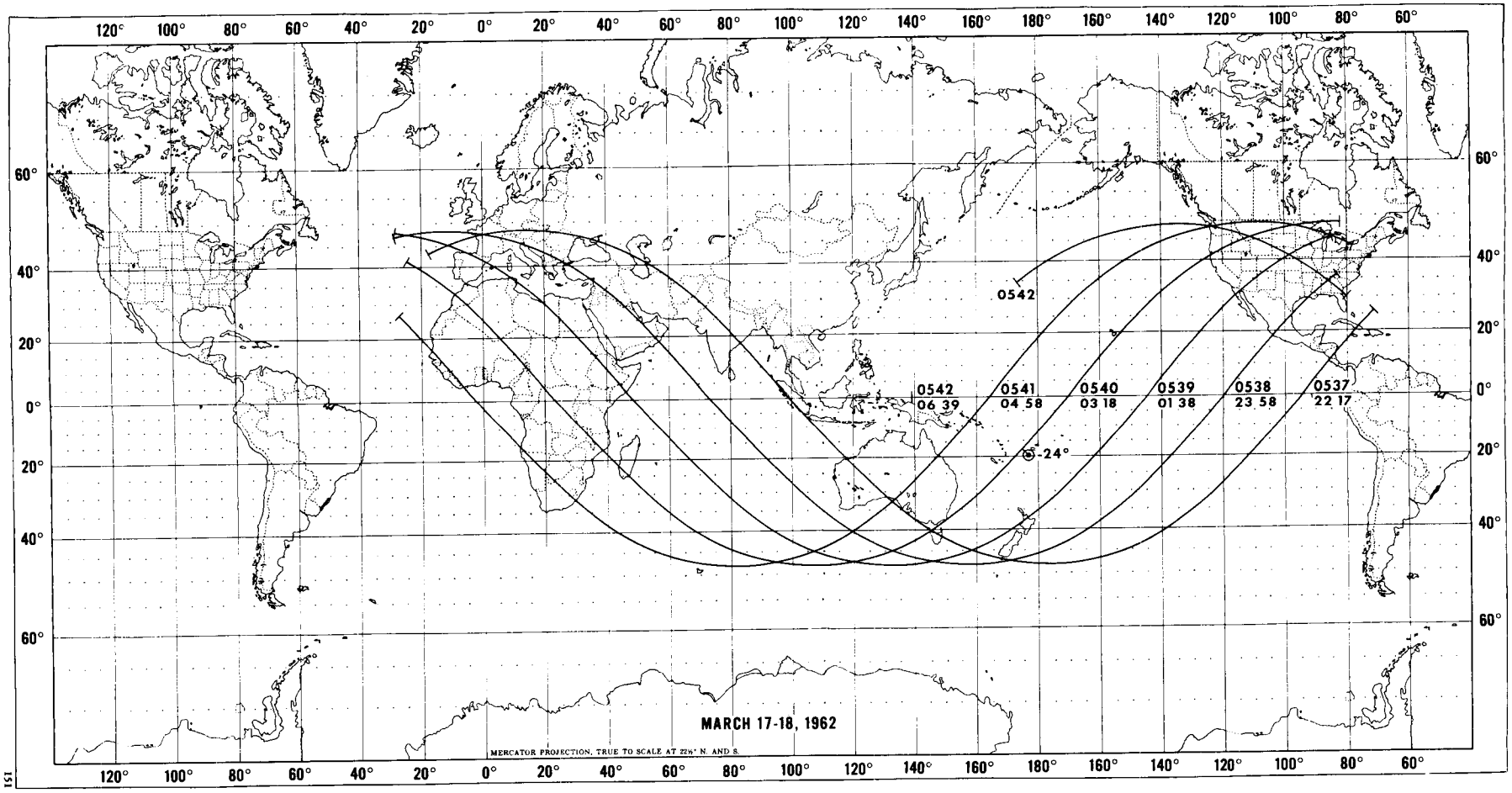
120° 100° 80° 60° 40° 20° 0° 20° 40° 60° 80° 100° 120° 140° 160° 180° 160° 140° 120° 100° 80° 60°
60°
40°
20°
0°
20°
40°
60°
0542
0542 06 39
0541 04 58
0540 03 18
0539 01 38
0538 23 58
0537 22 17
-24°
MARCH 17-18, 1962
MERCATOR PROJECTION, TRUE TO SCALE AT 22½° N. AND S.

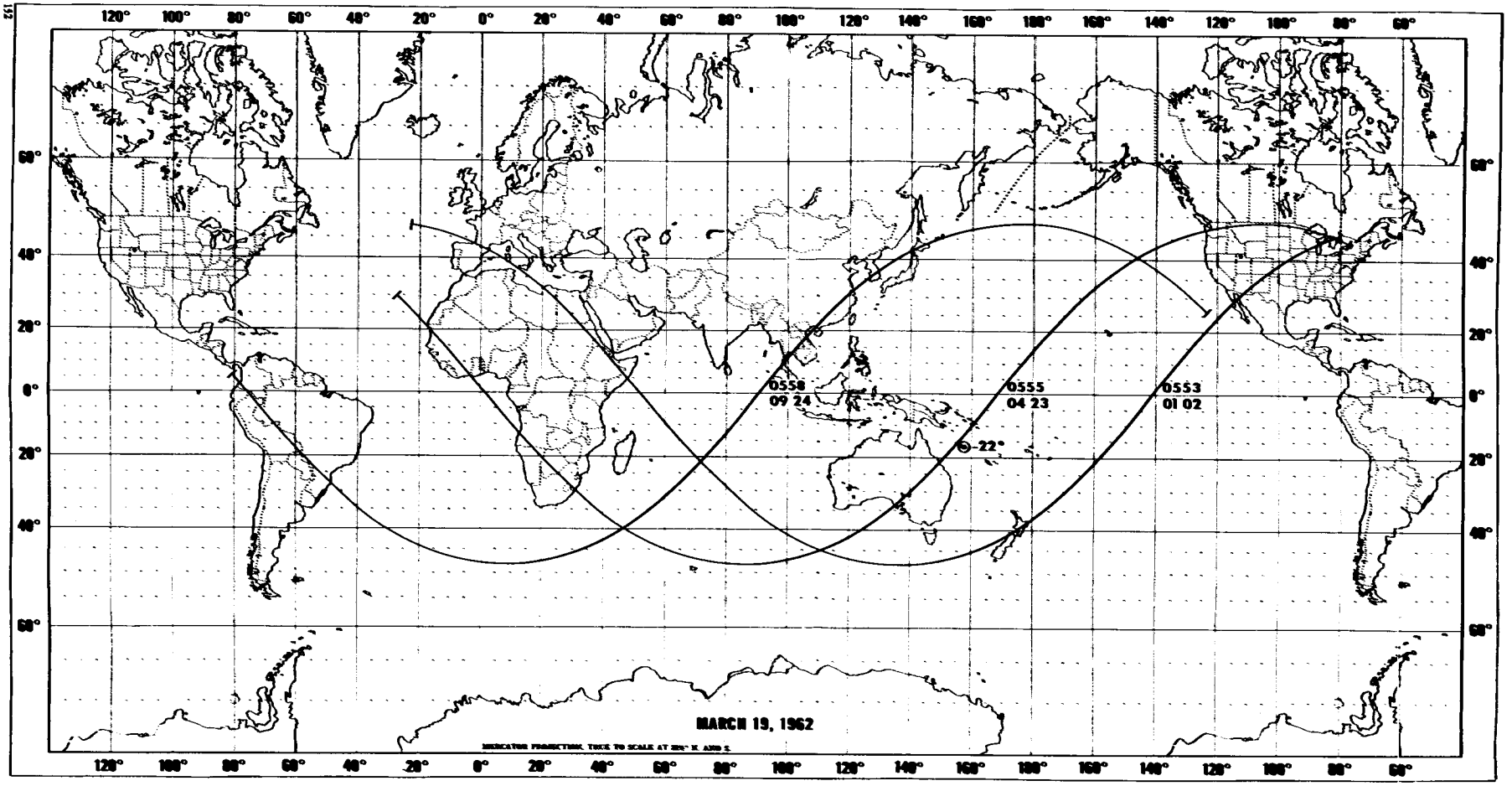
0558
09 24
0555
04 23
0553
01 02
22°
MARCH 19, 1962

728-166 O - 64 - 11

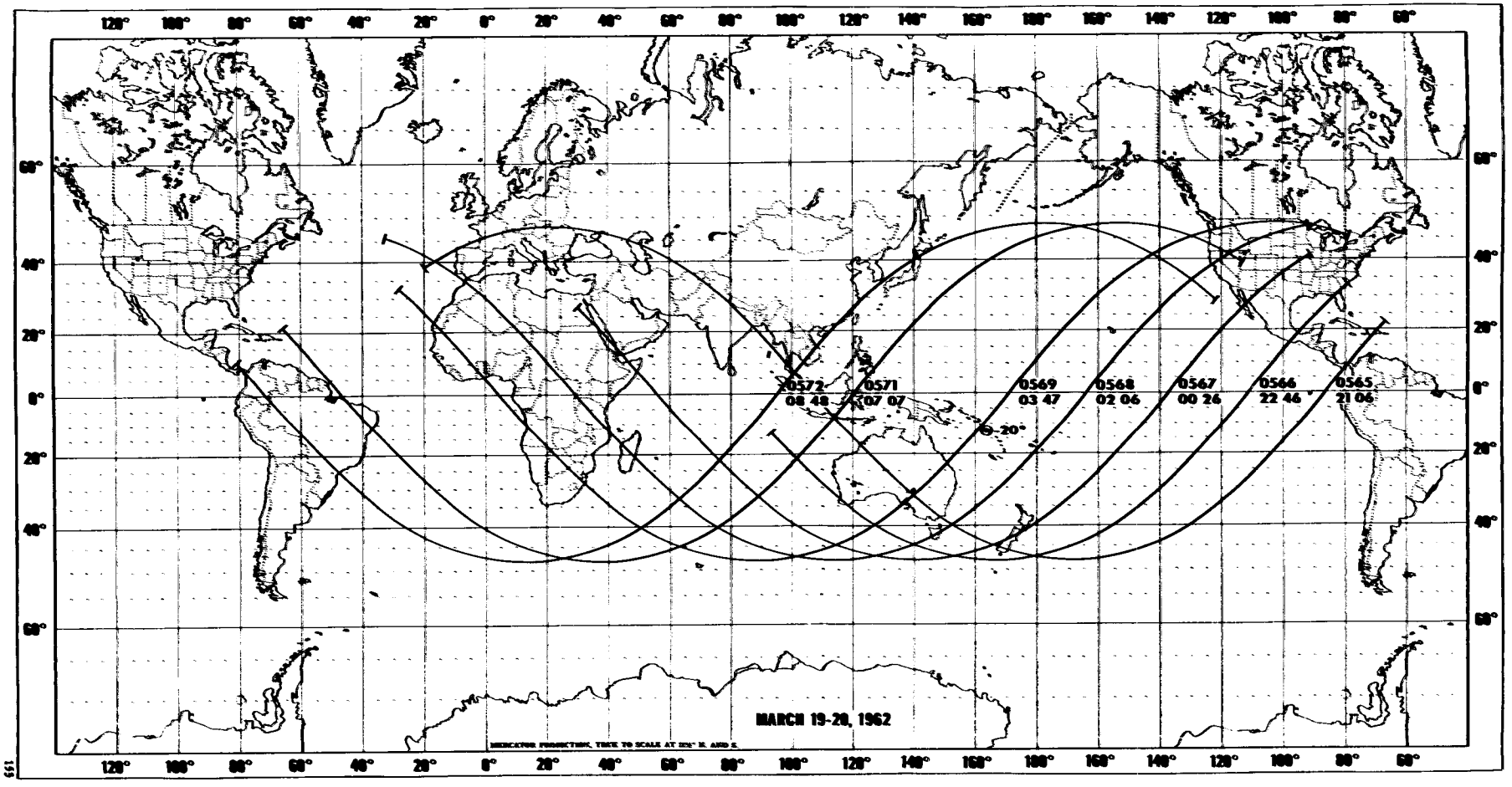

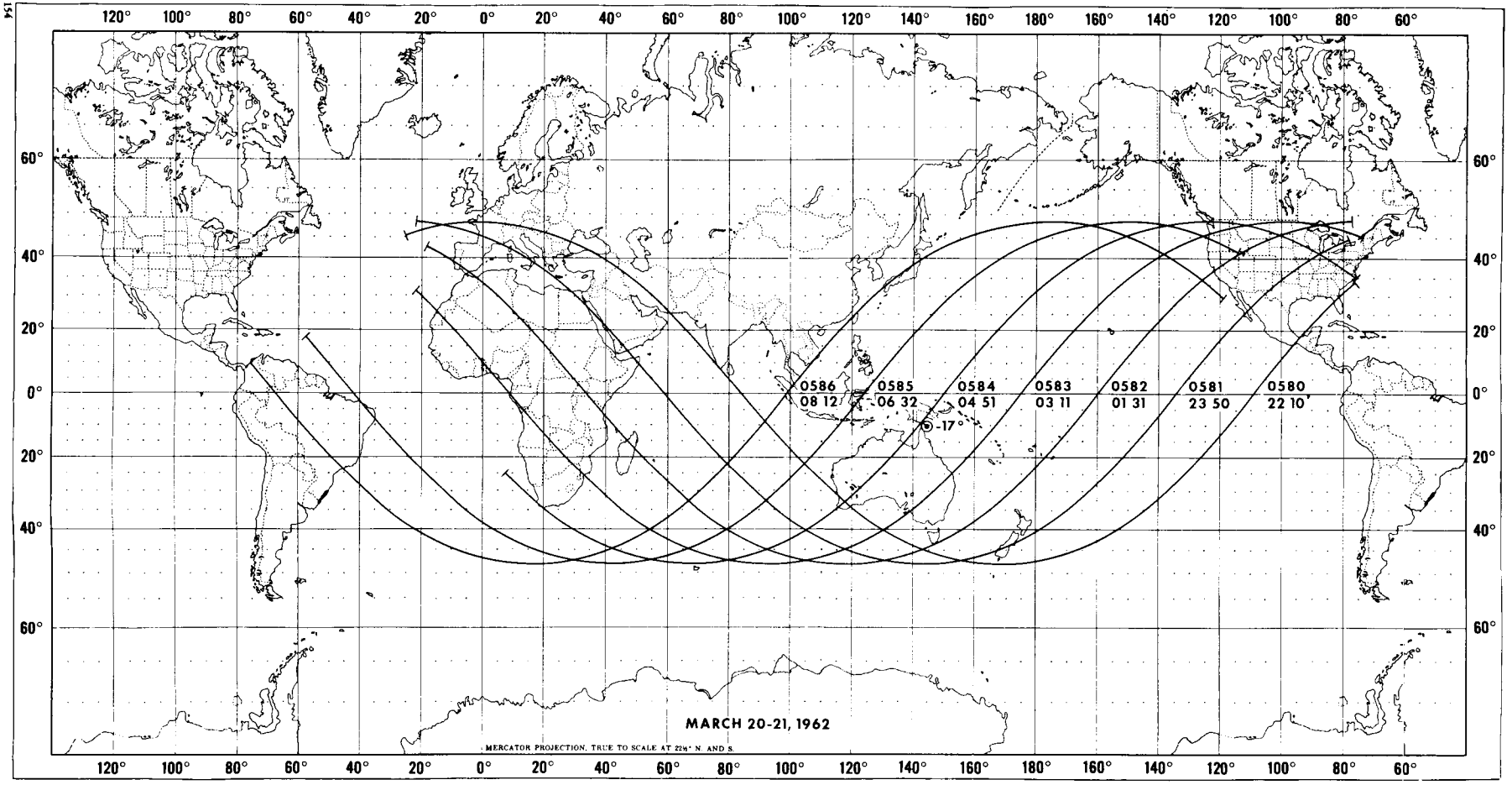
120° 100° 80° 60° 40° 20° 0° 20° 40° 60° 80° 100° 120° 140° 160° 180° 160° 140° 120° 100° 80° 60°
60°
40°
20°
0°
20°
40°
60°
0586
08 12
0585
06 32
0584
04 51
0583
03 11
0582
01 31
0581
23 50
0580
22 10
-17°
MARCH 20-21, 1962
MERCATOR PROJECTION. TRUE TO SCALE AT 22½° N. AND S.

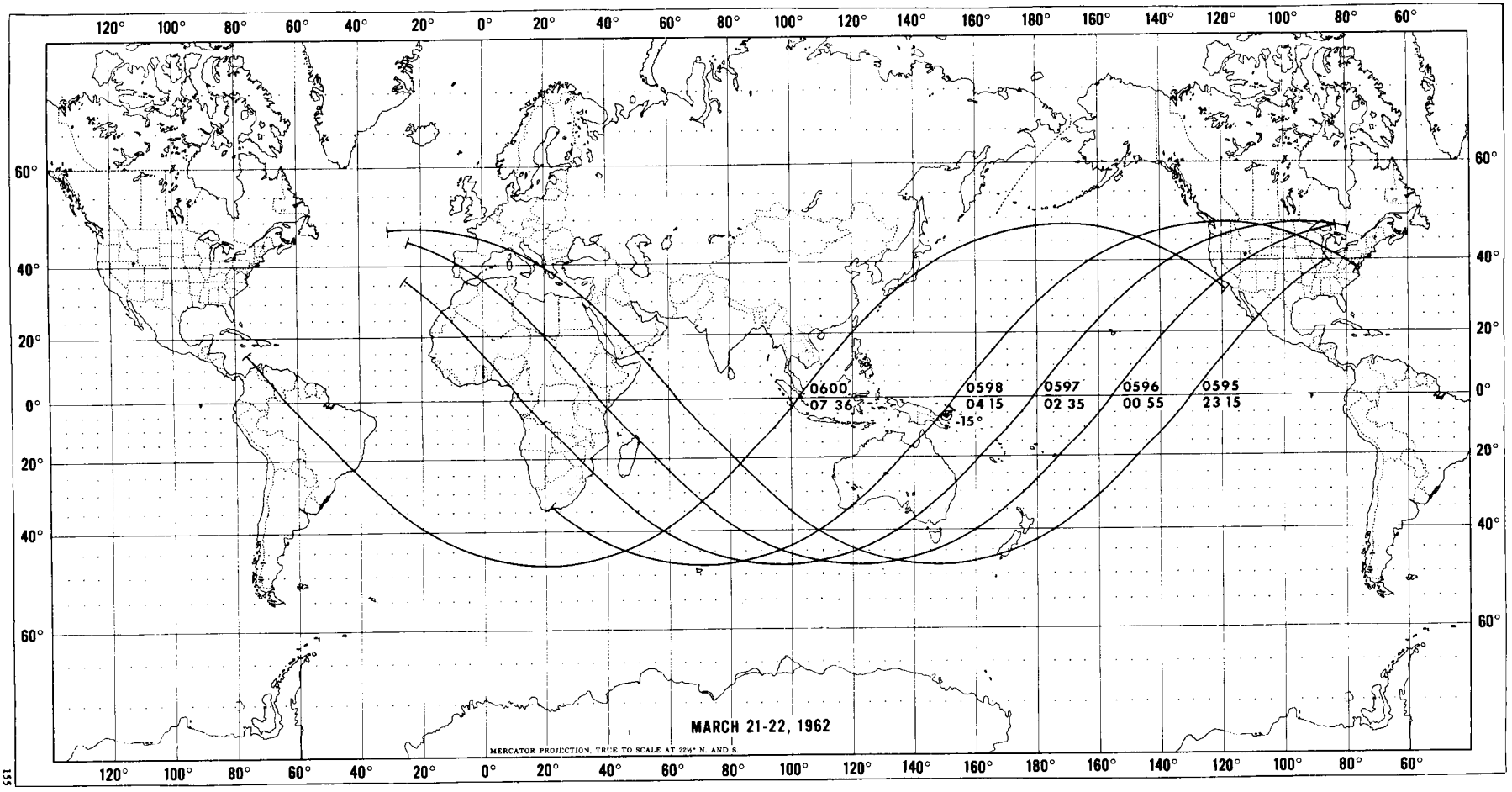
120° 100° 80° 60° 40° 20° 0° 20° 40° 60° 80° 100° 120° 140° 160° 180° 160° 140° 120° 100° 80° 60°
60°
40°
20°
0°
20°
40°
60°
0600
07 36
0598
04 15
-15°
0597
02 35
0596
00 55
0595
23 15
MARCH 21-22, 1962
MERCATOR PROJECTION, TRUE TO SCALE AT 22½° N. AND S.

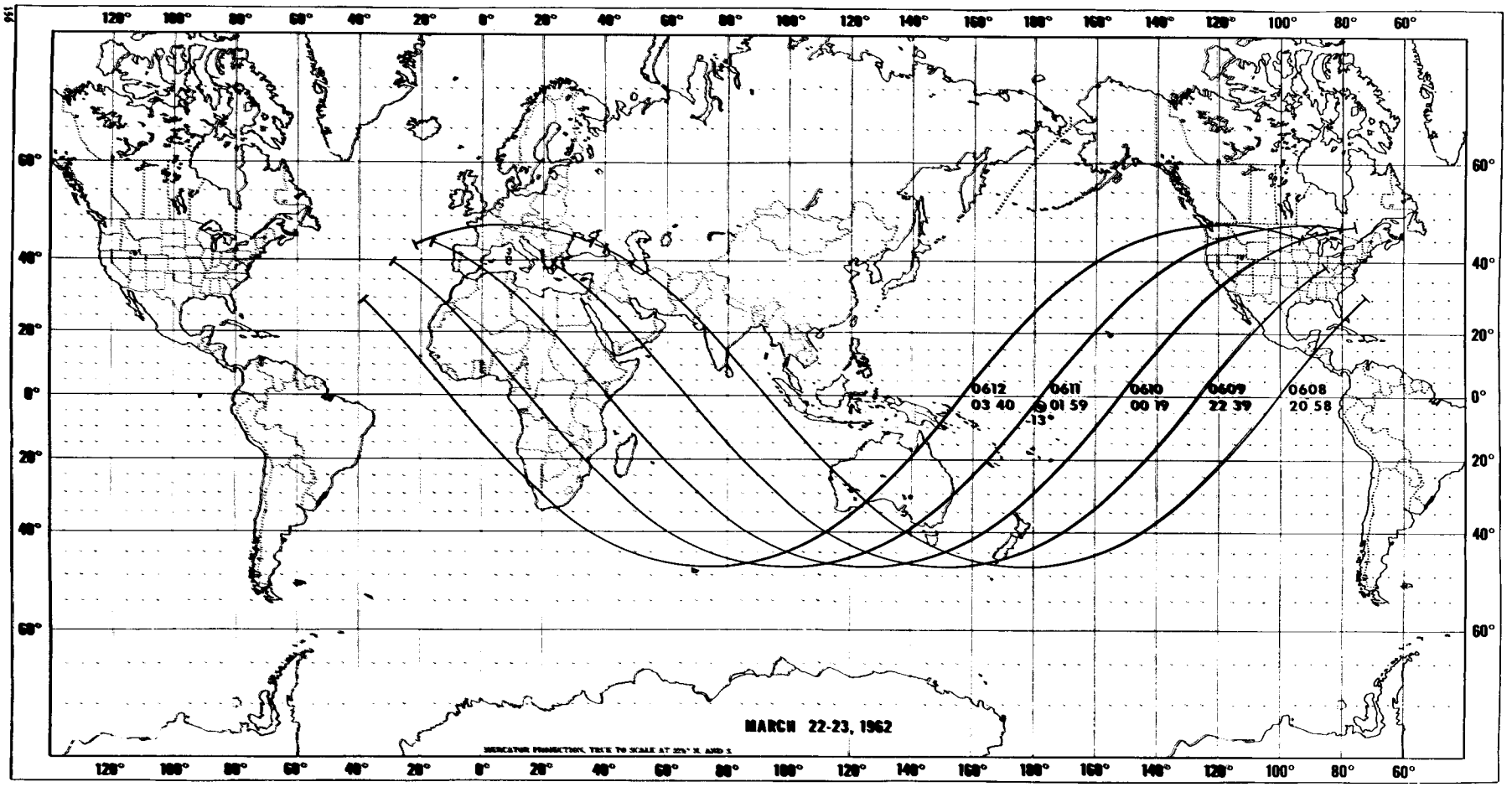
0612
03 40
0611
01 59
0610
00 19
0609
22 39
0608
20 58
-13°
MARCH 22-23, 1962

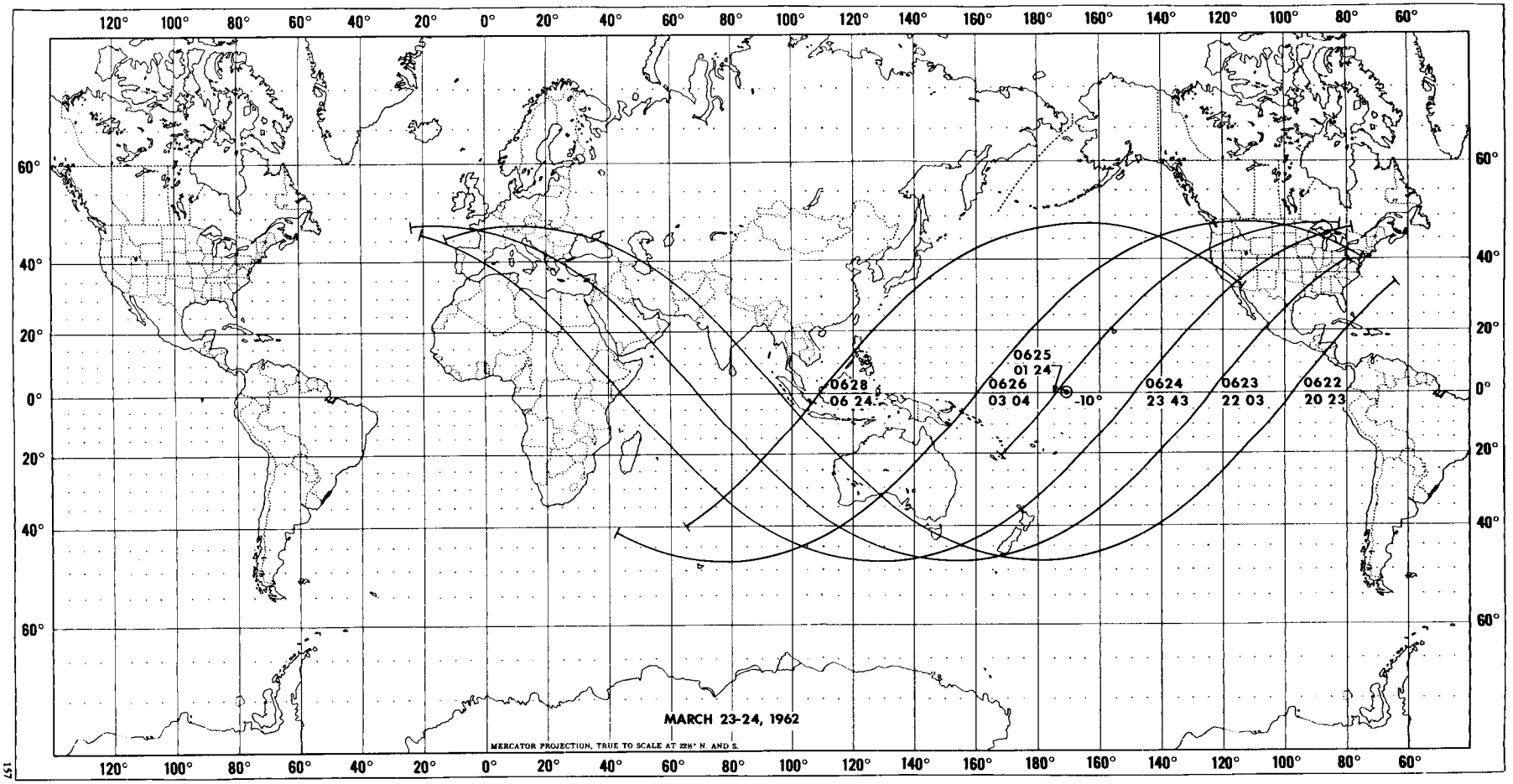
120° 100° 80° 60° 40° 20° 0° 20° 40° 60° 80° 100° 120° 140° 160° 180° 160° 140° 120° 100° 80° 60°
60°
40°
20°
0°
20°
40°
60°
0628
06 24
0625
01 24
0626
03 04
-10°
0624
23 43
0623
22 03
0622
20 23
MARCH 23-24, 1962
MERCATOR PROJECTION, TRUE TO SCALE AT 22½° N. AND S.

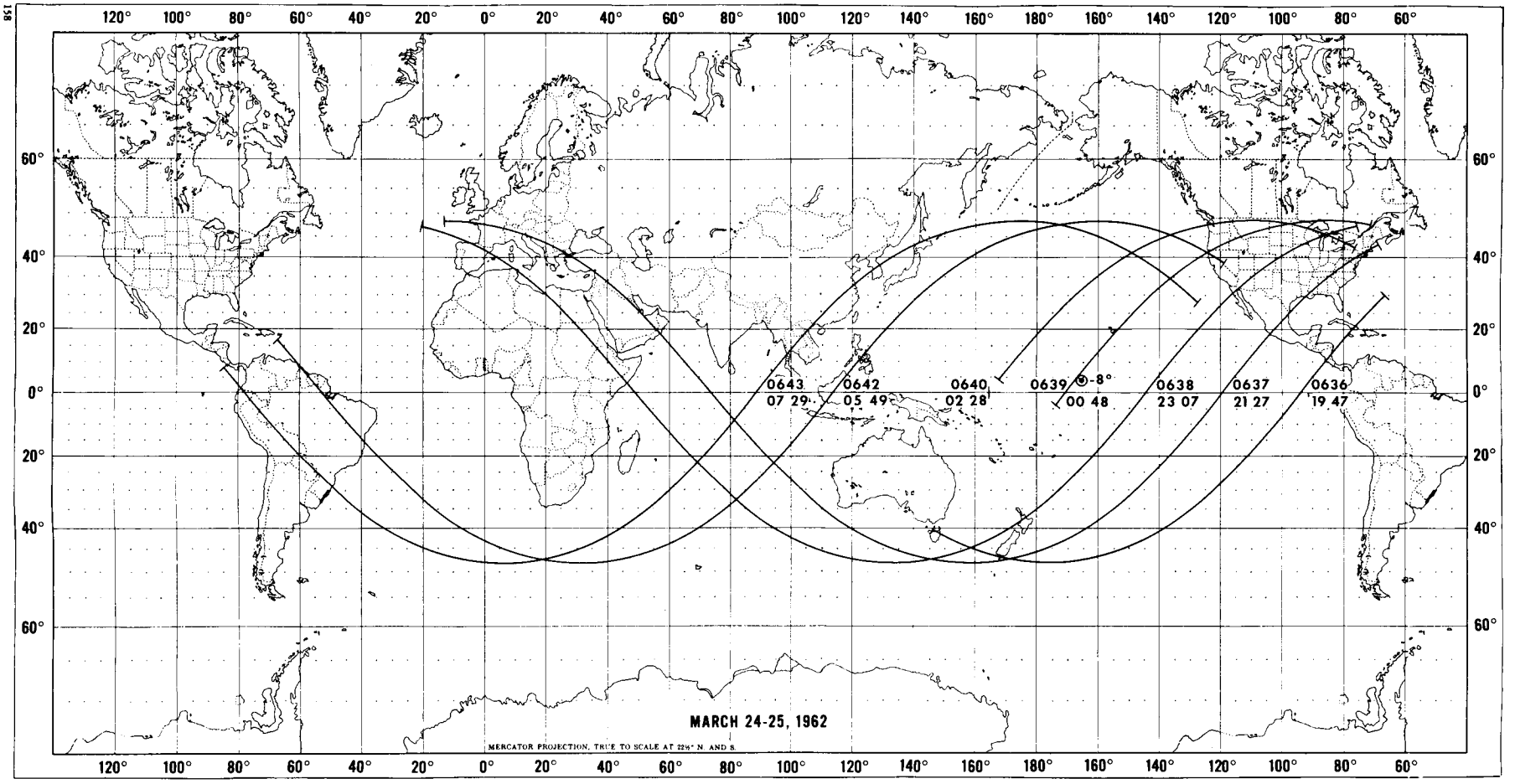
120° 100° 80° 60° 40° 20° 0° 20° 40° 60° 80° 100° 120° 140° 160° 180° 160° 140° 120° 100° 80° 60°
60°
40°
20°
0°
20°
40°
60°
0643
07 29
0642
05 49
0640
02 28
0639
00 48
-8°
0638
23 07
0637
21 27
0636
19 47
MARCH 24-25, 1962
MERCATOR PROJECTION, TRUE TO SCALE AT 22½° N. AND S.

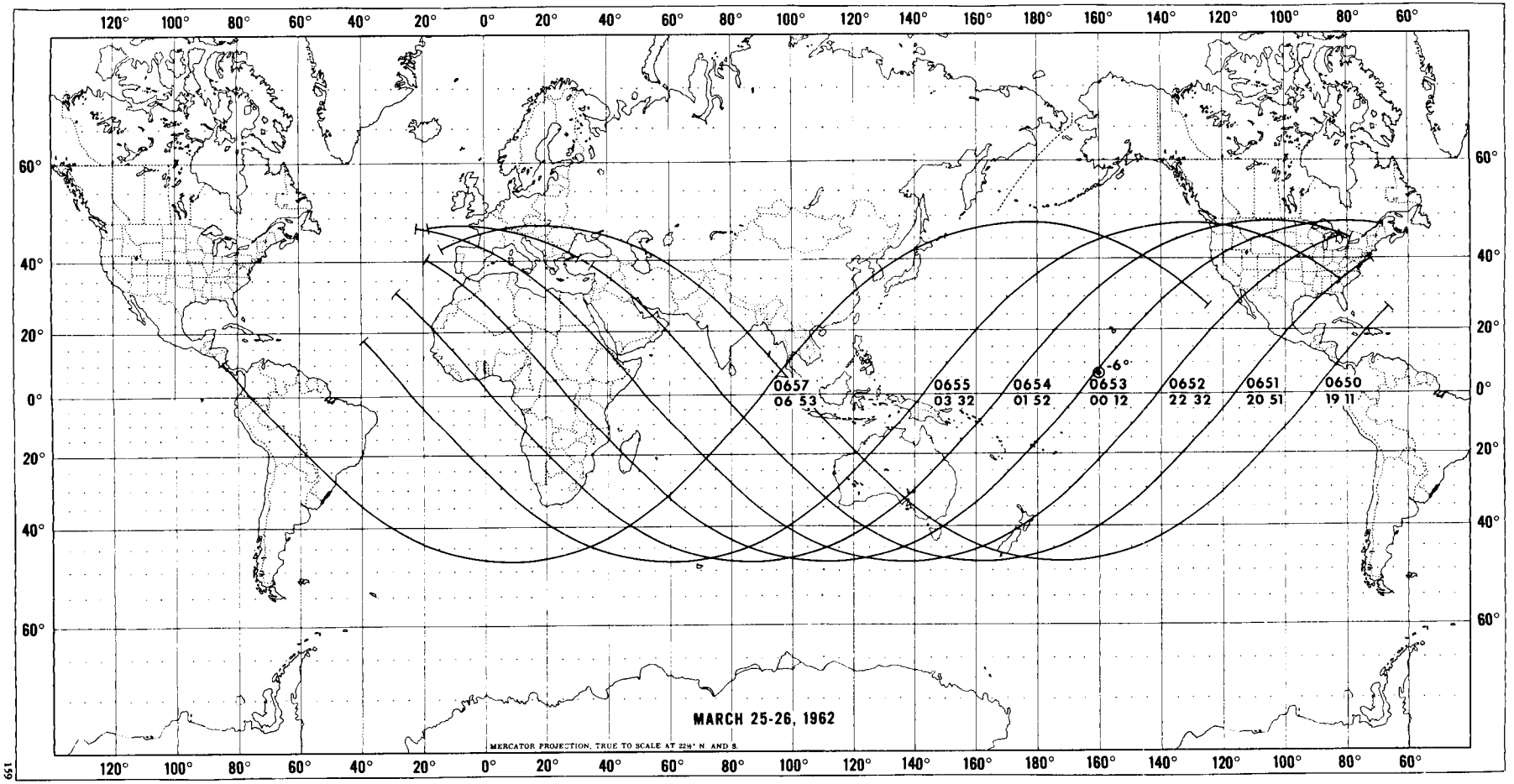
120° 100° 80° 60° 40° 20° 0° 20° 40° 60° 80° 100° 120° 140° 160° 180° 160° 140° 120° 100° 80° 60°
60°
40°
20°
0°
20°
40°
60°
0657
06 53
0655
03 32
0654
01 52
-6°
0653
00 12
0652
22 32
0651
20 51
0650
19 11
MARCH 25-26, 1962
MERCATOR PROJECTION, TRUE TO SCALE AT 22½° N. AND S.

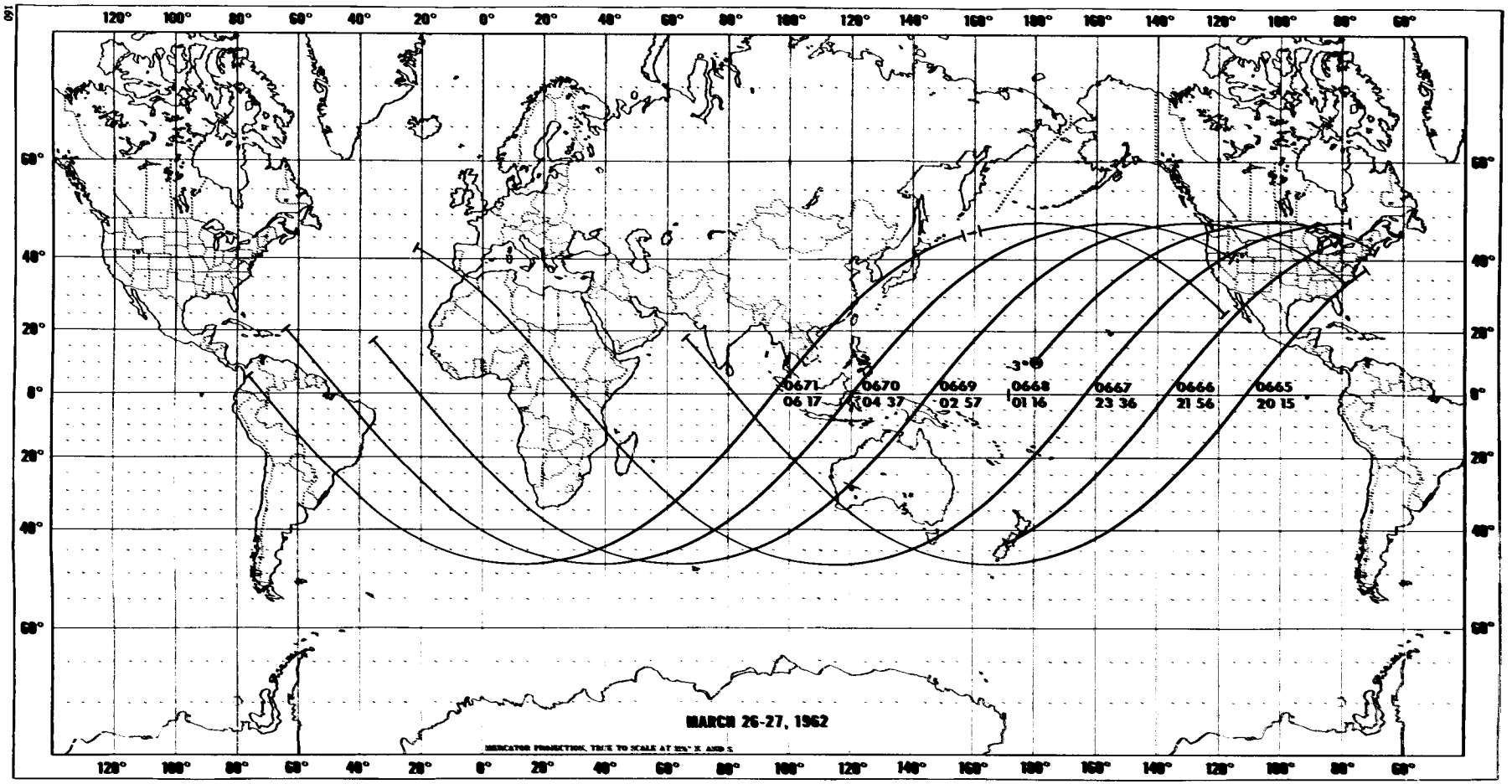
0671
06 17
0670
04 37
0669
02 57
0668
01 16
0667
23 36
0666
21 56
0665
20 15
MARCH 26-27, 1962

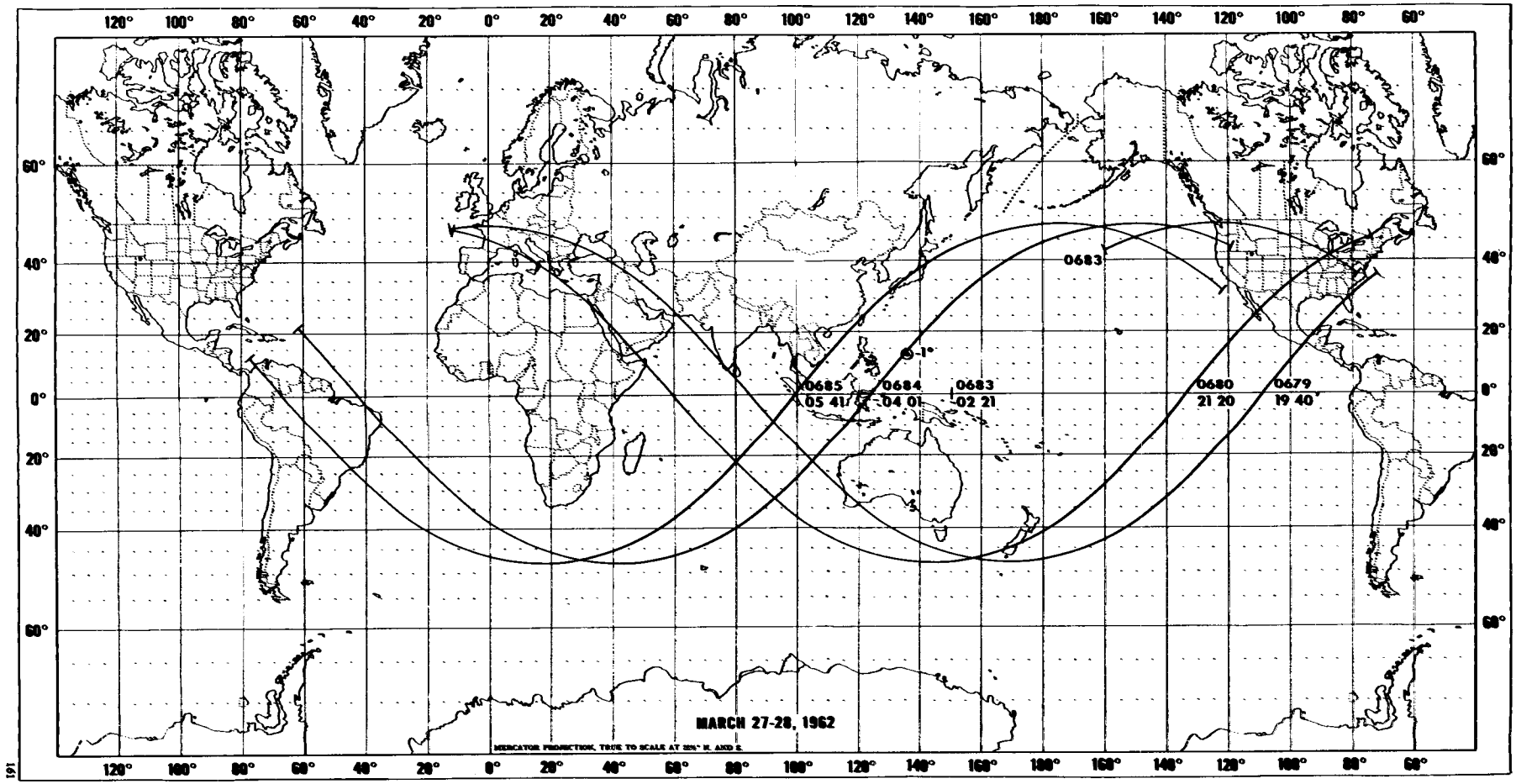
120° 100° 80° 60° 40° 20° 0° 20° 40° 60° 80° 100° 120° 140° 160° 180° 160° 140° 120° 100° 80° 60°
60°
40°
20°
0°
20°
40°
60°
0683
-1°
0685
05 41
0684
-04 01
0683
-02 21
0680
21 20
0679
19 40
MARCH 27-28, 1962
MERCATOR PROJECTION, TRUE TO SCALE AT 22½° N. AND S.

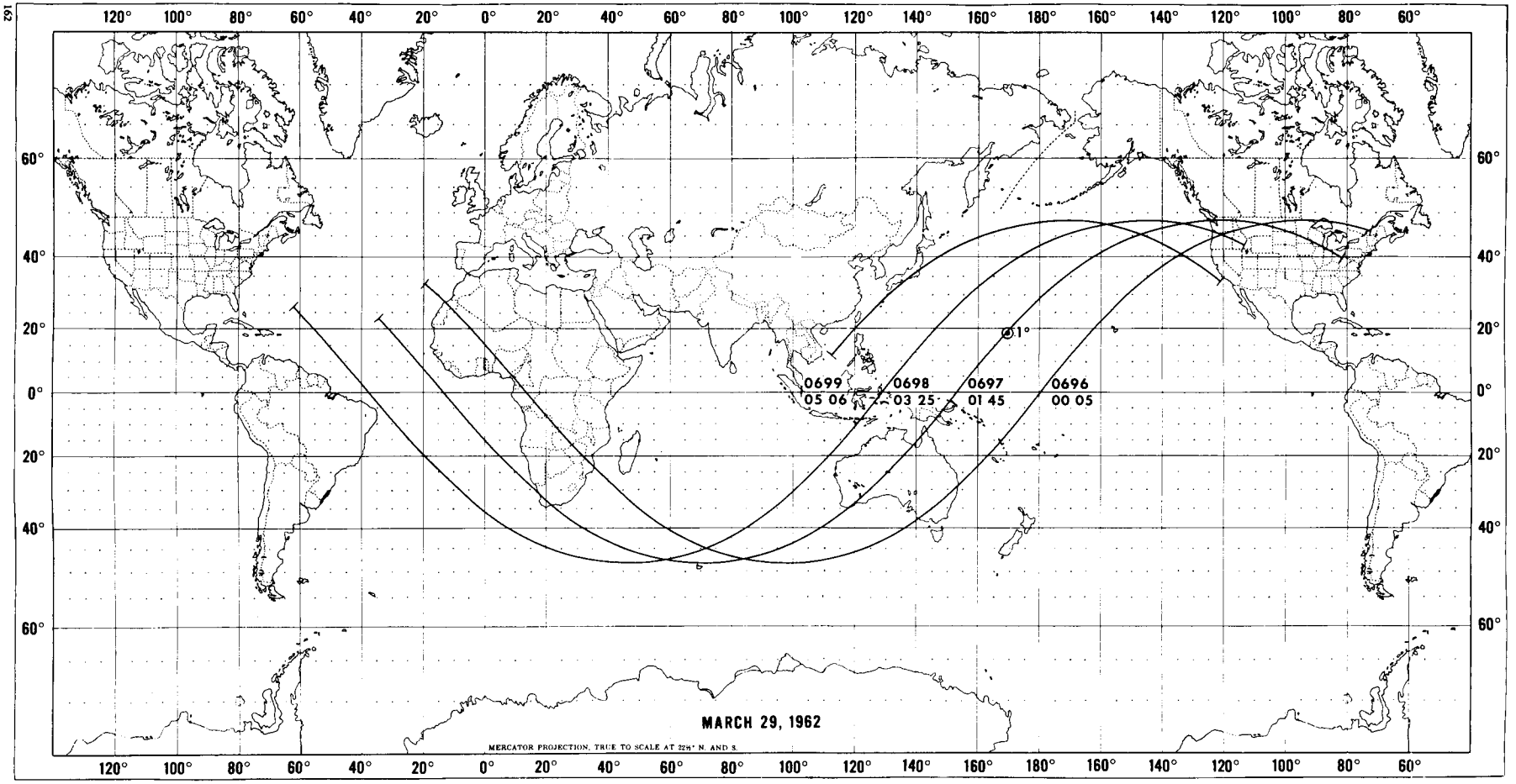
120° 100° 80° 60° 40° 20° 0° 20° 40° 60° 80° 100° 120° 140° 160° 180° 160° 140° 120° 100° 80° 60°
60°
40°
20°
0°
20°
40°
60°
0699
05 06
0698
03 25
0697
01 45
0696
00 05
1°
MARCH 29, 1962
MERCATOR PROJECTION, TRUE TO SCALE AT 22½° N. AND S.

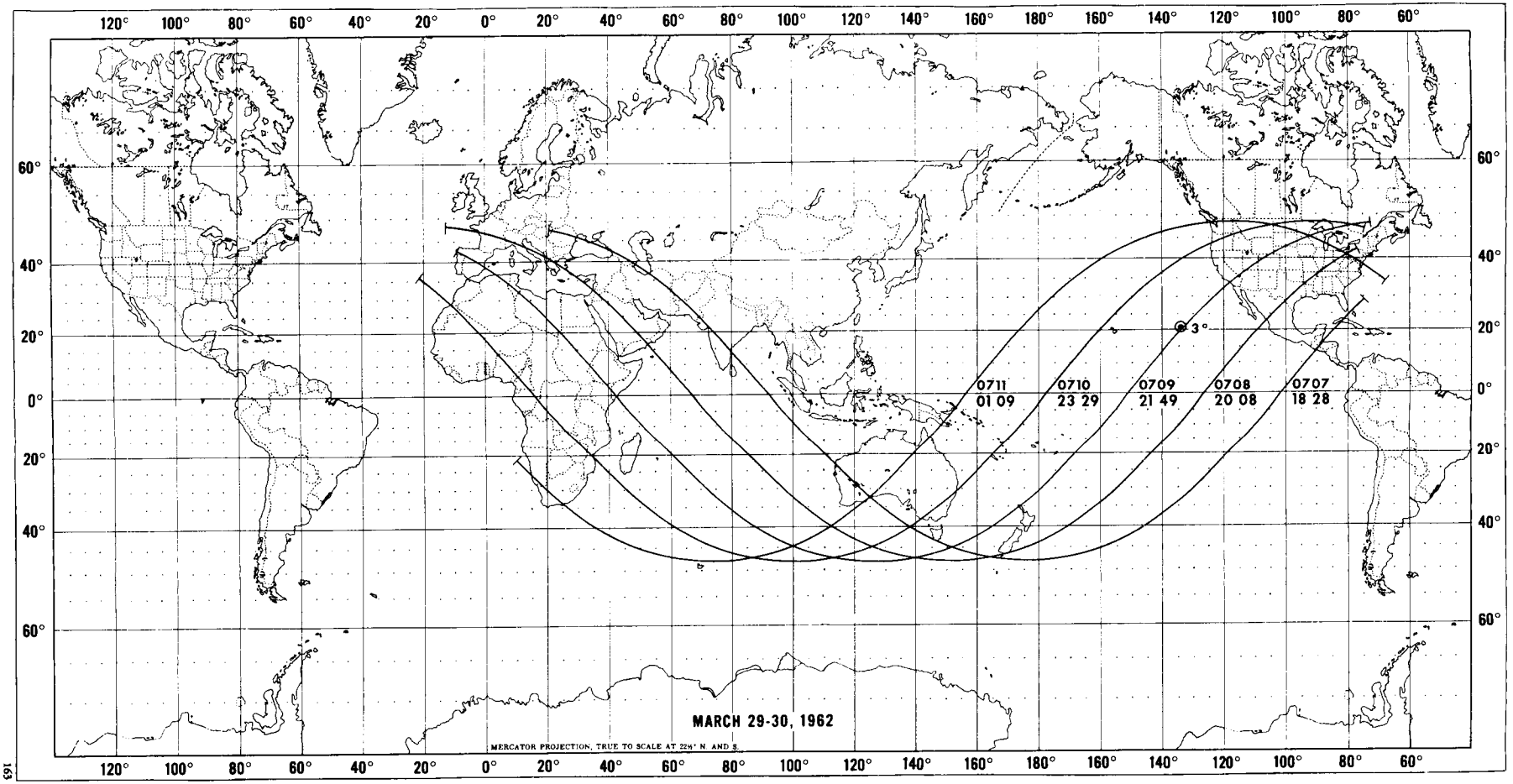
120° 100° 80° 60° 40° 20° 0° 20° 40° 60° 80° 100° 120° 140° 160° 180° 160° 140° 120° 100° 80° 60°
60°
40°
20°
0°
20°
40°
60°
3°
0711
01 09
0710
23 29
0709
21 49
0708
20 08
0707
18 28
MARCH 29-30, 1962
MERCATOR PROJECTION, TRUE TO SCALE AT 22½° N. AND S.

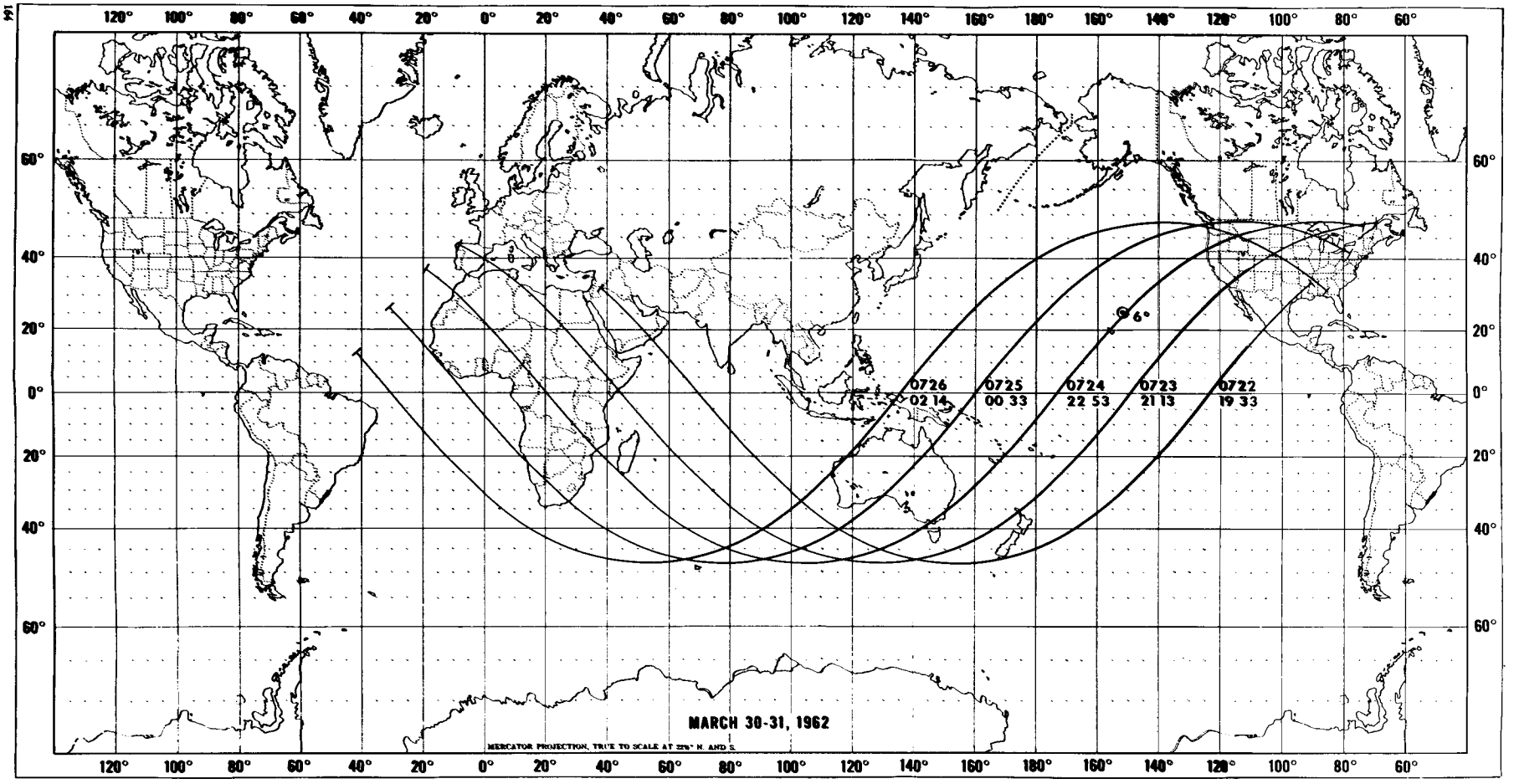
120° 100° 80° 60° 40° 20° 0° 20° 40° 60° 80° 100° 120° 140° 160° 180° 160° 140° 120° 100° 80° 60°
60°
40°
20°
0°
20°
40°
60°
0726
02 14
0725
00 33
0724
22 53
0723
21 13
0722
19 33
6°
MARCH 30-31, 1962
MERCATOR PROJECTION, TRUE TO SCALE AT 22½° N. AND S.

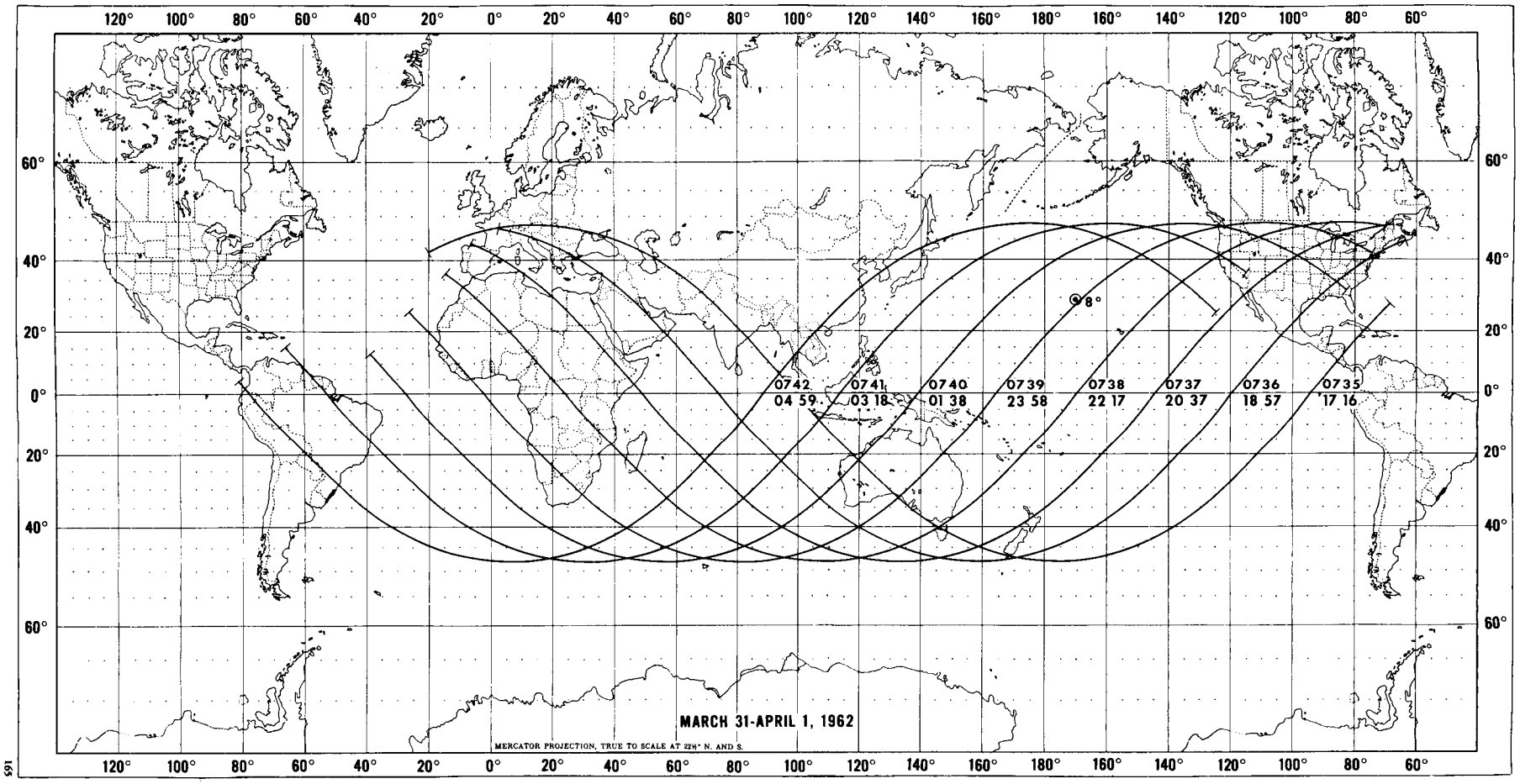
120° 100° 80° 60° 40° 20° 0° 20° 40° 60° 80° 100° 120° 140° 160° 180° 160° 140° 120° 100° 80° 60°
60°
40°
20°
0°
20°
40°
60°
8°
0742 0741 0740 0739 0738 0737 0736 0735
04 59 03 18 01 38 23 58 22 17 20 37 18 57 17 16
MARCH 31-APRIL 1, 1962
MERCATOR PROJECTION, TRUE TO SCALE AT 22½° N. AND S.

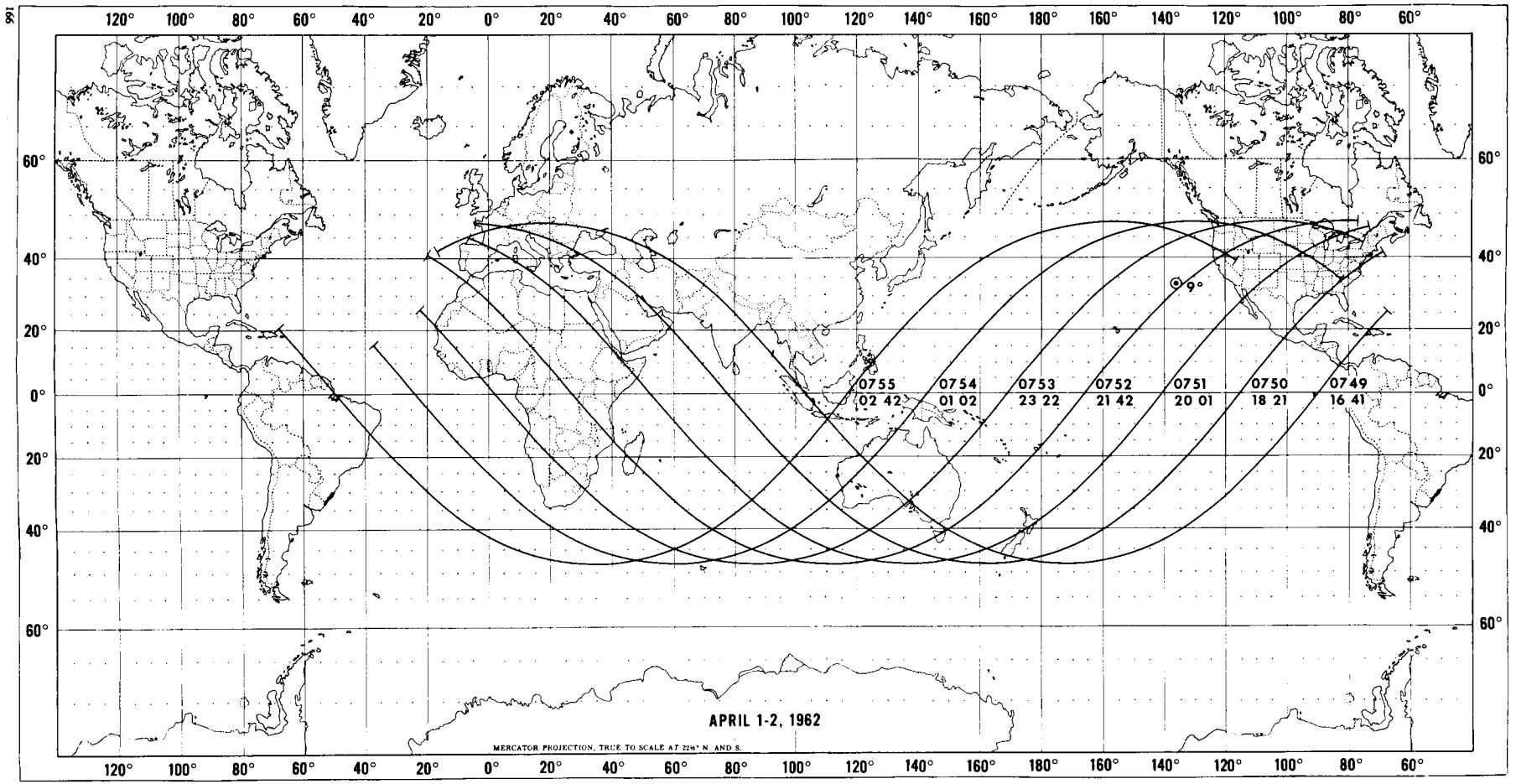
120° 100° 80° 60° 40° 20° 0° 20° 40° 60° 80° 100° 120° 140° 160° 180° 160° 140° 120° 100° 80° 60°
60°
40°
20°
0°
20°
40°
60°
0755
02 42
0754
01 02
0753
23 22
0752
21 42
0751
20 01
0750
18 21
0749
16 41
9°
APRIL 1-2, 1962
MERCATOR PROJECTION, TRUE TO SCALE AT 22½° N. AND S.

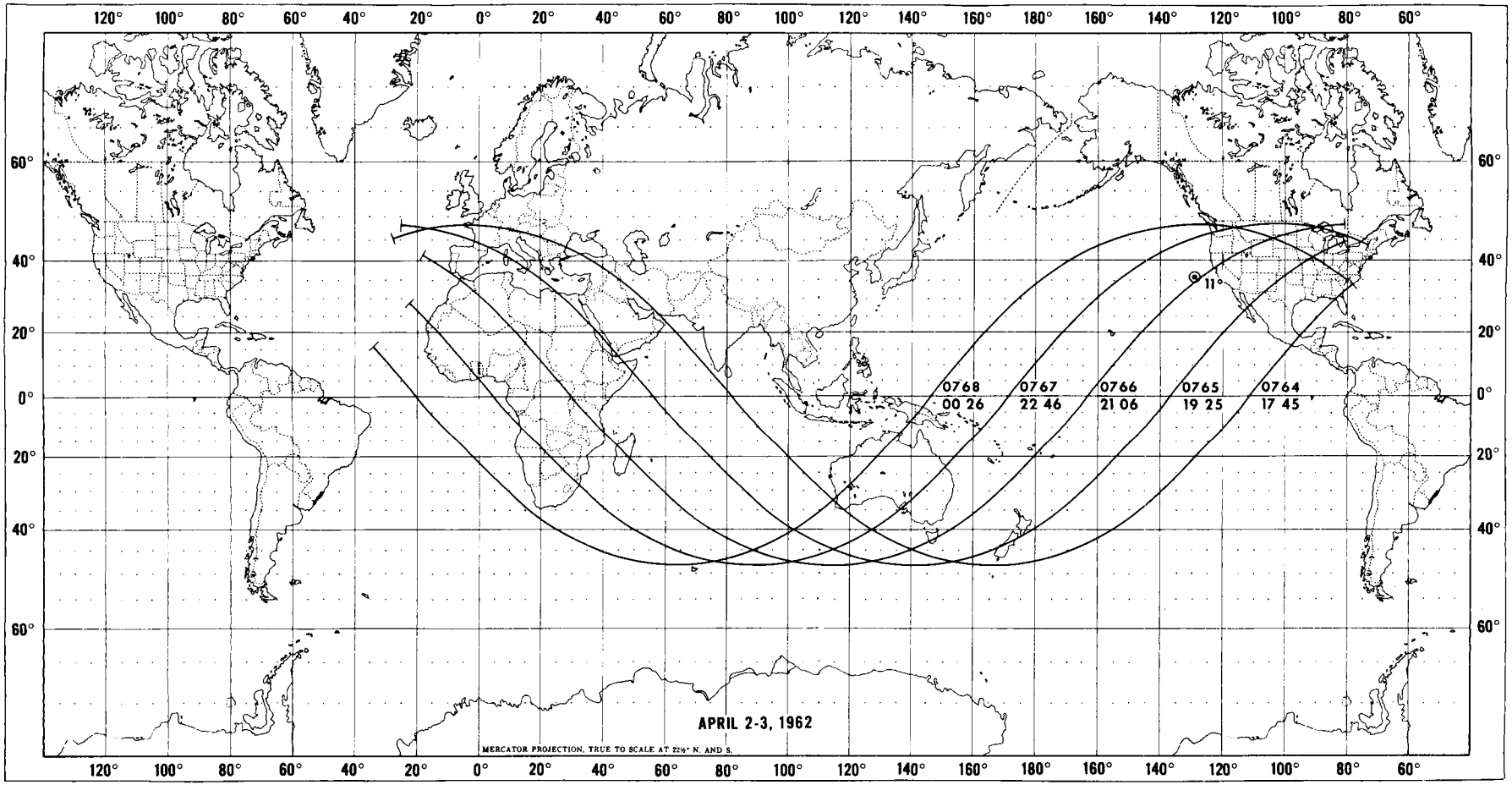
120° 100° 80° 60° 40° 20° 0° 20° 40° 60° 80° 100° 120° 140° 160° 180° 160° 140° 120° 100° 80° 60°
60°
40°
20°
0°
20°
40°
60°
11°
0768
00 26
0767
22 46
0766
21 06
0765
19 25
0764
17 45
APRIL 2-3, 1962
MERCATOR PROJECTION, TRUE TO SCALE AT 22½° N. AND S.

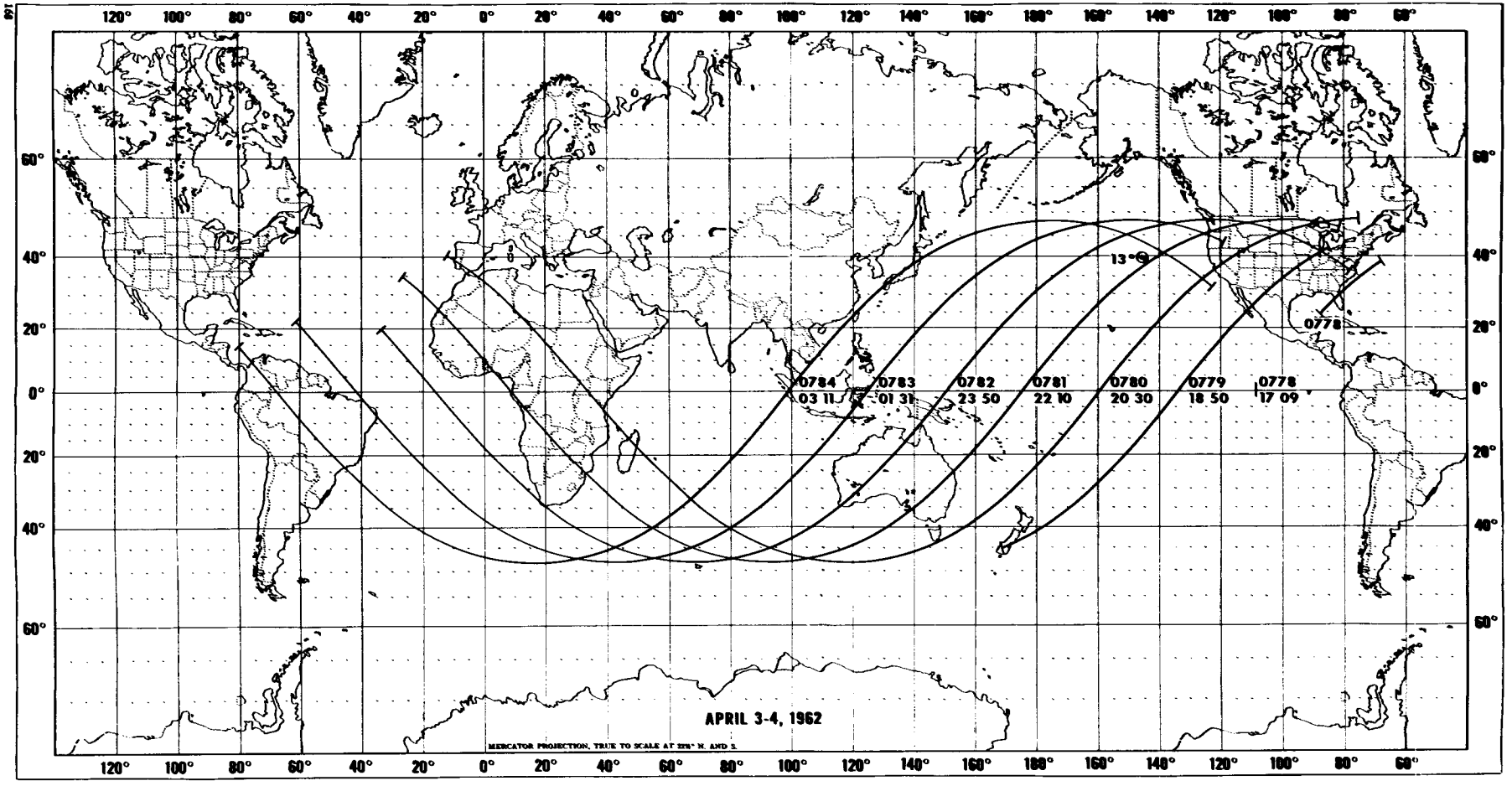
120° 100° 80° 60° 40° 20° 0° 20° 40° 60° 80° 100° 120° 140° 160° 180° 160° 140° 120° 100° 80° 60°
60°
40°
20°
0°
20°
40°
60°
13°S
0778
0784 03 11
0783 01 31
0782 23 50
0781 22 10
0780 20 30
0779 18 50
0778 17 09
APRIL 3-4, 1962
MERCATOR PROJECTION, TRUE TO SCALE AT 22½° N. AND S.

729-166 O - 64 - 12

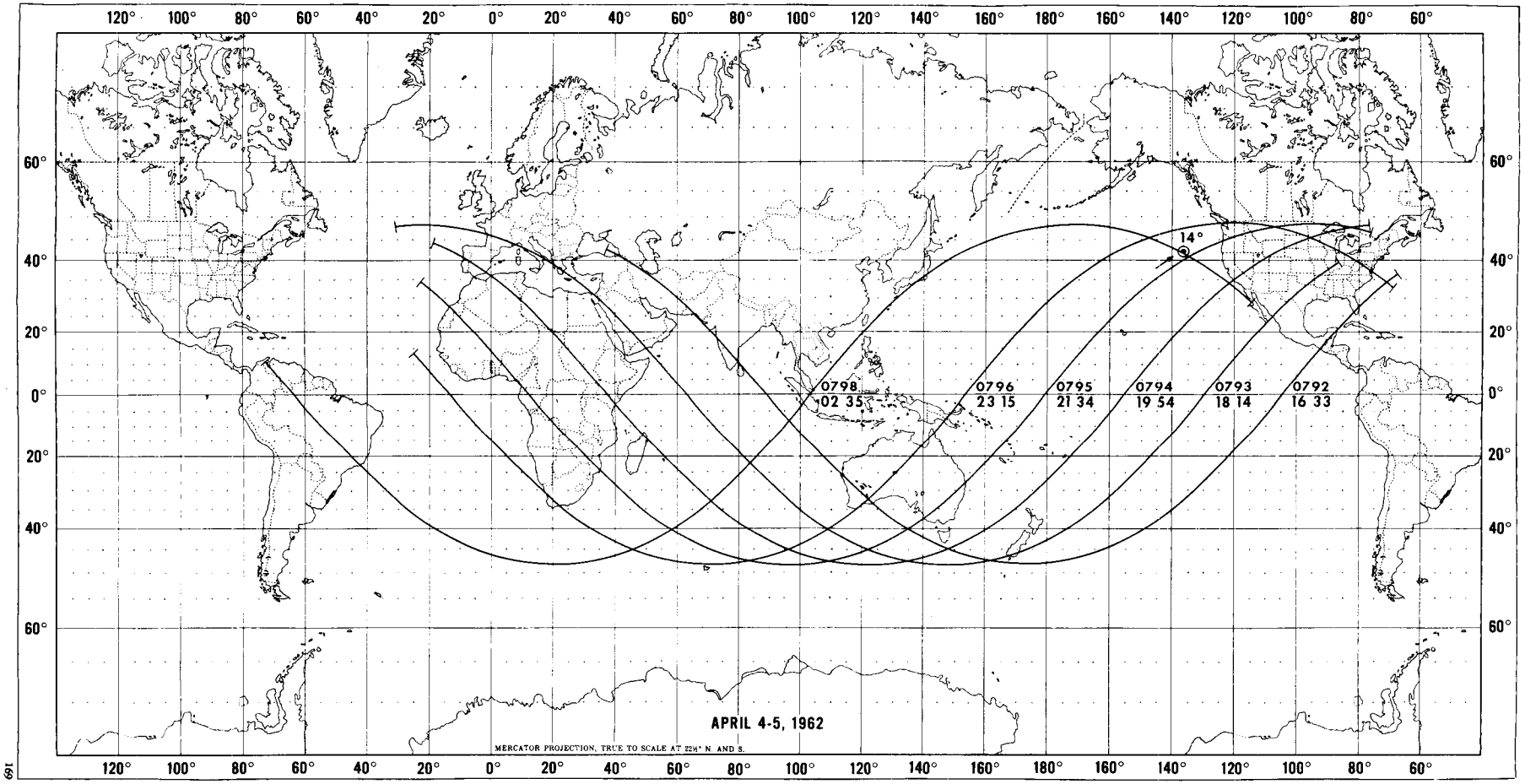

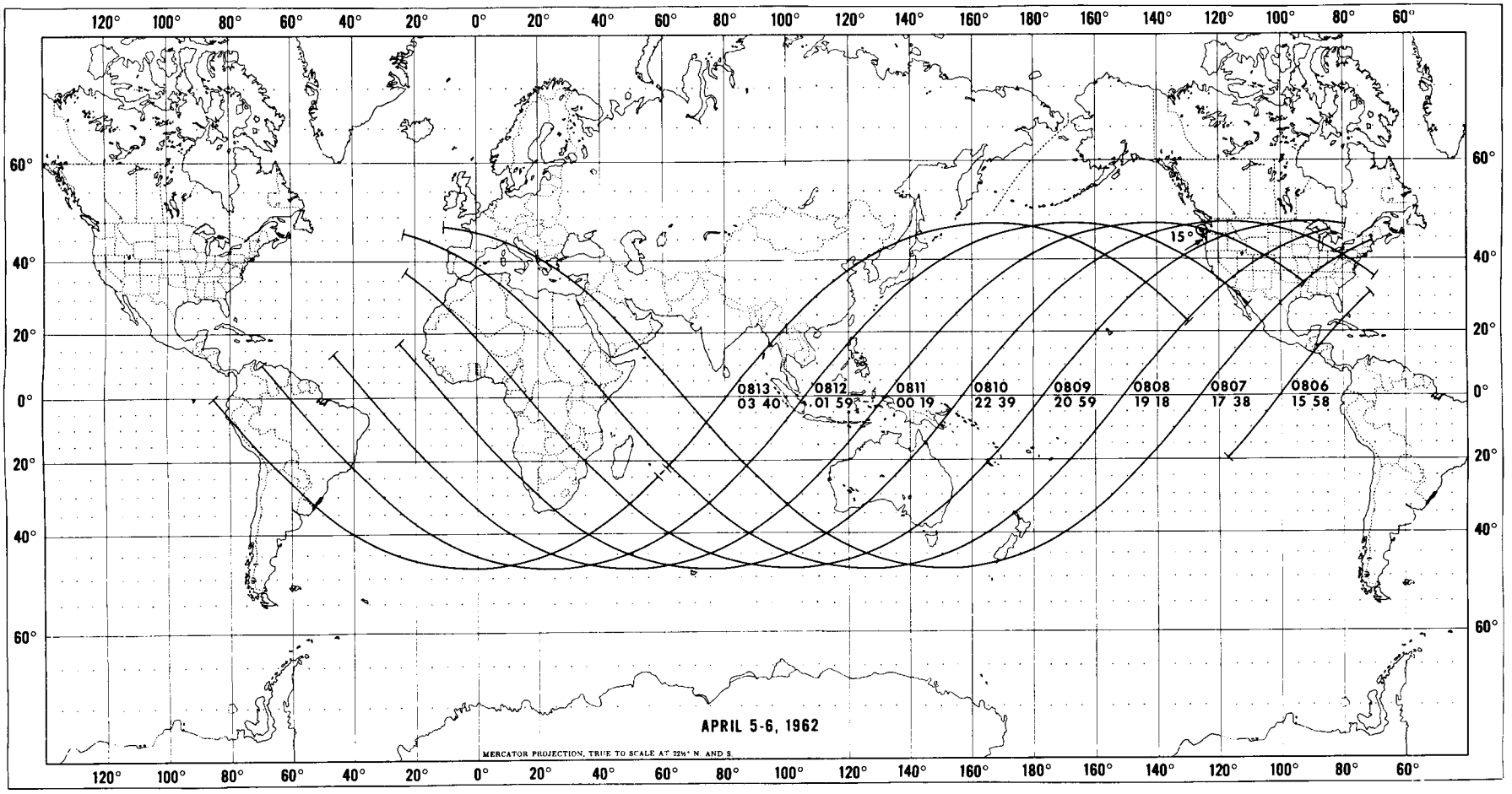
120° 100° 80° 60° 40° 20° 0° 20° 40° 60° 80° 100° 120° 140° 160° 180° 160° 140° 120° 100° 80° 60°
60°
40°
20°
0°
20°
40°
60°
15°
0813
03 40
0812
01 59
0811
00 19
0810
22 39
0809
20 59
0808
19 18
0807
17 38
0806
15 58
APRIL 5-6, 1962
MERCATOR PROJECTION, TRUE TO SCALE AT 22½° N. AND S.

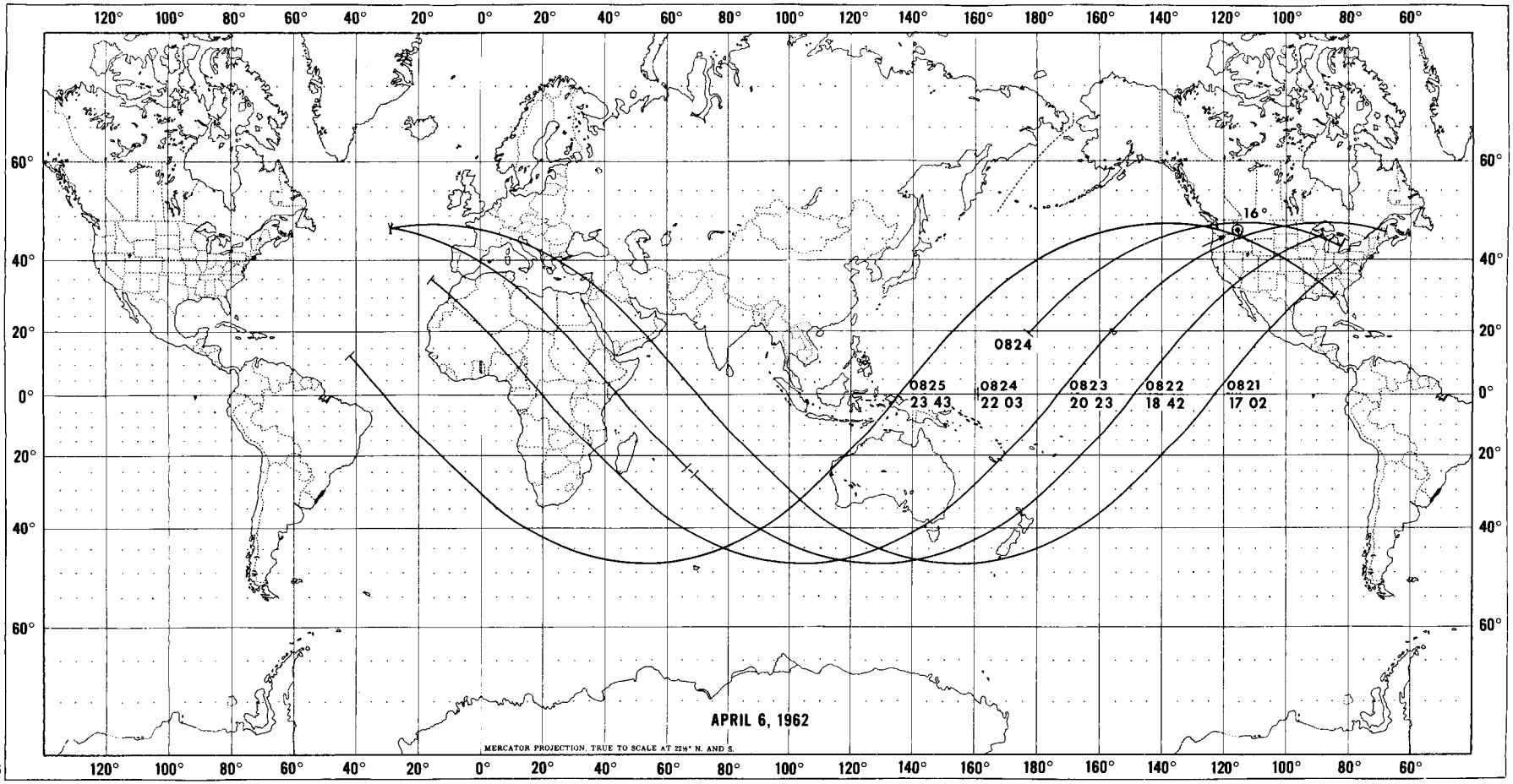
120° 100° 80° 60° 40° 20° 0° 20° 40° 60° 80° 100° 120° 140° 160° 180° 160° 140° 120° 100° 80° 60°
60°
40°
20°
0°
20°
40°
60°
16°
0824
0825
23 43
0824
22 03
0823
20 23
0822
18 42
0821
17 02
APRIL 6, 1962
MERCATOR PROJECTION, TRUE TO SCALE AT 22½° N. AND S.

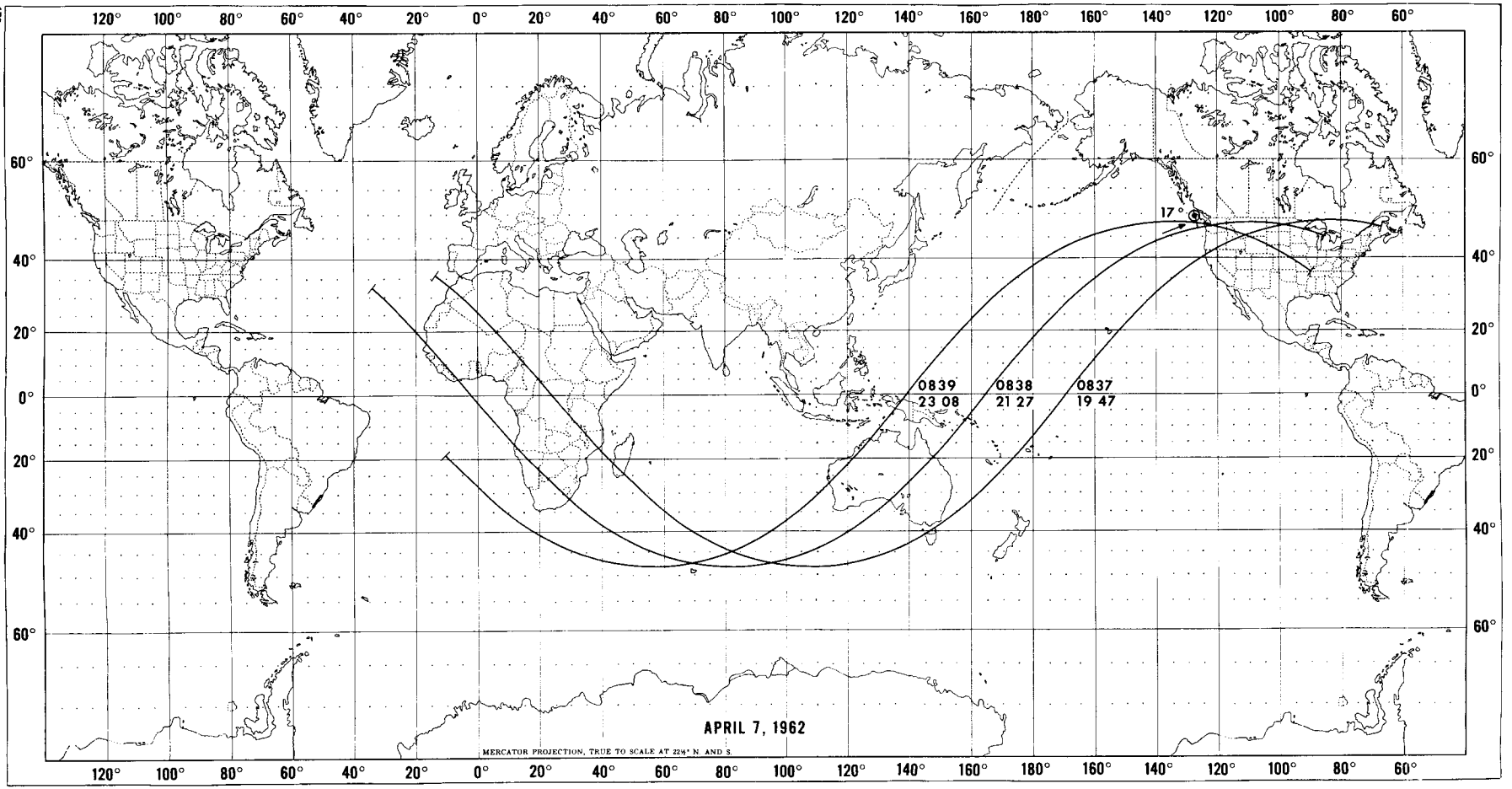
120° 100° 80° 60° 40° 20° 0° 20° 40° 60° 80° 100° 120° 140° 160° 180° 160° 140° 120° 100° 80° 60°
60°
40°
20°
0°
20°
40°
60°
17°
0839
23 08
0838
21 27
0837
19 47
APRIL 7, 1962
MERCATOR PROJECTION, TRUE TO SCALE AT 22½° N. AND S.

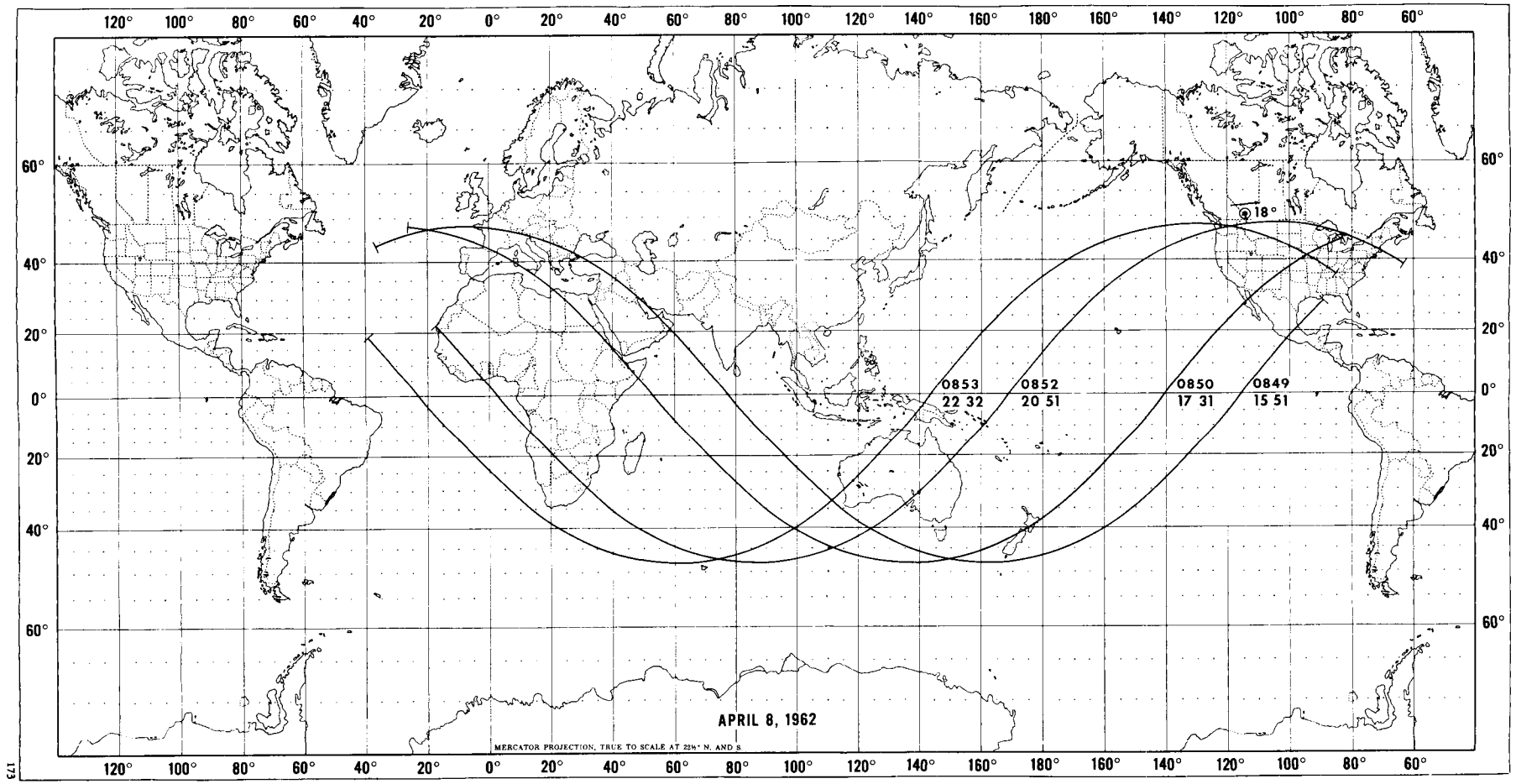
120° 100° 80° 60° 40° 20° 0° 20° 40° 60° 80° 100° 120° 140° 160° 180° 160° 140° 120° 100° 80° 60°
60°
40°
20°
0°
20°
40°
60°
18°
0853
22 32
0852
20 51
0850
17 31
0849
15 51
APRIL 8, 1962
MERCATOR PROJECTION, TRUE TO SCALE AT 22½° N. AND S.

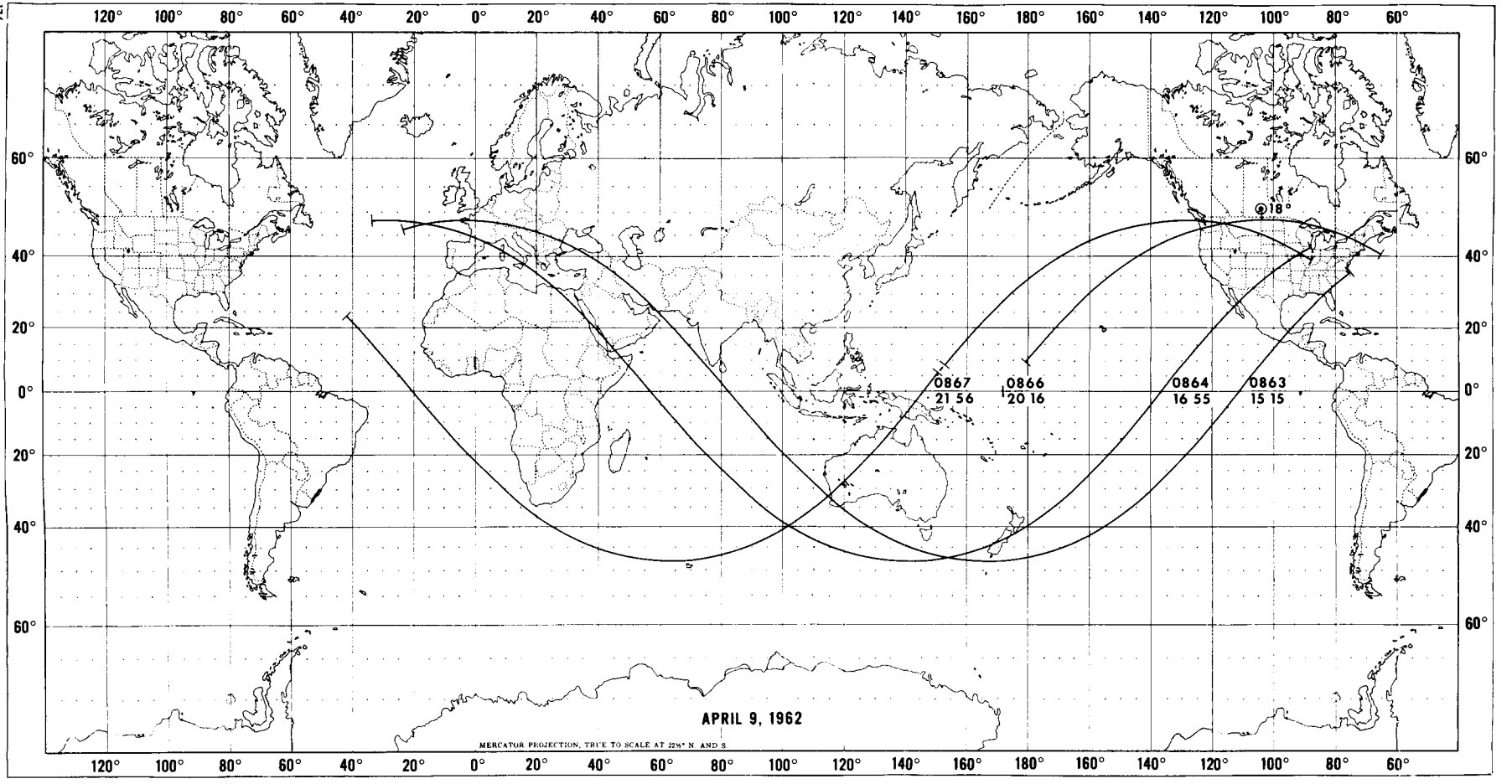
120° 100° 80° 60° 40° 20° 0° 20° 40° 60° 80° 100° 120° 140° 160° 180° 160° 140° 120° 100° 80° 60°
60°
40°
20°
0°
20°
40°
60°
18°
0867
21 56
0866
20 16
0864
16 55
0863
15 15
APRIL 9, 1962
MERCATOR PROJECTION, TRUE TO SCALE AT 22½° N. AND S.

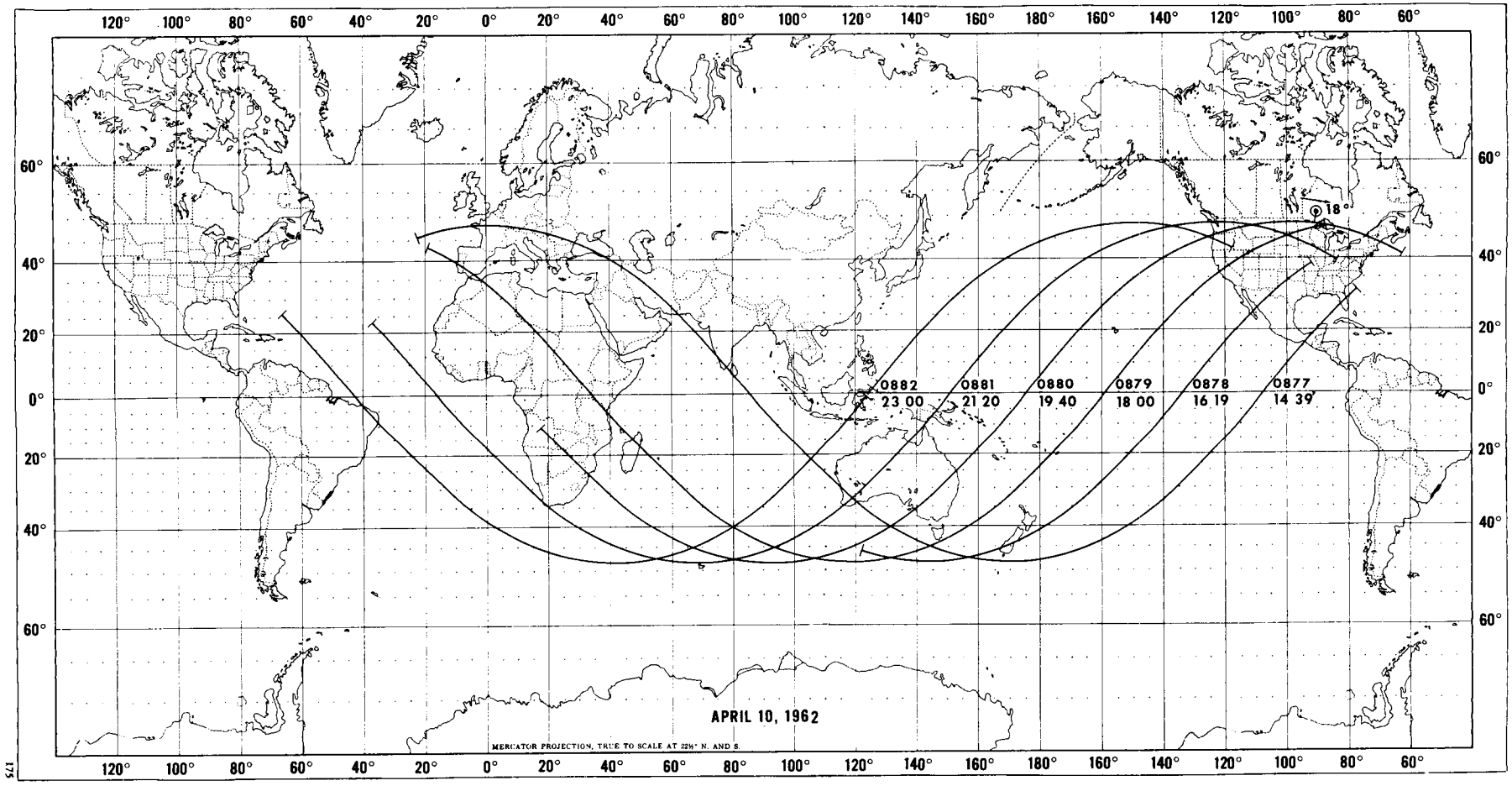
120° 100° 80° 60° 40° 20° 0° 20° 40° 60° 80° 100° 120° 140° 160° 180° 160° 140° 120° 100° 80° 60°
60°
40°
20°
0°
20°
40°
60°
18°
0882
23 00
0881
21 20
0880
19 40
0879
18 00
0878
16 19
0877
14 39
APRIL 10, 1962
MERCATOR PROJECTION, TRUE TO SCALE AT 22½° N. AND S.

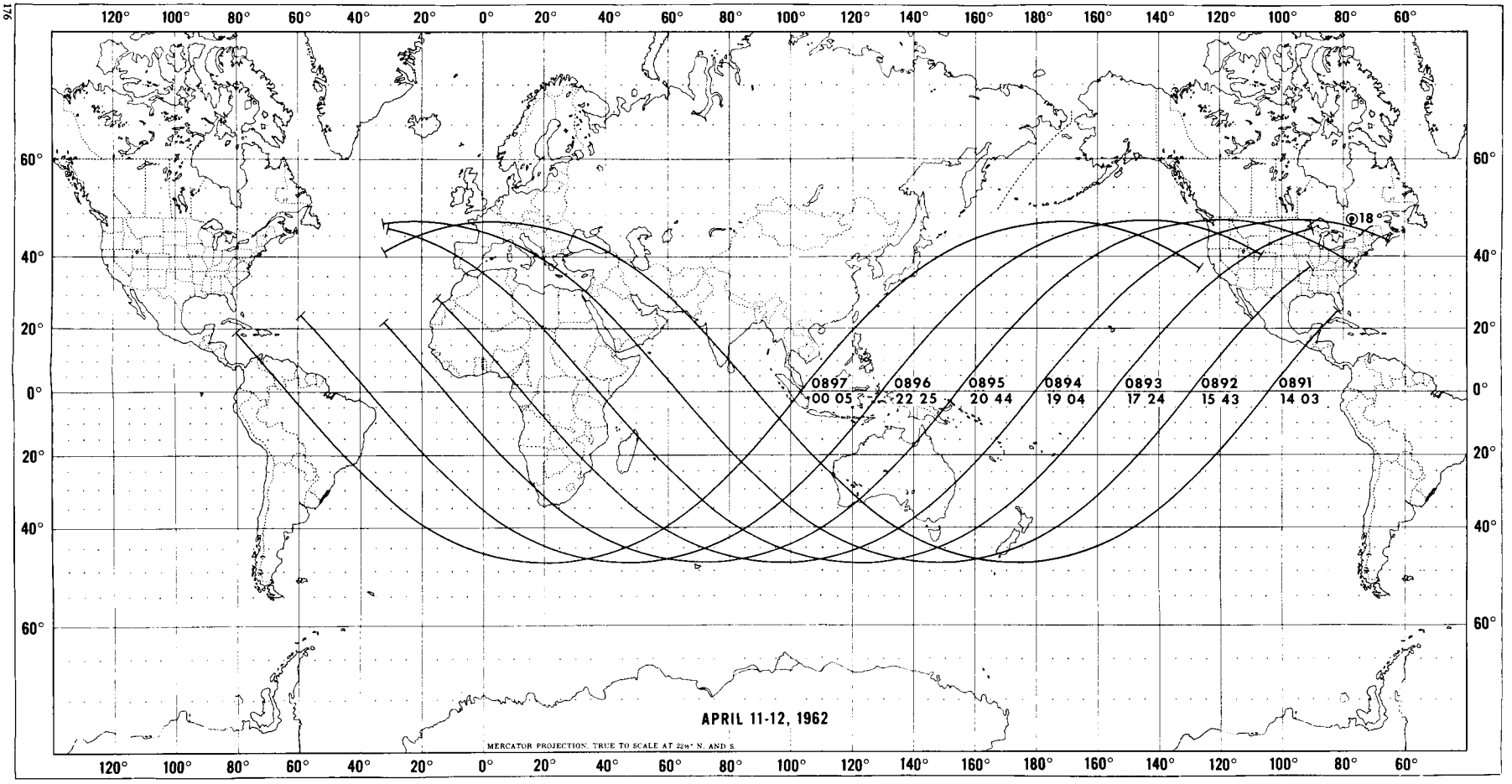
120° 100° 80° 60° 40° 20° 0° 20° 40° 60° 80° 100° 120° 140° 160° 180° 160° 140° 120° 100° 80° 60°
60°
40°
20°
0°
20°
40°
60°
18°
0897 00 05
0896 22 25
0895 20 44
0894 19 04
0893 17 24
0892 15 43
0891 14 03
APRIL 11-12, 1962
MERCATOR PROJECTION. TRUE TO SCALE AT 22½° N. AND S.

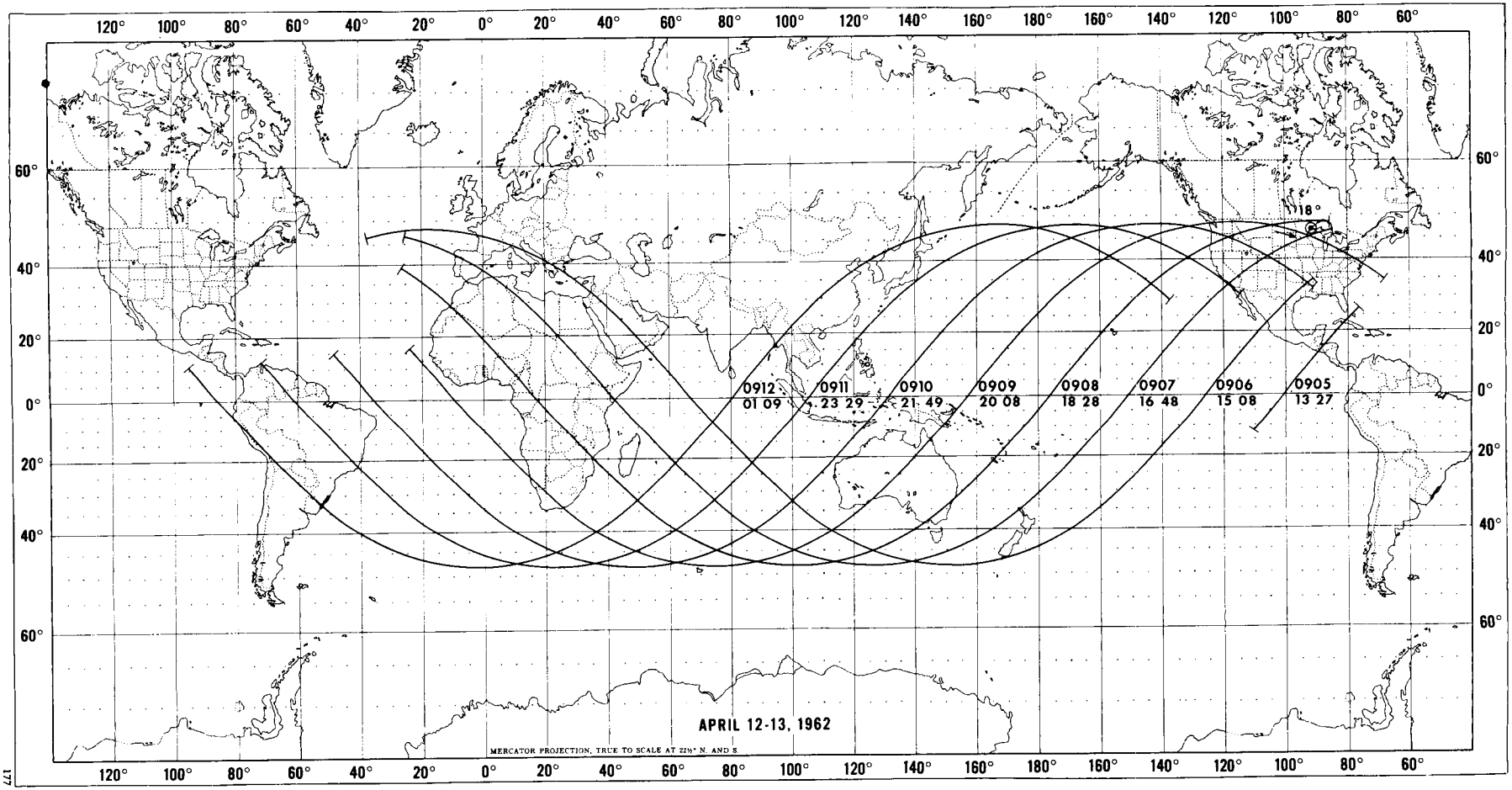
120° 100° 80° 60° 40° 20° 0° 20° 40° 60° 80° 100° 120° 140° 160° 180° 160° 140° 120° 100° 80° 60°
60°
40°
20°
0°
20°
40°
60°
18°
0912
01 09
0911
23 29
0910
21 49
0909
20 08
0908
18 28
0907
16 48
0906
15 08
0905
13 27
APRIL 12-13, 1962
MERCATOR PROJECTION, TRUE TO SCALE AT 22½° N. AND S.

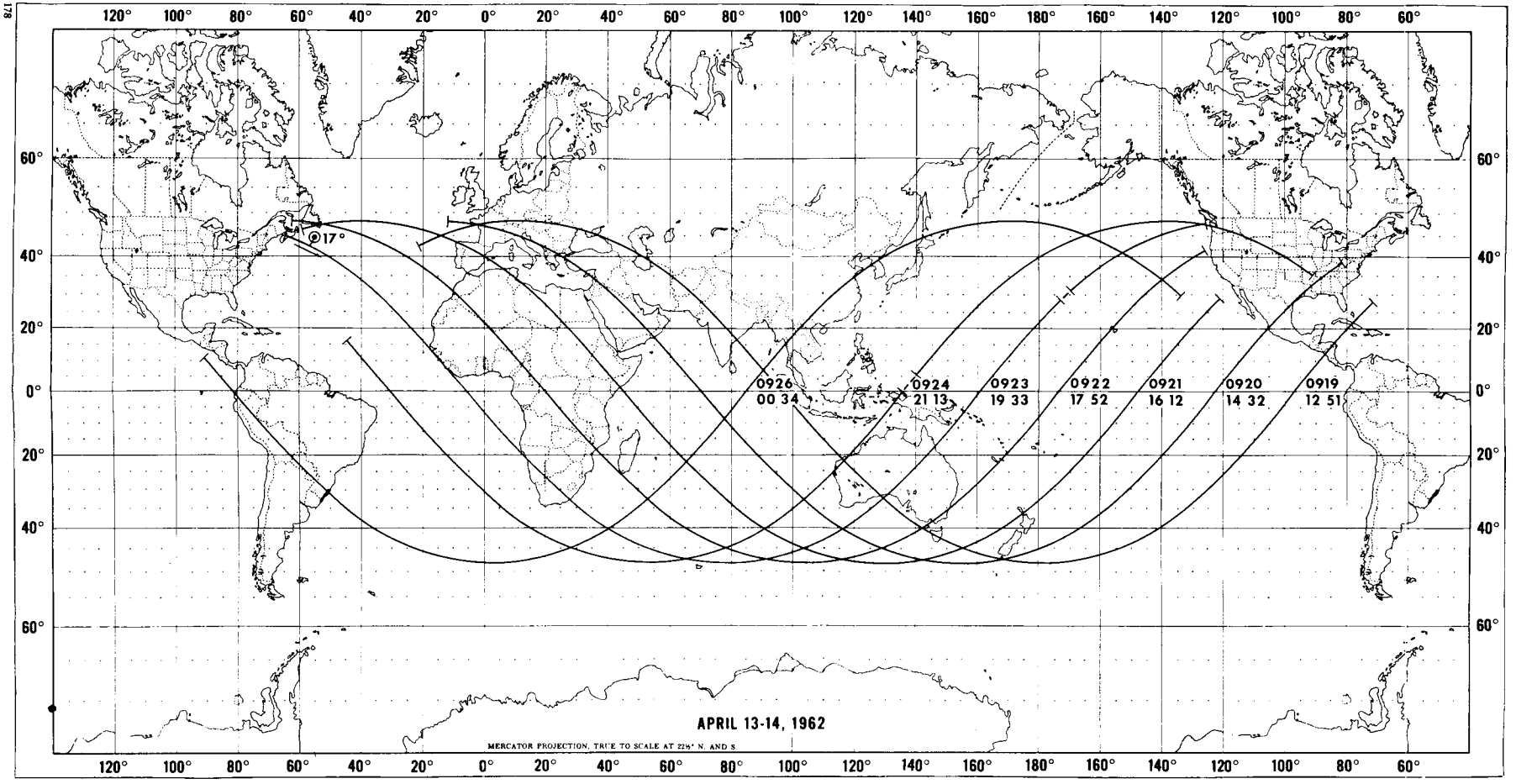
120° 100° 80° 60° 40° 20° 0° 20° 40° 60° 80° 100° 120° 140° 160° 180° 160° 140° 120° 100° 80° 60°
60°
40°
20°
0°
20°
40°
60°
17°
0926
00 34
0924
21 13
0923
19 33
0922
17 52
0921
16 12
0920
14 32
0919
12 51
APRIL 13-14, 1962
MERCATOR PROJECTION, TRUE TO SCALE AT 22½° N. AND S.

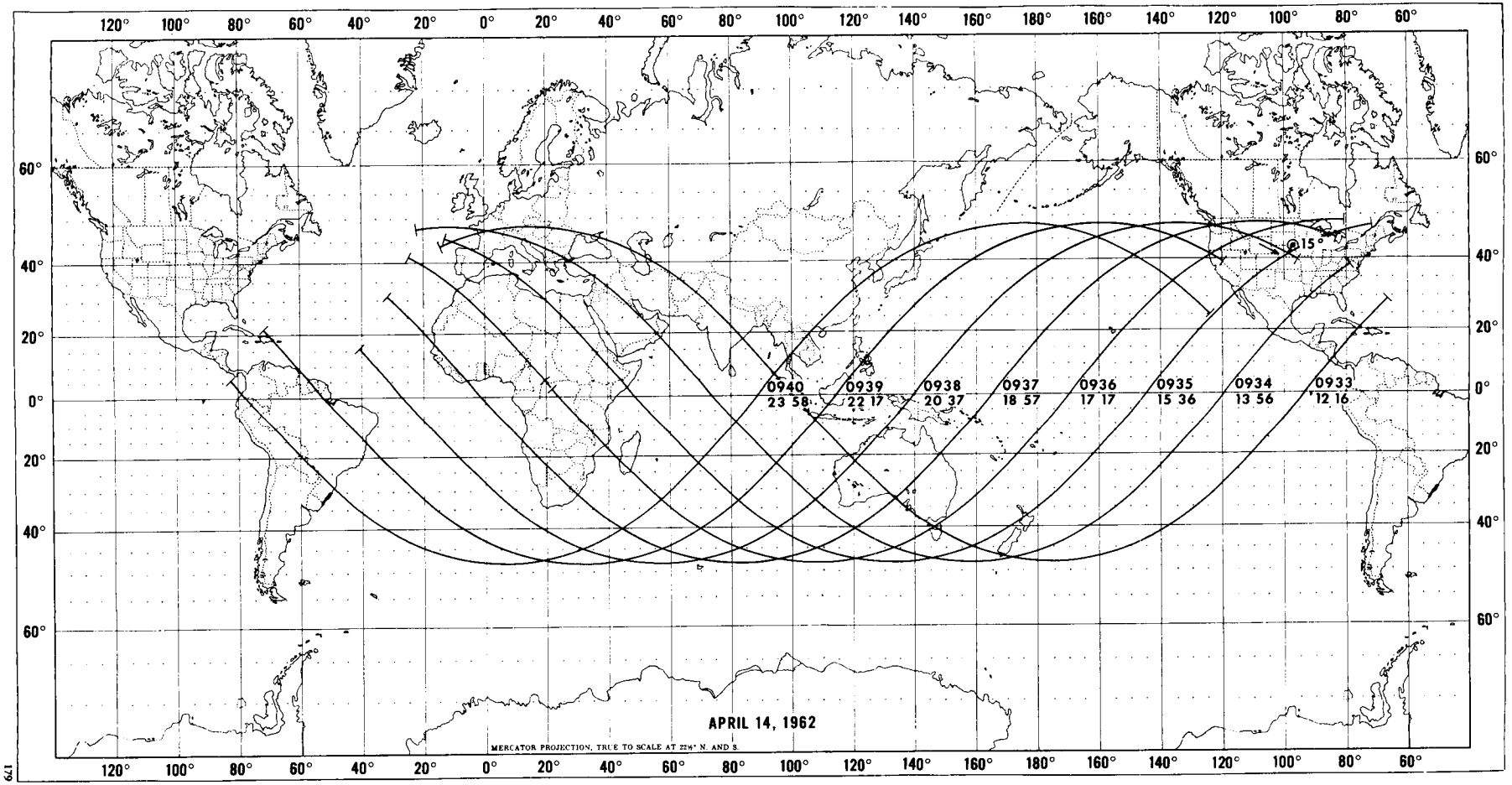
120° 100° 80° 60° 40° 20° 0° 20° 40° 60° 80° 100° 120° 140° 160° 180° 160° 140° 120° 100° 80° 60°
60°
40°
20°
0°
20°
40°
60°
15°
0940 23 58
0939 22 17
0938 20 37
0937 18 57
0936 17 17
0935 15 36
0934 13 56
0933 12 16
APRIL 14, 1962
MERCATOR PROJECTION, TRUE TO SCALE AT 22½° N. AND S.

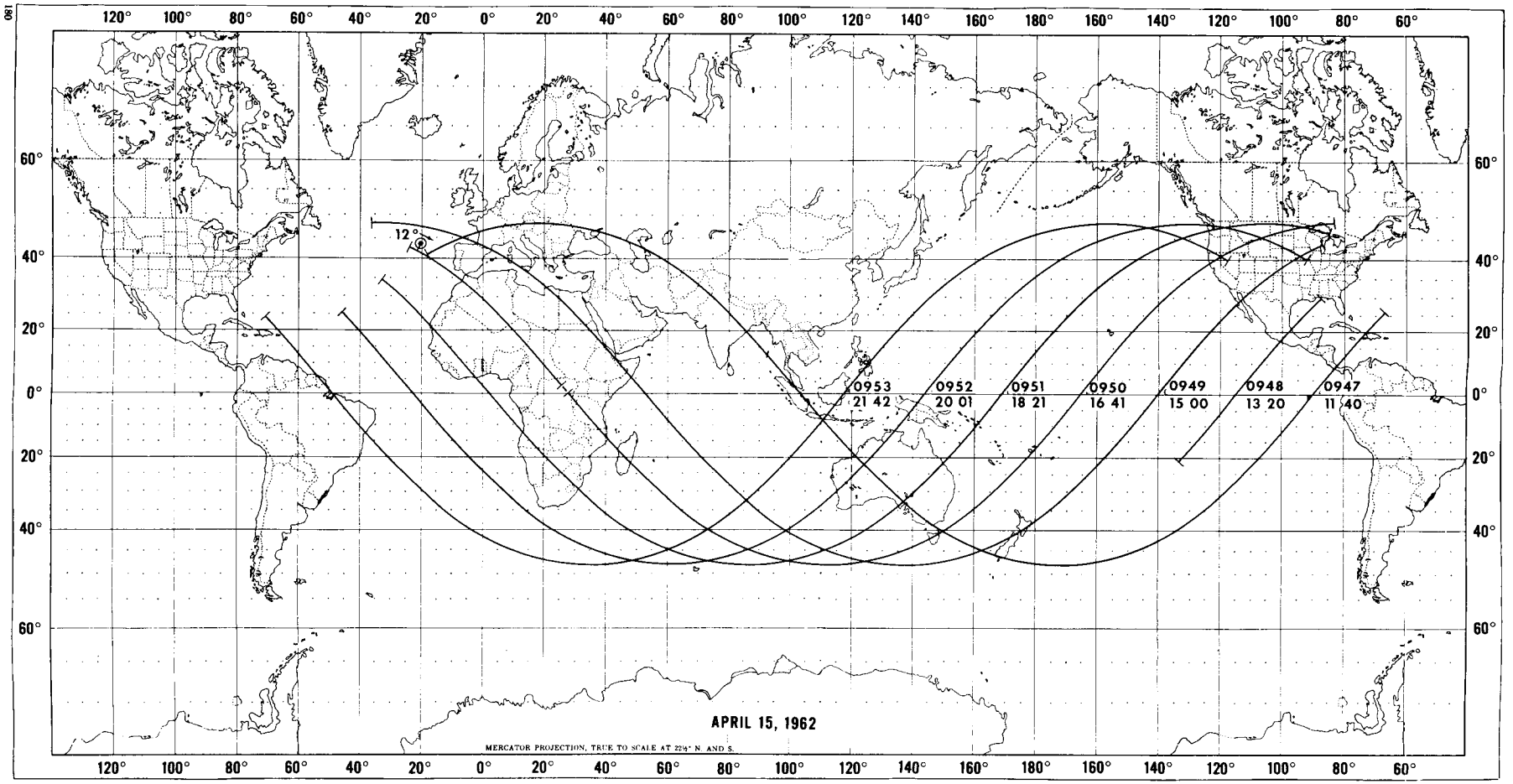
180
120° 100° 80° 60° 40° 20° 0° 20° 40° 60° 80° 100° 120° 140° 160° 180° 160° 140° 120° 100° 80° 60°
60°
40°
20°
0°
20°
40°
60°
12
0953 21 42
0952 20 01
0951 18 21
0950 16 41
0949 15 00
0948 13 20
0947 11 40
APRIL 15, 1962
MERCATOR PROJECTION, TRUE TO SCALE AT 22½° N. AND S.

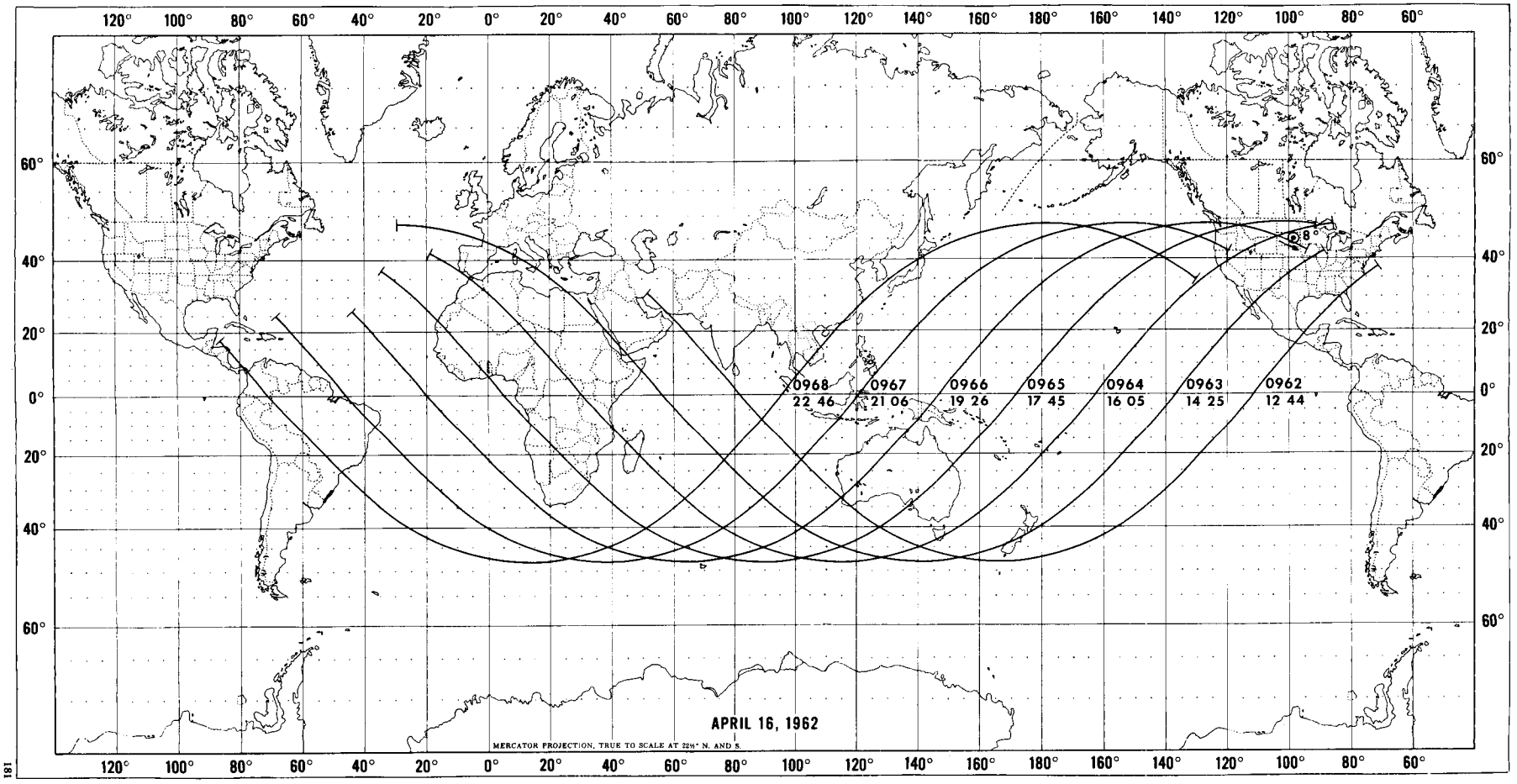
120° 100° 80° 60° 40° 20° 0° 20° 40° 60° 80° 100° 120° 140° 160° 180° 160° 140° 120° 100° 80° 60°
60°
40°
20°
0°
20°
40°
60°
0968
22 46
0967
21 06
0966
19 26
0965
17 45
0964
16 05
0963
14 25
0962
12 44
APRIL 16, 1962
MERCATOR PROJECTION, TRUE TO SCALE AT 22½° N. AND S.

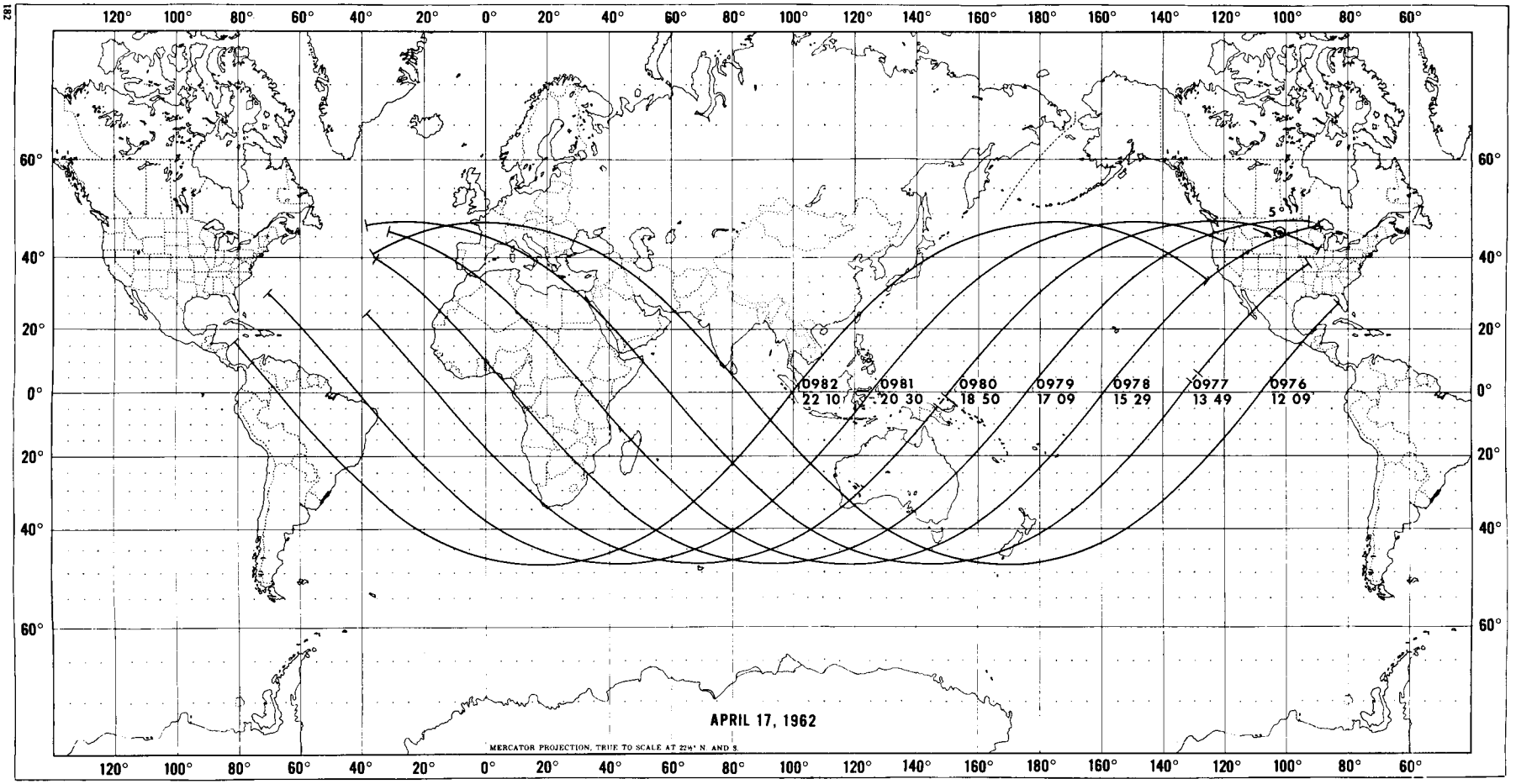
120° 100° 80° 60° 40° 20° 0° 20° 40° 60° 80° 100° 120° 140° 160° 180° 160° 140° 120° 100° 80° 60°
60°
40°
20°
0°
20°
40°
60°
5°
0982 22 10
0981 20 30
0980 18 50
0979 17 09
0978 15 29
0977 13 49
0976 12 09
APRIL 17, 1962
MERCATOR PROJECTION, TRUE TO SCALE AT 22½° N. AND S.

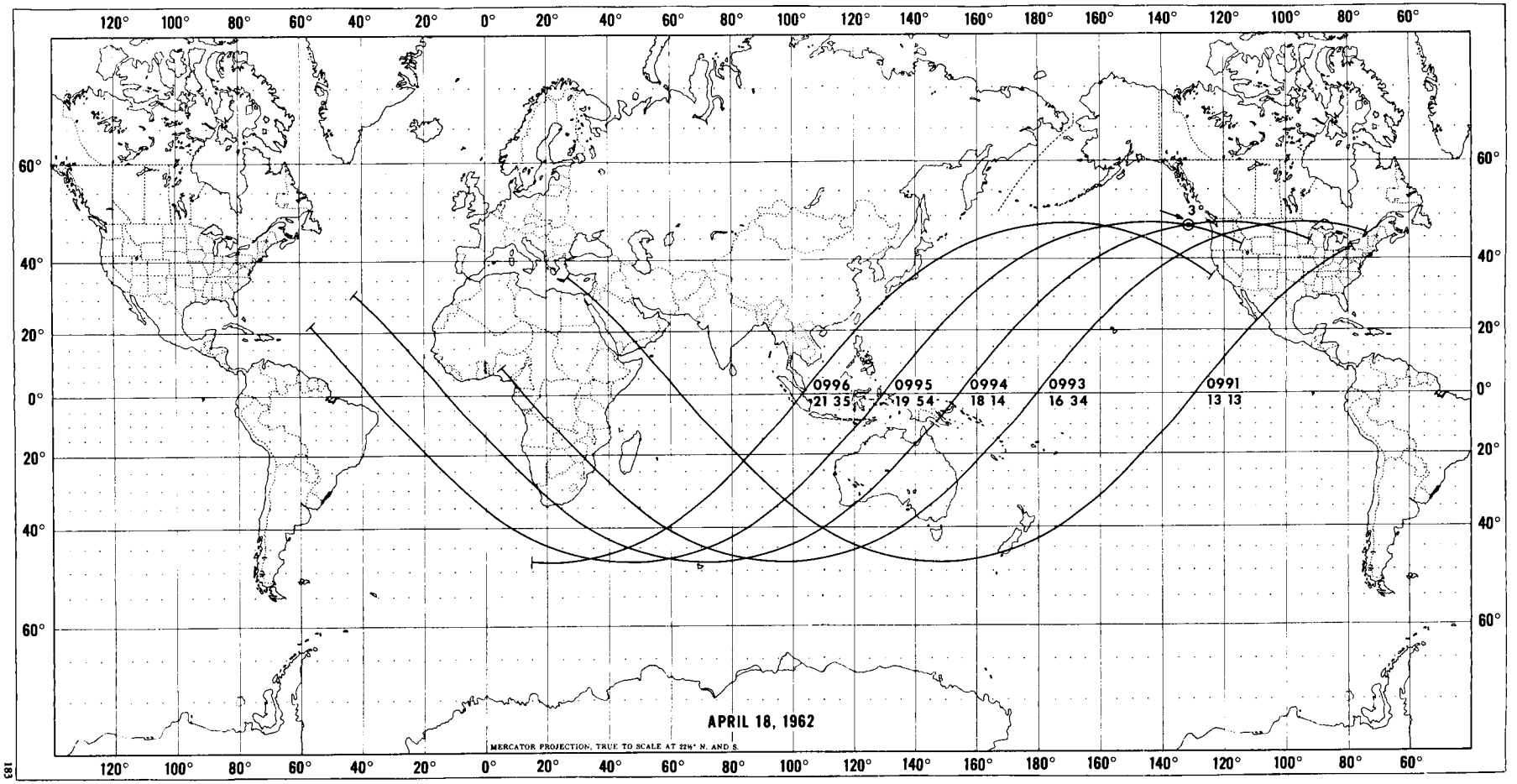
120° 100° 80° 60° 40° 20° 0° 20° 40° 60° 80° 100° 120° 140° 160° 180° 160° 140° 120° 100° 80° 60°
60°
40°
20°
0°
20°
40°
60°
3°
0996
21 35
0995
19 54
0994
18 14
0993
16 34
0991
13 13
APRIL 18, 1962
MERCATOR PROJECTION, TRUE TO SCALE AT 22½° N. AND S.

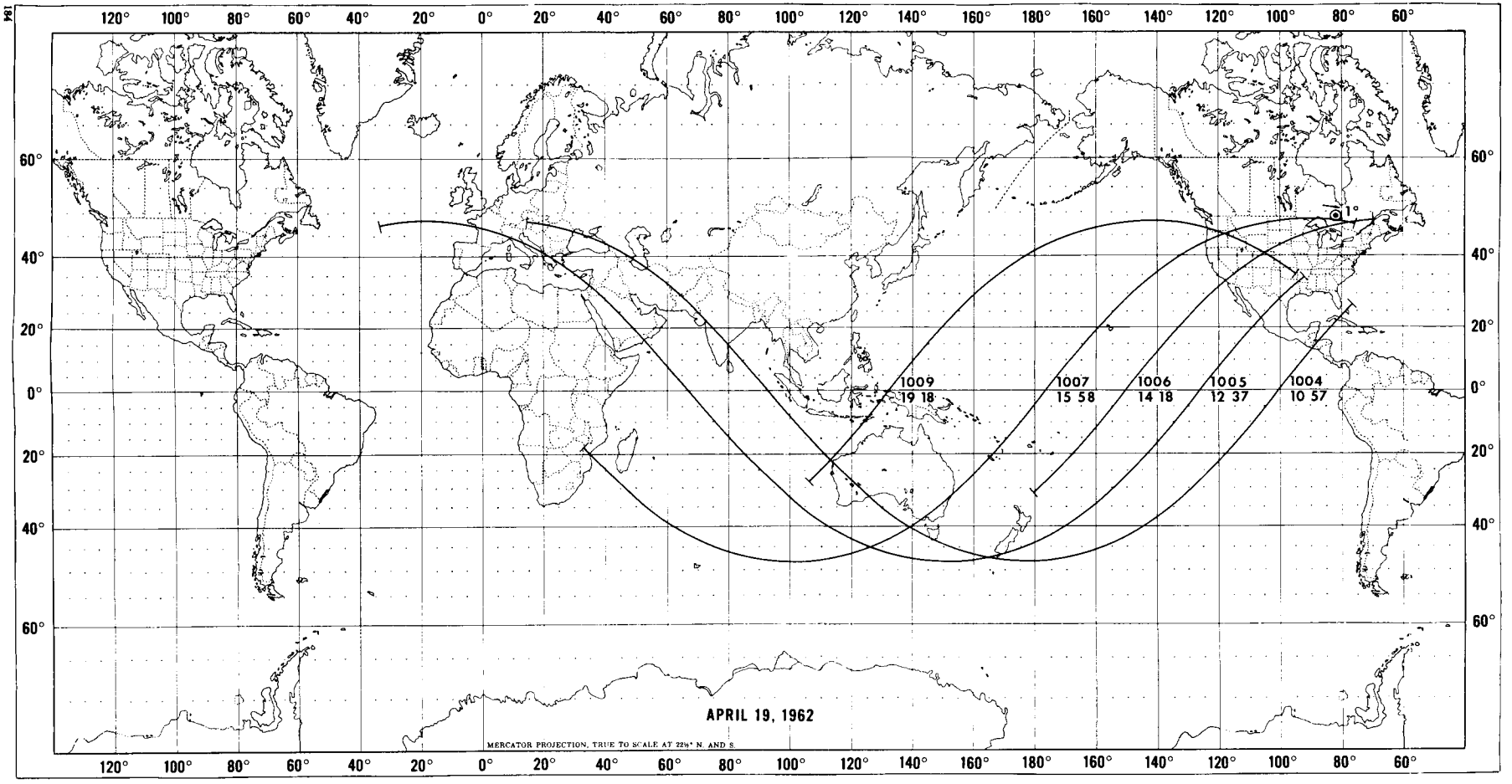
120° 100° 80° 60° 40° 20° 0° 20° 40° 60° 80° 100° 120° 140° 160° 180° 160° 140° 120° 100° 80° 60°
60°
40°
20°
0°
20°
40°
60°
1009
19 18
1007
15 58
1006
14 18
1005
12 37
1004
10 57
1°
APRIL 19, 1962
MERCATOR PROJECTION, TRUE TO SCALE AT 22½° N. AND S.

729-166 O - 64 - 13

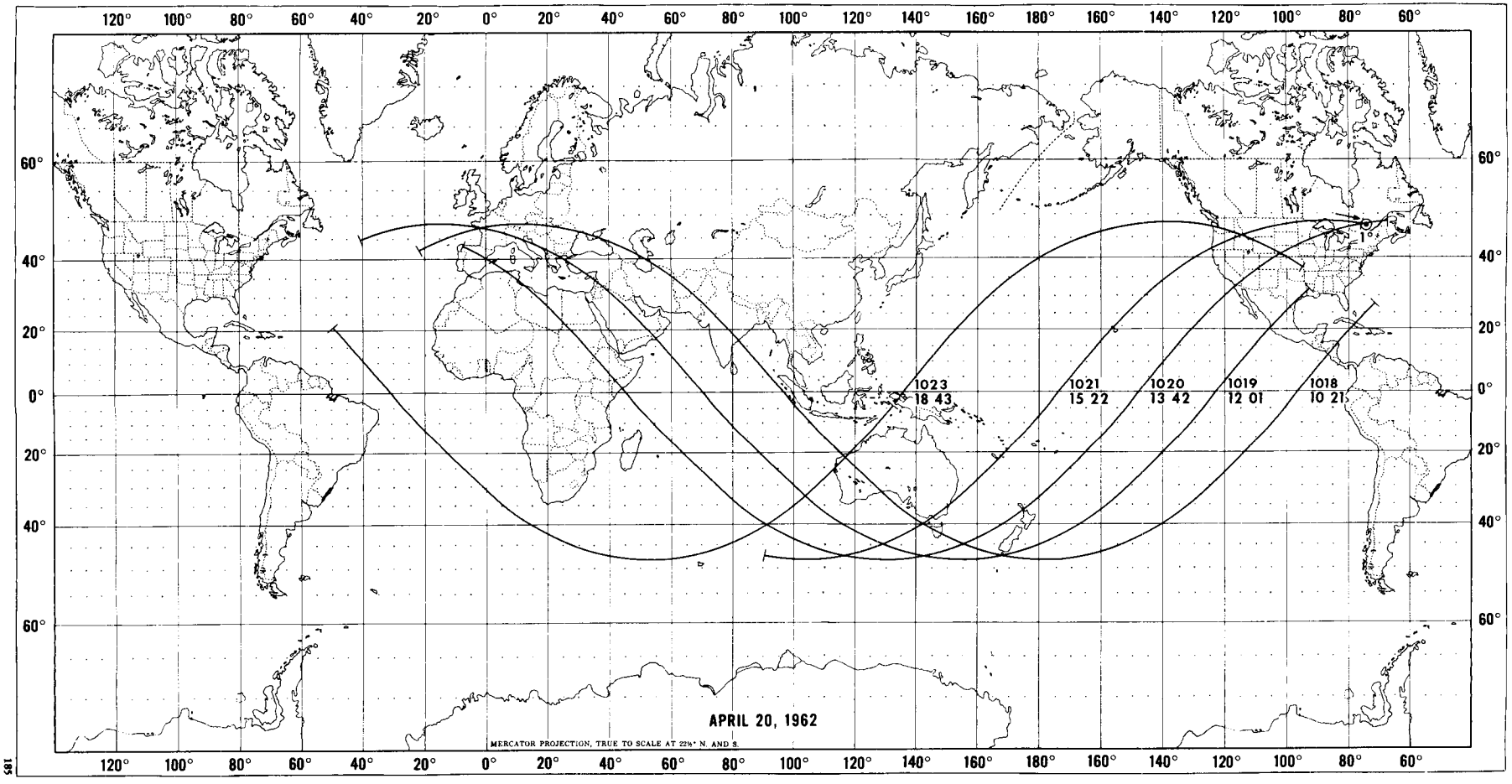

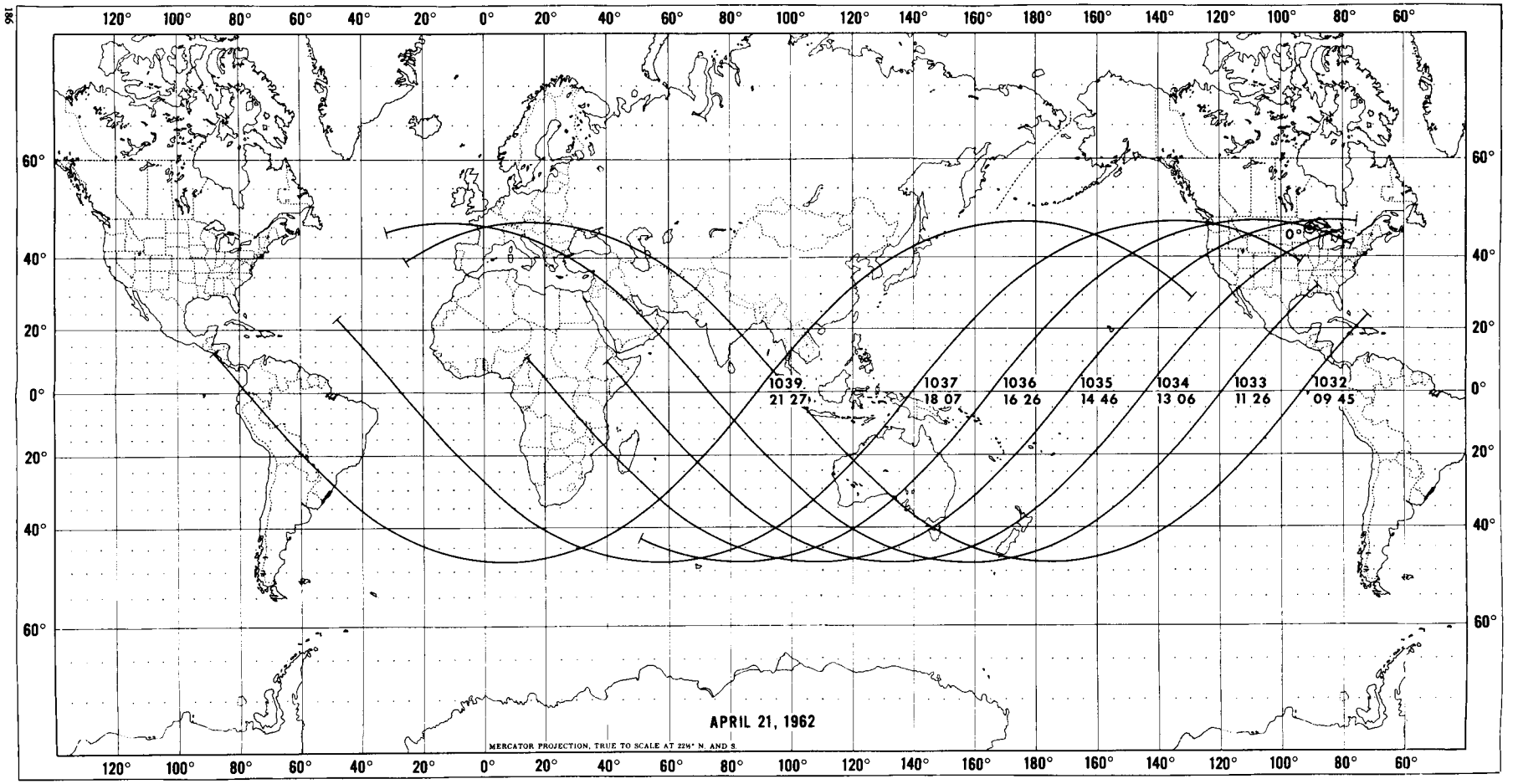
120° 100° 80° 60° 40° 20° 0° 20° 40° 60° 80° 100° 120° 140° 160° 180° 160° 140° 120° 100° 80° 60°
60°
40°
20°
0°
20°
40°
60°
0°
1039
21 27
1037
18 07
1036
16 26
1035
14 46
1034
13 06
1033
11 26
1032
09 45
APRIL 21, 1962
MERCATOR PROJECTION, TRUE TO SCALE AT 22½° N. AND S.

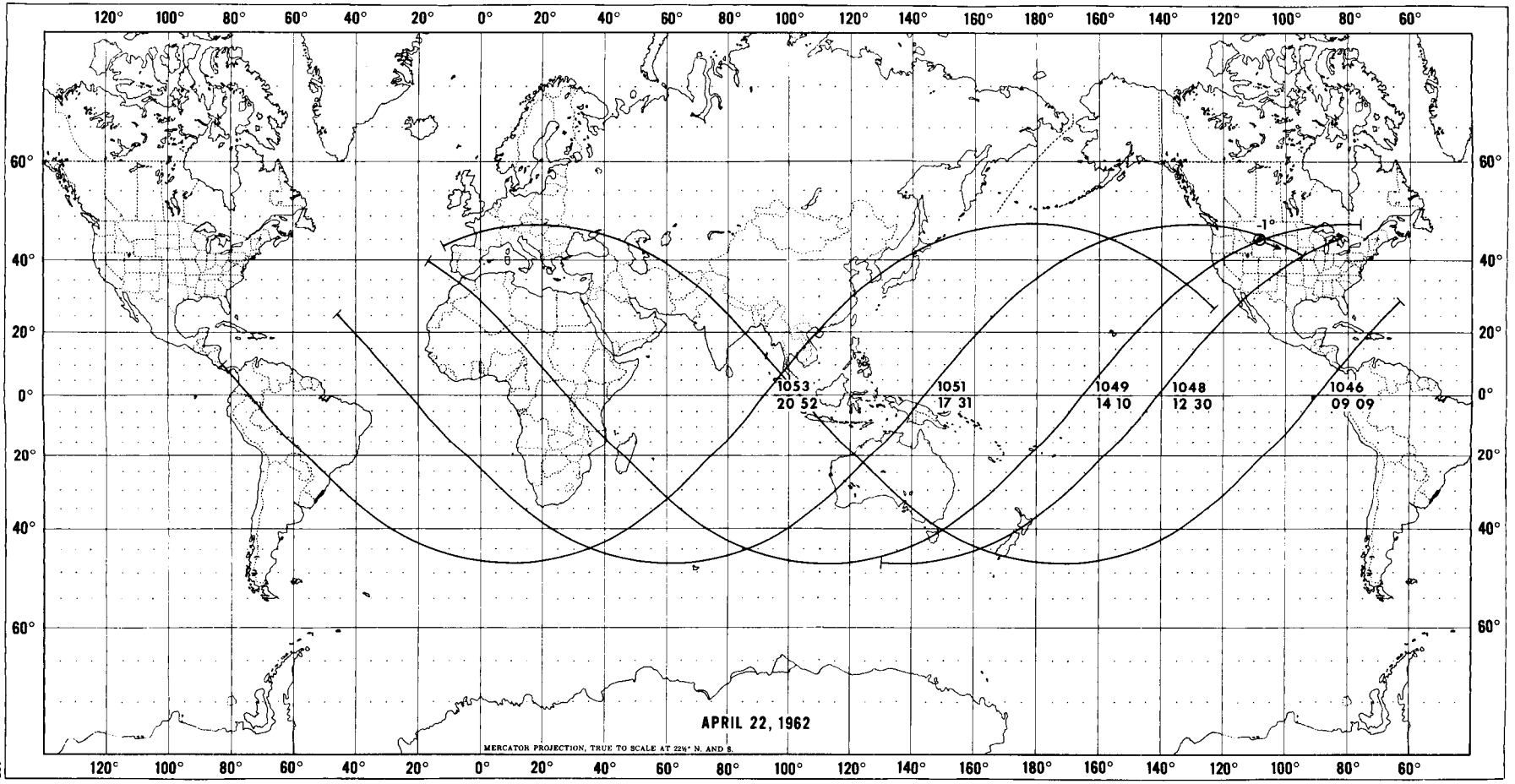
120° 100° 80° 60° 40° 20° 0° 20° 40° 60° 80° 100° 120° 140° 160° 180° 160° 140° 120° 100° 80° 60°
60°
40°
20°
0°
20°
40°
60°
1053
20 52
1051
17 31
1049
14 10
1048
12 30
1046
09 09
-1°
APRIL 22, 1962
MERCATOR PROJECTION, TRUE TO SCALE AT 22½° N. AND S.

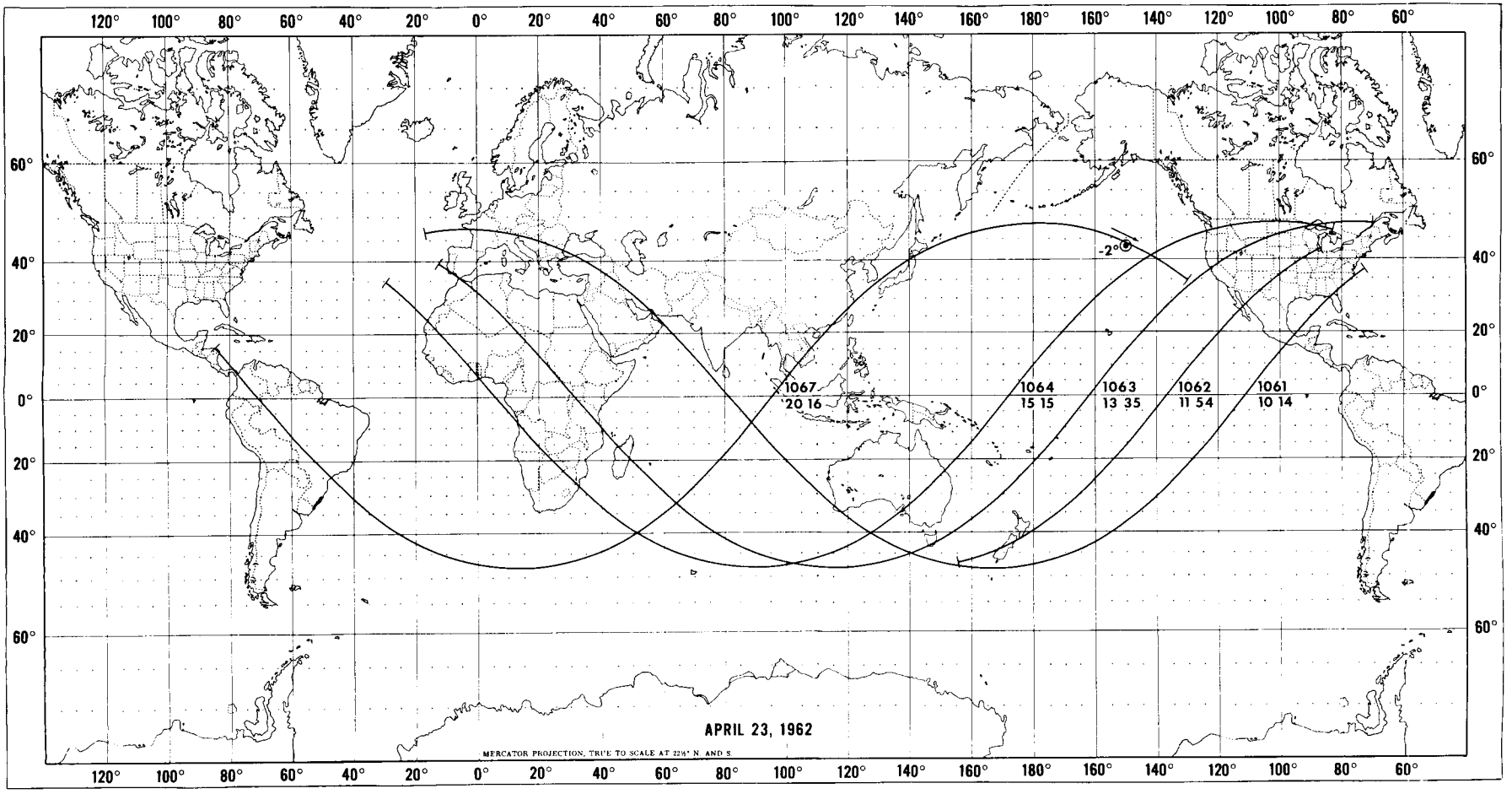
120° 100° 80° 60° 40° 20° 0° 20° 40° 60° 80° 100° 120° 140° 160° 180° 160° 140° 120° 100° 80° 60°
60°
40°
20°
0°
20°
40°
60°
-2°
1067
20 16
1064
15 15
1063
13 35
1062
11 54
1061
10 14
APRIL 23, 1962
MERCATOR PROJECTION, TRUE TO SCALE AT 22½° N. AND S.

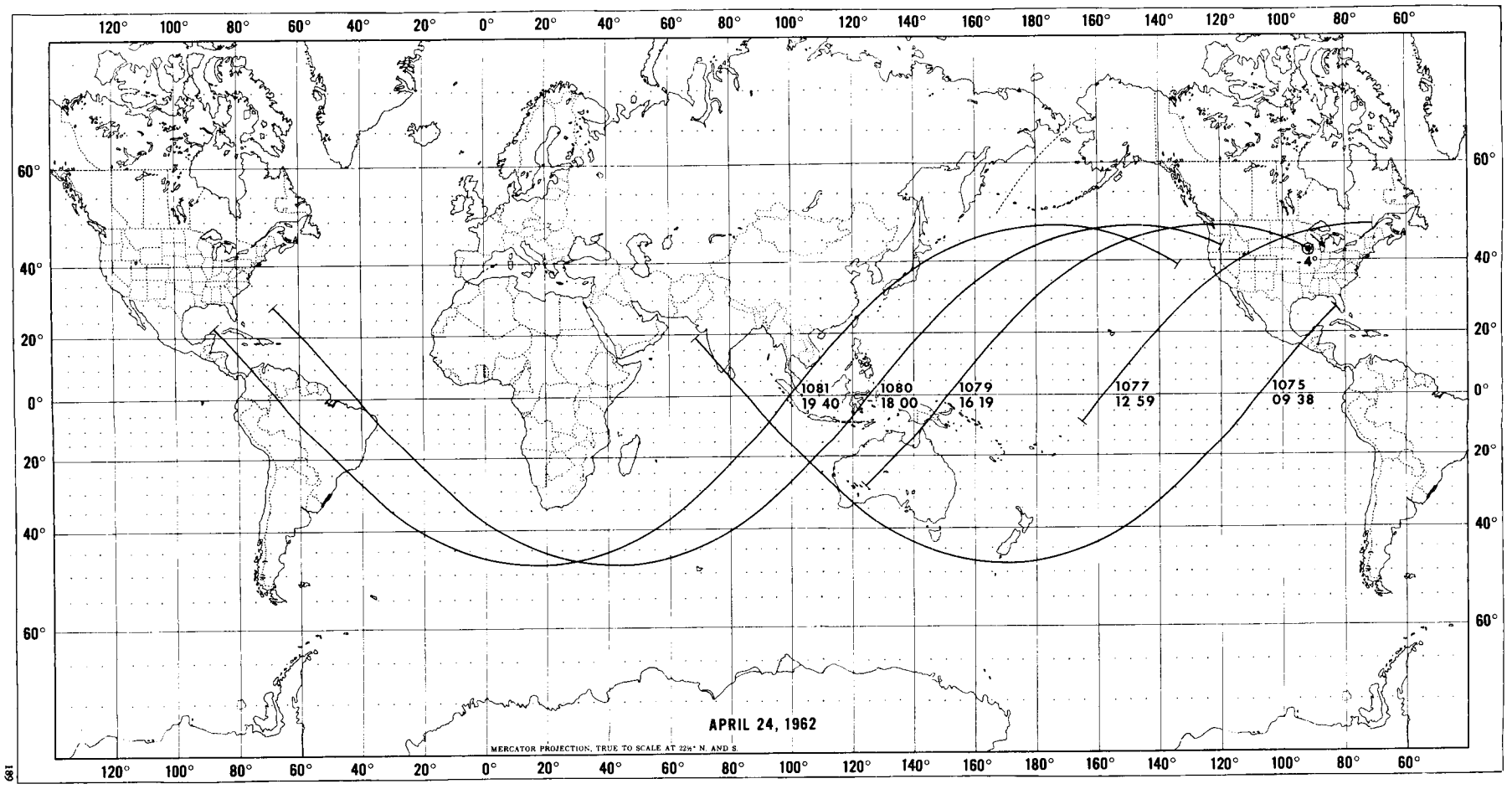
120° 100° 80° 60° 40° 20° 0° 20° 40° 60° 80° 100° 120° 140° 160° 180° 160° 140° 120° 100° 80° 60°
60°
40°
20°
0°
20°
40°
60°
1081
19 40
1080
18 00
1079
16 19
1077
12 59
1075
09 38
APRIL 24, 1962
MERCATOR PROJECTION, TRUE TO SCALE AT 22½° N. AND S.

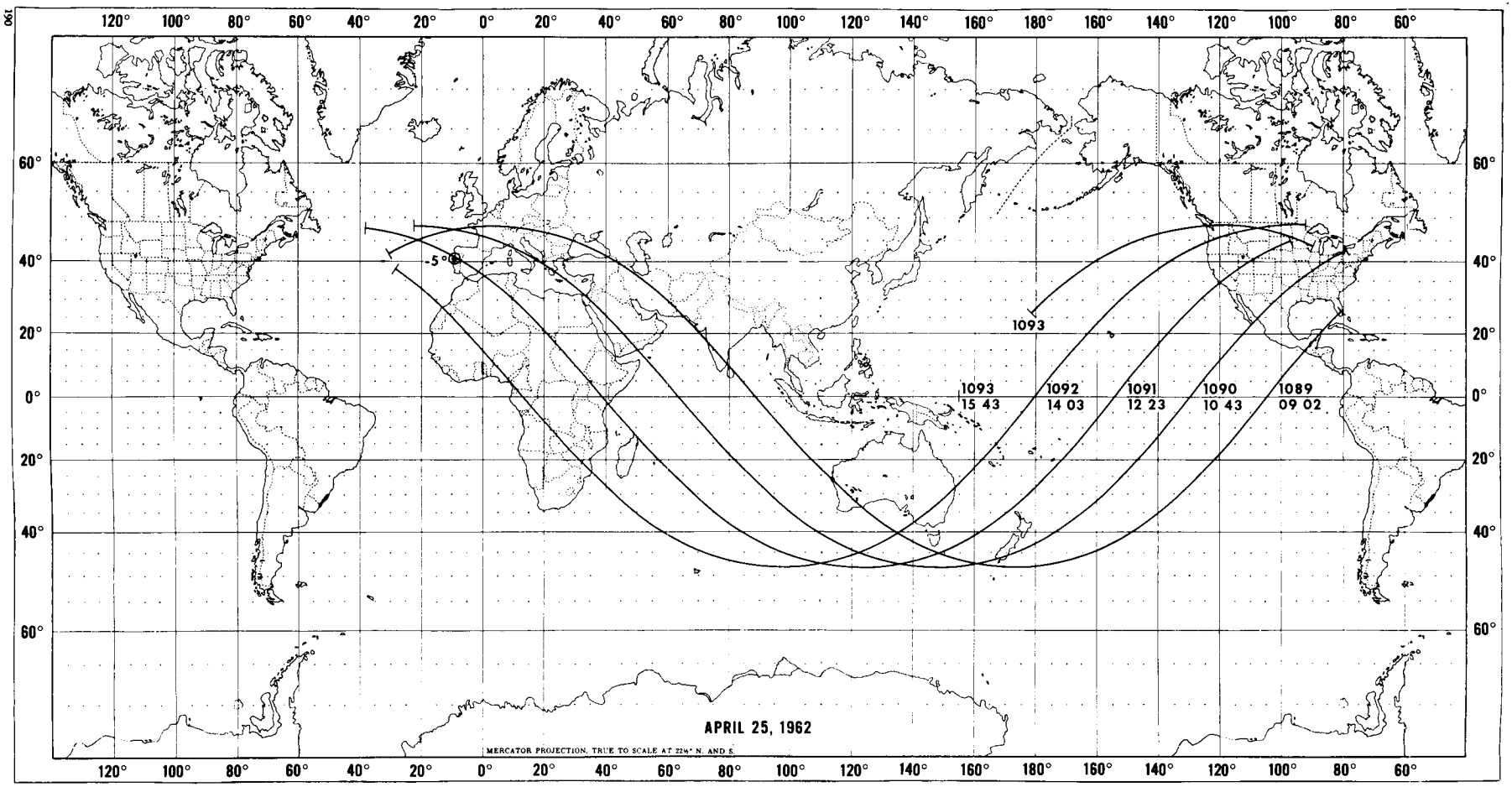
120° 100° 80° 60° 40° 20° 0° 20° 40° 60° 80° 100° 120° 140° 160° 180° 160° 140° 120° 100° 80° 60°
60°
40°
20°
0°
20°
40°
60°
-5°
1093
1093
15 43
1092
14 03
1091
12 23
1090
10 43
1089
09 02
APRIL 25, 1962
MERCATOR PROJECTION, TRUE TO SCALE AT 22½° N. AND S.

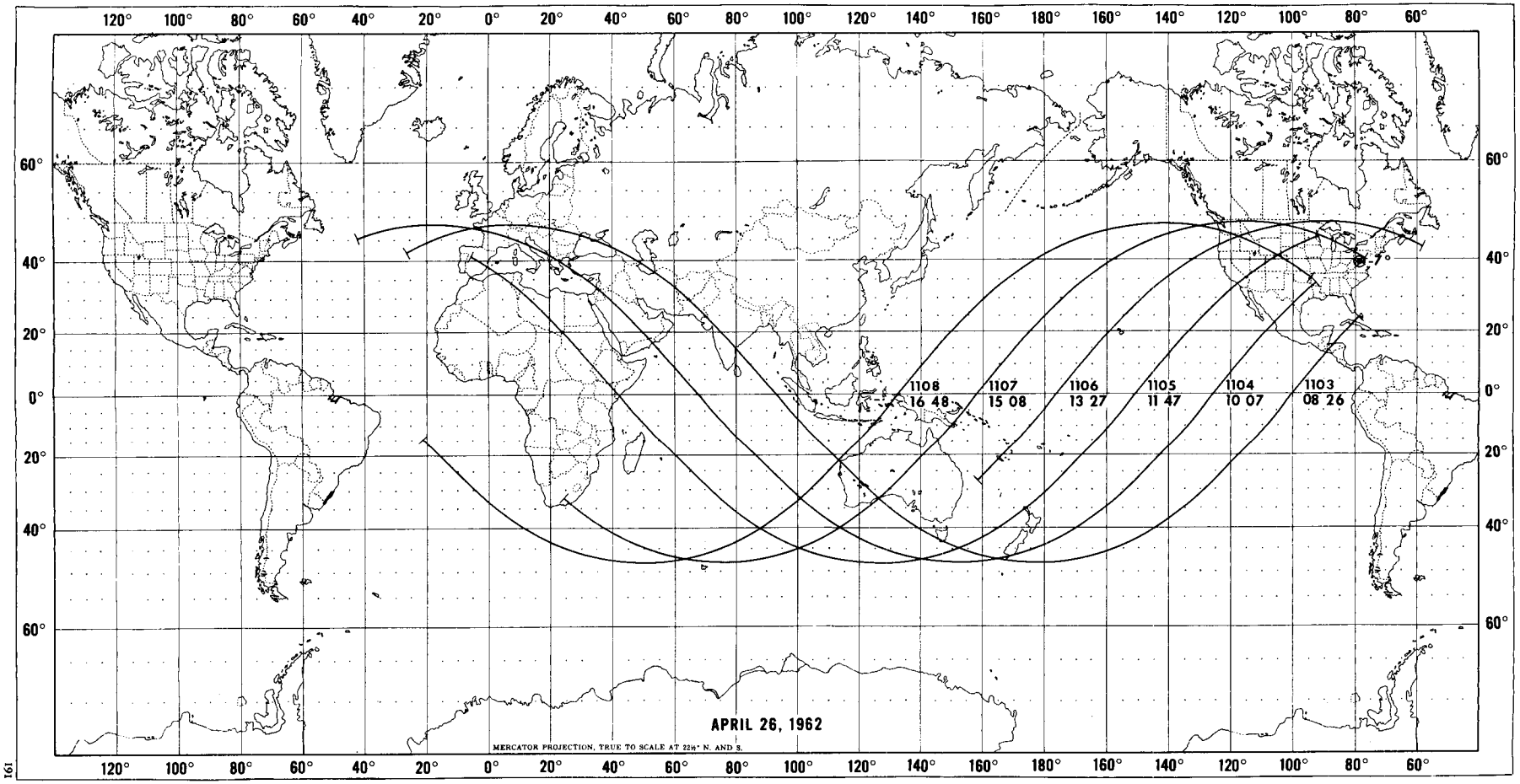
120° 100° 80° 60° 40° 20° 0° 20° 40° 60° 80° 100° 120° 140° 160° 180° 160° 140° 120° 100° 80° 60°
60°
40°
20°
0°
20°
40°
60°
1108
16 48
1107
15 08
1106
13 27
1105
11 47
1104
10 07
1103
08 26
APRIL 26, 1962
MERCATOR PROJECTION, TRUE TO SCALE AT 22½° N. AND S.

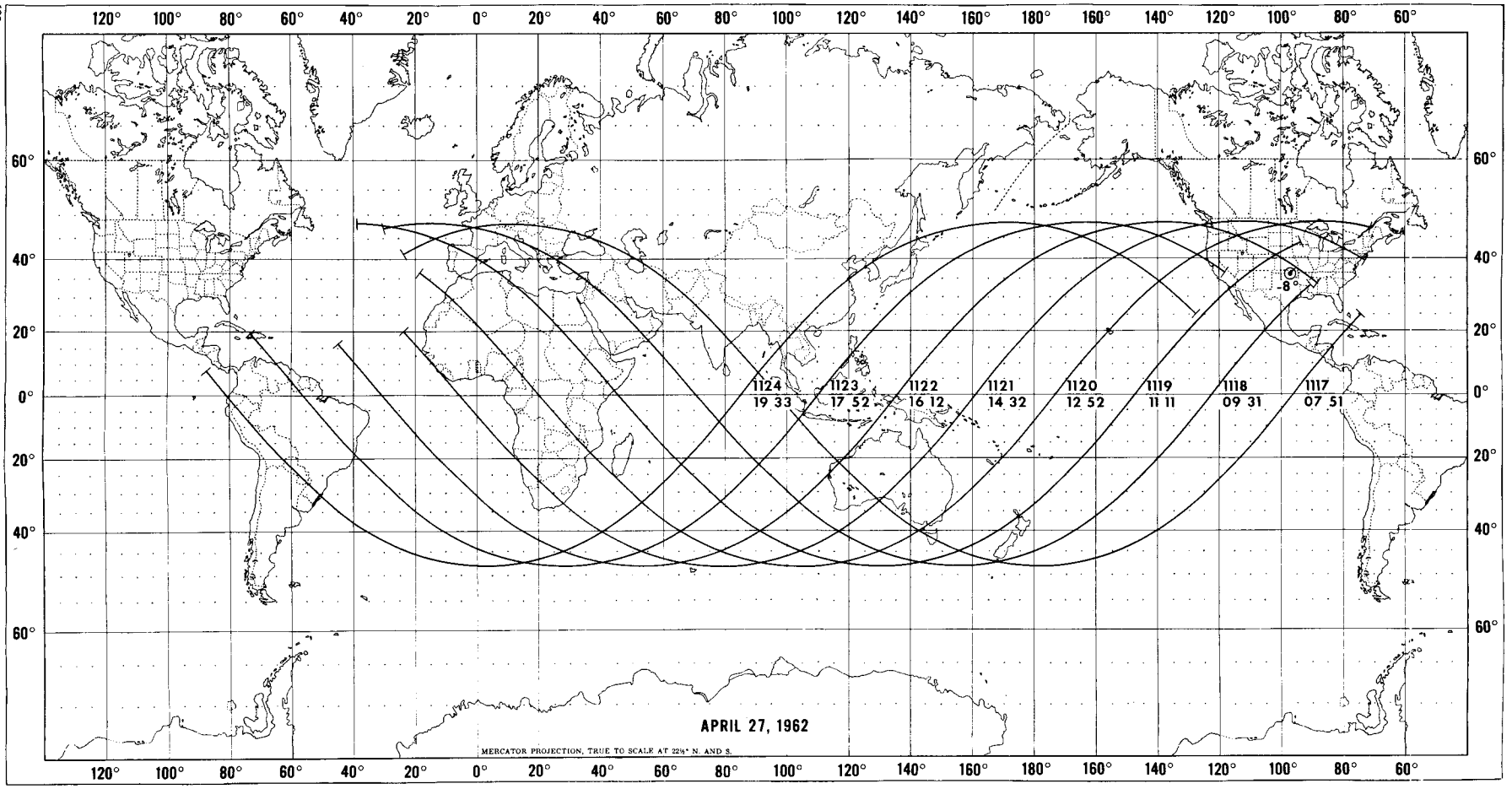
120° 100° 80° 60° 40° 20° 0° 20° 40° 60° 80° 100° 120° 140° 160° 180° 160° 140° 120° 100° 80° 60°
60°
40°
20°
0°
20°
40°
60°
-8°
1124
19 33
1123
17 52
1122
16 12
1121
14 32
1120
12 52
1119
11 11
1118
09 31
1117
07 51
APRIL 27, 1962
MERCATOR PROJECTION, TRUE TO SCALE AT 22½° N. AND S.

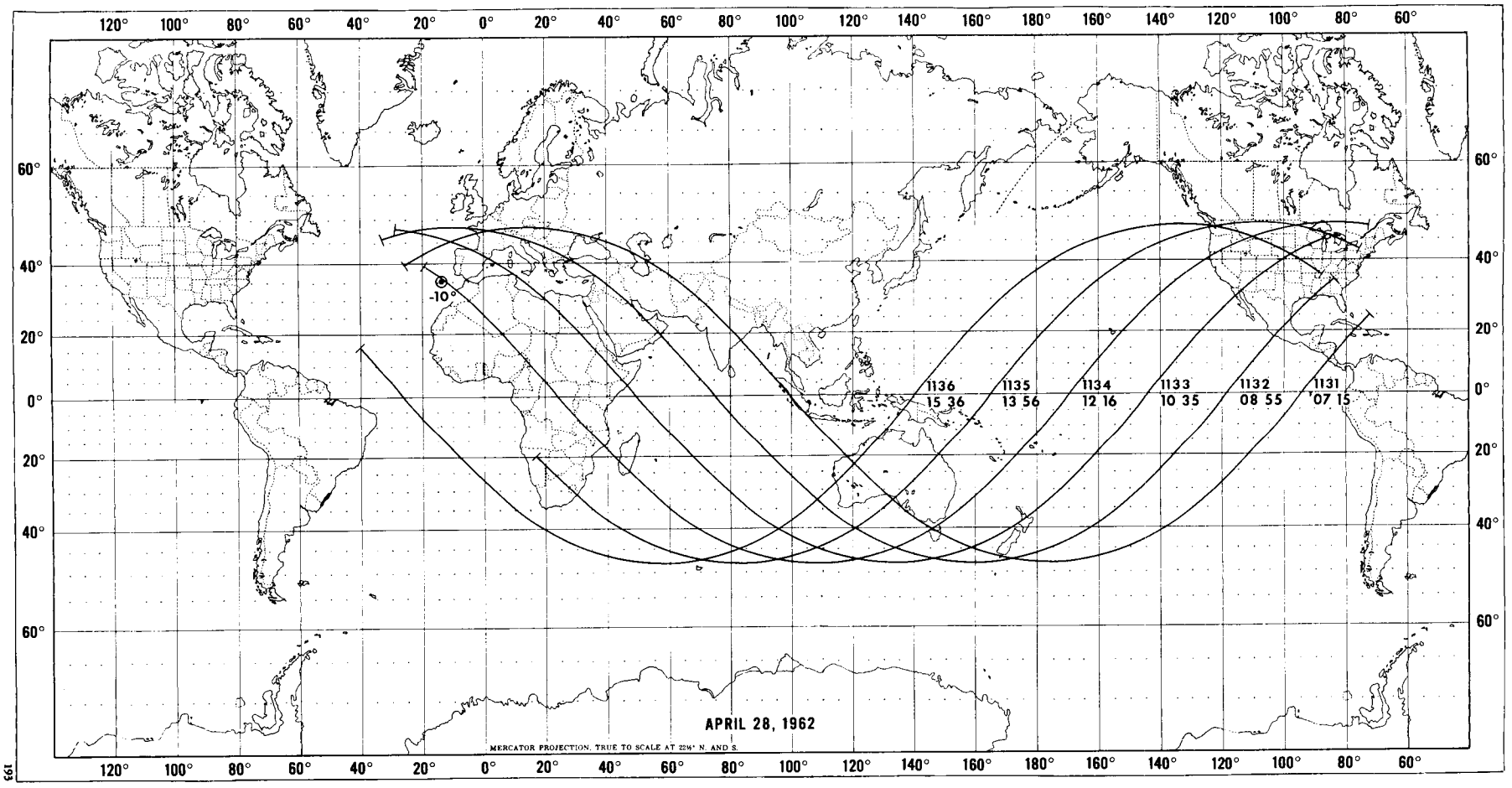
120° 100° 80° 60° 40° 20° 0° 20° 40° 60° 80° 100° 120° 140° 160° 180° 160° 140° 120° 100° 80° 60°
60°
40°
20°
0°
20°
40°
60°
-10°
1136
15 36
1135
13 56
1134
12 16
1133
10 35
1132
08 55
1131
07 15
APRIL 28, 1962
MERCATOR PROJECTION. TRUE TO SCALE AT 22½° N. AND S.

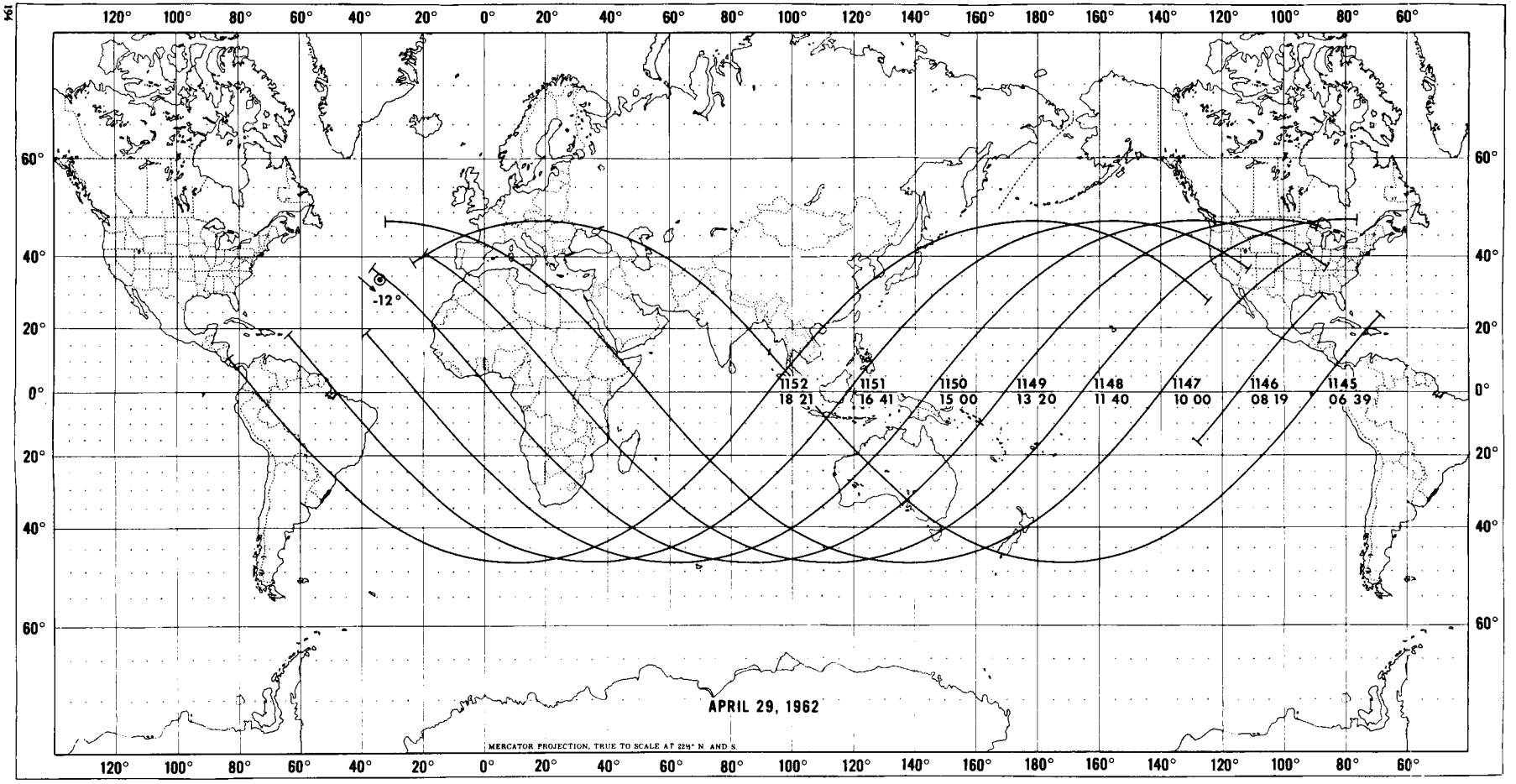
120° 100° 80° 60° 40° 20° 0° 20° 40° 60° 80° 100° 120° 140° 160° 180° 160° 140° 120° 100° 80° 60°
60°
40°
20°
0°
20°
40°
60°
-12°
1152 18 21
1151 16 41
1150 15 00
1149 13 20
1148 11 40
1147 10 00
1146 08 19
1145 06 39
APRIL 29, 1962
MERCATOR PROJECTION, TRUE TO SCALE AT 22½° N. AND S.

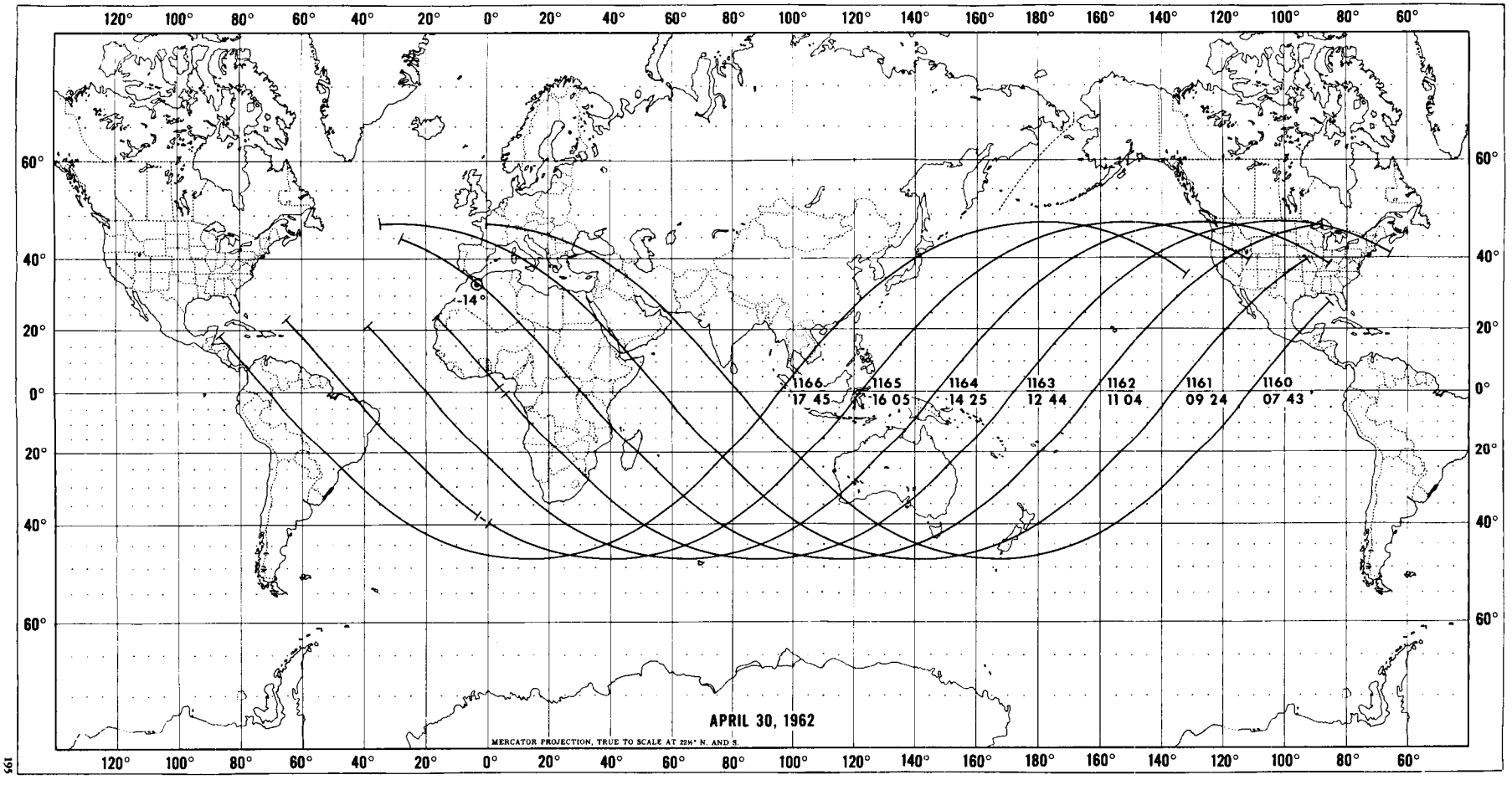
120° 100° 80° 60° 40° 20° 0° 20° 40° 60° 80° 100° 120° 140° 160° 180° 160° 140° 120° 100° 80° 60°
60°
40°
20°
0°
20°
40°
60°
-14°
1166
17 45
1165
16 05
1164
14 25
1163
12 44
1162
11 04
1161
09 24
1160
07 43
APRIL 30, 1962
MERCATOR PROJECTION, TRUE TO SCALE AT 22½° N. AND S.

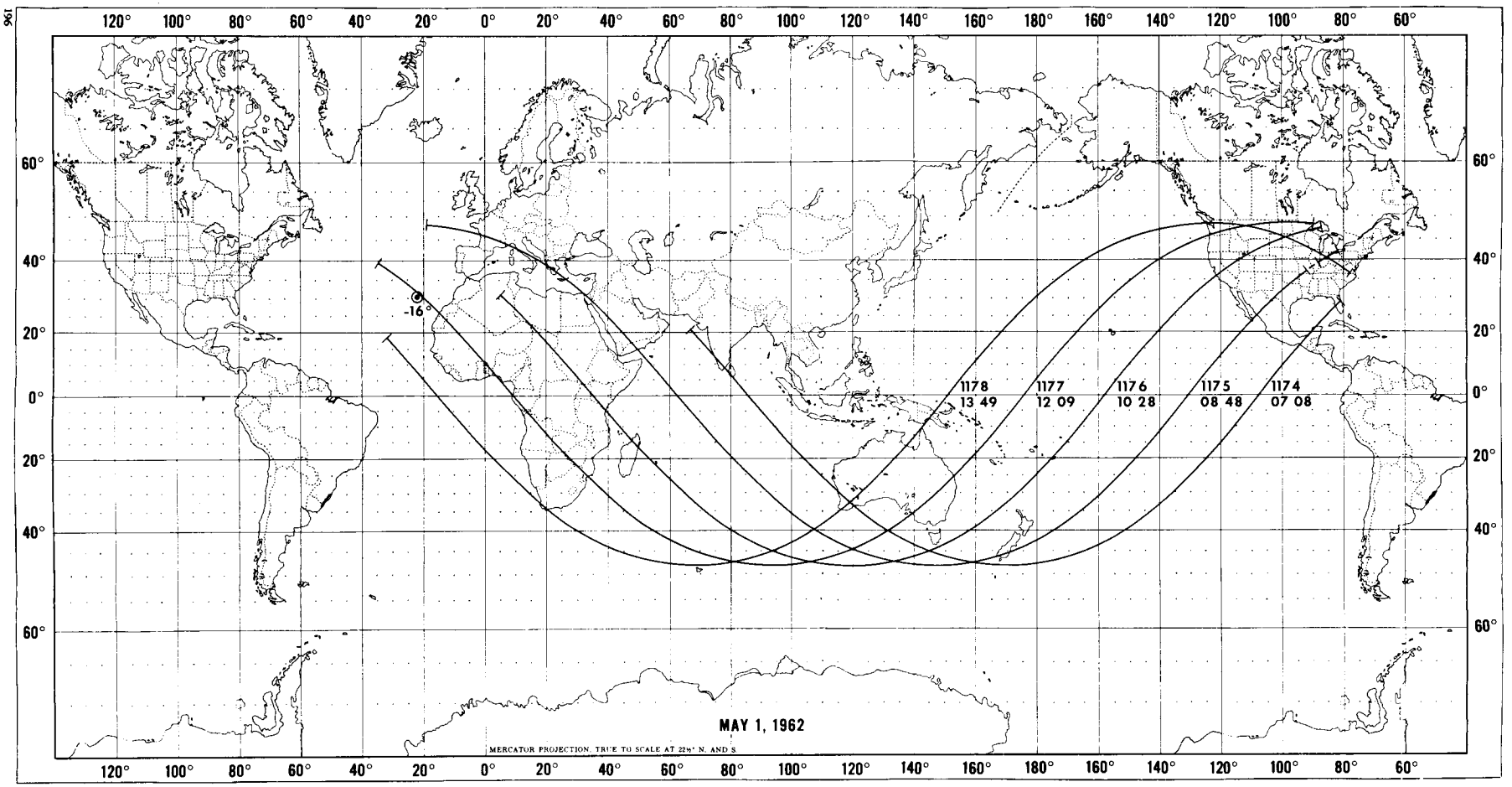
120° 100° 80° 60° 40° 20° 0° 20° 40° 60° 80° 100° 120° 140° 160° 180° 160° 140° 120° 100° 80° 60°
60°
40°
20°
0°
20°
40°
60°
-16°
1178
13 49
1177
12 09
1176
10 28
1175
08 48
1174
07 08
MAY 1, 1962
MERCATOR PROJECTION, TRUE TO SCALE AT 22½° N. AND S

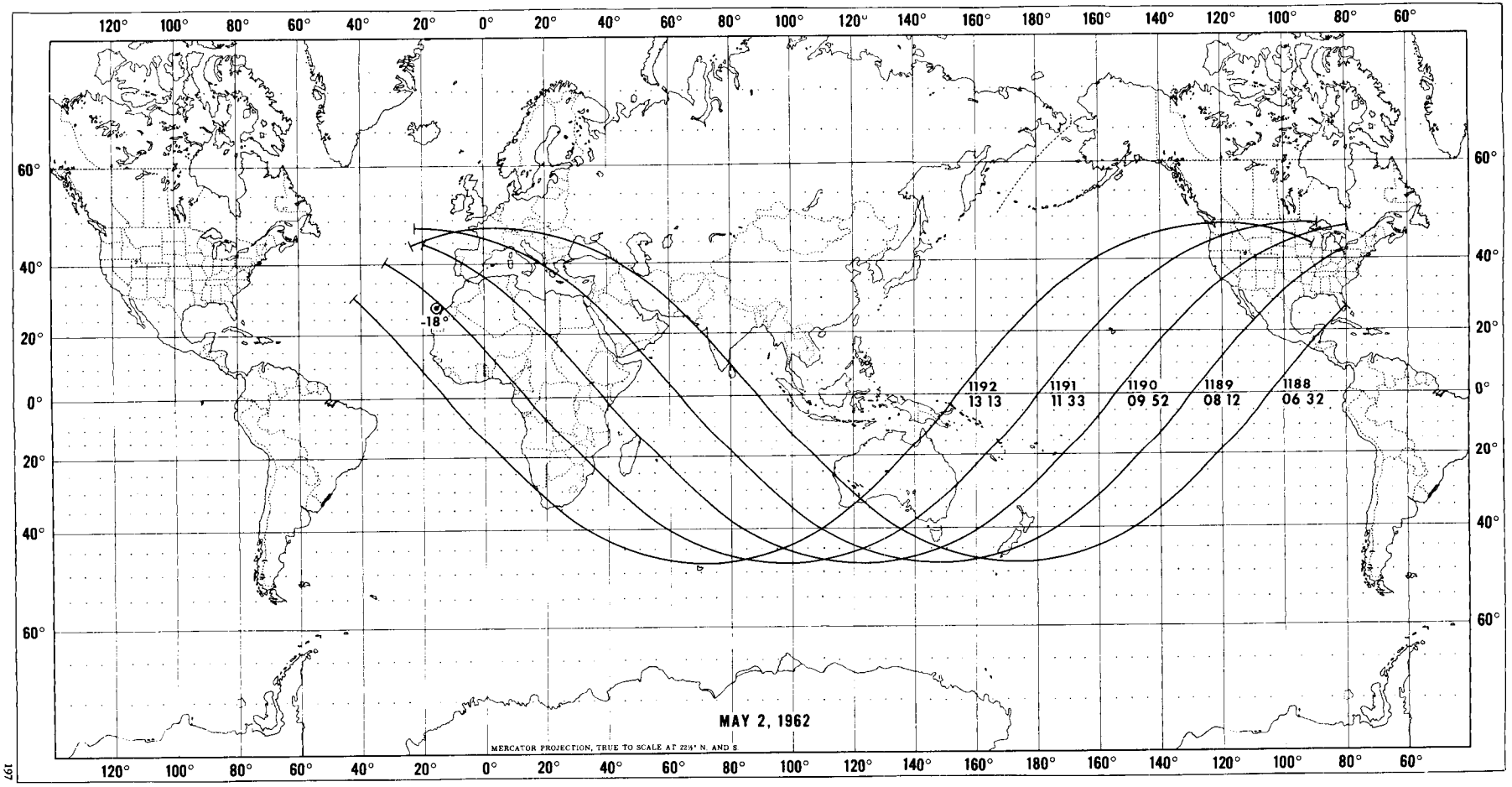
120° 100° 80° 60° 40° 20° 0° 20° 40° 60° 80° 100° 120° 140° 160° 180° 160° 140° 120° 100° 80° 60°
60°
40°
20°
0°
20°
40°
60°
-18°
1192
13 13
1191
11 33
1190
09 52
1189
08 12
1188
06 32
MAY 2, 1962
MERCATOR PROJECTION, TRUE TO SCALE AT 22½° N. AND S

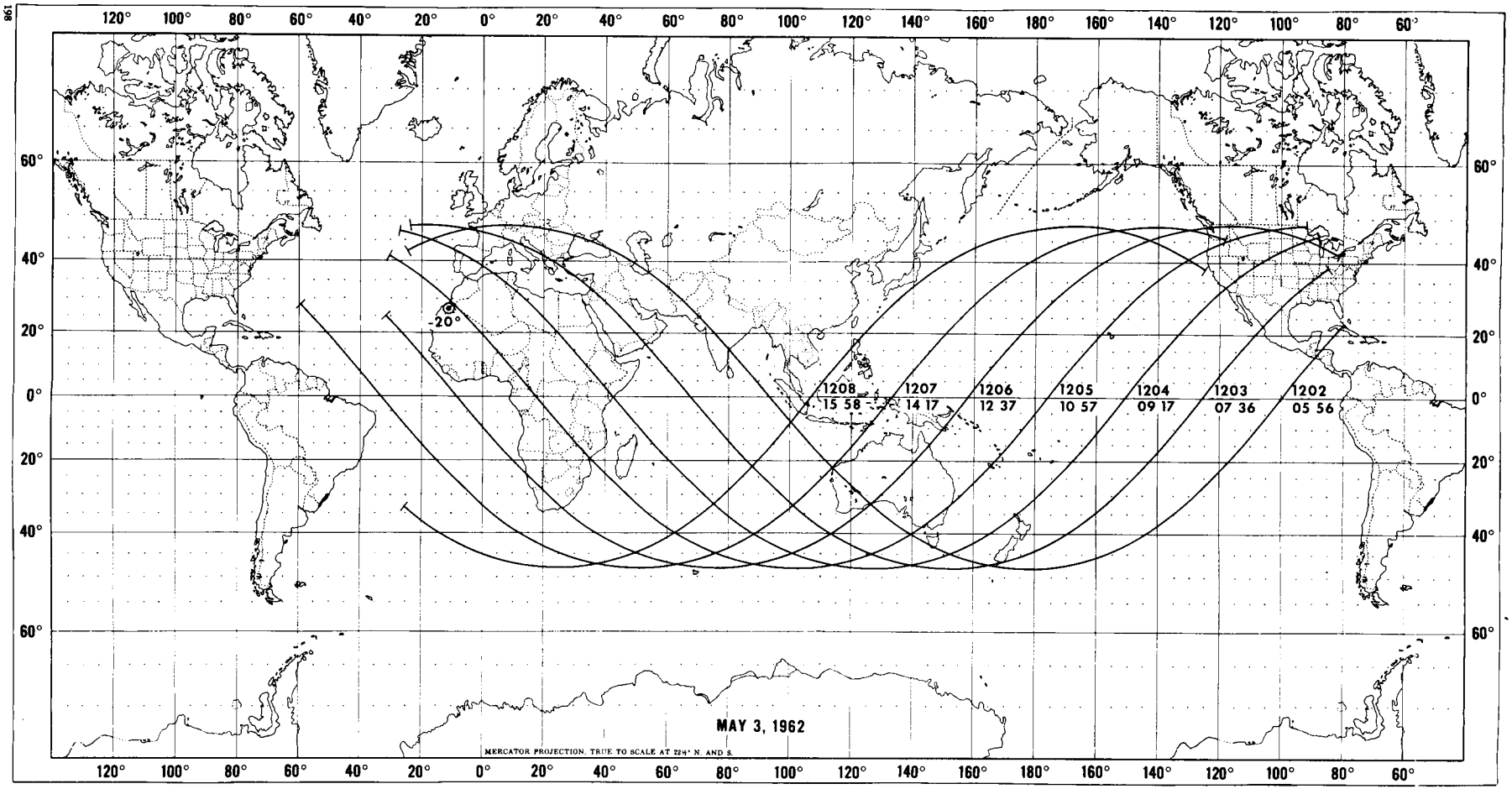
120° 100° 80° 60° 40° 20° 0° 20° 40° 60° 80° 100° 120° 140° 160° 180° 160° 140° 120° 100° 80° 60°
60°
40°
20°
0°
20°
40°
60°
-20°
1208
15 58
1207
14 17
1206
12 37
1205
10 57
1204
09 17
1203
07 36
1202
05 56
MAY 3, 1962
MERCATOR PROJECTION. TRUE TO SCALE AT 22½° N. AND S.

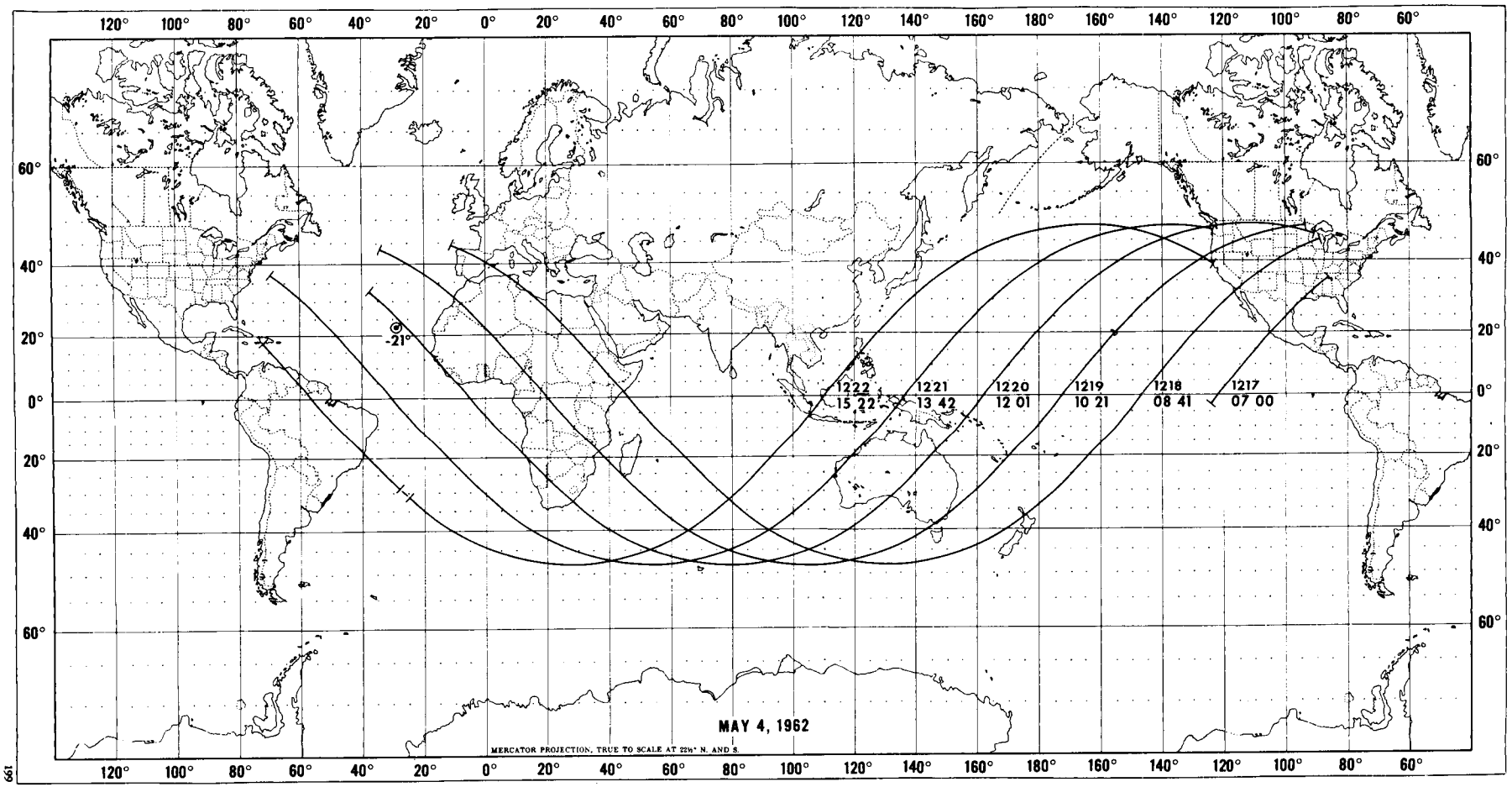
120° 100° 80° 60° 40° 20° 0° 20° 40° 60° 80° 100° 120° 140° 160° 180° 160° 140° 120° 100° 80° 60°
60°
40°
20°
0°
20°
40°
60°
-21°
1222
15 22
1221
13 42
1220
12 01
1219
10 21
1218
08 41
1217
07 00
MAY 4, 1962
MERCATOR PROJECTION, TRUE TO SCALE AT 22½° N. AND S.

661

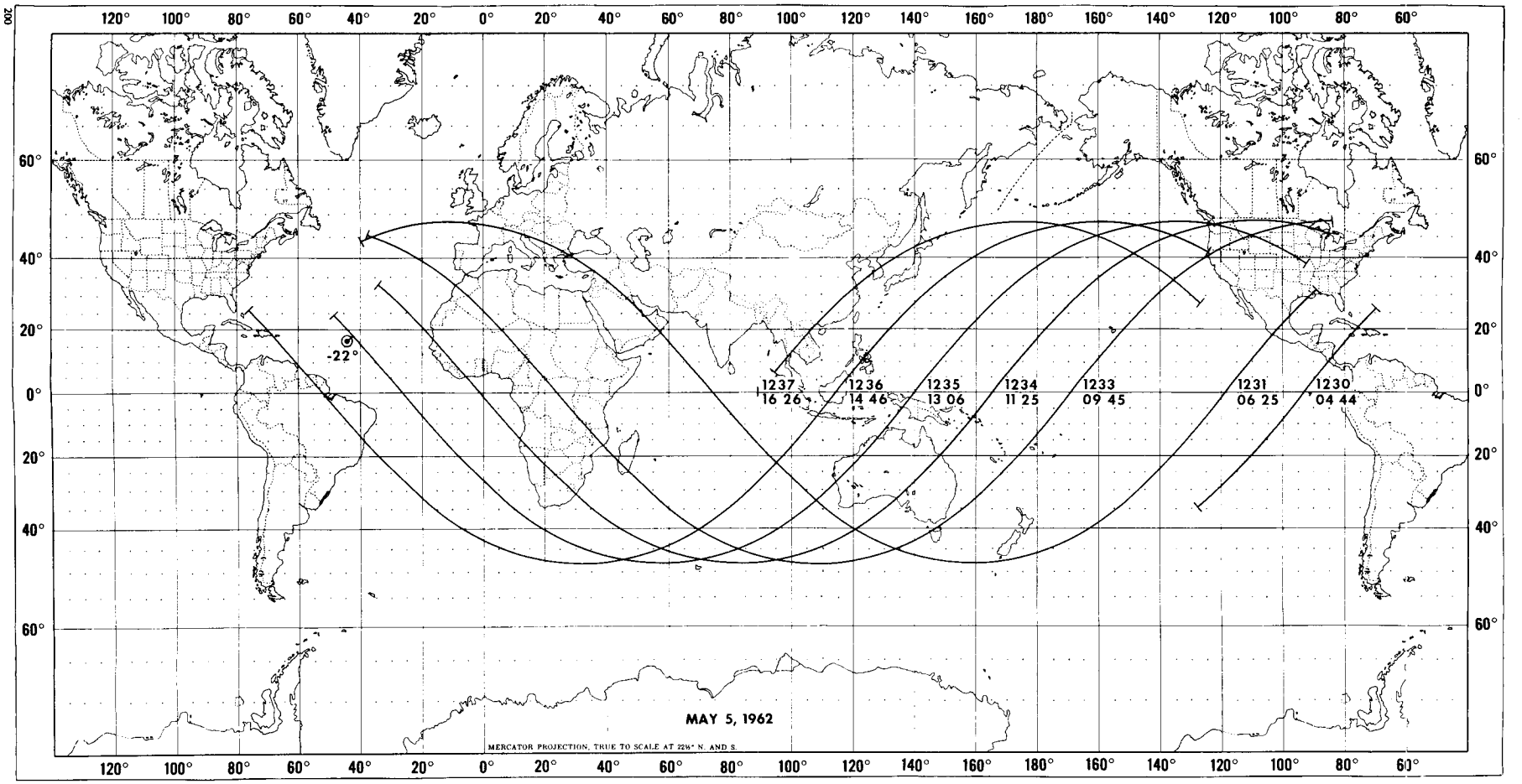
120° 100° 80° 60° 40° 20° 0° 20° 40° 60° 80° 100° 120° 140° 160° 180° 160° 140° 120° 100° 80° 60°
60°
40°
20°
0°
20°
40°
60°
-22°
1237
16 26
1236
14 46
1235
13 06
1234
11 25
1233
09 45
1231
06 25
1230
04 44
MAY 5, 1962
MERCATOR PROJECTION, TRUE TO SCALE AT 22½° N. AND S.

729-166 O - 64 - 14

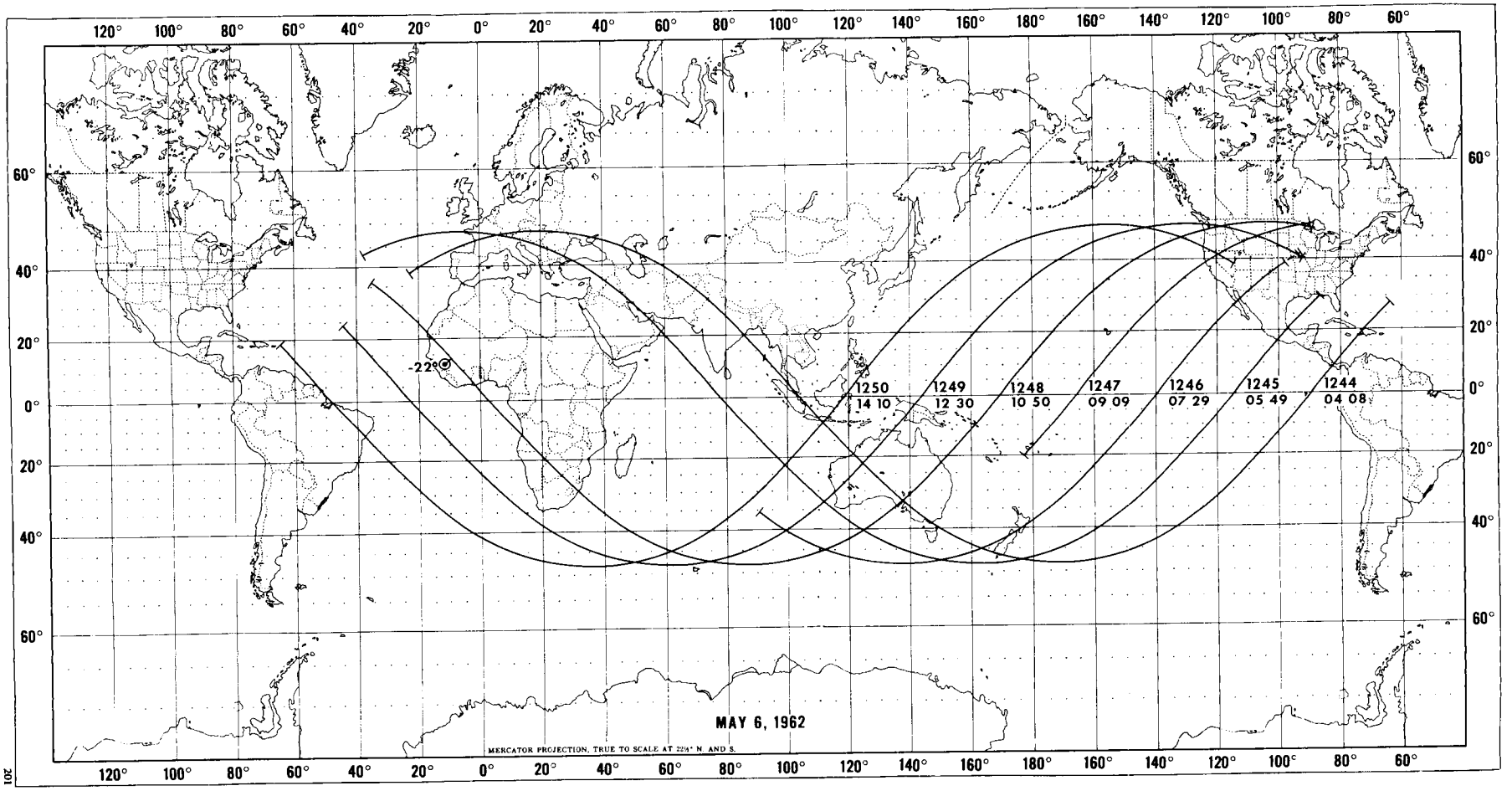

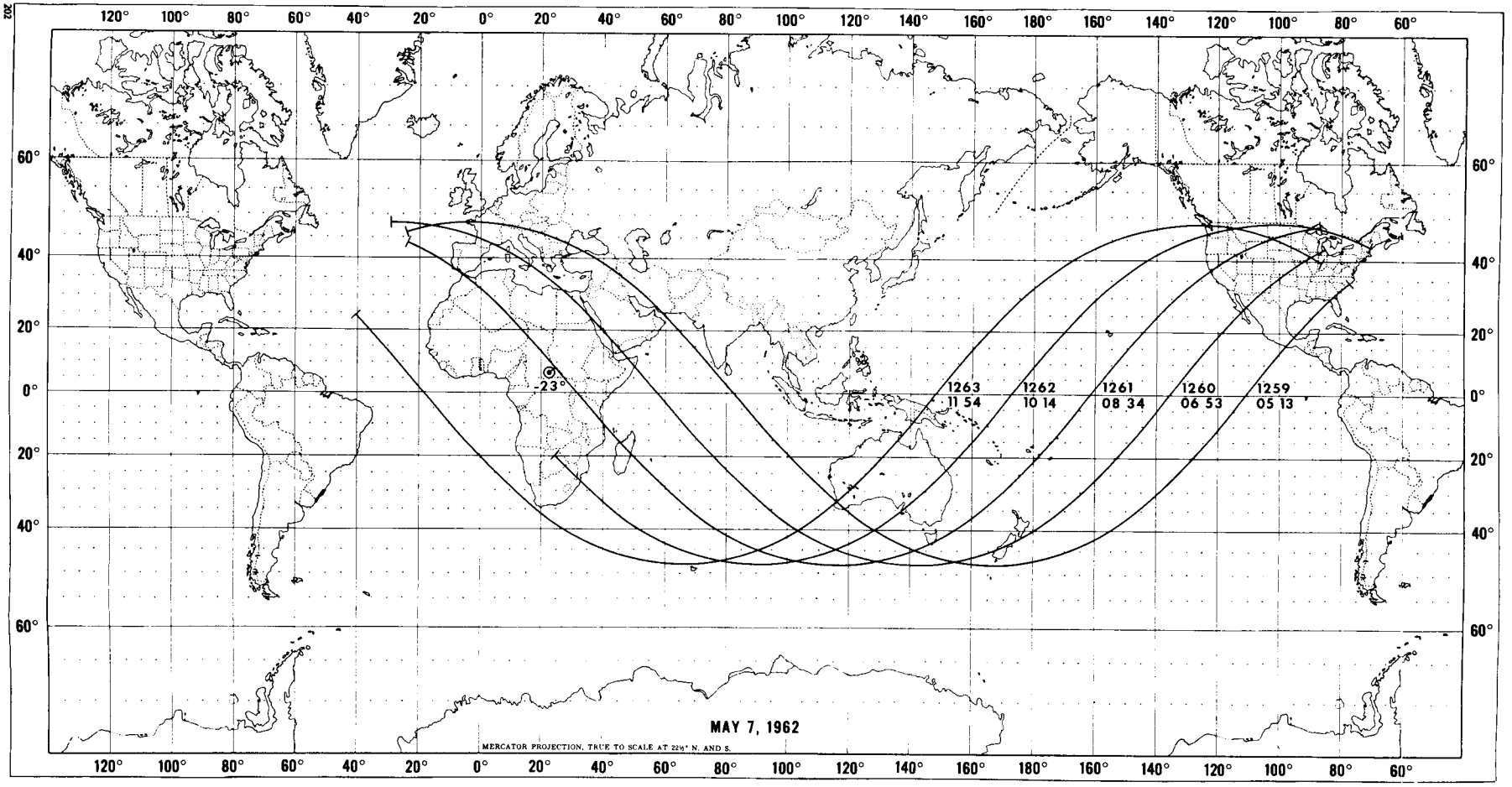
120° 100° 80° 60° 40° 20° 0° 20° 40° 60° 80° 100° 120° 140° 160° 180° 160° 140° 120° 100° 80° 60°
60°
40°
20°
0°
20°
40°
60°
-23°
1263
11 54
1262
10 14
1261
08 34
1260
06 53
1259
05 13
MAY 7, 1962
MERCATOR PROJECTION, TRUE TO SCALE AT 22½° N. AND S.

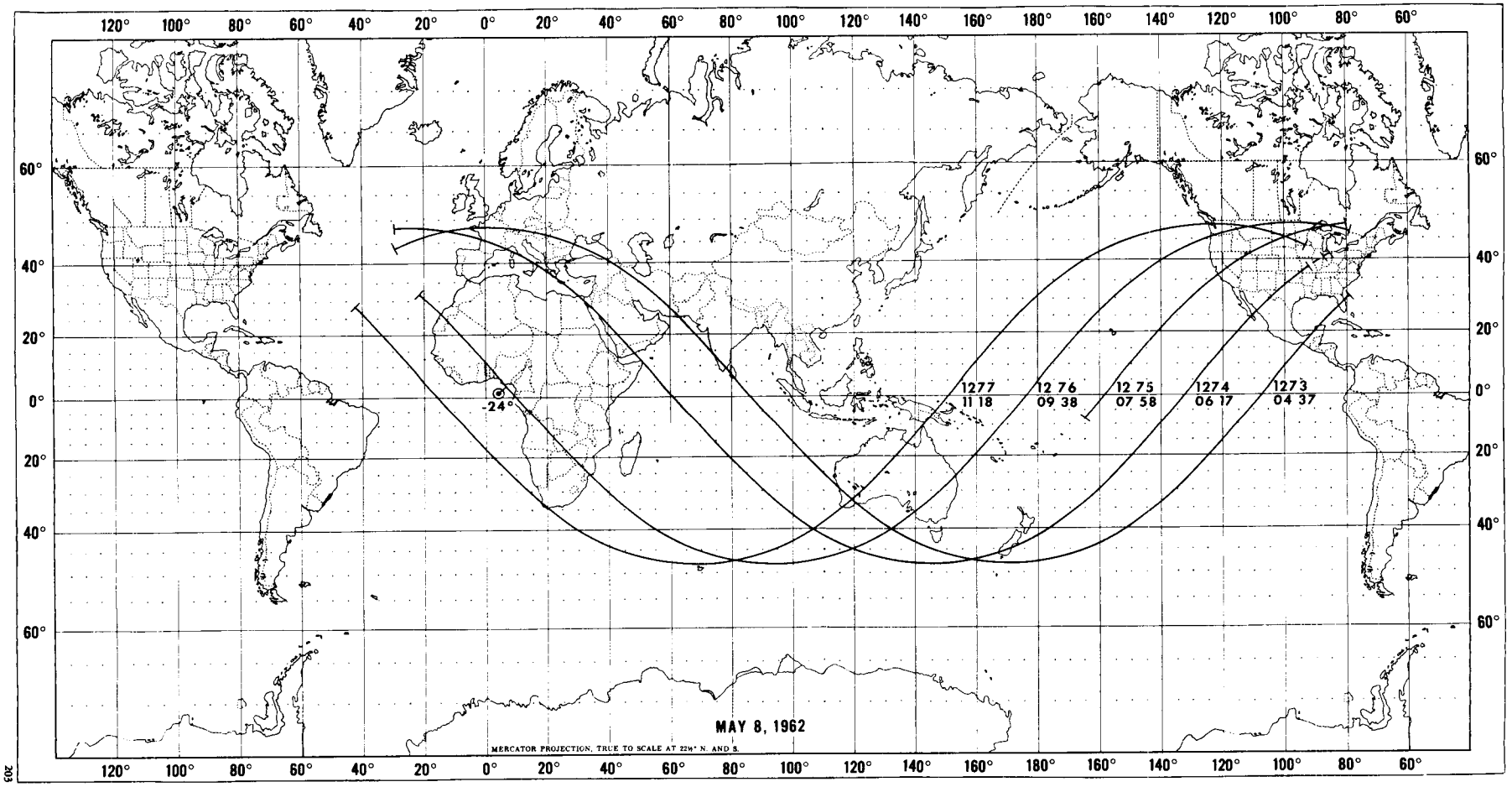
120° 100° 80° 60° 40° 20° 0° 20° 40° 60° 80° 100° 120° 140° 160° 180° 160° 140° 120° 100° 80° 60°
60°
40°
20°
0°
20°
40°
60°
-24°
1277
11 18
12 76
09 38
12 75
07 58
1274
06 17
1273
04 37
MAY 8, 1962
MERCATOR PROJECTION, TRUE TO SCALE AT 22½° N. AND S.

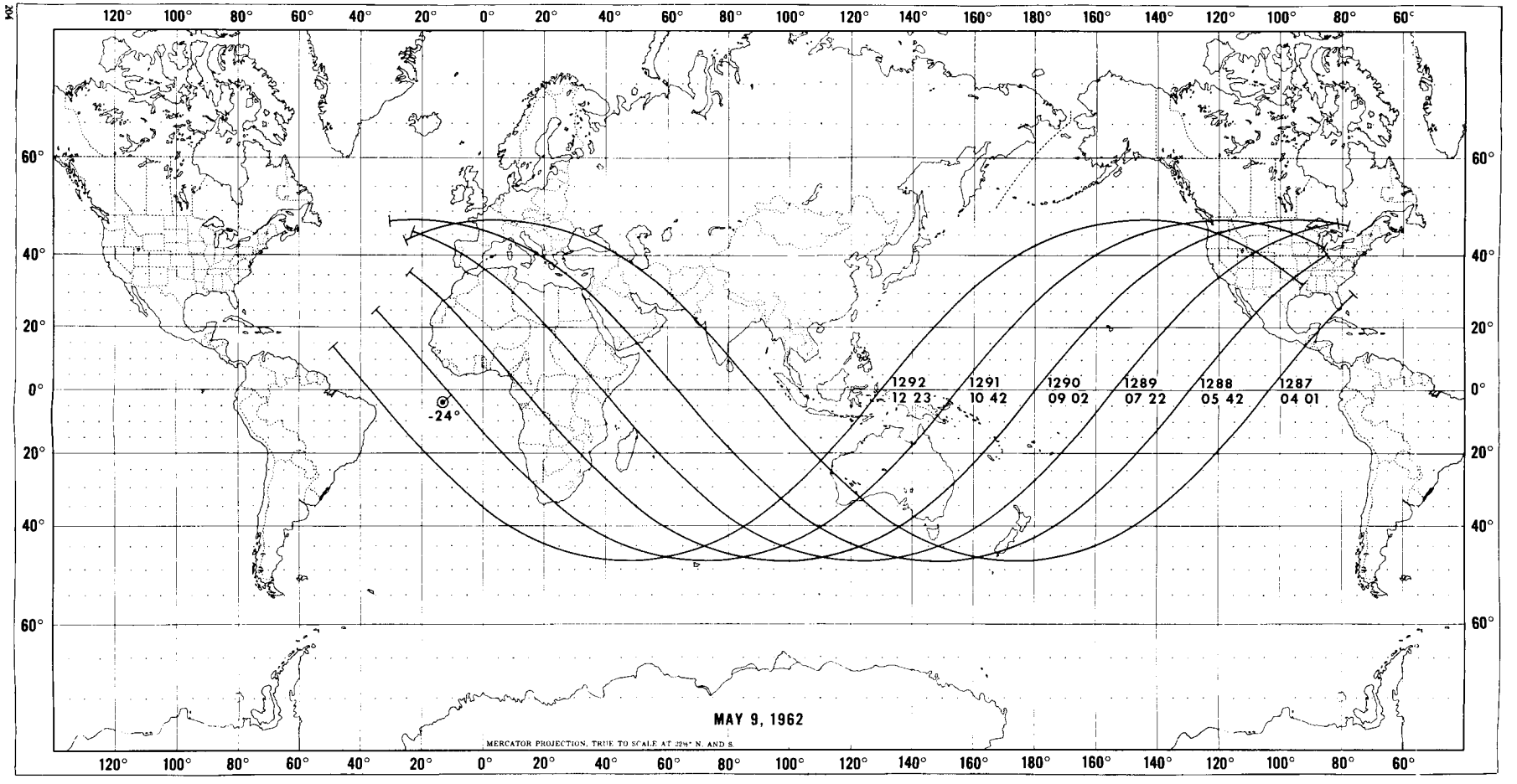
120° 100° 80° 60° 40° 20° 0° 20° 40° 60° 80° 100° 120° 140° 160° 180° 160° 140° 120° 100° 80° 60°
60°
40°
20°
0°
20°
40°
60°
1292
12 23
1291
10 42
1290
09 02
1289
07 22
1288
05 42
1287
04 01
-24°
MAY 9, 1962
MERCATOR PROJECTION, TRUE TO SCALE AT 22½° N. AND S.

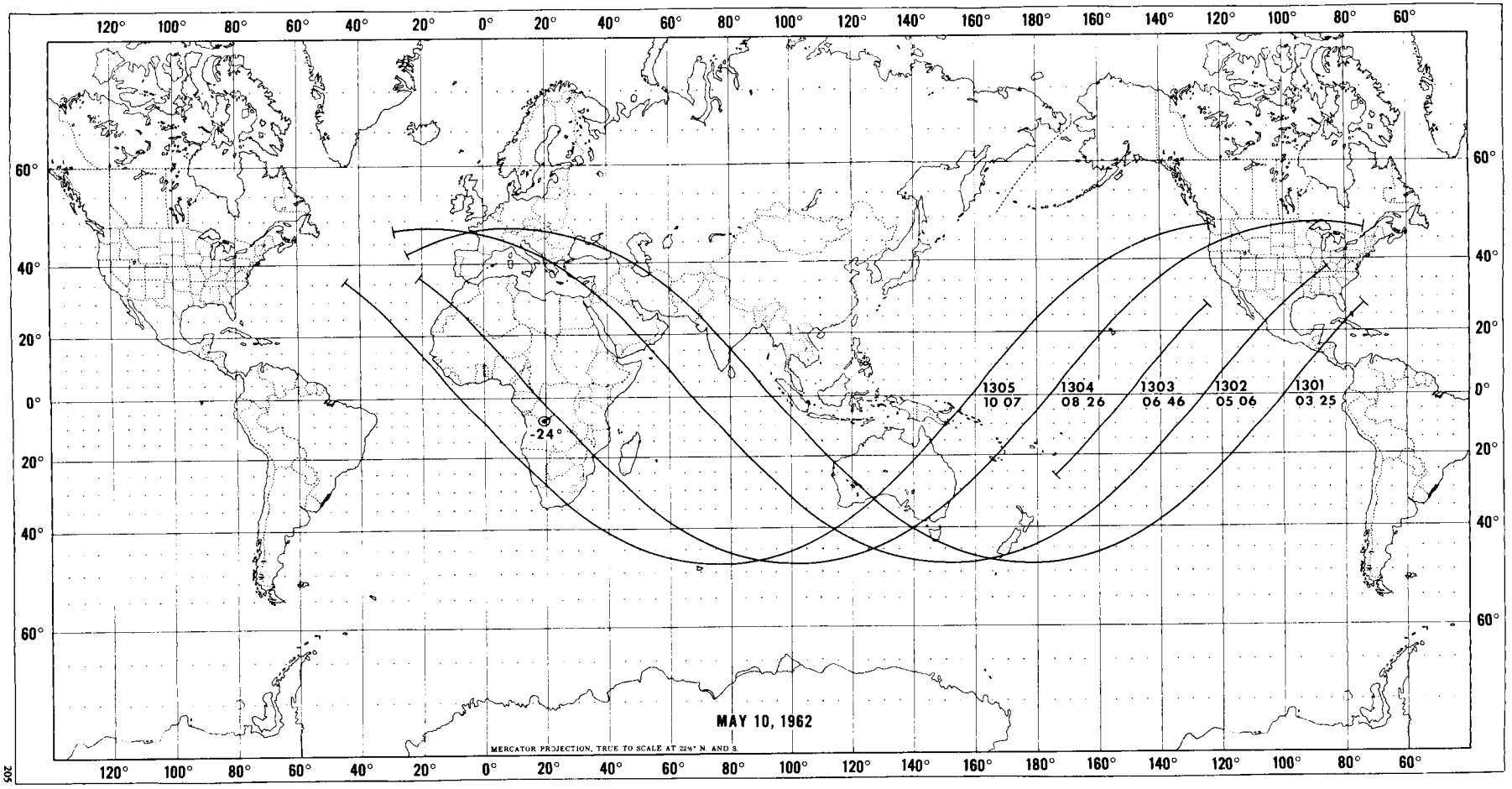
120° 100° 80° 60° 40° 20° 0° 20° 40° 60° 80° 100° 120° 140° 160° 180° 160° 140° 120° 100° 80° 60°
60°
40°
20°
0°
20°
40°
60°
1305
10 07
1304
08 26
1303
06 46
1302
05 06
1301
03 25
-24°
MAY 10, 1962
MERCATOR PROJECTION, TRUE TO SCALE AT 22½° N. AND S.

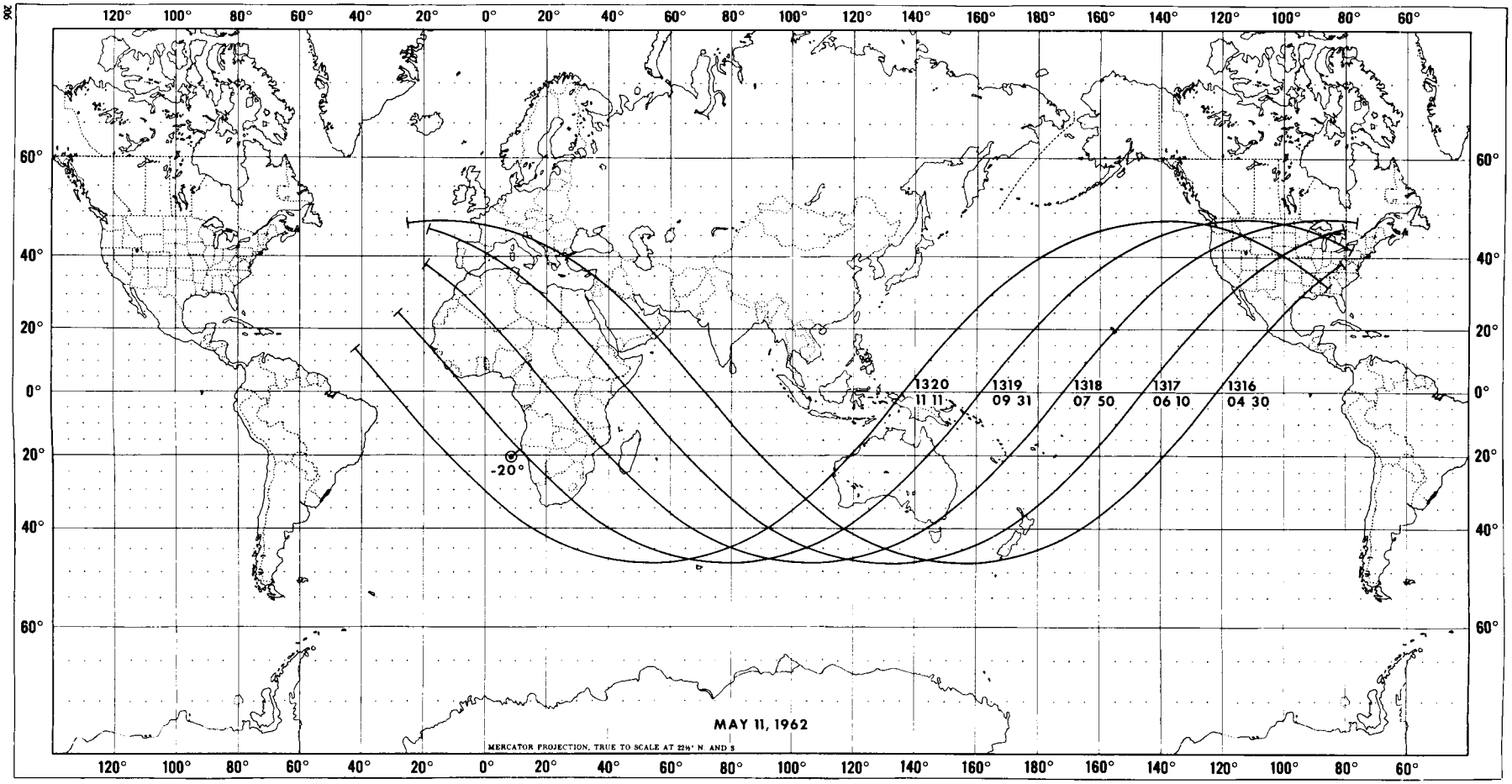
120° 100° 80° 60° 40° 20° 0° 20° 40° 60° 80° 100° 120° 140° 160° 180° 160° 140° 120° 100° 80° 60°
60°
40°
20°
0°
20°
40°
60°
1320
11 11
1319
09 31
1318
07 50
1317
06 10
1316
04 30
-20°
MAY 11, 1962
MERCATOR PROJECTION, TRUE TO SCALE AT 22½° N. AND S.

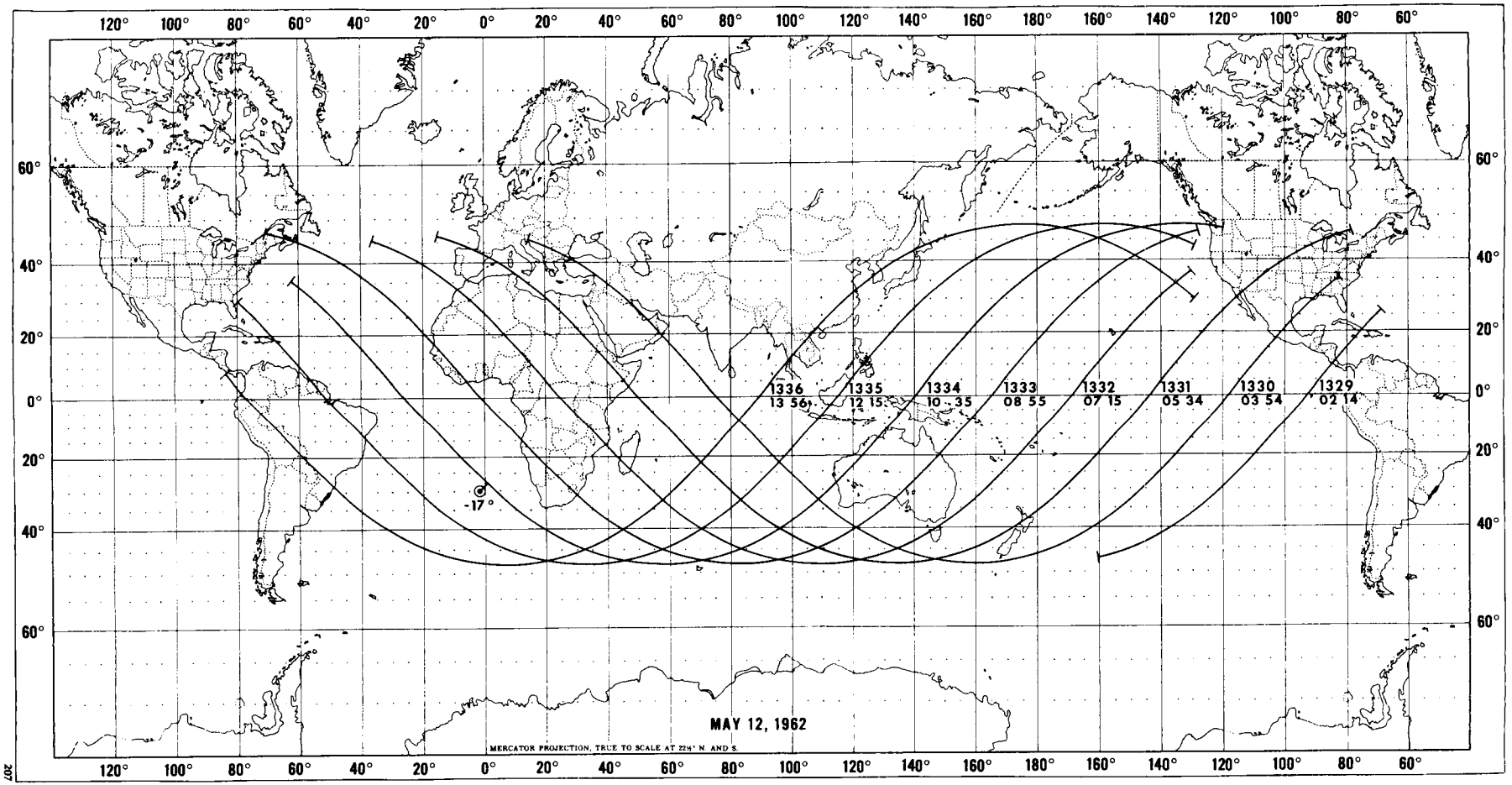
120° 100° 80° 60° 40° 20° 0° 20° 40° 60° 80° 100° 120° 140° 160° 180° 160° 140° 120° 100° 80° 60°
60°
40°
20°
0°
20°
40°
60°
1336
13 56
1335
12 15
1334
10 35
1333
08 55
1332
07 15
1331
05 34
1330
03 54
1329
02 14
-17°
MAY 12, 1962
MERCATOR PROJECTION, TRUE TO SCALE AT 22½° N. AND S.

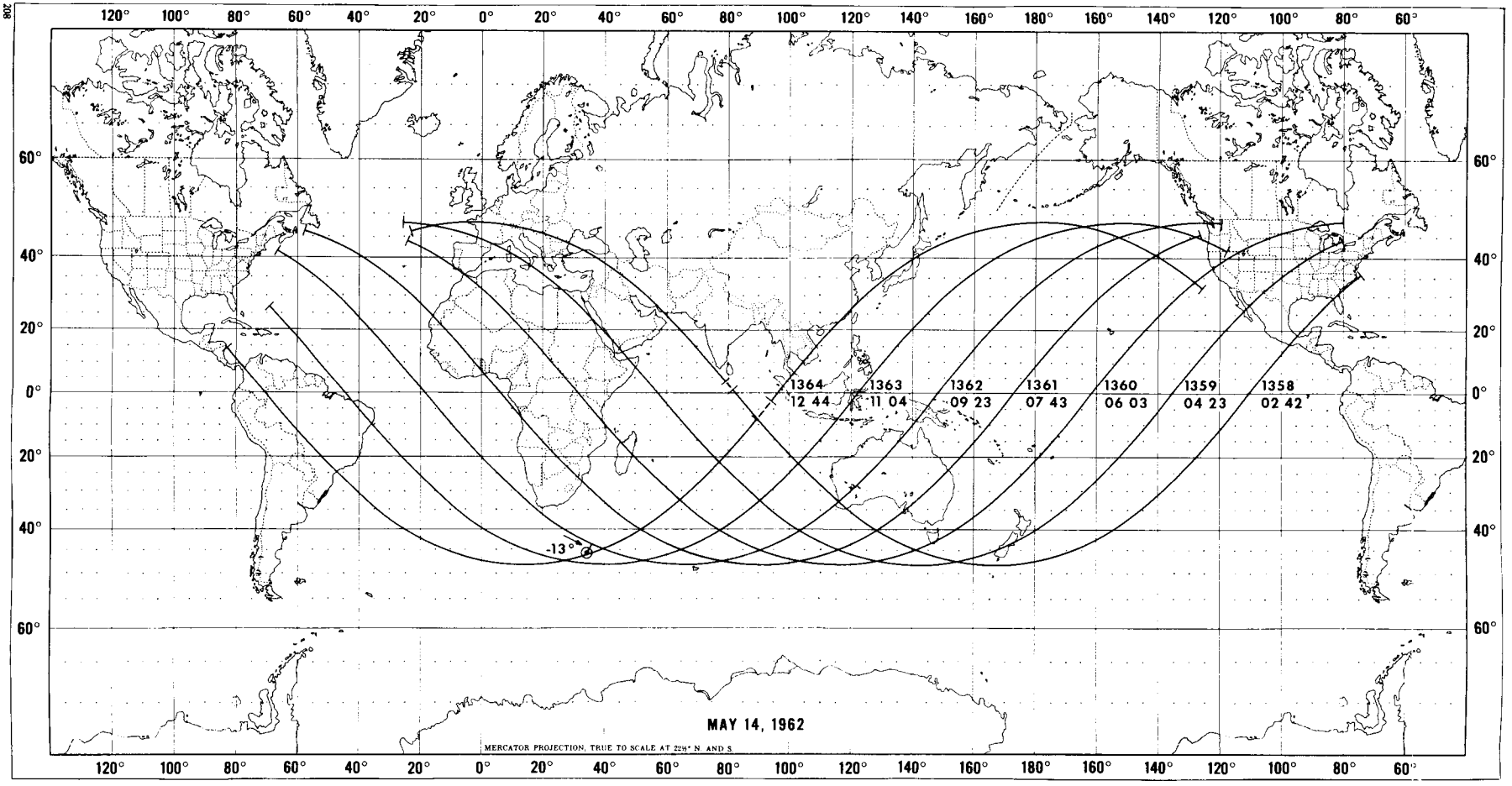
120° 100° 80° 60° 40° 20° 0° 20° 40° 60° 80° 100° 120° 140° 160° 180° 160° 140° 120° 100° 80° 60°
60°
40°
20°
0°
20°
40°
60°
1364
12 44
1363
11 04
1362
09 23
1361
07 43
1360
06 03
1359
04 23
1358
02 42
-13°
MAY 14, 1962
MERCATOR PROJECTION, TRUE TO SCALE AT 22½° N. AND S.

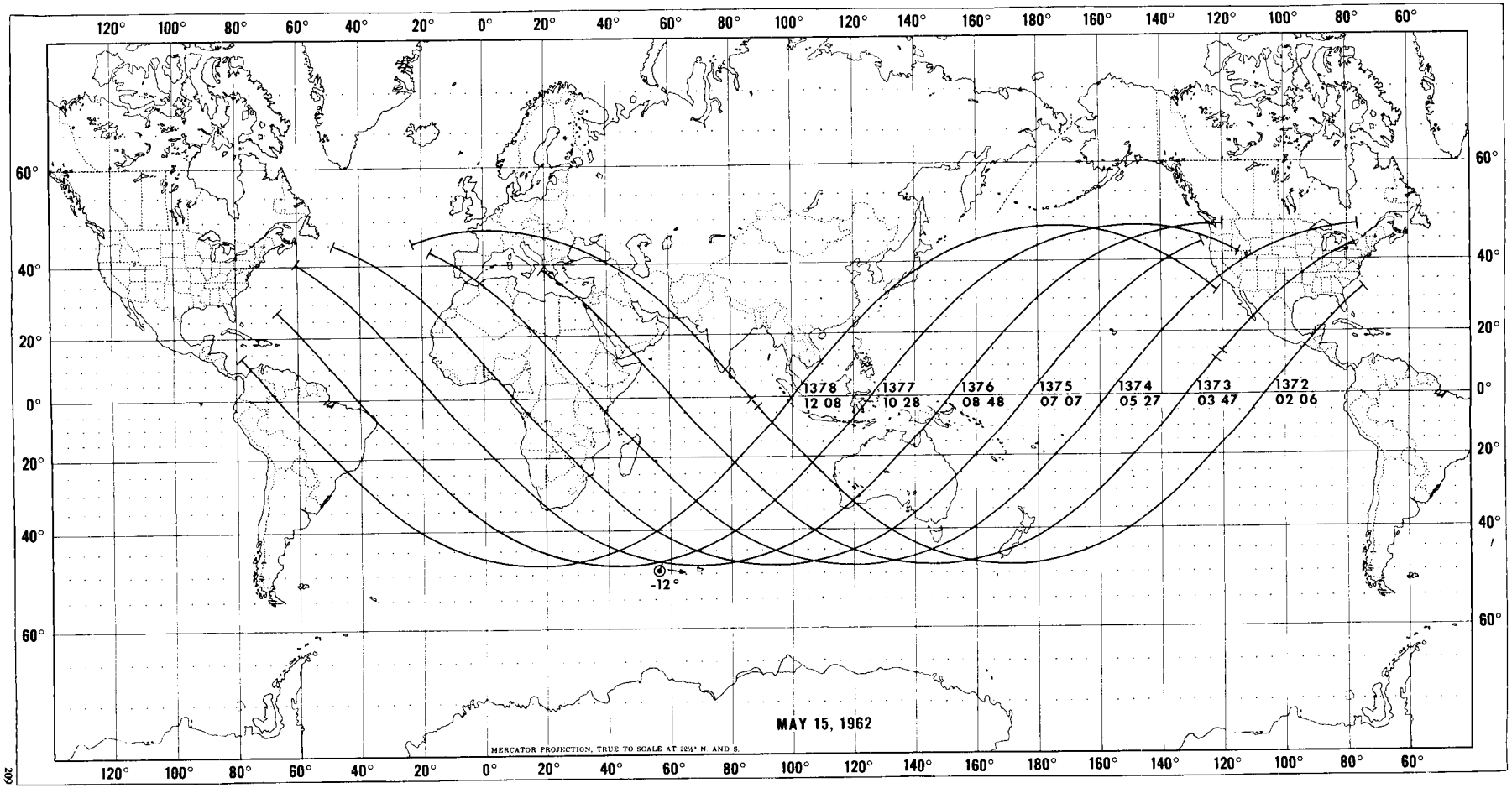
120° 100° 80° 60° 40° 20° 0° 20° 40° 60° 80° 100° 120° 140° 160° 180° 160° 140° 120° 100° 80° 60°
60°
40°
20°
0°
20°
40°
60°
1378
12 08
1377
10 28
1376
08 48
1375
07 07
1374
05 27
1373
03 47
1372
02 06
-12°
MAY 15, 1962
MERCATOR PROJECTION, TRUE TO SCALE AT 22½° N AND S.

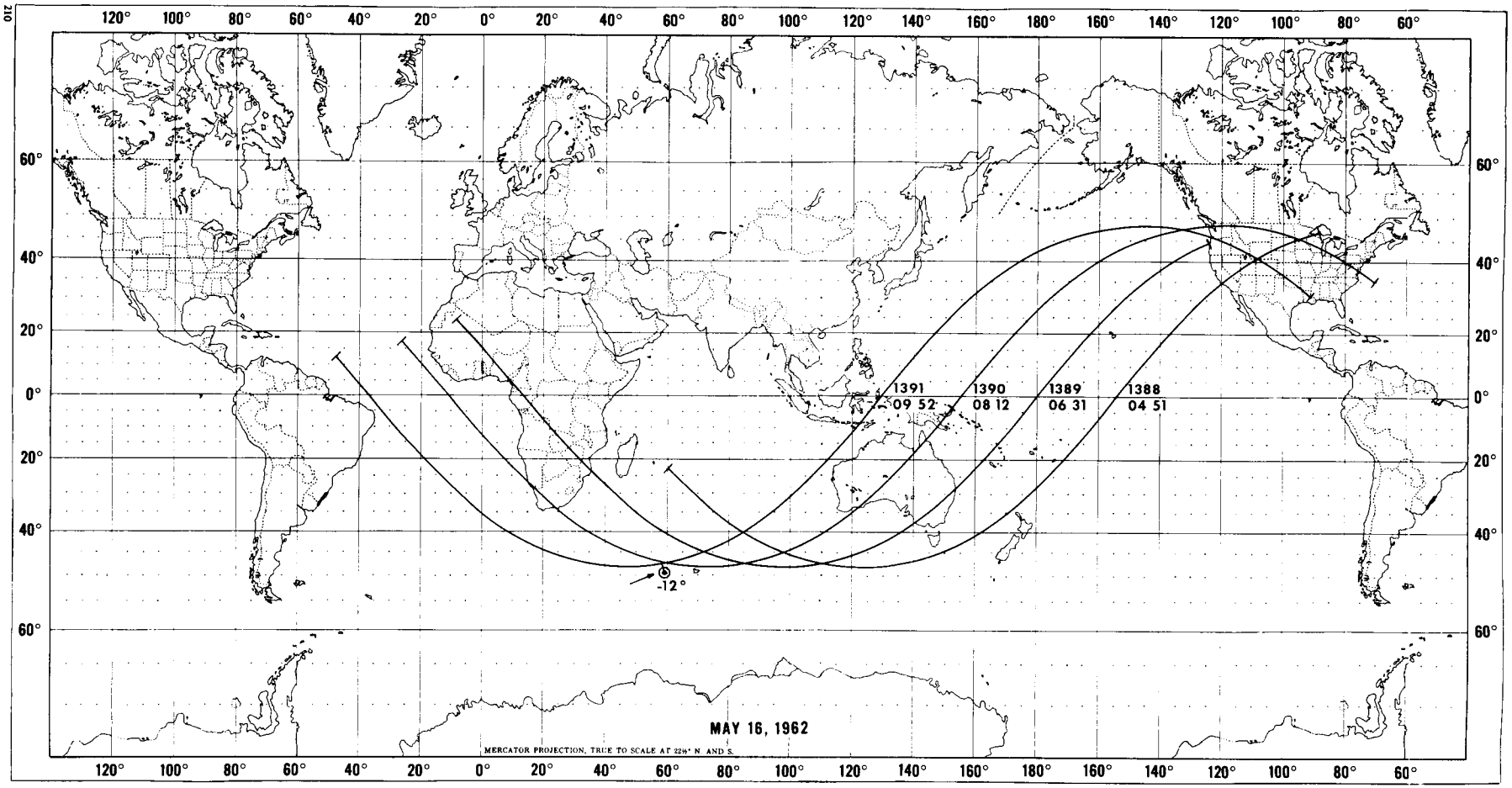
120° 100° 80° 60° 40° 20° 0° 20° 40° 60° 80° 100° 120° 140° 160° 180° 160° 140° 120° 100° 80° 60°
60°
40°
20°
0°
20°
40°
60°
1391
09 52
1390
08 12
1389
06 31
1388
04 51
-12°
MAY 16, 1962
MERCATOR PROJECTION, TRUE TO SCALE AT 22½° N. AND S.

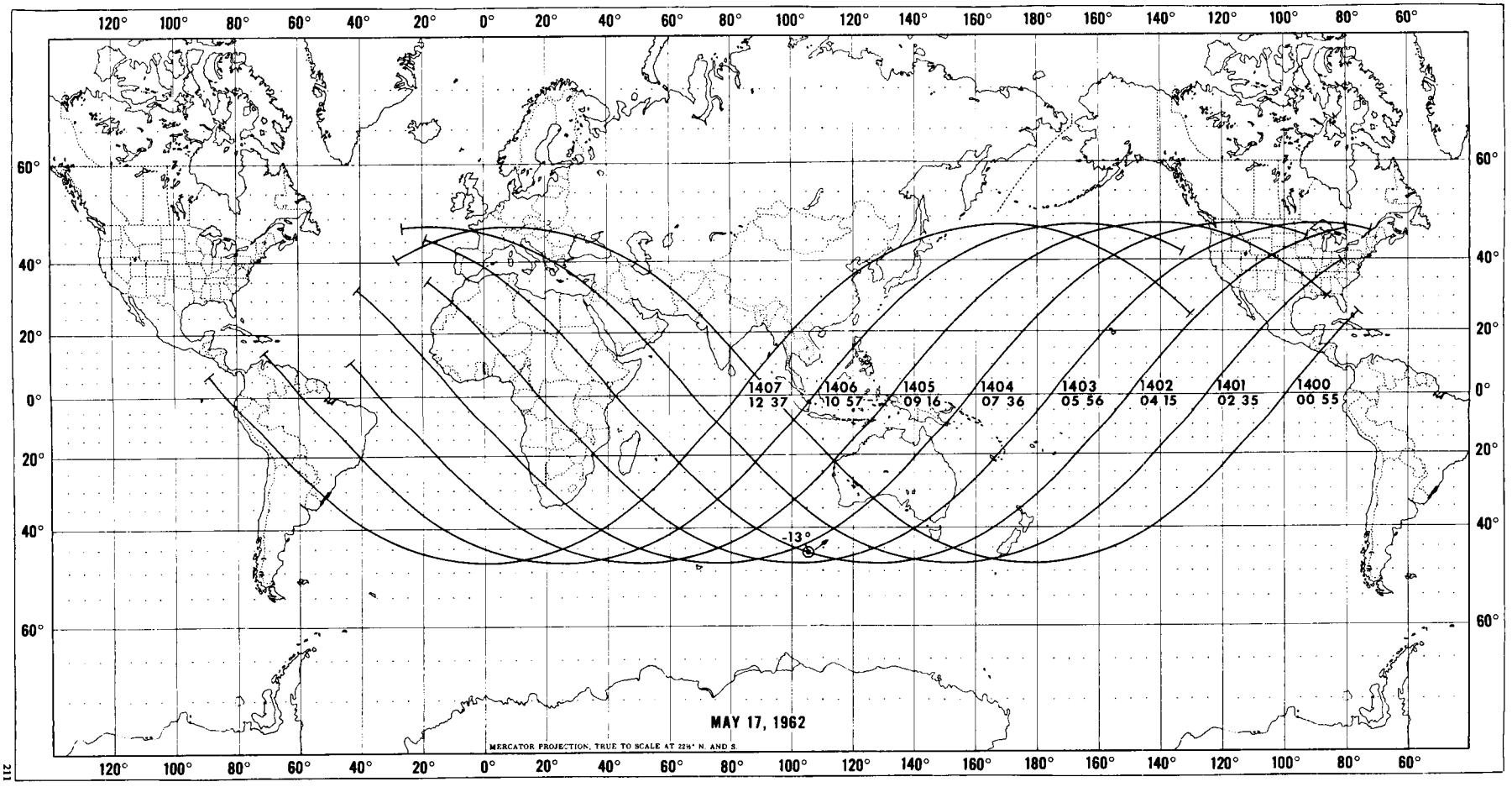
120° 100° 80° 60° 40° 20° 0° 20° 40° 60° 80° 100° 120° 140° 160° 180° 160° 140° 120° 100° 80° 60°
60°
40°
20°
0°
20°
40°
60°
1407
12 37
1406
10 57
1405
09 16
1404
07 36
1403
05 56
1402
04 15
1401
02 35
1400
00 55
-13°
MAY 17, 1962
MERCATOR PROJECTION, TRUE TO SCALE AT 22½° N. AND S.

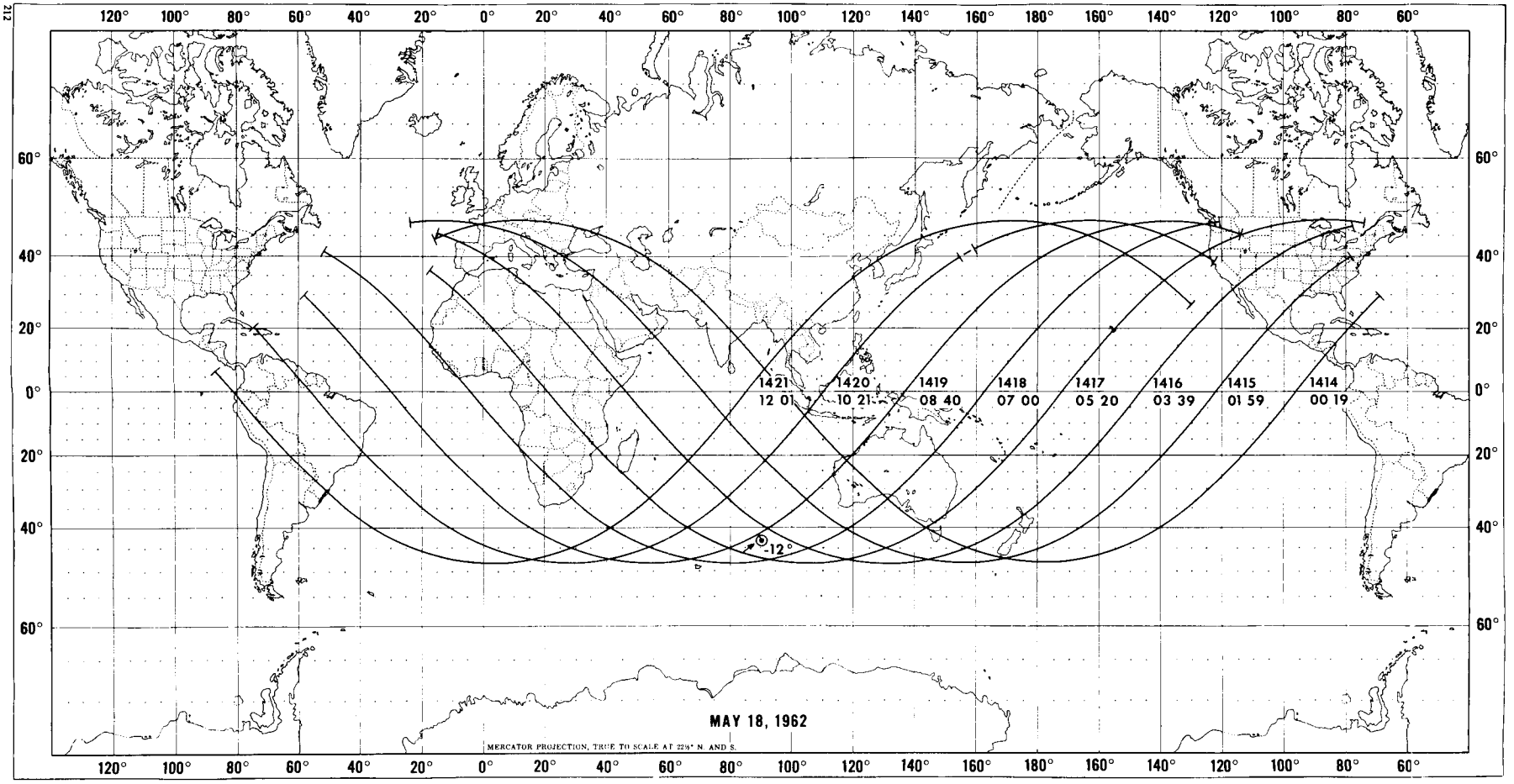
120° 100° 80° 60° 40° 20° 0° 20° 40° 60° 80° 100° 120° 140° 160° 180° 160° 140° 120° 100° 80° 60°
60°
40°
20°
0°
20°
40°
60°
1421
12 01
1420
10 21
1419
08 40
1418
07 00
1417
05 20
1416
03 39
1415
01 59
1414
00 19
-12°
MAY 18, 1962
MERCATOR PROJECTION, TRUE TO SCALE AT 22½° N. AND S.

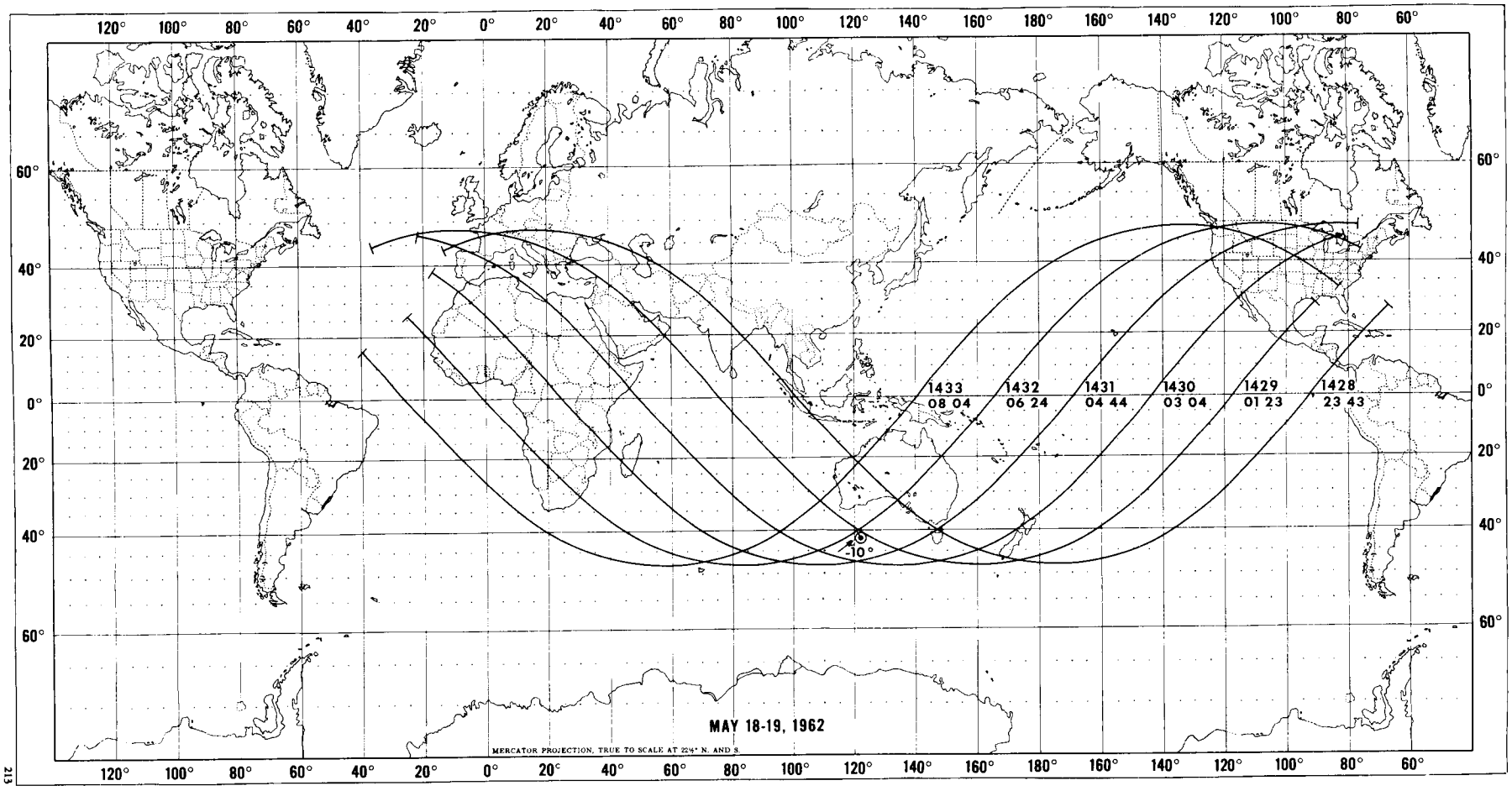
120° 100° 80° 60° 40° 20° 0° 20° 40° 60° 80° 100° 120° 140° 160° 180° 160° 140° 120° 100° 80° 60°
60°
40°
20°
0°
20°
40°
60°
1433
08 04
1432
06 24
1431
04 44
1430
03 04
1429
01 23
1428
23 43
-10°
MAY 18-19, 1962
MERCATOR PROJECTION, TRUE TO SCALE AT 22½° N. AND S.

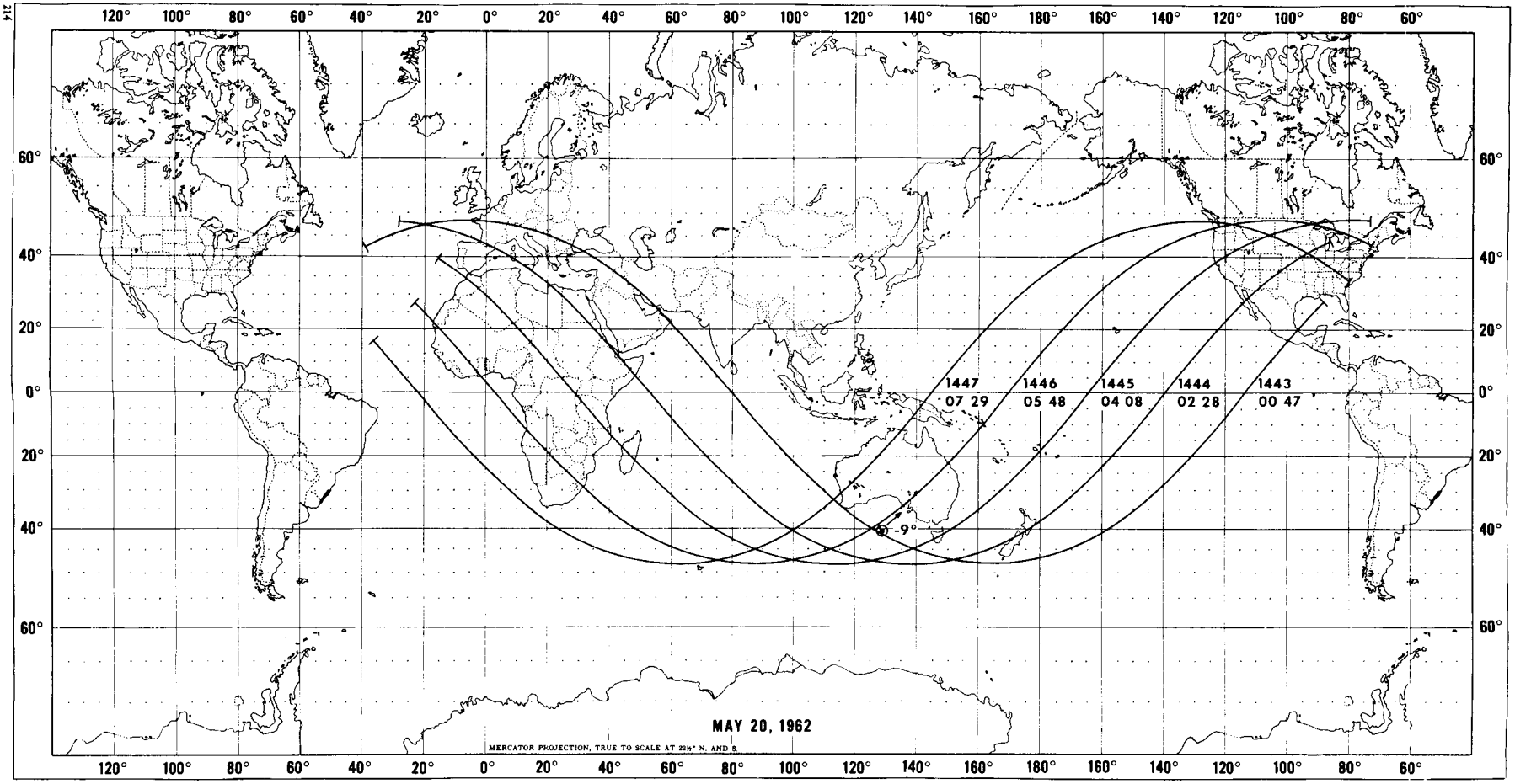
120° 100° 80° 60° 40° 20° 0° 20° 40° 60° 80° 100° 120° 140° 160° 180° 160° 140° 120° 100° 80° 60°
60°
40°
20°
0°
20°
40°
60°
1447
07 29
1446
05 48
1445
04 08
1444
02 28
1443
00 47
-9°
MAY 20, 1962
MERCATOR PROJECTION, TRUE TO SCALE AT 22½° N. AND S.

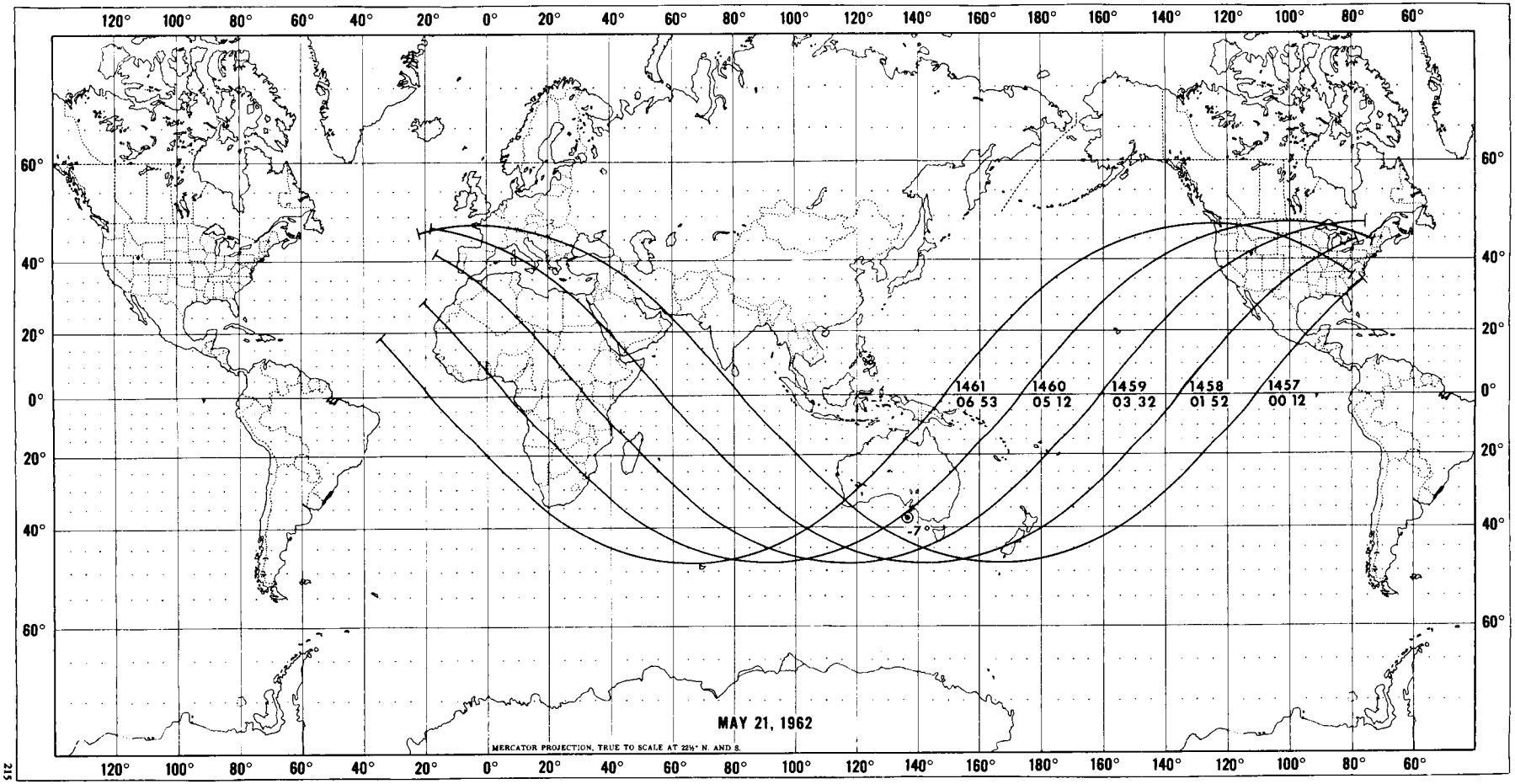
120° 100° 80° 60° 40° 20° 0° 20° 40° 60° 80° 100° 120° 140° 160° 180° 160° 140° 120° 100° 80° 60°
60°
40°
20°
0°
20°
40°
60°
1461
06 53
1460
05 12
1459
03 32
1458
01 52
1457
00 12
-7°
MAY 21, 1962
MERCATOR PROJECTION, TRUE TO SCALE AT 22½° N. AND S.

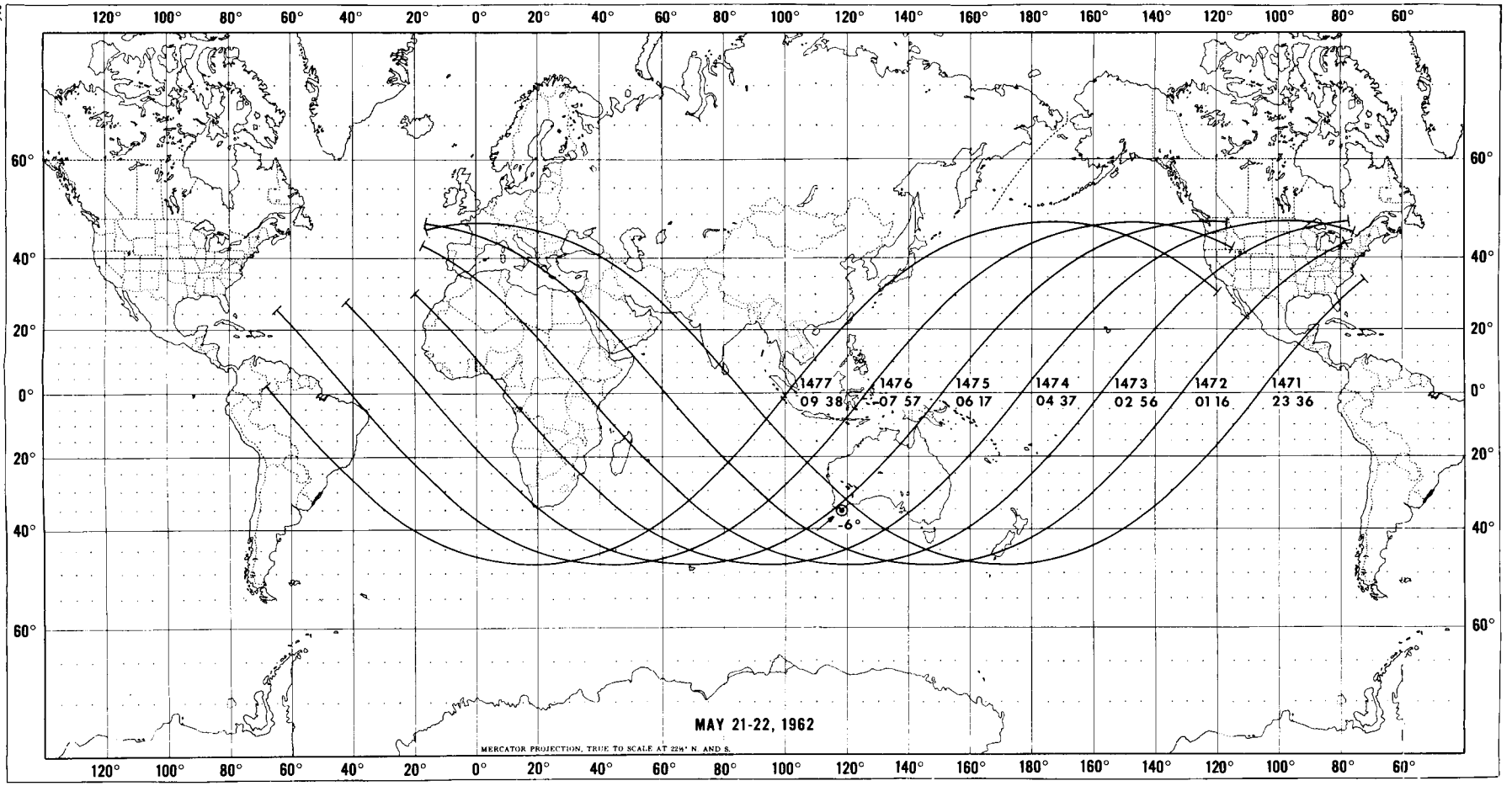
120° 100° 80° 60° 40° 20° 0° 20° 40° 60° 80° 100° 120° 140° 160° 180° 160° 140° 120° 100° 80° 60°
60°
40°
20°
0°
20°
40°
60°
1477 09 38
1476 07 57
1475 06 17
1474 04 37
1473 02 56
1472 01 16
1471 23 36
-6°
MAY 21-22, 1962
MERCATOR PROJECTION, TRUE TO SCALE AT 22½° N. AND S.

729-166 O - 64 - 15

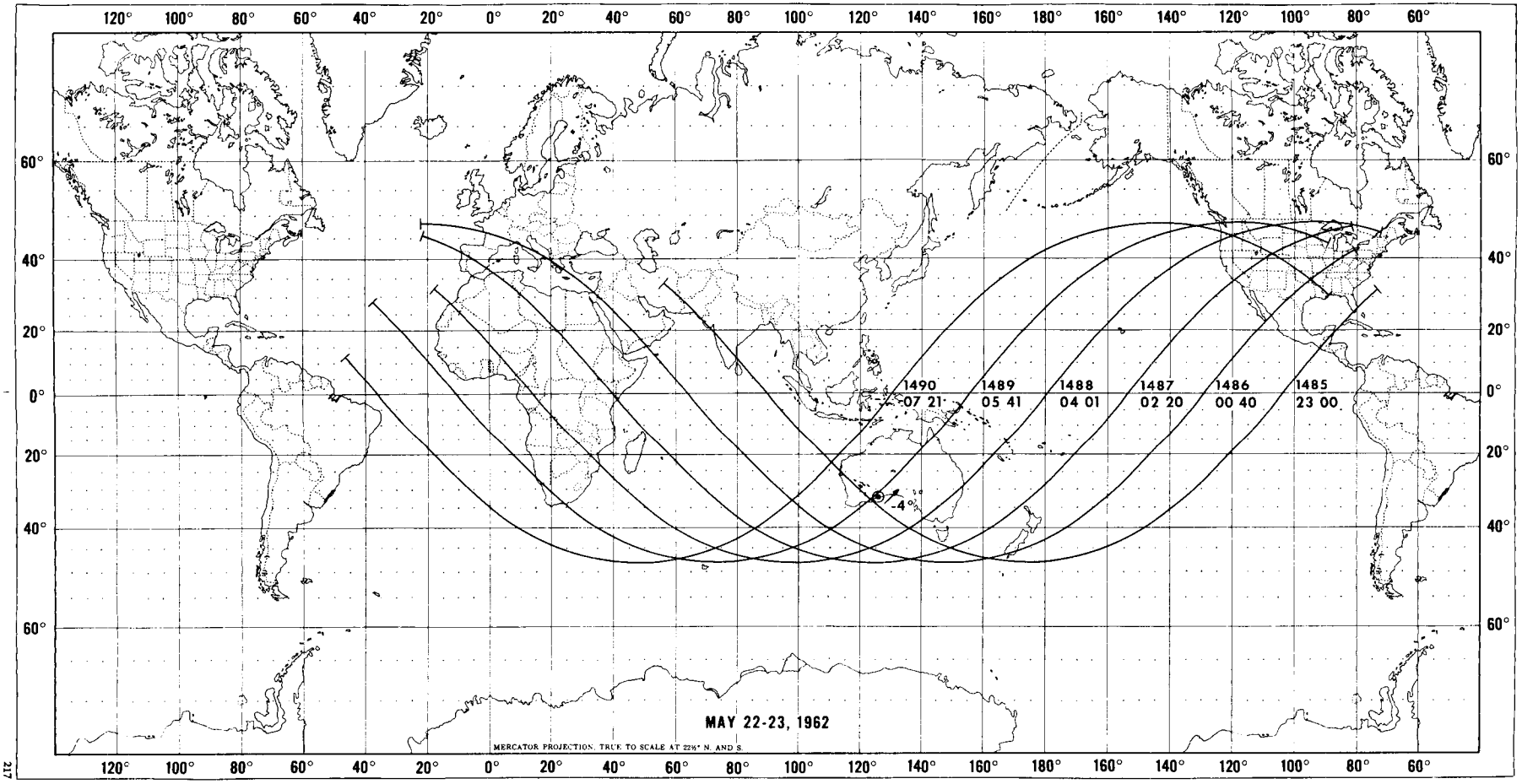

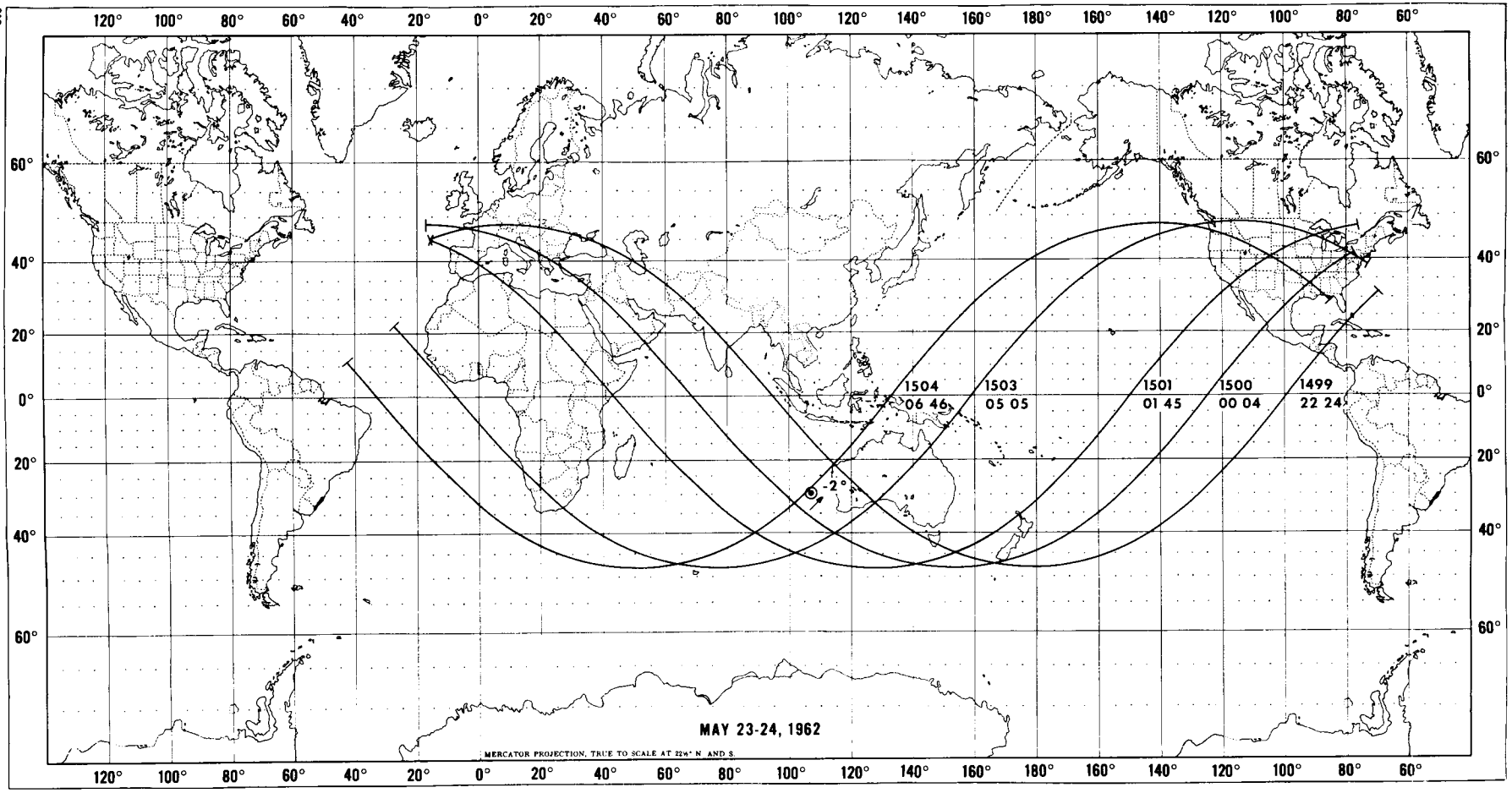
120° 100° 80° 60° 40° 20° 0° 20° 40° 60° 80° 100° 120° 140° 160° 180° 160° 140° 120° 100° 80° 60°
60°
40°
20°
0°
20°
40°
60°
1504
06 46
1503
05 05
1501
01 45
1500
00 04
1499
22 24
-2°
MAY 23-24, 1962
MERCATOR PROJECTION, TRUE TO SCALE AT 22½° N. AND S.

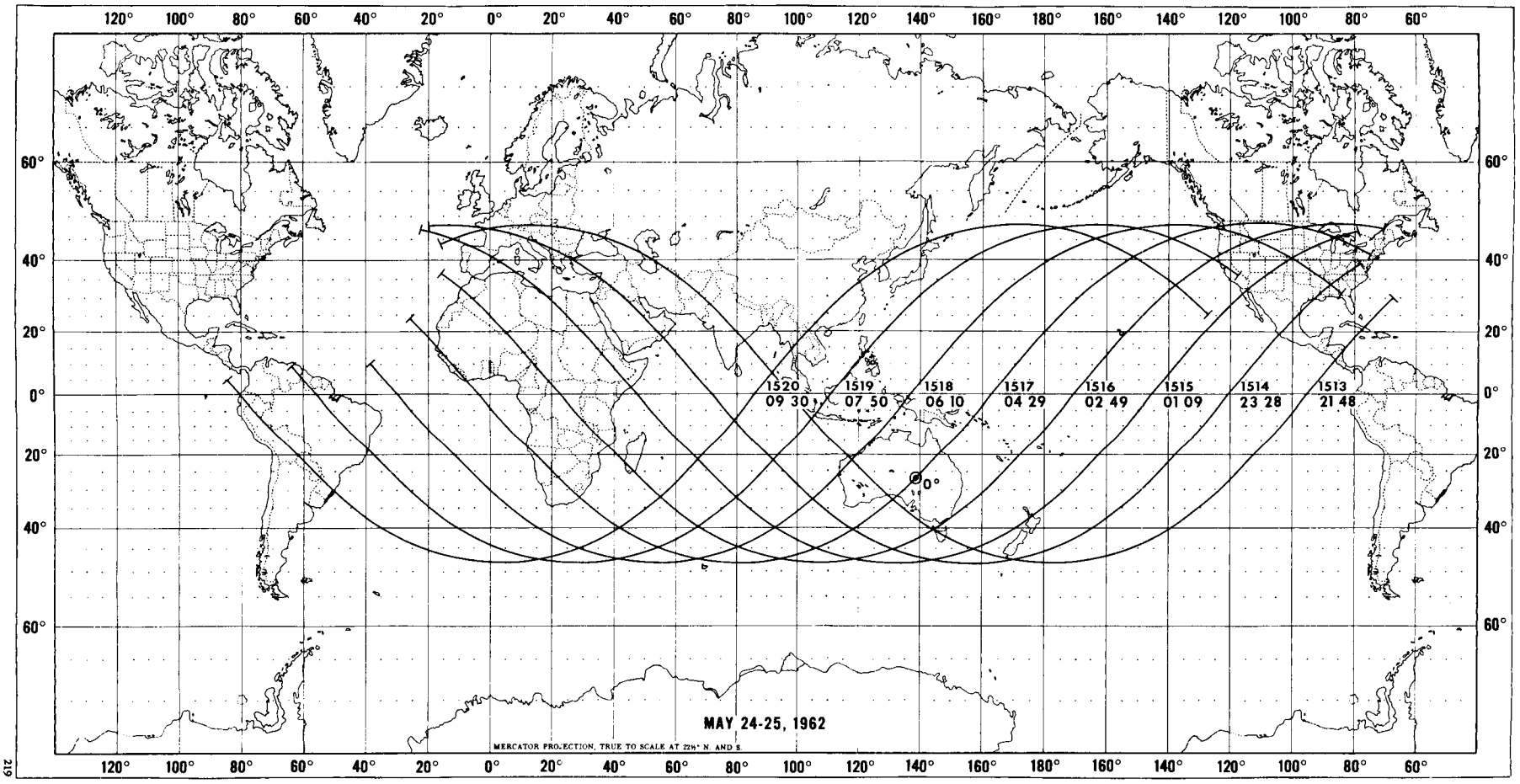
120° 100° 80° 60° 40° 20° 0° 20° 40° 60° 80° 100° 120° 140° 160° 180° 160° 140° 120° 100° 80° 60°
60°
40°
20°
0°
20°
40°
60°
1520 09 30
1519 07 50
1518 06 10
1517 04 29
1516 02 49
1515 01 09
1514 23 28
1513 21 48
0°
MAY 24-25, 1962
MERCATOR PROJECTION, TRUE TO SCALE AT 22½° N. AND S.

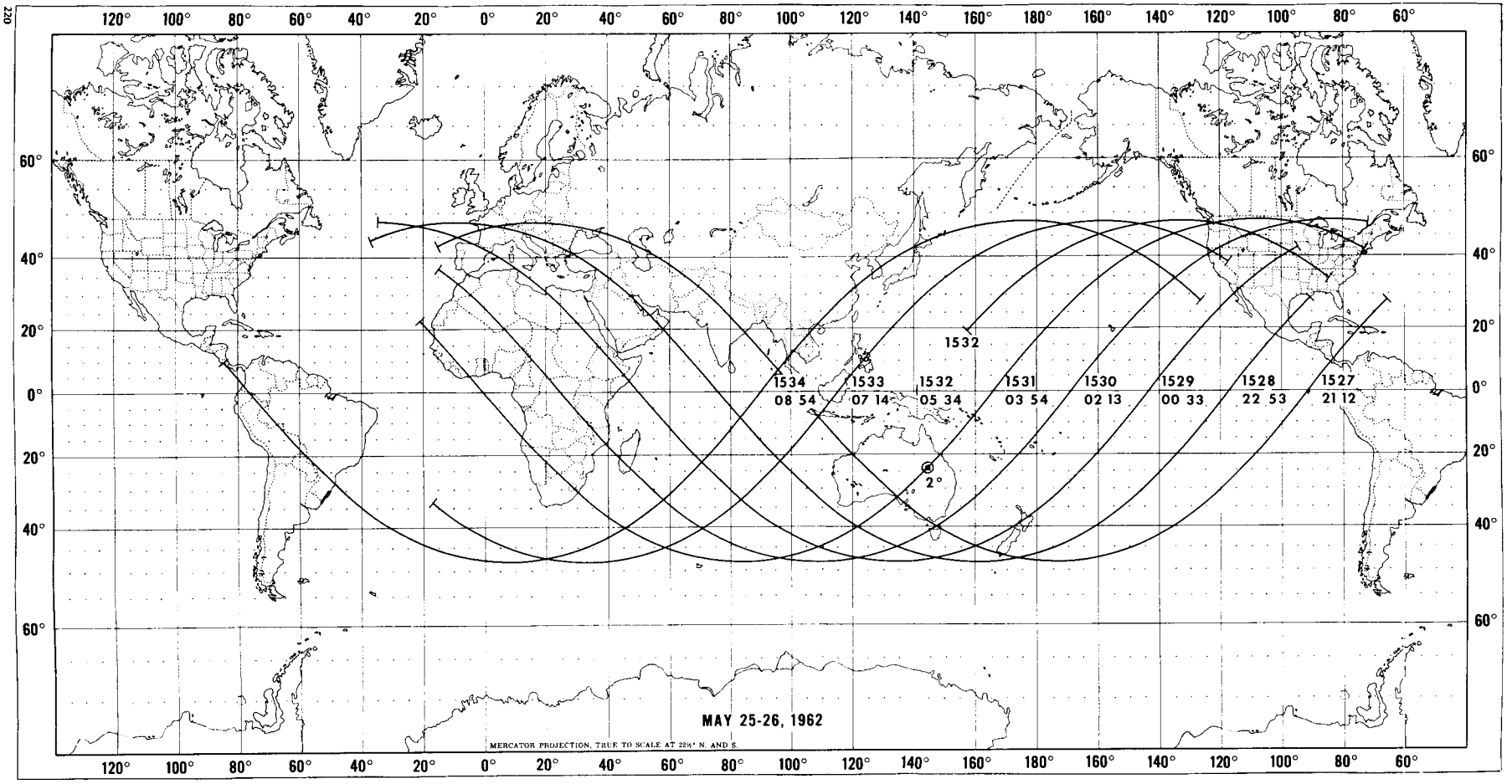
120° 100° 80° 60° 40° 20° 0° 20° 40° 60° 80° 100° 120° 140° 160° 180° 160° 140° 120° 100° 80° 60°
60°
40°
20°
0°
20°
40°
60°
1532
1534 08 54
1533 07 14
1532 05 34
1531 03 54
1530 02 13
1529 00 33
1528 22 53
1527 21 12
2°
MAY 25-26, 1962
MERCATOR PROJECTION, TRUE TO SCALE AT 22½° N. AND S.

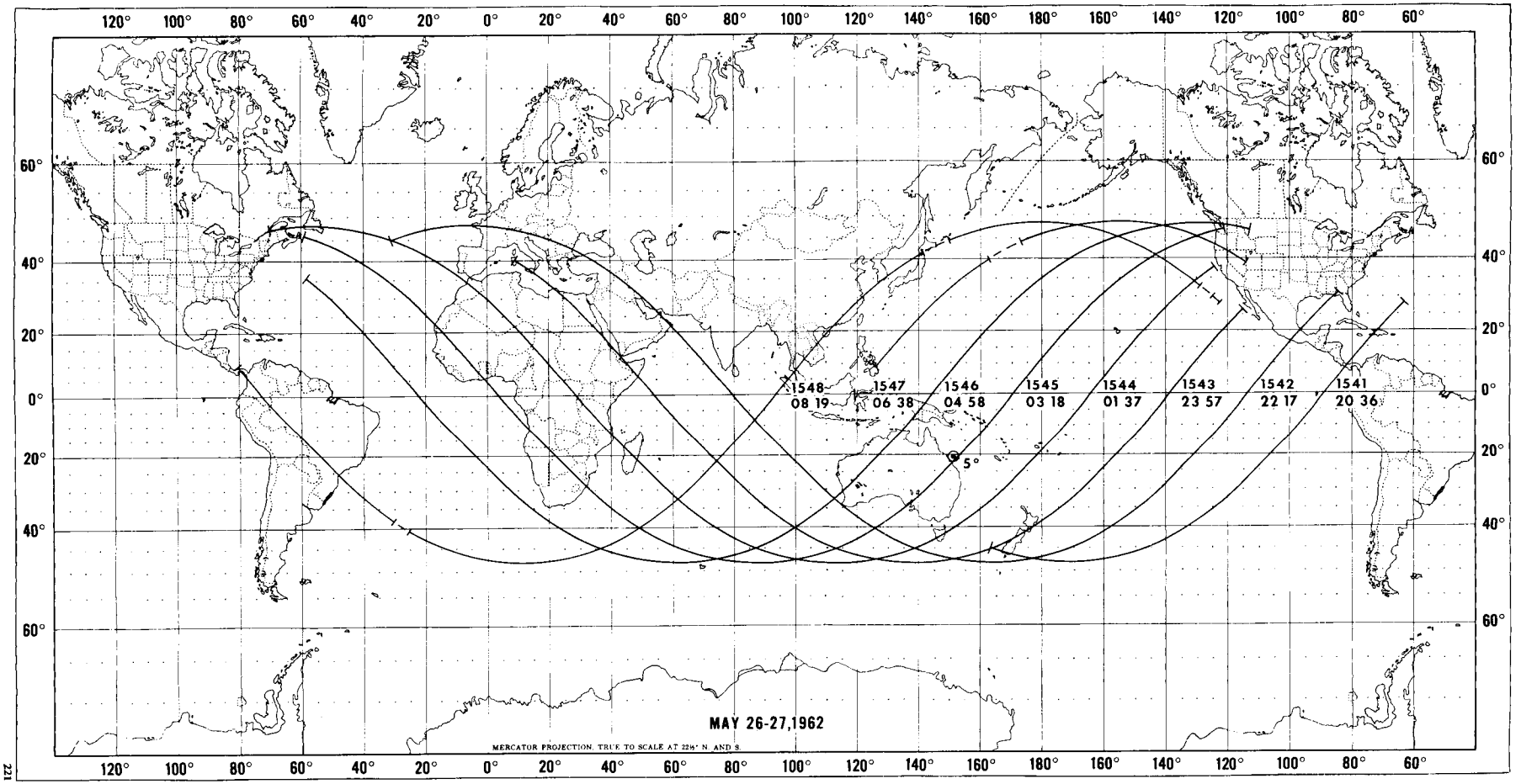
120° 100° 80° 60° 40° 20° 0° 20° 40° 60° 80° 100° 120° 140° 160° 180° 160° 140° 120° 100° 80° 60°
60°
40°
20°
0°
20°
40°
60°
1548 08 19
1547 06 38
1546 04 58
1545 03 18
1544 01 37
1543 23 57
1542 22 17
1541 20 36
5°
MAY 26-27,1962
MERCATOR PROJECTION, TRUE TO SCALE AT 22½° N. AND S.

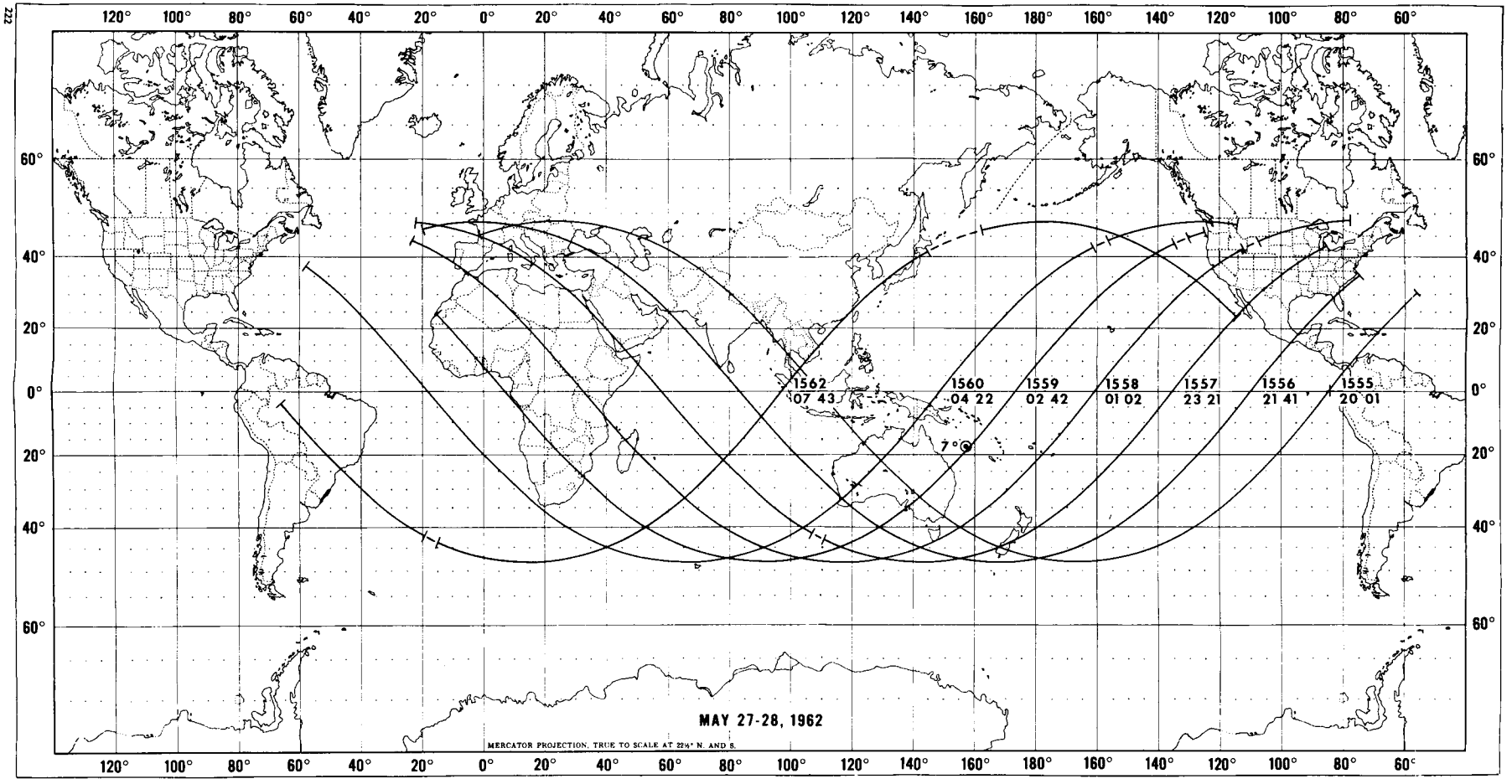
120° 100° 80° 60° 40° 20° 0° 20° 40° 60° 80° 100° 120° 140° 160° 180° 160° 140° 120° 100° 80° 60°
60°
40°
20°
0°
20°
40°
60°
1562
07 43
1560
04 22
1559
02 42
1558
01 02
1557
23 21
1556
21 41
1555
20 01
7°
MAY 27-28, 1962
MERCATOR PROJECTION, TRUE TO SCALE AT 22½° N. AND S.

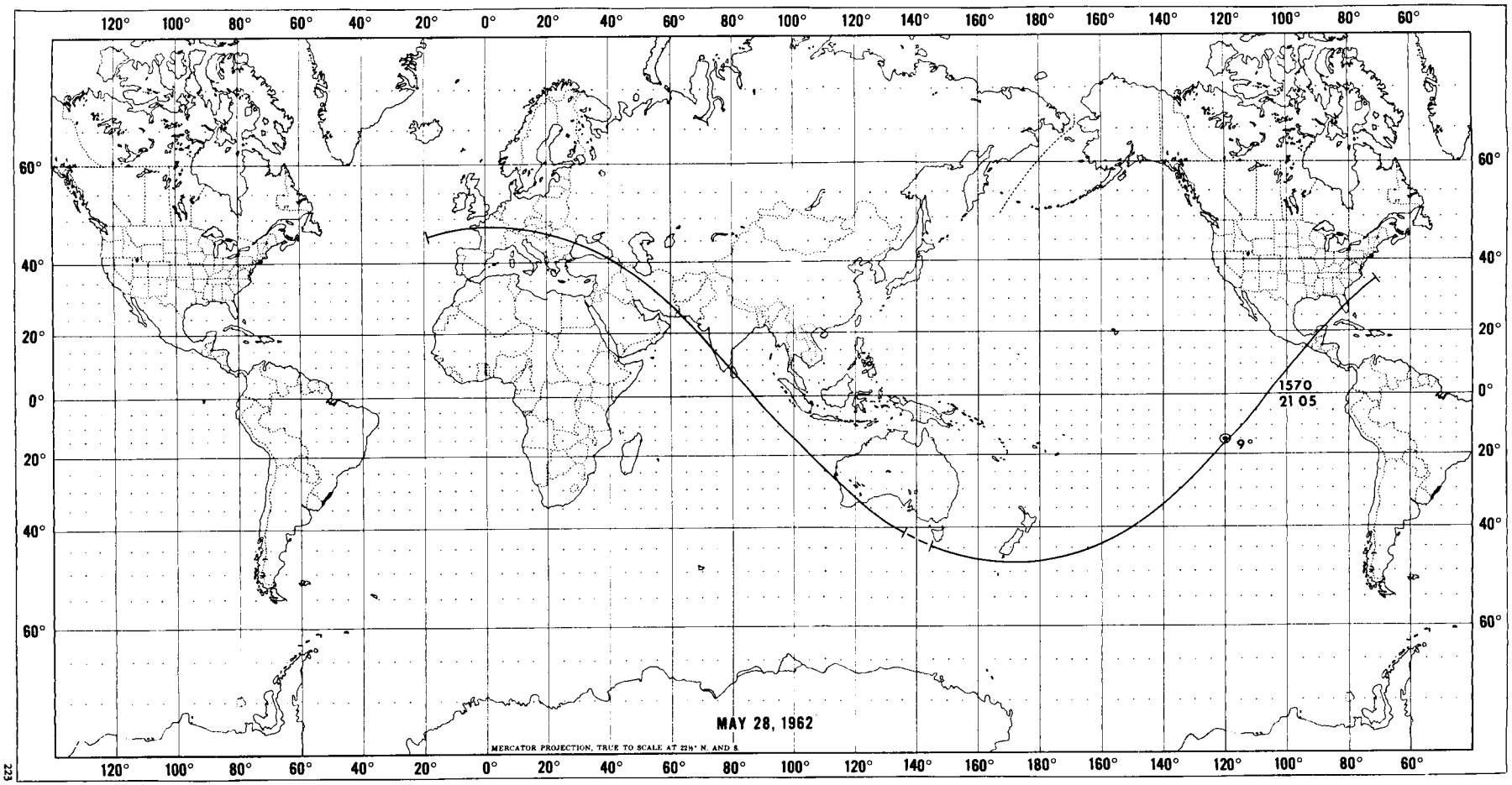
120° 100° 80° 60° 40° 20° 0° 20° 40° 60° 80° 100° 120° 140° 160° 180° 160° 140° 120° 100° 80° 60°
60°
40°
20°
0°
20°
40°
60°
1570
21 05
9°
MAY 28, 1962
MERCATOR PROJECTION, TRUE TO SCALE AT 22½° N. AND S.

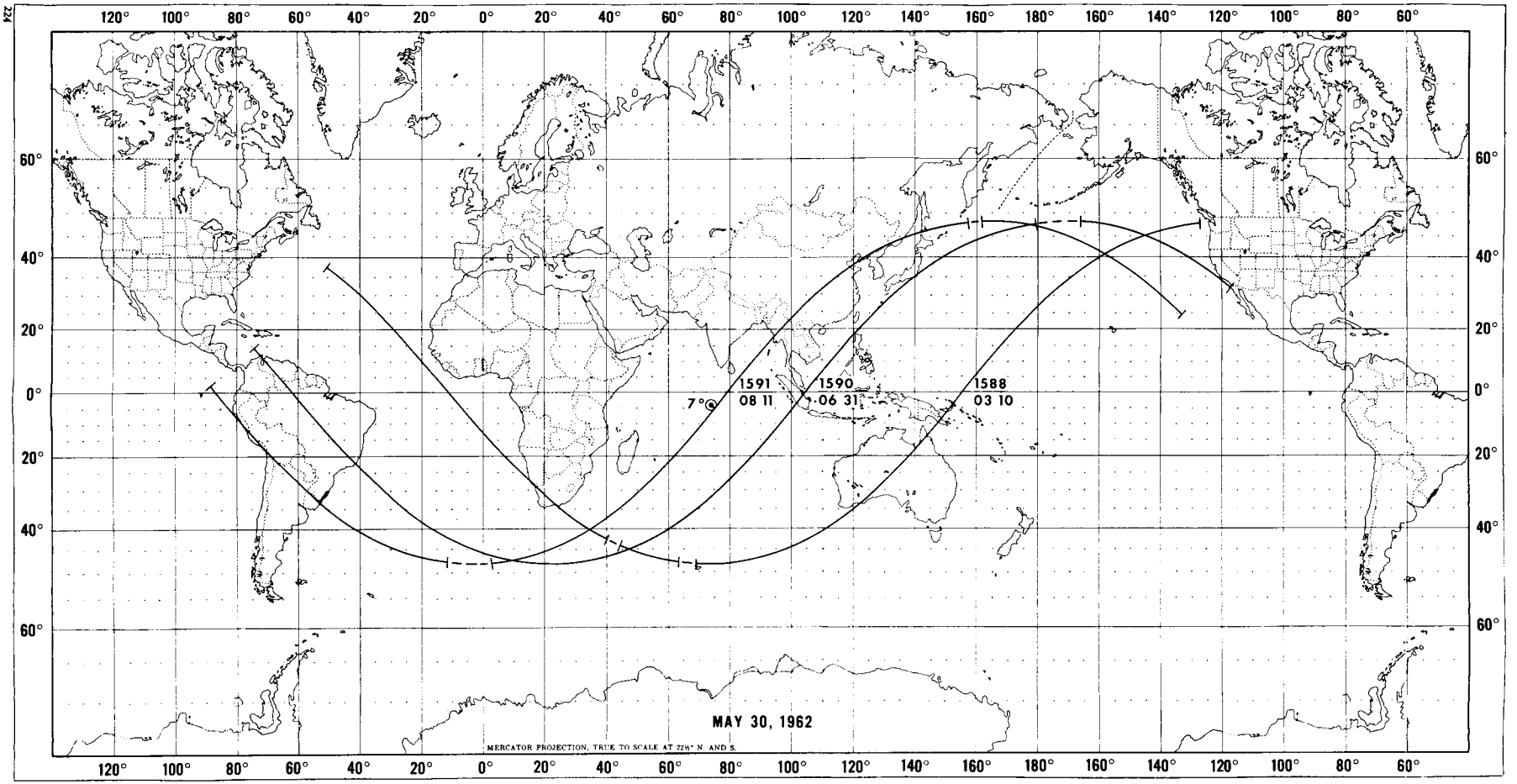
120° 100° 80° 60° 40° 20° 0° 20° 40° 60° 80° 100° 120° 140° 160° 180° 160° 140° 120° 100° 80° 60°
60°
40°
20°
0°
20°
40°
60°
7°
1591
08 11
1590
06 31
1588
03 10
MAY 30, 1962
MERCATOR PROJECTION, TRUE TO SCALE AT 22½° N. AND S.

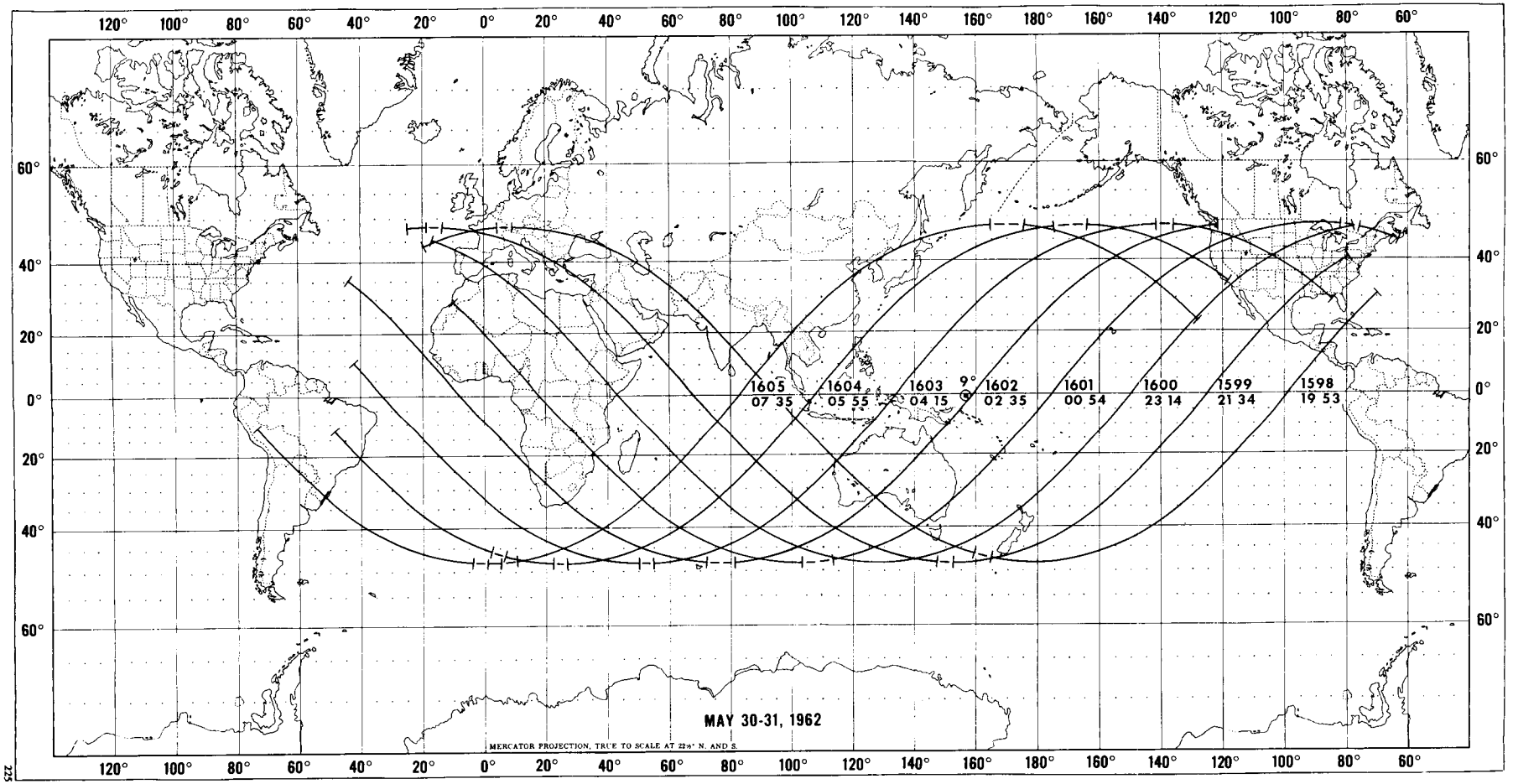
120° 100° 80° 60° 40° 20° 0° 20° 40° 60° 80° 100° 120° 140° 160° 180° 160° 140° 120° 100° 80° 60°
60°
40°
20°
0°
20°
40°
60°
1605
07 35
1604
05 55
1603
04 15
9°
1602
02 35
1601
00 54
1600
23 14
1599
21 34
1598
19 53
MAY 30-31, 1962
MERCATOR PROJECTION, TRUE TO SCALE AT 22½° N. AND S.

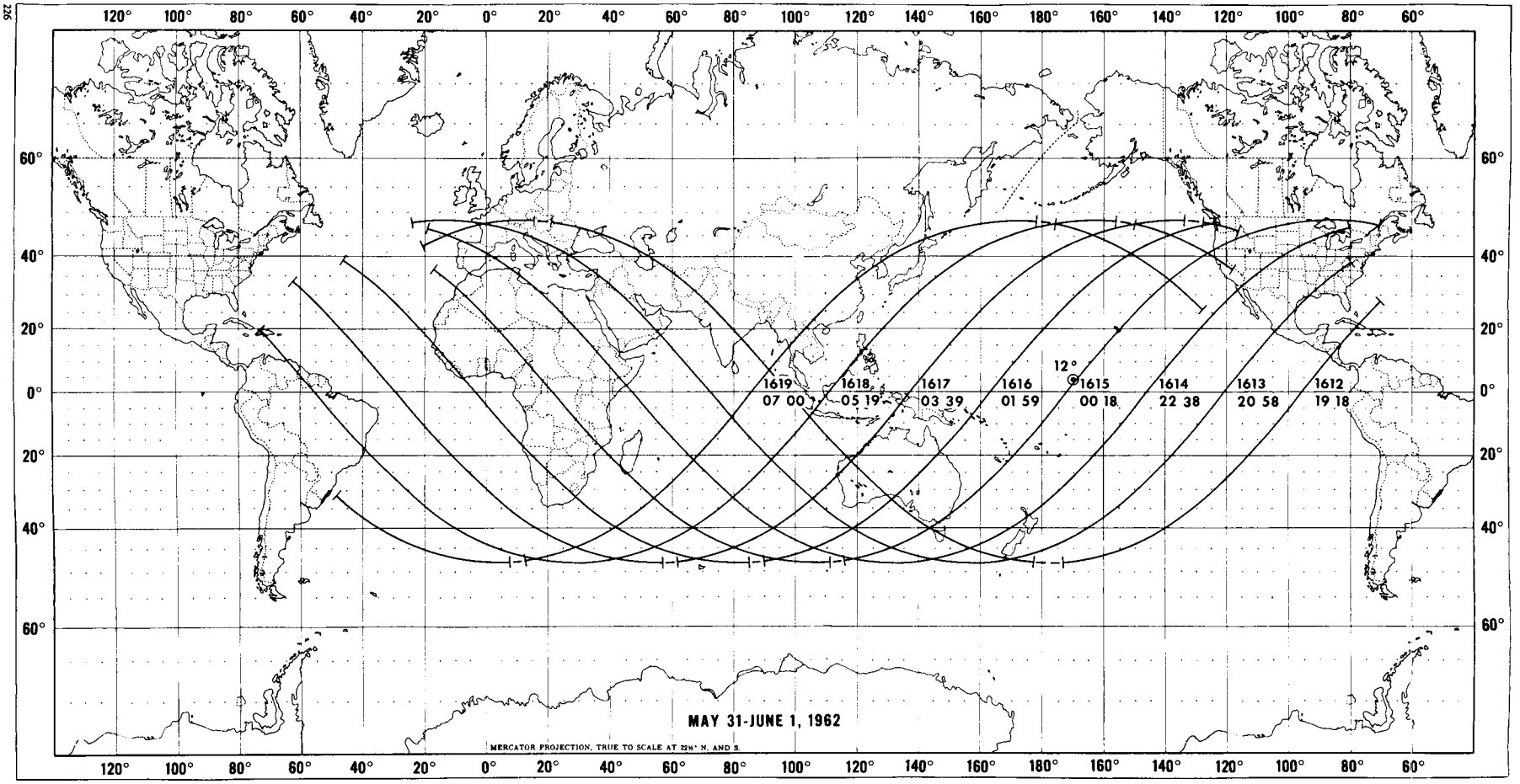
120° 100° 80° 60° 40° 20° 0° 20° 40° 60° 80° 100° 120° 140° 160° 180° 160° 140° 120° 100° 80° 60°
60°
40°
20°
0°
20°
40°
60°
12°
1619
07 00
1618
05 19
1617
03 39
1616
01 59
1615
00 18
1614
22 38
1613
20 58
1612
19 18
MAY 31-JUNE 1, 1962
MERCATOR PROJECTION, TRUE TO SCALE AT 22½° N. AND S.

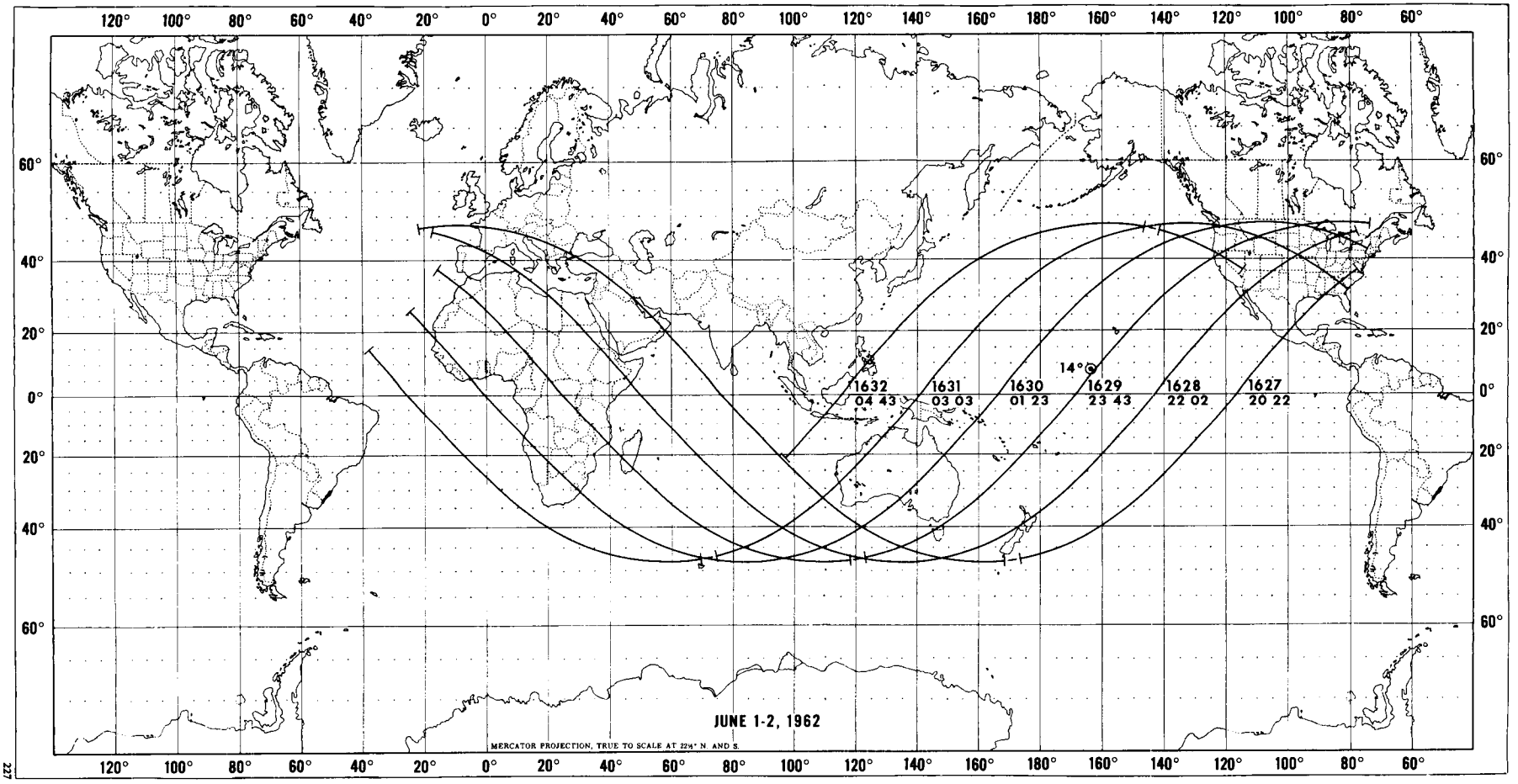
120° 100° 80° 60° 40° 20° 0° 20° 40° 60° 80° 100° 120° 140° 160° 180° 160° 140° 120° 100° 80° 60°
60°
40°
20°
0°
20°
40°
60°
14°
1632
04 43
1631
03 03
1630
01 23
1629
23 43
1628
22 02
1627
20 22
JUNE 1-2, 1962
MERCATOR PROJECTION, TRUE TO SCALE AT 22½° N. AND S.

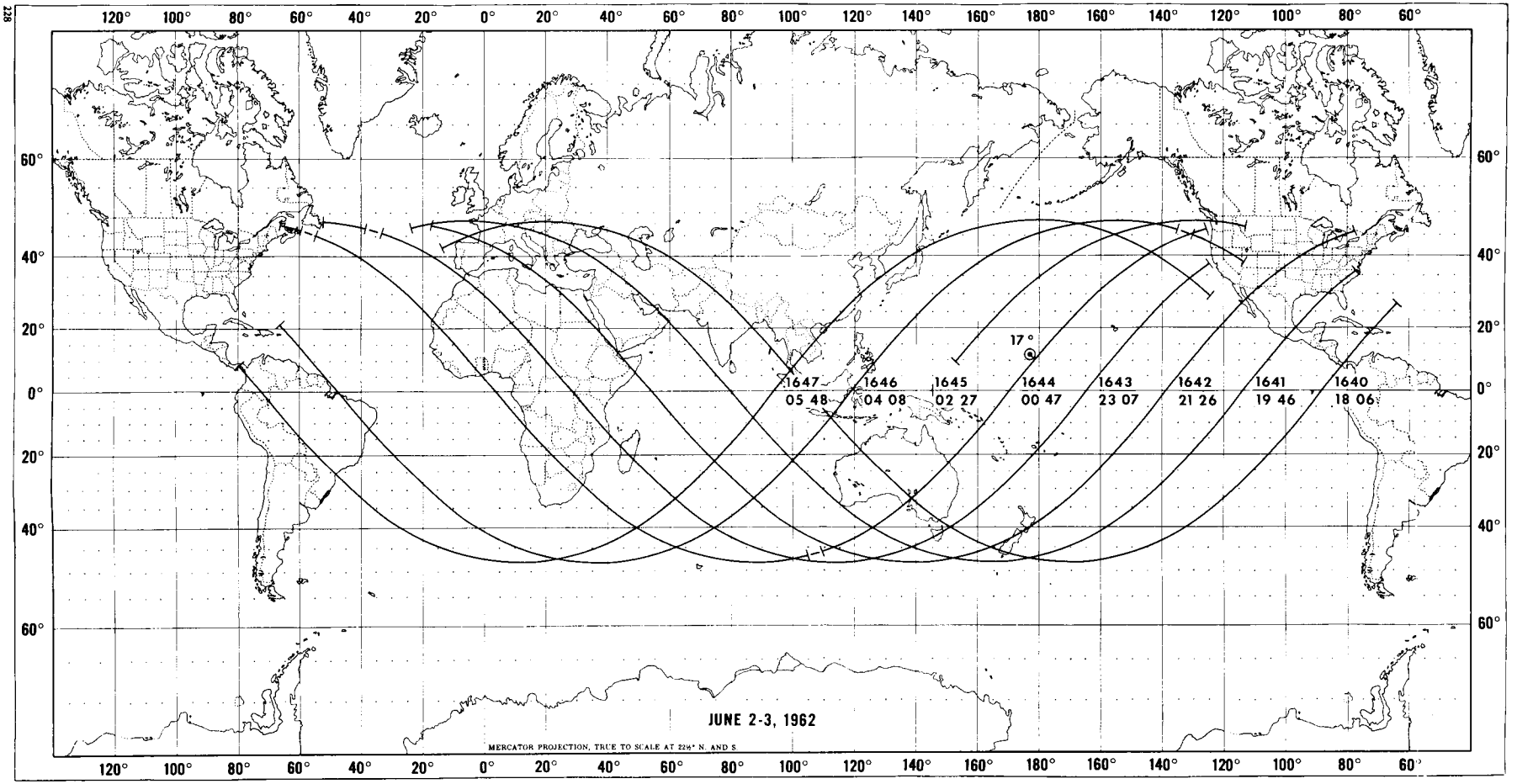
120° 100° 80° 60° 40° 20° 0° 20° 40° 60° 80° 100° 120° 140° 160° 180° 160° 140° 120° 100° 80° 60°
60°
40°
20°
0°
20°
40°
60°
17°
1647 05 48
1646 04 08
1645 02 27
1644 00 47
1643 23 07
1642 21 26
1641 19 46
1640 18 06
JUNE 2-3, 1962
MERCATOR PROJECTION, TRUE TO SCALE AT 22½° N. AND S.

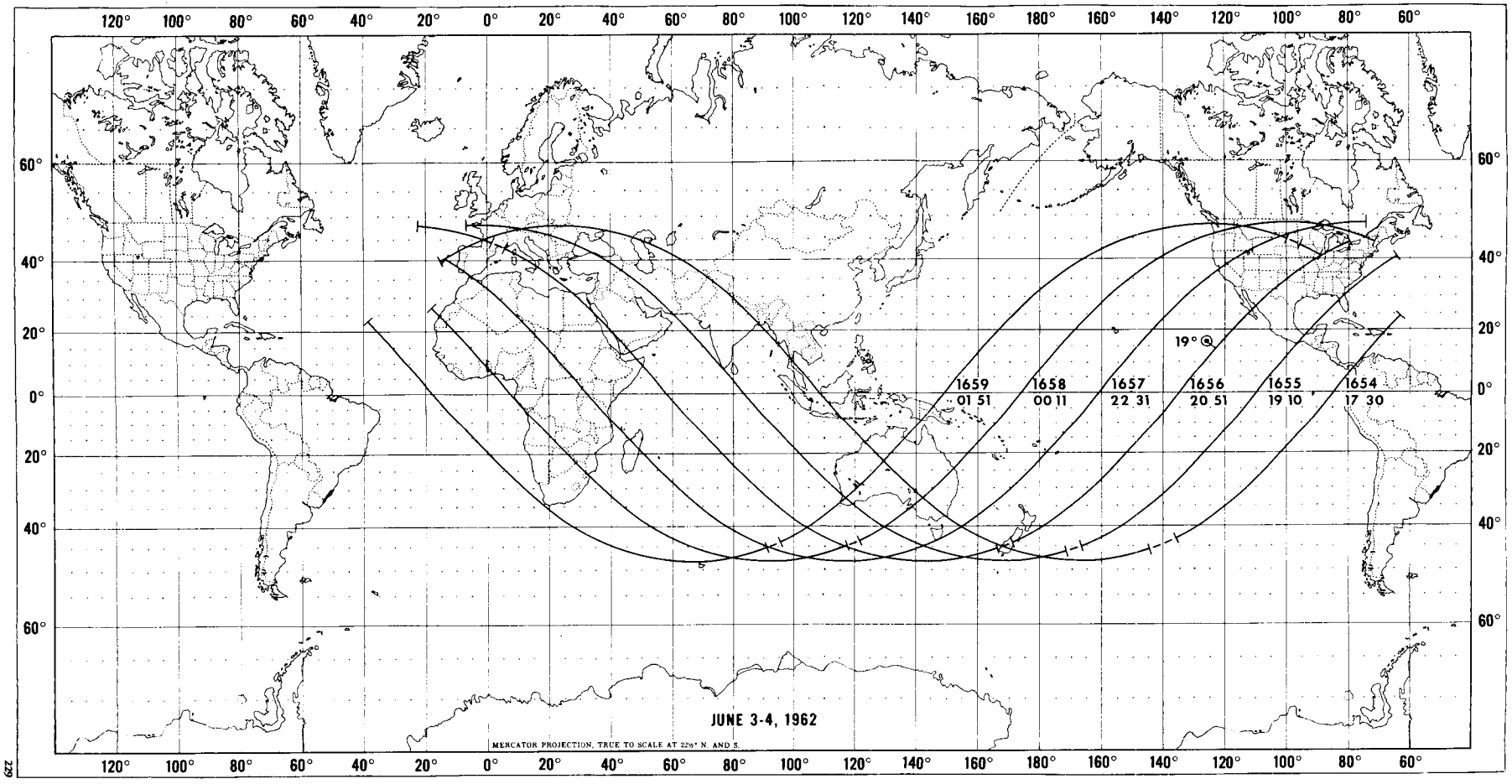
120° 100° 80° 60° 40° 20° 0° 20° 40° 60° 80° 100° 120° 140° 160° 180° 160° 140° 120° 100° 80° 60°
60°
40°
20°
0°
20°
40°
60°
19°
1659 01 51
1658 00 11
1657 22 31
1656 20 51
1655 19 10
1654 17 30
JUNE 3-4, 1962
MERCATOR PROJECTION, TRUE TO SCALE AT 22½° N. AND S.

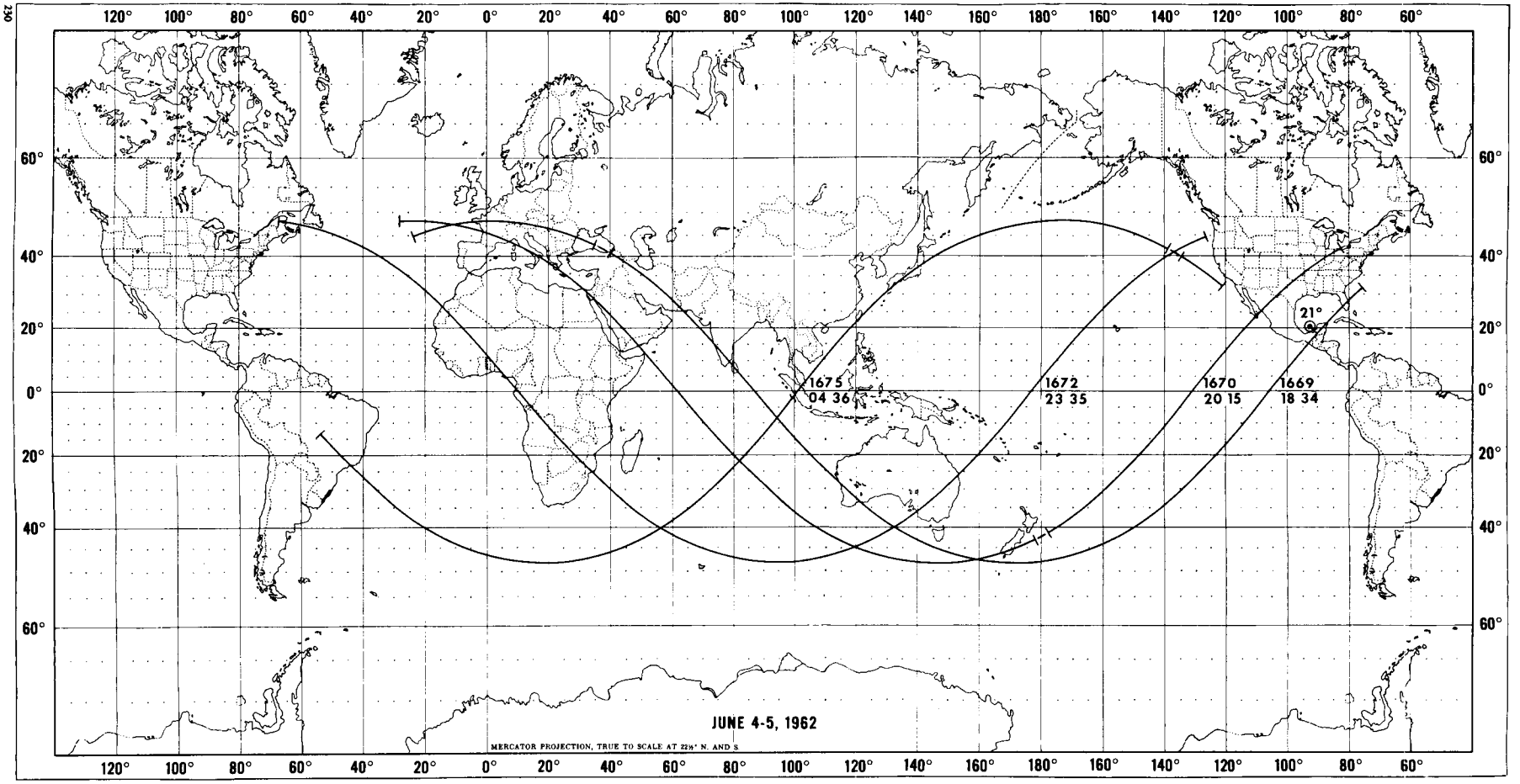
120° 100° 80° 60° 40° 20° 0° 20° 40° 60° 80° 100° 120° 140° 160° 180° 160° 140° 120° 100° 80° 60°
60°
40°
20°
0°
20°
40°
60°
1675
04 36
1672
23 35
1670
20 15
1669
18 34
21°
JUNE 4-5, 1962
MERCATOR PROJECTION, TRUE TO SCALE AT 22½° N. AND S.

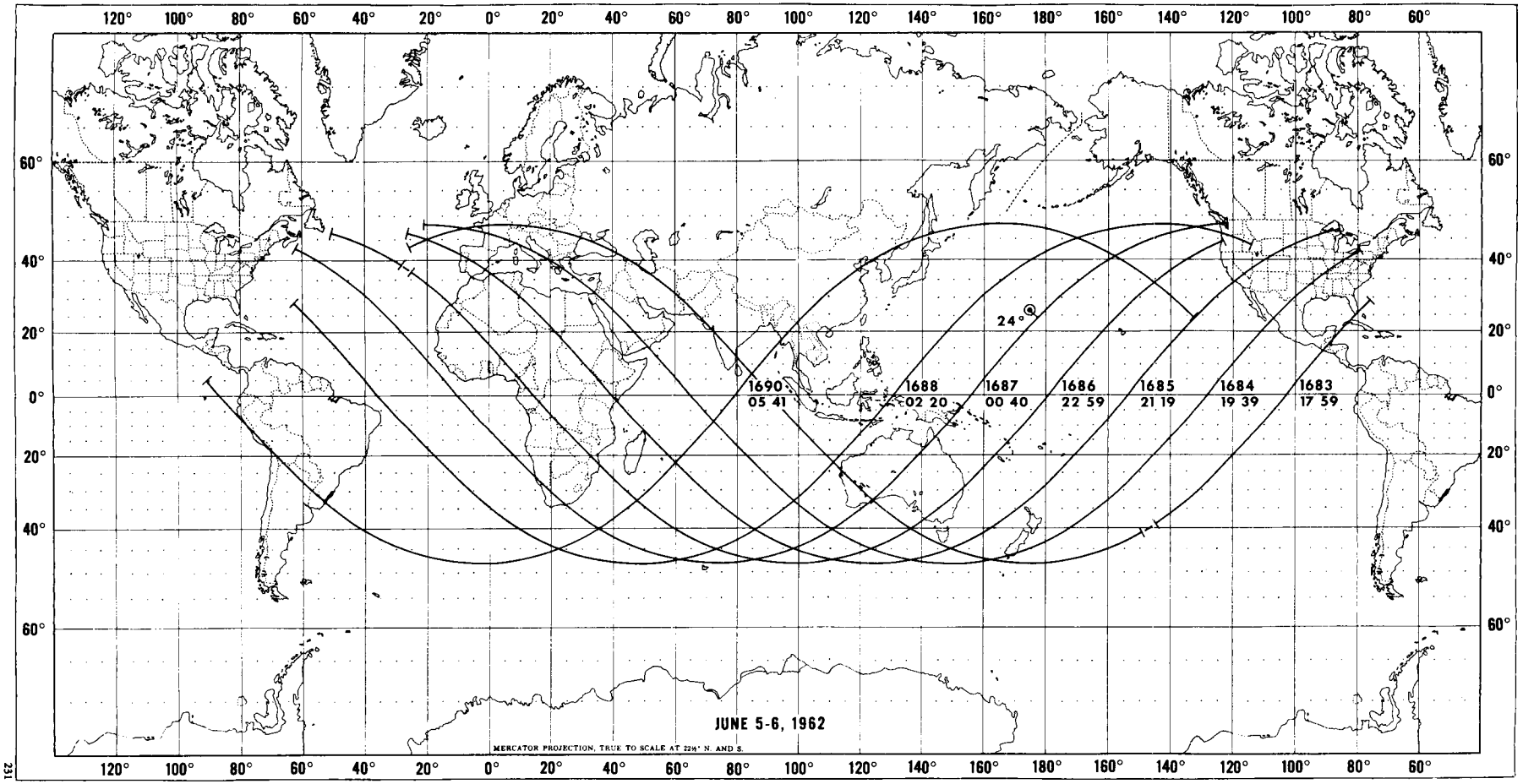
120° 100° 80° 60° 40° 20° 0° 20° 40° 60° 80° 100° 120° 140° 160° 180° 160° 140° 120° 100° 80° 60°
60°
40°
20°
0°
20°
40°
60°
24°
1690
05 41
1688
02 20
1687
00 40
1686
22 59
1685
21 19
1684
19 39
1683
17 59
JUNE 5-6, 1962
MERCATOR PROJECTION, TRUE TO SCALE AT 22½° N. AND S.

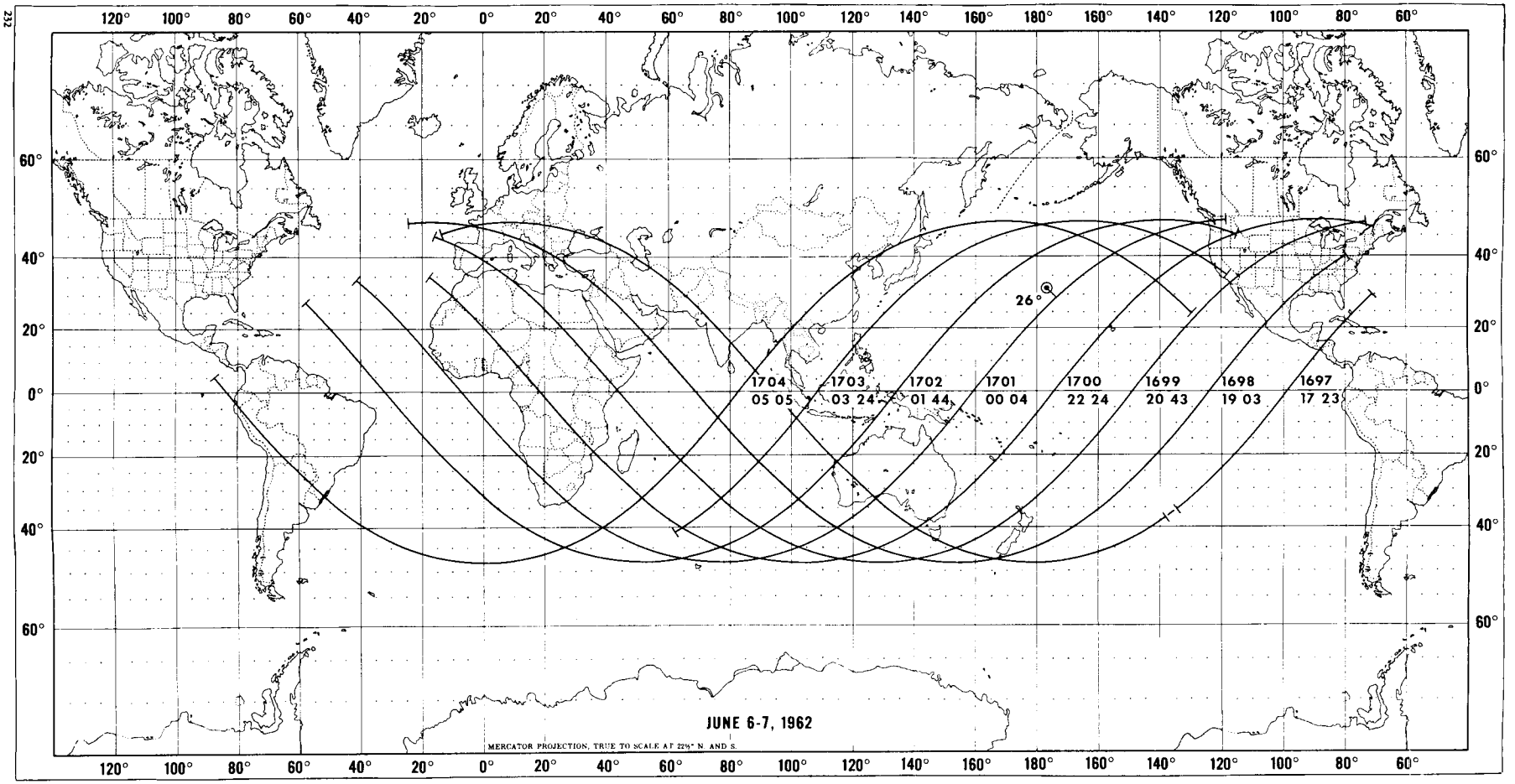
120° 100° 80° 60° 40° 20° 0° 20° 40° 60° 80° 100° 120° 140° 160° 180° 160° 140° 120° 100° 80° 60°
60°
40°
20°
0°
20°
40°
60°
26°
1704
05 05
1703
03 24
1702
01 44
1701
00 04
1700
22 24
1699
20 43
1698
19 03
1697
17 23
JUNE 6-7, 1962
MERCATOR PROJECTION, TRUE TO SCALE AT 22½° N. AND S.

729-166 O - 64 - 16

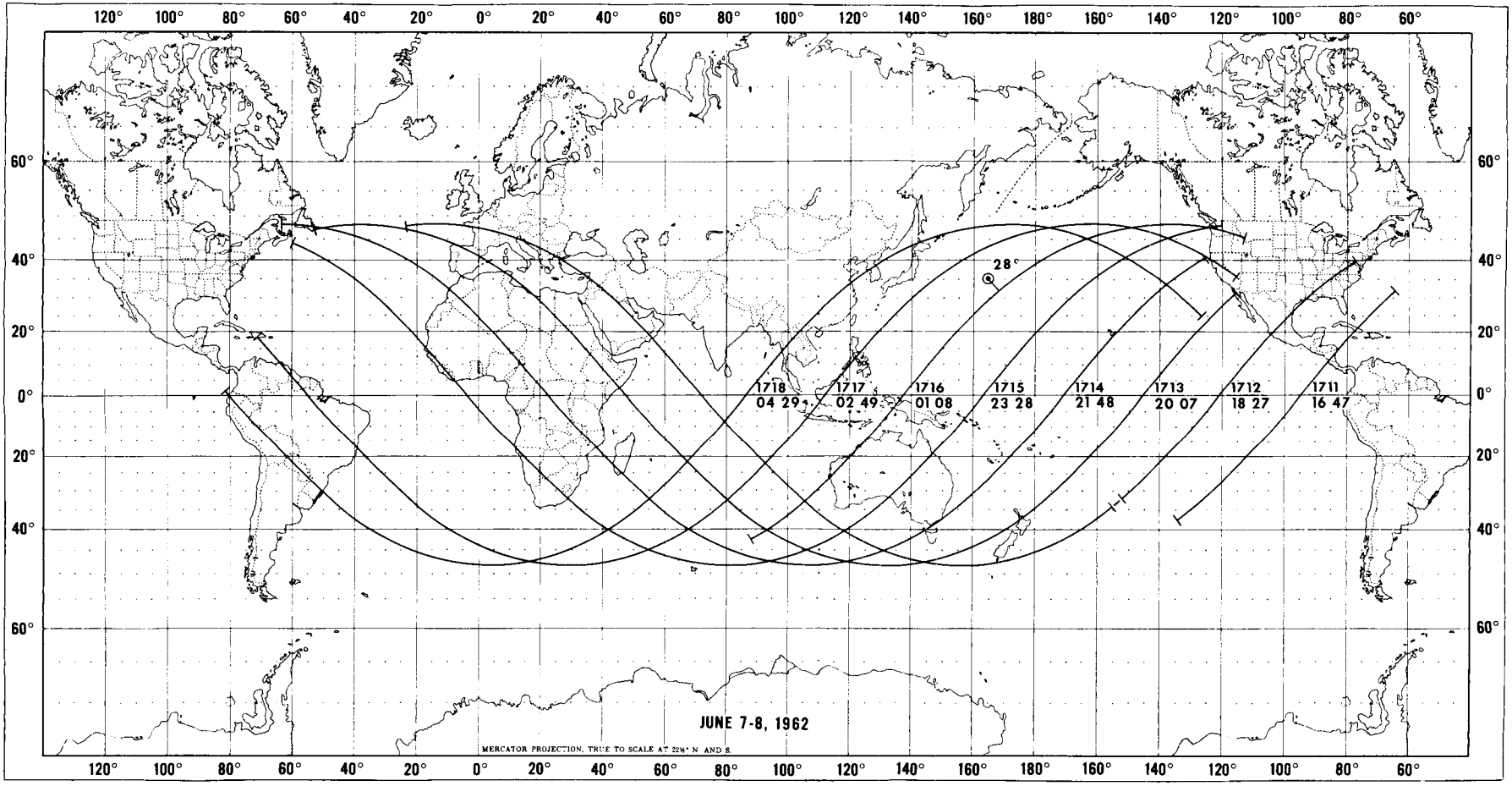

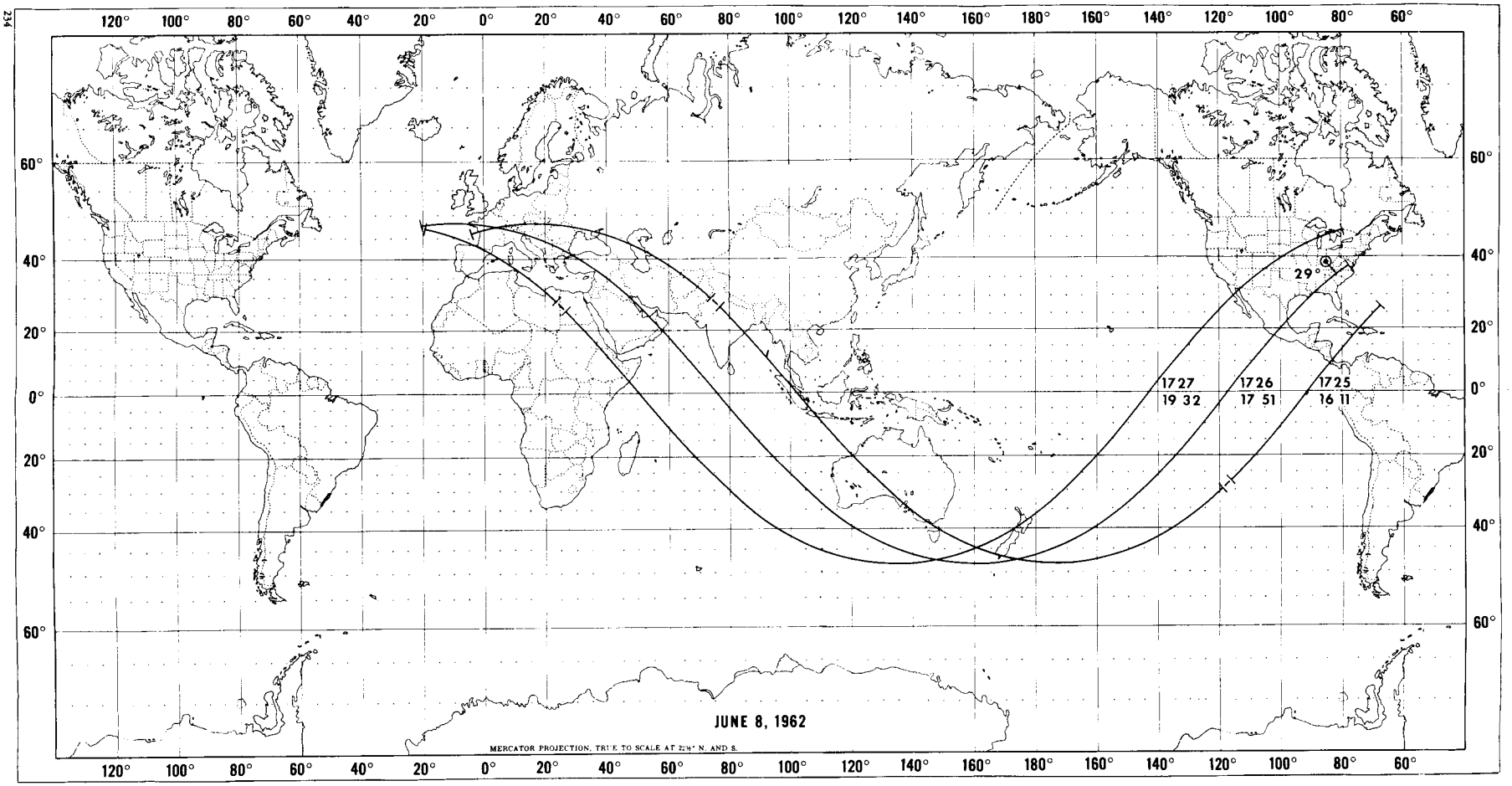
120° 100° 80° 60° 40° 20° 0° 20° 40° 60° 80° 100° 120° 140° 160° 180° 160° 140° 120° 100° 80° 60°
60°
40°
20°
0°
20°
40°
60°
29°
17 27
19 32
17 26
17 51
17 25
16 11
JUNE 8, 1962
MERCATOR PROJECTION, TRUE TO SCALE AT 2½° N. AND S.

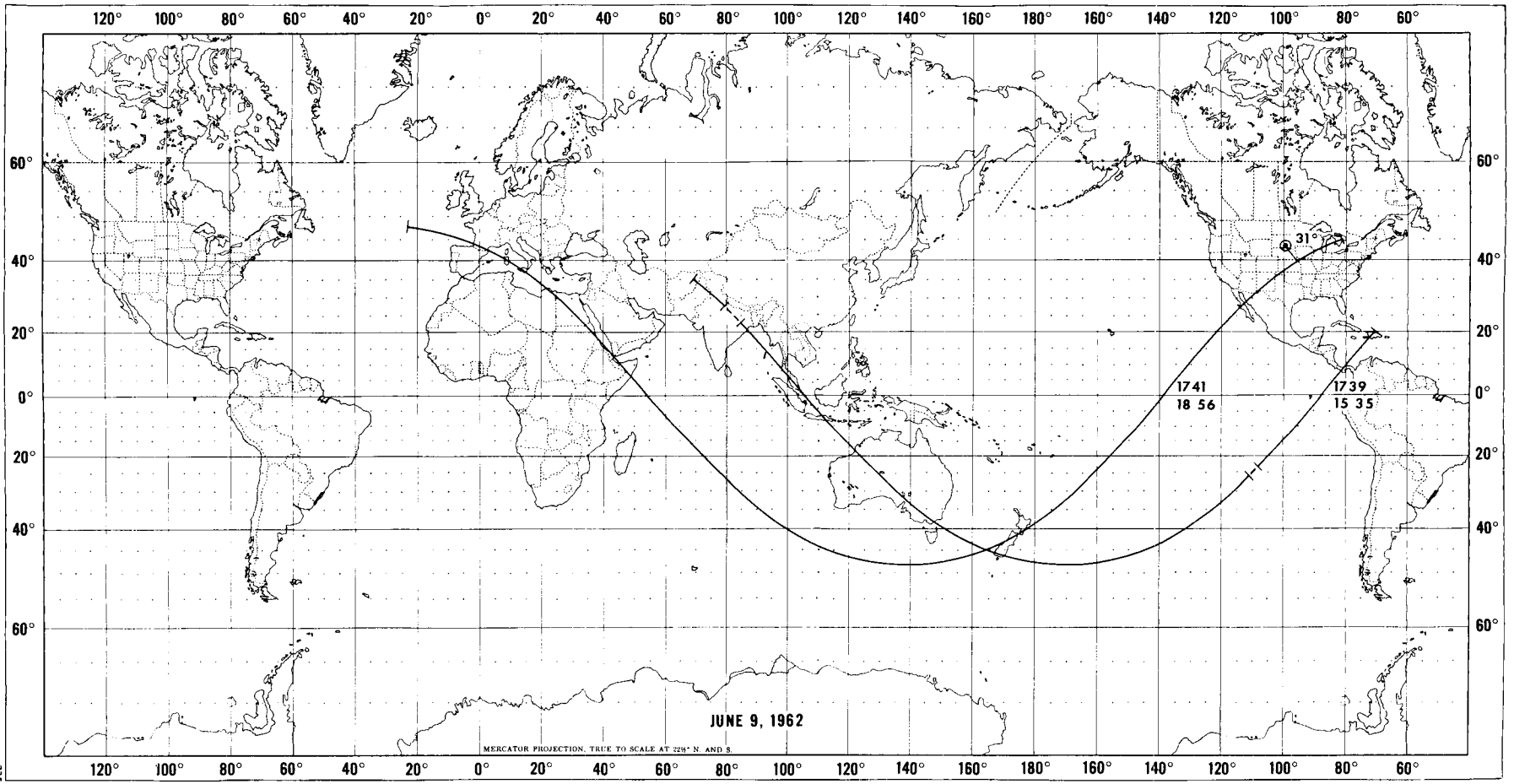
120° 100° 80° 60° 40° 20° 0° 20° 40° 60° 80° 100° 120° 140° 160° 180° 160° 140° 120° 100° 80° 60°
60°
40°
20°
0°
20°
40°
60°
31°
1741
18 56
1739
15 35
JUNE 9, 1962
MERCATOR PROJECTION, TRUE TO SCALE AT 22½° N. AND S.

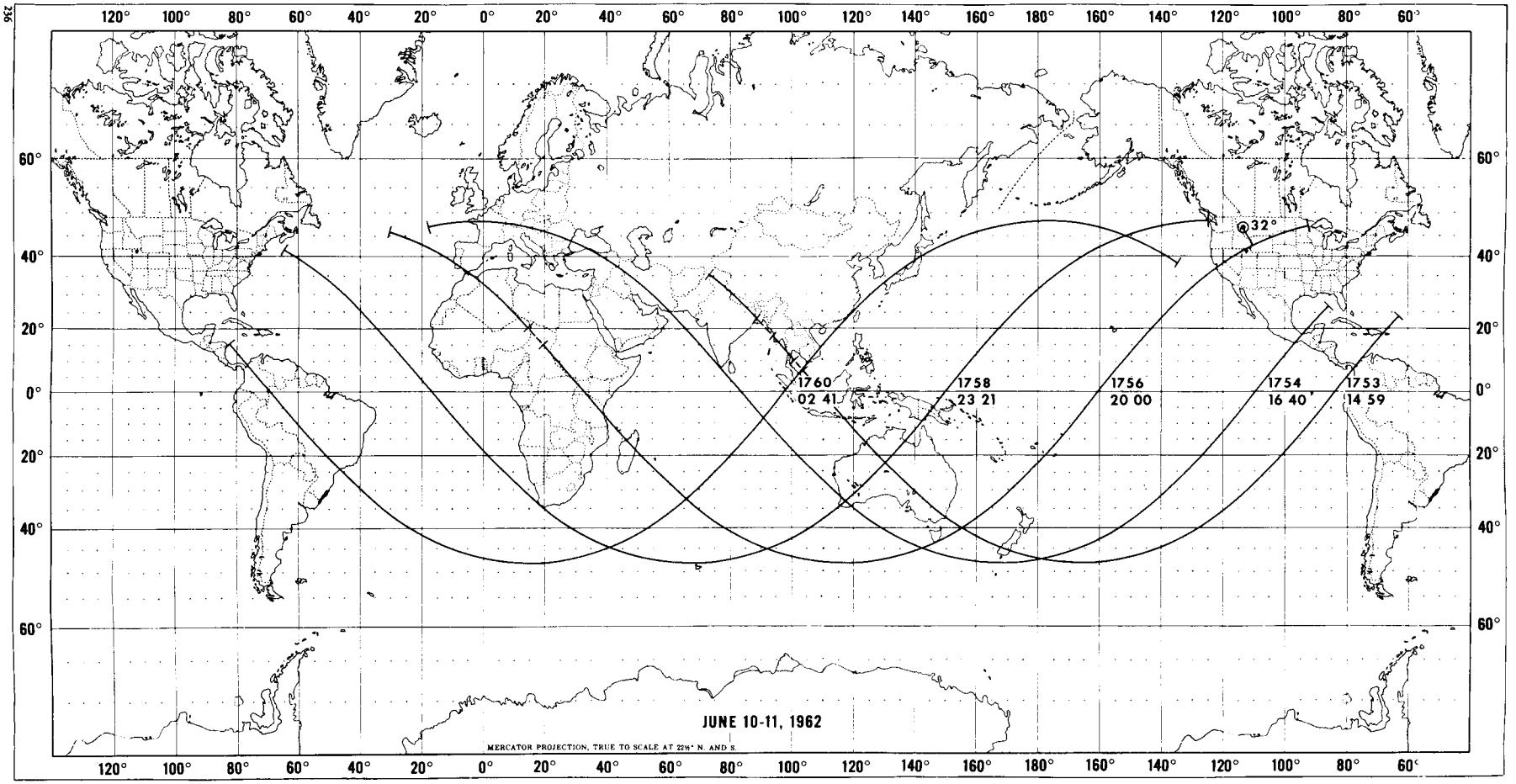
120° 100° 80° 60° 40° 20° 0° 20° 40° 60° 80° 100° 120° 140° 160° 180° 160° 140° 120° 100° 80° 60°
60°
40°
20°
0°
20°
40°
60°
32°
1760
02 41
1758
23 21
1756
20 00
1754
16 40
1753
14 59
JUNE 10-11, 1962
MERCATOR PROJECTION, TRUE TO SCALE AT 22½° N. AND S.

723-166 O - 64 - 17

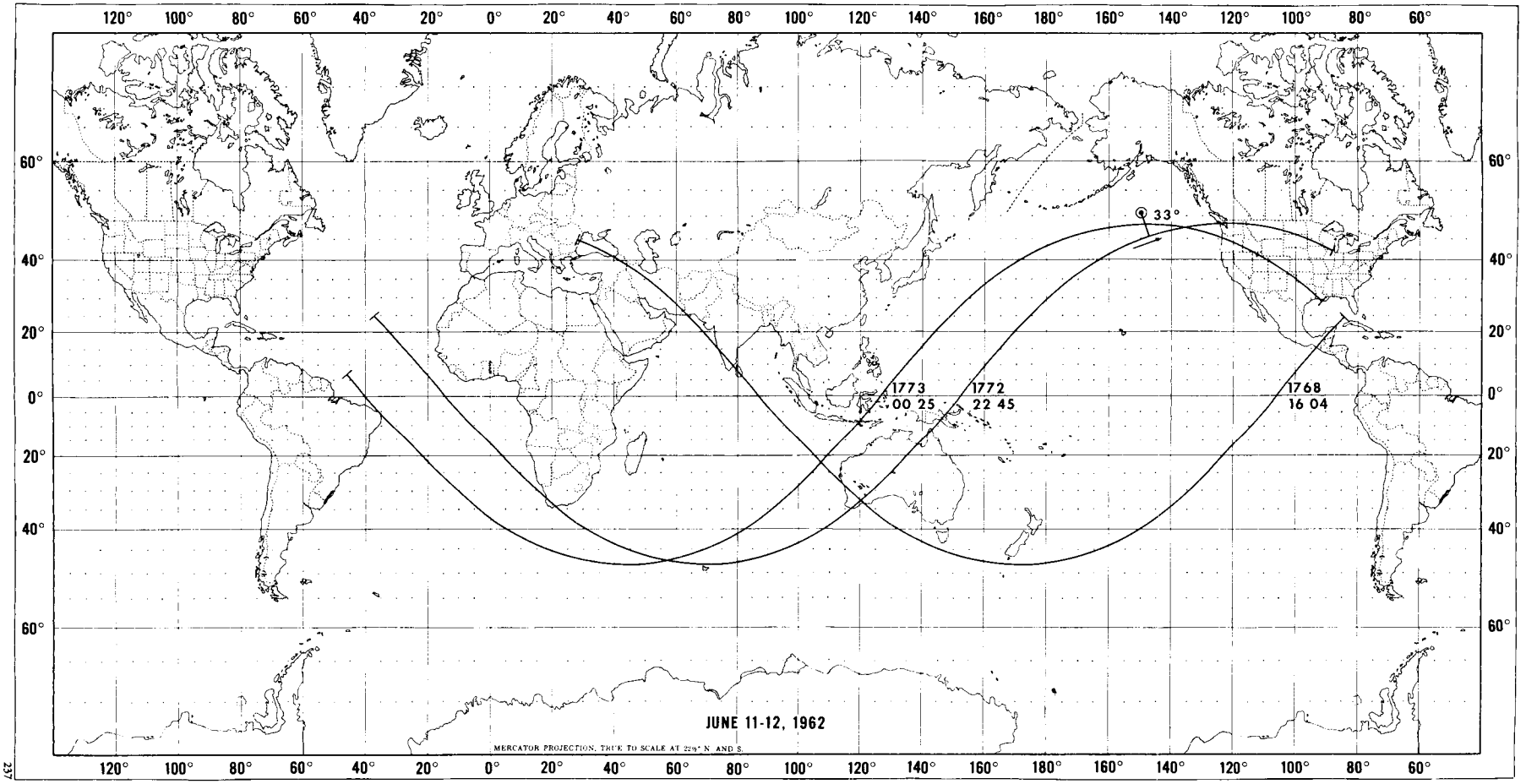

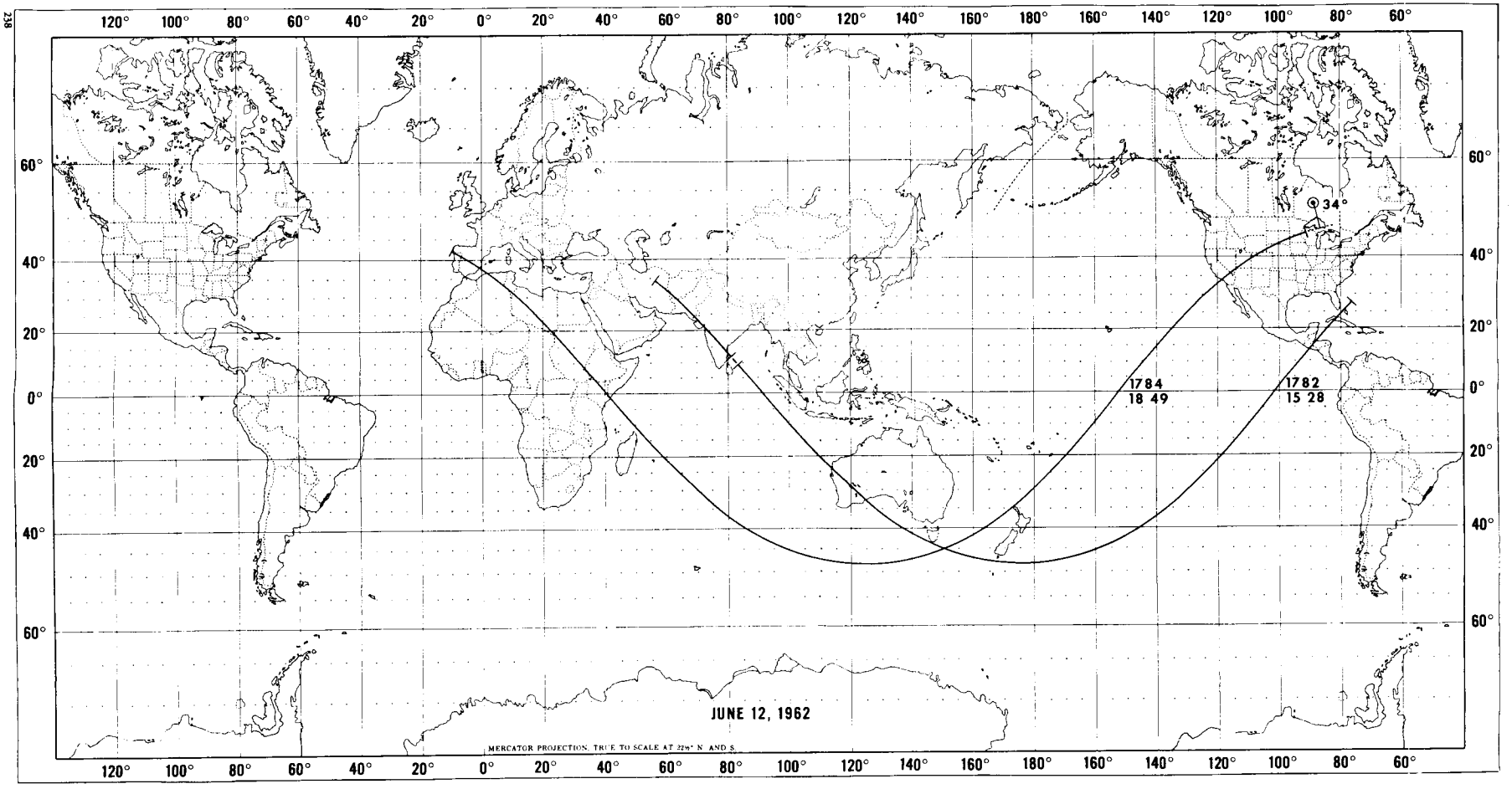
120° 100° 80° 60° 40° 20° 0° 20° 40° 60° 80° 100° 120° 140° 160° 180° 160° 140° 120° 100° 80° 60°
60°
40°
20°
0°
20°
40°
60°
34°
1784
18 49
1782
15 28
JUNE 12, 1962
MERCATOR PROJECTION. TRUE TO SCALE AT 22½° N. AND S.

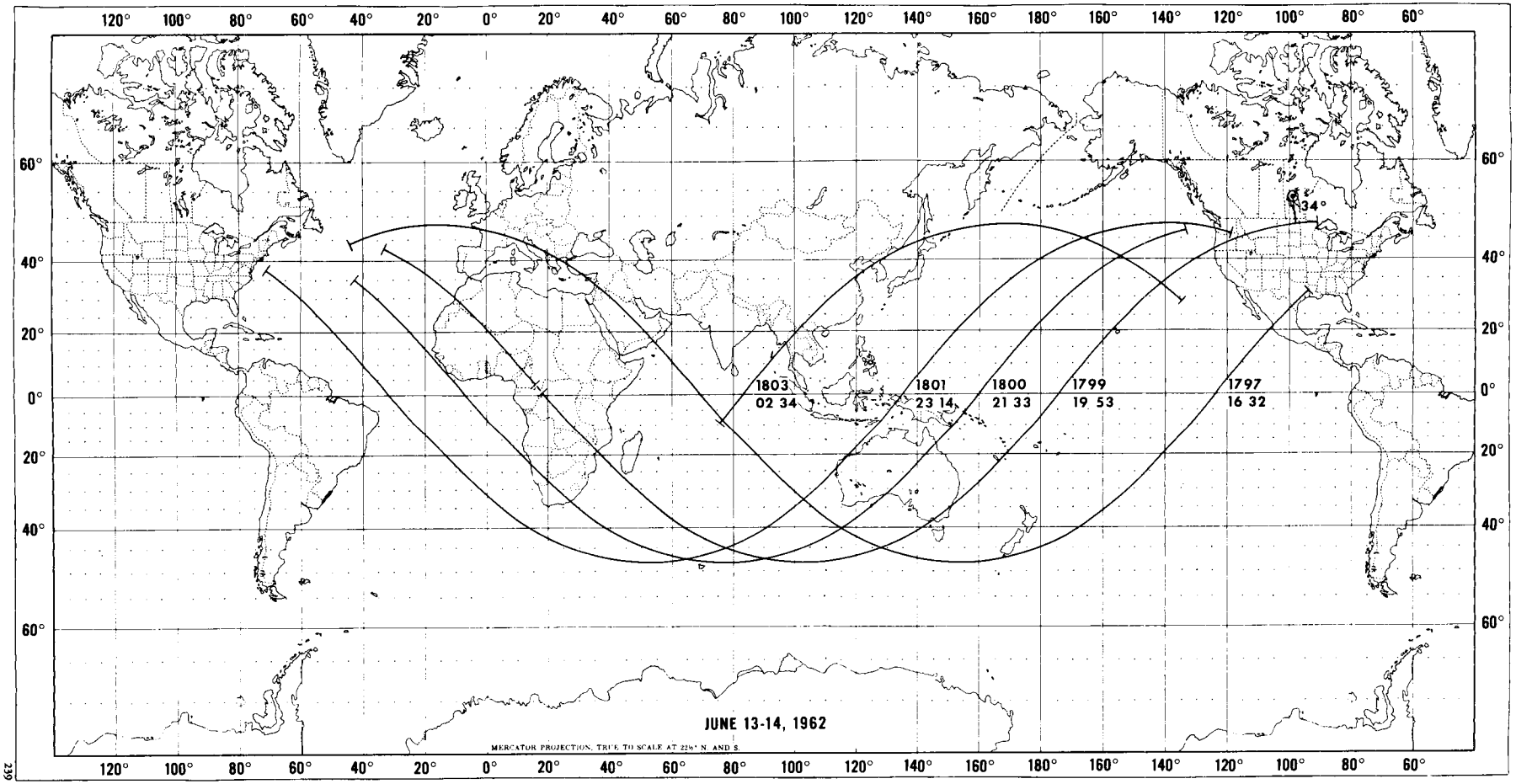
120° 100° 80° 60° 40° 20° 0° 20° 40° 60° 80° 100° 120° 140° 160° 180° 160° 140° 120° 100° 80° 60°
60°
40°
20°
0°
20°
40°
60°
34°
1803
02 34
1801
23 14
1800
21 33
1799
19 53
1797
16 32
JUNE 13-14, 1962
MERCATOR PROJECTION, TRUE TO SCALE AT 22½° N. AND S.

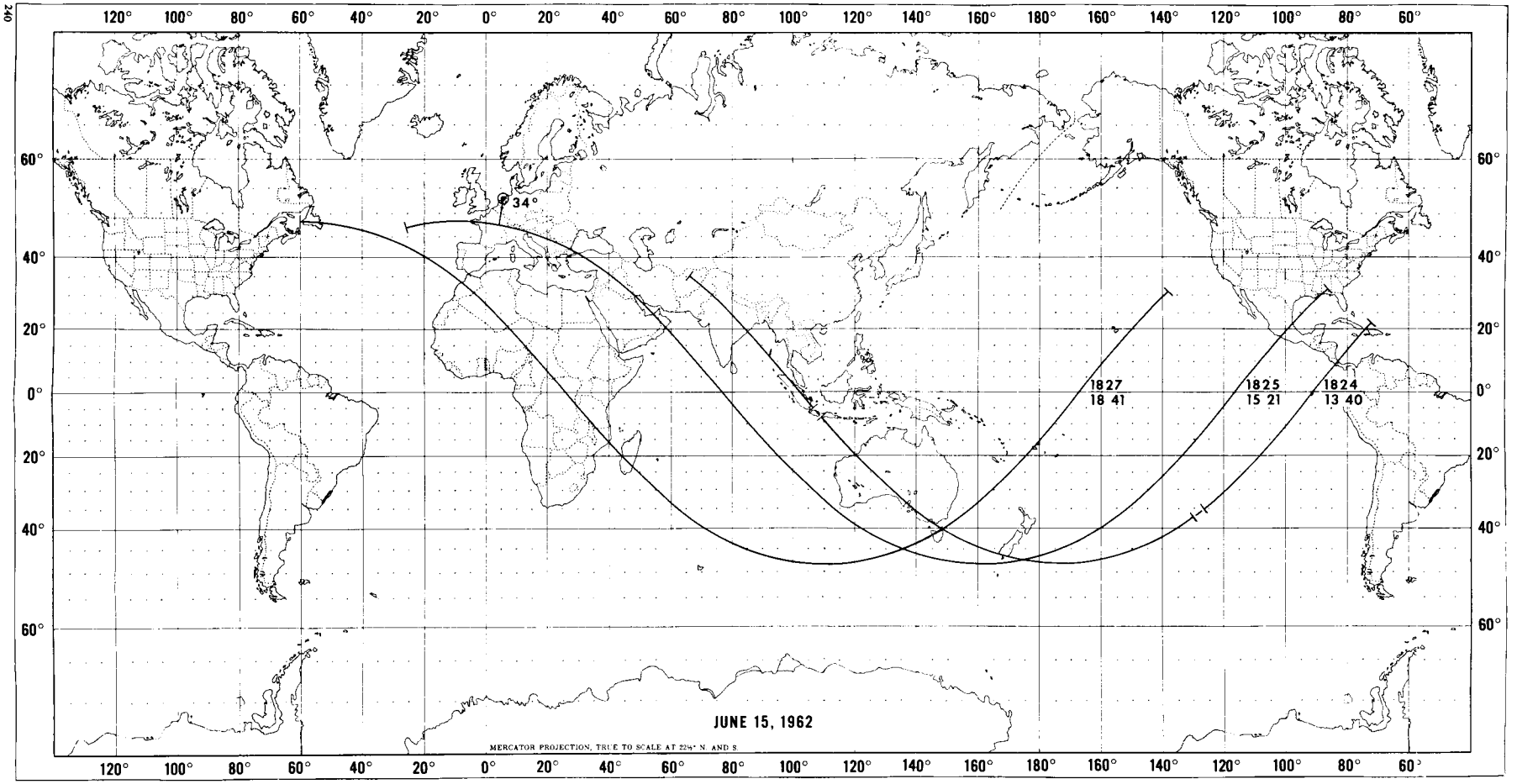
120° 100° 80° 60° 40° 20° 0° 20° 40° 60° 80° 100° 120° 140° 160° 180° 160° 140° 120° 100° 80° 60°
60°
40°
20°
0°
20°
40°
60°
34°
1827
18 41
1825
15 21
1824
13 40
JUNE 15, 1962
MERCATOR PROJECTION, TRUE TO SCALE AT 22½° N. AND S.

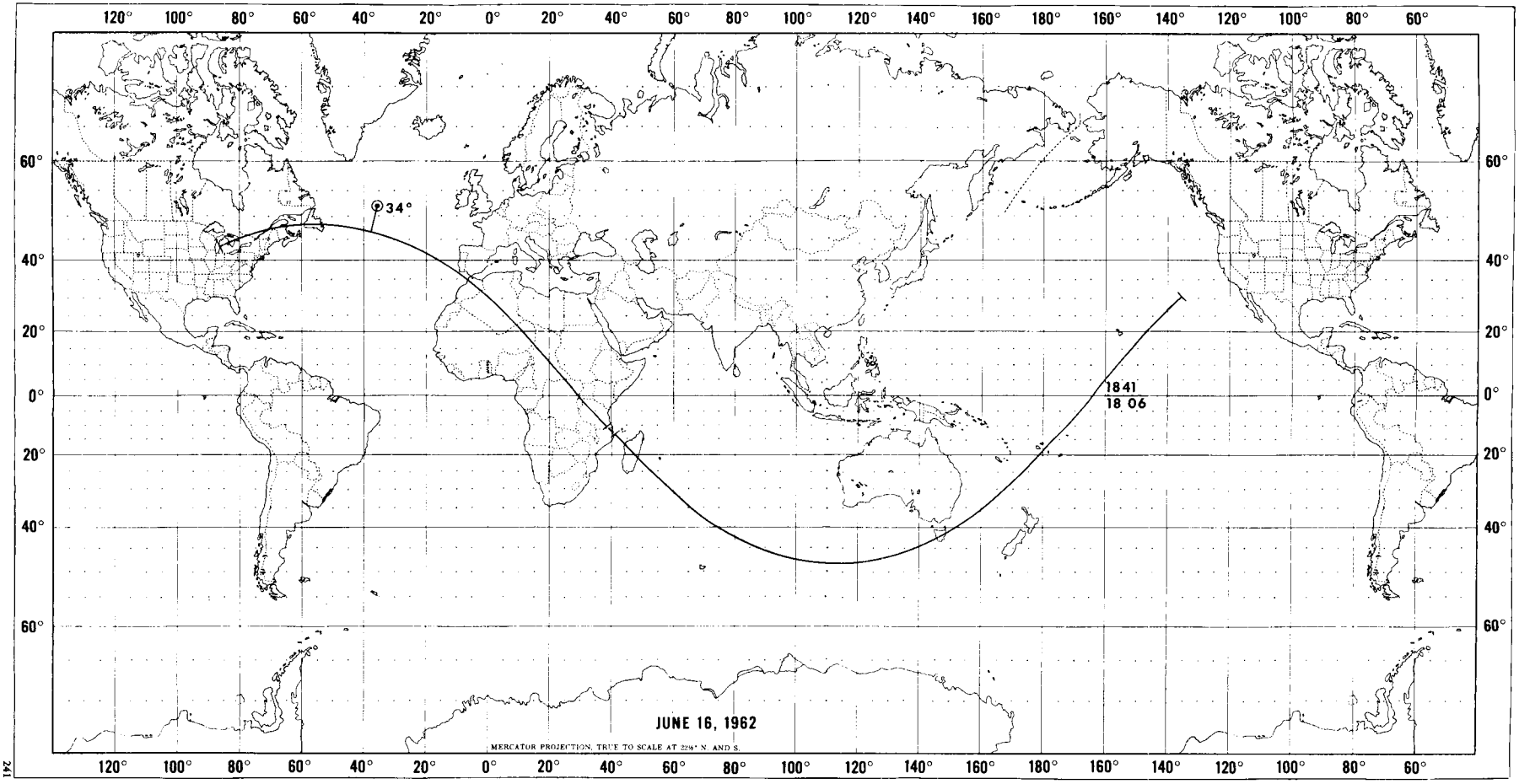
120° 100° 80° 60° 40° 20° 0° 20° 40° 60° 80° 100° 120° 140° 160° 180° 160° 140° 120° 100° 80° 60°
60°
40°
20°
0°
20°
40°
60°
34°
1841
18 06
JUNE 16, 1962
MERCATOR PROJECTION, TRUE TO SCALE AT 22½° N. AND S.

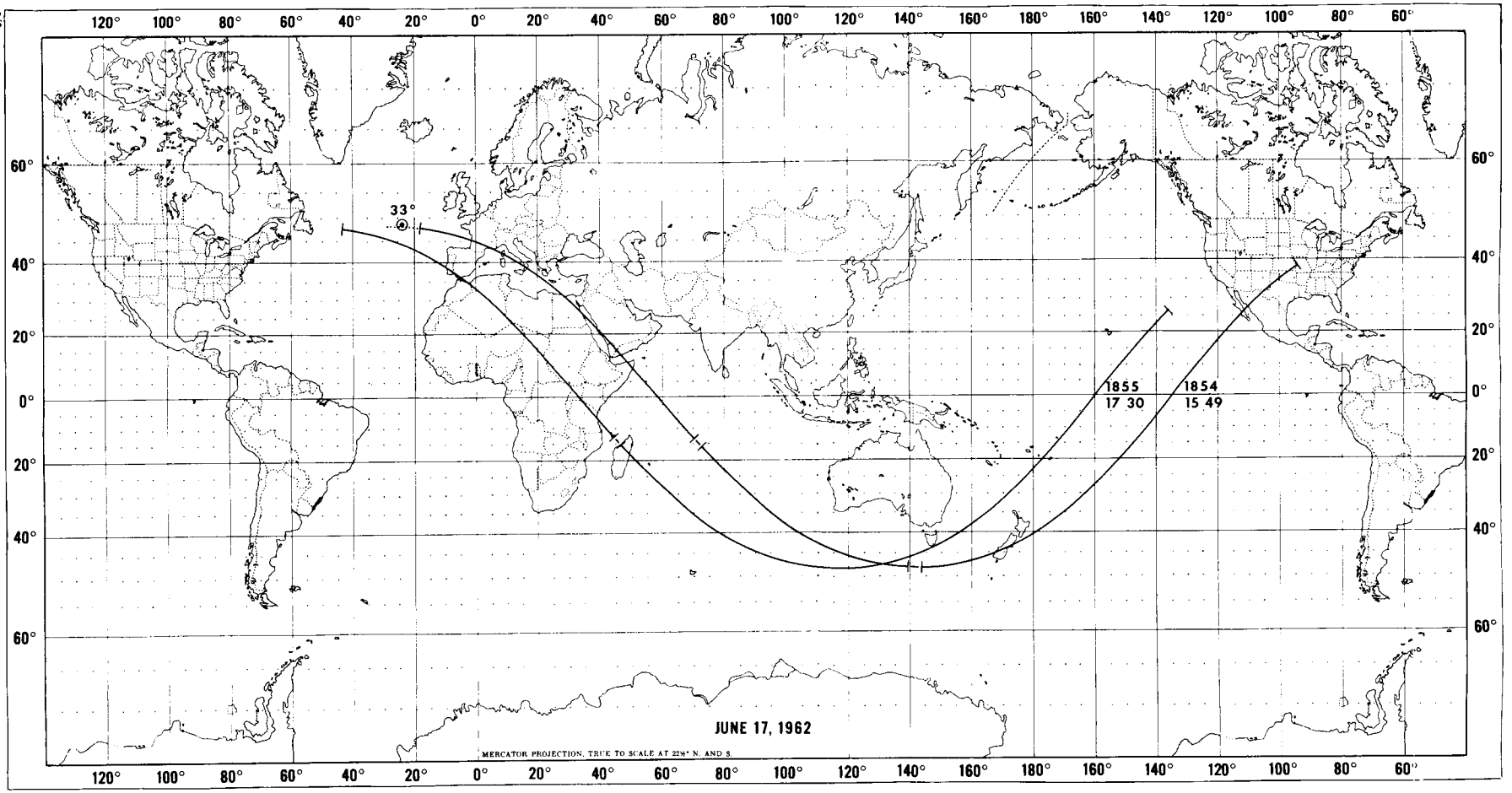
120° 100° 80° 60° 40° 20° 0° 20° 40° 60° 80° 100° 120° 140° 160° 180° 160° 140° 120° 100° 80° 60°
60°
40°
20°
0°
20°
40°
60°
33°
1855
17 30
1854
15 49
JUNE 17, 1962
MERCATOR PROJECTION, TRUE TO SCALE AT 22½° N. AND S.

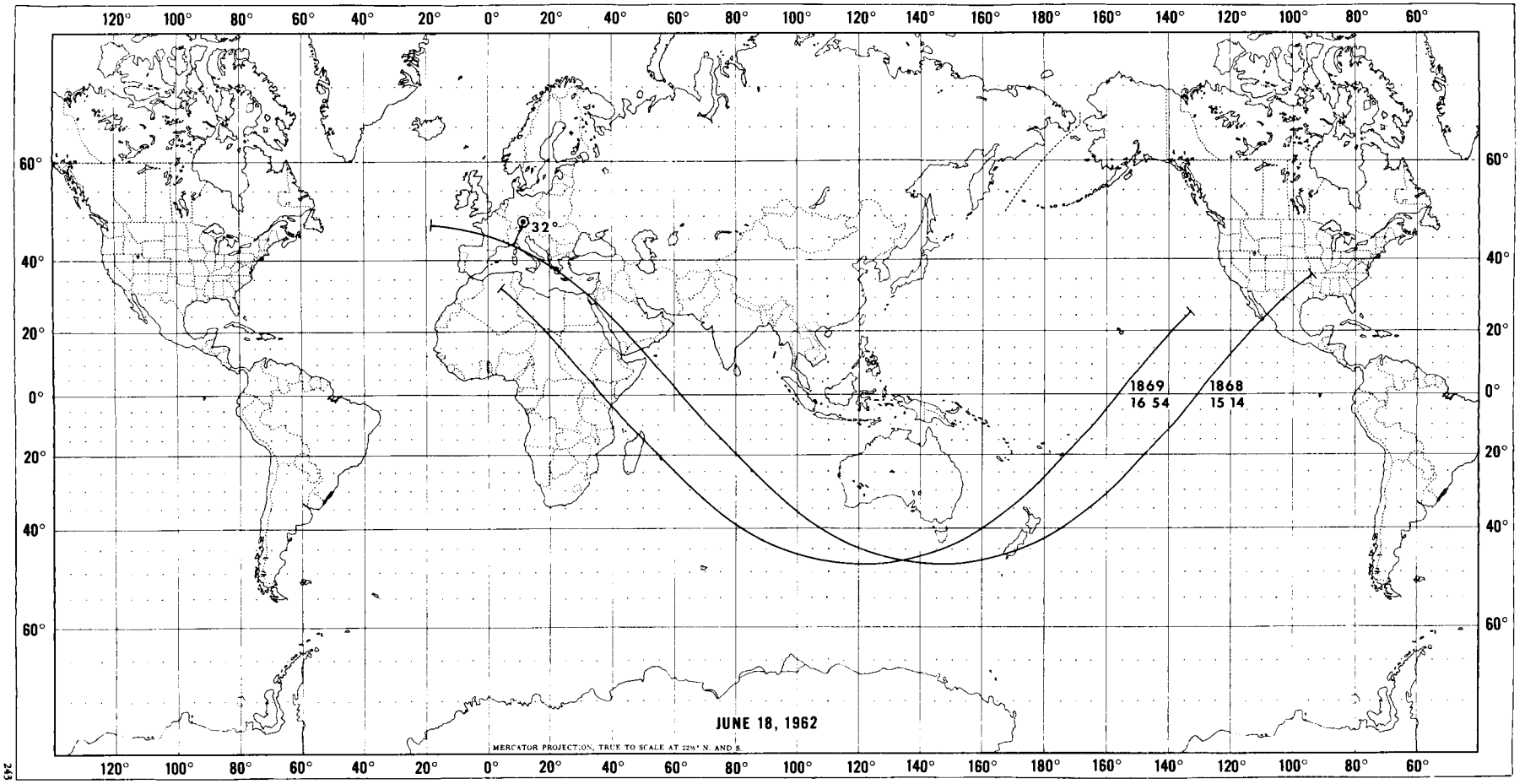
120° 100° 80° 60° 40° 20° 0° 20° 40° 60° 80° 100° 120° 140° 160° 180° 160° 140° 120° 100° 80° 60°
60°
40°
20°
0°
20°
40°
60°
32°
1869
16 54
1868
15 14
JUNE 18, 1962
MERCATOR PROJECTION, TRUE TO SCALE AT 22½° N. AND S.

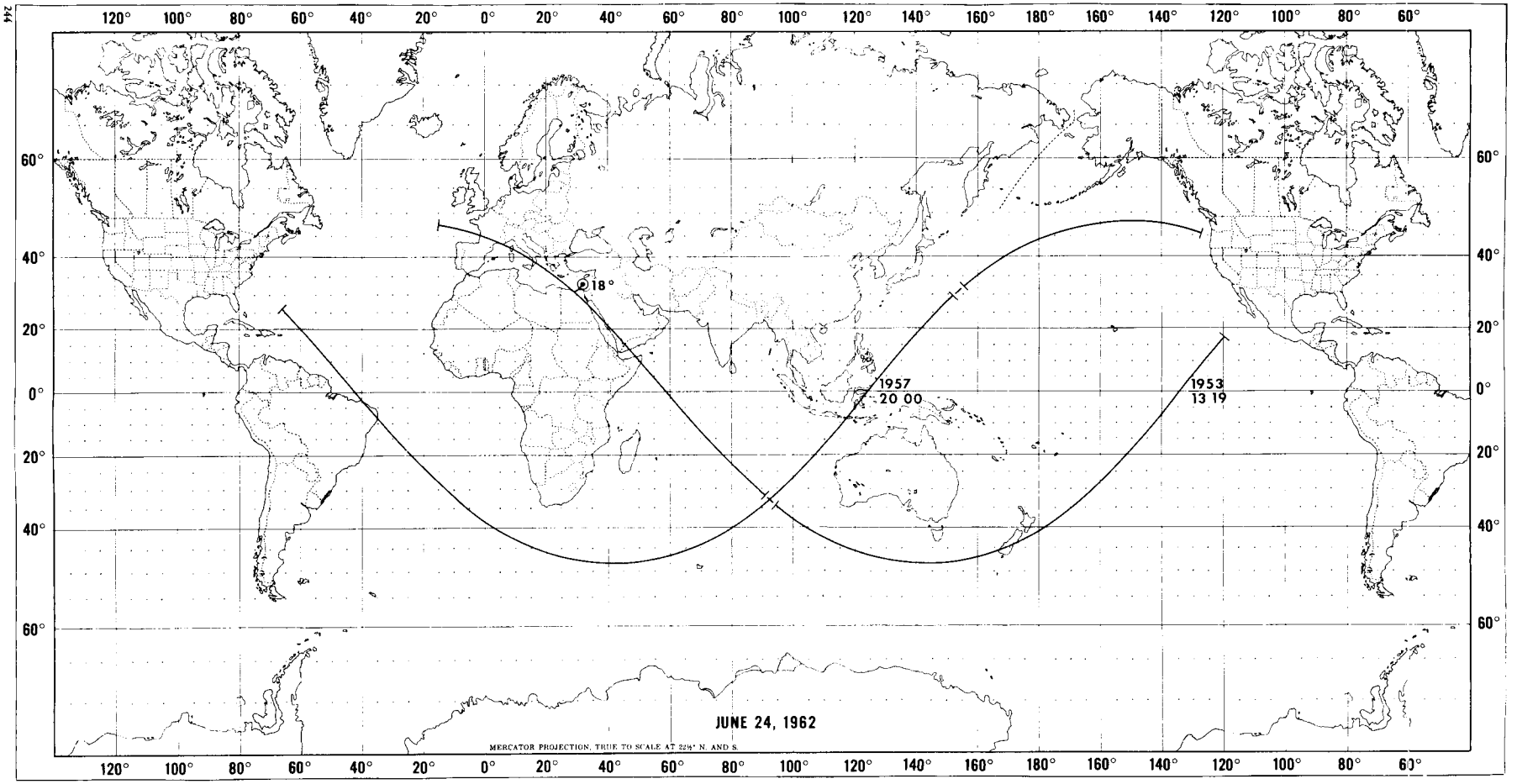
120° 100° 80° 60° 40° 20° 0° 20° 40° 60° 80° 100° 120° 140° 160° 180° 160° 140° 120° 100° 80° 60°
60°
40°
20°
0°
20°
40°
60°
18°
1957
20 00
1953
13 19
JUNE 24, 1962
MERCATOR PROJECTION, TRUE TO SCALE AT 22½° N. AND S.

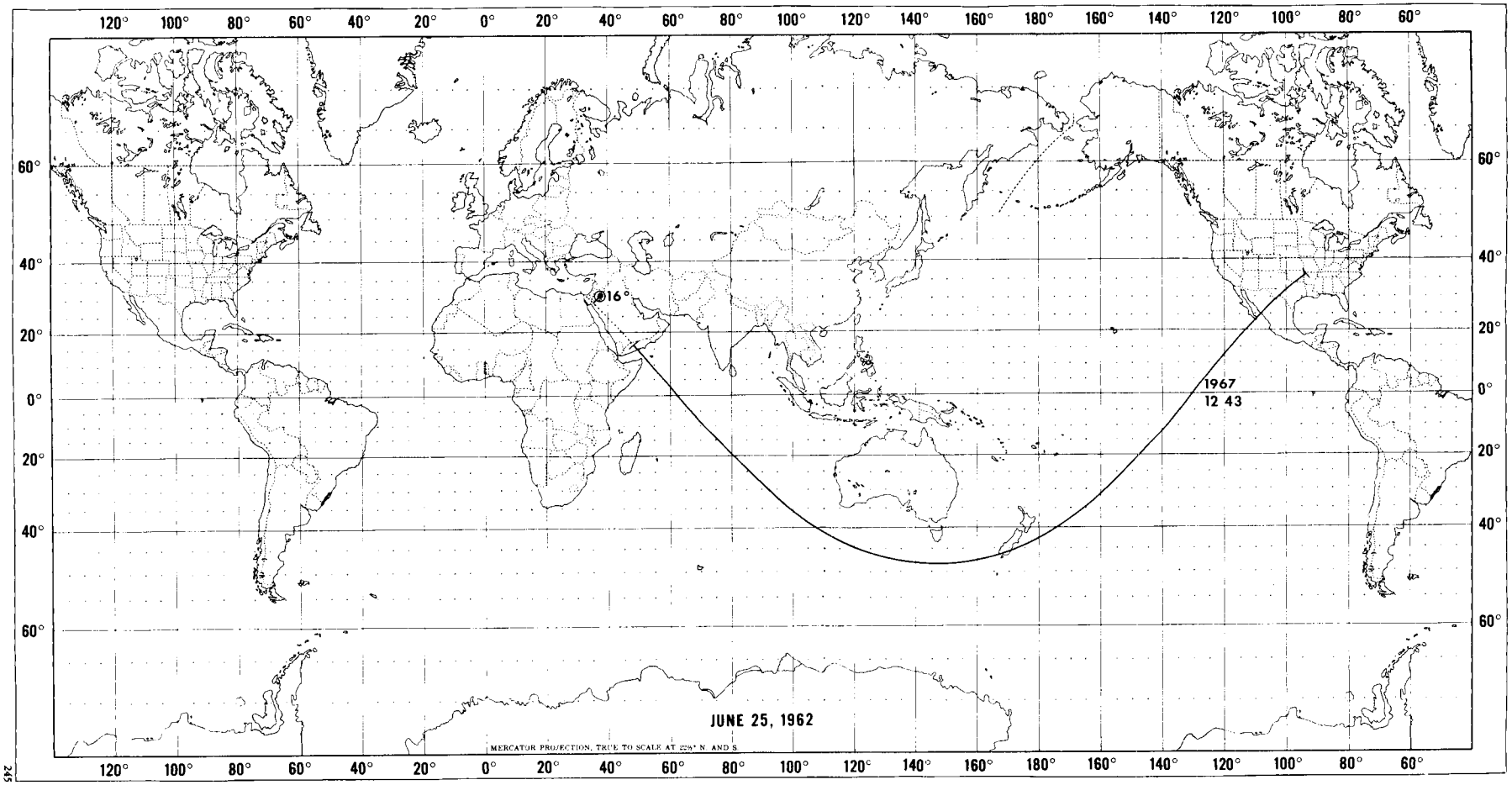
120° 100° 80° 60° 40° 20° 0° 20° 40° 60° 80° 100° 120° 140° 160° 180° 160° 140° 120° 100° 80° 60°
60°
40°
20°
0°
20°
40°
60°
16°
1967
12 43
JUNE 25, 1962
MERCATOR PROJECTION, TRUE TO SCALE AT 22½° N. AND S.

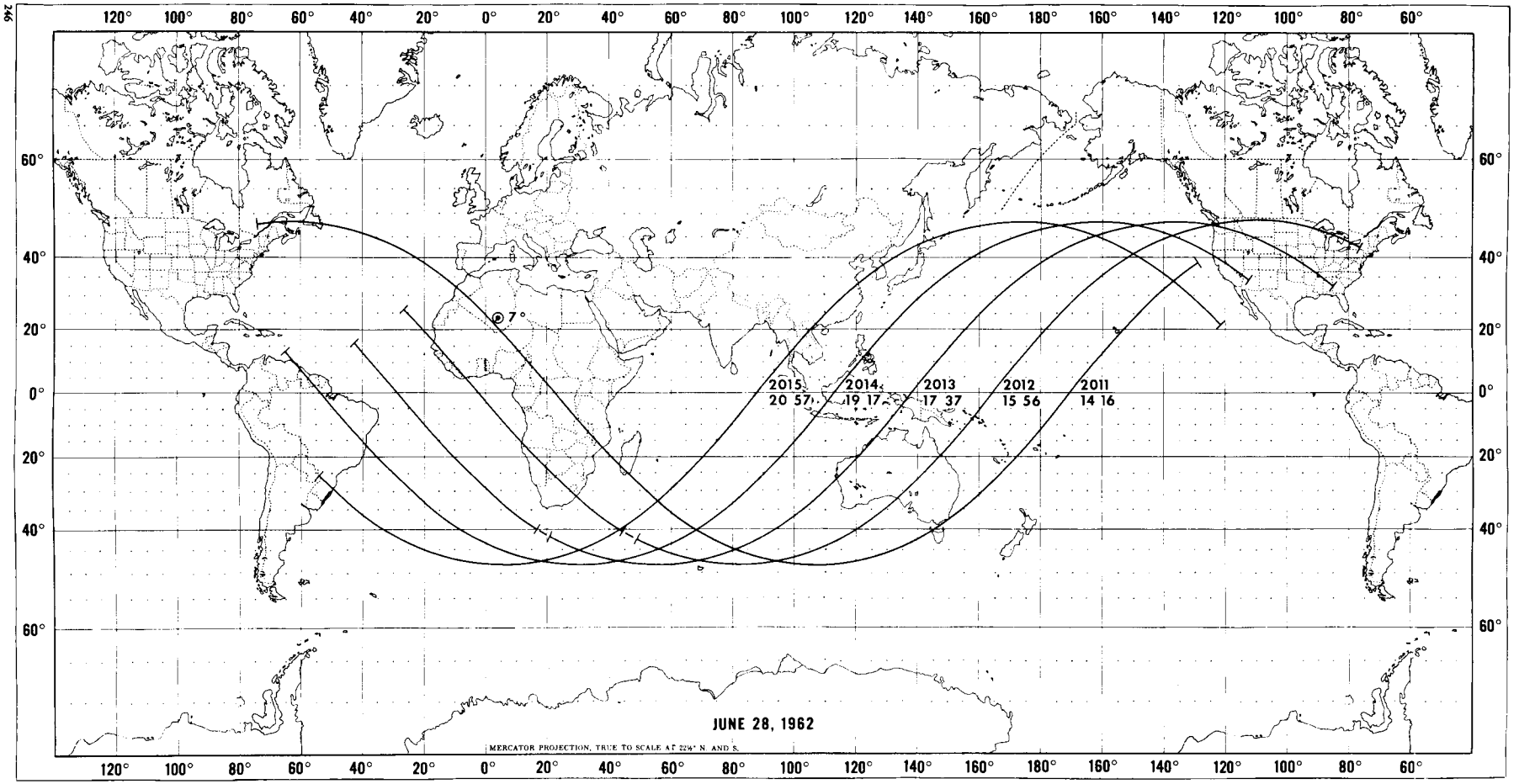
120° 100° 80° 60° 40° 20° 0° 20° 40° 60° 80° 100° 120° 140° 160° 180° 160° 140° 120° 100° 80° 60°
60°
40°
20°
0°
20°
40°
60°
7°
2015
20 57
2014
19 17
2013
17 37
2012
15 56
2011
14 16
JUNE 28, 1962
MERCATOR PROJECTION, TRUE TO SCALE AT 22½° N. AND S.

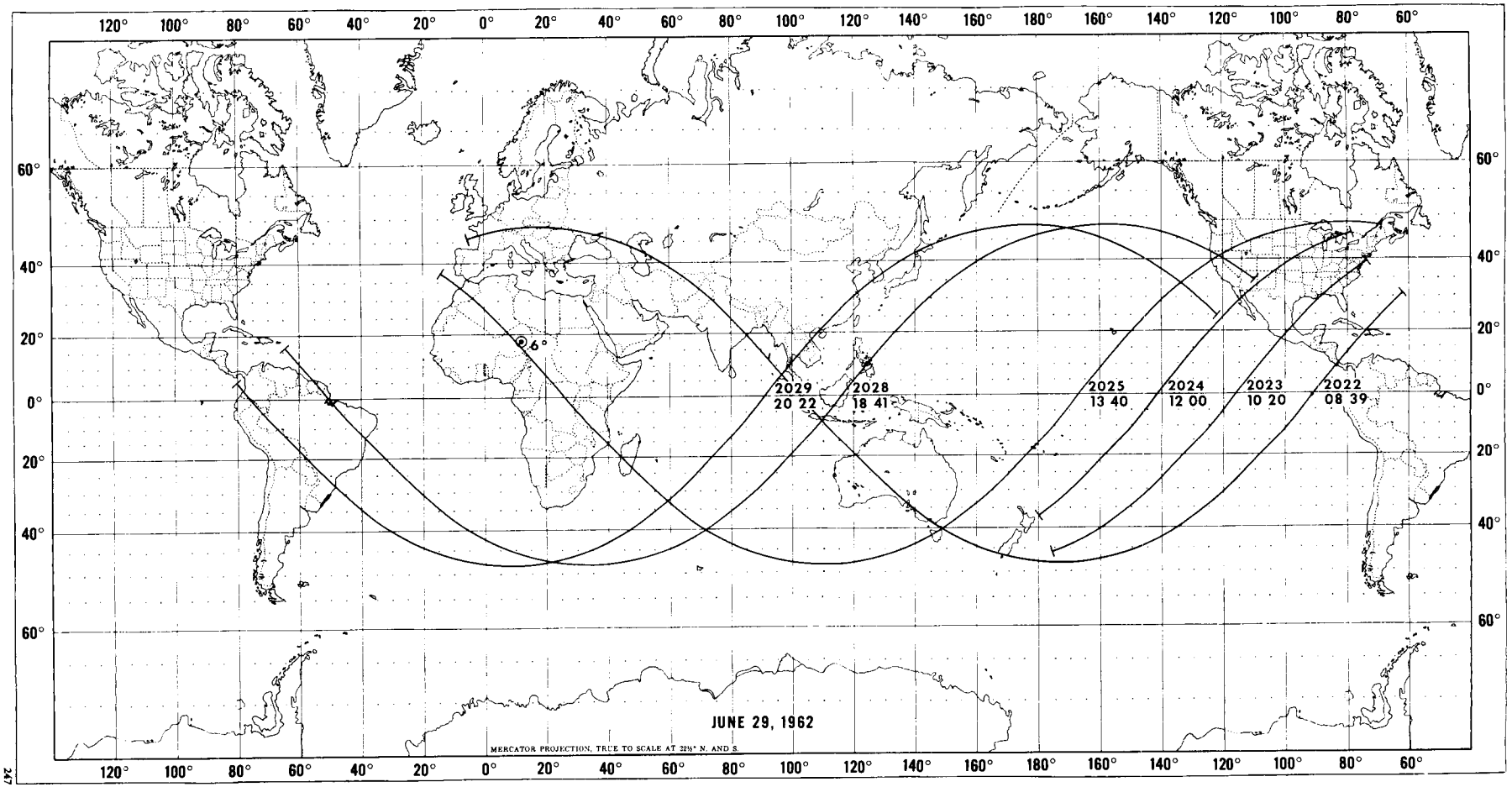
120° 100° 80° 60° 40° 20° 0° 20° 40° 60° 80° 100° 120° 140° 160° 180° 160° 140° 120° 100° 80° 60°
60°
40°
20°
0°
20°
40°
60°
6°
2029
20 22
2028
18 41
2025
13 40
2024
12 00
2023
10 20
2022
08 39
JUNE 29, 1962
MERCATOR PROJECTION, TRUE TO SCALE AT 22½° N. AND S.

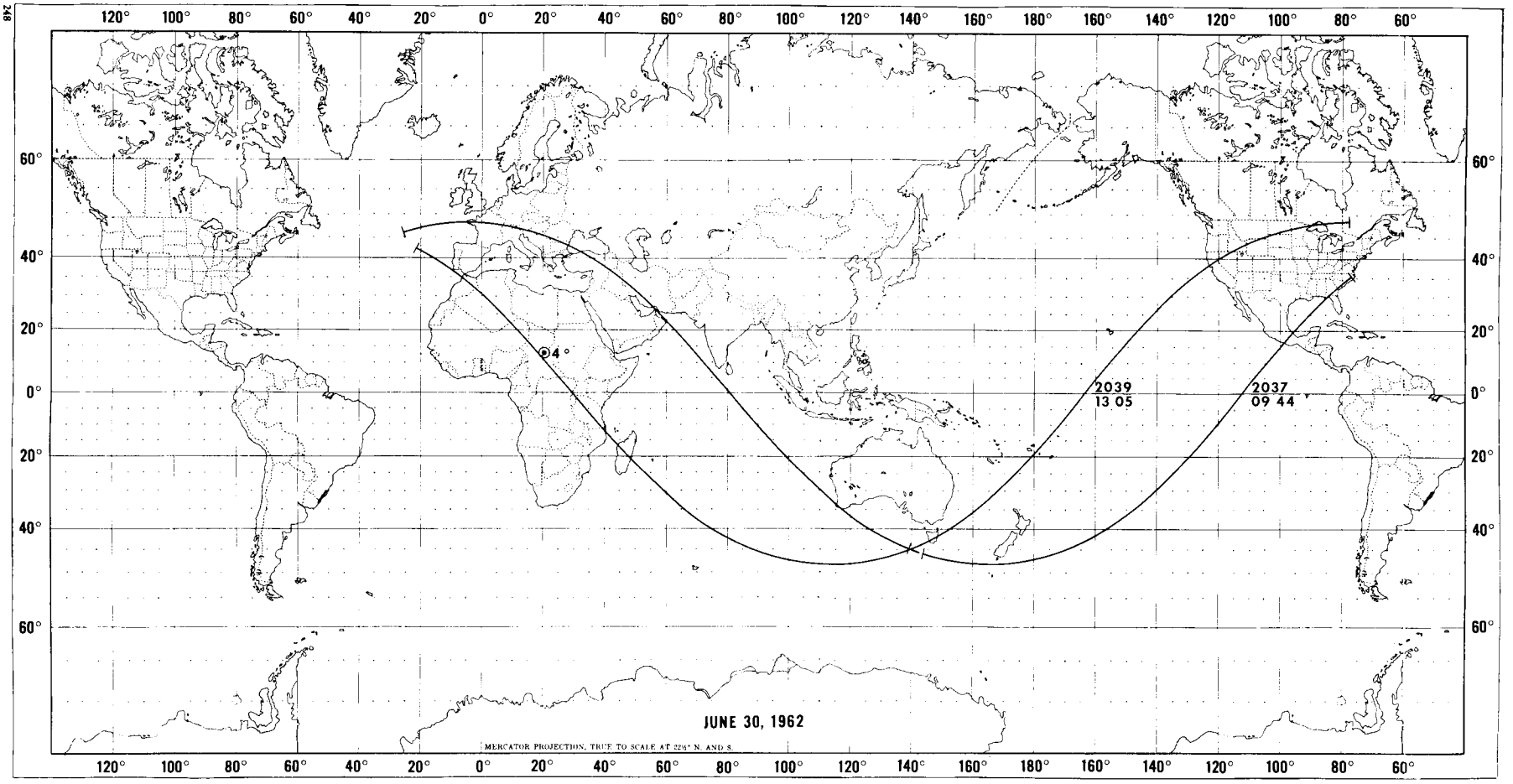
120° 100° 80° 60° 40° 20° 0° 20° 40° 60° 80° 100° 120° 140° 160° 180° 160° 140° 120° 100° 80° 60°
60°
40°
20°
0°
20°
40°
60°
4°
2039
13 05
2037
09 44
JUNE 30, 1962
MERCATOR PROJECTION, TRUE TO SCALE AT 22½° N. AND S.

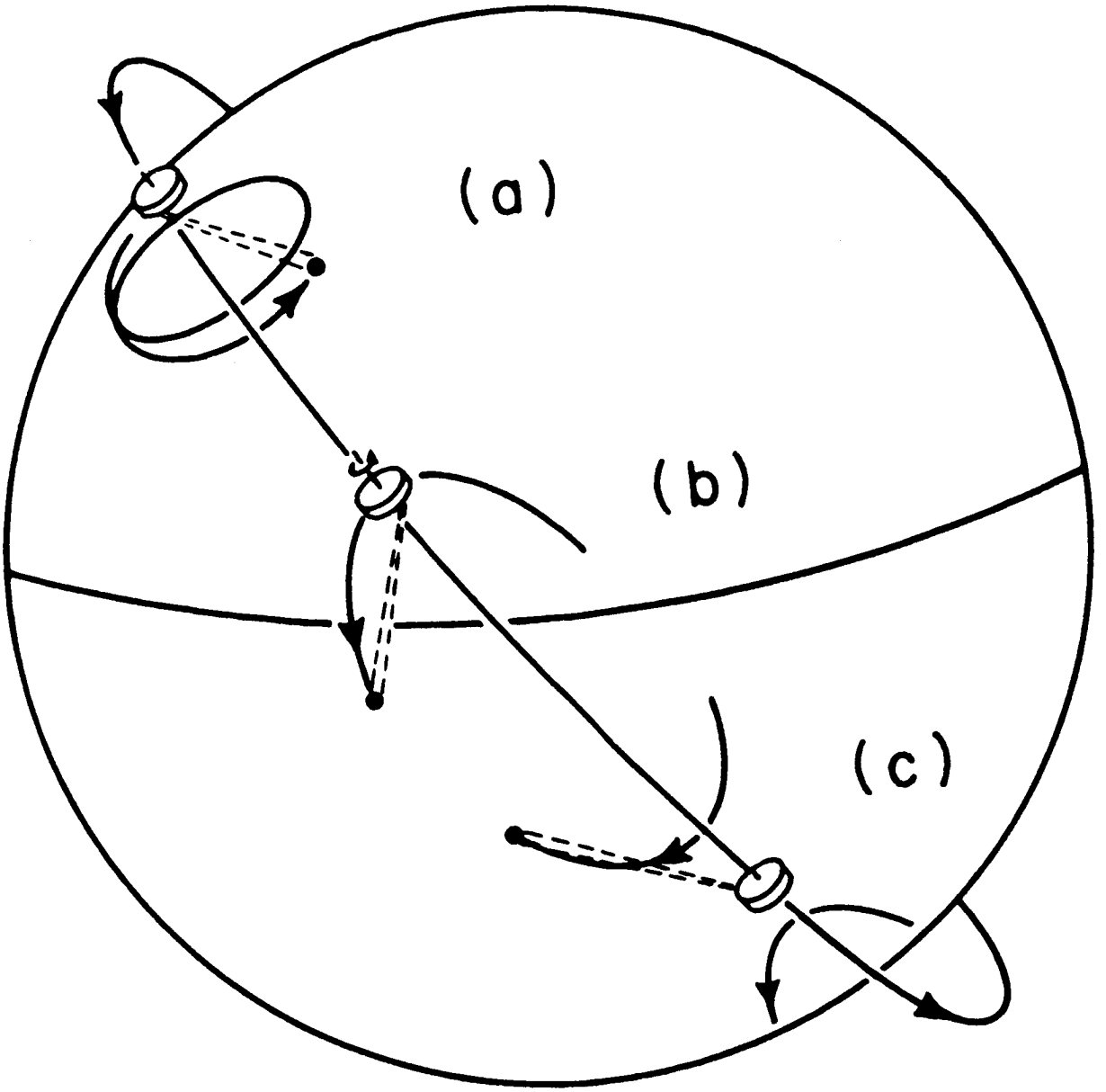

Figure B1—Scanning modes of the TIROS Radiometer: (*a*) Closed Mode, (*b*) Single Open Mode, and (*c*) Alternating Open Mode

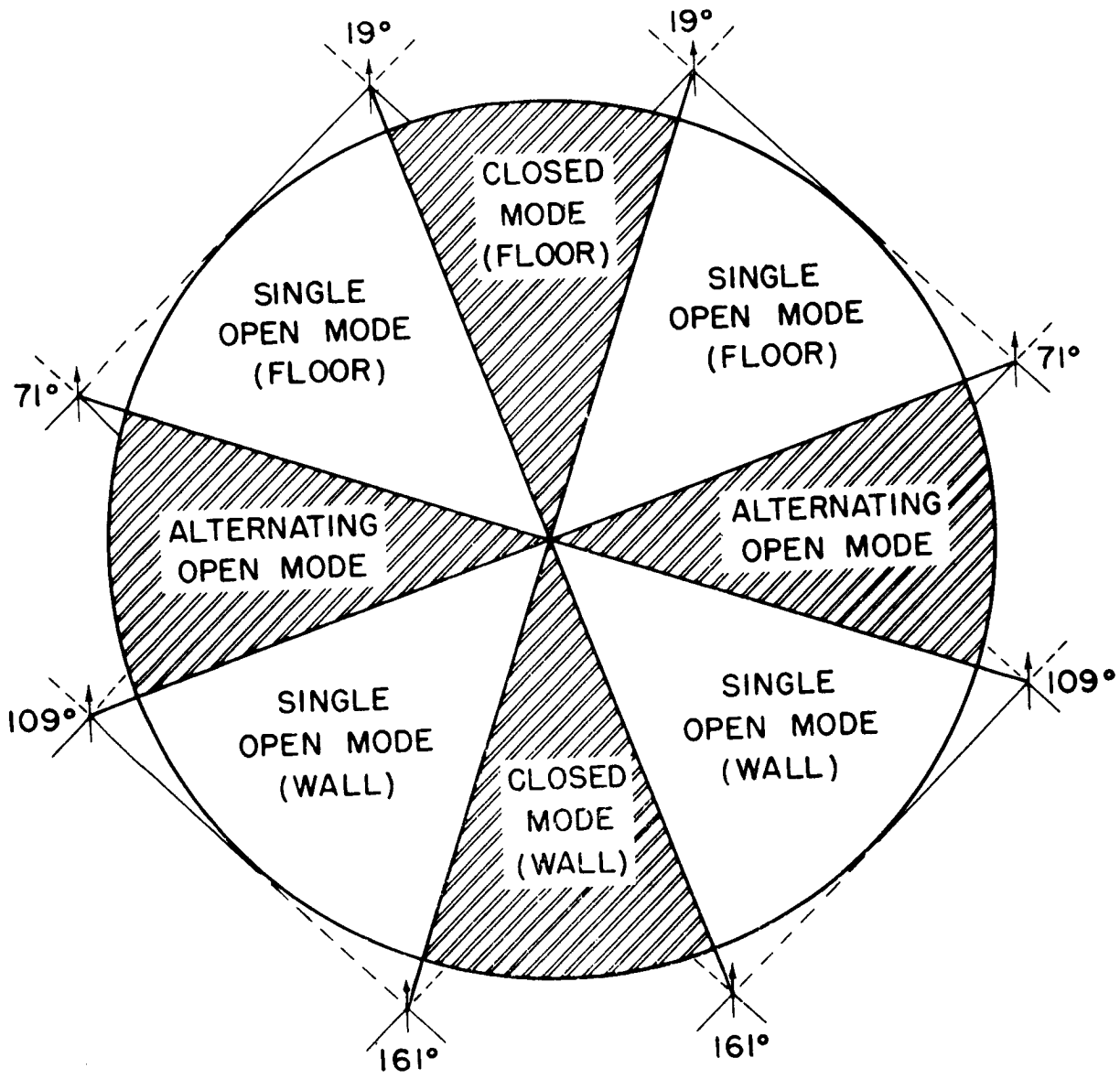

Figure B2—Nominal boundary satellite nadir angles for the various scanning modes at a height of about 717 km. Arrows indicate the spin vector through the top of the satellite, and the nadir angles refer to the opposite direction, viz., the spin (camera) axis. Solid lines at 45° to the arrows indicate the floor and dashed lines the wall scan of the radiometer.

U. S. GOVERNMENT PRINTING OFFICE : 1964 O - 729-166